Durham University

Durham E-Theses

Development of Novel Stem Cell Based Neurite Outgrowth Models and their Application to Study Neurite Inhibition in Neurological Disorders

KIRSTY ELIZABETH GONCALVES

How to cite:

GONCALVES, KIRSTY ELIZABETH (2017) Development of Novel Stem Cell Based Neurite Outgrowth Models and their Application to Study Neurite Inhibition in Neurological Disorders. Doctoral thesis, Durham University.

Use policy

The full-text may be used and/or reproduced, and given to third parties in any format or medium, without prior permission or charge, for personal research or study, educational, or not-for-profit purposes provided that:

- a full bibliographic reference is made to the original source
- a https://etheses.durham.ac.uk/id/eprint/12414/ is made to the metadata record in Durham E-Theses
- the full-text is not changed in any way

The full-text must not be sold in any format or medium without the formal permission of the copyright holders.

Please consult the full Durham E-Theses policy for further details.

Academic Support Office, The Palatine Centre, Durham University, Stockton Road, Durham, DH1 3LE
e-mail: e-theses.admin@durham.ac.uk Tel: +44 0191 334 6107
https://etheses.durham.ac.uk

Department of Biosciences

Development of Novel Stem Cell Based Neurite Outgrowth Models and their Application to Study Neurite Inhibition in Neurological Disorders

Kirsty Elizabeth Goncalves

A thesis submitted for the degree of Doctor of Philosophy

2017

Abstract

The inability of central nervous system (CNS) neurons to regenerate results in lost neural connectivity and is common to many neurological disorders. This loss of connectivity results in functional deficit following trauma such as spinal cord injury (SCI) and has been implicated in many neurodegenerative diseases including Alzheimer's disease (AD). Throughout this project a robust, reliable and physiologically relevant 3D model of human neuritogenesis was developed and applied to investigate the process of neurite inhibition, along with its underlying signalling mechanisms.

SCI results in the formation of a glial scar; involving the activation of astrocytes and secretion of inhibitory molecules that act through receptors to inhibit neurite growth thereby reducing neural connectivity. This project describes several approaches used to investigate this process including growth substrate coating, biomimetic 2D/3D functionalised growth surfaces and the development of a co-culture model to study reactive astrocyte-neuron interactions. Each approach has successfully led to neurite inhibition, and we have also demonstrated the ability of small molecules to restore neurite outgrowth despite the presence of inhibitory stimuli.

Inhibition of neurite growth is also associated with β-amyloid (Aβ) deposition, a hallmark of AD. Neurites that pass through deposits become dystrophic and their ability to form connections is reduced. This study has also focussed on elucidating the molecular mechanisms that underpin Aβ-mediated inhibition, through growth substrate coating, exogenous Aβ application and the development of a disease-specific neurite outgrowth model based on iPSC technology, all of which successfully led to inhibition of neurite outgrowth. Small molecules that target specific downstream signalling events were used to restore neurite growth in the presence of inhibitory Aβ. This has helped identify common signalling pathways involved in neurite inhibition in both SCI and AD.

Activation of the Rho A and ROCK signalling pathway is common to neurite inhibition in the glial scar and AD. This thesis provides compelling evidence as to the common role of Rho A activation in neurite inhibition. A ROCK inhibitor, Y-27632 and ibuprofen, an inhibitor of Rho A, were used to restore neurite outgrowth in the inhibitory models described throughout this project. These data suggest a common role for Rho A and ROCK activation in neurite inhibition, inhibition of which may provide a useful therapeutic strategy to promote regeneration in the CNS and enhance neuronal connectivity in many neurological disorders.

List of Contents

Chapter I: Introduction

Chapter II: Materials & Methods

Chapter III: Development of Robust and Reproducible Human Pluripotent Stem Cell Derived Models of Neurite Outgrowth

Chapter IV: Investigation into the Molecular Mechanisms that Underpin Neurite Inhibition in the Glial Scar

Chapter V: Investigation into the Role of β-amyloid in Neurite Inhibition within Alzheimer's Disease

Chapter VI: Application of Biomimetic Surfaces to Study the Role of Extracellular Molecules in Neurite Outgrowth and Inhibition

List of Figures

Chapter I: Introduction

Chapter II: Materials & Methods

Chapter III: Development of Robust and Reproducible Human Pluripotent Stem Cell Derived Models of Neurite Outgrowth

Chapter IV: Investigation into the Molecular Mechanisms that Underpin Neurite Inhibition in the Glial Scar

Chapter V: Investigation into the Role of β-amyloid in Neurite Inhibition within Alzheimer's Disease

Chapter VI: Application of Biomimetic Surfaces to Study the Role of Extracellular Molecules in Neurite Outgrowth and Inhibition

Chapter VII: Discussion

List of Tables

Chapter II: Materials & Methods

Chapter IV: Investigation into the Molecular Mechanisms that Underpin Neurite Inhibition in the Glial Scar

Chapter V: Investigation into the Role of β-amyloid in Neurite Inhibition within Alzheimer's Disease

Chapter VI: Application of Biomimetic Surfaces to Study the Role of Extracellular Molecules in Neurite Outgrowth and Inhibition

Abbreviations

All-*trans* retinoic acid	ATRA
Alzheimer's disease	AD
American spinal injury association	ASIA
Amyloid precursor protein	APP
Atomic force microscopy	AFM
Bone morphogenetic protein	BMP
Bovine serum albumin	BSA
Brain-derived neurotrophic factor	BDNF
Carbon dioxide	CO_2
Central nervous system	CNS
Cerebellar granular neurons	CGN
Cerebrospinal fluid	CSF
Chondroitin sulphate	CS
Chondroitin sulphate proteoglycan	CSPG
Chondroitinase ABC	Ch'ase
Coefficient of variance	CV
Collapsin response mediator protein-2	CRMP-2
Cyclic adenosine monophosphate	cAMP
Degrees celsius	°C
Dimethyl sulfoxide	DMSO
Dockkopf-1	Dkk-1
Dorsal root ganglion	DRG
Dulbecco's modified Eagle's medium with high glucose	DMEM-HG
Embryoid bodies	EBs
Embryonal carcinoma cell	EC
Embryonic stem cell	ES
Engelbreth-holm-swarm	EHS
Enzyme-linked immunosorbent assay	ELISA
European collection of authenticated cell cultures	ECACC
Extracellular matrix	ECM
Fibroblast growth factor	FGF
Focal adhesion kinase	FAK
Foetal bovine serum	FBS
Glial fibrilary acid protein	GFAP
Glial-derived neurotrophic factor	GDNF
Glycosaminoglycan	GAG

Gram	g
GTPase activating proteins	GAPs
Guanine-nucleotide exchange factors	GEFs
Guanine-nucleotide-dissociation inhibitors	GDIs
Haemotoxylin and eosin	H&E
Heparan sulphate proteoglycan	HSPG
High internal phase emulsion	HIPE
In vitro fertilisation	IVF
Induced pluripotent stem cell	iPSC
Kilodalton	kDa
Leucine rich repeat	LRR
Litre	L
Mammalian protein extraction reagent	MPER™
Microgram	µg
Microlitre	µL
Micrometer	µm
Micromolar	µM
Microtubule	MT
Microtubule associated protein	MAP
Microtubule-associated protein 2	MAP2
Microtubules	MTs
Millilitre	mL
Millimolar	mM
Minimum essential Eagle's medium with Earle's salts solution	EMEM
Myelin associated glycoprotein	MAG
Nanometer	nm
Nanomolar	nM
Nerve growth factor	NGF
Neural tube defects	NTDs
Neurofibrillary tangle	NFT
Neurofilament	NF
No significant difference	ns
Nogo extracellular peptide	NEP 1-40
Nogo receptor	NgR
Non-essential amino acids	NEAA
Non-receptor tyrosine kinase	NTK
Non-steroidal anti-inflammatory drug	NSAID
Nuclear factor κ B	NFκB
Oligodendrocyte-myelin glycoprotein	OMGP

Paraformaldehyde	PFA
Parkinson's disease	PD
Peripheral nervous system	PNS
Peroxisome proliferator-activated receptor γ	PPARγ
Phosphate buffered saline	PBS
Picogram	pg
Picomolar	pM
Pluripotent stem cell	PSC
Presenilin 1	PS1
Presenilin 2	PS2
Protein kinase C ε	PKCε
Retinaldehyde dehydrogenase	RALDH
Retinoic acid	RA
Retinoic acid receptor	RAR
Retinoic acid response element	RARE
Retinoic X receptor	RXR
Retinol dehydrogenase 10	RDH10
Retinol-binding protein 1	RBP1
Retinol-binding protein 4	RBP4
Rho A kinase	ROCK
Sonic hedgehog	Shh
Spinal cord injury	SCI
Stage specific embryonic antigen 3	SSEA-3
Standard error of the mean	SEM
Surface binding unit	SBU
Three-dimensional	3D
Two-dimensional	2D
Water	H_20
β-amyloid	Aβ
β-III-tubulin	TUJ-1

Declaration

The work described herein was carried out in the Department of Biosciences, Durham University between October 2013 and August 2017. All of the work is my own, except where specifically stated otherwise. No part has previously been submitted for a degree at this or any other university.

Statement of Copyright

The copyright of this thesis rests with the author. No quotations from it should be published without prior written consent and information derived from it should be acknowledged.

Publications Arising from this Work

Original Research

K. Clarke, D. Tams, A. Henderson, M. Roger, A. Whiting, S. Przyborski, A robust and reproducible human pluripotent stem cell derived model of neurite outgrowth in a three-dimensional culture system and its application to study neurite inhibition, Neurochemistry International (2017), doi: 10.1016/j.neuint.2016.12.009

K. Clarke, M. Roger & S. Przyborski, An investigation into the role of β-amyloid-mediated neurite inhibition in an Alzheimer's disease patient-derived model of neuritogenesis – *In Preparation*

K. Clarke, M. Roger & S. Przyborski, Application of biomimetic 2D and 3D growth substrates to study the role of extracellular stimuli in neurite outgrowth and inhibition – *In Preparation*

K. Clarke, M. Roger & S. Przyborski, Investigation into the role of chondroitin sulphate proteoglycan (CSPG) induced neurite inhibition in a novel 3D model of human neuritogenesis – *In Preparation*

Abstract

K. E. Clarke, A. Whiting & S. Przyborski, Optimisation of a novel neurite outgrowth model to study the role of inhibition in human stem cell derived neurons, European Cells and Materials (2014) 28(4):49

Review

K. Clarke, V. Christie, A. Whiting & S. Przyborski, Using Small Molecules to Control Stem Cell Growth and Differentiation, TOCRIS Review Series (2014)

Book Chapter

K. Clarke & S. Przyborski, Stem Cells in Neuroregeneration, Neuroscience: Past, Present & Future (2017) *In Partnership with the British Neuroscience Association*

Oral Presentations

2016 **White Rose Biotechnology & Tissue Engineering Group:** "*An Investigation into the Process of Neurite Inhibition in the Glial Scar using a Human Pluripotent Stem Cell Based Model of Neurite Outgrowth*"

2014 **White Rose Biotechnology & Tissue Engineering Group:** "*Optimsation of a Novel Neurite Outgrowth Model to Study the Role of Neurite Inhibition in Human Stem Cell Derived Neurons*"

Poster Presentations

2017 **International Society for Stem Cell Research (ISSCR) Annual Meeting:** Presentation "*Application of Patient-Derived Induced Pluripotent Stem Cells (iPSCs) to Study the Role of Neurite Inhibition and Mechanisms of Recovery in Alzheimer's Disease*"

2016 **ISSCR International Symposium – Models of Neural Regeneration and Disease**: "*The Development of a Novel Human Pluripotent Stem Cell Based Model of Neuritogenesis and its Application to Study Disorders of the Central Nervous System*"

2015 **British Neuroscience Association Festival of Neuroscience:** "*Development of a Robust and Reproducible Method of Human Neurite Outgrowth and its application to study the Mechanisms of Neurite Inhibition within the Glial Scar*"

2014 **Tissue and Cell Engineering Society:** "*Optimisation of a Novel Neurite Outgrowth Model to Study the Role of Neurite Inhibition in Human Stem Cell Derived Neurons*"

Acknowledgements

This research was supported by a BBSRC funded studentship.

I would like to thank the following people for helping me make this work possible:

Firstly, my supervisor Prof. Stefan Przyborski for the guidance and inspiration that he has offered me throughout my PhD.

I would also like to thank Dr. Mathilde Roger for her friendship, guidance, and mentoring, throughout my project.

Thank you to Sion Phillips, Dale Athey and Deepan Shah at Orla Protein Technologies Ltd, for their help and collaboration.

Thank you to all of the SAP lab members past and present that have supported me throughout my PhD:

Bek, for being there for me right from (almost) the beginning and reminding me what comes after *1.9* when numbering my thesis chapters.

Lydia, for watching the same TV shows as me, and providing me with someone to gossip to about them during those long hours spent in the lab.

Matt, for providing comic relief and always helping me put things into perspective.

Lucy, thank you for being my bus companion and for making me realise that reading does not have to be confined to one book at a time.

Eve, thank you for your friendship, support, and straight talking.

Nicole, thank you for always being kind, supportive and providing a shoulder to lean on.

Antonio, thank you for always being so cool and laid back, helping me realise that being stressed never helps in any situation.

Steve, thank you for your help with GraphPad Prism and for always knowing which bank accounts have the latest cash back offers.

Thank you also to Dr. Nicola Fullard, Dr. Fred Tholozan, Pamela Ritchie, Henry Hoyle & Ben Allcock for their endless support in and out of the lab.

I would also like to give special thanks to my parents. Thank you Mam and Dad for always loving and supporting me. Thank you for being so proud of this achievement.

Finally, I would like to thank my husband Daniel. Dan, thank you for loving me, caring for me and supporting me throughout the past four years. You have made my dreams come true.

Chapter I: Introduction

1.1 Development of the Central Nervous System

The central nervous system (CNS) is comprised of two main organs, the brain that processes received information, and the spinal cord, which transmits sensory information from the peripheral nervous system (PNS) to the brain. The role of the CNS is to receive and process information resulting in an appropriate response to the signal received along with controlling essential processes such as motor function.

Three connective tissue membranes, the meninges, protect the entire CNS; the outer membrane is the *dura mater* followed by the *arachnoid mater* with the inner most membrane being the *pia mater*[1]. Cerebrospinal fluid (CSF) fills the subarachnoid space (the space between the *arachnoid* and *pia mater*) while the epidural space (the space between the *dura mater* and periosteum) is filled with fibrous and adipose connective tissue, providing protection to the tissue of the CNS[2].

The spinal cord ranges from 43 – 45 cm in length and extends from the base of the brain to the first lumbar vertebrae (L1), as the vertebral column grows faster than the spinal cord[2]. A cross-section of the spinal cord reveals a central core of grey composed of interneurons, cell bodies, dendrites and glial cells. The grey matter is surrounded by white matter composed of mostly myelinated axons. Ascending tracts relay information from the PNS to brain, while descending tracts transmit information from the brain to the periphery[2].

The brain is the most complex organ in the human body and contains a heterogenic population of cell types including neurons and supporting glial cells[4]. The mature brain is composed of more than 100 billion neurons that form complex neuronal networks, with the adult brain being estimated to have more than 60 trillion connections[5]. The brain is also composed of a series of interconnected cavities that form the CSF filled ventricular system that provides protection to the brain and is also involved in the removal of waste and the transport of substances[5].

In embryonic development, the nervous system begins to form as the embryo reorganises into the three germ layers (ectoderm, mesoderm and endoderm)[6]. Signalling from the posterior margin of the embryo induces formation of the neural plate, which develops bilateral neural folds that fuse at the midline creating the neural tube[7,8]. Development and closure of the neural tube usually completes by 28 days post-conception and failure to close can result in neural tube defects (NTDs) such as spina bifida and anecephaly[7].

Dorsoventral patterning of the neural tube depends on the relative quantities of dorsalizing factors such as bone morphogenetic protein (BMP) from the non-neural ectoderm and ventralizing factors including sonic hedgehog (Shh) from the notochord and floor plate[6]. Retinoic acid (RA) is a patterning factor that contributes to both dorsoventral and anteroposterior patterning of the neural plate and along with WNTs and fibroblast growth factors (FGFs) is involved in organisation of the spinal cord and posterior hindbrain[9]. The relative quantities of morphogens such as RA, Shh and BMP in the developing neural tube gives rise to the cell types that develop from resident stem cells. Therefore, fully understanding the signalling pathways activated by such morphogens can help elucidate the mechanisms behind neural differentiation of stem cells and can be used *in vitro* to generate populations of cells for use in disease modelling to further understand pathogenic mechanisms or to generate pools of cells for regenerative medicine purposes.

1.1.1 Neuritogenesis

Neuritogenesis is a process that occurs during the development of the individual neuron and results in the formation of complex neuronal circuitry that is essential for nervous system function. Neurites are cytoskeletal processes that extend from the cell body of the developing neuron and with a growth cone at the distal tip, later become the axon and dendrites of the mature neuron[10]. The ability of neurites to sprout and form at the right time and in the correct orientation forms the basis of neuronal connectivity, which in turn ensures correct brain functioning.

Neurite formation occurs in three distinct phases; first budding occurs, where the initial bud begins to protrude from the cell breaking the original round, spherical cellular shape. The bud then develops into a neurite, which later matures into an axon or dendrite, a process that is summarised in Figure 1-1[10].

Neuritogenesis is heavily influenced by external stimuli, particularly extracellular-matrix (ECM) proteins such as tenascins[11], collagen, and laminin, which all have important roles in axonal development and navigation. Cell signalling events initiated by extra-cellular stimuli result in cytoskeletal modulation, which ultimately induces neurite guidance and elongation[12]. Laminin is thought to induce neurite development by forming a complex with integrin receptors that dimerise at the cell membrane transmitting signals to the actin cytoskeleton. This is thought to induce micro-domain and receptor induced calcium rises that stimulate membrane changes leading to neurite protrusion[10].

The initial sprouting of a neurite from the cell body of a developing neuron depends on force generated from within the cell. Microtubules and membrane addition are known to be important in the elongation, polarity and speed of neurite development, however

alone, these processes do not generate enough force required for initial neurite extension, this is thought to be driven by the actin cytoskeleton[10].

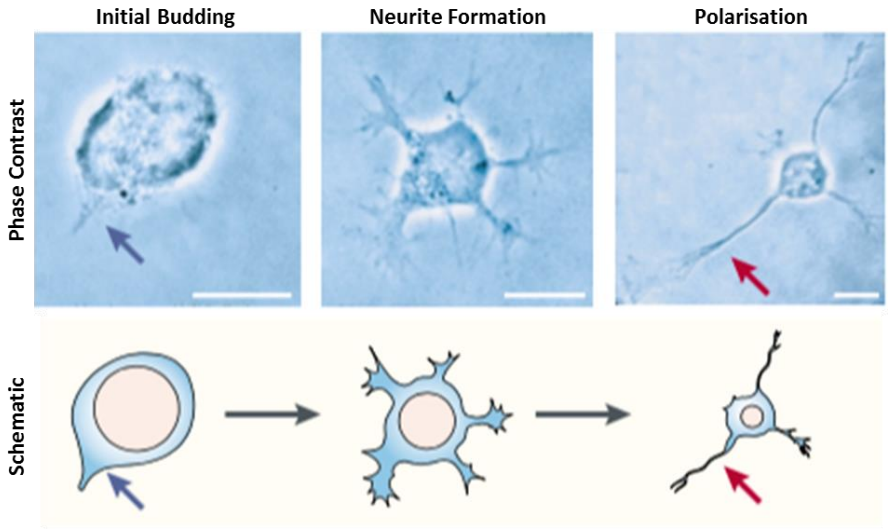

Fig 1-1: Stages of neurite development.
Initial stages of neurite development as shown by phase contrast images of rat embryonic hippocampal neurons in culture along with a schematic depicting the stages of neurite outgrowth. The initial budding stage highlights the neurite sprout with a blue arrow. Neurites then extend as the cell differentiates and as the cell matures, morphological polarisation leads to the formation of the mature axon (highlighted by the red arrow) and dendrites. Adapted from Da Silva & Dotti.

1.1.1.1 The Role of the Actin Cytoskeleton in Neuritogenesis

The growth cone, located at the distal tip of the developing neurite is rich in cytoskeletal components, predominantly actin fibrils. The growth cone contains a central core that is filled with organelles and growing microtubules (MTs) essential for the development of the neurite[13]. The peripheral area of the growth cone that surrounds the central region is made up of actin-based lamellipodia and filopodia, which drive neurite extension[10]. Lamellipodia consist of an actin meshwork that has adhesion functions, and induces the tension necessary for growth cone movement and neurite extension. Whereas fliopodia consist of actin bundles that promote rapid extension of developing neurites. Within the growth cone, actin is thought to polymerise at the leading edge, before disassembling and receding to the peripheral area where it can re-polymerise, driving the protrusion of the neurite[10].

The Rho pathway is a well-characterised signalling pathway involved in the control of actin dynamics and Rho GTPases are ubiquitously expressed proteins that are heavily involved in this signalling cascade. The Rho family of proteins includes: Rho A, Rac1 and Cdc42 all of which play a role in neurite outgrowth and guidance. Rho A negatively

regulates the process, as activation of Rho A inhibits neurite outgrowth[10,14], whereas, activation of Rac and Cdc42 is required for neurite outgrowth. Rho GTPases impact neurite outgrowth through inducing actin remodeling and they achieve this through the formation of multi-molecular complexes that contain regulatory proteins and actin-binding proteins. Actin-binding proteins include Ena/VASP that couple actin to the cell surface, Arp2/3 that nucleates actin, proteins that promote actin depolymerisation (ADF/cofilin) and proteins that promote polymerisation at the barbed end of the actin filament (profilin) along with many more proteins.[10]

The exact molecular pathway that controls actin dynamics in neurite extension and growth remains relatively unknown; however, through studies focusing on cell migration and Rho GTPase binding partners, a potential signalling pathway has been outlined in Figure 1-2[10]. The extracellular, neurite-initiating stimulus such as a component of the ECM is thought to bind to a cell surface receptor, inducing activation of downstream signaling molecules. Receptor activation is thought to transmit signals through guanine-nucleotide exchange factors (GEFs) or guanine-nucleotide-dissociation inhibitors (GDIs) and GTPase activating proteins (GAPs) to a series of effector proteins such as Rho A and its downstream effector Rho A Kinase (ROCK), WASP, and Arp2/3, inducing actin instability[10]. Relaxation of the actin meshwork allows microtubules to penetrate the area, altering membrane dynamics and promoting neurite sprouting.

Although the general signalling pathway remains relatively unclear, the molecular signalling pathway that follows receptor activation by specific stimuli is beginning to be uncovered. For example, nerve growth factor (NGF) induces neurite formation in cells cultured *in vitro*[15,16] and is associated with an increase in Rac 1 and Cdc42 activity. This is associated with Rho A inactivation, resulting in signalling events that are associated with neuritic growth. This is thought to be induced by activation of the Ras-linked tyrosine kinase receptor (TrkA) by NGF which in turn activates Ras and PI 3-kinase followed by activation of Cdc42 and Rac 1 and deactivation of Rho A and ROCK[17]. This signalling cascade results in the induction of neurite outgrowth. However, although much of the signalling pathway, upstream of Cdc42, Rac 1 and Rho A has been elucidated for the NGF ligand, this is not the case for all ligands that influence neuritogenesis and the complexities of this cascade remain unclear.

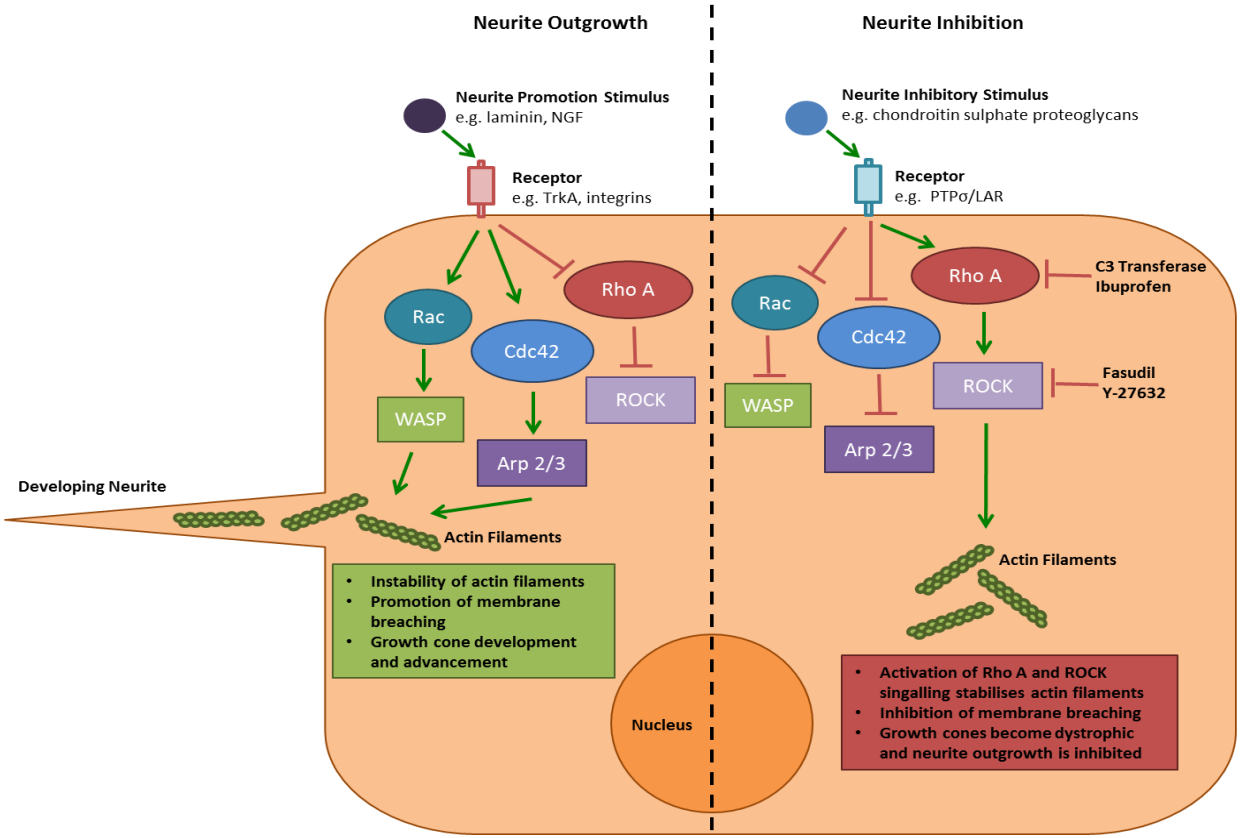

Fig 1-2: The role of the Rho signalling pathway in neurite development and inhibition.
Extracellular signals act through a receptor dependent mechanism leading to activation of Rho GTPases (Rac and Cdc42) and inhibition of Rho A. Activation of Rac, Cdc42 and their downstream signalling partners, WASP and Arp2/3 combined with inhibition of Rho A and downstream ROCK, induces neurite development. This results in instability allowing the intrusion of microtubules to the area and membrane breaching promoting neurite growth. Efforts have been made promote neurite regeneration by using small molecules to inhibit Rho A (C3 transferase, ibuprofen) or ROCK (fasudil, Y-27632).

The complexity of this signalling pathway can be highlighted by the protein Arp2/3 the role of which in neurite development is not fully understood, however it is known to promote branching of actin filaments by promoting actin nucleation[18]. Loss of function of Arp2/3 through siRNA in cultured neurons does not inhibit neurite outgrowth, but actually increases the number of shorter, more irregular neurites[19]. However, overexpression of N-WASP an activator of Arp2/3 increases the number of neurites[20], which demonstrates the complex role of Arp2/3 signalling in neurite outgrowth[18] and demonstrates how so many aspects of this pathway may remain not fully understood.

Although the detailed molecular mechanism of this signalling pathway in neuritogenesis remains relatively unknown, manipulation of this pathway is still commonly used to enhance neurite outgrowth in *in vitro* cultures. Activation of Rho A and its downstream signalling molecule ROCK, inhibits neurite outgrowth, therefore inhibition of Rho A and ROCK signalling can be used as a strategy to enhance neurite outgrowth. ROCK inhibitors such as, Y-27632[21–24] and fasudil[21,25] are commonly used to enhance neurite outgrowth cultures *in vitro*, and have even been shown to overcome inhibitory stimuli in non-permissive environments[26,27].

Inhibition of Rho A signalling is another commonly used strategy to enhance neurite outgrowth cultures, C3-transferase (an inhibitor of Rho A), can be used to increase neurite outgrowth[28,29]. Interestingly, Roloff *et al*, demonstrate the ability of the non-steroidal anti-inflammatory drug (NSAID), ibuprofen, to enhance neurite outgrowth in cultures derived from human pluripotent stem cells differentiated toward a neural linage[21]. This study found that ibuprofen not only targets cyclooxygenase enzymes resulting in its anti-inflammatory function, but also suppresses Rho A activity to induce neurite outgrowth[21,30,31]. Therefore, understanding the detailed molecular mechanism that underpins neurite development can be important to help enhance neuronal cultures *in vitro* and also to develop therapeutic interventions in the context of neurite inhibition that is common to many CNS disorders.

1.1.1.2 Neurite Outgrowth in Disease

Inability of neurites to regenerate and restore lost neuronal connections is common to many nervous system disorders ranging from trauma[32–34] to neurodegenerative diseases[35–38]. Neurite inhibition results in growth cones becoming dystrophic and left unable to form connections with other cells, which has a major impact in connectivity and the transmission of nervous signals[39].

Trauma to central nervous system results in the formation of a glial scar, which is a large obstacle in the treatment of spinal cord injury (SCI). The glial scar involves the secretion

of inhibitory molecules from reactive astrocytes and the release of inhibitory molecules from myelin debris, which act through receptors to activate Rho A signalling, in turn inducing neurite inhibition[33,34,39]. Similarly, the β-amyloid (Aβ) peptide implicated in Alzheimer's disease (AD) pathogenesis, has also been found to induce neurite inhibition through a Rho A dependent signalling mechanism[36,40]. The α-synuclein peptide associated with Parkinson's disease (PD) has been linked with neurite inhibition *in vitro*[37] and inhibition of neurite outgrowth has even been implicated in neurological conditions such as schizophrenia[41,42] and Down's syndrome[43,44].

Understanding the molecular mechanisms that underpin neurite outgrowth and inhibition is important, as neurite inhibition is so widespread throughout disorders of the CNS. Further insights into the molecular pathways that govern neurite inhibition can lead to the development of mechanisms that intervene within the process, resulting in rational therapeutic design. Consequently, there is a need for physiologically relevant *in vitro* models of neuritogenesis to help elucidate the downstream signalling events that induce neurite inhibition and to screen potential molecules that may be able to overcome inhibition in the presence of inhibitory stimuli.

1.1.2 The Retinoic Acid Pathway in Neural Development

Retinoic acid (RA) is a derivative of vitamin A that cannot be synthesised and must be obtained from the diet, from meat in the form of retinyl esters or β-carotene from plant sources[45]. RA belongs to a family of molecules known as retinoids, of which it is the most active naturally occurring substance[46]. It is an important signalling molecule involved in embryonic development, and has a particularly important role in the patterning and differentiation of the developing nervous system. Deficiencies in vitamin A, historically, have resulted in defects in a wide range of biological systems including: keratinisation of epithelia, anaemia, blindness and loss of immune function. Vitamin A deficiency in animals has also been found to lead to nerve degeneration and symptoms similar to that of motor neuron disease[46]. This large range of symptoms highlights the importance of RA as a signalling molecule in development, especially in development of the nervous system.

1.1.2.1 Retinoic Acid Metabolism and Signalling

Retinoids are obtained from the diet and stored in the liver, lungs, bone marrow and kidneys. Retinoids are transported from these storage sites to target cells as retinol, which is released into the bloodstream and transported bound to retinol-binding protein 4 (RBP4) in the plasma[46]. Target cells, through an interaction between RBP4 and its membrane receptor, STRA6, take up retinol, allowing it to enter the cytoplasm[9]. Once in the cell, retinol is bound to retinol-binding protein 1 (RBP1) and metabolised in a two-

step process by retinol dehydrogenase 10 (RDH10) and retinaldehdye dehydrogenases (RALDHs) to produce all-*trans* retinoic acid (ATRA)[47].

Usually two retinoic-acid-binding proteins (CRABP1 and CRABP2) bind to ATRA in the cytoplasm and assist translocation of RA to the nucleus. Once in the nucleus, RA binds to a transcription complex, that includes a pair of ligand-activated transcription factors: the RA receptor (RAR) and retinoic X receptor (RXR)[9]. This complex can be made up from three different RAR (RARα, RARβ and RARγ) and three different RXRs (RXRα, RXRβ and RXRγ) with each molecule having several different isoforms[46]. Together this receptor heterodimeric pair binds to a DNA sequence, the retinoic acid response element (RARE). This results in induction of gene expression with over 500 genes having been observed to be retinoic acid inducible[9]. Following induction of RARE, ATRA exits the nucleus and is broken down in the cytoplasm by CYP26 and P450 enzymes[47]. A schematic overview of the RA signalling pathway is shown in Figure 1-3.

Retinoic acid can act by both paracrine and autocrine mechanisms to induce expression of genes essential to neuronal development and differentiation[9]. For this reason it is an important signalling molecule involved in embryonic development and as also been harnessed for use *in vitro* to promote neuronal differentiation of human pluripotent stem cells[45].

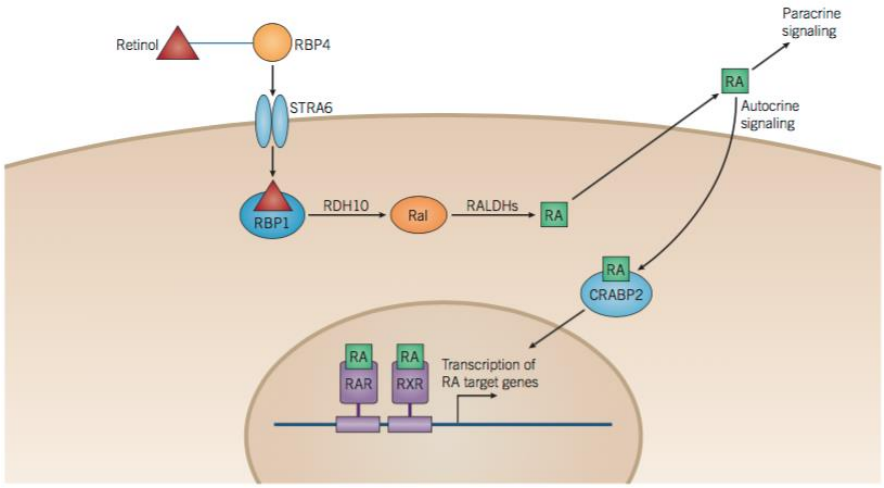

Fig 1-3: Metabolism and molecular mechanism of retinoic acid signalling.
Retinol binding protein 4 (RBP4) transports retinol to its target cells where it enters the cytoplasm with the help of the transmembrane receptor, STRA6. Retinol then binds to retinol binding protein 1 (RBP1) and is metabolised to Ral by retinol dehydrogenase 10 (RDH10) and then to retinoic acid (RA) by retinaldehyde dehdryogenases (RALDHs). RA either acts in a paracrine fashion on other target cells or through an autocrine mechanism. RA is translocated to the nucleus by cellular retinoic-acid binding protein 2 (CRPB2) where it can bind to retinoic acid receptors (RARs) and retinoic X receptors (RXRs) that form heterodimers and bind to DNA at the retinoic acid response element (RARE) inducing transcription of target genes. Taken from Clarke *et al*.

1.1.2.2 Retinoic Acid in Nervous System Development

Retinoic acid is heavily involved in the patterning and differentiation of the nervous system *in vivo*. It contributes toward both dosoventral[46] and anteroposterior[48] patterning of the neural plate and tube during the early development events of the nervous system. The role of RA in anteroposterior patterning is to induce posterior hindbrain and anterior spinal cord organisation, along with other signalling molecules including WNTs and FGFs. In the absence of RA signalling, the posterior hindbrain is missing and spinal cord abnormal[46]. This process is tightly regulated due to the generation of RA in the posterior mesoderm, which is tightly controlled by the CYP26C1 enzyme that breaks down RA resulting in a concentration gradient. Newly formed somites in the developing neural tube release RA along with other signalling molecules that include Shh and BMPs dorsally, which act together to determine cellular fate of sensory, motor and interneurons[46].

The role of RA in the patterning of neuraxis was first studied by the treatment of developing embryos with an excess of RA in species including *Xenopus*[48–50], zebrafish, mice and rats[46]. In the case of RA treatment, anterior structures were lost (including the forebrain and eyes) and the hindbrain and spinal cord expanded to compensate for this loss[48]. A repression in anterior genes such as *Otx2, Emx1* and *Dlx1* and an induction in posterior genes such as *Krox20, Hox* and *Pax2,* which explains the observed expansion of the hindbrain and spinal cord[46]. Alteration of RA signaling through selective ligands for the RAR and RXR receptors causes an upregulation in posterior gene expression, similar to that seen with RA excess[49]. Therefore, it is thought that a gradient of RA within the developing nervous system is responsible for patterning and that shifting the gradient anteriorly by increasing RA signalling can reduce forebrain and midbrain formation. Whereas, shifting the gradient posteriorly by decreasing RA signaling results in an enlargement of the forebrain and midbrain[46]. This dramatic effect on neural development highlights the important role that RA plays in the developmental process and the importance of a delicate signalling gradient that leads to successful neural development.

RA induces differentiation of cells toward glia and neuronal lineages through the induction of transcription of many genes that encode: transcription factors, structural proteins, enzymes, cell surface receptors and other signalling molecules. RA inducible genes include transcription factors such as nuclear factor κB (NFκB), SOX1 and SOX6, along with proteins such as protein kinase Cε (PKCε) and microtubule-associated protein 2 (MAP2) and elements of the canonical WNT pathway[9]. RA may also function to suppress particular signalling pathways in its role to induce neuronal differentiation, as shown by Verani *et al*, whose study identifies an increase in the WNT pathway inhibitor Dickkopf-1 (Dkk-1) upon RA induction of neural differentiation in mouse stem cells[51].

The number of primary neurons that develop in fish and amphibians is controlled by RA signalling and the addition of RA to the embryo results in an increase in primary neuron number and a change in their positioning[52,53]. An inhibition in RA signalling in these species results in a decrease in primary neuron number and embryos are left unable to respond to physical stimulation[46]. Similarly, in retinoid-deficient mice, neurons of the hippocampal denate gyrus are reduced; suggesting RA signalling is an important step in the early differentiation pathway of hippocampal neurons[45]. Therefore, promotion of neuronal differentiation by RA makes it a useful tool to generate neurons *in vitro.*

1.1.2.3 Retinoic Acid in the Mature Nervous System

Peripheral neurons are capable of regeneration following injury, however, neurons in the CNS are unable to regenerate, which poses an obstacle in the treatment of CNS injury. Following a peripheral nerve injury, RA signalling is induced, to promote neuronal regrowth and regeneration by activating the same signalling mechanisms involved in neuronal development[9]. The receptor, RARβ2, is upregulated following peripheral nerve injury, however is not expressed in the adult spinal cord, suggesting that an upregulation in this receptor is involved in the neurite outgrowth promoting response to peripheral nerve injury[9,54].

RA is thought to act upon neurons promoting the protrusion of neurites from the cell body, however expression of RARβ2 within Schwann cells and macrophages, may suggest that RA also acts upon surrounding cells to promote the formation of a more permissive environment for neurite outgrowth[9]. A proposed mechanism for this is the secretion of neurite promoting factors such as neurotrophin and NGF, however, the signalling events that follow peripheral nerve injury appear to be complicated and not well understood. A potential mechanism is outlined in Figure 1-4. RA is also thought to promote neuronal regeneration by inhibiting the pro-inflammatory effects of macrophages that upregulate RARs following injury[9]. Understanding the role of RA in peripheral nerve regeneration is important in the development of therapeutics aimed at targeting this pathway to promote neural regeneration in both the PNS and CNS.

Injury to the CNS such as spinal cord injury (SCI) induces an increase in RA signalling activity that peaks 4 – 7 days post-injury[9]. However, unlike injury to the PNS, neurons are unable to regenerate following CNS injury, due to the formation of a glial scar, an environment that is inhibitory to neurite outgrowth[39]. Wong *et al* demonstrate the potential neurite-promoting role of RA following spinal injury, by inducing over expression of RARβ2 in rat dorsal root ganglion (DRG) cultures *in vitro* and in injured rats *in vivo*, which resulted in significant neurite outgrowth and functional recovery following SCI[55]. This highlights the potential role of RA for use in therapeutic interventions in both

CNS and PNS injury and the need for further understanding of the signalling pathways that govern tissue and cellular regeneration, as RA signalling has also been implicated in limb and lung regeneration[56].

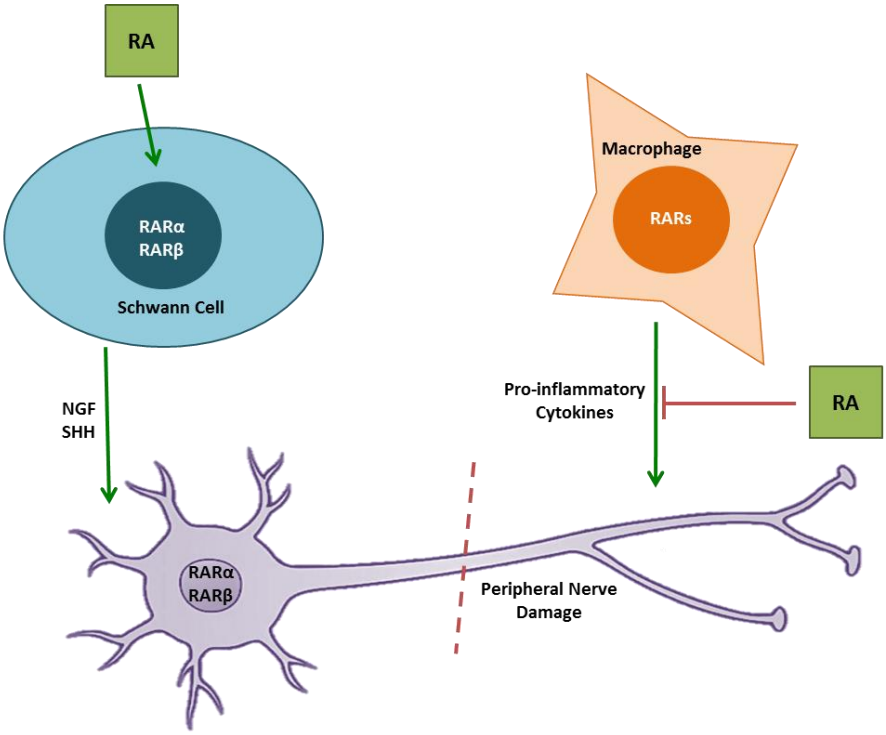

Fig 1-4: The potential role of retinoic acid in regeneration following peripheral nerve injury.
Retinoic acid (RA) inhibits the secretion of inflammatory cytokines from macrophages, which express retinoic acid receptors (RARs). Schwann cells also express RARs and RA induces secretion of neurotrophins including nerve growth factor (NGF) and signalling molecules such as sonic hedgehog (SHH). The secretion of neurotrophins supplements the beneficial effects of RA on neuronal regeneration, and also enhances production of RA from damaged neurons.

One of the roles of RA in the mature nervous system is thought to be the maintenance of neuronal plasticity. Vitamin A deprived mice and rats have been found to show signs of cognitive impairment and memory deficits that can be reversed by the restoration of vitamin A to the diet. This suggests an important role for RA in the maintenance of memory functions[57–59]. A similar memory loss phenotype is observed in ageing animals and can be restored by induced RA signalling[60,61], which has even been found to effectively rescue memory deficits in a mouse model of Alzheimer's disease[62]. This further emphasises the need to better understand RA signalling in the mature nervous system.

1.2 In Vitro Models of Neurite Outgrowth

Neurite outgrowth is an important developmental process, impairment of which is common to many neurological disorders, which in turn has a detrimental effect on neuronal connectivity. Neurite inhibition poses an obstacle in the treatment of many diseases; therefore, the development of accurate *in vitro* models to study the mechanisms that underpin the process is an extremely active area of research. Applications of neurite outgrowth models range from the screening of potential drug candidates to investigations into molecular developmental and pathological mechanisms. Such models are often used for toxicology studies to determine the neurotoxicity of compounds and in drug discovery. Most *in vitro* neurite outgrowth assays rely on analysis and quantification of micrographs to determine neurite elongation and regression, which can be inaccurate and time consuming[63]. Therefore, there is a need for improved models of neuritogenesis that can be adapted for high throughput screening techniques to enable rapid identification and screening of compounds.

1.2.1 Limitations of the Use of Retinoic Acid In Vitro

Retinoic acid, due to its role in the development of the nervous system, is often used *in vitro* to promote neuronal differentiation and neurite outgrowth in cell cultures[64,65]. Neuronal models based on the differentiation of pluripotent stem cells, such as embryonic stem (ES) cells and embryonal carcinoma (EC) cells, often harness the neuronal differentiation properties of ATRA to generate functional neurons for studies[21,66–72]. Similarly, SH-SY5Y neuroblastoma cells, a cell line commonly used for neurite outgrowth assays, are usually treated with ATRA to induce a more neuronal phenotype along with the outgrowth of neurites[73–77]. However, ATRA induction of differentiation in SH-SY5Y cells has recently come into question as it is thought to effect cell susceptibility to neurotoxins, therefore may not be suitable for use in neurotoxicity screening assays[78].

Although ATRA is commonly used to induce neuronal differentiation *in vitro*, its use is limited as it readily breaks down when exposed to light and heat[79]. ATRA contains five unsaturated double bonds, which leaves it prone to isomerisation and results in the formation of breakdown products such as, *9-cis* and *13-cis* retinoic acids, which may have an unwanted biological activity[80]. Therefore, as ATRA can readily breakdown, its use *in vitro* is limited, as the exact concentration of ATRA in a particular solution is variable and high concentrations may be needed to induce the desired differentiation and to account for the breakdown of the compound over the culture period. For this reason, synthetic more stable retinoid compounds have been developed for use in induction of neuronal differentiation studies.

1.2.1.1 Synthetic Retinoid Analogues

As light and heat exposure is unavoidable during cell culture, much effort has been placed in the development of synthetic retinoid analogues that are more stable and practical for use *in vitro* than the naturally occurring ATRA. Previously, it has been demonstrated that only 37 % of ATRA remains in solution following a 3-day exposure to laboratory fluorescent light, due to instability that is thought to arise from the conjugated linker region[81]. However, synthetic retinoids have been developed such as EC23 that replace sections of the polyene chain with an acetylene moiety and phenyl rings providing complete stability, with 100 % EC23 remaining following a 3-day exposure period to light[81]. Another synthetic retinoid analogue was developed to better resemble the structure of the ATRA molecule, AH61, which shows signs of isomerisation following exposure to light, but only one other isomer was detected and 86 % of the original compound remained[81]. The structure of retinoid analogues including ATRA, EC23, EC19 and AH61, are shown in Figure 1-5.

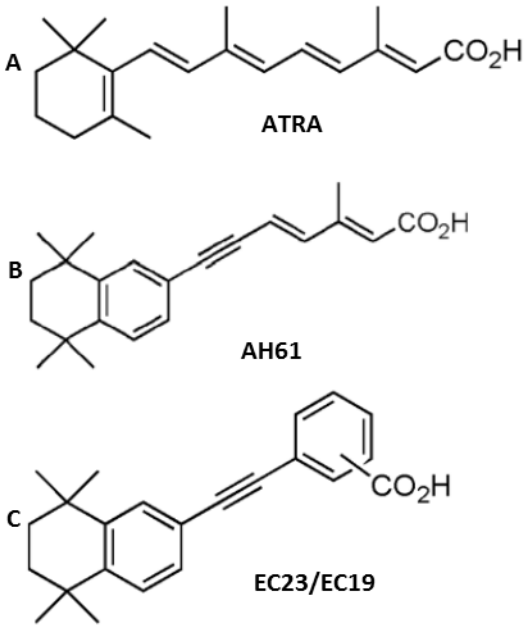

Fig 1-5: Chemical structures of synthetic retinoid analogues.
Naturally occurring ATRA (A) readily isomerises when exposed to light and heat i.e laboratory conditions. Therefore synthetic retinoid compounds have been developed that are more stable and practical for use *in vitro*, AH61 (B) shares a similar structure with ATRA but is more stable and does not break down as readily as ATRA. EC23 (C) (CO_2H in position 4) is completely stable with no evidence of degradation and is a potent inducer of neural differentiation, whereas EC19 (C) (CO_2H in position 3) induces non-neural, epithelial-like differentiation in human pluripotent stem cells.

Christie *et al*, addressed the biological activity of the synthetic retinoid, EC23 by determining that neuronal differentiation in both human neuroprogenitor and human embryonic stem cells was enhanced by the molecule[82]. EC23 was found to induce expression of neuronal markers such as β-III-tubulin (TUJ-1) and NF-200 to a greater extent at lower concentrations (10 nM) than ATRA and to a similar extent at high concentrations (100 nM) in ReN cell 197VM progenitor cells[82]. Similarly, the biological activity of AH61 was assessed by Clemens *et al*, and it was found that AH61 has similar neuronal differentiation inducing properties to the naturally occurring ATRA, in an embryonal carcinoma (EC) cell model of neuronal development[81]. AH61 was found to induce loss of stem cell markers such as SSEA-3 and TRA-1-60 along with induction of the early neuronal marker A2B5 to a similar level as ATRA, as measured by flow cytometry[81]. Therefore both AH61 and EC23 have previously been found to induce neuronal differentiation in culture to a similar extent to ATRA with significantly enhanced stability when exposed to light.

Subtle variations in retinoid structure can significantly impact the biological function of the molecule, as can be demonstrated by the synthetic molecule, EC19. Similarly to EC23, when exposed to light for a 3-day period, EC19 remains completely unaltered[83]. However, the biological function of EC19 differs from that of EC23 in that EC19 appears to induce epithelial-like differentiation of embryonal carcinoma cells, as opposed to neuronal differentiation. In another study, Christie *et al*, demonstrate that EC cells exposed to 10 μM of each retinoid for a 21-day period exhibit completely distinct morphological appearances[83]. Cells treated with ATRA appear heterogeneous with areas of neural rosettes and areas containing flat epithelial-like cells, however, EC23 induced cells appear to contain more neural rosettes and less epithelial-like areas, whereas, EC19 treated cells contain large areas of flat epithelial-like cells with no evidence of neural rosettes[83]. Expression of cytokeratin-8 (an epithelial marker) was induced to a greater degree by EC19, whereas, expression of TUJ-1 (a neuronal marker) was induced to a greater degree by EC23[83,84]. Therefore, the differences in biological activity between EC19 and EC23 are induced by only subtle variations in their structure, highlighting the importance in structural design during the development of novel synthetic retinoid molecules.

The development of novel, synthetic, retinoid molecules has provided advances in the field of stem cell biology and the development of differentiation protocols, particularly neuronal differentiation. Stable, synthetic retinoids do not isomerise as readily when exposed to light and heat compared with the naturally occurring ATRA, therefore, are more practical for use *in vitro*, as exposure to these factors cannot be avoided.

Retinoid compounds are often used *in vitro* to promote neuronal differentiation and maturation. However, this is not a requirement of all commonly used cell types to ensure

neurite development *in vitro*, as primary cell types derived from animal tissue, such as DRG often contain mature neurons. However certain cancer cell lines, including the commonly used SH-SY5Y along with pluripotent cells, require RA-induced maturation to develop neurites and mature in culture. Each neurite-forming cell type often has its own distinct set of advantages and disadvantages, therefore, the appropriateness of a particular cell type should be considered when developing *in vitro* models.

1.2.2 Dorsal Root Ganglia

Dorsal root ganglia (DRG) refers to a collection of cell bodies from afferent sensory fibres located where the cervical, thoracic, lumbar and sacral spinal nerves enter the spinal cord[85]. As the soma of such cells is located on a side branch of the main axon it is easily accessible for patch clamp recordings, therefore this cell type is often considered for neurological studies[86]. *In vitro* culture of DRG neurons within hours of seeding, result in the development of several long, thin and uniform axons tipped with growth cones that express axonal marker proteins[87]. However, long-term culture results in a more mature morphology that better reflects that of DRG neurons *in vivo*[87]. For this reason, DRG neurons are often explanted from many animals, including chick[88,89], mouse[90,91] and rat[89,92–94] for use in *in vitro* models of neurite outgrowth.

DRG neurons are primary cultures, explanted from experimental animals and are thought to overcome some of the disadvantages associated with immortalised cell lines. For example, immortalised cell lines that have been genetically manipulated may result in an altered phenotype and variations from their native functions[95]. The continual passaging of cell lines can also lead to further genetic variation, resulting in a phenotype that may be far removed from the native *in vivo* cell type[95]. Szpara *et al* characterised the gene expression of neurites generated from DRG cultures and found that many transcripts expressed during *in vivo* development are also expressed during neurite extension *in vitro*[96]. Therefore, *in vitro* neurite outgrowth assays based on explanted DRG neurons are thought to provide a reliable model to study the process of neurite outgrowth.

Although neurite outgrowth from primary DRG cultures has been compared favorably with neurite outgrowth *in vivo*, there are some disadvantages to the use of such cells in neurite outgrowth assays. Isolation of primary cells may be difficult, resulting in a heterogeneous population of cells that may include glial subtypes and neurons that vary in response to stimuli, signal conduction and neurochemistry[85]. Similarly, the method of isolation along with the age of the animal, may contribute to phenotypic variations in the resultant cellular population[97]. Such variation is problematic in the development of robust neurite outgrowth assays for use in pharmaceutical development and drug discovery, where a standardised and reproducible assay is essential.

1.2.3 Cerebellar Granular Neurons

Cerebellar granular neurons (CGN) constitute the largest homogenous population of neurons within the mammalian brain and provide the basis of many well-characterised primary *in vitro* culture models[98]. Primary CGN cultures are a popular *in vitro* model used to study many aspects of neurobiology including developmental, functional and pathological processes. Unlike DRG neurons, cellular isolation is particularly efficient resulting in more homogenous populations of cells with an estimated 90 % purity of cultures[98]. CGN cells are usually explanted from post-natal rats[99,100] for use *in vitro;* however, animal derived cells may not be suitable for studying certain aspects of human biology due to physiological differences between the species. This is a factor that should be considered when selecting an appropriate neurite outgrowth assay for a particular study.

CGN form the basis of many *in vitro* models of neurite outgrowth and have been used to study many aspects of neuritogenesis. For example, Wantanabe *et al*, use primary mouse CGNs to study the role of the cell adhesion molecule L1 and its downstream signalling events in neurite outgrowth[101]. Many studies that focus on the role of specific hormones in neurite outgrowth do so by the use of CGN *in vitro* models. For example, Farwell *et al* focus on the role of thyroxine in brain development and neurite outgrowth, elucidating a novel actin-dependent mechanism by which the hormone drives neurite outgrowth[102]. Similarly, a study by Tankiwaki and Schwartz investigates the role of somatostatin in the induction of neurite outgrowth, concluding that the hormone is involved in neurite initiation[103]. Studies such as these highlight the valuable role of CGN-based *in vitro* models.

1.2.4 SH-SY5Y Neuroblastoma Cells

A major limitation in the use of primary mammalian neurons such as DRG and CGN is that once terminally differentiated, neurons lose their proliferative capability. For this reason, immortalised cell lines provide an appealing alternative. The SH-SY5Y neuroblastoma sub-line was derived from the parental line SK-N-SH which itself was derived from a human metastatic bone tumour biopsy[104]. SH-SY5Y cells differentiate in response to retinoic acid and are one of the most common cell types used routinely for neurite outgrowth studies[105–108].

Prior to differentiation, SH-SY5Y cell populations can be expanded on a large scale with ease and using low cost medium, which is an advantage compared with primary cell types[109]. Similarly, SH-SY5Y cells are of human origin therefore their physiology may be

more relevant when studying human disease as opposed to animal derived explanted cell types. However, SH-SY5Y cells themselves present limitations. Original SH-SY5Y cultures were heterogeneous containing both adherent and floating cell types, many studies focus only upon adherent populations of SH-SY5Y with floating cells being discarded without mention in media changes[109]. Similarly, the original SK-N-SH population contained both neuron-like and epithelial-like sub-populations of cells that were later isolated in the development of the SH-SY5Y sub-line[110].

Although the relevance of SH-SY5Y for neurite outgrowth studies has been called into question[109], they still form the basis of one of the most popular *in vitro* models of neuritogenesis and are commonly used to study the process. Nicolini *et al* used retinoic acid differentiated SH-SY5Y cells to assess the neurotoxic effect of chemotherapy drugs along with their effect on neurite outgrowth[111]. In this study it was found that results obtained *in vitro* within the SH-SY5Y model of neurite development, were similar to those found previously *in vivo*[111]. Therefore, it was concluded that SH-SY5Y cells could provide a reliable model for the screening of neurotoxicity induced by chemotherapy drugs[111]. However, although commonly used, there are many limitations associated with the use of SH-SY5Y cells *in vitro* including their neoplastic nature, mixed morphology and limited capacity for neuritogenesis and these factors must be considered when using SH-SY5Y cells[109].

1.2.5 PC12 Cells

The PC12 cell line was derived from a transplantable rat adrenal pheochromocytoma and generates neurites reversibly upon induction by nerve growth factor (NGF)[112]. Induction of PC12 cell differentiation by NGF results in a peripheral sympathetic phenotype[113] and the synthesis of catecholamines[112], therefore the use of this model to study central nervous system disorders may be limited.

Due to the ability of PC12 cells to readily differentiate and generate neurites upon induction by NGF, their main application *in vitro* has been to study the role of NGF in neurite development[15,114,115]. Initially, Gunning *et al*[116] and later Richter-Landsberg & Jastroff[117] used the NGF – PC12 induction model to investigate the role of cyclic adenosine monophosphate (cAMP) in NGF-mediated signalling. Although PC12 cells are a suitable model for the study of NGF signalling, their neoplastic nature and short neurites may result in limitations for use in certain applications.

1.2.6 Pluripotent Stem Cells

Pluripotent stem cells (PSCs) are unspecialised cells that can differentiate into cell types from each of the three germ layers[118–120]. There are three main types of pluripotent stem cell commonly used in neuronal differentiation studies (outlined in Figure 1-6) including, embryonic stem (ES) cells derived from the inner core of the developing blastocyst, along with their malignant counterpart, the embryonal carcinoma (EC) cell derived from teratoma tumours[69]. More recently induced pluripotent stem cell (iPSC) technology involving the reprogramming of adult somatic cells[121–123] has gained popularity as this cell type avoids the ethical considerations associated with ES cells and malignant characteristics associated with EC cells.

The ability of PSCs to self-renew and differentiate into specialised subtypes including mature neurons has resulted in PSCs forming the basis of many *in vitro* models[124]. PSCs also have the potential to generate a population of neuronal subtypes for the purpose of cell replacement therapies[125] used to treat neurodegenerative diseases and clinical trials are underway for the application of this technology in the treatment of Parkinson's disease[125–128]. Many groups have focused on the development of robust and reproducible neuronal differentiation protocols to generate functional, mature neurons for use both *in vitro* and *in vivo.*

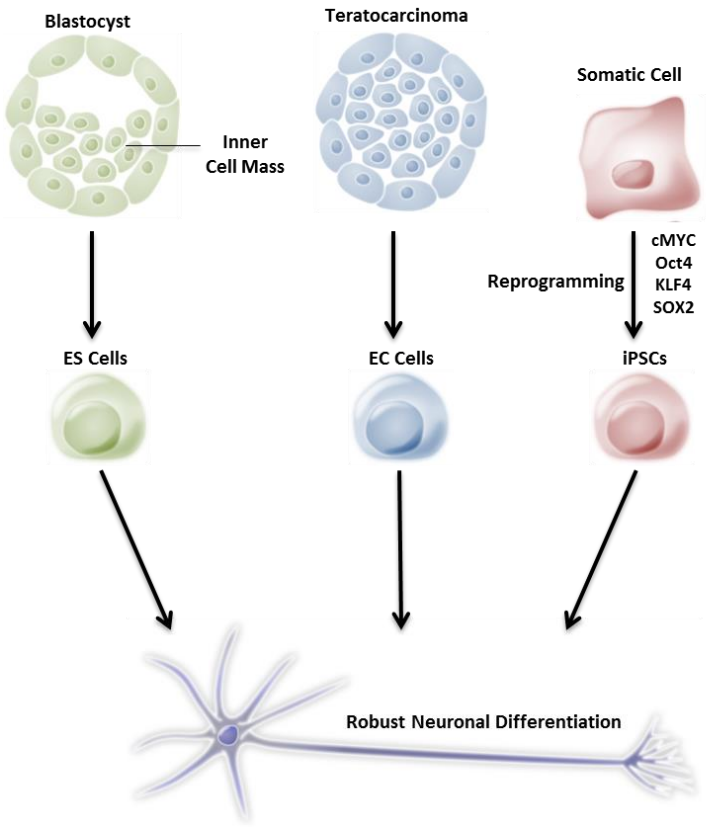

Fig 1-6: Types of pluripotent stem cell commonly used in neural differentiation studies.
Embryonic stem (ES) cells are derived from the inner cell mass of the developing blastocyst, whereas embryonal carcinoma (EC) cells are derived teratocarcinomas. EC cells are the malignant counterparts of ES cells and both cell types are commonly used to generate neuronal cell populations. Induced pluripotent stem cells (iPSCs) are generated through reprogramming of adult somatic cells resulting in an undifferentiated phenotype. iPSCs overcome some of the ethical implications associated with ES cells and the malignant phenotype associated with EC cells, along with having potential applications for personalised medicine

1.2.6.1 Embryonic Stem Cells

Embryonic stem (ES) cells are pluripotent stem cells derived from the inner cell mass of the blastocyst from surplus embryos generated by *in vitro* fertilisation (IVF)[129]. They are characterised by their expression of pluripotency markers including extracellular markers such as SSEA-3, SSEA-4 and TRA-1-60 and transcription factors including Oct 4 and Nanog[129]. When injected into immunocompromised mice, ES cells form teratomas containing tissue from each germ lineage, an assay used to determine the differentiation potential of newly isolated cell lines[130,131].

Neuronal differentiation of ES cells is not only an important process to generate functional neurons for *in vitro* models and *in vivo* cell replacement, but can be used as a tool to understand the signalling mechanisms involved in neuronal development. Application of morphogens such as retinoic acid (RA) can be used to direct ES cells toward a neural lineage. The combination and concentration of morphogens used in a differentiation protocol determines the phenotype of the resultant neuronal population[132], as shown in Figure 1-7.

The generation of specific neuronal subtypes is important in the production of cell populations for transplantation and also to study disease mechanisms *in vitro*. For example, RA exposure followed by sonic hedgehog (Shh) treatment results in the differentiation of motoneurons *in vitro* as described by Li *et al*[132,133]. Harper *et al* demonstrate a potential application of the resultant motoneurons to study the process of neurite outgrowth *in vitro* in a comparison with motoneuron injured rats[134]. Other neuronal differentiation procedures include the culture of ES cells as embryoid bodies (EBs)[135], dual-SMAD inhibition[136] and FGF induction[137], combinations of which can be used to obtain specific neuronal subtypes.

Although there are many differentiation protocols available that generate functional neurons from ES cells, few are used to study neurite outgrowth. ES cell-derived neurons are usually used for drug screening, cell replacement therapy or to study developmental processes. However, ES cell popularity for use in neurite outgrowth assays may now increase due to the publication of a methodology by Harril *et al* that details the use of an ES cell-derived neuronal cell line, hN2™, in an automated, high-throughput neurite outgrowth assay[138]. This study compares the effects of known inhibitors of neurite outgrowth in standard assays such as DRG cultures with hN2™ cells analysed using automated image analysis techniques[138]. It was found that neurites from both models behaved in a similar manner when exposed to inhibitory compounds, therefore it was concluded that hN2™ cells could provide a reliable model of neurite outgrowth suitable for high-throughput screening[138].

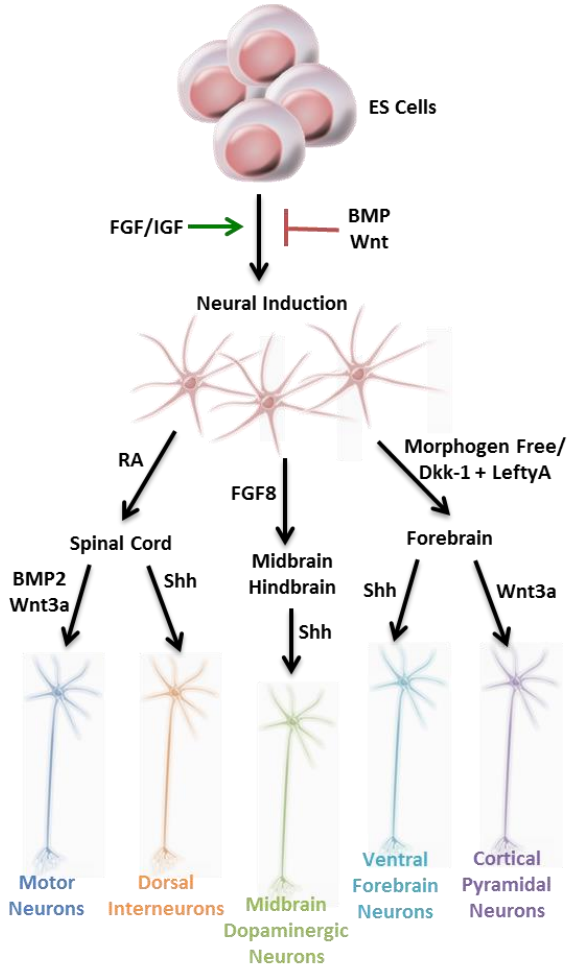

Fig 1-7: Morphogen induction of specific neuronal phenotypes.
The fate of embryonic stem (ES) cells can be directed toward a neural phenotype by the application of morphogens that induce signalling pathways involved in embryonic development. The order and combination in which morphogens are applied, determines the specific subset of neurons generated. This schematic depicts some of the major stages in the generation of common neuronal subtypes.

1.2.6.2 Embryonal Carcinoma Cells

Embryonal carcinoma (EC) cells are the malignant counterpart of the ES cells derived from teratocarcinomas, malignant germ cell tumours[69]. They offer a robust and simple model to study developmental pathways due to their pluripotent nature and ability to form teratomas in immunocompromised mice[69]. Unlike ES cells, their maintenance is relatively simple and growth medium inexpensive. They also overcome the ethical implications involved in the derivation of ES cells from viable embryos.

There are two main EC-cell lines commonly used in neural differentiation and outgrowth studies, P19 mouse derived cells[139–142] and N-TERA2 human derived EC cells[21,66,143,144].

Both lines differentiate into functional neurons when exposed to RA and are commonly used to study the process of neurite outgrowth, however, the N-TERA2 line has the advantage of being human derived, therefore is more applicable to medical applications such as drug screening and investigations into pathological mechanisms.

The original N-TERA2 EC cell line was derived from a lung metastasis of a male germ cell tumour and many clonal lines have now been derived from the original parental line. For example, in 1984 Andrews derived the NTERA2.cl.D1 subline that when exposed to RA loses expression of pluripotency markers such as SSEA-3 and results in a heterogeneous cell population containing neuronal subtypes[145]. Similarly, in 2000 Przyborski derived another subline, TERA2.cl.SP12 from the original N-TERA2 parent line through immunomagnetic sorting based on expression of SSEA-3[146]. The TERA2.cl.SP12 subline was found to respond to RA and differentiate readily, displaying enhanced differentiation compared with other clonal lines and resulting in the production of both neurons and glia[146].

Since its derivation, the TERA2.cl.SP12 clonal subline has formed the basis of many well-characterised neurite outgrowth models[82,147–150], as RA exposure leads to the generation of mature[70,71], electrophysiolocially active neurons[72] that are suitable for many applications. Stewart *et al* demonstrate the culture of TERA2.cl.SP12 cells as spheroid structures that when exposed to RA generate neurites that radiate from the central cellular aggregate[148]. This overcomes some of the difficulties posed by traditional monolayer neurite outgrowth cultures, where neurites form a network of overlapping, branching processes that are difficult to trace and quantify, as shown in Figure 1-8. This cellular aggregate approach to neurite generation allows for efficient neurite quantification as each neurite originates from a single perikaryon.

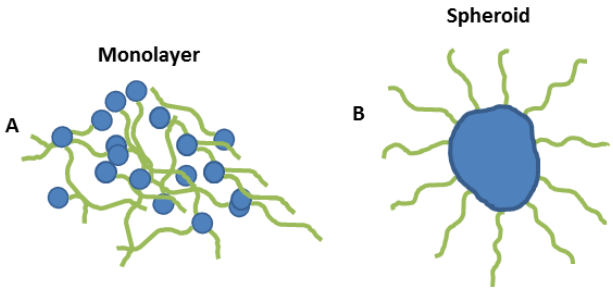

Fig 1-8: Neurite outgrowth from monolayer and spheroid cultures of EC cells.
Embryonal carcinoma (EC) cells can be cultured as monolayers or spheroids and neurites can be generated in either culture system. Neurite outgrowth (green) from monolayers (A) of cells results in the formation of complex neuronal circuitry, however, when tracing neurites for quantification it is difficult to determine the perikaryon (blue) associated with each neurite. Spheroid (B) culture offers a solution to this, as neurites radiate from one central point, allowing for more accurate quantification.

1.2.6.3 Induced Pluripotent Stem Cells

Induced pluripotent stem cells (iPSCs), unlike ES and EC cells, are derived from adult somatic cells. The generation of iPSCs involves the reprogramming of cells[151,152] such as skin fibroblasts, typically this is achieved through retroviral transfection of a cocktail of transcription factors usually including: Oct3/4, c-Myc, Klf4 and Sox2[122,153]. This results in a pluripotent cellular population with similar properties and expression of pluripotency markers as ES cells[153] whilst avoiding the ethical implications associated with the use of embryonic tissue. Pioneering studies by Takahashi *et al,* first describe the reprogramming of mouse fibroblasts[154] and then apply the same principles to successfully reprogram human fibroblasts, forming one of the first human iPSC lines[121].

Due to their ability to indefinitely self-renew and when stimulated, differentiate into functional cell types including neurons, there has been a focus on the development of robust iPSC neural differentiation protocols[124,125,155]. Neural differentiation procedures used to direct the fate of iPSCs, generally adhere to the same principles as those used in ES culture. Morphogens are used to stimulate developmental pathways and to induce neuronal phenotypes. For example, Hu *et al*, demonstrate the ability of iPSCs to differentiate in a comparison with ES cell differentiation[156]. This study found that when differentiated using common techniques such as RA and Shh induction, iPSCs generated functional neural and glial subtypes to the same extent as ES cells[156].

Although iPSC-derived neurons are rarely used in specific neurite outgrowth studies, the development of iPSC technology has resulted in many opportunities to study complex disease states *in vitro*. Neurodegenerative diseases such as Alzheimer's disease and Parkinson's disease are multifaceted, complex disorders; therefore the ability to produce disease specific *in vitro* models based on patient derived cells has led to many advancements in this field.

Yagi *et al* describe the isolation of fibroblasts from two Alzheimer's disease patients with mutations in presenilin 1 and 2 components of γ-secretase, which is involved in the generation of β-amyloid species[157]. This study then describes the subsequent reprogramming of the fibroblasts into iPSCs and induction of neuronal differentiation to produce neurons with disease specific characteristics such as an elevated $A\beta_{42}$:$A\beta_{40}$[157]. Similarly, patient obtained iPSC-derived neurons have been used to study the molecular pathogenesis associated with Parkinson's disease and have been shown to accumulate α-synuclein, a hallmark of the disease[158,159].

The development of iPSC based complex disease models *in vitro* not only has implications in the development of more reliable drug screening models[160] but also has applications in

the field of personalised medicine[124]. Patient specific cells can be generated using iPSC technology to produce a pool of differentiated cells for transplantation purposes or personalised drug screening that are genetically identical to the individual (summarised in Figure 1-9)[124,125]. This can lead to personalised *in vitro* models with an enhanced predictive value that can be used to determine the effect of a drug on a specific individual.

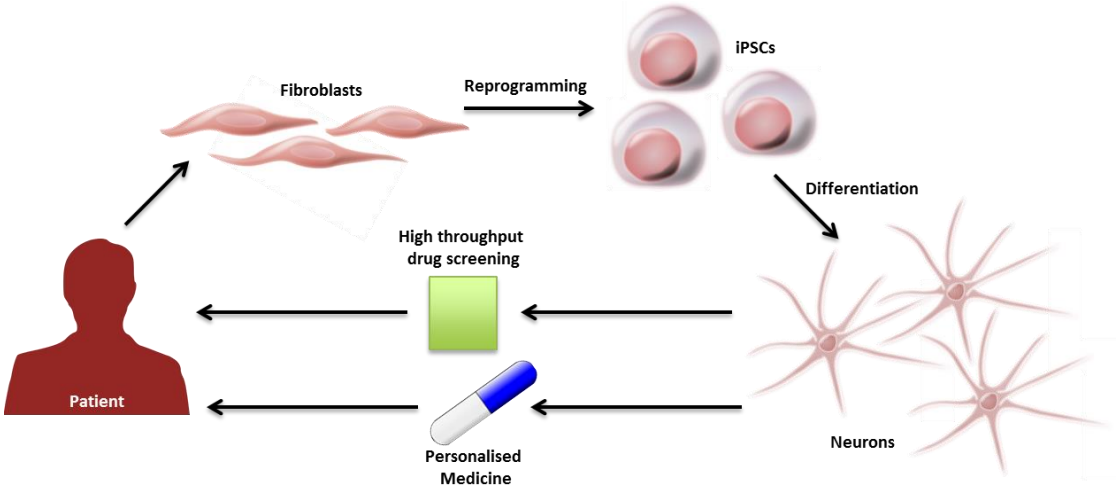

Fig 1-9: Application of induced pluripotent stem cell technology in drug development.
A schematic representing the development of induced pluripotent stem cell (iPSC) populations and their application in drug development. Patient derived somatic cells such as fibroblasts can be reprogrammed to form iPSCs that can subsequently be differentiated into mature neurons. iPSC-derived neurons then have applications in personalised medicine, as patient specific models can be generated for drug screening. iPSCs also have applications in the *in vitro* modelling of complex diseases that can be used for high throughput screening and identification of specific drug candidates.

1.3 3D Cell Culture Technologies

Cells are the building blocks of complex, three-dimensional (3D) tissues within the body; however, *in vitro,* cells are often cultured in a two-dimensional (2D) environment. Cells cultured on flat, 2D growth substrates can often differ significantly from their *in vivo* counterpart as their morphology, cell-to-cell contacts, cell-to-matrix contacts and differentiation may all be altered[161]. Cells cultured in 2D adapt to their microenvironment, resulting in cell flattening and cytoskeletal remodelling[162]. This leads to changes in the internal structure of the cell along with nuclear shape, ultimately resulting in altered gene and protein expression, impacting cellular behaviour due to the close relationship between cell structure and function[162]. Many aspects of the cellular microenvironment impact the function of the cell, including three-dimensionality and nutritional status

(summarised in Figure 1-10), all of which should be considered when developing an *in vitro* cell-based model[161].

This is of particular importance, as 3D culture technology can help to restore a cytoskeletal architecture more reminiscent of native cells, which in turn effects cellular function, as the two are so closely connected[162]. Similarly, nutritional status, is also an important consideration when developing an *in vitro* model or engineering a tissue-like construct. This depends on the tissue of interest, as development of a "*healthy*" tissue construct may require adequate oxygenation and nutritional excess. However, there are other occasions such as tumour development, when *in vivo* tissues are exposed to hypoxia and nutrient insufficiency that can lead to necrosis[161]. This is of particular relevance in the screening of chemotherapeutic drugs, specifically as some are hypoxia-targetting, and the level or absence of necrosis in a tumour model may convey resistance to such drugs, which would not be the case *in vivo*[162]. Therefore, when developing an *in vitro* cell-based model, the culture parameters that are the most consistent with the native cellular microenvironment should be considered, which will differ depending on the tissue of interest.

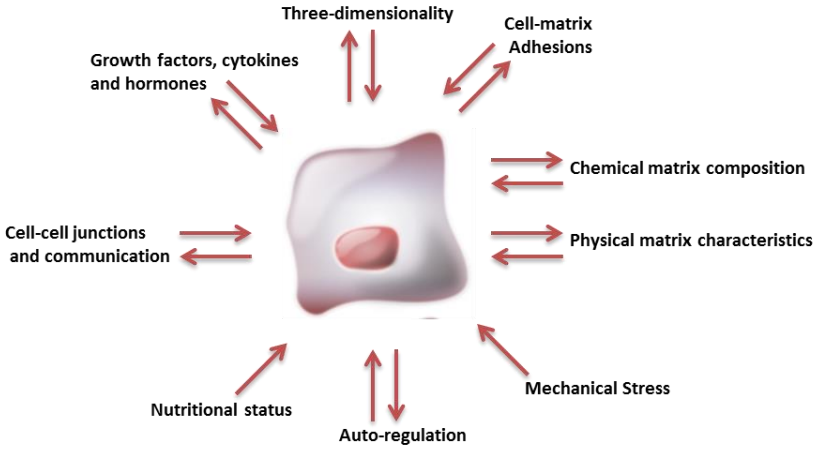

Fig 1-10: Microenvironmental factors that affect cellular behaviour.
A schematic representing aspects of the cellular microenvironment that effect cellular function and behavior. Most aspects of the microenvironment affect the way in which a cell behaves and in turn should be considered when developing *in vitro* cell-based models. For example, 3D cell culture technology is becoming more widely adopted as traditional 2D growth substrates induce changes in cellular structure that effect the function and protein expression of a cell. Equally, the oxygen availability of each culture model should be considered as many physiological tissues exist in hypoxic conditions. To produce the most accurate *in vitro* model possible that best reflects the *in vivo* environment, each aspect of the physiological microenvironment should be considered.

One of the hurdles faced by the pharmaceutical industry is that many of the drugs that show promising effects *in vitro,* fail to demonstrate the required clinical safety and efficacy for approval for human use[163,164]. Most *in vitro,* cell-based models commonly used in drug development and safety testing, routinely adopt 2D cell culture conditions, such as the Caco-2 monolayer model of intestinal permeability[165,166] and HepG2 model of hepatotoxicity[167,168]. However, due to cellular inconsistencies *in vitro* and *in vivo,* when candidate drugs are tested in animal models, drugs that were initially thought to be suitable may exhibit unwanted effects[162]. This is thought to be due to the altered cellular structure and function associated with 2D culture and there is now much focus on the development 3D cell-based, *in vitro* models with better predictive value[161,169,170].

There are many 3D cell culture technologies commonly used in the development of *in vitro* models, each has its own advantages and disadvantages that should be assessed prior to use. Spheroid culture systems are perhaps the most basic method of recreating a 3D environment and are most commonly used in stem cell culture, whilst scaffold based technologies can provide support and 3D growth cues to cultures and range from ECM-based hydrogels to solid polymer scaffolds[161,162]. However, all 3D technologies aim to provide a more physiologically relevant microenvironment maintaining native cellular structure and function, to provide more reliable insights into biological processes[161,162].

1.3.1 Spheroid Cultures

The most simple 3D cell culture system is that of the spheroid culture, which is a scaffold free methodology that promotes the culture of cells as multi-cellular aggregate structures. Within spheroids, cells form cell-to-cell contacts and secrete their own ECM components providing a more favourable microenvironment than the traditional 2D culture setting[162]. The most traditional methodology of aggregate induction is that of the hanging drop technique, whereby cells are cultured within a suspended droplet on the lid of a tissue culture plate and aggregates form at the apex of the drop[171]. However, other aggregate induction methodologies (outlined in Figure 1-11) also include the culture of cells on low adherent substrates allowing them to form cellular aggregates in suspension[172]. Alternatively, specialised tissue culture plates are available that contain microwells that force the cells into close proximity resulting in spheroids of a controlled size, such as the AggreWell™ plate[173].

Spheroid culture techniques are most commonly employed in the culture of pluripotent stem cells. Cellular aggregates composed of ES cells, known as embryoid bodies (EBs), can provide insight into the mechanisms of early differentiation events that occur during embryonic development[174]. The culture of EBs mimics many of the events involved in early embryonic development and therefore can be a very valuable tool in the study of

developmental mechanisms, however, there are a number of problems associated with spheroid cultures[174]. For example, a lack of diffusion both of gasses and nutrients into the centre of large EBs can result in a hypoxic environment that may lead to necrosis[162].

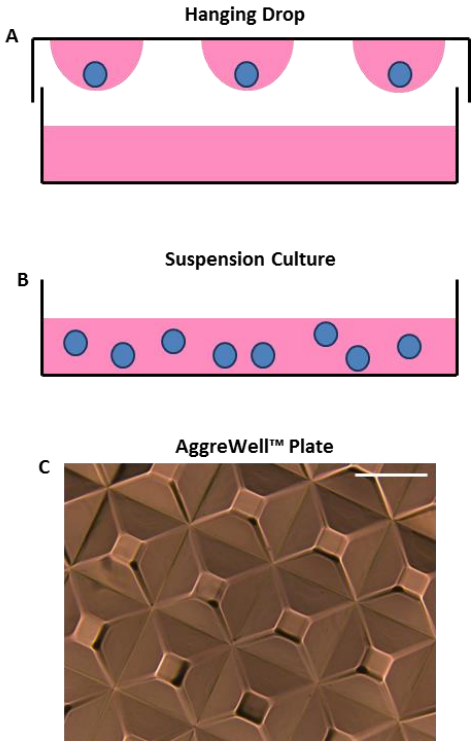

Fig 1-11: Spheroid culture methodologies.
Schematics representing each method of cellular aggregate induction used routinely in spheroid culture systems. The hanging drop methodology (A) involves the culture of cells in drops of growth medium, suspended from the lid of a tissue culture plate and cellular aggregates (blue) form at the apex of each drop. Low adherent substrates can be used to culture cells in suspension (B) and cells begin to form clumps that develop into cellular aggregates over the culture period. A micrograph (C) demonstrates the microwells visible at the bottom of each culture well within an AggreWell™ plate. Cells that are cultured within the microwells are forced into close proximity and ultimately spheroids can be harvested from the plate. Scale bar: 500 μm.

The formation of EBs mimics the initial stages in embryogenesis, and therefore this technique is often used in differentiation protocols to provide a more physiologically relevant setting[174]. Particularly, neural differentiation of ES cells is commonly achieved through EB culture combined with the application of morphogens to direct stem cell fate toward a neural lineage. EB neural differentiation methodologies result in the generation of neurons, through the dissociation of differentiated spheroid structures[135] that can subsequently be used for transplantation[137] or *in vitro* purposes[175–177] such as neurite outgrowth assays. An example application of spheroid differentiation cultures is highlighted by a study from Doers *et al* that describes the isolation of iPSCs from patients with fragile X syndrome and their subsequent neural differentiation as spheroids to

provide a disease specific *in vitro* model[178]. Differentiated neurospheres were dissociated and re-plated as neuronal cultures and the ability of patient-derived neurons to form neurites was found to be impaired[178].

1.3.2 Hydrogel Technology

Scaffold structures are often used to provide a 3D environment for cell growth and development *in vitro*. Hydrogels are an example of scaffold-based technology and are comprised of a loose framework of cross-linked molecules usually of natural origin such as agarose, fibrin, collagen or hyaluronic acid in a high water content gel[162]. These materials contain cell adhesion sites and provide a biochemically favourable environment by re-capitulating some aspects of the native ECM, along with providing a 3D environment for cell growth, both of which are important factors in providing a physiologically relevant microenvironment (summarised in Figure 1-10)[162,179].

As with all 3D cell culture technology, there are some limitations to the use of hydrogels that must be considered prior to use. Cells are usually encapsulated into the gels through a process that may require exposure to UV light to cure the gel and promote polymerisation, which may have adverse effects upon the cells[180]. Difficulty of nutrient diffusion throughout the gel may limit the length of time cultures are able to be maintained for, resulting in cells being cultured for relatively short periods of time[162]. However, there are also many advantages in the use of hydrogels, particularly in the field of tissue engineering. Once cells are encapsulated within the hydrogel, they are able to grow and develop cell-cell interactions with the potential to result in tissue formation[180]. Once a tissue has developed within the gel, the gel can be degraded through enzymatic digestion resulting in a scaffold-free tissue-like structure, as described in Figure 1-12[180].

Common applications of hydrogel technology include the study of cellular migration and branching[162] such as neuritogenesis, therefore hydrogels are commonly used in neurite outgrowth studies[179,181,182]. Tibbet *et al*, demonstrate the differences between neural cells cultured as a monolayer and within a hydrolytically degradable polyethylene glycol based hydrogel[179]. Within the hydrogel, cells form a spheroid-like structure and neurites radiate from the central sphere within the 3D space[179]. This has advantages over the traditional monolayer culture, as neurite quantification is more simple and precise, as neurites do not form complex networks, along with providing a more physiologically relevant 3D geometry to study the development of neurites.

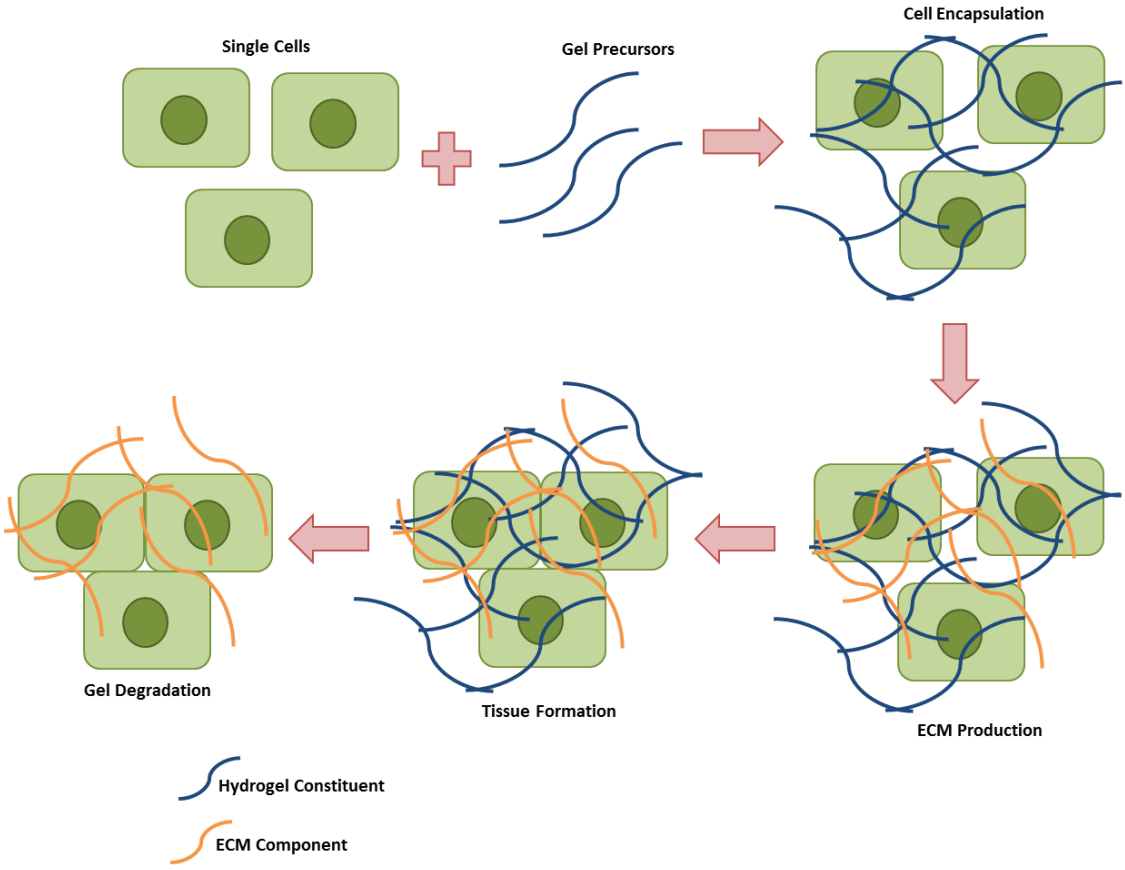

Fig 1-12: Development of tissue-like structures within hydrogels.
A schematic representing the development of tissue-like structures within hydrogel scaffolds. Single cells are initially encapsulated within the gel through the polymerisation of gel precursors (blue). Within the gel, cells begin to secrete their own ECM components (orange) and form cell-to-cell contacts resulting in tissue-like structures. The gel can then be enzymatically degraded, leaving a scaffold-free, tissue-like structure remaining.

Hydrogel based approaches are currently being considered for use in the repair of nerve injuries, particularly as they can be biodegradable, proving a suitable candidate for cellular delivery *in vivo*. Assuncao-Silva *et al*, propose a strategy that combines a co-culture approach of neurons with adipose derived stem cells and glial derived neurotrophic factor within a hydrogel based culture system to enhance neurite outgrowth in the context of peripheral nerve injury (PNI)[181]. Similarly, Shepard *et al* describe the combination of gene delivery with biodegradable hydrogels to promote neurite outgrowth and to potentially overcome the obstacles that limit regeneration in the nervous system[182].

1.3.3 Fibrous Scaffolds

Similarly to hydrogels, fibrous scaffolds provide a 3D support for developing cells and electro-spinning is used to generate the most commonly used fibrous scaffolds[162].

Electrospinning allows for the generation of nanofibrous scaffolds that can be made from either synthetic or natural polymers that can have a bioactive function[183]. Passing a polymer jet through an electric field and collecting the resultant material on a grounded surface[162] results in the formation of 3D mesh of non-woven nano and microfibres[183]. Nanofibrous scaffolds are highly porous and have a high surface area to volume ratio along with providing a large range of topological features that encourage cellular adhesion and proliferation[183].

One of the major advantages of the electrospinning technique is that the orientation of fibres can be determined. Fibres within the scaffold can be aligned producing directional scaffolds on which cells can adhere and elongate, providing alignment and directionality to cultures[162]. This particularly has applications in the generation of neuronal grafts for implantation in the case of PNI[184–186]. The alignment of nanofibre scaffolds is also thought mimic the structure of certain aspects of the ECM, including the arrangement of collagen fibrils[162]. Nanofibres can also be functionalised by the incorporation of ECM motifs such as laminin into the scaffold that promotes the outgrowth of neurites and enhances neuronal cultures, providing a more physiologically relevant environment[187].

However, the 3D support which nanofibres provide has been called into question as cells adhere to the surface of the scaffold with minimum penetration[183]. Therefore, some may believe that there is little difference between 2D cell culture and cells cultured within a nanofibre scaffold. However, although cells do not migrate into the scaffold, they receive nutrients and growth cues from the 3D topography of the scaffold, providing a uniquely 3D culture environment[183].

Electrospun nanofibres are commonly used in the field of neural tissue engineering and due to their aligned nature, are often used to direct neurite outgrowth. A study by Xie *et al* describes a combined approach to enhance the neural differentiation of ES cells[188]. This study combines two different forms of 3D technology through differentiation of ES cells as spheroids (EBs) before seeding neural progenitor cells onto an electrospun biodegradable polymer for the repair of nerve injuries. In this case the electrospun scaffold was found to not only enhance neural differentiation but also to provide growth cues and guidance for the developing neurites themselves[188].

Nanofibrous scaffolds are routinely used in neurite outgrowth studies, with the composition of the scaffold such as its diameter and surface properties determining the extent to which neurites develop[189,190]. Therefore, variability in the production of such scaffolds impacts the reproducibility of a particular neurite outgrowth assay, preventing its widespread adoption within the pharmaceutical industry. However, this offers flexibility that may be required in an academic setting, as modifications may be made to

the production to enable investigations into the effect of certain aspects of the material (surface coupling with ECM components, structure/order, directionality, diameter, conduction, etc.) upon neuritogenesis.

1.3.4 Porous Scaffolds

Porous scaffolds provide a 3D microenvironment in which cells can infiltrate and retain a morphology reminiscent of the *in vivo* tissue. Within porous scaffolds, cells form contacts with neighbouring cells resulting in structures that resemble the native tissue[162]. Various materials have been used to generate porous scaffolds for cell culture applications, however, inert, non-degradable materials perhaps seem to be the most widely adopted for *in vitro* purposes[162]. These consist of internal pore structures connected by voids in which cells can grow and growth medium can diffuse throughout[191]. There are many mechanisms employed in the generation of such scaffolds including: emulsion templating, leachable particles and gas foam technology[191].

Most non-degradable scaffolds are polystyrene based and as polystyrene is inert and stable. These products have a long shelf life particularly in comparison to hydrogels or biodegradable scaffolds made from natural sources[191]. Conventional 2D tissue culture plastic-ware is usually polystyrene based, therefore 3D polystyrene scaffolds offer an opportunity for direct comparison between 2D and 3D culture, allowing investigation specifically into the effect of a 3D geometry on cellular function[191]. However, polystyrene is not a particularly physiologically relevant material, as cells are never exposed to this material *in vivo* and polystyrene scaffolds fail to recapitulate the *in* vivo biochemical environment. This can be overcome by adsorption of ECM proteins[192] to the scaffold, or by the functionalisation of such scaffolds[193] to provide a more biochemically favourable environment.

Emulsion templating is a production technique used in the manufacture of porous, polystyrene scaffolds such as Alvetex® Scaffold. Alvetex® Scaffold is a commercially available, inert, polystyrene scaffold manufactured using a biphasic emulsion[191]. The scaffold is created through a polymerisation reaction consisting of an aqueous and non-aqueous monomer/surfactant phase[191,194–196]. The resultant scaffold is termed a poly-HIPE (high internal phase emulsion) and consists of a network of voids and interconnecting windows (internal structure of Alvetex® is shown in Figure 1-13)[191]. Alvetex® is manufactured into a 200 µm thick disc and is available in insert formats that are compatible with standard tissue culture plastic-ware, as shown in Figure 1-13. Scaffolds such as this provide a highly porous 3D cell culture microenvironment that promotes the exchange of nutrients, waste products and gasses[191].

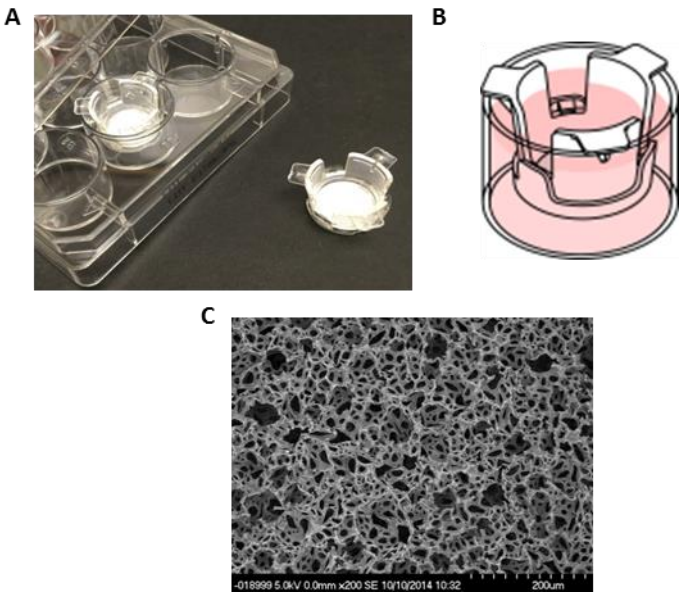

Fig 1-13: Alvetex® Scaffold: A porous polystyrene scaffold for 3D cell culture.
Alvetex® Scaffold inserts (A) are compatible with standard tissue culture plastic-ware. Within the culture well (B), growth medium connects the outer and inner chambers providing an abundance of nutritional material. An electron micrograph (C) reveals the internal porous, structure of scaffold with internal voids of 40 μm on average and interconnecting windows of approximately 13 μm.

Similarly to the other 3D cell culture technologies discussed thus far, polystyrene scaffolds such as Alvetex® have applications in the field of neuroscience. Specifically, Alvetex® Scaffold is commonly used in the development of *in vitro* models including differentiation methodologies and neurite outgrowth models based upon stem cell derived neurons. In a study by Hayman *et al* the ability of Alvetex® to provide a 3D environment for the growth and differentiation of human stem cell derived neurons was established[150]. In a later study by Hayman *et al* it was found that neuritogenesis was actually enhanced by the culture of neurons within a 3D environment compared with traditional 2D culture, as evidenced by elevated expression of known markers of neurite outgrowth including, nestin, MAP2 and NeuroD[147]. The ability of glial and neuronal populations to form functional circuitry within a 3D environment was assessed by Smith *et al,* who found that cells cultured within Alvetex® Scaffold exhibited a more physiologically relevant phenotype in terms of morphology, pharmacology and electrophysiology[197].

1.4 Conclusions

In conclusion, neurite outgrowth is an important developmental process, essential to the maintenance of proper neural connectivity. Inhibition of neurite outgrowth is common to many disorders of the nervous system including trauma such as spinal cord injury and

neurodegeneration including Alzheimer's disease. For this reason, the development of reliable, robust and reproducible *in vitro* neurite outgrowth models is essential, not only to study the underlying mechanisms of neurite inhibition, but also to screen potential compounds that may be able to recover neurite growth.

As described in this chapter, 3D cell culture technology can provide a more physiologically relevant environment to study cellular processes, and polystyrene scaffolds have even been previously demonstrated to enhance neuritogenesis. Although neurite outgrowth models currently exist, there are many limitations in their application to routinely test the ability of compounds to induce neurite degeneration or regeneration. Perhaps most importantly quantification of neurite outgrowth currently relies on neurite tracing using image analysis software. This can be laborious and error prone, which is why there is need for a novel model of neurite outgrowth that can be more easily and accurately quantified, amenable to high throughput applications. Synthetic retinoid compounds can induce robust neuronal differentiation from human pluripotent stem cells, and have been shown to reproducibly induce neuritogenesis. 3D cell culture technology in combination with the robust neuronal differentiation of human pluripotent stem cells induced by synthetic retinoid analogues, may provide a novel *in vitro* model of neuritogenesis that better recapitulates *in vivo* neurite development, with greater efficiency and accuracy. This model may then be applied to specific disease pathways to uncover the molecular signalling events common to the process of neurite inhibition.

1.4.1 Project Aims

This project aims to build upon current knowledge of neurite induction, to develop a novel 3D *in vitro* model of human neuritogenesis, combining human pluripotent stem cells, synthetic retinoid analogues and 3D cell culture technology in the form of Alvetex® Scaffold. This physiologically relevant model of human neurite outgrowth can be applied to study the role of neurite inhibition in the context of spinal cord injury and Alzheimer's disease, identifying signalling pathways common to both pathologies. We hypothesise that combining the aforementioned technology will allow us to develop an improved, novel model of human neurite development that better mimics the *in vivo* developmental process. Once developed, we then plan to apply this model to several neurological pathologies to begin to dissect the molecular signalling events that govern neurite inhibition and regeneration in the CNS.

Furthermore, the identification of such signalling mechanisms can allow for the identification of critical points where intervention by small molecules may result in the restoration neurite growth. This demonstrates the application of such a model in the screening of potential compounds and the assessment of neurotoxicity of potential drug

candidates. We hypothesise that inhibition in the Rho A/ROCK signalling cascade may lead to neurite regeneration, despite the presence of inhibitory stimuli, aiding our understanding of the inhibitory pathways involved in loss of neuronal connectivity within the CNS.

To further enhance the model, protein surface technology will be employed to functionalise 2D and 3D growth substrates to improve the physiological relevance and standardise the model. This technology can then be used to further identify neurite inhibitory/enhancing motifs and to enhance our understanding of the molecular processes involved in neurite growth and inhibition.

1.4.2 Project Objectives

- Develop and characterise a robust and reproducible, novel *in vitro* model of human neurite outgrowth by combining human pluripotent stem cell, synthetic retinoid and 3D cell culture technologies.

- Apply the novel 3D model of neuritogenesis to study the molecular mechanisms underpinning neurite inhibition in the context of the glial scar that forms following spinal cord injury.

- Investigate the ability of the β-amyloid peptide involved in Alzheimer's disease to induce neurite inhibition and potential mechanisms of recovery.

- Identify potential neurite enhancing and inhibitory motifs through the use of protein surface technology to produce functionalised growth substrates that can be used to further enhance and standardise the novel 3D model of neurite outgrowth.

Chapter II: Materials & Methods

2.1 Introduction

A number of scientific techniques were used throughout this thesis, in order to investigate and probe neurite development and inhibition. These range from advanced cell culture techniques, to immunofluorescence and histological processing analyses, which have allowed for the development of the novel human neurite outgrowth model described and applied throughout the chapters of this work. This chapter outlines the main scientific techniques that have been utilised throughout this study.

2.2 Cell Culture

2.2.1 Maintenance of Human Pluripotent Stem Cells

The human embryonal carcinoma (EC) stem cell line, TERA2.cl.SP12 is a sub-line of the original TERA-2 line isolated by Prof. Stefan Przyborski (Durham University). The original TERA-2 line was isolated from a lung metastasis of a primary malignant embryonal carcinoma in the testis. The TERA2.cl.SP12 sub-line was isolated from the original TERA-2 line based on expression of the pluripotency marker SSEA-3 and exhibits enhanced neural differentiation when exposed to retinoic acid[146].

TERA2.cl.SP12 pluripotent stem cells were maintained in Dulbecco's modified Eagle's medium with high glucose (DMEM-HG, Gibco, Cramlington, UK) supplemented with 10 % heat-treated foetal bovine serum (FBS, Gibco), 2 mM L-glutamine (Gibco) and 20 active units of Penicillin and Streptomycin (Gibco). Cells were incubated at 37 °C and 5 % CO_2 in a humidified environment. Cells were maintained at high confluence in 75 cm^2 culture flasks (BD Falcon, Erembodegem, Belgium) to ensure their pluripotent phenotype and passaged every 3 – 4 days. Cells were dissociated using acid washed glass beads (ThermoFisher, Cramlington, UK) to mechanically dislodge cells, which were then split in a 1:3 ratio and seeded into further 75 cm^2 culture flasks.

TERA2.cl.SP12 cells were stored at -140 °C in FBS supplemented with 10 % dimethyl sulfoxide (DMSO, Sigma-Aldrich, Dorset, UK). Cells were frozen at a 1:3 ratio from a confluent 75 cm^2 culture flask and resuspended in freezing medium before being slowly frozen at a rate of -1 °C per minute. Revival of cells was preformed rapidly and cells were transferred immediately from -140 °C storage into a 37 °C water bath to thaw. Cells were then transferred into 9 mL of warm maintenance medium before being centrifuged at 1000 rpm for 3 mins. DMSO containing supernatant was then aspirated and the remaining

cell pellet was resuspended in 10 mL maintenance medium before being seeded into a 25 cm^2 (BD Falcon) culture flask. Revived cells were incubated at 37 °C and 5 % CO_2 in a humidified environment for 2 – 3 days and passaged at a 1:1 ratio into a 75 cm^2 culture flask.

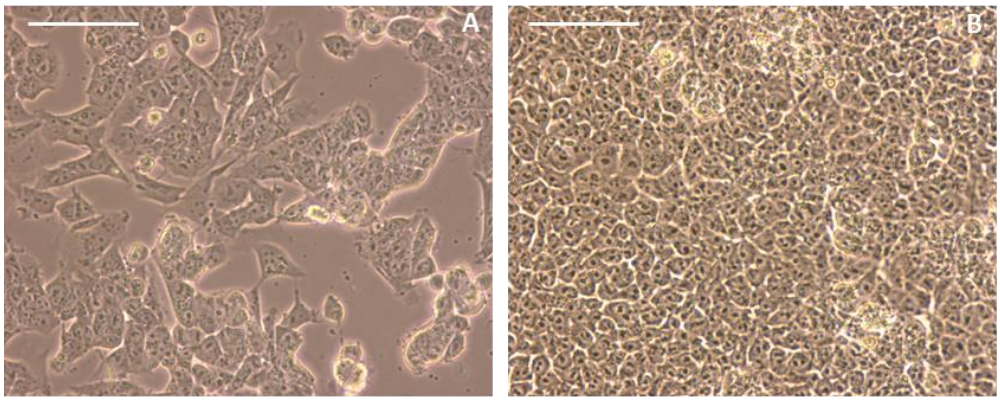

Fig 2-1: TERA2.cl.SP12 human pluripotent stem cells at low and high confluence.
Phase contrast micrographs of the embryonal carcinoma cell line, TERA2.cl.SP12 at low (A) and high confluence (B). Cells are maintained at high confluence to ensure their pluripotent phenotype. Scale bars: 100 µm.

2.2.2 Maintenance of U-251MG Human Glioblastoma/Astocytoma Cells

U-251MG (formerly known as U-373MG) cells (European Collection of Authenticated Cell Cultures, Salisbury, UK) are adherent human glioblastoma astrocytoma cells, derived from a malignant glioblastoma tumour by explant technique. Cell morphology is pleomorphic, astrocytoid[198].

U-251MG cells were maintained in Minimum Essential Eagle's Medium with Earle's Salts Solution (EMEM, Gibco) and supplemented with 10 % heat-treated FBS, 2 mM L-glutamine, 1 % Non-Essential Amino Acids (NEAA, Gibco), 1 mM Sodium Pyruvate (Gibco) and 20 active units of Penicillin and Streptomycin. Cells were maintained in 75 cm^2 culture flasks (Greiner Bio One, Gloucester, UK) and sub-confluent cultures (70 – 80 %) were split every 3 – 4 days at a ratio of 1:3 – 1:6. Passaging of cells involved the detachment of cells via trypsinisation with 3 mL of 0.25 % trypsin/2 mM EDTA solution (Gibco). Loosely adhered cells were then washed off the surface of the flask with 7 mL maintenance medium, which also acts to neutralise trypsin solution. The whole 10 mL cell suspension was then collected and centrifuged at 1000 rpm for 3 mins and cells were resuspended in 3 mL maintenance medium before being split and seeded in further 75 cm^2 culture flasks containing 15 mL of maintenance medium.

U-251MG cells were stored at -140 °C in FBS containing 10 % DMSO. A single cell suspension was obtained via trypsinisation as previously described from a confluent 75 cm^2 culture flask and split 1:3 for freezing and storage at -140 °C. Cells were revived as previously described in section *2.1.1* for TERA2.cl.SP12 cells.

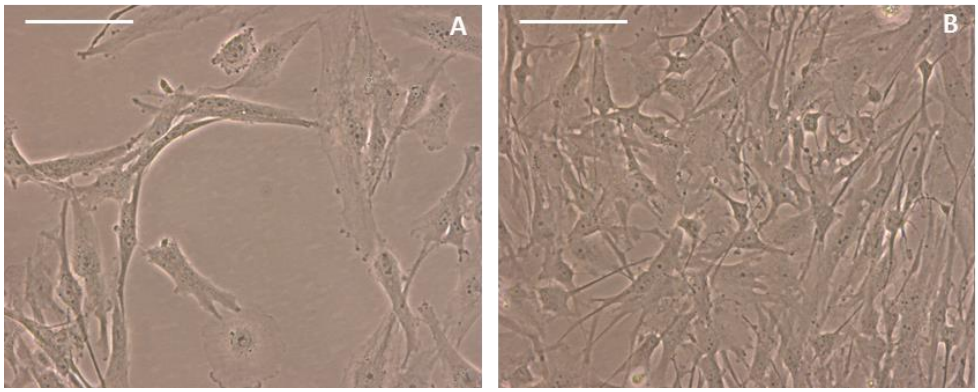

Fig 2-2: U-251MG human astroglioma cells at low and high confluence.
Phase contrast micrographs of the glioma cell line, U-251MG at low (A) and high confluence (B). Scale bars: 100 µm.

2.2.3 Maintenance of U-118MG Glioblastoma/Astrocytoma Cells

U-118MG (ATCC, Manassas, USA) cells are adherent human glioblastoma cells of mixed morphology. The cell line was derived from a grade IV human brain glioblastoma, astrocytoma and cells are tumorigenic in nude mice[199].

U-118MG cells were maintained in DMEM-HG supplemented with 10 % heat-treated FBS, 2 mM L-glutamine and 20 active units of Penicillin and Streptomycin. Cells were incubated at 37 °C and 5 % CO_2 in a humidified environment. Cells were maintained in 75 cm^2 tissue culture flasks and passaged every 3 – 4 days at 70 – 80 % confluence. Passaging of cells was by trypsinisation with 3 mL 0.25 % trypsin/2 mM EDTA solution and loosely adhered cells were washed from the surface of the culture flask with 7 mL maintenance medium. The whole 10 mL cell suspension was then collected and centrifuged at 1000 rpm for 3 mins and cells were resuspended in 3 mL maintenance medium before being split and seeded in further 75 cm^2 flasks containing 15 mL of maintenance medium.

Storage of U-118MG cells was at -140 °C in FBS containing 10 % DMSO. A single cell suspension was obtained via trypsinisation as previously described from a confluent 75 cm^2 culture flask and split 1:3 for freezing and -140 °C storage. Cells were revived as previously described in part 2.1.1 for TERA2.cl.SP12 cells.

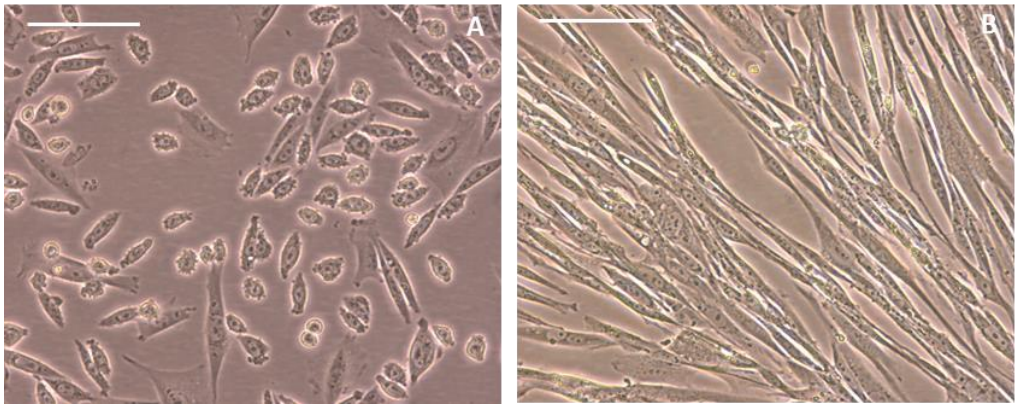

Fig 2-3: U-118MG human astroglioma cells at low and high confluence.
Phase contrast micrographs of the glioma cell line, U-118MG at low (A) and high confluence (B). Scale bars: 100 μm.

2.2.4 Induction of Differentiation of Human Pluripotent Stem Cells in 2D Monolayer Cultures

For 2D monolayer differentiation studies, human pluripotent stem cells (TERA2.cl.SP12) were seeded at a density of 200,000 cells per 25 cm^2 culture flask and incubated for 24 hours to allow cells to adhere to the culture surface. Following 24 hours incubation, the culture medium was replaced with medium containing retinoid compounds: ATRA (Sigma-Aldrich), EC23 (ReproCELL Europe, Sedgefield, UK) or AH61 (Chemistry Department, Durham University, Durham) at concentrations of 0.001 μM, 0.01 μM, 1 μM and 10 μM. Cells were cultured for a further 7 days with a media change on the 4^{th} day of culture. Cell surface marker expression was then analysed by flow cytometry following 7-day retinoid treatment.

2.2.5 Formation of Neurospheres from Human Pluripotent Stem Cells

Confluent cultures of TERA2.cl.SP12 human pluripotent stem cells were trypsinised using 0.25 % trypsin/2 mM EDTA solution to create a single cell suspension before viable cells were counted using a trypan blue (Sigma-Aldrich) exclusion assay and a haemocytometer. Cells were then seeded in suspension culture at a density of 1.5 x 10^6 cells per sterile, untreated, biological, 90 mm Petri dish (ThermoFisher). Cells were incubated in 20 mL maintenance medium for 24 hours at 37 °C and 5 % CO_2 in a humidified environment to promote cell aggregation.

Following 24 hours in culture, cells began to aggregate and retinoid compounds were added directly to the 24 hour-old culture medium from the time of cell seeding, to avoid disaggregation of newly formed cellular aggregates. To achieve a final concentration of 0.01 μM EC23, 20 μL of 0.01mM EC23 stock solution was added to 20 mL maintenance

medium forming the basis of the differentiation medium. Cell aggregates were further maintained in suspension for 21 days at 37 °C and 5 % CO_2 in a humidified environment. Differentiation medium was changed every 3 – 4 days by transferring the suspension culture to a 50 mL conical tube (Greiner Bio One) allowing the cell aggregates to collect at the bottom of the tube. The old differentiation medium was then carefully aspirated away, leaving a sediment of cell aggregates at the bottom of the tube. Fresh differentiation medium was then added to the tube and the cell aggregates were resuspended and seeded into a fresh 90 mm untreated Petri dish. Following 21 days culture, human pluripotent stem cell aggregates become fully matured neurospheres capable of forming neurites.

2.2.6 Induction of Neurite Outgrowth from Stem Cell Derived Neurospheres

Following 21 days differentiation, stem cell derived neurospheres were cultured on 2D and 3D (Alvetex® Scaffold) growth substrates coated with laminin and poly-D-lysine to promote neurite outgrowth, as described by Clarke *et al*[149].

2.2.6.1 Coating of Growth Substrates for Neurite Outgrowth Studies

Alvetex® Scaffold 12-well format inserts (ReproCELL Europe) were prepared by plasma treatment using the K1050X Plasma Asher at a power level of 40 W, for 5 mins. Treated scaffolds and conventional 48-well tissue culture treated plates were coated overnight at room temperature with 10 μgmL^{-1} poly-D-lysine (Sigma-Aldrich) and laminin (Sigma-Aldrich) solution. Coating solution was prepared by adding 500 µL of 1 $mgmL^{-1}$ Laminin from Engelberth-Holm-Swarm murine sarcoma membrane and 500 µL of 1 $mgmL^{-1}$ poly-D-lysine solution (poly-D-lysine powder (Sigma-Aldrich) reconstituted in 1 mL phosphate buffered saline (PBS)) to 49 mL PBS without Ca^{++}, Mg^{++} (Lonza, Basel, Switzerland). To each well of a 48 well tissue culture plate, 150 µL coating solution was added and 300 µL coating solution was added to each Alvetex® Scaffold. Following overnight incubation at room temperature, coating solution was removed and growth substrates were washed three times with PBS and stored in PBS prior to neurosphere seeding.

2.2.6.2 Seeding of Neurospheres for Neurite Outgrowth Assays

Following 21 days differentiation, neurospheres were collected using a 20 mL serological pipette (Greiner) and passed through a 100 µm cell strainer (BD Falcon) to remove any single cells or cellular debris. Neurospheres were then washed with fresh maintenance media (without retinoid compounds) and backwashed into a new 90 mm Petri dish. Maintenance media containing mitotic inhibitors: 1 µM cytosine arabinose (Sigma-Aldrich), 10 µM 5'fluoro 2'deoxyuridine (Sigma-Aldrich) and 10 µM uridine (Sigma-Aldrich) was added to each well of a poly-D-lysine and laminin coated 48-well plate (500

μL per well) or to a 12-well culture plate containing poly-D-lysine and laminin coated 12-well format Alvetex® Scaffold inserts (4 mL per scaffold). A 200 μL pipette tip was used to transfer 20 μL of media containing 1 – 2 neurospheres into each 2D well or 50 μL containing 5 – 10 neurospheres onto each Alvetex® Scaffold. Neurospheres were then incubated for 10 days at 37 °C and 5% CO_2 in a humidified environment. Throughout this time, the culture medium was not changed to avoid disruption to the developing neurites. Following 10 days incubation, the cell aggregates were fixed with 4% paraformaldehyde (PFA, Sigma-Aldrich) and stored in PBS prior to immunofluorescence analysis.

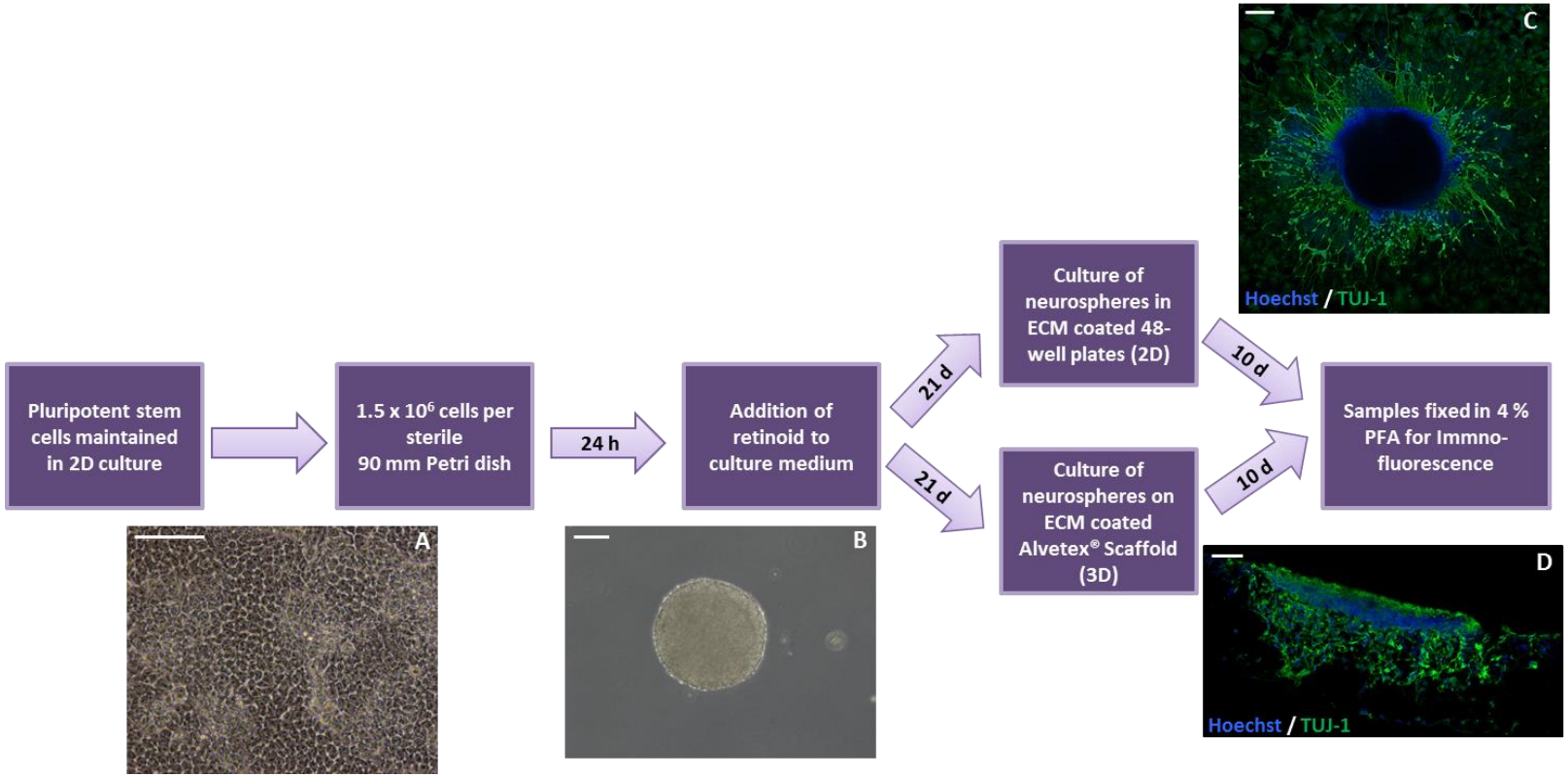

Fig 2-4: Flow chart summarising the stages of the neurite outgrowth process in both 2D and 3D culture. Human pluripotent stem cells are maintained in 2D culture (A, scale bar: 100 µm), seeded in suspension culture at a density of 1.5 x 10^6 cells per Petri dish and allowed to aggregate for 24 hours. Retinoid compounds are then added directly to the culture medium to induce neural differentiation for 21 days (B, scale bar 100 µm), following which, neurospheres are seeded either into either 2D culture plates (C, scale bar: 200 µm) or onto Alvetex® Scaffolds for 3D culture (D, scale bar: 200 µm). Neurospheres are maintained for a further 10 days with mitotic inhibitors before being fixed for immunofluorescence analysis.

2.2.7 Image Analysis

2.2.7.1 Neurite Quantification

To quantify neurite outgrowth, neurospheres were stained for the pan-neuronal marker, β-III-tubulin (TUJ-1) that highlights neurites radiating from the aggregate. Digital images (TIFF format) of the staining were recorded and opened in the image analysis software, Image J (imagej.nih.gov). The scale was set in the software by tracing the scale bar on the image and selecting Analyze > Set Scale and entering the length of the scale bar in μm. Neurites were then traced using the "Freehand Line" tool and recorded by selecting Analzye > Measure, followed by Analyze > Draw. This produced a table containing the number assigned to each neurite and the length of each neurite in μm. This raw data was then analysed to give the total number of neurites per neurosphere, the average neurite length, and the neurite density, which is the number of neurites normalised to aggregate perimeter.

A sampling method of quantification was developed to ensure efficient and accurate neurite quantification. This involved overlaying a grid onto each image and using a random number generator (random.org) to select three squares per image to quantify. This method was found to produce data that was not significantly different to counting every neurite per neurosphere and deemed adequate to be used throughout this project.

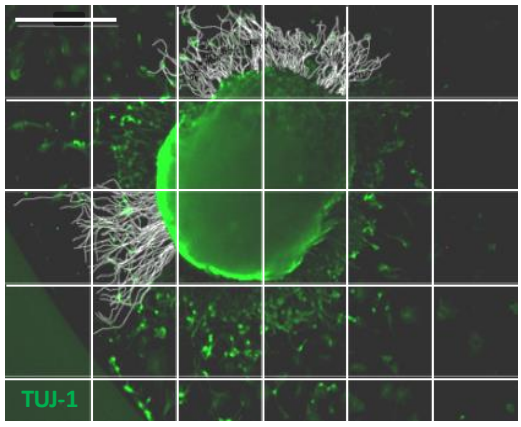

Fig 2-5: Quantification of neurite outgrowth using Image J software.
A grid overlay was placed over the original image to be quantified in Image J and three squares per image were randomly chosen using a random number generator to be quantified. The neurites radiating from the central aggregate in the selected squares were traced using the "freehand line" tool and measured. Scale bar: 500 μm.

2.2.7.2 Migration Analysis

Image J software was also used to analyse the area of migration around an aggregate. The scale was calibrated in the software as described in section *2.2.7.1.* Images of the nuclear stain Hoechst were opened in image J to highlight the aggregate body along with the nuclei of cells that had migrated away from the main bulk of the aggregate. The "Freehand Selection" tool was then used to trace the perimeter of the aggregate and also the zone of nuclei that had clearly migrated from the aggregate (Figure 2-6). Each selection was then measured by selecting Analyze > Measure which produced a table containing the area of each measurement. The zone of migration was then calculated as a percentage of aggregate area.

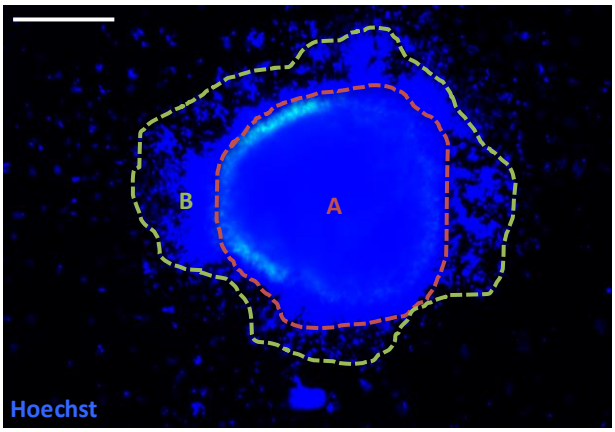

Fig 2-6: Analysis of area of migration using Image J software.
The area of central body of the aggregate was measure using Image J (A, red) followed by the area of the zone of migration (B, green). This allowed calculation of the percentage zone of migration. Scale bar: 500 μm.

2.2.8 Media Supplementation

Throughout this thesis, a number of small molecules were used to direct the differentiation of pluripotent potent stem cells or to influence neurite outgrowth. Retinoid compounds used to promote neural differentiation were added to suspension cultures of pluripotent stem cell aggregates during the differentiation period of culture or to 2D monolayer cultures and replaced every 3 – 4 days. Molecules that were used to manipulate neurite outgrowth, were added to the culture medium containing mitotic inhibitors during the neurite outgrowth period of culture and not replaced for the entirety of the 10-day culture (unless otherwise stated).

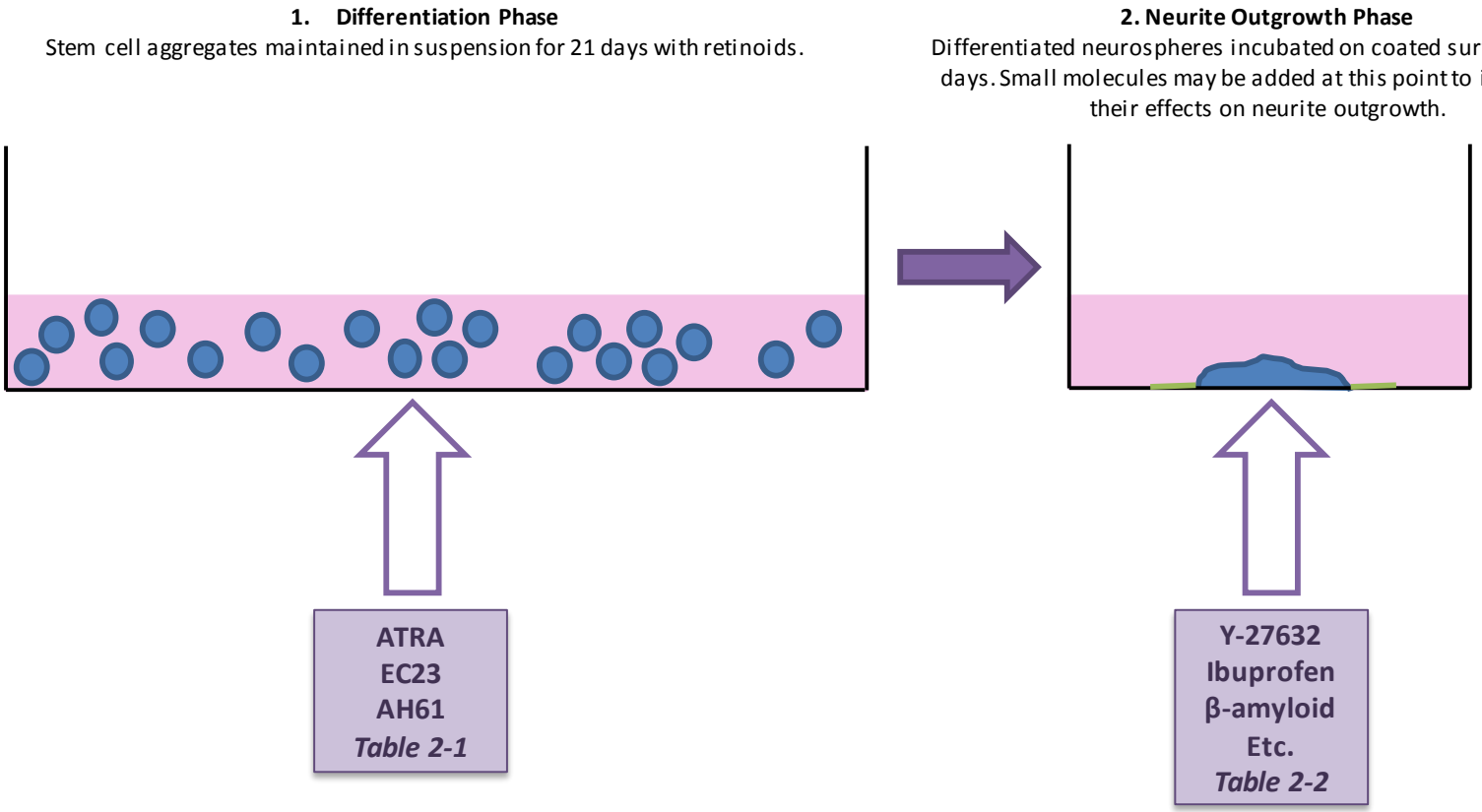

Fig 2-7: Generation of neurite outgrowth from human pluripotent stem cells is a two-step process.
Initially, stem cell aggregates were maintained in suspension with retinoid molecules for 21 days to promote their differentiation (*1. Differentiation Phase*). Fully differentiated neurospheres were then placed on ECM coated 2D and 3D surfaces and maintained for a further 10 days with mitotic inhibitors, at which point neurites begin to protrude from the body of the neurosphere (*2. Neurite Outgrowth Phase*). During the neurite outgrowth phase a variety of molecules were added to cultures to determine their effect on neurite outgrowth.

Stock solutions of each compound were aliquoted and stored at -20 °C. An example of a calculation used to determine the volume of vehicle in which to dissolve a compound producing a desired stock solution is given below. A similar calculation was used to determine the stock solution parameters of each molecule used throughout this study by altering the molecular weight, known mass and required concentration.

Stock Solution Example – EC23

MW = 332 g
Known Mass = 10 mg
Desired Concentration = 10 mM

1M = 332 g in 1,000 mL
(÷ 100) 10mM = 3.32 g in 1,000 mL
x = (0.01 g (known mass) / 3.32 g) x 1,000
x = 3.01 mL DMSO to dissolve 10 mg to give 10 mM stock solution

Compound	Structure	Molecular Weight /g	Vehicle	Supplier
ATRA	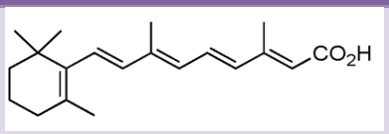	300.44	DMSO	Sigma-Aldrich
EC23	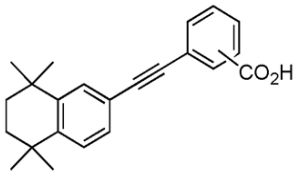	332.44	DMSO	ReproCELL Europe
AH61	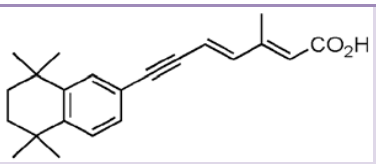	322.19	DMSO	Chemistry Department (Durham University)

Table 2-1: Small molecules used to direct pluripotent stem cell differentiation.
The details of retinoid molecules added either at the suspension culture stage to promote neuronal differentiation of human pluripotent stem cell aggregates or to 2D monolayer cultures for differentiation studies.

Compound	Molecular Weight /g	Vehicle	Supplier	Description
Chondroitinase ABC	120,000	0.01 % BSA	Sigma-Aldrich	Enzyme that cleaves GAG chains from chondroitin sulphate proteoglycans rendering them inactive
Y-27632 dihydrochloride	320.26	H_2O	Tocris	Selective p160 ROCK inhibitor
Ibuprofen	206.28	DMSO	Sigma-Aldrich	Non-steroidal anti-inflammatory drug
β-amyloid 1-40	4329.8	1 % acetic acid	Sigma-Aldrich	β-amyloid fragment most abundant in healthy brain
β-amyloid 1-42	4514.08	50 mM Tris Buffer	Tocris	β-amyloid fragment closely linked to Alzheimer's disease pathogenesis
NEP 1-40	4626.14	H_20	Sigma-Aldrich	Antagonist peptide to the Nogo-66 receptor

Table 2-2: Agents used to manipulate neurite outgrowth.
The details of supplements added to culture media containing mitotic inhibitors during neurite outgrowth phase of culture.

2.2.9 Culture of ReproNeuro Glu Cells

ReproNeuro Glu cells (ReproCELL, Kanagawa, Japan) are iPSC derived neuroprogenitor cells that have a propensity to form mature glutamatergic neurons. Somatic cells obtained from a healthy individual are reprogrammed to form iPSCs that in turn are differentiated to form neuroprogenitor cells. These cells are revived from frozen as neuroprogenitors and cannot be passaged or propagated, so must be used directly in an experimental procedure upon revival.

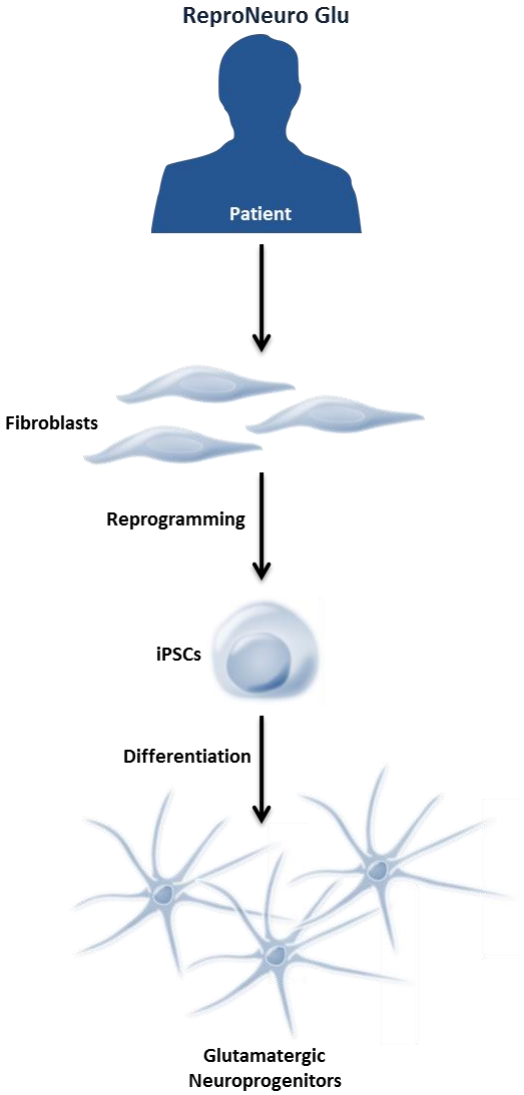

Fig 2-8: Schematic depicting the derivation of ReproNeuro Glu cells.
Somatic cells are obtained from a healthy individual and reprogrammed to form iPSCs. iPSCs are then differentiated to form a pool of glutamatergic precursor cells (ReproNeuro Glu) that upon revival and culture in Glu Maturation Medium, ultimately form mature neurons with glutamatergic properties.

2.2.9.1 Revival of ReproNeuro Glu Cells from Cryopreservation

Cells were stored in vapour phase liquid nitrogen and were transferred to a Dewar containing liquid nitrogen for revival. To revive cells the lid of the frozen cell vial was partially opened to release the pressure and frozen cells were thawed at 37 °C for 90 seconds while gently swirling. If cells are thawed for longer than 90 seconds, there is a significant loss of viability. The contents of the vial were decanted into 10 mL of pre-warmed Glu Thawing Medium (ReproCELL) and the vial was rinsed with 1 mL of Glu Thawing Medium to ensure all cells were collected. The cells were then centrifuged at 350 g for 5 minutes at room temperature and gently re-suspended in 2 mL of Glu Maturation Medium (ReproCELL) supplemented with 120 µL of Glu Additive (ReproCELL) and 100 active units of penicillin/streptomycin. The cell suspension was then topped up with 1 mL Glu Maturation Medium to give a final concentration of 1.0 x 10^6 cells per mL for cell seeding.

2.2.9.2 2D Monolayer Culture of ReproNeuro Glu Cells

For 2D monolayer cultures, cells were seeded onto 16 mm diameter glass coverslips in a 12-well tissue culture plate. Coverslips were coated in 0.002 % poly-L-lysine solution (Sigma-Aldrich) (0.01 % poly-L-lysine solution diluted in PBS), for 3 hours at 37 °C. Poly-L-lysine solution was then removed and the coverslips were washed twice in PBS prior to coating in 200 µL Glu Coat (ReproCELL) solution (150 µL of Glu Coat diluted in 5 mL PBS) overnight at 37 °C.

Prior to cell seeding, Glu Coat solution was removed and 280 µL of cell suspension following revival from cryopreservation was added to each well of the 12-well culture plate containing a glass coverslip. This achieved a final seeding density of 2.8 x 10^5 cells per well and wells were topped up with Glu Maturation Medium to give a final volume of 1.4 mL. Cells were incubated at 37 °C and 5 % CO_2 in a humidified atmosphere for 14 days to allow the development of mature neurons with a 50 % media change on the 3rd and 7th day of culture. Following the 14 day culture period, cells were washed in PBS and fixed in 4 % PFA for immunofluorescent analysis.

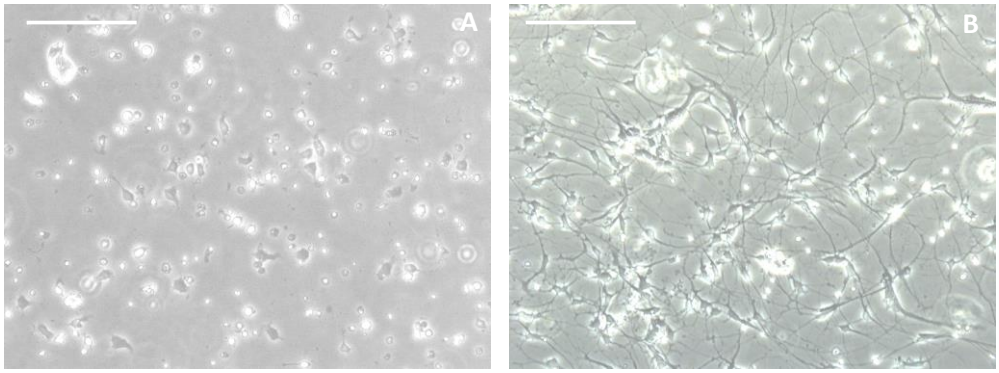

Fig 2-9: ReproNeuro Glu cells mature over a 14-day culture period.
Phase contrast micrographs depicting ReproNeuro Glu cells cultured in 2D immediately following seeding (A) and following 14 days in culture (B), cells have adopted a more neural morphology. Scale bars: 100 µm

2.2.9.3 3D Culture of ReproNeuro Glu Cells

Alvetex® Scaffold 12-well format inserts were prepared by plasma treatment using the K1050X Plasma Asher at a power level of 40 W, for 5 mins. Treated scaffolds were washed in PBS and incubated in 300 µL of 0.002 % poly-L-lysine solution at 37 °C for 3 hours. Scaffolds were then washed in PBS twice before being coated in 300 µL Glu Coat solution overnight at 37 °C.

Coated scaffolds were placed in a 12-well tissue culture plate and a cloning cylinder with an internal diameter of 3.4 mm was placed on the scaffold. Into the cylinder 40 µL of cell suspension was placed, resulting in a seeding density of 4 x 10^5 cells per scaffold. The cloning cylinder containing the cell suspension was incubated upright on the scaffold for 10 mins at 37 °C and 5 % CO_2 in a humidified environment. Following 10 minutes the cloning cylinder was then removed and the scaffold was incubated for a further 30 mins at 37 °C and 5 % CO_2 in a humidified environment before being topped up with 4 mL Glu Maturation Media. Scaffolds were then incubated for 14 days to allow the maturation of the neurons with a 50 % media change on day 3 and 7 of culture. Following 14 days incubation, scaffolds were fixed in 4 % PFA for analysis.

Fig 2-10: Concentrated seeding of ReproNeuro Glu on Alvetex® Scaffold using a cloning cylinder.
To achieve concentrated seeding on Alvetex® Scaffold, a 3.4 mm diameter cloning cylinder was used. The cell suspension was added directly to the cloning cylinder, which was incubated vertically on the scaffold for 10 minutes before removal. The scaffold was then incubated for a further 30 minutes without the cloning cylinder before being topped up with 4 mL Glu Maturation Medium.

2.2.9.4 Neurosphere Formation from ReproNeuro Glu Cells

AggreWell 800 plates (STEMCELL Technologies, Cambridge, UK) were used to induce spheroid formation from ReproNeuro Glu cells. The plates contain microwells that force the cells into close proximity promoting the formation of spheroid structures. The plates were prepared by rinsing each well in 2 mL Glu Maturation Medium. This was then removed and 0.5 mL Glu Maturation Medium was added to each well and the plate was centrifuged at high speed (2000 g for 5 mins) to displace any bubbles from the microwells. Cells were then seeded into each well with 1 mL of cell suspension (1×10^6 cells) added to each well. Cells were then pipetted up and down gently, to ensure even distribution of cells throughout the well, and each well was topped up with 0.5 mL Glu Maturation Medium. The plate was then centrifuged at 100 g for 3 minutes to capture the cells in the microwells and incubated at 37 °C and 5 % CO_2 in a humidified environment for 24 hours to allow spheroid formation. Following 24 hours incubation, spheroids were harvested from microwells using a p1000 pipette to gently pipette the medium within the wells up and down, forcing the spheroids from their microwells. Cell aggregates were collected and passed through a 100 μm cell strainer; aggregates collected in the strainer (aggregates > 100 μm) were then backwashed into a sterile 90 mm Petri dish prior to seeding for neurite outgrowth assays.

2.2.9.5 Neurite Outgrowth Assay from ReproNeuro Glu derived Neurospheres

Following the formation of neurospheres, cell aggregates were plated onto either 48-well tissue culture plates or 12-well format Alvetex® Scaffold. 48-well plates were coated with 150 µL per well of 0.002 % poly-L-lysine solution for 2 hours at 37 °C and washed twice in PBS before being coated in 150 µL Glu Coat solution overnight at 37 °C. Scaffolds were prepared as per section *2.2.9.3 3D Culture*.

Coating solution was removed from 48-well tissue culture plates and 12-well format Alvetex® Scaffolds, wells were then topped up with 500 µL Glu Maturation Medium and scaffolds were placed in 12-well culture plates with 4 mL Glu Maturation Medium. Neurospheres were seeded using a 200 µL pipette tip to transfer 20 µL containing 2-3 neurospheres into each 2D well, and 40 µL containing 5-10 neurospheres onto each scaffold. Neurospheres were then cultured for 10 days in Glu Maturation Medium during which time neurites begin to protrude from the neurospheres. The medium was not changed throughout the neurite outgrowth period to avoid disruption of the developing neurites. Following 10 days culture, the neurospheres were fixed in 4 % PFA for analysis.

2.2.10 Culture of ReproNeuro Cells

ReproNeuro cells (ReproCELL) differ from ReproNeuro Glu cells in that they are a mixed population of iPSC derived neuroprogenitor cells. Somatic cells obtained from a healthy individual are reprogrammed to form iPSCs and in turn differentiated to generate neuroprogenitor cells. The cells are revived from frozen as neuroprogenitors and cannot be passaged or propagated, so must be used directly in an experiment upon revival.

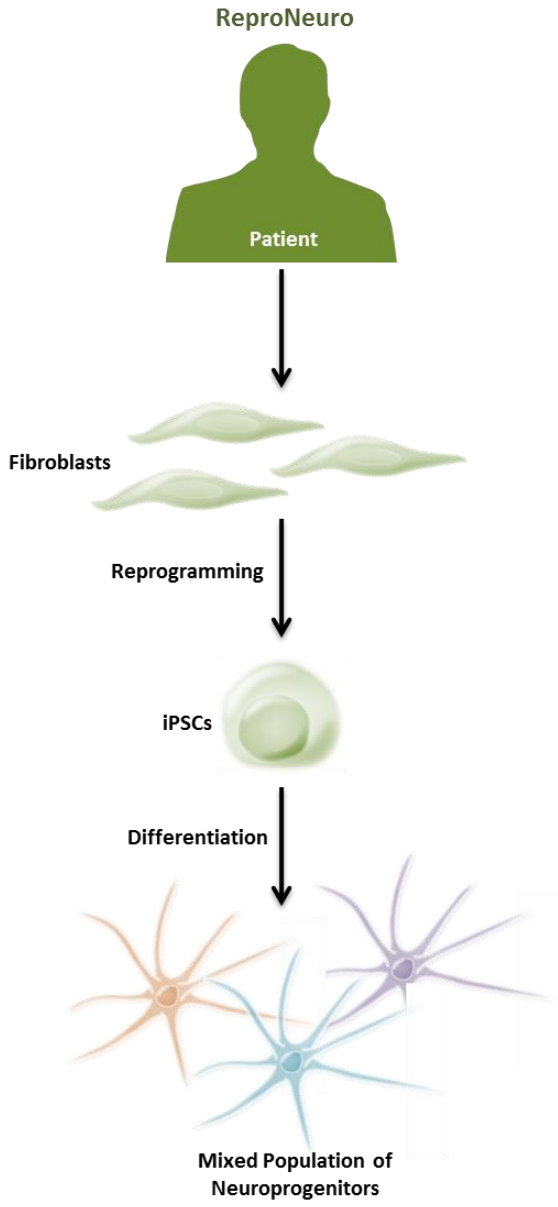

Fig 2-11: Schematic depicting the derivation of ReproNeuro cells.
Somatic cells obtained from a healthy individual were reprogrammed to form iPSCs. The iPSCs were differentiated to form a pool of mixed precursor cells (ReproNeuro) that upon revival and culture in Maturation Medium, ultimately form a mixed population of mature neurons.

2.2.10.1 Revival of ReproNeuro Cells from Cryopreservation

Cells were stored and revived as per section *2.2.9.1 Revival of ReproNeuro Glu Cells from Cryopreservation,* however the composition of Maturation Medium (ReproCELL) differed. Maturation Medium was prepared by adding 520 µL of Additive A (ReproCELL) and 100 active units of penicillin/streptomycin to each 40 mL bottle of Maturation Medium.

2.2.10.2 2D Monolayer Culture of ReproNeuro Cells

For 2D monolayer cultures, cells were seeded onto 16 mm diameter glass coverslips in a 12-well tissue culture plate. Coverslips were coated with 0.002 % poly-L-lysine (diluted 0.01 % poly-L-lysine solution (Sigma-Aldrich) in PBS) for 2 hours at 37 °C. Poly-L-lysine solution was then removed and the coverslips were washed twice in PBS prior to coating with 200 µL ReproCoat (ReproCELL) solution (150 µL of ReproCoat diluted in 5 mL PBS), overnight at 37 °C.

Prior to cell seeding, coating solution was removed and 280 µL of cell suspension following revival from cryopreservation was added to each well, achieving a final seeding density of 2.8×10^5 cells per well. Wells were topped up with Maturation Medium to give a final volume of 1.4 mL and cells were incubated at 37 °C and 5 % CO_2 in a humidified atmosphere for 14 days. This promotes the development of mature neurons and cells received a 50 % media change on the 3rd and 7th day of culture. Following the 14 day culture period, cells were washed in PBS and fixed in 4 % PFA for immunofluorescent analysis.

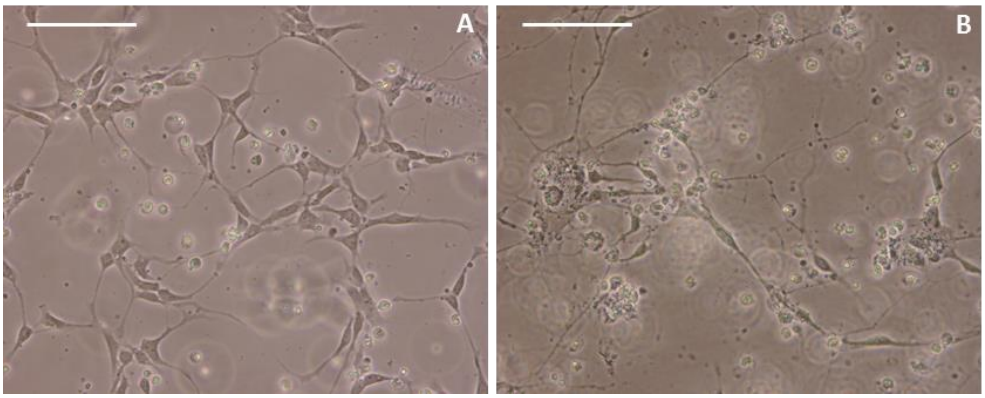

Fig 2-12: ReproNeuro cells mature over a 14-day culture period.
Phase contrast micrographs showing ReproNeuro Glu cultured in 2D 24 hours following seeding (A) and following 14 days in culture (B), cells have adopted a more neural morphology. Scale bars: 100 µm

2.2.10.3 Neurosphere Formation from ReproNeuro Cells

Neurospheres were formed using AggreWell plates using the same methodology described for ReproNeuro Glu cells. The protocol is described in section *2.2.9.4.4 Neurosphere Formation from ReproNeuro Glu Cells*.

2.2.10.4 Neurite Outgrowth Assay from ReproNeuro derived Neurospheres

Following the formation of neurospheres, cell aggregates were seeded onto either 48-well tissue culture plates or 12-well format Alvetex® Scaffold. Alvetex® Scaffolds were prepared by plasma treatment using the K1050X Plasma Asher at a power level of 40 W, for 5 mins. Treated scaffolds and 48-well plates were coated with 0.002 % poly-L-lysine solution for 2 hours at 37 °C and washed twice in PBS before being coated in ReproCoat solution overnight at 37 °C.

Coating solution was removed from 2D and 3D growth substrates. 2D wells were then topped up with 500 µL Maturation Medium and scaffolds were placed in 12-well culture plates with 4 mL Maturation Medium. Neurospheres were seeded using a 200 µL pipette tip to transfer 20 µL containing 2-3 neurospheres into each 2D well, and 40 µL containing 5-10 neurospheres onto each scaffold. 2D cultures were maintained for 24 hours post-seeding, whilst 3D cultures were maintained for 10 days prior to fixation in 4 % PFA for analysis.

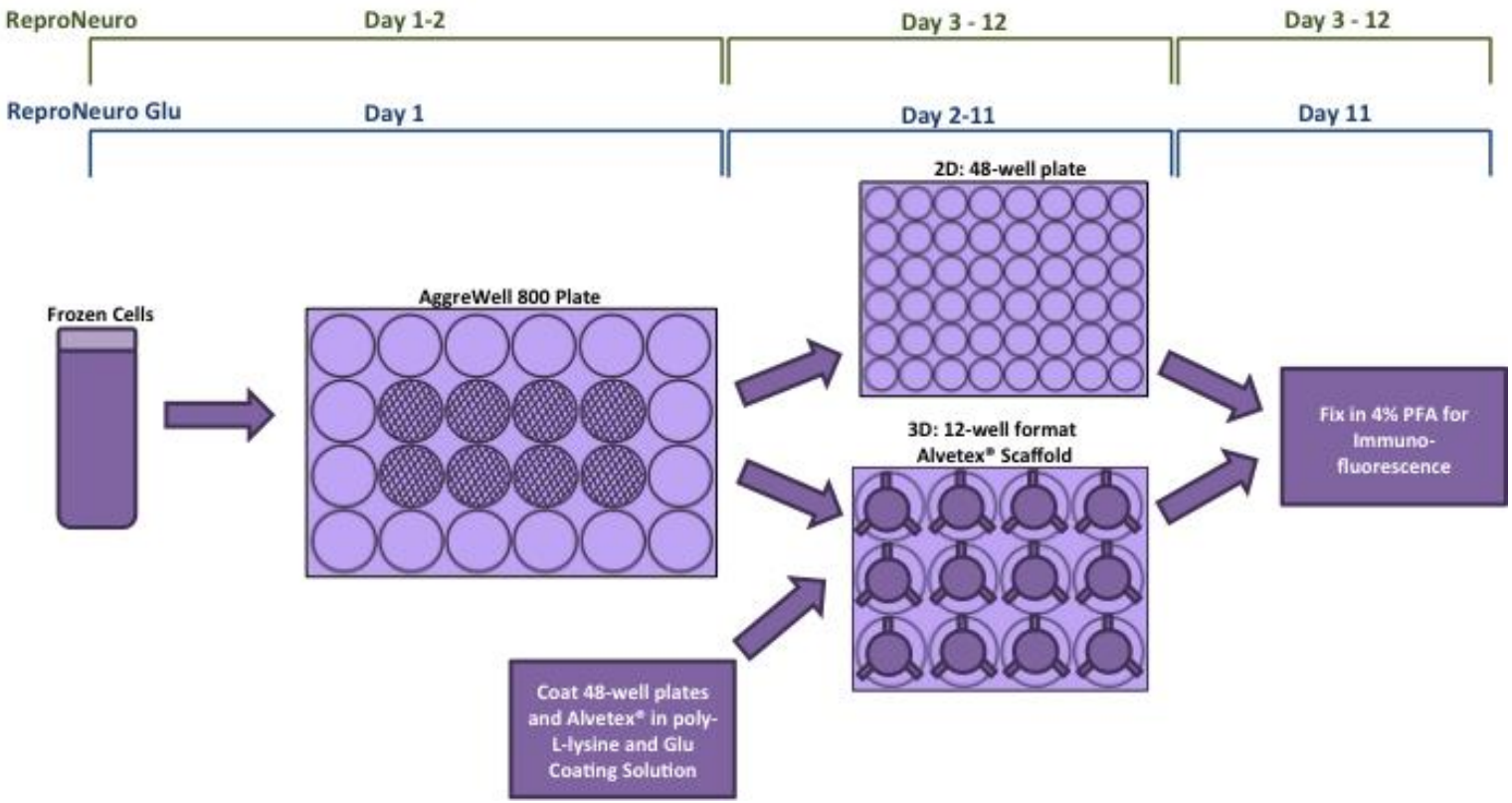

Fig 2-13: Schematic summarising neurosphere formation and neurite outgrowth from ReproNeuro cell lines.
ReproNeuro and ReproNeuro Glu cells are revived from frozen directly into an AggreWell™ 800 plate. The plate is then centrifuged to capture the cells in the microwells and incubated for 24-48 hours to form spheroid structures. Neurospheres are then harvested and seeded on coated coated 2D (48-well tissue culture plate) and 3D (12-well format Alvetex® Scaffold) surfaces. 2D cultures are then maintained for a further 24 hours (ReprNeuro) or 10 days (ReproNeuro Glu), whereas 3D cultures are maintained for a 10 day period to promote neurite outgrowth. Following the neurite outgrowth phase of culture samples are then fixed with 4 % PFA and immunofluorescence analysis.

2.3 Flow Cytometry

Flow cytometry was used to determine the expression of cell surface antigens using fluorescent antibodies. Cells tagged with fluorescent antibodies were quantified using a flow cytometer to determine average percentage expression of an antigen in a population of cells. This technique was used to analyse the expression of stem cell and differentiation markers in populations of pluripotent stem cells exposed to various differentiation conditions.

2.3.1 Sample Preparation

Pluripotent stem cells were differentiated as described in section *2.2.4 Induction of Differentiation of Human Pluripotent Stem Cells in 2D Monolayer Cultures* and a single cell suspension obtained via trypsinisation as previously described. Cells were then washed in PBS and re-suspended in 1 mL blocking buffer (0.1 % bovine serum albumin (BSA, Sigma-Aldrich) in PBS). Cells were then centrifuged at 800 rpm for 3 minutes, counted using a haemocytometer and seeded in a 96-well round-bottomed, untreated flow cytometry plate at a density of 150,000 cells per well. The plate was then centrifuged at 800 rpm at 4 °C for 3 minutes to pellet cells.

2.3.2 Immunostaining of Cell Suspension

Following centrifugation, cells were then re-suspended in 50 µL of the appropriate primary antibody diluted in blocking buffer and incubated for 1 hour on ice. Primary antibodies and their dilutions are shown in Table 2-3.

Antibody	Dilution	Supplier
SSEA-3	1:5	DSHB
A2B5	1:20	Abcam
P3X	1:10	P. Andrews (University of Sheffield)

Table 2-3: Primary antibodies used to stain extracellular markers for flow cytometric analysis.

Following incubation with the primary antibody, cells were washed three times in 100 µL blocking buffer and centrifuged at 800 rpm at 4 °C for 3 minutes. The cells were then incubated for 1 hour in the dark with an anti-mouse IgM secondary antibody (Sigma-Aldrich) diluted 1:50 in blocking buffer. Cells were then washed three times in blocking buffer and re-suspended in 200 µL blocking buffer for flow cytometric analysis.

2.3.3 Flow Cytometric Analysis

The Millipore GuavaCyte Plus Flow Cytometer (Millipore, Consett, UK) was calibrated using the Guava Check Kit (Millipore). This involved passing quality control beads of known size, fluorescence and shape, through the machine to determine a percentage coefficient of variance (CV). A percentage CV of less than 5 % should be obtained before sample analysis.

Cell clumps and debris were eliminated from analysis using forward and side-scatter gates to ensure fluorescence detected was from single cells. Settings were adjusted to the negative control (P3X) which is an antigen expressed only on mouse cells and should not react with the human cells, as shown in Figure 2-15.

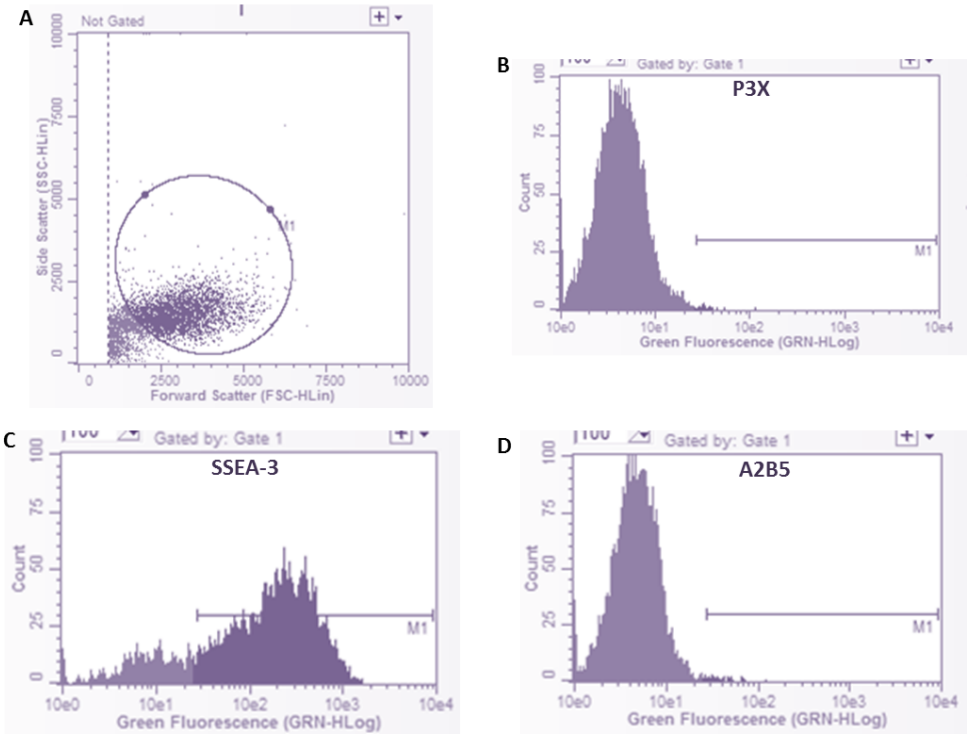

Fig 2-14: Settings used to analyse expression of extracellular markers of human pluripotent stem cells using flow cytometry.
Side scatter and forward scatter plots (A) were used to gate for intact cells, and eliminate signal caused by cellular debris. The circle (M1) represents the cells that have been selected for analysis. P3X is an antigen expressed by mouse cells and acts as a negative control when analysing samples of human cells (B). Settings were adjusted to P3X fluorescence using a histogram marker (M1) to select the population of cells that did not fluoresce when stained for this marker, as any fluorescence is likely to be background, non-specific signal. These settings were then applied to all other samples. The stem cell marker SSEA-3 (C) is highly expressed in undifferentiated human pluripotent stem cells, and the positive population of cells is highlighted by the histrogram marker. The early neuronal differentiation marker, A2B5 (D) is expressed at extremely low levels in undifferentiated cells, with its histogram closely resembelling that of the negative control, P3X.

2.4 Histology and Immunofluorescence Staining

2.4.1 Fixation of 2D Cultures

To fix 2D cultures, media was aspirated and cultures were washed in PBS before being incubated in 4 % PFA at room temperature. 2D neurite outgrowth cultures were incubated in PFA for 1 hour to allow penetration of the fixative into the mass of cells, while 2D monolayer cultures were incubated in PFA for 30 minutes. Following fixation cells were washed 3 times in PBS and stored in PBS prior to processing.

2.4.2 Fixation of 3D Alvetex® Scaffolds

Avetex® Scaffolds were unclipped from their plastic settings and washed in PBS prior to fixation in 4 % PFA overnight at 4 °C. Scaffolds were then washed three times in PBS prior to either wax embedding or whole mount immunofluorescence analysis.

2.4.3 Paraffin Wax Embedding and Sectioning of 3D Alvetex® Scaffolds

Fixed scaffolds were dehydrated through a series of ethanol baths: 30, 50 70, 80, 90, 95 and 100 % ethanol for 15 minutes each. In the case of 3D neurite outgrowth cultures the 70 % ethanol step was substituted with 0.1 % crystal violet (Sigma-Aldrich) dissolved in 70 % ethanol to stain aggregates and aid visualisation during the sectioning process.

Following dehydration, samples were transferred to histoclear (National Diagnostics, East Riding, UK) for 15 minutes. Samples were then incubated at 60 °C in a 1:1 mixture of melted paraffin wax (ThermoFisher) and histoclear, for 30 minutes followed by an incubation at 60 °C for an hour with melted paraffin wax only. Scaffolds were then cut in half and embedded in paraffin wax using plastic moulds (CellPath, Newton, UK) and embedding cassettes (ThermoFisher) to allow for transverse sectioning. Wax blocks were allowed to solidify overnight.

Alvetex® Scaffolds embedded in paraffin wax were sectioned at 6 µm using a Leica Microtome RM2125RT and mounted onto charged superfrost microscope slides (ThermoFisher). 3D neurite outgrowth cultures were stained with crystal violet to allow visualisation and to ensure aggregate sample is within wax section.

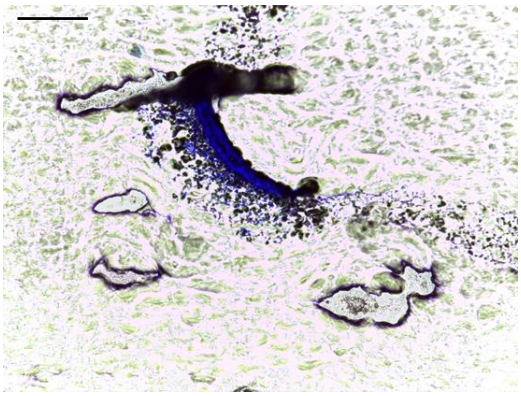

Fig 2-15: Crystal violet visualisation of cell aggregates cultured in 3D, embedded in paraffin wax.
Cell aggregates cultured on Alvetex® Scaffold were embedded in paraffin wax for sectioning. To visualise cell aggregates during the sectioning process, they were stained with crystal violet solution. Each section was mounted onto a microscope slide and examined for the presence of a cellular aggregate prior to processing. Scale bar: 200 μm.

2.4.4 Haematoxylin and Eosin (H&E) Staining

Paraffin wax sections containing Alvetex® Scaffold were deparaffinised in histoclear before being rehydrated through a series of ethanols: 100 % ethanol for 2 minutes and 95 % followed by 70 % ethanol for 1 minute each. Samples were then washed in deionised water for 1 minute followed by staining in Mayer's Haematoxylin (Sigma-Aldrich) for 5 minutes. Slides were then washed in deionised water for 30 seconds, followed by alkaline ethanol for 30 seconds to blue the nuclei. Samples were then dehydrated through 70 % and 95 % ethanol for 30 seconds each and stained in eosin solution (Sigma-Aldrich) for 1 minute. Slides were then dehydrated in 95 % ethanol twice for 10 seconds each, 100 % ethanol for 15 seconds then 30 seconds and cleared twice in histoclear for 3 minutes each. Slides were then mounted in DPX (ThermoFisher) ready for microscopy using a Leica ICC50 high definition camera mounted on a Leica microscope.

2.4.5 Immunofluorescent Analysis of 3D Cultures

2.4.5.1 Scaffold Whole Mounts

Fixed, whole Alvetex® Scaffolds were permeablised in 0.1 % Triton X-100 (Sigma-Aldrich) for 20 minutes at room temperature. Scaffolds were then blocked for 30 minutes in a blocking solution consisting of: 1 % normal goat serum (NGS, Sigma-Aldrich) and 0.01 % Tween (Sigma-Aldrich) in PBS. Scaffolds were then placed on a microscope slide and a hydrophobic barrier pen (Vector Laboratories, Peterbrough, UK) was used to draw a circle around the scaffold membrane to contain the antibody solution. Scaffolds were

incubated on microscope slides with the relevant primary antibody solution diluted in blocking buffer for 2 hours at room temperature and then washed three times for 10 minutes in blocking buffer. Scaffolds were once again placed on microscope slides and incubated with the relevant secondary antibody diluted in blocking buffer with the addition of the nuclear dye Hoechst 33342 (ThermoFisher) for 1 hour at room temperature. Scaffolds were then washed 3 times for 10 minutes in blocking buffer prior to mounting on microscope slides with Vectashield anti-fade mounting medium (Vector Laboratories).

2.4.5.2 Scaffold Cross-Sections

Paraffin wax sections were deparaffinised in histoclear for 15 minutes and rehydrated in 100 % ethanol, 70 % ethanol and PBS for 5 minutes each. To retrieve antigens, samples were then incubated in a 95 °C water bath for 20 minutes with citrate buffer. The slides were allowed to cool and then blocked in a solution of 20 % NGS and 0.4 % Triton X-100 in PBS for an hour at room temperature. Slides were then incubated with the primary antibody diluted in blocking buffer overnight at 4 °C. Samples were then washed 3 times in PBS for 10 minutes each and incubated with the secondary antibody, diluted in blocking buffer with the nuclear dye Hoechst at room temperature for an hour. Slides were washed 3 times in PBS for 10 minutes each prior to mounting with Vectashield anti-fade mounting medium.

2.4.6 Immunofluorescence Staining of 2D Cultures

Fixed samples of cells cultured in 2D were permeabilised with 0.1 % Triton-X100 in PBS for 10 minutes followed by blocking on ice for 1 hour in 1 % NGS, 0.01 % Tween in PBS. Primary antibody was then added to samples and incubated for 1 hour whilst gently rocking. Samples were then washed three times in blocking buffer for 10 minutes each followed by incubation with the fluorescent secondary antibody and nuclear dye Hoechst 33342 for 1 hour, which was specific for the primary antibody used. Cells were then washed for a further 3 times for 10 minutes each in blocking buffer prior to microscopy. Antibodies were diluted in blocking buffer and are listed in section *2.4.7 Summary of Antibodies used in Immunofluorescence*.

2.4.7 Summary of Antibodies used in Immunofluorescence

Target	Dilution	Host Species	Supplier	Product Code
β-III-tubulin	1:600	Rabbit	Cambridge Bioscience	3525-100
Nestin	1:100	Mouse	Abcam	ab22035
Neurofilament-L	1:100	Mouse	Life Technologies	130400
Neurofilament-M	1:100	Mouse	Sigma-Aldrich	N2787
Neurofilament-H	1:500	Rabbit	Abcam	ab8135
GFAP	1:100	Mouse	Sigma-Aldrich	G3893
Chondroitin Sulphate	1:100	Mouse	Abcam	ab11570

Table 2-4: Primary antibodies used in immunofluorescence.
Primary antibodies used for immunofluorescence, with their working dilution and the host species. All antibodies were diluted in blocking buffer.

Antibody	Dilution	Emission (max) Wavelength /nm	Supplier	Product Code
Alexafluor anti-rabbit 488	1:600	525	ThermoFisher	A-11034
Alexafluor anti-mouse 488	1:600	525	ThermoFisher	A-11001
Alexafluor anti-mouse 594	1:600	617	ThermoFisher	A-21203
Hoechst 33342	1:1000	461	ThermoFisher	H3570

Table 2-5: Secondary antibodies and dyes used in immunofluorescence.
Secondary fluorescent conjugated antibodies and their respective emission wavelengths and the fluorescent nuclear dye hoechst 33342. All antibodies were diluted in blocking buffer.

2.5 Western Blotting

2.5.1 Generation of Cellular Lysates

2.5.1.1 Formation of Lysates from 2D Cultures

Cellular lysates were generated using a lysis buffer that consisted of Mammalian Protein Extraction Reagent (MPER™, ThermoFisher) with 1 % protease inhibitor cocktail (Sigma-Aldrich). Flasks of cells cultured in 2D were washed in ice-cold PBS and incubated with lysis buffer on ice, on a rocking platform for 15 minutes. Following incubation, cells were then detached using a cell scraper (ThermoFisher) and collected in a microcentrifuge tube (StarLab, Milton Keynes, UK) for centrifugation at 4 °C, 12,000 g for 15 minutes. The supernatant was then collected and stored at - 80 °C until use.

2.5.1.2 Formation of Lysates from 3D Alvetex® Scaffold Cultures

Alvetex® Scaffolds were unclipped from their plastic casing and washed in ice-cold PBS prior to incubation with lysis buffer (composition described in *2.5.1.1 Formation of Lysates from 2D Cultures*). Scaffolds were incubated on ice for 30 minutes in lysis buffer and vortexed for 10 seconds, every 5 minutes during this time. Samples were then centrifuged at 4 °C, 12,000 g for 15 minutes and the supernatant was collected and stored at - 80°C until use.

2.5.2 Bradford Protein Assay

A Bradford Assay was used to determine the concentration of protein present in each cellular lysate, to ensure that equal protein levels of each sample were compared. To a 96-well flat-bottomed plate, 250 µL of Quick Start™ Bradford 1 x Dye Reagent (Bio-Rad, Hertfordshire, UK) and 5 µL of each BSA Protein Standard (Bio-Rad) were added. Protein standards range in concentration from 0.125 to 2.0 $mgmL^{-1}$ to produce a standard curve that unknown samples can then be compared to. Lysates were thawed on ice and 5 µL of each sample was added to a well containing 250 µL of Bradford reagent and samples/standards were incubated with the reagent for 5 minutes before absorbance was determined at 590 nm using a BioTek, ELx800 microplate reader.

Quantification of lysate protein content was obtained through plotting a linear regression through the standard curve data using GraphPad Prism software. The equation of the straight line could then be obtained and rearranged to find the x value (protein concentration) by substituting the y value (absorbance) for each sample. An example is shown below:

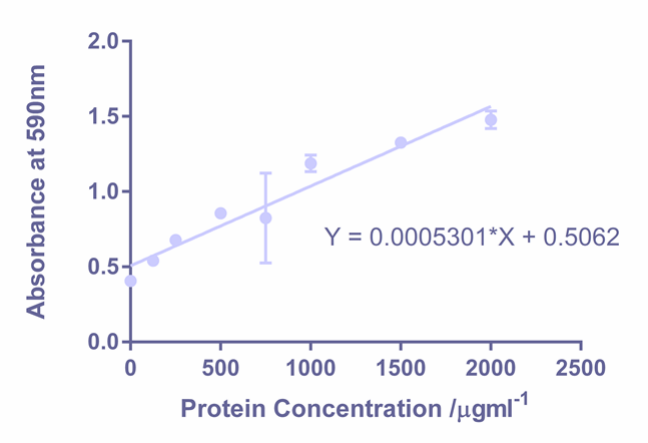

Fig 2-16: Typical standard curve for protein quantification by Bradford Assay.
A typical standard curve plotted from absorbance at 590 nm for a series of protein standards. A linear regression was plotted through the data set and an R^2 value obtained (0.8731 for this data set) which demonstrates the relationship between the two variables, the closer to 1, the more the variables correlate. Plotting a linear regression determines the equation of the line, which can then be rearranged and the absorbance of protein lysates of unknown concentration can be substituted into the equation to determine their concentration.

Equation of Linear Regression: $y = 0.0005301x + 0.5062$

Rearranged to make x the subject: $x = \frac{y - 0.5062}{0.0005301}$

Sample of unknown protein concentration with an average absorbance of 1.429 at 590 nm

$y = 1.429$; $x = \frac{1.429 - 0.5062}{0.0005301}$

$x = 1740\ \mu gmL^{-1}$

2.5.3 SDS Polyacrylamide Gel Electrophoresis

Protein lysates were prepared for electrophoresis by incubation with 4 x Laemmli sample buffer (Bio-Rad) and 10 % 2-mercaptoethanol (Sigma-Aldrich) at 95 °C for 5 minutes. Samples were then loaded into an any-kD pre-cast polyacrylamide gel (Bio-Rad) and run at 120 V for 1-2 hours in 1 x TGS buffer (Biorad).

2.5.4 Protein Transfer

Electrophoresed samples were then transferred onto a nitrocellulose membrane (GE Healthcare, Buckinghamsire, UK) by constructing the following onto the black side of a transfer cassette: sponge, blotting paper, gel, nitrocellulose membrane, blotting paper, sponge. The transfer sandwich was then rolled using a roller to remove any bubbles and placed into the transfer tank with an ice block in transfer buffer (3.03 g tris, 14.41 g glycine, 200 mL methanol in 1 L H_20). The transfer was for overnight at 4 °C at 15 V followed by 2 hours the following day at 30 V.

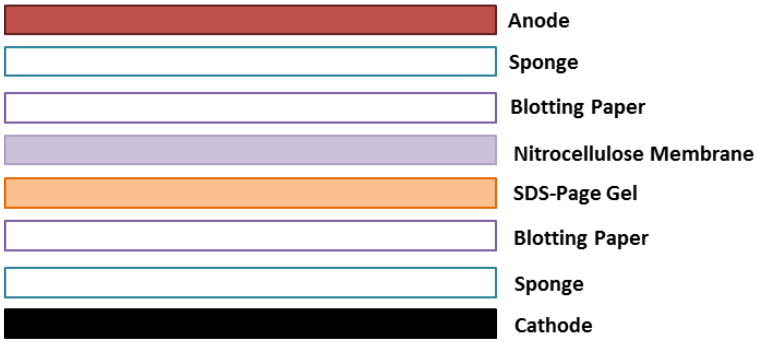

Fig 2-17: Schematic representing the transfer sandwich used in western blotting. The transfer sandwich is assembled in transfer buffer and involves the stacking of sponges and blotting paper with the SDS-Page gel containing the electrophoresed samples and a nitrocellulose membrane sandwiched between the layers.

2.5.5 Immunostaining and Exposure of Membrane

Following protein transfer, membranes were blocked at room temperature for an hour in 5 % milk powder dissolved in 0.1 % Tween in PBS. Primary antibodies were then diluted in 5 % milk solution and incubated with the membrane overnight at 4 °C. Membranes were washed 3 times for 5 minutes in 0.1 % Tween and incubated with the secondary antibody diluted in 5 % milk solution for an hour at room temperature. This was followed by 3 washes for 5 minutes in 0.3 % Tween solution and 3 washes for 5 minutes in 0.1 % Tween solution. The Clarity™ ECL detection kit (Biorad) was used for detection as per the manufacturer's instruction, the two solutions were mixed in a 1:1 ratio and incubated for 5 minutes with the membrane followed by exposure with photographic film (ThermoFisher).

2.5.6 Summary of Antibodies

Target	Dilution	Host Species	Supplier	Product Code
Versican	1:2,500	Rabbit	Abcam	ab177480
GFAP	1:4,000	Mouse	Sigma	G3893
β-actin	1:10,000	Mouse	Abcam	ab8224
Anti-rabbit-HRP	1:4,000	Goat	Santa Cruz Biotechnology	SC-2030
Anti-mouse-HRP	1:4,000	Goat	Sigma-Aldrich	A4416

Table 2-6: Antibodies used in western blotting.
Primary and secondary antibodies used in western blotting. Secondary antibodies are HRP conjugated and all antibodies were diluted in 5 % milk solution.

2.6 Microscopy

2.6.1 Phase Contrast Imaging of Live Cultures

Phase contrast images of live cell cultures were obtained using the Leica DFC 310FX with digital camera DMI 3000B with objectives: x5, x10, x20.

2.6.2 Brightfield Imaging

Histology samples were imaged using a Leica ICC50 High Definition camera mounted onto a Leica microscope and objectives: x5, x10, x20 and x40. Images were captured using Leica EZ software.

2.6.3 Fluorescence Imaging

2.6.3.1 Conventional Fluorescence Imaging

Fluorescent images used for quantification of neurite outgrowth were obtained using the Leica DFC 310FX with digital camera DMI 3000B and objectives: x5, 10 and x20. Filters: DAPI, 488 nm. Images were captured using Leica V4 software.

2.6.3.2 Confocal Imaging

Leica SP5 confocal laser scanning microscope was used to obtain high-resolution representative images with objectives: x10 HCX PL APO CS, x20 HCX PL APO oil UV, x40

HCX PL APO Oil UV and x63 HCX PL APO Oil UV. Images were captured using Leica AF software.

The Zeiss 880 confocal laser scanning microscope with airy scan was also used to obtain high-resolution images with objectives: x10 EC Plan Neo DC I, x20 Plan Apochromat DIC II, x40 EC Plan Neo DIC II and x63 Plan Aprochromat DIC II. The tile scan feature was used to obtain high-resolution images of whole neurospheres and their surrounding neurite outgrowth by capturing a 3x3 tiled area from the centre of the cell aggregate. Images were captured using Zeiss Zen software.

Please note that, dark areas in the centre of neurospheres are an artifact of using confocal microscopy to obtain high quality images, as the light has difficulty penetrating the large mass of the neurosphere. When images are captured using conventional fluorescence microscopy this phenomenon is not observed.

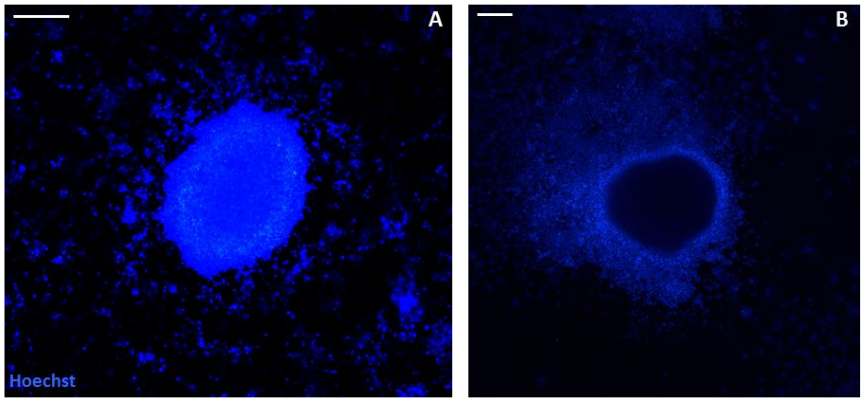

Fig 2-18: Hoechst staining of cell aggregates imaged using conventional and confocal microscopy.
Hoechst staining highlights the nuclei of the cells that reside within the cellular aggregate; therefore staining is mainly confined to aggregate body, with a small number of nuclei that have migrated from the cell aggregate. When imaged using conventional fluorescence microscopy (A) the hoechst staining appears solid. However, when imaged using confocal microscopy (B), there appears to be a dark region in the centre of the aggregate. This is an artifact of confocal microscopy, due to the inability of the light to penetrate the aggregate mass and is enhanced by the scattering of out of focus light from the confocal microscope. Scale bars: A = 500 µm, B = 200 µm

2.7 Statistical Analysis

GraphPad Prism v7 was used to assess statistical significance of results and the relevant statistical test was used depending on the data set including: Student's T-test, One-way ANOVA and Two-way ANOVA and unless otherwise stated a Gaussian distribution is assumed. Significance is depicted graphically for each data set with * = $p \leq 0.05$, ** = $p \leq 0.01$, *** = $p \leq 0.001$, **** = $p \leq 0.0001$.

Chapter III: Development of Robust and Reproducible Human Pluripotent Stem Cell Derived Models of Neurite Outgrowth

3.1 Introduction

Neuritogenesis is an important developmental process, essential to the formation of complex neuronal networks and connections[10]. Inhibition of neurite outgrowth is common to many disorders of the central nervous system (CNS)[40–44] ranging from trauma in the form of spinal cord injury[33,39] to neurodegenerative diseases including Alzheimer's disease[35,36] and Parkinson's disease[37]. For this reason, the development of *in vitro* models that recapitulate the process of neuritogenesis has been a highly active area of research. However, there is still need for a physiologically relevant, robust and reproducible model of neurite outgrowth that can be applied to study the molecular processes that underpin neurite inhibition in the context of a variety of disorders of the nervous system. In addition to this, robust *in vitro* neurite outgrowth models, also offer the ability to routinely screen compounds, to test their neurotoxic or regeneration promoting properties. For this reason, the development of a robust, reproducible, and physiologically relevant model of neuritogenesis is essential, to provide a tool for routine use in the screening of such compounds.

3.1.1 Embryonal Carcinoma (EC) Cells as a Model of Neuritogenesis

Embryonal carcinoma (EC) cells are pluripotent stem cells that form the basis of many neural differentiation studies and are well characterised[69]. Stefan Przyborski first isolated the TERA2 sub-line, TERA2.cl.SP12 in 2001, which has since formed the basis of many neurological studies[146]. The TERA2.cl.SP12 subline was identified as expressing high levels of pluripotency markers such as SSEA-3/4 and TRA-1-60 in the undifferentiated state and high levels of differentiation markers such as A2B5 and VIN-IS-56 upon retinoic acid induction[146]. Therefore, due to their high expression of early neuronal markers such as A2B5 upon retinoic acid exposure, TERA2.cl.SP12 cells are thought to undergo neuronal differentiation more readily than other clonal lines such as NTERA2.cl.D1 or the heterogeneous parental line itself, TERA2[146].

Due to their pluripotent nature EC cell-based models offer insight into the developmental processes involved in human embryonic development[69]. As cells derived from the TERA2 lineage readily undergo robust neuronal differentiation, they have been used to study the molecular processes involved in neuronal differentiation and development. Przyborski *et*

al describe a transcriptional profiling analysis that compared TERA2-derived, retinoic acid induced neurons with *in vivo* and *in vitro* developing neural cells[71]. It was found that neurons differentiated from TERA2 cultures express similar genes and proteins to developing neurons *in vivo*. Various individual neuron-specific genes, including: *nestin*, *Pax6* and *NKx6.1* along growth-related proteins known to be involved in vertebrate neurogenesis (SCG10, GAP43) were expressed in differentiated TERA2 cultures and aligned closely with gene expression of developing neural cells both *in vitro* and *in vivo*[71]. Therefore, it was demonstrated that neurogenesis upon retinoic acid induction of human pluripotent stem cells is conserved and the resultant neurons share similarities with their *in vivo* counterpart. Similarly, TERA2 derived neurons have also been characterised in terms of functionality and have been found to be electrophysiologically active[72]. Therefore EC cells can provide a source of functional, well-characterised neurons for use in *in vitro* neuronal models such as those used to study neurite outgrowth.

One of the main limitations of standard models of neurite outgrowth lies within the quantification methodology, as most models rely on the tracing of individual neurites using image analysis software[63,200]. When neurons are cultured as traditional monolayers, they form a network of overlapping, branching neurites that prove difficult to trace and subsequently quantify[63]. Stewart *et al* describe two distinct methodologies for the induction of neuronal differentiation by retinoic acid in TERA2.cl.SP12 cells, first as monolayer cultures and secondly as spheroids cultured in suspension[148]. Both methodologies induced successful neuronal differentiation, measured by downregulation of stem cell markers and upregulation of neuronal markers. However, when differentiated spheroids were cultured on ECM coated surfaces, neurites were found to radiate from the central spheroid structure[148]. This may provide a more easily quantifiable alternative, as each neurite radiates from a central point with no evidence of branching, therefore promoting easier, less time consuming and more accurate neurite tracing.

Therefore, EC cells can offer insights into the developmental processes that are involved in human embryonic development. They form the basis of many robust neuronal differentiation studies and the mature neurons that they generate have been characterised and found to express similar proteins as their *in vivo* counterpart[71], as well as displaying functional electrophysiological characteristics[72]. For this reason, EC cell-derived neurons have been extensively studied and characterised and are commonly used to generate *in vitro* neuronal cell-based models[21,66,69,70,72,84,145,146,148].

3.1.2 Enhancement of Neurite Outgrowth by 3D Culture Technology

When developing *in vitro* cell-based models, many aspects of the microenvironment should be considered in order to generate the most physiologically relevant model

possible[161,162]. Particularly, many studies now focus on the use of 3D cell culture technology to provide a more physiological geometry and growth cues for cultured cells[161,162,191]. One way in which this may be achieved is through the use of specifically designed 3D scaffolds, such as the commercially available Alvetex® scaffold. Alvetex® scaffold is a porous, polystyrene polyHIPE with an internal structure comprised of pores and interconnecting windows that promote the influx of culture medium into the scaffold[191]. The use of Alvetex® has been demonstrated in a wide variety of *in vitro* models ranging from the generation of skin equivalents[201] to the enhancement of hepatocyte function[202].

Polystyrene, 3D scaffolds such as Alvetex® have previously been demonstrated to enhance neuronal differentiation and neurite outgrowth as described by Hayman *et al*[147]. This study focused on the culture of retinoic acid treated TERA2.cl.SP12 cells either in 2D conditions or within the 3D scaffold and found that 3D cultures had developed a more extensive network of individual neuritic processes compared with their 2D counterpart[147]. A molecular analysis revealed that expression of markers associated with developing neurons were up-regulated in 3D cultures indicating an ongoing expansion of the neuronal network with continuing neurite development[147]. Similarly, the protein MAP2ab, associated with maturation of the neuronal cytoskeleton was enhanced by 3D culture, indicating maturation of the 3D neural network and the development of more extensive neurite networks compared with 2D cultured cells[147].

Therefore, 3D cell culture technology has applications in the development of more physiologically relevant culture models, to maintain a more *in vivo*-like geometry in which to culture cells. Furthermore, this technology has been demonstrated to further enhance current models of neurite outgrowth and to provide a favourable environment for the development of complex neuronal networks.

3.1.3 Enhancement of Neurite Outgrowth by Manipulation of Rho Signalling

The process of neuritogenesis *in vivo*, involves extensive remodelling of the actin cytoskeleton, and relies heavily upon the Rho signalling cascade[10,13], as described in Chapter I. As actin dynamics provide the driving force that induces neurite extension, manipulation of this process is a common strategy employed in the enhancement of current neurite outgrowth *in vitro* models. For example, Roloff *et al* describe inhibition of Rho and its downstream target, ROCK, to enhance their current N-TERA2 derived model of neuritogenesis[21]. This study found that inhibition of Rho by the analgesic, ibuprofen, enhanced neurite outgrowth significantly[21]. Similarly, fasudil and Y-27632, both inhibitors of Rho's downstream effector, ROCK, significantly enhanced neurite outgrowth in NTERA-2 derived neurons[21].

Inhibition of ROCK is a strategy to enhance neurite outgrowth that has also been applied to other model systems including those base on PC-12 cells. Both Y-27632 and H-1152 are inhibitors of ROCK that have been demonstrated to enhance neurite outgrowth from PC-12 cells in a time and dose-dependent manner[203]. However, this effect is not conserved within all neuronal subtypes, as Y-27632 alone has limited neurite-enhancing effect in retinal ganglion cells and only when in combination with ciliary neurotrophic factor is this enhancement observed[204].

Although inhibition of Rho and ROCK signalling can enhance *in vitro* neurite outgrowth in some models of neuritogenesis, its suitability in neurite inhibition studies should be considered. Inhibition of Rho and ROCK is commonly used to overcome neurite inhibition in a non-permissive environment such as the presence of inhibitory molecules associated with spinal cord injury[25–27,30,32]. Therefore, if for example, Y-27632 is already incorporated in the basic model, the addition of inhibitory stimuli may not result an inhibitory response, as the intrinsic presence of Y-27632 may recover and mask any such effect. Therefore, the suitability of incorporation of any Rho/ROCK pathway inhibitor should be assessed prior to incorporation into any model with particularly consideration of the particular application of such model.

3.1.4 Applications of a Physiologically Relevant Neurite Outgrowth Model

Neuritogenesis is an important developmental process, essential in the formation of neuronal circuitry and connections[205]. Impairment of neurite outgrowth is common to many pathologies of the nervous system, including spinal cord injury[33,39,206], Alzheimer's disease[35,36], Parkinson's disease[37], schizophrenia[41] and Down's syndrome[43]. For this reason there is need for a physiologically representative model of neuritogenesis that can be used to probe the underlying molecular mechanisms that underpin neurite inhibition and generation. Furthermore, *in vitro* models of neurite outgrowth can be used to screen the potential for agents to overcome neurite inhibition and aid in the discovery of new drugs to intervene and recover the process[124]. Also, as new drugs are developed, part of their safety assessment requires any neurotoxic effects to be identified and measured, therefore neurite outgrowth models may provide useful tools for this[63]. Therefore, there is great demand and need for an *in vitro*, cell-based model of neuritogenesis that better reflects the *in vivo* process of neurite development.

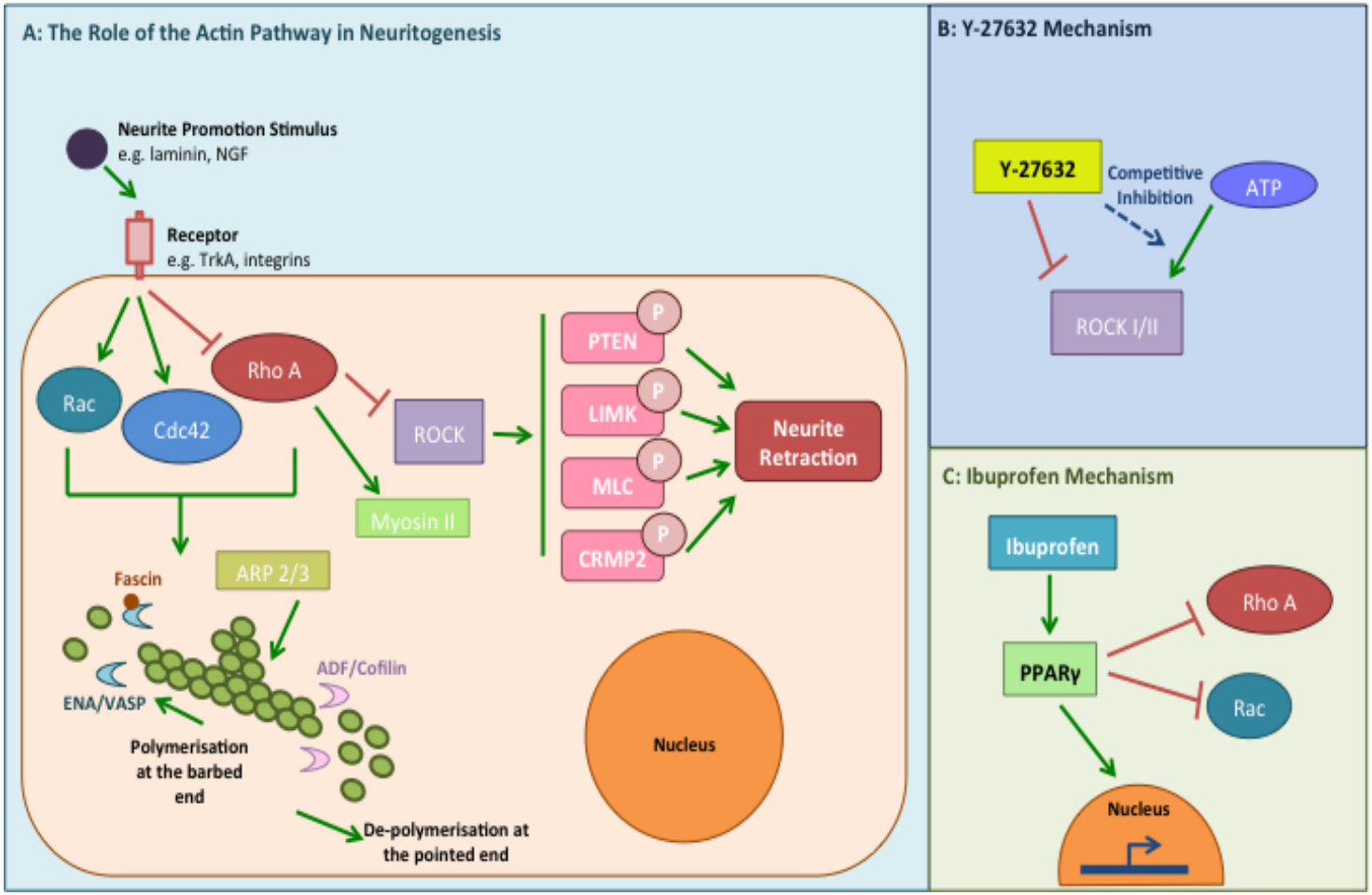

Fig 3-1: The mechanisms by which Y-27632 and ibuprofen promote neurite generation.
A schematic representation of how activation of Rac and Cdc42, along with inhibition of Rho A leads to neurite elongation (A). Activation of Rac and Cdc42 enhances *de novo* elongation through the promoting of polymerisation at the barbed end of the actin filament through anti-capping proteins ENA/VASP enhanced by fascin. Convergent elongation is also promoted, whereby Arp2/3 drives actin branching and the bundling of filaments. ADF/cofilin depolymerises actin at the pointed end, freeing G-actin monomers for polymerisation at the barbed end, whilst also driving propulsion of the growth cone. This depolymerisation also allows for actin re-organisation, which promotes microtubule penetration into the growth cone of the developing neurite. Inhibition of Rho A results in activation of Myson II which leads to myosin driven contractility and neurite elongation. Rho A and ROCK activation is inhibited when neurite outgrowth is active, however in the presence of an inhibitory stimulus, ROCK leads to the phosphorylation of a number of downstream targets, which has an inhibitory effect upon neurite outgrowth. A schematic representation depicts the mechanism by which Y-27632 inhibits ROCKI/II (B), through competitive inhibition of ATP binding. Ibuprofen however, induces activation of the transcription factor PPARγ, which inhibits Rho A and promotes the transcription of anti-inflammatory associated genes (C).

3.1.5 Conclusions

Due to the importance of neuritogenesis in neuronal development and its implications in neurological pathologies, there is a need for the development of a robust and reproducible model of neuritogenesis. In this chapter we describe the combination of 3D cell culture technology in the form of Alvetex® Scaffold with human pluripotent stem cells and synthetic retinoid analogues to produce a robust and reproducible model of human neuritogenesis that can be applied to study the process of neurite inhibition in the context of different nervous system disorders.

3.1.5.1 Chapter Aims

This chapter aims to investigate and optimise the role of synthetic retinoid analogues (EC23 and AH61) in differentiation and neurite development from the human embryonal carcinoma cell line, TERA2.cl.SP12. Synthetic retinoids have previously been reported to readily induce neural differentiation of TERA2.cl.SP12 cells[81–84,149] and this chapter aims to optimise this process with a specific focus on the induction of neuritogenesis from spheroid cultures in a similar manner as described by Stewart *et al*[148], along with a thorough characterisation of the resultant neurites. Furthermore, this chapter aims to adapt the spheroid neurite outgrowth culture system outlined by Steward *et al*[148], into a 3D culture environment using Alvetex® Scaffold, to produce a more physiologically relevant model to apply to the study of neurite inhibitory mechanisms. In addition to this EC cell-derived model of neuritogenesis, this chapter also aims to apply the principles of spheroid induction of neuritogenesis to an iPSC-derived neurite outgrowth model. Throughout this chapter the ability of inhibitors of Rho/ROCK signalling to enhance neurite outgrowth within these models will be assessed and their appropriateness for use in applications to study neurite inhibition will be discussed.

3.1.5.2 Chapter Objectives

- Evaluate the effect of natural and synthetic retinoid compounds on neural differentiation of TERA2.cl.SP12 cells.

- Optimise the concentration and retinoid compound most appropriate for use in TERA2.cl.SP12 derived spheroid model of neurite outgrowth.

- Develop and evaluate a novel quantification methodology to reduce time-consuming neurite tracing.

- Fully characterise the resultant neurites obtained from retinoid-induced differentiation of TERA2.cl.SP12 cells, to determine if the expression of cytoskeletal markers is conserved within the system.

- Adapt the 2D spheroid based model of neuritogenesis into a 3D culture system using Alvetex® Scaffold to produce a more physiologically relevant model of neurite outgrowth.

- Use iPSC technology to develop another novel model of neurite outgrowth in 2D and 3D culture systems.

- Examine the ability of Rho and ROCK inhibition to enhance neurite outgrowth in both EC and iPSC-derived neurite outgrowth models.

3.2 Materials & Methods

The methodologies used throughout this chapter are detailed in the main Materials & Methods section of this thesis (Chapter II). The main aim of this chapter was to develop robust and reproducible models of human neurite outgrowth, one of which was based on a human embryonal carcinoma cell line. This model was well developed and characterised throughout this chapter. In addition to this, a novel method of neurite quantification was also developed to further enhance the reliability of this model as an assay. A Standard Operating Procedure (SOP) for this methodology was established and can be found in Appendix I.

3.3 Results

3.3.1 Neural Differentiation of Human Pluripotent Stem Cells Induced by Synthetic Retinoid Compounds

To determine the ability of synthetic retinoids EC23 and AH61, along with the naturally occurring ATRA to induce neural differentiation of human pluripotent stem cells, TERA2.cl.SP12 EC cell monolayers were incubated with the compounds for 7 days. As can be seen in Figure 3-2 (A), phase contrast micrographs reveal typical stem cell morphology of undifferentiated TERA2.cl.SP12 cells and cells are packed tightly into colonies at high confluence. Monolayers differentiated with 0.01 μM ATRA (Figure 3-2B) however, appear to contain areas where cells appear larger and lose their typical stem cell morphology with monolayers appearing heterogenous. Similarly, monolayers treated with synthetic compounds (EC23 and AH61) appear to lose their characteristic stem cell-like morphology and adopt a more differentiated phenotype with monolayers appearing more homogenous than those differentiated with ATRA.

To compare the ability of each compound to induce neural differentiation of TERA2.cl.SP12 monolayers, cell surface marker expression by flow cytometry was measured. This analysis revealed changes in expression of the stem cell marker SSEA-3 (Figure 3-2E) and the early neuronal marker A2B5 (Figure 3-2F) with retinoid treatment. The pluripotency marker SSEA-3 is highly expressed in undifferentiated cells and declines with increasing concentration of each compound tested (0.001 – 10 μM). At all concentrations, treatment with the synthetic retinoids EC23 and AH61 results in significantly less expression of SSEA-3 than ATRA treatment, and AH61 also induced SSEA-3 loss to a significantly greater extent than EC23 at each concentration.

A2B5, an early neuronal antigen is found at extremely low levels in the undifferentiated TERA2.cl.SP12 population and expression is induced by retinoid treatment. Lower concentrations of synthetic retinoids (0.001 – 0.01 μM) induce expression of A2B5 to a significantly higher degree than ATRA, indicating greater neural induction. However, increasing retinoid concentration results in a smaller difference between the compounds and at 1 μM there is no significant difference in A2B5 expression amongst the compounds tested.

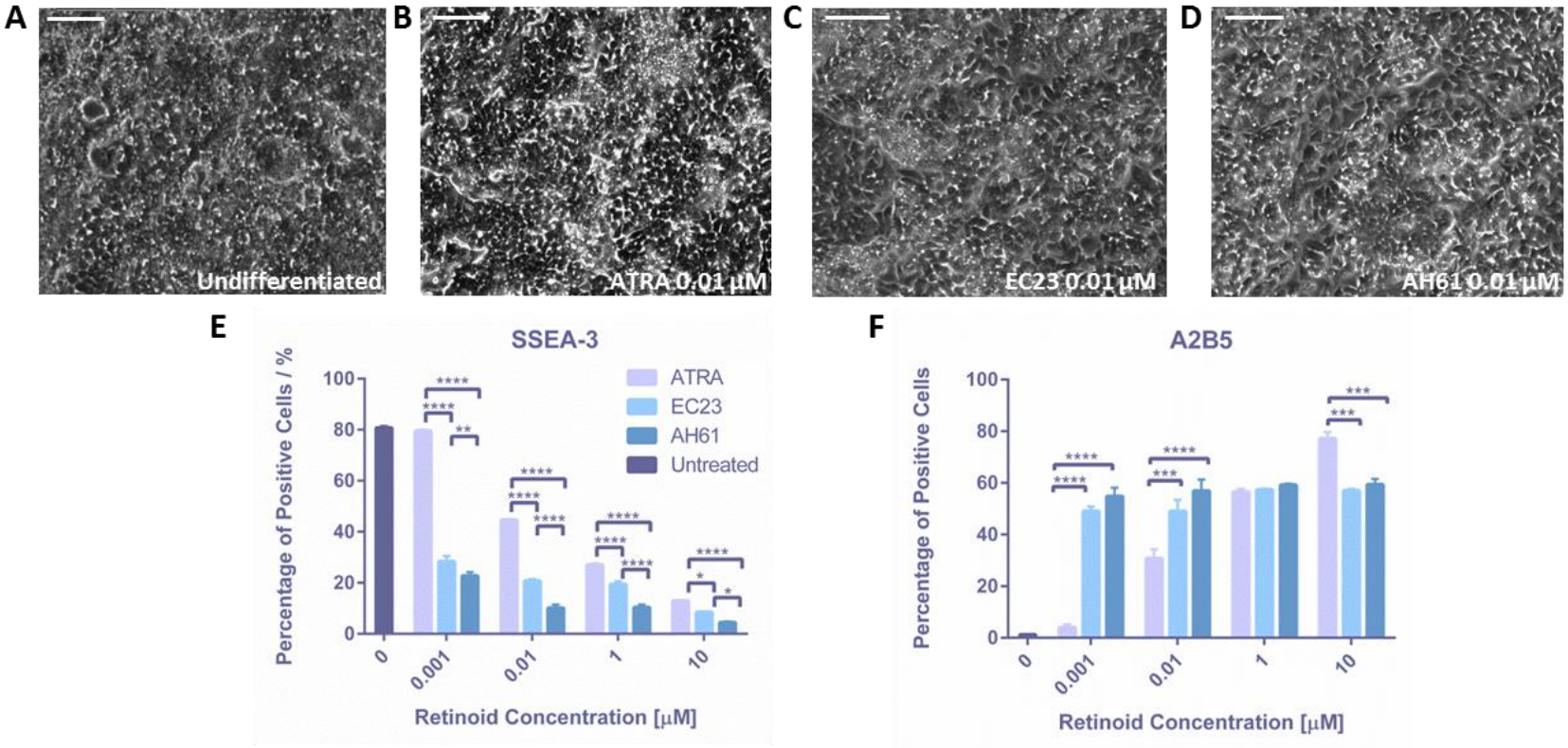

Fig 3-2: Induction of differentiation of human pluripotent stem cells with retinoid compounds.
Representative phase contrast images of TERA2.cl.SP12 cells cultured as 2D monolayers (A) and treated with ATRA (B), EC23 (C) and AH61 (D) for 7 days. Flow cytometry (E) analysis of cellular expression of the stem cell marker, SSEA-3 (E) and the early neuronal marker, A2B5 (F) from 2D monolayers treated with retinoid compounds for 7 days (data represent mean ± SEM, n=9; 3 samples of cells were stained from 3 independent differentiation studies). Synthetic retinoids induce loss of SSEA-3 expression and induction of A2B5 expression to a greater extent than ATRA at low concentrations. Two way ANOVA with Tukey's multiple comparisons test: * = $p \leq 0.05$, ** = $p \leq 0.01$, *** = $p \leq 0.001$, **** = $p \leq 0.0001$. Scale bars: 200 µm.

3.3.2 Development and Characterisation of a Robust and Reproducible Model of Human Neurite Outgrowth in 2D Culture

To develop a spheroid-based human pluripotent stem cell-derived model of neurite outgrowth, a two-step culture methodology was developed. The methodology of which is outlined in Chapter II (*2.2.5 Formation of neurospheres from human pluripotent stem cells*, *2.2.6 Induction of neurite outgrowth from stem cell derived neurospheres*). In brief, monolayers of TERA2.cl.SP12 cells were dissociated and seeded in suspension to promote aggregation and then differentiated with retinoid compounds for 21 days to form mature neurospheres. Neurospheres were cultured on poly-D-lysine and laminin coated surfaces for a further 10 days, during which time neurospheres adhered to the growth substrates and neurites began to protrude from the neurospheres in a radial fashion. During the 10-day neurite outgrowth period, retinoids were not included in the growth medium, however mitotic inhibitors were added to prevent excess cell proliferation.

Quantification of neurite outgrowth was achieved by examination of TUJ-1 positive staining, a pan-neuronal marker that highlights neurite outgrowth. Neurites were then traced using image analysis software (Image J), however tracing each individual neurite is an extremely time consuming process that can be prone to error. For this reason, a sampling procedure was developed to establish an accurate and efficient quantification methodology. TERA2.cl.SP12 derived neurospheres were differentiated with increasing concentrations of ATRA and quantified by tracing every neurite (Figure 3-3A). The same data set was then analysed using a sampling method that involved the overlay of a grid onto the image and the random selection of three squares per image to quantify (Figure 3-3B). Data sets from both quantification methods were compared and a statistical analysis demonstrated that there was no significant difference (ns) in the number of neurites per neurosphere (Figure 3-3C) or the neurite density (Figure 3-3D) of each neurosphere when using either quantification method. Therefore the sampling method of quantification was deemed a satisfactory method of neurite quantification for use throughout this study.

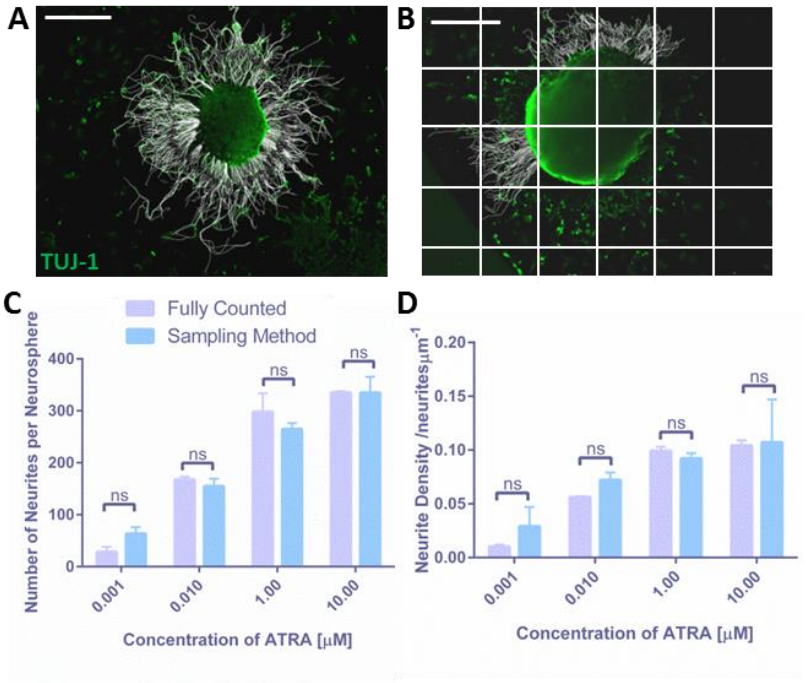

Fig 3-3: Development of an efficient method for the quantification of neurite outgrowth.
Representative images showing TUJ-1 positive neurites (green) radiating from neurospheres and neurites were traced using Image J software (white). All neurites protruding from each neurosphere were counted (A) and compared with a sampling method (B) whereby a grid was overlaid onto each image and three squares were selected randomly to quantify. Scale bars: 500 µm. Quantification of the number of neurites per neurosphere (C) and neurite density (D) for cell aggregates differentiated with a range of concentrations of ATRA (0.001 µM – 10 µM), and quantified by both fully counting neurite outgrowth and by employing the sampling method described. No significant (ns) difference was found between counting all neurites (fully counted) and the efficient sampling method developed through two-way ANOVA analysis and Tukey's multiple comparison test (data represent mean ± SEM, n=6-9; 2-3 neurospheres were quantified from 3 independently differentiated pools of neurospheres).

In order to optimise the differentiation process, the ability of synthetic retinoids to induce neurite generation from human pluripotent stem cell aggregates was analysed over a range of concentrations (0.001 – 10 µM). Neurite outgrowth was identified by immunofluorescence (Figure 3-3A) whereby nuclei (blue) remained within the central cellular aggregate whilst neurites (green, TUJ-1+) extended radially from the central aggregate body. Neurospheres differentiated with ATRA (Figure 3-4Aa,d) appear to have generated less neurites and neurite growth appears to be less uniform than those neurospheres differentiated with the same concentration EC23 (Figure 3-4Ab,e) or AH61 (Figure 3-4Ac,f).

Quantification of neurite outgrowth from neurospheres differentiated with each retinoid compound revealed that at lower concentrations (0.001 – 0.01 µM) those neurospheres differentiated with EC23 and AH61 produced significantly more neurites (Figure 3-4B)

than those differentiated with ATRA. Similarly, when normalised to aggregate size, the neurite density (Figure 3-4C) of neurospheres differentiated with synthetic compounds was significantly higher than those differentiated with ATRA. However, the difference in neurite outgrowth between the compounds tested becomes less pronounced at higher retinoid concentrations (1 – 10 μM) with no significant difference in the neurite density between compounds at these concentrations. This is thought to be due to the maximal capacity of neurite outgrowth from the neurospheres being reached, particularly as increasing the concentration of retinoid molecules further did not increase neurite outgrowth. Therefore, it was determined that 0.01 μM EC23 was the optimum condition for inducing neuritogenesis from stem cell derived neurospheres. This is because 0.01 μM EC23 induced the generation of significantly more neurites per neurosphere and neurospheres were of a greater neurite density than those aggregates differentiated by ATRA and AH61. The optimal set of conditions was used to induce neuronal differentiation and neurite generation for the remainder of this study.

To further characterise the neurites generated from stem cell-derived neurospheres induced by 0.01 μM EC23, expression of known cytoskeletal markers were analysed over time. It was found that nestin, an intermediate filament protein found in neural stem cells and progenitors, was expressed early in culture (Figure 3-5A-D). Maximal expression of nestin was observed at day 2, whereas more intermediate neurite outgrowth markers such as neurofilament-L (Figure3-5E-H) and neurofilament-M (Figure 3-5I-L) are expressed later in culture, during the intermediate time points analysed (days 4 – 10). The marker of neurite maturation, neurofilament-H (Figure 3-5Q-T), was expressed maximally at day 20 in extended cultures. The pan-neuronal marker TUJ-1 highlights the extension of neurites from the neurospheres over time (Figure 3-5Q-T) with neurites beginning to protrude from the neurosphere at day 2 and increasing in length over the 20-day culture period.

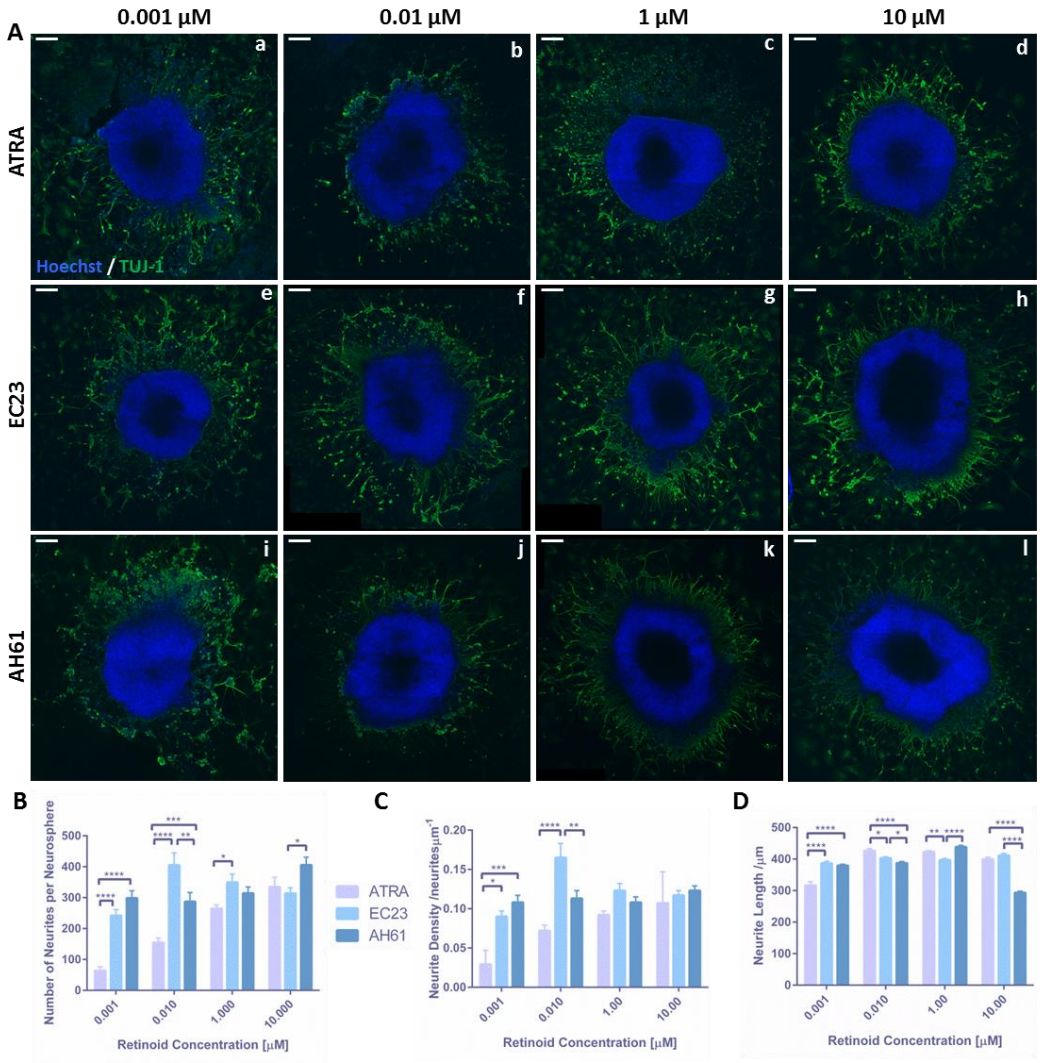

Fig 3-4: Induction of neurite outgrowth using natural and synthetic retinoid compounds.
Representative confocal images of neurospheres (A) differentiated with a range of concentrations (0.001 µM – 10 µM) of ATRA (a-d), EC23 (e-h) and AH61 (i-l) and subsequently cultured in 2D. TUJ-1 positive neurites are highlighted in green and radiate from the central body of the neurosphere with nuclei being stained blue. Scale bars: 200 µm. Quantification examining the number of neurites per neurosphere (B) (data represent mean ± SEM, n=15-24; between 5-8 neurospheres were quantified from 3 independently differentiated pools of neurospheres), the number of neurites per µm of aggregate circumference, neurite density (C) (data represent mean ± SEM, n=15-24 between 5-8 neurospheres were quantified from 3 independently differentiated pools of neurospheres) and neurite length (D) (data represent mean ± SEM, n=100; 33 neurites from 3 independently differentiated neurospheres were measured). Synthetic molecules induce greater neuritogenesis at lower concentrations than the naturally occurring ATRA and 0.01 µM EC23 was found to be the optimum differentiation condition in terms of neurite number and density. This condition was therefore selected for use throughout the project. Data was analysed using a two-way ANOVA with Tukey's multiple comparison test: * = $p < 0.05$, ** = $p < 0.01$, *** = $p < 0.001$, **** = $p < 0.0001$.

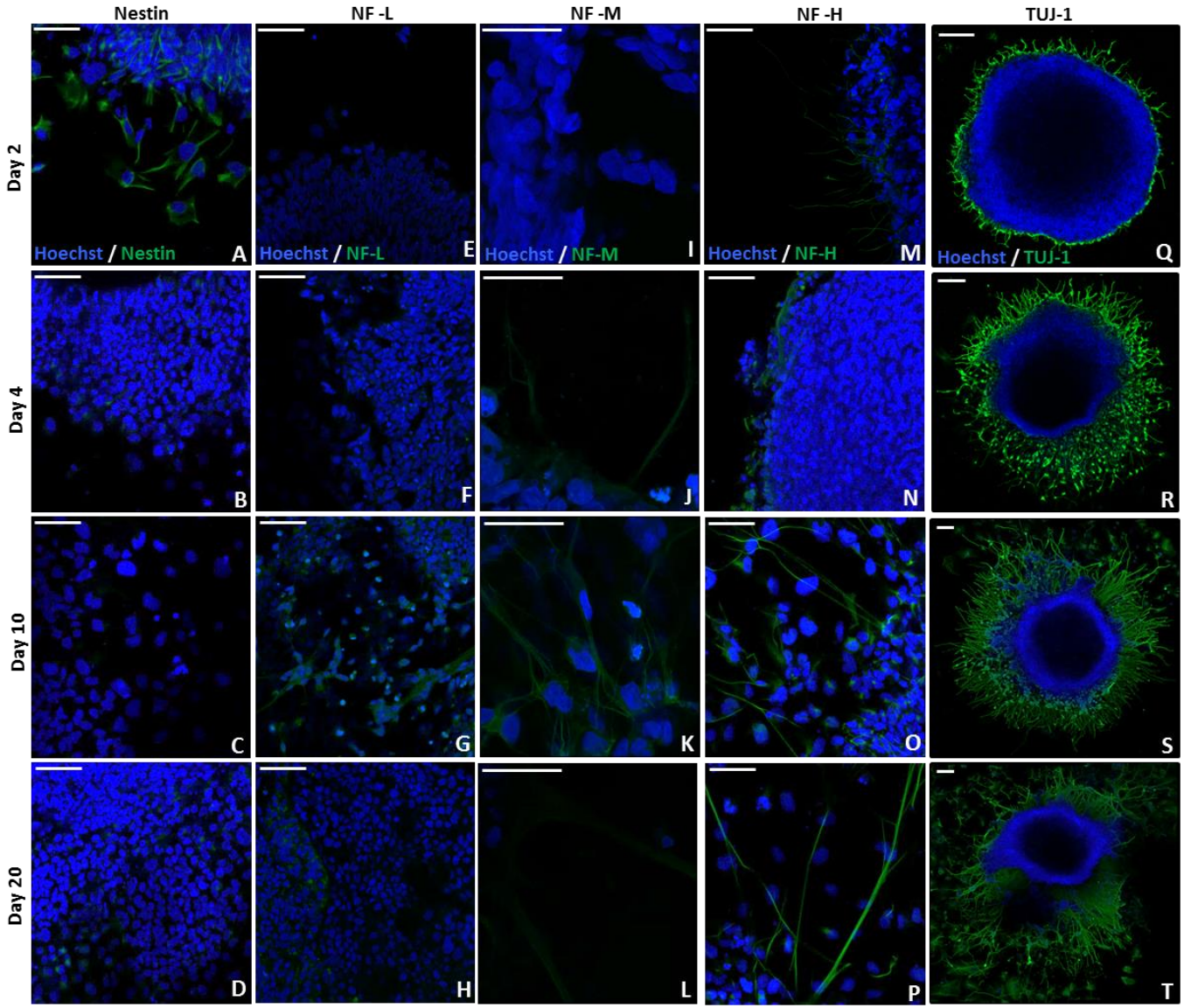

Fig 3-5: Characterisation of neuronal differentiation through the stages of neurite outgrowth from neurospheres over 20 days in 2D culture.
Neurospheres were cultured on poly-D-lysine and laminin coated 2D surfaces for up to 20 days. Representative confocal images of expression over time of nestin (A-D), neurofilament-L (E-H), neurofilament-M (I-L), neurofilament-H (M-P), and TUJ-1 (Q-T). Scale bars: (A-P): 50 µm , (Q-T): 100 µm. Nestin, a marker of neuronal stem cells is expressed early in culture, whereas more intermediate markers of neurite outgrowth such as NF-L and NF-M are expressed midway through culture and NF-H, a mature marker of neurite outgrowth is expressed at later stages of culture. This suggests that neurite outgrowth within this model, shares similarities with neurite outgrowth during development of the nervous system.

3.3.3 Development of a Novel Stem Cell Derived Neurite Outgrowth Model within a 3D Culture System

This 2D fully optimised and characterised model of neuritogenesis was then combined with well-established 3D cell culture technology to provide a more physiologically representative model of neurite development. Building on previous work that has demonstrated enhanced neuritogenesis on 3D Alvetex® Scaffold membranes[147,150]. This study has utilised the same technology to produce a more characterised and advanced model of neuritogenesis with many applications to study neurite growth and inhibition.

Alvetex® scaffold is a highly porous cell culture scaffold specifically developed for 3D cell culture applications and is compatible with traditional tissue culture plastic-ware (Figure 3-6A). The internal structure of Alvetex® scaffold is visible under scanning electron microscopy (SEM, Figure 3-6B) and comprises of voids with an average size of 40 μm and interconnecting windows of 13 μm. Alvetex® membranes are suspended in well inserts providing an appropriate substrate on which to perform 3D cell culture.

Neurospheres differentiated with the optimal 0.01 μM EC23, were cultured on Alvetex® scaffold coated with poly-D-lysine and laminin for 10 days with the addition of mitotic inhibitors. A cross-section of Alvetex® scaffold (Figure 3-6C) reveals that the neurosphere predominantly remains on top of the scaffold with only a few nuclei (hoechst stained blue) penetrating the material. In contrast, extensive neurite outgrowth (TUJ-1 positive staining – green) can be observed within the 3D material. The scaffold provides a more physiologically relevant environment and physical 3D space for neurites to grow and develop.

A view from above the scaffold indicates that the neurosphere itself remains on top of the scaffold (Figure 3-6D) whereas, neurites can be visualised from the bottom surface of the scaffold (Figure 3-6E), having penetrated the entire 200 μm depth of the material. A schematic demonstrates the difference in neurite development from neurospheres cultured in 2D (Figure 3-6F) and 3D (Figure 3-6G). When cultured in 2D neurites (green) radiate from the central cellular aggregate (blue), whereas in 3D culture, the body of the aggregate remains on top of the scaffold whilst the neurites penetrate the depth of the material and are visible from the underside, providing a novel means of quantification.

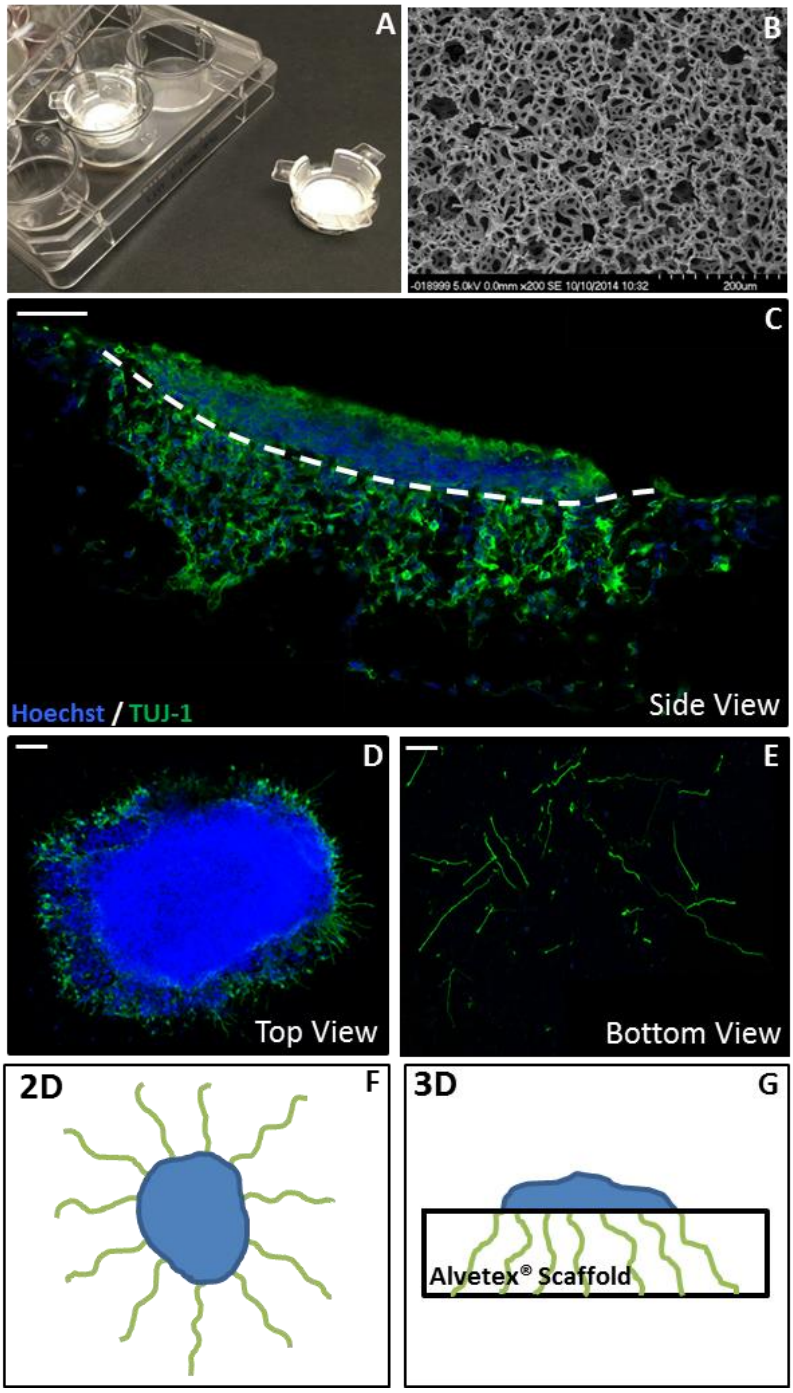

Fig 3-6: Development of a novel 3D model of neurite outgrowth.
Image of Alvetex® Scaffold 12-well inserts (A) and a scanning electron micrograph demonstrating the internal structure of the scaffold (B) with voids of 40 µm and interconnecting windows of 13 µm. Extensive neurite outgrowth can be observed within the 3D scaffold (C) with TUJ-1 positive neurites staining green and nuclei blue, imaged using confocal microscopy. The majority of the neurosphere remains on top of the scaffold (D) with neurites growing into the 3D material. Neurites can be visualised on the bottom of the scaffold (E), having extended through 200 µm of Alvetex® Scaffold. A schematic depicts the difference in neurite development between 2D (F) and 3D (G) culture. Neurospheres are depicted blue and neurites green. In 2D culture neurospheres radiate from the central neurosphere, whereas in 3D the neurites penetrate the depth of Alvetex® scaffold. Scale bars: 100 µm.

3.3.4 Investigation into the Role of Rho A/ROCK Signaling in Neurite Outgrowth

Neurite growth is controlled by a balance between signalling pathways involving the neurite promoting effects of Rac/Cdc42 and Rho A-mediated inhibitory signalling, which have opposing effects upon the actin cytoskeleton resulting in neurite growth or inhibition[10,13,207], as shown in Figure 3-6. For this reason many *in vitro* models of neurite outgrowth involve the addition of inhibitors of Rho A and ROCK to enhance neurite growth by reducing inhibitory signalling[21–24,29,30,203,204,208,209]. Such molecules include ibuprofen, an inhibitor of Rho A and the selective ROCK inhibitor, Y27632. To investigate the effect of Rho A/ROCK signaling within the human pluripotent stem cell derived model of neurite outgrowth described herein, Y-27632 and ibuprofen were added to 2D and 3D neurite outgrowth cultures.

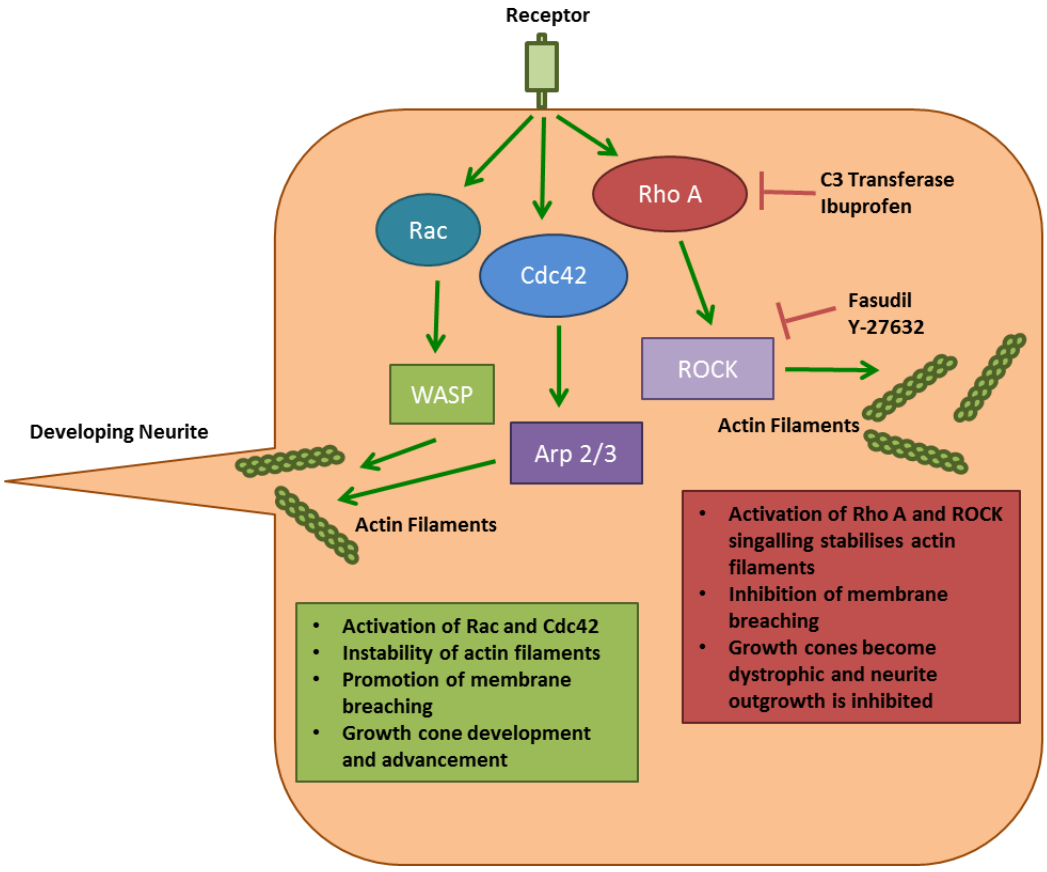

Fig 3-7: A balance between Rac and Rho signalling controls neurite growth.
Activation of Rac and Cdc42 drives neurite protrusion, whereas activation of Rho A promotes growth cone collapse. Neurite growth is dependent upon the balance between these two opposing signaling mechanisms due to their actions upon the actin cytoskeleton. Rac and Cdc42 activation promotes actin polymerisation and destabalises actin filaments resulting in membrane breaching, whereas Rho A activation results in stabalisation of actin filaments and inhibition of membrane breaching.

3.3.4.1 Inhibition of ROCK by Y-27632

To investigate the role of ROCK inhibition and to potentially enhance neuritogenesis within this stem cell derived model, the selective ROCK inhibitor Y-27632, was added to the culture medium of neurospheres at a range of concentrations (0.5 – 50 μM), during the 10-day neurite outgrowth phase of culture. Neurite outgrowth (TUJ-1+, green) from neurospheres cultured in 2D (Figure 3-8A) with 0.5 μM Y-27632 (Figure 3-7Ac,d) appears to differ only slightly from neurite outgrowth from untreated neurospheres (Figure 3-8Aa,b). However, higher concentrations such as 10 μM – 50 μM of Y-27632 have a drastic effect on neurite outgrowth, with a significantly greater number of TUJ-1 positive neurites visibly radiating from the central neurosphere. It also appears that at 10 μM – 50 μM Y-27632, fewer nuclei and cell bodies are visible outside of the cellular aggregate than in untreated and 0.5 μM treated neurospheres.

Quantification of the number of neurites per neurosphere (Figure 3-8B) and neurite density (Figure 3-8C) of the neurospheres (neurite number normalised to neurosphere size) reveals that both parameters increase in a dose dependent manner with increasing Y-27632 concentration. Treatment with 0.5 μM Y-27632 increases neurite number and density slightly, however this increase is not statistically significant. Whereas, treatment with 10 – 50 μM Y-27632 results in a significant increase in neurite number and density compared with the control. Neurite length (Figure 3-8D) however, decreases in a dose dependent manner with increasing Y-27632 treatment. There is little difference in the length of neurites produced by neurospheres treated with 0.5 μM Y-27632, however higher concentrations such as 10 – 50 μM Y-27632 resulted in a dose dependent inhibition of neurite length. Similarly, as observed in the fluorescence micrographs, the migration of nuclei from the central neurosphere (Figure 3-8E) was inhibited by Y-27632 treatment. Migration was significantly inhibited compared with the control at 10 – 15 μM Y-27632.

Neurospheres cultured in 3D were also treated with Y-27632 to potentially enhance neurite outgrowth within the 3D culture system (Figure 3-9). Neurospheres are visible from the top view of the scaffold (Figure 3-8Aa,c,e,g,i) whilst TUJ-1 (green) positive neurites have visibly penetrated the depth of the scaffold as viewed from below (Figure 3-9Aa,b,d,f,h,j). In the absence of Y-27632 significant neurite outgrowth can be viewed from the bottom of the scaffold (Figure 3-9Ab) and with increasing Y-27632 concentration, particularly at 15 – 50 μM Y-27632 treatment (Figure 3-8g-j) it appears that neurite outgrowth penetrating the scaffold is significantly enhanced. This is reflected in quantification of the number of neurites penetrating the scaffold (Figure 3-9B), which demonstrates little difference in neurite outgrowth between untreated neurospheres and those treated with 0.5 μM Y-27632. However, treatment with 10 – 50 μM Y-27632

resulted in an increase in the number of neurites penetrating the 3D material and 50 μM treatment resulted in a statistically significant increase in neurite outgrowth compared with the control.

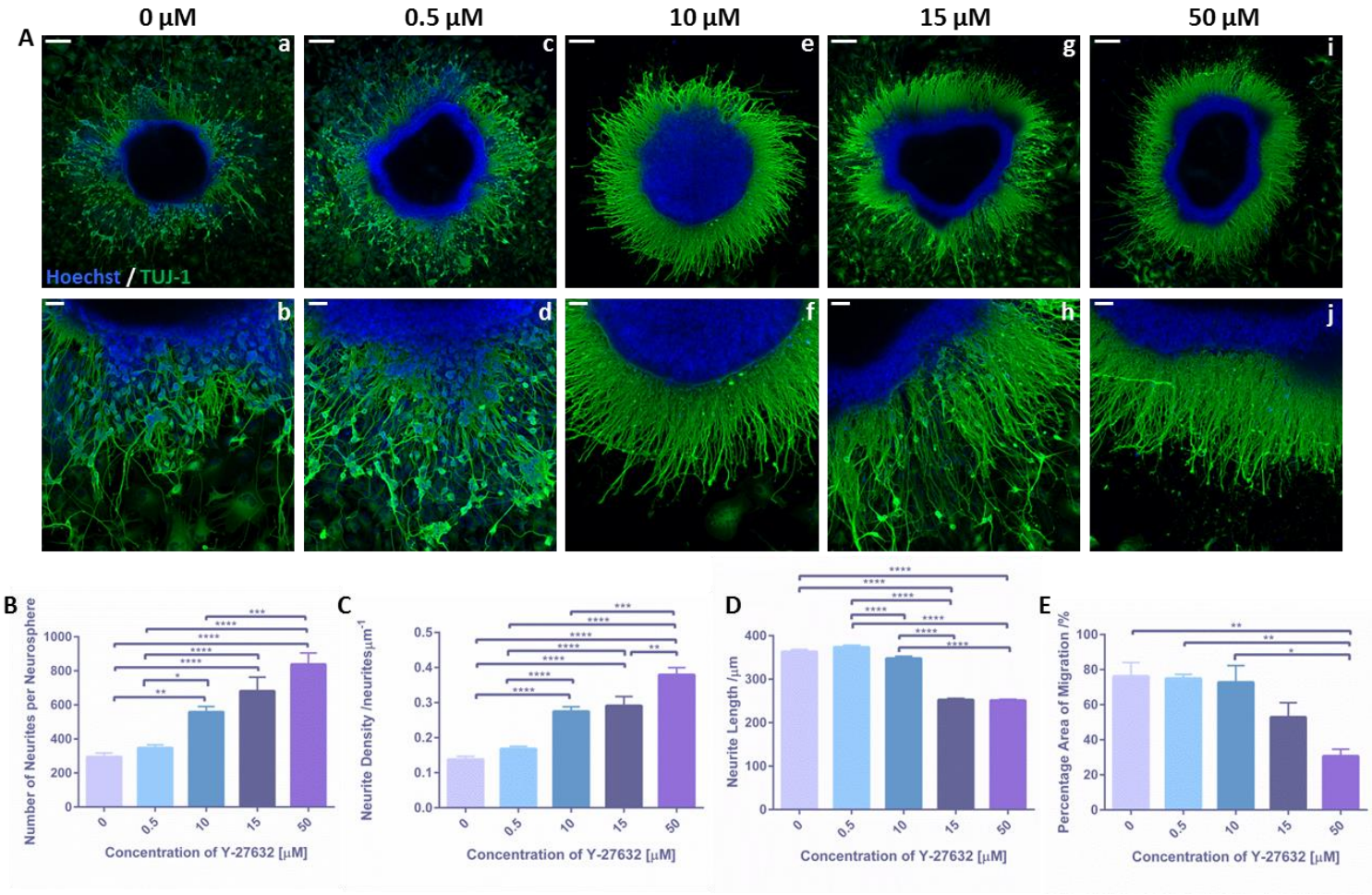

Fig 3-8: Enhancement of 2D neurite outgrowth by the selective ROCK inhibitor, Y-27632.
Representative confocal images (A) of TUJ-1 positive (green) neurite outgrowth from neurospheres cultured in 2D with a range of concentrations (0 – 50 µM) of Y-27632, a selective inhibitor of the ROCK enzyme. Nuclei are highlighted in blue. Scale bars: (Aa,c,e,g,i): 200 µm, (Ab,d,f,h,j): 50 µm. Number of neurites per neurosphere (B) (data represent mean ± SEM, n=15-18; 3 repeats from independent pools of cells were conducted, from which 15-18 neurospheres were quantified) and neurite density (C) (data represent mean ± SEM, n=15-18; 3 repeats from independent pools of cells were conducted, from which 15-18 neurospheres were quantified) are both greatly increased in a dose dependent manner by the addition of Y-27632 to the culture medium during the neurite outgrowth phase of culture. However, neurite length (D) (data represent mean ± SEM, n=457-984; between 457-984 neurites were measured from 15-18 neurospheres differentiated on 3 separate occasions) and percentage area of migration from the central body of the aggregate (E) (data represent mean ± SEM, n=9; 3 neurospheres were samples from 3 independent differentiation studies) are both inhibited by increasing concentrations of Y-27632. Data analysed by an ordinary one-way ANOVA with Tukey's multiple comparisons test: * = $p < 0.05$, ** = $p < 0.01$, *** = $p < 0.001$, **** = $p < 0.0001$.

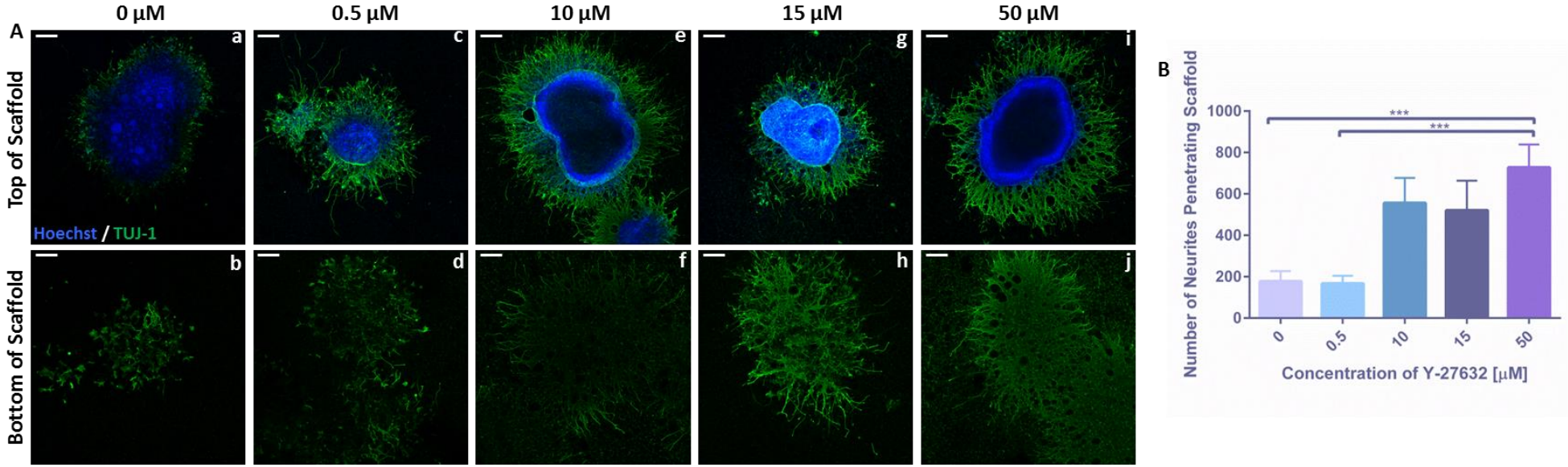

Fig 3-9: Enhancement of 3D neurite outgrowth by the selective ROCK inhibitor, Y-27632.
Representative confocal images (A) of neurospheres sitting on top of Alvetex® Scaffold (Aa,c,e,g,i) and TUJ-1 (green) positive neurites are visible from the underside of the scaffold (Ab,d,f,h,j). Nuclei are highlighted in blue. Scale bars: 200 µm. Neurospheres were cultured with a range of concentrations (0 – 50 µM) of Y-27632 throughout the 10 day neurite outgrowth phase of culture, and quantification of neurites that have penetrated the scaffold (B) (data represent mean ± SEM, n=6-9; neurite outgrowth was analysed from 2-3 neurospheres from 3 independently differentiated pools of neurospheres) demonstrates the ability of the molecule to enhance neurite outgrowth in a dose dependent manner. Data analysed by an ordinary one-way ANOVA with Tukey's multiple comparisons test: * = $p < 0.05$, ** = $p < 0.01$, *** = $p < 0.001$, **** = $p < 0.0001$.

3.3.4.2 Inhibition of Rho A by Ibuprofen

To investigate the ability of inhibition of Rho A to potentially enhance neurite outgrowth within this stem cell-derived model of neuritogenesis, ibuprofen the non-steroidal anti-inflammatory drug and inhibitor of Rho A[30], was added to the neurosphere culture medium for the duration of the 10-day neurite outgrowth period. A range of ibuprofen concentrations were tested (0 – 750 μM) and neurospheres cultured in 2D (Figure 3-10A) appear to generate more TUJ-1 positive (green) neuritic extensions at higher concentrations of ibuprofen such as 750 μM (Figure 3-10Ak,l). Similarly to Y-27632 treatment, 750 μM ibuprofen treatment seems to result in fewer nuclei migrating from the central cellular body. However, the effect upon neurite generation does not seem as profound as that of Y-27632, neurospheres treated with higher concentrations of ibuprofen (500 – 750 μM) do appear to generate more neurites than untreated aggregates.

Quantification of neurite outgrowth from ibuprofen treated neurospheres reveals that both neurite number (Figure 3-10B) and density (Figure 3-10C) increase in a dose dependent manner with ibuprofen treatment. Treatment with higher concentrations of ibuprofen, ranging from 100 – 750 μM result in a statistically significant increase in both neurite number and density compared with untreated neurospheres. Similarly to Y-27632 treatment, neurite length (Figure 3-10D) decreases with increasing ibuprofen concentration resulting in a significant inhibition in neurite length with 500 – 750 μM ibuprofen. An inhibition in migration of cells from the central neurosphere (Figure 3-10E) was also documented and appeared to respond to ibuprofen treatment in a dose-dependent fashion, although a slight (not statistically significant) increase in migration was observed with 10 μM ibuprofen.

In 3D culture neurospheres are visible on top of the scaffold (Figure 3-11Aa,c,e,g,i,k) and significant neurite penetration is observed from the bottom view of the scaffold (Figure 3-11Ab,d,f,h,j,l). In the absence of ibuprofen treatment (Figure 3-11 Aa,b) significant neuritogenesis can be observed from the underside of the scaffold. As ibuprofen treatment increases in concentration (10 – 100 μM) it appears that the number of TUJ-1 positive (green) neurites penetrating the 3D material increases. However at the highest concentrations of ibuprofen tested (500 – 750 μM) fewer neurites appear to be visible on the underside of the scaffold, as opposed to 100 μM ibuprofen.

Similarly, quantification (Figure 3-11B) reveals an increase in the number of neurites penetrating the scaffold with increasing ibuprofen concentration, in a dose-dependent manner up to 500 μM. However, as ibuprofen concentration increases to 750 μM, the number of neurites penetrating the 3D material dramatically declines. This could be due

to the fact that ibuprofen inhibits neurite length in 2D culture (Figure 3-10), therefore at the highest concentrations of ibuprofen tested, fewer neurites are able to penetrate the 200 μm depth of the scaffold, thus are visible from the underside. Concentrations of 100 μM and 500 μM ibuprofen were found to significantly enhance neurite outgrowth in 3D culture compared with untreated controls.

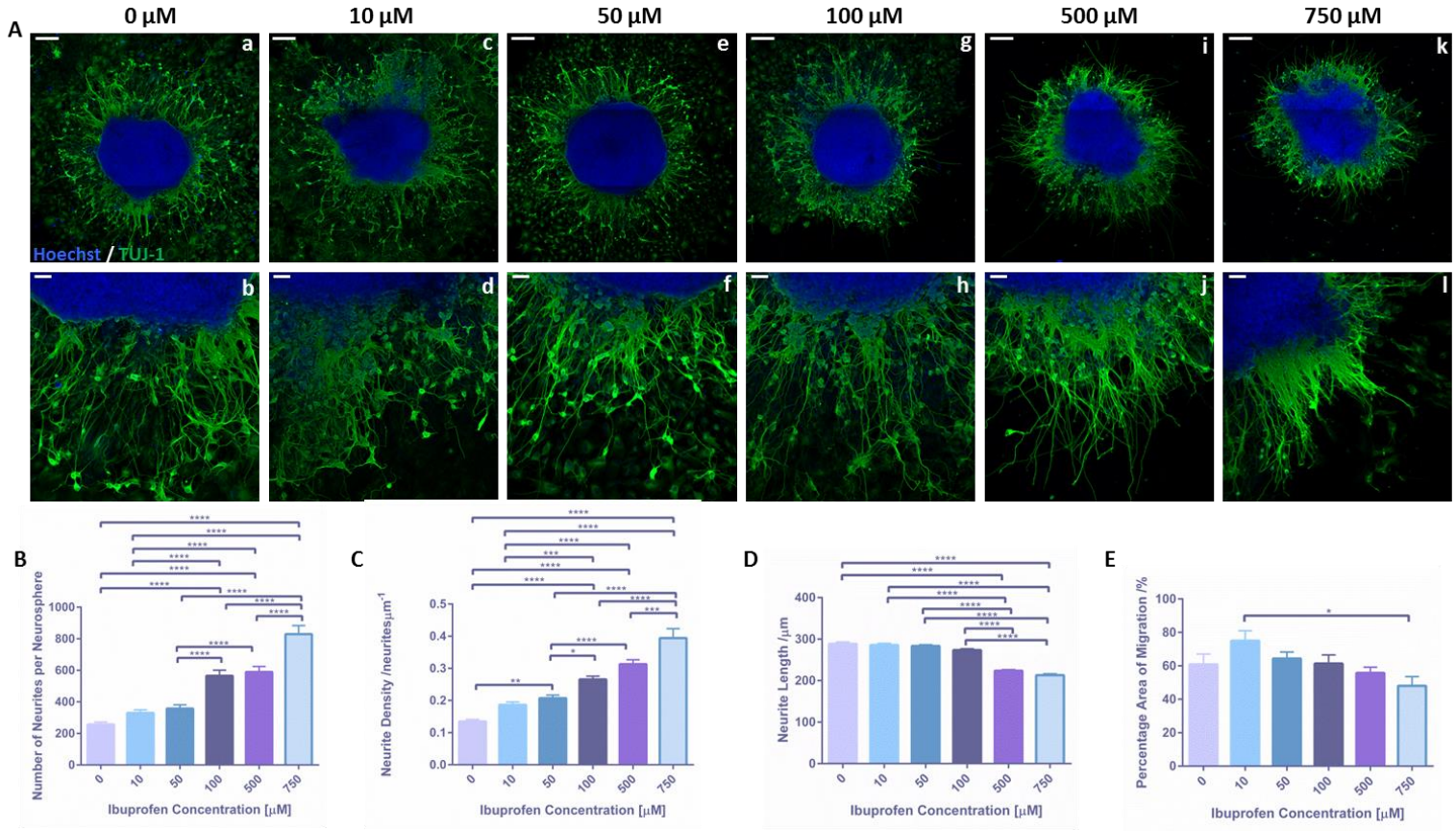

Fig 3-10: Enhancement of 2D neurite outgrowth by ibuprofen, an inhibitor of Rho A.
Representative confocal images (A) of neurospheres cultured in 2D with increasing concentrations of ibuprofen (0 – 750 µM). The pan-neuronal marker TUJ-1 is stained in green and nuclei are highlighted in blue and form the body of the aggregate. Scale bars: (Aa,c,e,g,i,k): 200 µm (Ab,d,f,h,j,l): 50 µm. Quantification of neurite outgrowth revealed that with increasing concentrations of ibuprofen, the number of neurites per neurosphere (B) (data represent mean ± SEM, n=15-24; between 5-8 neurospheres were quantified from 3 independently differentiated cell populations) and the density of the neurites (C) (data represent mean ± SEM, n=15-24; between 5-8 neurospheres were quantified from 3 independently differentiated cell populations) increased in a dose dependent manner with ibuprofen concentration. However, neurite length (D) (data represent mean ± SEM, n=521-1273; between 521-1273 neurites were measured from 5-8 neurospheres sampled from 3 independently differentiated neurosphere populations) and migration of cells from the aggregate (E) (data represent mean ± SEM, n=7-9) decrease with increasing ibuprofen concentration, particularly at higher concentrations. One-way ANOVA with Tukey's multiple comparisons: * = $p < 0.05$, ** = $p < 0.01$, *** = $p < 0.001$, **** = $p < 0.0001$.

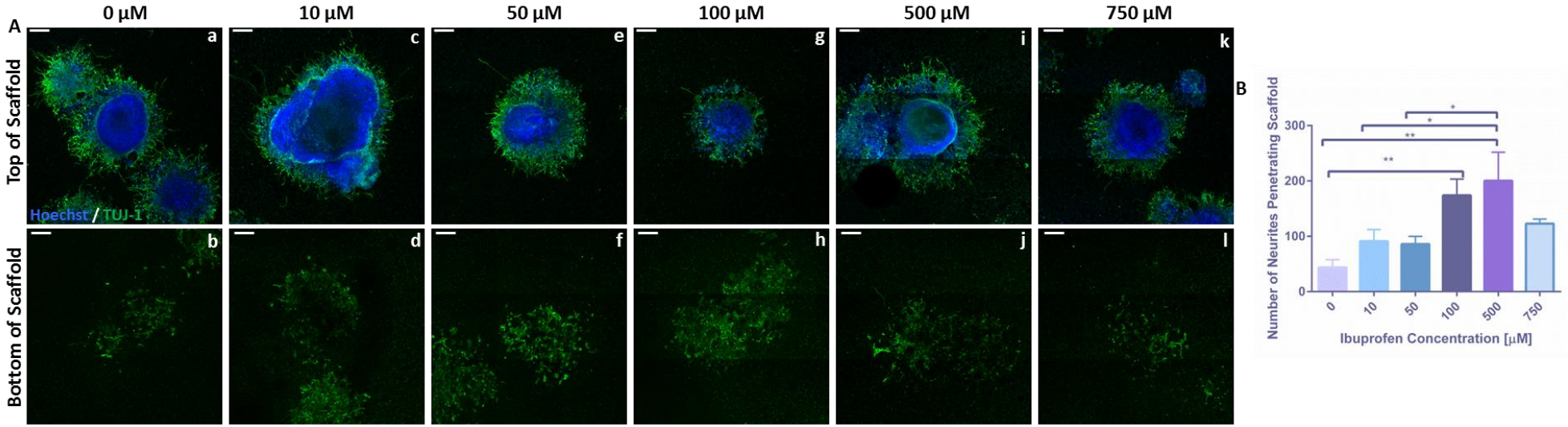

Fig 3-11: Enhancement of 3D neurite outgrowth by ibuprofen, an inhibitor of Rho A.
Representative confocal images (A) of neurospheres cultured in 3D with increasing concentrations of ibuprofen (0 – 750 µM). The body of the neurosphere is visible from the top view of the scaffold (Aa,c,e,g,i,k) and neurites that have penetrated the 3D material are visible from below the scaffold (Ab,d,f,h,j,l). TUJ-1 highlights neurite outgrowth in green and hoechst stains nuclei in blue. Scale bars: 200 µm. Quantification of the neurites that have penetrated the scaffold (B) (data represent mean ± SEM, n=6-9; neurite outgrowth was quantified from 2-3 neurospheres from each of 3 independently differentiated populations of neurospheres) demonstrates that ibuprofen enhances neurite outgrowth up to high concentrations, however, this effect is lost at 750 µM. Data analysed using an ordinary one-way ANOVA with Tukey's multiple comparisons test: * = $p < 0.05$, ** = $p < 0.01$, *** = $p < 0.001$, **** = $p < 0.0001$.

3.3.5 Development of a Novel iPSC Derived Model of Neurite Outgrowth

In addition to the development and characterisation of a robust and reproducible EC-cell derived model of neurite outgrowth, an iPSC-derived neurite outgrowth model was also developed. This required the use of ReproNeuro, iPSC-derived neuroprogenitor cells[210,211] which were cultured as neurospheres and subsequently neurite outgrowth was observed. Two different populations of ReproNeuro cells were used for the development of this model, ReproNeuro Glu cells which are glutamatergic neuroprogenitor cells and ReproNeuro cells which form a mixed population of neuroprogenitors (Figure 3-12)[212]. ReproNeuro cells do not require differentiation by EC23, as the cells are received as differentiated neuroprogenitor cells that mature through the course of the culture period through the use of ReproNeuro Maturation medium.

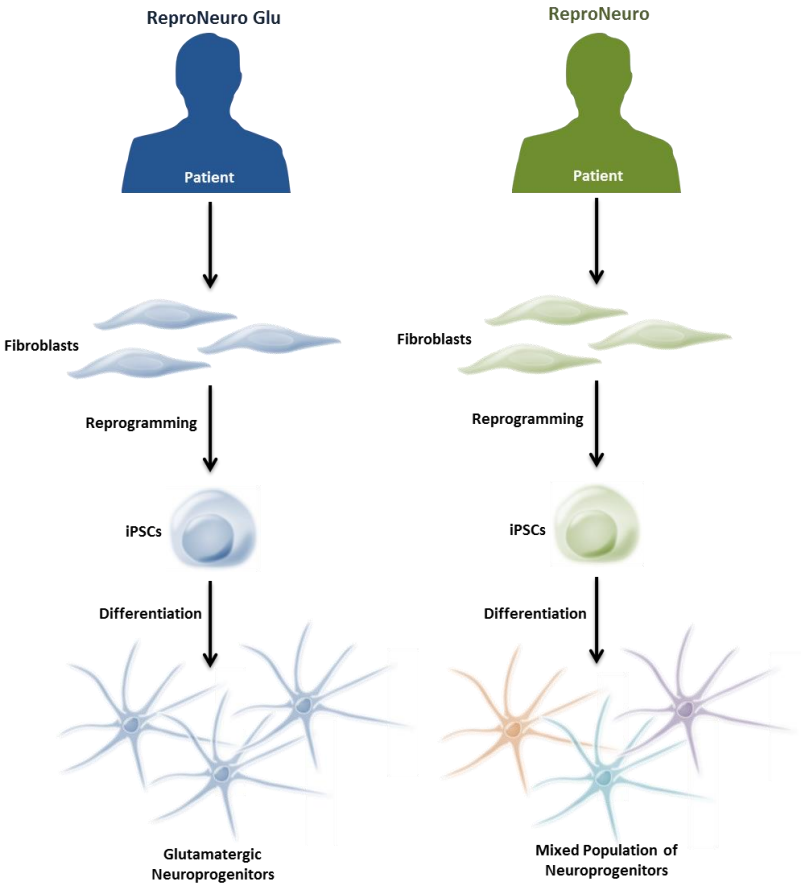

Fig 3-12: Derivation of ReproNeuro cell lines.
ReproNeuro Glu and ReproNeuro cells are both derived from fibroblasts isolated from human donors. The fibroblasts are then reprogrammed to form populations of iPSCs that subsequently undergo differentiation to promote the formation of neuroprogenitor cells. However different differentiation procedures are used to generate the two cell lines. This results in the formation of ReproNeuro Glu, a population of predominantly glutamatergic neuroprogenitors, and ReproNeuro, a mixed population of neuroprogenitor cells.

3.3.5.1 Development of a ReproNeuro Glu Derived Model of Neurite Outgrowth

In order to form spheroid structures from ReproNeuro Glu cells, AggreWell™ plates were used to force cells into close proximity with one another (Figure 3-13). AggreWell™ plates contain microwells, initially filled with bubbles (Figure 3-13A), which can be removed by centrifugation (Figure 3-13B). ReproNeuro Glu cells were then seeded within the plates and incubated for 24 hours, during which time cells form 3D spherical structures due to the nature of the microwells forcing cells into close contact with one another (Figure 3-13C,D). ReproNeuro Glu-derived neurospheres were then harvested (Figure 3-13E) and seeded onto ECM-coated growth substrates for a 10-day neurite outgrowth period (Figure 3-13F,G) during which, neurites began to radiate from the central neurosphere, similar to the TERA2.cl.SP12 derived model of neuritogenesis described previously.

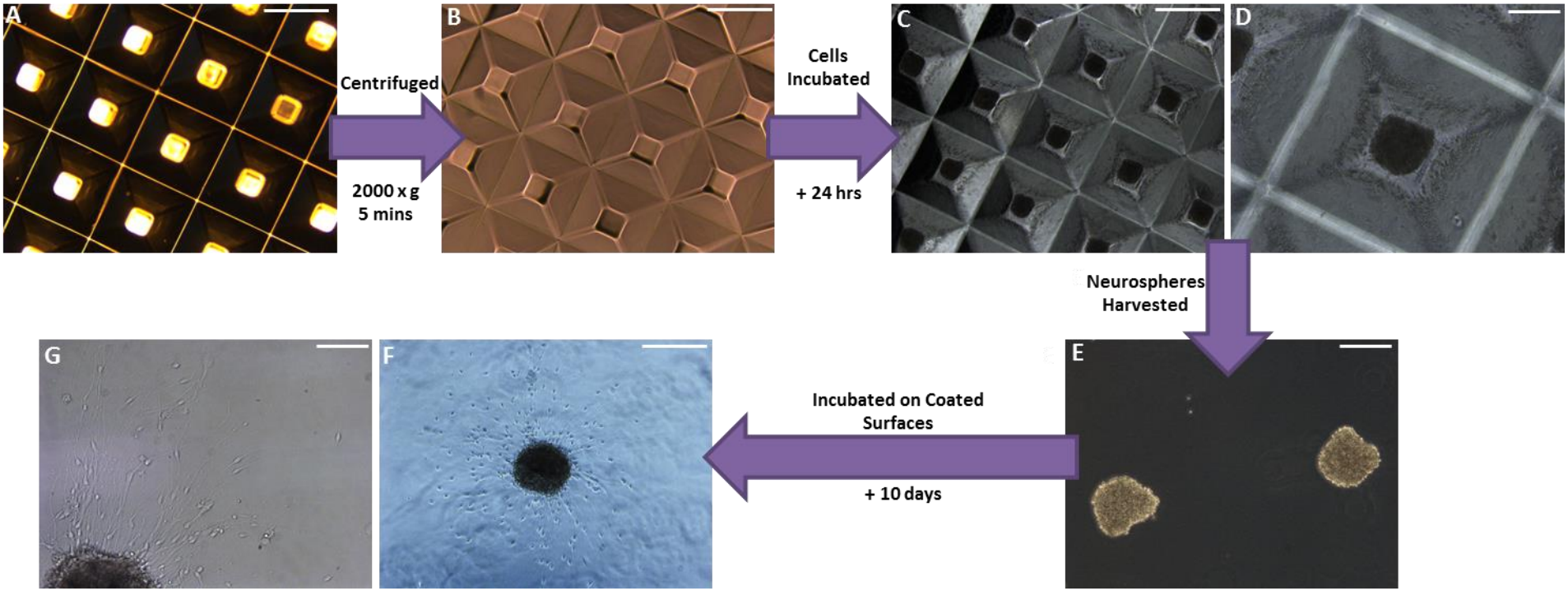

Fig 3-13: Formation of neurospheres from ReproNeuro Glu, iPSC derived neuroprogenitor cells and induction of 2D neurite outgrowth.
AggreWell™ 800 plates prior to centrifugation (A) have small bubbles at the bottom of each microwell, following the addition of culture medium and centrifugation at high speed; bubbles are removed from the microwells (B). ReproNeuro Glu cells were revived and immediately seeded into AggreWell™ plates. Following 24 hours incubation, cells formed spheroid structures in each microwell (C,D), which were then harvested from the plate (E). Neurospheres were then seeded on 2D surfaces coated in ReproNeuro Glu coating solution and cultured for 10 days (F,G). Scale bars: A-D: 500 µm, E-G: 200 µm.

In order to characterise the cell line, ReproNeuro Glu cells were also cultured as a monolayer (Figure 3-14A) and were found to express the pan-neuronal marker TUJ-1 (Figure 3-14B) whilst forming an extensive neuronal network as visible by both phase contrast and fluorescence microscopy. ReproNeuro Glu-derived neurospheres formed via AggreWell™ plates were cultured for a 10-day neurite outgrowth period, during which time neurites can be seen to visibly radiate from the central sphere by phase contrast microscopy (Figure 3-14C). Similarly, staining for the pan-neuronal marker TUJ-1 (Figure 3-14D) highlights the vast expanse of neurites generated by the neurosphere during this culture period. Significant neurite outgrowth can be observed radiating from the central cellular aggregate and neurites appear extremely long. Most nuclei appear to have remained within the central spheroid with few nuclei appearing to have migrated from the cellular mass. ReproNeuro Glu cells cultured within Alvetex® scaffold form complex networks of TUJ-1 positive neurons (Figure 3-14E,F) within the 3D microenvironment. From the top view of the scaffold (Figure 3-14E) a large volume of intertwining neurons are visible and the bottom view of the scaffold (Figure 3-14F) reveals those neurites that have penetrated the entire 200 µm depth of the 3D material.

To compare both 2D models of neurite outgrowth described thus far in this chapter, neurite outgrowth from ReproNeuro Glu-derived neurospheres (Figure 3-15Aa) and TERA2.cl.SP12 derived neurospheres differentiated with 0.01 µM EC23 (Figure 3-15Ab) was compared. Neurites that stain positive for TUJ-1 (green) can be seen to protrude from both neurospheres in a radial manner. However, ReproNeuro Glu-derived neurospheres are extremely small in size compared with TERA2.cl.SP12-derived neurospheres. In both cases nuclei appear restricted to the central cellular mass with little migration from the neurosphere. ReproNeuro Glu-derived neurospheres appear to produce many more and longer neurites than TERA2.cl.SP12 cell derived neurospheres, as visible via fluorescence microscopy.

Quantification reveals a similar number of neurites per neurosphere from both 2D cultured models (Figure 3-15B), however the difference in aggregate size between the two models results in this being a poor reflection of the neurite generation properties of each type of neurosphere. The neurite density (Figure 3-15C), gives a more reliable comparison of the ability of each type of neurosphere to produce neurites, and reveals that ReproNeuro Glu-derived neurospheres produce significantly more neurites per µm of neurosphere circumference compared with TERA2.cl.SP12-derived neurospheres. Similarly quantification of neurite length (Figure 3-15D) reveals that neurites generated by ReproNeuro Glu-derived neurospheres are significantly longer than their TERA2.cl.SP12 derived counterparts.

Although neurite outgrowth appears to be enhanced in ReproNeuro Glu-derived neurospheres, the TERA2.cl.SP12-derived model of neuritogenesis will still be used throughout this study for a number of reasons. Primarily, the ability of TERA2.cl.SP12 cells to produce functional neurons and differentiate in response to retinoid compounds has been clearly documented previously along with their ability to form neurites in 3D, and this model is a well-known robust model of neurogenesis. Furthermore, EC cells are widely available and their consumables more economically favourable than the specialised media and supplements required for ReproNeuro Glu culture. Therefore the TERA2.cl.SP12 model was continually used throughout the remainder of the project.

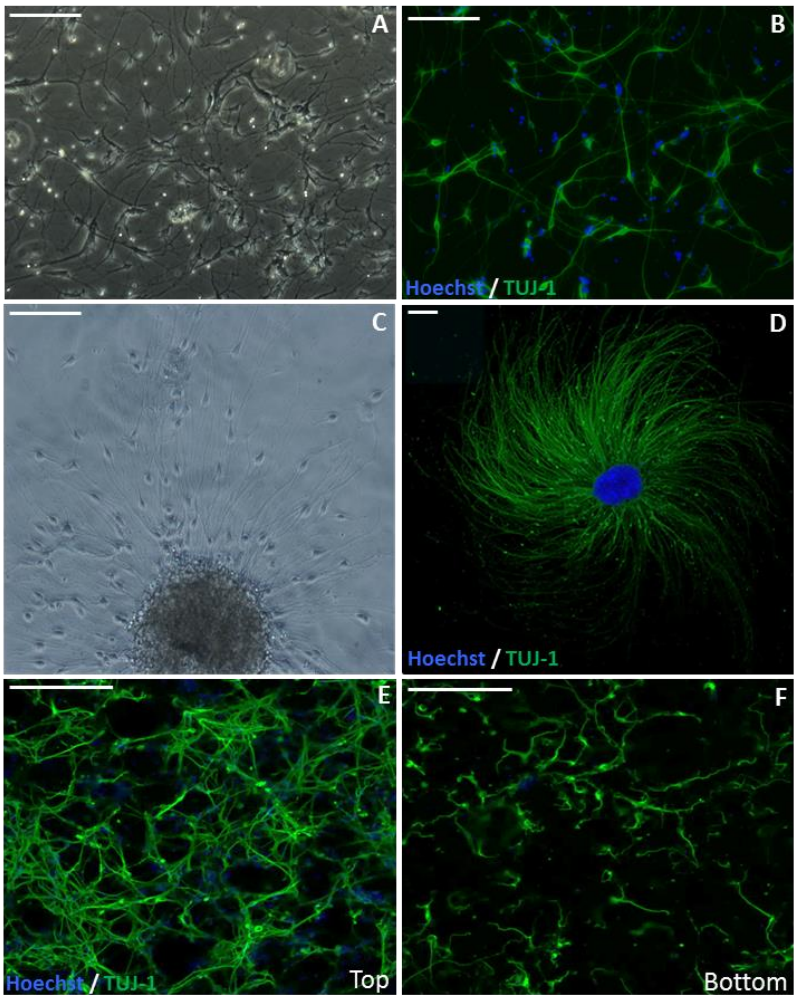

Fig 3-14: Development of a neurite outgrowth model from ReproNeuro Glu, iPSC derived neuroprogenitor cells.
A representative phase contrast image of ReproNeuro Glu cells cultured as a 2D monolayer (A) and stained for the pan-neuronal marker, TUJ-1 (green) with nuclei being highlighted in blue (B). Extensive neurite outgrowth can be observed from neurospheres cultured in 2D under phase contrast microscopy (C) and TUJ-1 (green) staining (D) highlights the full extent of neurite outgrowth from the neurosphere. ReproNeuro Glu cells were also cultured in 3D in Alvetex® scaffold and stained for TUJ-1 expression (green). Cells can be seen forming neuronal networks on the top of the scaffold (E) and neurites have even penetrated the 3D material, as visible from the underside view of the scaffold (F). Scale bars: A-D: 200 µm, E-F: 100 µm.

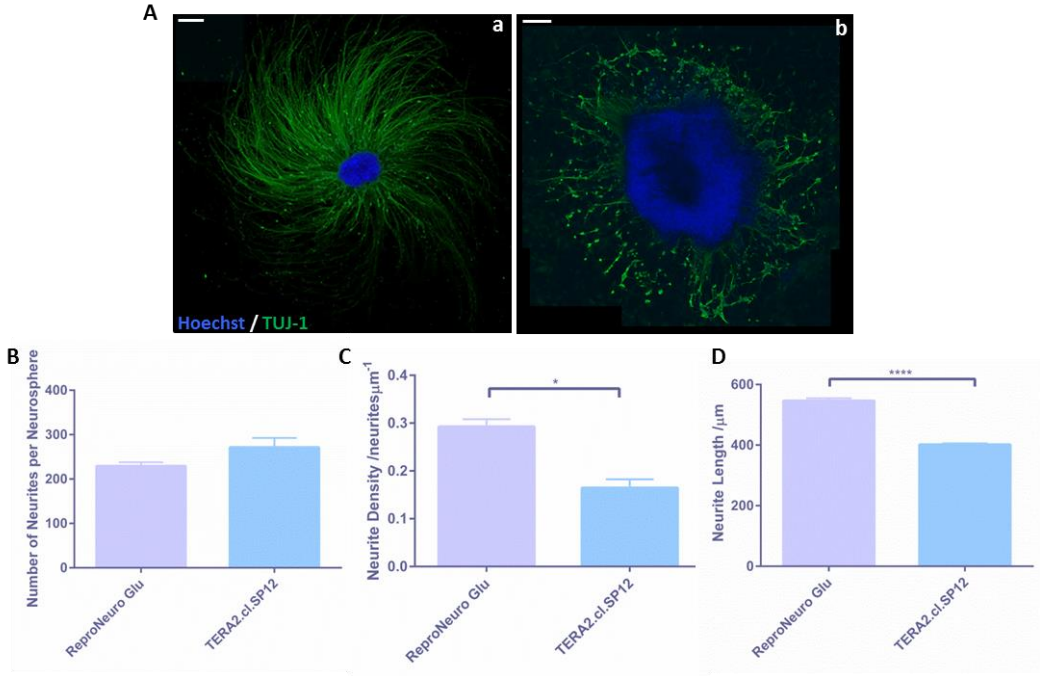

Fig 3-15: Comparison of two novel human pluripotent stem cell derived models of neurite outgrowth in 2D culture.
Representative confocal images (A) of neurite outgrowth from a neurosphere formed from iPSC derived neuroprogenitor cells (Aa) and from the optimised neurite outgrowth methodology for TERA2.cl.SP12 differentiation (Ab). The pan-neuronal marker TUJ-1 (green) highlights neurite outgrowth and nuclei (blue) are restricted to the cell aggregate. Scale bars: 200 µm. TERA2.cl.SP12 derived neurospheres produce more neurites per neurosphere (B) (data represent mean ± SEM, n=3-27; 1-9 neurospheres were quantified from 3 independently cultured cell populations) than ReproNeuro Glu cell aggregates when cultured in 2D on ECM coated surfaces. However, when this is normalised to aggregate size by measuring neurite density (C) (data represent mean ± SEM, n=3-27; 1-9 neurospheres were quantified from 3 independently cultured cell populations), ReproNeuro Glu cell aggregates produce significantly more neurites per µm of aggregate circumference. The average neurite length (D) (data represent mean ± SEM, n=114-1343; between 114-1343 neurites were measured from a total of 3-27 neurospheres obtained from 3 independent cell cultures), is significantly greater in ReproNeuro Glu cultures than TERA2.cl.SP12 cultures. Data analysed using an unpaired T-test assuming a Gaussian distribution: * = $p < 0.05$, ** = $p < 0.01$, *** = $p < 0.001$, **** = $p < 0.0001$.

3.3.5.2 Development of a ReproNeuro Derived Model of Neurite Outgrowth

Spheroids were generated from ReproNeuro neuroprogenitor cells through a similar methodology as ReproNeuro Glu cells, however a number of differences feature in the two methodologies. AggreWell™ plates are prepared in the same manner as previously described, the air bubbles present in the microwells (Figure 3-16A) were removed via centrifugation (Figure 3-16B). ReproNeuro cells are then seeded within the plates, however unlike with ReproNeuro Glu cells, ReproNeuro cells are cultured for 48 hours rather than 24 hours. The length of this incubation period was doubled, as cells had not appeared to form tight spheroids within the microwells of the plate at 24 hours, and following 48 hours incubation, clear 3D structures were visible within the plate (Figure 3-16C).

Following the 48-hour incubation period, neurospheres were harvested from the plate (Figure 3-16D) and seeded onto ECM-coated 2D and 3D surfaces to promote the induction of neurite outgrowth. Neurospheres were observed daily following seeding and at 24 hours in culture significant neurite outgrowth could be observed to radiate from the central cellular mass, under phase contrast (Figure 3-16E). However following the additional 9 days in culture, (a total of 10 days neurite outgrowth the same length of time as ReproNeuro Glu) the cellular aggregate completely lost its structure as the majority of cells had migrated from the neurosphere (Figure 3-65F). For this reason it was decided that cultures should be fixed at day 1 post-neurosphere seeding in 2D as both neurites and structural integrity were observed at this time point. However, a neurite outgrowth period of 24 hours is unsuitable for 3D neurite outgrowth cultures as this time interval does not allow for neurites to traverse the entire 200 μm depth of the 3D scaffold. Therefore 3D cultures were maintained for 10 days, as there is no evidence of cellular migration in 3D culture. The optimised methodology developed for neurite outgrowth from ReproNeuro cells differs then from ReproNeuro Glu cells in the AggreWell™ plate incubation time (48 hours rather than 24 hours) and in the neurite outgrowth period for 2D cultures (24 hours rather than 10 days).

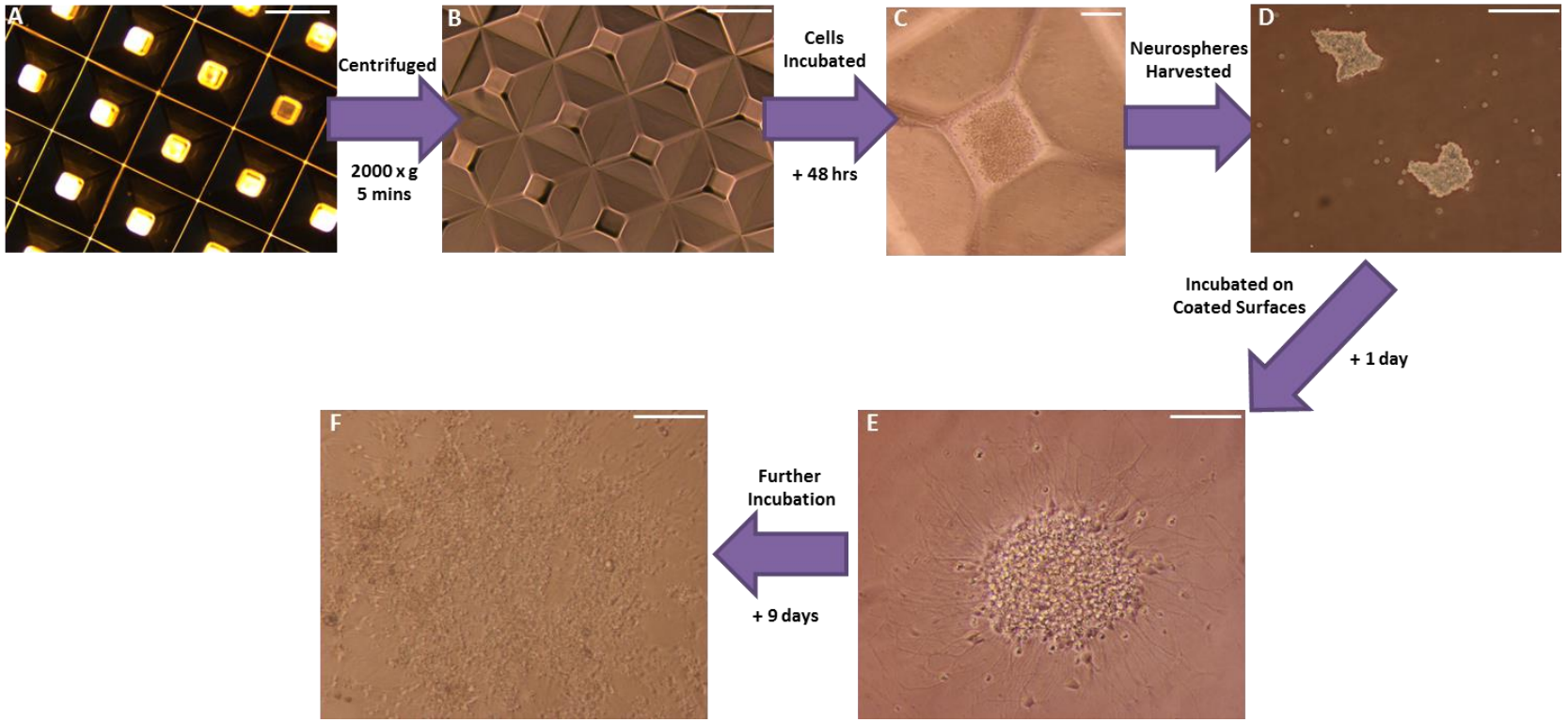

Fig 3-16: Formation of neurospheres from ReproNeuro, iPSC derived neuroprogenitor cells and 2D neurite outgrowth.
Phase contrast images showing the stages of neurosphere formation from ReproNeuro neuroprogenitor cells. AggreWell™ 880 plates were centrifuged at high speed to remove air bubbles from the microwells (A,B). ReproNeuro cells were seeded into the AggreWell™ plate and centrifuged to collect the cells in each microwell, they were then incubated for 48 hours to form spheroid structures (C) and harvested from the plate (D). Neurospheres were then cultured on 2D surfaces coated with ReproNeuro coating solution and incubated for 24 hours (E). Following 24 hours incubation, significant neurite outgrowth was visible under phase contrast; therefore cultures were fixed at this point. However, if further incubated for the full 10 day duration, neurospheres lost their structure as significant migration of cells from the spheroid structure was evident (F). Scale bars: A-B: 500 µm, C-F: 200 µm.

To characterise the growth and development of ReproNeuro neuroprogenitor cells, the cells were cultured as a monolayer in addition to neurospheres. Monolayer cultures of ReproNeuro cells examined via phase contrast microscopy (Figure 3-17A) reveal a large number of cells that have not adhered to the growth substrate, despite the adhesion promoting ECM-coating. This could be due to a loss of cell viability, as the manufacturer's cellular revival protocol states that a loss of viability may be likely during the revival of cells from cryopreservation. However, a number of cells have adhered to the 2D growth substrate and have extended long neuritic-like processes. Immunofluorescence staining for the pan-neuronal marker TUJ-1 (Figure 3-17B) highlights the extent of the cellular processes and confirms that they are in fact neurites. A large number of nuclei (blue) within the cellular monolayer appear to reside within colonies with TUJ-1 positive (green) extensions protruding from each colony.

Neurospheres formed from ReproNeuro cells and subsequently cultured in 2D conditions for 24 hours demonstrate extensive neurite outgrowth visible by phase contrast microscopy (Figure 3-17C). A large number of cellular processes can be observed to radiate from the central cellular mass and a few non-adherent cells are visible outside of the neurosphere. Immunofluorescence analysis of neurospheres cultured for 24 hours in 2D (Figure 3-17D) reveals TUJ-1 positive neurites (green) extending from the central neurosphere in a radial manner, whilst nuclei (blue) remain within the aggregate mass with no evidence of cellular migration.

ReproNeuro-derived neurospheres cultured in 3D (Figure 3-17E,F) upon ECM-coated Alvetex® scaffold, generate neurites that rather than radiating from the central cellular mass in 2D culture, penetrate the depth of the 3D material following 10 days in culture. The mass of the neurosphere containing a multitude of nuclei (blue) remains on top of the 3D material with no evidence of nuclear infiltration into the scaffold (Figure 3-17E). Neurites do not visibly radiate from the central scaffold as with 2D culture, but the bottom view of the scaffold (Figure 3-17F) confirms that neurites have penetrated the entire 200 μm depth of the material having exited the bottom of the scaffold.

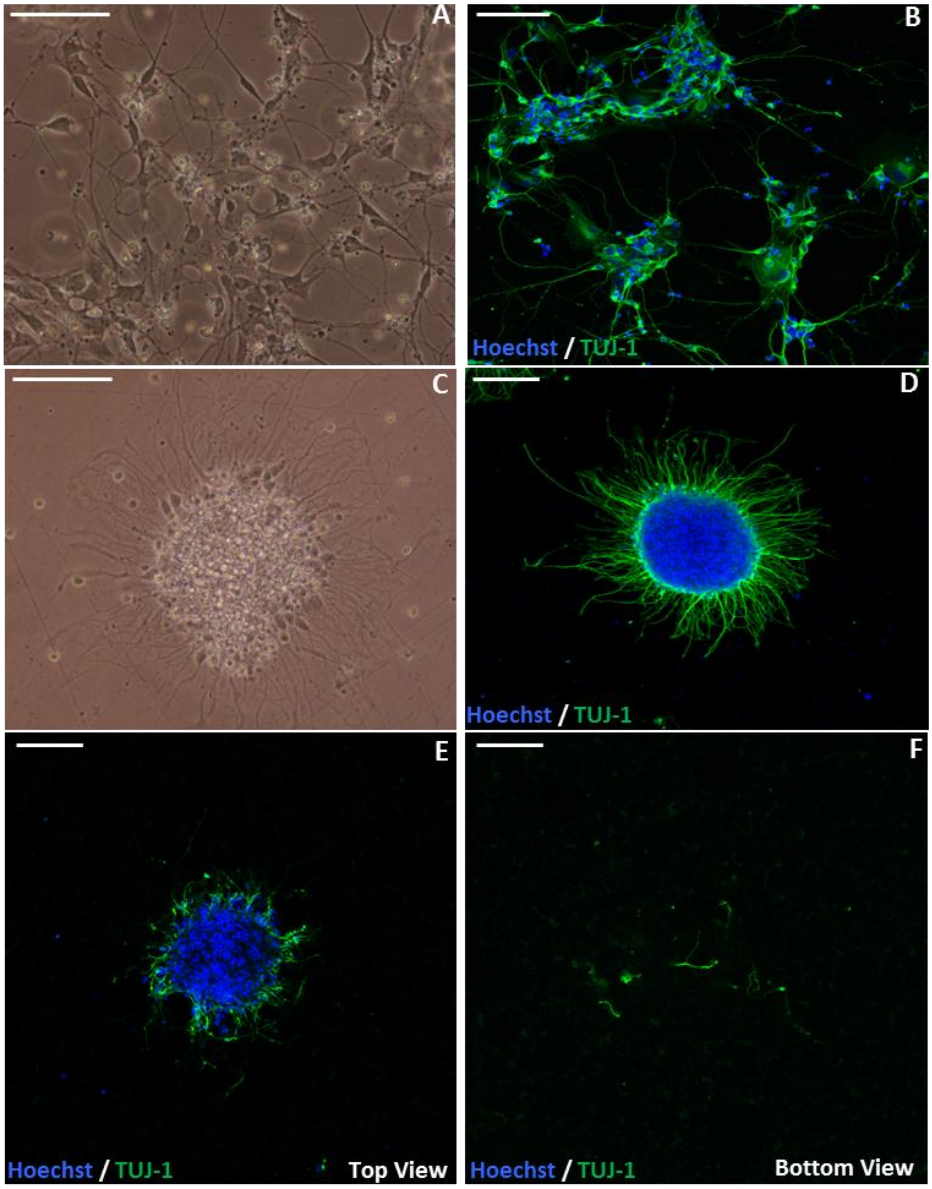

Fig 3-17: Development of a neurite outgrowth model from ReproNeuro, iPSC derived neuroprogenitor cells.
A representative phase contrast image of ReproNeuro cells cultured as a 2D monolayer (A) and an immunofluorescence image highlighting the pan-neuronal marker TUJ-1 (green) and nuclei (blue) (B). Extensive neurite outgrowth can be observed from neurospheres cultured in 2D conditions under phase contrast (C) and TUJ-1 (green) positive neurites can be seen extending from the central cellular aggregate, with nuclei (blue) mainly being confined to the spheroid structure (D). In 3D culture the neurospheres can be seen from the top view (E) of scaffold with nuclei being highlighted blue and TUJ-1 expression in green. From the bottom view of the scaffold (F) neurites can be seen to have penetrated the depth of the 3D material having exited from the bottom of the scaffold. Scale bars: 100 µm.

3.3.5.3 Potential Mechanisms to Enhance Neurite Outgrowth from iPSC-derived Neurospheres

This chapter also aims to identify the potential of Rho A and ROCK inhibition to enhance neurite outgrowth in iPSC-derived neurons. This involved the addition of Y-27632 and ibuprofen to inhibit ROCK and Rho A respectively, to 2D and 3D cultures of ReproNeuro-derived neurospheres. As described previously, 2D cultures were maintained with each compound only for 24 hours due to issues with cellular migration, whereas 3D cultures were maintained with compounds for the 10-day duration of the neurite outgrowth period. In addition to this, the neurotrophic effects of astrocytes within the CNS and the effect of this upon neurite outgrowth were also investigated due to the use of ReproNeuro MQ astrocyte conditioned medium.

3.3.5.3.1 Inhibition of ROCK by Y-27632

To investigate the ability of Y-27632 to enhance neuritogenesis, the small molecule inhibitor of ROCK was added to the culture medium of 2D ReproNeuro cultures at varying concentrations (0 – 15 μM) for the 24-hour neurite outgrowth phase of culture. Immunofluorescence staining (Figure 3-18A) highlighting expression for the pan-neuronal marker TUJ-1 (green) reveals little obvious difference in neurite extension between the concentrations tested. This could be due to the reduced culture period of 24-hours which may not be long enough to elicit the dramatic effects of Y-27632 as observed in the EC-cell derived model of neuritogenesis. However neurites that have extended from neurospheres cultured with 15 μM Y-27632 (Figure 3-17Ag,h) appear longer than those that were generated from neurospheres in the absence of the molecule (Figure 3-17Aa,b).

Quantification of the number of neurites per neurosphere (Figure 3-18B) reveals little difference between 0 μM and 0.5 μM treatment, however, 10 μM Y-27632 induced a significant increase in the average number of neurites per neurosphere. This enhancing effect of Y-27632 was lost at the highest concentration tested (15 μM). Similarly, the density of neurites surrounding each neurosphere (Figure 3-18C) appears to increase with Y-27632 concentration up to 10 μM Y-27632. The observation of 15 μM resulting in a reduction in the number of neurites per neurosphere was not observed when normalised to neurosphere size and expressed as neurite density.

The observation of neurite length increasing with Y-27632 treatment made during the analysis of the immunofluorescence images (Figure 3-18A) was confirmed by quantification detailing the average length of neurites (Figure 3-18D). All concentration of Y-27632 tested were found to induce a significant increase in neurite length compared with the untreated control, with 15 μM treatment resulting in the greatest enhancement

of neurite length. Although there is little evidence of cellular migration from ReproNeuro-derived neurospheres in 2D culture, Y-27632 was found to inhibit the little migration that does occur (Figure 3-18E). All concentrations of Y-27632 tested resulted in a distinct inhibition of cellular migration with 15 μM Y-27632 treatment resulting in a statistically significant inhibition.

ReproNeuro-derived neurospheres were also cultured in 3D (Figure 3-19A) for 10 days with the same range of concentrations of Y-27632 (0 – 15 μM). Neurospheres remain on top of the scaffold (Figure 3-19Aa,c,e,g) whilst TUJ-1 positive (green) neurites penetrate the depth of the 3D material and are visible from the underside of the scaffold (Figure 3-19Ab,d,f,h). Without Y-27632 treatment (Figure 3-19Aa,b), few neurites can be seen to have penetrated the depth of the 3D material and with 0.5 μM treatment (Figure 3-19Ac,d) almost no neurites are visible from the bottom view of the scaffold. However increasing Y-27632 concentration to 10 μM (Figure 3-18Ae,f) and 15 μM (Figure 3-19Ag,h) results in a larger number of visible neurites from the underside of the scaffold.

This is further evidenced by quantification of the number of neurites penetrating Alvetex® scaffold for each treatment condition (Figure 3-19B). Neurospheres cultured in 3D without Y-27632 treatment are seen to produce a small number of neurites that are able to fully penetrate the 3D material. Treatment with 0.5 μM Y-27632 resulted in an inhibition of neurite penetration, which was evident from the representative immunofluorescence images (Figure 3-19A) and treatment with 10 – 15 μM Y-27632 resulted in an enhancement of neurite outgrowth within the 3D culture environment. The highest concentration of Y-27632 tested, 15 μM resulted in a statistically significant increase in neurite penetration throughout the 200 μm depth of the scaffold in comparison to 0 – 0.5 μM Y-27632.

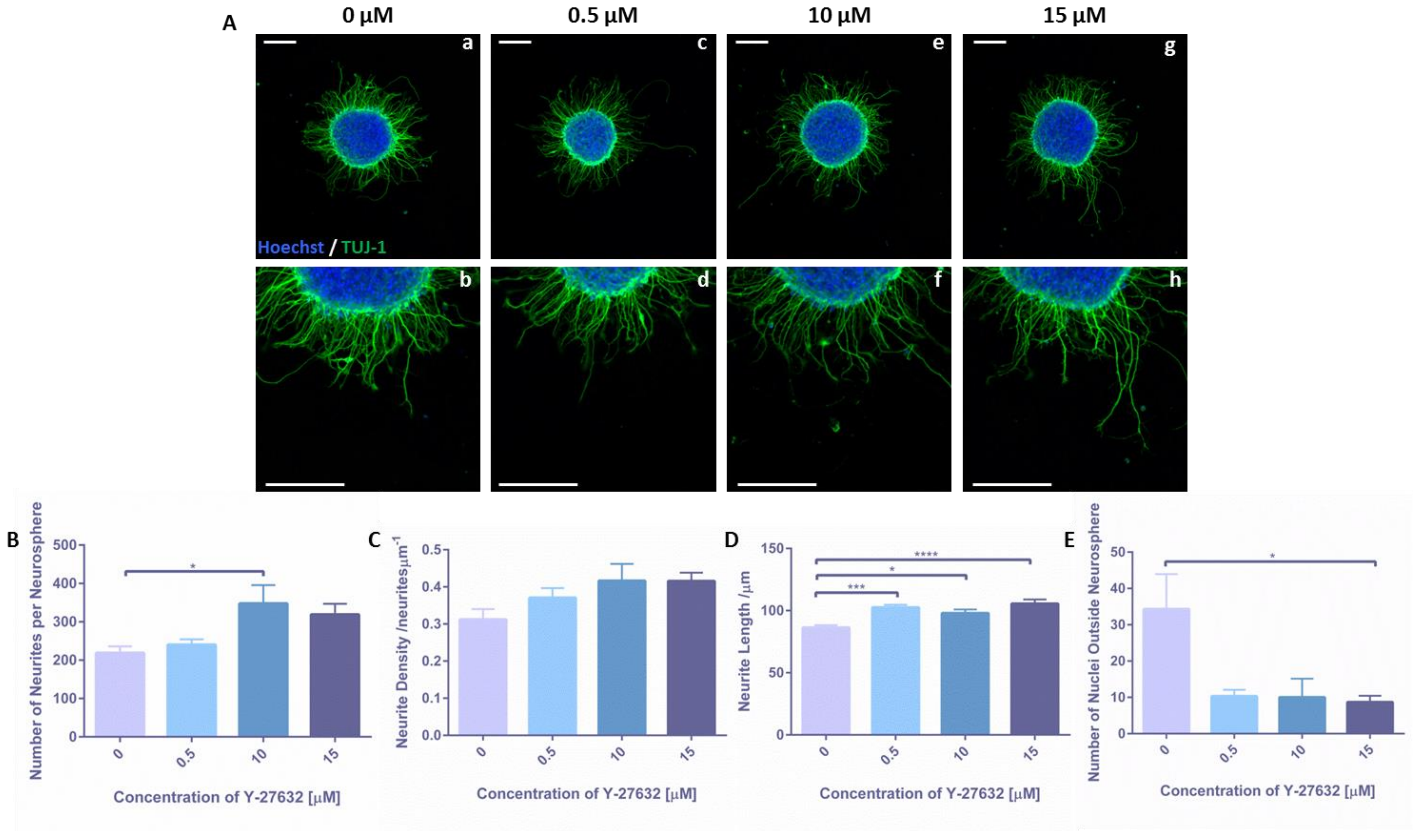

Fig 3-18: Enhancement of neurite outgrowth from ReproNeuro derived neurospheres by the selective ROCK inhibitor, Y-27632 in 2D culture.
Representative confocal images of ReproNeuro derived neurospheres cultured in 2D conditions with supplementation of the culture medium with increasing concentrations (0 – 15 µM) of Y-27632 (A). TUJ-1 positive neurites (green) can be seen to radiate from the central cellular aggregate with nuclei (blue) mainly being restricted to the aggregate body. Scale bars: 100 µm. The number of neurites per neurosphere (B) (data represent mean ± SEM, n=9; 3 neurospheres from 3 individual vials of frozen cells from the supplier) is significantly enhanced with the addition of 10 µM Y-27632 to the culture medium and when this is normalised to aggregate size, neurite density (C) (data represent mean ± SEM, n=9; 3 neurospheres from 3 individual vials of frozen cells from the supplier) increases in a dose dependent manner with increasing Y-27632 concentration. Similarly, neurite length (D) (data represent mean ± SEM, n=171-225; between 171-225 neurites were measured from 3 neurospheres obtained from 3 individual vials of frozen cells from the supplier) is enhanced with the supplementation of the culture medium with Y-27632, whereas migration of cells from the neurosphere (E) (data represent mean ± SEM, n=3; migration was measured from 1 neurosphere per vial of frozen cells from the supplier) significantly decreases with Y-27632 supplementation. Ordinary one-way ANOVA with Tukey's multiple comparison test: * = $p < 0.05$, ** = $p < 0.01$, *** = $p < 0.001$, **** = $p < 0.0001$.

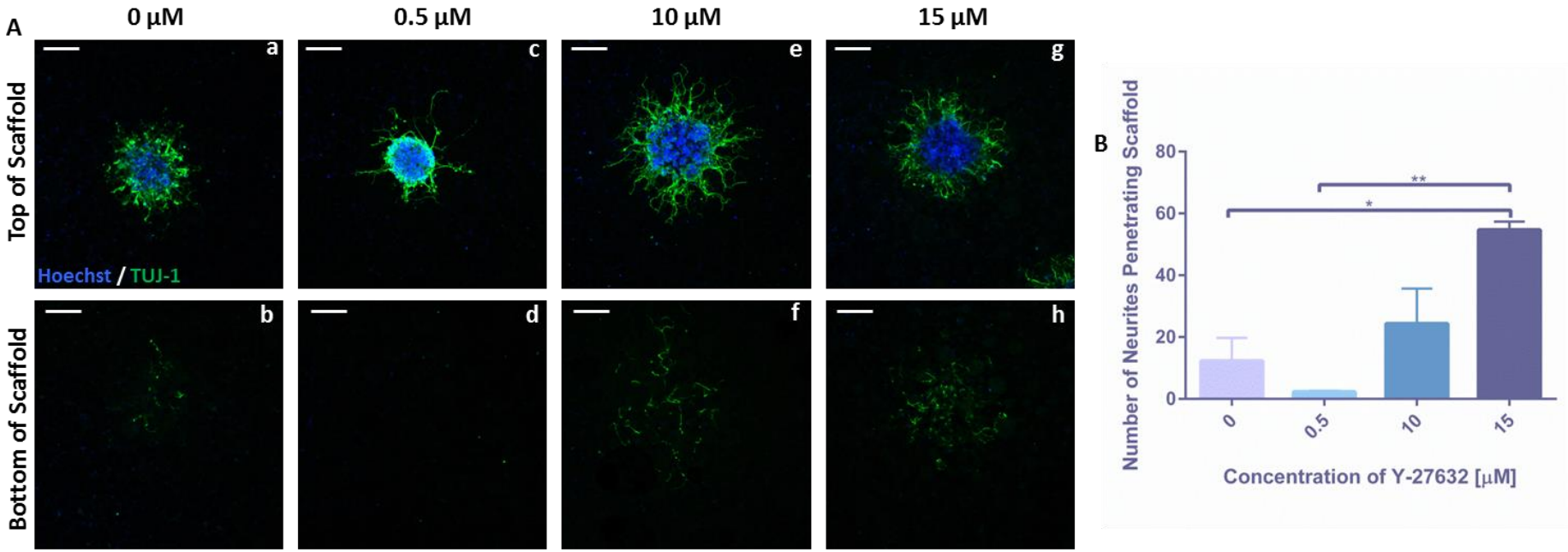

Fig 3-19: Enhancement of neurite outgrowth from ReproNeuro Glu derived neurospheres by the selective ROCK inhibitor, Y-27632 in 3D culture.
Representative confocal images of ReproNeuro derived neurospheres cultured in 3D with supplementation of the culture medium with increasing concentrations (0 – 15 µM) of Y-27632 (A). Neurosphere bodies can be seen from the top view of the scaffold (Aa,c,e,g) with nuclei (blue) being restricted to the cellular aggregate and TUJ-1 positive neurites (green) can be seen to have penetrated the depth of the 3D material from the bottom view of the scaffold (Ab,d,f,h). Scale bars: 100 µm. Quantification of the number of neurites that have penetrated the scaffold (B) (data represent mean ± SEM, n=3; neurite outgrowth from 3 neurospheres per scaffold was quantified and due to limited cell availability this was not repeated with multiple cell populations) with each Y-27632 concentration reveals that at higher concentrations (10 – 15 µM) neurite outgrowth is significantly enhanced within this 3D model of neuritogenesis. One-way ANOVA with Tukey's multiple comparisons: * = $p < 0.05$, ** = $p < 0.01$, *** = $p < 0.001$, **** = $p < 0.0001$.

3.3.5.3.2 Inhibition of Rho A by Ibuprofen

To investigate the ability of ibuprofen, an inhibitor of Rho A, to promote neurite growth from ReproNeuro-derived neurospheres in 2D culture, varying concentrations (0 – 500 μM) of the compound were added to the culture system for the 24-hour duration of the neurite outgrowth period. Immunofluorescence data (Figure 3-20A) highlighting expression of the pan-neuronal marker TUJ-1 (green) reveals the extent of neurite outgrowth from neurospheres cultured in each condition. Significant neurite outgrowth can be seen to radiate from neurospheres cultured in the absence of ibuprofen (Figure 3-19Aa,b) and ibuprofen treatment (10 – 500 μM) appears to result in the development of shorter neurites. Treatment with 500 μM (Figure 3-20Ag,h), particularly, appears to result in fewer, extremely short neurites.

Ibuprofen treatment results in an increase in the number of neurites per neurosphere (Figure 3-20B) with increasing concentration of ibuprofen, until the highest concentration of 500 μM is reached and neurite number reverts to a similar level as the untreated control. Treatment with 100 μM ibuprofen resulted in significantly more neurites per neurosphere than the untreated control, however this effect was lost at 500 μM, as significantly fewer neurites were generated than with 500 μM treatment. A similar effect was noted when this was normalised to neurosphere size and expressed as neurite density (Figure 3-20C), possibly as the size of neurospheres is well controlled due to the use of AggreWell™ plates during their formation. In terms of neurite density 100 μM induced a significant increase compared with the untreated control, which was lost at 500 μM, as neurite density returned to a level that was similar to the control.

Quantification of the average neurite length (Figure 3-20D) reveals a similar trend to that observed from the immunofluorescence data (Figure 3-19A). Ibuprofen treatment at all concentrations tested (10 – 500 μM) was found to significantly inhibit neurite length. Similarly, the migration (Figure 3-20E) of cells from the central cellular mass was also inhibited with all concentrations of ibuprofen treated.

Ibuprofen treatment was also found to have a similar effect in ReproNeuro-derived neurospheres cultured in 3D conditions. Neurospheres remained on top of the scaffold (Figure 3-21Aa,c,e,g) whilst TUJ-1 positive (green) neurites visible from the underside of the scaffold (Figure 3-20 Ab,d,f,h). Neurospheres cultured without ibuprofen treatment (Figure 3-21Aa,b) generate few neurites were visible from the bottom of the scaffold. Low concentrations of ibuprofen 10 μM (Figure 3-20Ac,d) appear to reduce the number of neurites visible from the underside of the scaffold, whereas 100 μM (Figure 3-21Ae,f) treatment appears to enhance the number of neurites that have visibly penetrated the

scaffold. Interesting 500 μM (Figure 3-21Ag,h) treatment, again appears to result in a reduction of the number of neurites that are visible from the underside of the scaffold.

Quantification of the number of neurites that have penetrated the scaffold (Figure 3-21B) demonstrates that low concentrations of ibuprofen such as 10 μM, result in a slight increase in neurite penetration into the scaffold. However, increasing the concentration of ibuprofen 10-fold to 100 μM results in a significant increase in neurite penetration of the scaffold. The highest concentration of ibuprofen tested, 500 μM, resulted in a decline in neurite penetration, with neurite outgrowth returning to a similar level as the control. This could be due to the reduction of neurite length observed in 2D culture, as if neurite length is inhibited then the number of neurites long enough to span the 200 μm depth of the scaffold will be reduced.

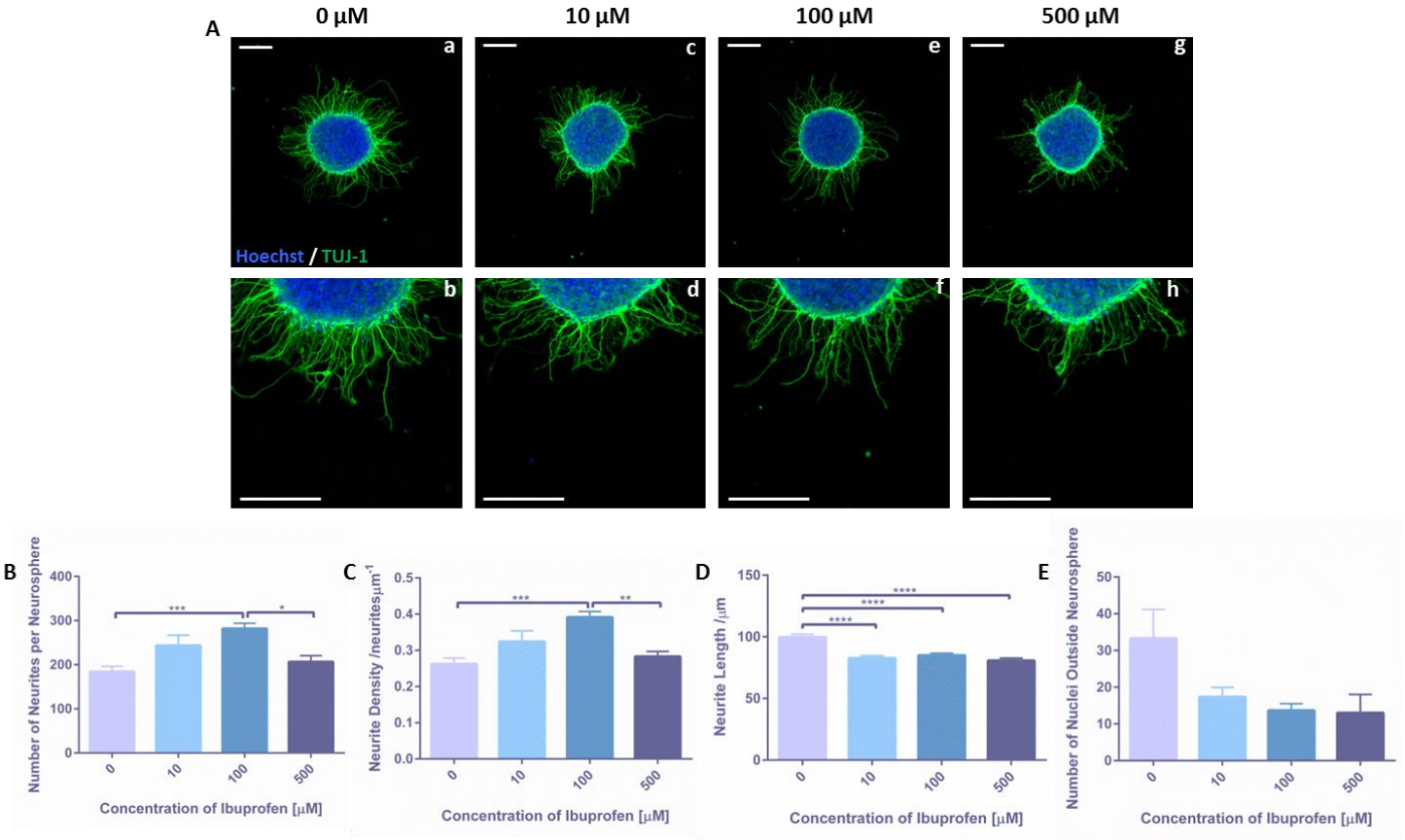

Enhancement of neurite outgrowth from ReproNeuro derived neurospheres in 2D culture by ibuprofen, an inhibitor of Rho A.
Representative confocal images of ReproNeuro derived neurospheres cultured in 2D with a range of concentrations (0 - 500 µM) of ibuprofen (A). Nuclei are stained in blue and the pan-neuronal marker, TUJ-1 in green, highlights neurites. Scale bars: 100 µm. Quantification of the number of neurites per neurosphere (B) (data represent mean ± SEM, n=9; 3 neurospheres from 3 independent vials of cryopreserved cells from the supplier) and the neurite density of the neurospheres (C) (data represent mean ± SEM, n=9; 3 neurospheres from 3 independent vials of cryopreserved cells from the supplier) reveals that neurite outgrowth is enhanced with ibuprofen up to the highest concentration tested, 500 µM, at which point the level of neuritogenesis returns to that of the control. However, neurite length (D) (data represent mean ± SEM, n=141-256; between 141-256 neurites in total were measured from 3 neurospheres each from 3 independent vials of cells) and cellular migration from the neurospheres (E) (data represent mean ± SEM, n=3; due to limited cell availability 3 neurospheres from 1 population of cells were quantified) are both inhibited by the supplementation of the culture medium with ibuprofen. One-way ANOVA with Tukey's multiple comparisons: * = $p < 0.05$, ** = $p < 0.01$, *** = $p < 0.001$, **** = $p < 0.0001$.

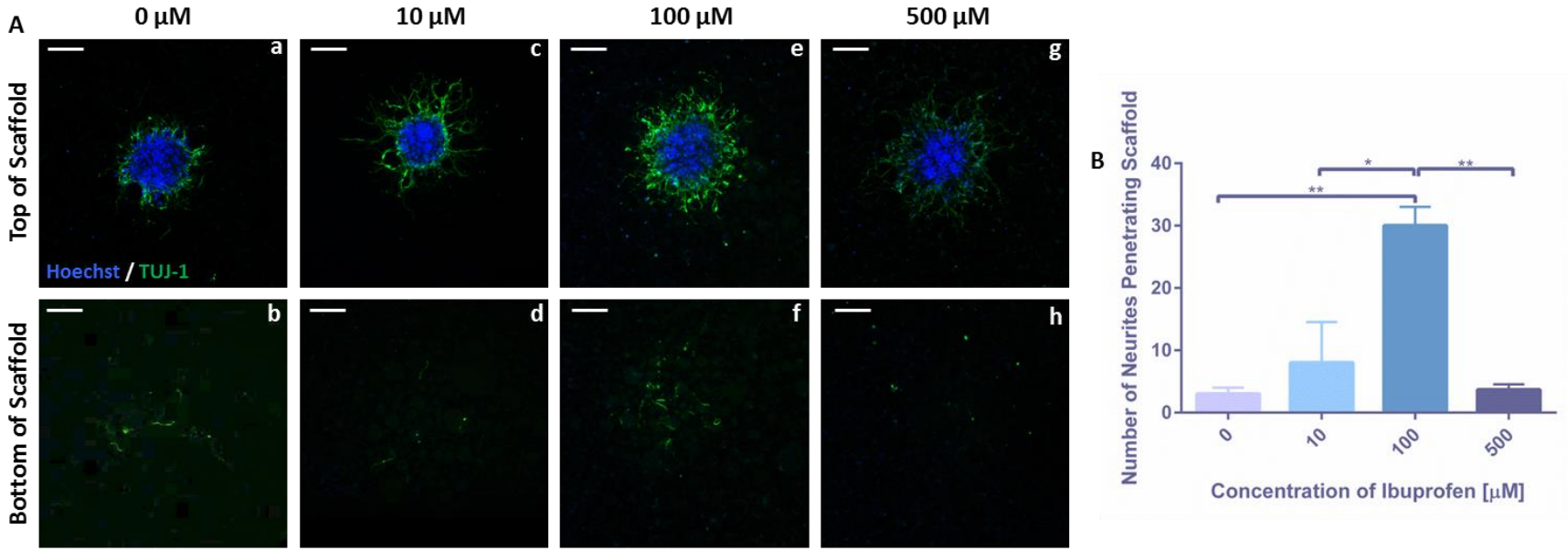

Fig 3-21: Enhancement of neurite outgrowth from ReproNeuro derived neurospheres in 3D culture by ibuprofen, an inhibitor of Rho A.
Representative confocal images of ReproNeuro derived neurospheres cultured in 3D with a range of concentrations (0 - 500 µM) of ibuprofen (A). Neurospheres can be seen to remain on top of the scaffold (Aa,c,e,g) with nuclei being stained blue, and TUJ-1 positive neurite (green) can be observed to have penetrated the depth of the 3D material and are visible from the bottom view of the scaffold (Ab,d,f,h). Scale bars: 100 µm. Quantification of the number of neurites to have penetrated the scaffold (B) (data represent mean ± SEM, n=3; neurite outgrowth from 3 neurospheres per scaffold was quantified and due to limited cell availability this was not repeated with multiple cell populations) reveals that at lower concentrations of ibuprofen (10 – 100 µM) neurite outgrowth is enhanced from the control, however at the highest concentration of ibuprofen (500 µM) neurite outgrowth returns to a similar level as the control. One-way ANOVA with Tukey's multiple comparisons: * = $p < 0.05$, ** = $p < 0.01$, *** = $p < 0.001$, **** = $p < 0.0001$.

3.3.5.3.3 Neurotrophic Effects of Astrocyte Conditioned Medium

Astrocytes within the CNS are known for the metabolic support that they provide to neurons, particularly glutamate metabolism[213–216]. It is also well known that astrocytes secrete trophic factors such as soluble growth factors including nerve growth factor (NGF) that promote and support the growth of neurons[217–219]. For this reason astrocyte conditioned medium such as ReproNeuro MQ medium is thought to contain neurotrophic factors and has been designed for use with ReproNeuro cells. Previously ReproNeuro MQ medium has been demonstrated to enhance electrophysiological recordings from ReproNeuro cells[212]. This sub-section aims to address the role of MQ astrocyte conditioned medium within the ReproNeuro model of neurite outgrowth, and its ability to potentially enhance neurite outgrowth.

Therefore, the hypothesis that ReproNeuro MQ medium, conditioned by astrocytes, contains soluble factors that may promote neurogenesis and enhanced functionality of the cultured neurons, led to the theory that this medium may also be able to enhance neurite outgrowth within this ReproNeuro-based model of neuritogenesis. This was first assessed within the 2D culture environment and immunofluorescence staining for TUJ-1 (green) (Figure 3-22A) revealed that those neurospheres cultured in MQ medium (Figure 3-22Ac,d) appear to produce more neurites which are longer compared to the their control medium counterparts (Figure 3-22Aa,b). Supplementation of MQ medium with 10 μM Y-27632 (Figure 3-22Ae,f) or 100 μM ibuprofen (Figure 3-22g,h) did not appear to make any noticeable difference in the neurite outgrowth except perhaps Y-27632 treated neurites may be a little longer than those cultured in MQ medium alone.

Quantification of the number of neurites per neurosphere (Figure 3-22B) supports the observations made on the basis of the immunofluorescence data. Neurospheres cultured in MQ medium produce significantly more neurites than those cultured in control ReproNeuro medium and Y-27632 supplementation of MQ medium further enhances neurite outgrowth. Supplementation of MQ medium with ibuprofen however, appears to induce inhibition of neurite outgrowth compared with MQ medium alone. Similarly neurite density (Figure 3-22C) is enhanced significantly by MQ medium alone and with and Y-27632 supplementation. However the neurite density of the neurospheres is significantly reduced to a level that is similar to ReproNeuro control medium, in the presence of 100 μM ibuprofen.

Similarly, neurite length (Figure 3-22D) is significantly enhanced by MQ medium and further enhanced by the addition of 10 μM Y-27632. Although the average neurite length is inhibited with the addition of ibuprofen to MQ medium, neurites are still significantly

longer than those generated in control ReproNeuro medium, however the neurite enhancing effects of MQ medium are reduced.

A similar observation was made in 3D culture, as those neurospheres cultured in control ReproNeuro medium appear to produce few neurites capable of penetrating the entire depth of the scaffold, as visible from the bottom view (Figure 3-23Aa,b). However neurospheres cultured in MQ medium appear to generate a large amount of neurites that are visible from the underside of the scaffold (Figure 3-23Ac,d). MQ medium supplementation with both 10 μM Y-27632 (Figure 3-23Ae,f) and 100 μM ibuprofen (Figure 3-23Ag,h) seem to have an inhibitory effect upon neurite outgrowth in 3D culture, as fewer neurites are visible from the underside of the scaffold.

The number of neurites penetrating the scaffold (Figure 3-23B) for each condition resulted in both ReproNeuro and MQ media producing a similar amount of neurites capable of complete penetration of the scaffold. However, both supplementation with Y-27632 and ibuprofen was found to significantly inhibit neurite penetration compared with MQ medium alone. This could perhaps be due to Y-27632 or ibuprofen induced inhibition of neurite length as demonstrated in the 2D TERA2.cl.SP12-based model of neuritogenesis however, this effect has not been observed in ReproNeuro derived neurites cultured in 2D.

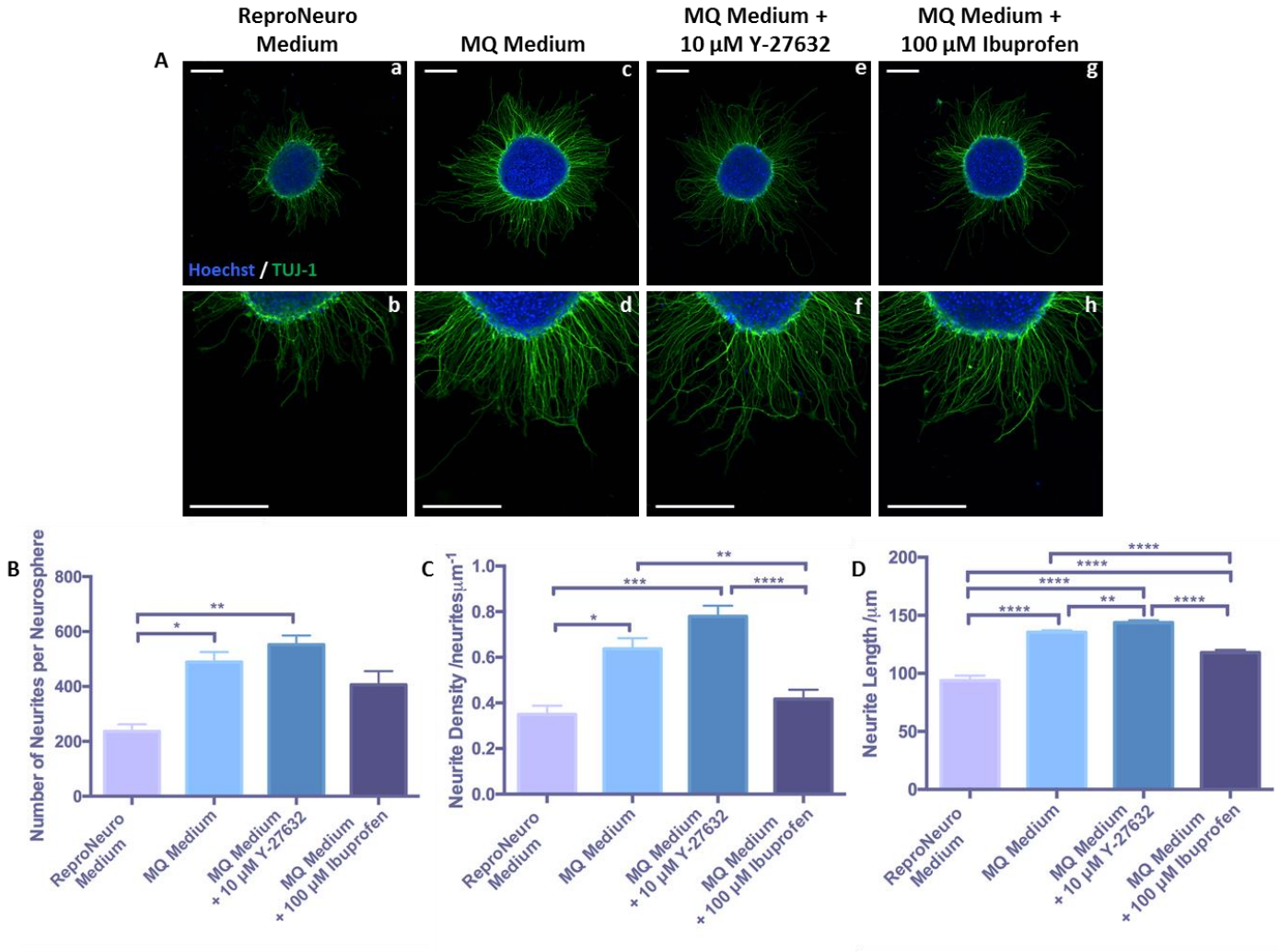

Fig 3-22: Enhancement of neurite outgrowth from ReproNeuro derived neurospheres through a combination of conditioned medium and inhibition of Rho/ROCK signalling in 2D culture. Representative confocal images (A) of ReproNeuro derived neurospheres cultured in 2D with standard ReproNeuro medium (Aa,b) or astrocyte conditioned, MQ medium (Ac,d) in combination with the selective ROCK inhibitor, Y-27632 (Ae,f) or ibuprofen (Ag,h). Neurite outgrowth is highlighted by staining for the pan-neuronal marker, TUJ-1 and nuclei are stained in blue. Scale bars: 100 µm. Quantification of the number of neurites per neurosphere (B) (data represent mean ± SEM, n=3-9; neurite outgrowth from 1-3 neurospheres was quantified per vial of cells from the supplier, of which there were 3), neurite density of the neurospheres (C) (data represent mean ± SEM, n=3-9; neurite outgrowth from 1-3 neurospheres was quantified per vial of cells from the supplier, of which there were 3) and neurite length (D) (data represent mean ± SEM, n=64-463; the length of 64-463 neurites was measured from 1-3 neurospheres per vial of cells from the supplier, of which there were 3) demonstrate that all three aspects of neurite outgrowth are enhanced with the MQ medium and can be further enhanced by Y-27632 supplementation. One-way ANOVA with Tukey's multiple comparisons: * = $p < 0.05$, ** = $p < 0.01$, *** = $p < 0.001$, **** = $p < 0.0001$.

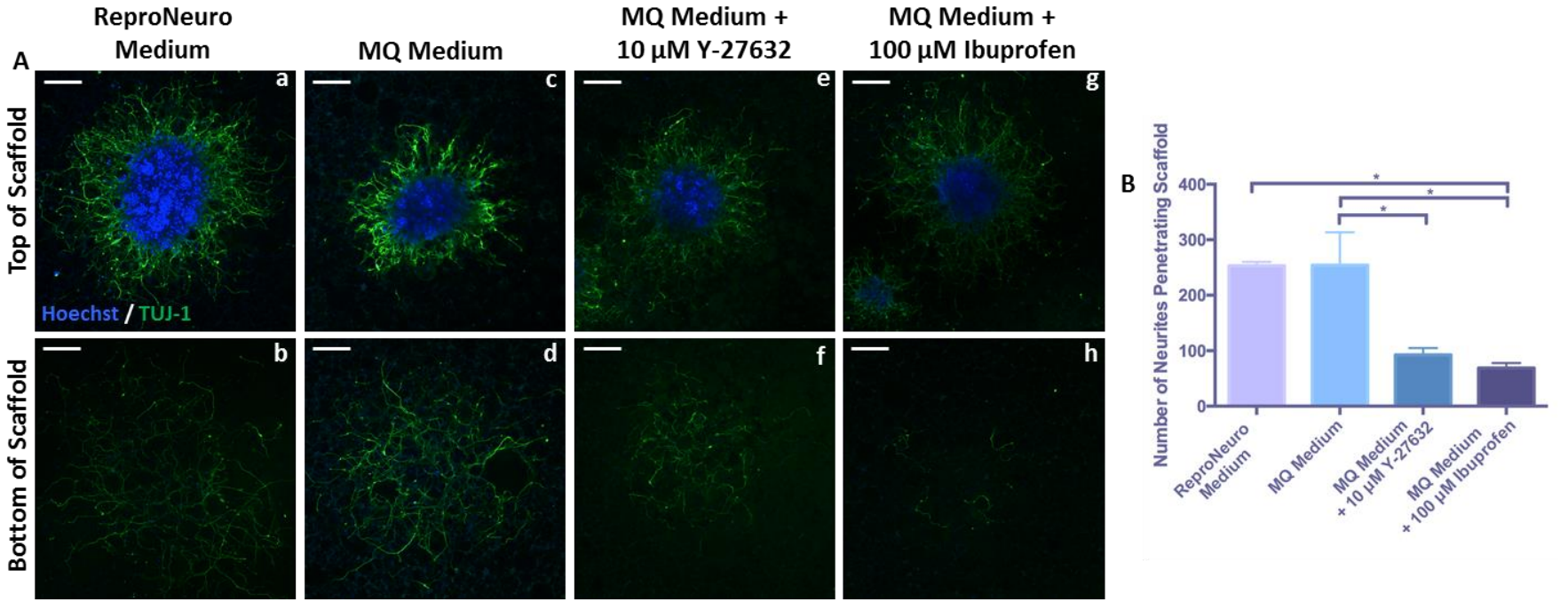

Fig 3-23: The effect of astrocyte-conditioned medium on 3D neurite outgrowth from ReproNeuro derived neurospheres.
Representative confocal images (A) of ReproNeuro derived neurospheres cultured in 3D with standard ReproNeuro medium (Aa,b) or astrocyte conditioned, MQ medium (Ac,d) supplemented with Y-27632 (Ae,f) or ibuprofen (Ag,h). Neurospheres remain on the top of the scaffold (Aa,c,e,g) with nuclei being stained blue, whilst TUJ-1 positive (green) neurites can be seen to have penetrated the depth of the 3D material (Ab,d,f,h). Scale bars: 100 µm. Quantification of neurite penetration (B) (data represent mean ± SEM, n=3; neurite outgrowth from 3 neurospheres per scaffold was quantified and due to limited cell availability this was not repeated with multiple cell populations) reveals that a similar number of neurites penetrate the scaffold with both ReproNeuro and MQ media but supplementation with Y-27632 and ibuprofen inhibits the number of neurites that penetrate the scaffold. One-way ANOVA with Tukey's multiple comparisons: * = $p < 0.05$, ** = $p < 0.01$, *** = $p < 0.001$, **** = $p < 0.0001$.

3.4 Discussion

Neuritogenesis is an important developmental process that promotes the formation of complex neuronal signalling pathways, essential to the proper functioning of the nervous system. Inability of neurons to undergo neuritogenesis and the resultant inhibition in neuronal connectivity is common to many nervous system disorders. Impaired neurite outgrowth has been implicated in a wide range of nervous system pathologies including spinal cord injury[26,33,34,39,220], Down's syndrome[43,221] and schizophrenia[42] along with Alzheimer's[35,36] and Parkinson's disease[37]. As neurite inhibition is common to such a large variety of nervous system disorders, there is need for a well-characterised and physiologically representative model of neuritogenesis that has the ability to screen potential drug candidates and recover inhibitory responses to provide possible therapeutic strategies.

Current *in vitro* neurite outgrowth models are usually based on the culture of stem cells[21,66–68], cancer cells[104–106] or primary animal derived cells[64,222,223] in monolayers. However, monolayer cultures can prove difficult to quantify, as it may not be possible to trace each individual neurite back to its parental cell body within an intricate neurite network using image analysis software[224]. The neurite outgrowth methodologies described within this chapter involve the application of spheroid culture techniques to generate neurite outgrowth radially from a single cellular aggregate. This produces a neurite outgrowth assay where neurites can be easily traced, combined with an efficient sampling method to enhance quantification, which is more amenable to scaling up and high throughput screening.

3.4.1 Development of a Novel Human Pluripotent Stem Cell Derived Model of Neuritogenesis

3.4.1.1 Embryonal Carcinoma Cell Based Model of Neurite Outgrowth

The first neurite outgrowth model described within this chapter is based upon neural differentiation of a human embryonal carcinoma cell line TERA2.cl.SP12. The initial optimisation process in the development of this model of neuritogenesis involved the selection of appropriate differentiation conditions.

Retinoic acid (ATRA), the naturally occurring metabolite of vitamin A has traditionally been used to promote neural differentiation *in vitro*[45,64,67,75,78,111,145]. However, there are many problems associated with ATRA use including chemical instability, which results in the breakdown of the compound when exposed to light and heat i.e laboratory conditions[79]. This can give rise to many inconsistencies and variations within culture

models. For this reason the ability of synthetic retinoid analogues to induce neural differentiation and neurite outgrowth from TERA2.cl.SP12 cells was addressed. Both EC23 and AH61 have previously been demonstrated to significantly enhance neural differentiation compared with ATRA[83,84] and the findings within this Chapter support this. The synthetic retinoid EC23 was found to be a potent inducer of neurite outgrowth to a much greater extent than AH61 and EC23. This was particularly noted at lower concentrations, as EC23 had a greater effect upon reduction of stem cell markers and induction of neuronal markers. The increased neuronal differentiation effects of EC23 evidenced within this Chapter are most likely due to increased stability of the molecule and potency in comparison with ATRA, as EC23 contains a non-isomerisable conjugated linker unit that does not readily isomerise[83,84]. The optimum differentiation conditions of 0.01 μM EC23 were selected for use throughout the remainder of the project.

This TERA2.cl.SP12 based model of neuritogenesis also has the advantage of being derived from human cells, therefore is more relevant for the study of human diseases that those models based on primary animal cells. Characterisation of this model and assessment of markers associated with neurite development *in vivo* is consistent with previously published evidence[69–72,146,148]. Expression of known cytoskeletal markers over time indicate that neurite outgrowth observed in the model shares similarities with the early stages of nervous system development. Neurofilament (NF) proteins are expressed heterogeneously throughout the developing nervous system[225–229] and expression of NFs throughout the culture period is as expected. Similarly, nestin a known marker of neural stem cells[230–233] is expressed very early in the neurite outgrowth period of culture, prior to neurite extension, as would be expected. Therefore, this suggests that neurite outgrowth within the model is conserved and undergoes a similar process as developing neurons *in vivo*.

Many widely adopted *in vitro* models of neurite outgrowth generally utilise conventional 2D cell culture methods, however this is not physiologically representative as neurites develop within 3D space *in vivo*. Traditional 2D culture techniques have their limitations as the growth of cells upon 2D substrates is far removed from the complex environment that cells experience *in vivo*[161,162]. When cultured in a 2D environment, cells flatten and their cytoskeleton becomes remodeled resulting in changes that do not resemble the function of their *in vivo* counterparts[161,162].

Previously, 3D cell culture technology has been used to enhance neuritogenesis from a stem cell-derived model[147,150]. Therefore, the development of a physiologically relevant model of neurite outgrowth within this Chapter has involved the combination of stable synthetic retinoids with a robust neurosphere generation technique and quantifiable neurite outgrowth in 2D and 3D culture. The culture of neurospheres within a 3D

environment results a more physiologically relevant geometry for the development of neurites, limiting some of the problems associated with 2D culture. This is particularly important to enable confidence that findings obtained *in vitro* are representative of *in vivo* processes such as predictions as to the suitability of molecules as potential therapeutics[162].

There is need for a robust and reproducible, physiologically relevant model of human neurite development, as this process is impaired in such a vast range of neurological pathologies. A reliable model of neuritogenesis such as the EC-derived model described in this chapter, has many applications ranging from screening of potential drug candidates for neurotoxicity or the ability of drugs to overcome inhibitory stimuli, investigations into the molecular signalling events that underpin neurite inhibition in disease and also studies into the developmental process of neuritogenesis itself.

3.4.1.2 Induced Pluripotent Stem Cell Based Model of Neurite Outgrowth

In addition to the TERA2.cl.SP12 model of neurite development, this chapter also describes the optimisation and development of an iPSC-derived model of neurite outgrowth. iPSC-based *in vitro* models have many advantages over other systems including that they are human derived[124]. In addition to this as, iPSC cells can be obtained directly from patients in a minimally invasive manner, there is an opportunity to provide patient specific *in vitro* models for drug screening[124,234] and disease specific *in vitro* models of complex neurological diseases[157,235–238], that otherwise would be modeled by more basic systems that are unable to recapitulate multiple aspects of the disease.

The cells described in this chapter are iPSC-derived neuroprogenitor cells that include ReproNeuro Glu cells, and ReproNeuro cells. ReproNeuro Glu cells produce a population of predominantly glutamatergic neurons, whereas ReproNeuro cells produce a population of neurons containing mixed subtypes[212,234]. ReproNeuro are the first commercially available human iPSC-derived neuroprogenitor cells and since their isolation have been used in electrophysiology[212], dopamine metabolism[210], oxidative stress[239] and brain development studies[211]. However, they have yet to be reported to form the basis of a study with the primary objective of assaying neurite outgrowth.

As described previously, spheroid-based neurite outgrowth models where neurites radiate from the central aggregate structure have advantages over traditional monolayer assays in terms of quantification. For this reason AggreWell™ technology was employed to generate ReproNeuro-derived spheroid structures. AggreWell™ plates are often used to generate embryoid bodies in the culture of ES cells[240–244], however here; the plates have been used to generate neurospheres from differentiated neuroprogenitor cells. At this

point potential differences between the two ReproNeuro cell lines became evident. ReproNeuro Glu cells readily formed spheroids within 24 hours whereas, ReproNeuro cells required at least a 48-hour incubation before 3D structures were visible. This perhaps suggests an inherent difference in cell-cell adherence between the two cell lines.

Furthermore, once spheroids were seeded for the neurite outgrowth phase of culture, differences in cellular migration became apparent. Cultures of both cell lines were observed daily by phase contrast microscopy to track the progress of 2D cultures. Following 24 hours in culture, both cell lines had produced a large number of neurites, visibly radiating from the neurosphere. However as the neurite outgrowth period progressed, ReproNeuro Glu neurospheres cultured in 2D retained their structure and cultures were analysed at 10 days. Whereas, ReproNeuro neurospheres cultured in 2D had completely lost their structural integrity as a large mass of cells had migrated from the cellular aggregate. ReproNeuro cultures were therefore analysed at 24 hours post neurosphere seeding rather than the standard 10-day neurite outgrowth period. This may be a limitation of the ReproNeuro model, as depending upon the application, cultures may need to be maintained for a duration greater than 24 hours and the effects of certain molecules may require a longer culture period to become evident.

Therefore, ReproNeuro cells appear to exhibit variations in cellular adhesion and migration compared with ReproNeuro Glu cells. This could be due to the inherent differences between the cell lines, in that the ReproNeuro lineage gives rise to a heterogenous population of neuronal subtypes that may express variances in adhesion and migration behaviour[212,234]. It could also be due to differential expression of components in key biological pathways that underpin these important cellular processes. For example Rac/cdc[245–248], integrins[249–253], focal adhesions[254–257] and cellular junctions[258] are all involved in cellular adhesion and migration. Interestingly, cellular adhesion, migration and neurite outgrowth are all interconnecting processes[259–261], and an impaired ability of cells to form adhesions and migrate, may impact their ability to form neurites.

In addition to this 2D model of neuritogenesis, similarly to the TERA2.cl.SP12 outgrowth model, ReproNeuro derived neurospheres were also cultured in a 3D environment to produce a more physiologically relevant model[162]. The aim of this was to produce a more physiologically accurate depiction of the process of neuritogenesis that occurs *in vivo* and provide a more reliable model with which to study the developmental process and to screen potential drug candidates.

iPSC-derived *in vitro* models are useful in the study of complex diseases, as iPSCs can be obtained from patients with specific mutations or phenotypes and subsequently differentiated into the cell type of interest[124,125,234]. This is particularly relevant in terms of

neurobiology, as neurodegenerative diseases including Alzheimer's and Parkinson's disease are multi-faceted, complex diseases[262–266] and *in vitro* modelling generally only recapitulates limited aspects of the disease. Similarly, interest in personalised medicine is increasing, as iPSC technology allows for the isolation of a somatic cell from a patient, reprogramming and differentiation, to produce patient specific *in vitro* models that can be used to assess the suitability of a drug on a patient-to-patient basis[124]. However iPSC-based models also have limitations such as expensive consumables associated with their culture and production difficulties in terms of their manufacture. For these reasons the use of iPSC-derived neurospheres throughout this project is limited to the areas where it was thought to be most beneficial (Alzheimer's disease modelling – Chapter V) and the most widely used neurite outgrowth assay throughout this project is the better-characterised TERA2.cl.SP12-based model.

3.4.2 Mechanisms to Enhance Neurite Outgrowth from Existing Neurite Outgrowth Models

Many studies that focus on the development of robust models of neurite outgrowth also assess potential mechanisms by which to enhance their models. This can be achieved through a number of approaches including reducing inhibitory signalling (inhibition of Rho A-mediated signalling)[21], electrical stimulation[267–270], providing a permissive growth substrate (ECM coatings)[271–275], co-culture with supporting cells[276–278] or addition of exogenous growth factors to cultures[15,279–282]. Another focus of this chapter is to assess the effect of inhibition of Rho A and its downstream signalling pathway along with the use of astrocyte conditioned medium as methodologies to enhance neurite outgrowth in both EC and iPSC-based models of neuritogenesis.

3.4.2.1 Inhibition of Rho A and ROCK Signalling

The actin cytoskeleton along with the signalling events that control its function, are integral in the formation and extension of neurites within the nervous system. Rac 1 and Cdc42 are responsible for the promotion of membrane breaching by stimulating actin destabilisation and polymeration[14,17,283,284]. Whereas, activation of Rho A and downstream ROCK is responsible for stabalisation of actin filaments, inhibition of membrane breaching and growth cone stalling[14,17,283,284]. Neurite growth is dependant upon a balance between these two signalling pathways. As a strategy to enhance neurite outgrowth within their models many *in vitro* assays opt for the inclusion of inhibitors of Rho A (C3 transferase, ibuprofen) or ROCK (fasudil, Y-27632) in their basic methodology[21,23,203]. Data within this chapter addresses the use of ibuprofen and Y-27632 to enhance neurite outgrowth within both TERA2.cl.SP12 and ReproNeuro 2D and 3D models of neuritogenesis.

In 2D neurite outgrowth cultures of TERA2.cl.SP12 treated with both Y-27632 and ibuprofen, a similar effect is observed. This is as expected as both Y-27632 and Rho A inhibit different components of the same signalling pathways. Both molecules are noted to enhance neurite number and density significantly but significantly inhibit neurite length, particularly at high concentrations. This may suggest reciprocal control of neurite number and length, perhaps due to the role of Rho A and ROCK in the stabilisation of actin filaments. Inhibition of these signalling events may enhance membrane breaching and neurite formation, however as actin filament stabilisation is reduced, filament extension, thus neurite length may also be reduced. However, a more in depth analysis of the actin dynamics in Y-27632 and ibuprofen treated neurites would be required to confirm this.

A similar effect is noted in the ReproNeuro 2D model of neuritogenesis as both Y-27632 and ibuprofen were generally found to enhance neurite number and density but only ibuprofen was found to inhibit neurite length. This variation in response to Y-27632 in ReproNeuro cells could be due to altered Rho A and ROCK signalling within the cell line, as hypothesised previously. However, other *in vitro* models based upon foetal-derived neurons or DRG cultures provide evidence that Rho A and ROCK inhibition can enhance neurite length[28,285–287]. This could be due to the fact that most studies incubate their cultures with such supplements for short time frames with the incubation period described by Fuentes *et al* only consisting of 8 hours[286]. The data described within this chapter was obtained following a 10-day incubation with each molecule. It could therefore be hypothesised that inhibition of Rho A and ROCK may enhance neurite length in short-term cultures, but neurite extension may slow over time resulting in a reduction in length in longer-term cultures.

An inhibition in migration of cells from the central body of the neurosphere is consistently observed in 2D cultures of TERA2.cl.SP12 and ReproNeuro cultures treated with Y-27632 and ibuprofen. This may be expected as GTPase signalling and actin dynamics are both heavily implicated in the process of cellular migration. During cell migration activation of Rac is required at the front edge of the cell to promote actin polymerisation and membrane protrusion, similar to its role in neurite extension[288–290]. However, Rho A is thought to regulate the contraction and retraction forces required for cellular propulsion at the rear of the cell and its cellular distribution is inverse to that of Rac[288–290]. The role of Rho A in cellular migration supports the observations made in this chapter as inhibition of Rho A may lead to inhibition of cellular propulsion forces required for migration. There is little focus in the literature on the role of Rho A/ROCK inhibition in cellular migration. However evidence to support this finding is described in a study by Wang *et al* who use Y-27632 to inhibit migration in tongue squamous cell carcinoma cells[291]. Similarly, Imamura *et al* describe the ability of Y-27632 to suppress tumour cell invasion[292].

More physiologically relevant 3D models of neuritogenesis based upon TERA2.cl.SP12 and ReproNeuro cells are also described in this chapter. 3D cell culture in the form of Alvetex® scaffold provides a more physiological geometry and microenvironment for the development of neurites, therefore this is thought to overcome some of the problems associated with 2D culture and provide experimental outcomes more representative of the *in vivo* situation[162]. Treatment of 3D cultures with Y-27632 and ibuprofen produced consistent results amongst the two cell lines. Y-27632 was found to enhance neurite outgrowth in 3D in a dose dependent manner, whilst ibuprofen was found to enhance neurite outgrowth in a similar manner, however at the highest concentrations tested was found to reduce neurite outgrowth. A reason for this apparent reduction in neurite outgrowth by ibuprofen in 3D culture could be that the 3D system involves the quantification of neurites that have penetrated the 200 μm depth of the scaffold. In 2D culture ibuprofen was found to inhibit neurite length, therefore in 3D cultures fewer neurites may be able to traverse the 200 μm depth of the 3D material for quantification.

Therefore, data within this chapter demonstrates the ability of a range of inhibitors of Rho A and ROCK to enhance neurite outgrowth in two human pluripotent stem cell derived models of neurite outgrowth in 2D and 3D culture. The addition of Y-27632 and ibuprofen to the culture medium could be incorporated into the model methodology to provide an enhanced neurite outgrowth model for applications such as neurotoxicity testing and study of neurite inhibition. However, the main aim of this project and application of such models is to study the role of neurite inhibition in neurological disorders and both Y-27632 and ibuprofen have been well documented in the literature to promote neurite regeneration in the presence of inhibitory stimuli[26,27,36]. Therefore the decision was made not to include small molecule supplementation (Y-27632 and ibuprofen) in the basic model protocol, as this could reduce the sensitivity of the model to inhibitory molecules and also have adverse effects upon neurite length.

3.4.2.2 Neurotrophic Effects of Astrocytes

Astrocytes are glial cells that are distributed throughout the nervous system and provide metabolic support to neurons through a number of functions including, regulation of blood flow, ion homeostasis, synapse function and metabolism[293,294]. The effects of soluble factors secreted by astrocytes and astrocyte-conditioned medium, upon a range of biological functions have been investigated including, the blood brain barrier and brain vasculature[295–298], oligodendrocye development[299] and ion transport[300]. However little is known about the effect of astrocyte-conditioned medium upon neurite outgrowth and elongation.

The constituents of astrocyte-conditioned medium depend upon the phenotype of the astrocytes cultured within the medium. For example, astrocytes that have adopted a reactive phenotype secrete chondroitin sulphate proteoglycans (CSPGs) that are inhibitory to neurite development[33,39,220,301]. However, astrocyte conditioned-medium has also been found to contain growth factors such as an insulin-like factor thought to promote neuronal survival and nerve growth factor[302–305]. Therefore if the state of the astrocytes used to generate the conditioned medium is not known, then it becomes difficult to hypothesise the effects of the medium upon neurite outgrowth.

Data within this chapter describe the ability of ReproNeuro MQ astrocyte-conditioned medium to enhance neurite outgrowth from iPSC-derived neurospheres in 2D culture. Neurospheres cultured within the astrocyte-conditioned medium produced significantly more and significantly longer neurites than their control counterparts, this could further be slightly enhanced by the supplementation of Y-27632 to the culture medium, although this effect was not found to be statistically significant. Furthermore, the addition of ibuprofen to astrocyte-conditioned medium was found to reverse the neurite promoting effects of the medium, restoring neurite outgrowth to a similar level as the control. This could be due to an adverse effect of the NSAID upon some unknown signalling pathway or an interaction with the soluble factors within the medium rendering them less potent. However, in 3D culture the effect of the astrocyte-conditioned medium was less apparent and both Y-27632 and ibuprofen were found to inhibit neurite penetration.

However, as ReproNeuro MQ medium is commercially available and little information is given by the manufacturer as to its constituents, understanding the signalling processes at play in this system is difficult. Due to the neurite enhancing effects observed in 2D culture, it is thought that the astrocytes used to condition this medium are not reactive in nature, although due to its undefined composition, ReproNeuro MQ medium was not used elsewhere in the project.

3.5 Conclusion

This chapter has described the development of two novel pluripotent stem cell-based models of neurite outgrowth and their applications to study neurite growth in 2D or 3D culture. The optimisation of synthetic retinoid compounds and their use in the induction of differentiation and neurite outgrowth from human EC cells was identified and a robust and reproducible model of neuritogenesis developed. This model was then characterised to ensure that protein expression was similar *in vitro* and *in vivo*. Furthermore, this calso describes the translation of this model into a 3D culture environment to potentially provide a more physiological representation of neurite development.

Although this neurite outgrowth assay improves on those currently used throughout the literature, there are some limitations associated with this assay. Particularly in the 3D culture assay, as to be quantified neurites must traverse the 200 μm depth of the 3D material, therefore, assay sensitivity is limited to those neurites long enough to penetrate the scaffold. Similarly, it is assumed that little sprouting occurs in 3D as there is no evidence of this in 2D culture. However, if sprouting were to occur within the scaffold, this would significantly impact neurite quantification, as neurites would not have originated from a single perikaryon. The 3D environment, in which neurites develop within this model, provides scaffolding that allows neurites to adopt a more physiological geometry; however, it does not recapitulate other aspects of the developing nervous system such as stiffness and biochemical environment. Despite these limitations, in this chapter, we present a well-characterised and versatile model that has been applied to study neurite inhibition in a variety of neurological disorders.

In addition to the EC-derived model of neuritogenesis, an iPSC-derived model was also developed based upon the same spheroid culture principles. Both models have advantages for use in specific applications. For example, the EC-derived model is more robust and well characterised therefore versatile and suitable for a wide range of applications. However the iPSC-based model of neurite outgrowth provides opportunities to study complex diseases and personalised drug screening. The development of both models represents significant advances in the field and each model provides a useful *in vitro* tool to enhance our understanding of the process of neuritogenesis.

Furthermore the ability of small molecules and potential growth factor infused medium to enhance outgrowth in these models was analysed. It was found that inhibition of Rho A and ROCK can enhance some aspects of neurite growth, whilst inhibiting others, suggesting a complex role for this signalling pathway in neurite development. The suitability of incorporation of such supplements in the basic model protocol was

considered and it was decided that this could impact the opportunity to study neurite inhibition so Y-27632 and ibuprofen will not be included in the basic protocol.

Therefore, two robust and reproducible models of neurite growth have been developed in 2D and 3D culture systems. Future work outlined within the remaining chapters of this thesis will focus on applications of such models to study the role of neurite growth and inhibition within the context of neurological diseases.

Chapter IV: Investigation into the Molecular Mechanisms that Underpin Neurite Inhibition in the Glial Scar

4.1 Introduction

4.1.1 Spinal Cord Injury

Traumatic spinal cord injury (SCI) is a debilitating condition that can result in paralysis and have a significant impact on the quality of life of an individual[206]. There are thought to currently be between 183,000 – 230,000 people living in the USA with SCI with around 10,000 new cases reported each year[306]. The main causes of SCI include motor vehicle accidents (36-48 %) followed by violence (5-19 %), falls (17-21 %) and recreational activities (7-16 %)[306]. The average cost of treating an individual with SCI over a lifetime is thought to be between $0.5 – $2 million[306]. Therefore SCI places not only a significant amount of strain upon patients and their families in terms of emotional and financial burdens but also on healthcare systems.

Other neurological impairments often accompany SCI and traumatic brain injury is associated with nearly half of all SCI. Therefore, a thorough neurological assessment is essential in the diagnosis of SCI and should include an evaluation of mental status, cranial nerves, motor, sensory and autonomic systems along with coordination and gait[306]. The American Spinal Injury Association (ASIA) impairment scale is used clinically to determine the severity of injury and consists of five grades depending upon the level of functional deficit (Table 4-1)[306]. The level of paralysis is determined by the position of the injury within the spinal cord (Figure 4-1) with injury to the cervical level segments often resulting in full or partial quadriplegia[307].

Current SCI treatment remains largely palliative and includes preventing the progression of injury, handling pain syndromes, implementing bowel and bladder training regimes, managing sensory loss and teaching patients how to cope with their disabilities[2]. The main obstacle in the treatment of SCI is the inability of neurons to regenerate and reinnervate damaged nerves. This occurs due to the formation of an inhibitory environment known as the glial scar that forms a non-permissive barrier, preventing the development of neurites and restoration of lost neuronal connections[34,39].

Grade	Description
A	Complete paralysis: no sensory or motor function preserved in the sacral segments S4 – S5
B	Incomplete paralysis: sensory but not motor function preserved below the neurological level and extending through the sacral segments S4 – S5
C	Incomplete paralysis: motor function preserved below the neurological levels and most key muscles have a grade < 3
D	Incomplete paralysis: motor function preserved below the neurological level and most key muscles have a grade > 3
E	Normal motor and sensory function

Table 4-1: ASIA impairment scale for SCI.
A table detailing the main characteristics of each grade of SCI as determined by the ASIA impairment scale, used in clinical practices to determine the extent of injuy[306].

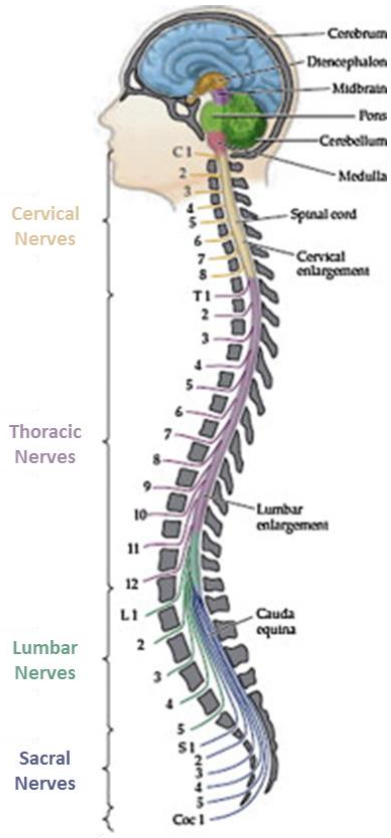

Fig 4-1: Degrees of spinal cord injury.
The human spinal cord comprises of 31 spinal nerve segments divided into four groups dependent upon the area of the body that they control, and damage to nerves in each area of the spinal cord effects specific areas of the body. The cervical nerves control the function of muscles and glands, whilst also receiving sensory input from the neck, shoulder arms and hands. The thoracic nerves are associated with chest and abdominal walls whereas the lumbar nerves are associated with the lower body, specifically hips and legs. The sacral nerves control the genitals and functioning of the lower digestive tract and the coccygeal nerve supplies the skin over the coccyx. Image modified from Silva *et al*.

4.1.2 Development of the Glial Scar

Damage to the spinal cord results in a series of cellular and molecular events that evolve over several days resulting in a chronic glial scar. The glial scar is a dynamic structure with different cell types participating in different events resulting in an inhibitory environment that prevents the reinnervation of neurons. Macrophages from the blood and microglia from the surrounding tissues represent the first cell types to respond in the hours following CNS injury[33]. In the days following injury large numbers of oligodendrocyte precursor cells are then recruited from the surrounding tissue[33]. The area of insult finally forms a glial scar containing a large number of reactive astrocytes that proliferate and slowly migrate to the injury site, eventually filling the vacant space left by the injury[33]. Within the glial scar, intact and damaged neurons develop dystrophic growth cones and scarring is often associated with the development of a fluid-filled cyst, as shown in Figure 4-2[39].

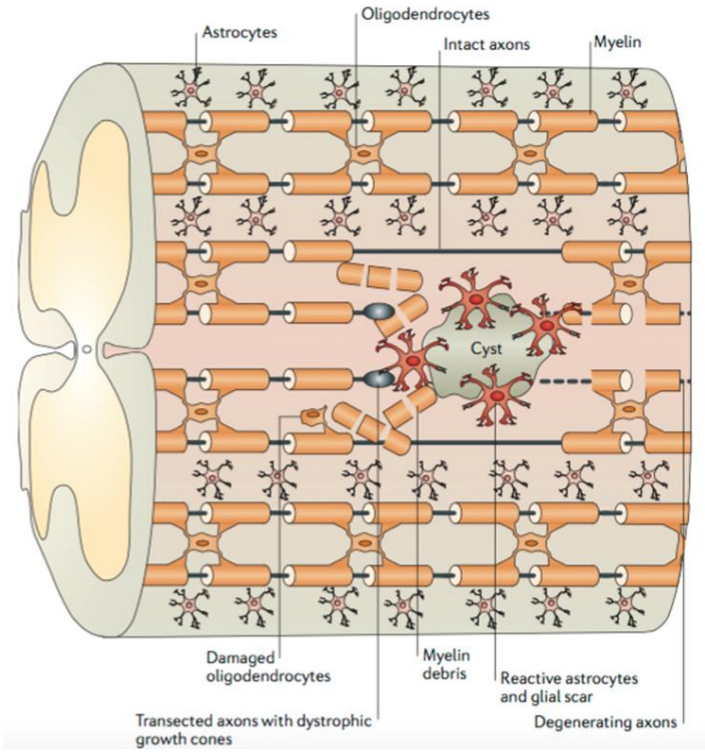

Fig 4-2: Formation of the glial scar following CNS injury.
Damage to nerve fibres and their surrounding tissues in the adult CNS results in the formation of an inhibitory environment known as the glial scar. The severed ends of axons form characteristic dystrophic growth cones and are exposed to the inhibitory mechanisms that are involved in glial scar formation. Inflammatory cells and reactive astrocytes are recruited to the site of injury and over time this leads to the formation of a glial scar, often accompanied by the formation of a fluid-filled cyst. This results in the formation of a hostile glial environment for axonal repair. Image taken from Yiu and He[2].

Glial scar development results in the formation of an inhibitory environment that suppresses neurite outgrowth. There are many mechanisms that contribute toward inhibition of neurite outgrowth in the glial scar including mechanical inhibition in the form of a meshwork of reactive astrocytes, and biochemical inhibition in the form of inhibitory molecules present on damaged myelin or secreted from reactive astrocytes[33,34,39].

4.1.2.1 Physical Inhibition of Neurite Outgrowth

One of the major inhibitory components of the glial scar is the accumulation of reactive astrocytes that mechanically block the outgrowth of neurites from developing neurons within the injured area. Following injury, astrocytes become hypertrophic and undergo cell division. They acquire a reactive phenotype associated with upregulation of the intermediate filament protein, glial fibrillary acidic protein (GFAP) and their morphology becomes hyperfilamentous[33]. Reactive astrocytes form a meshwork of tightly interwoven processes, bound together by tight and gap junctions, which provides a barrier, mechanically blocking the outgrowth of neurites in the area of the scar[33].

Understanding the role of reactive astrocytes in glial scar development is important in the development of novel therapeutic targets to intervene in the process. This is highlighted by Tian *et al* who demonstrate that the cell cycle inhibitor, olomoucine, can reduce the number of GFAP positive cells in a rat model of SCI associated with a recovery in functional deficit and reduction in the release of pro-inflammatory cytokines[308].

4.1.2.2 Chemical Inhibition of Neurite Outgrowth

Biochemical inhibition of neurite outgrowth is also a main contributing factor toward the inhibitory environment that arises post-injury. There are two main groups of inhibitory molecules implicated in the glial scar: chondroitin sulphate proteoglycancs (CSPGs) secreted from reactive astrocytes and inhibitory molecules found on damaged myelin (MAG, Nogo, OMGP)[33,34,39]. Although CSPGs and the myelin inhibitors act through different receptors, they are thought to converge on a similar signalling pathway involving Rho and ROCK activation that ultimately disrupt the actin cytoskeleton, resulting in growth cone collapse and neurite retraction[25,26,309,310].

4.1.2.2.1 Chondroitin Sulphate Proteoglycans

Reactive astrocytes inhibit neurite outgrowth in the glial scar through multiple mechanisms including mechanical blockage and the secretion of inhibitory chondroitin sulphate proteoglycans (CSPGs). CSPGs (aggrecan, brevican, neurocan, versican and

phosphacan)[39] are a family of inhibitory ECM molecules and are composed of a protein core with large, highly sulphated glycosaminoglycan (GAG) chains attached[311], as shown in Figure 4-3. The inhibitory effects of CSPGs are thought to depend upon the GAG side chains, as treatment with chondroitinase ABC, an enzyme that cleaves GAG chains from the protein core, has resulted in functional recovery in animal models of SCI[312–314].

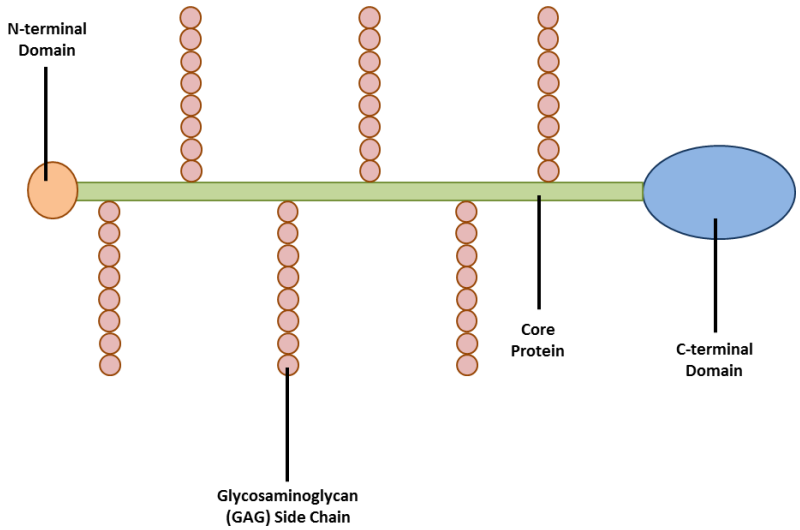

Fig 4-3: Chondroitin sulphate proteoglycan structure.
Chondroitin sulphate proteoglycans (CSPGs) are a family of single core proteins. Their structure includes the addition of glycosaminoglycan (GAG) (red) sidechains, attached to a single protein core (green) at serine residues by a tetrapeptide linker. The N-terminal domain (orange) binds through linker proteins to hyaluronan and the C-terminal domain (blue) that can associate with ECM components.

One of the proposed mechanisms by which CSPGs are thought to induce inhibition of neurite outgrowth is through the masking of neurite-promoting motifs within the ECM. CSPGs are thought to mask adhesion sites found throughout the ECM, impacting neurite outgrowth and inhibiting the neurite enhancing effects of certain ECM components such as laminin[261,315,316]. In a study by Mckeon *et al*, antibodies targeted against components of the laminin molecule were found to inhibit chondroitinase ABC-mediated rescue of neurite outgrowth in an *in vivo* model of the glial scar[317]. This suggests a potential interaction between CSPG and laminin-mediated effects on neurite outgrowth, and it is thought that one action of CSPGs may be to block the neurite promoting effects of laminin.

Although CSPGs are thought to interact with the ECM, they are also known to induce an intracellular signaling cascade resulting in growth cone collapse through the activation of cell surface receptors. Several CSPG receptors have been reported, including PTPσ, LAR phosphatase, NgR1 and NgR3[318]. A transgenic study by Xu *et al* demonstrated the role of the LAR receptor following injury, and found that deletion of LAR resulted in improved

functional recovery following SCI in mice[319]. Similarly, Shen *et al* evidenced binding of CSPGs to the PTPσ receptor along with recovery of neurite outgrowth in a receptor knockout, cell-based model[320]. The Nogo receptors (NgR) plays a crucial role in the induction of neurite inhibition as mediated by the myelin inhibitors; however, NgR1 and NgR3 are also thought to be activated by CSPGs. Dickendesher *et al* demonstrate the binding of the GAG domain of CSPG molecules to NgR1 and NgR3 in a cell-based neuronal model, and further evidence the functional role of these receptors through a knockout study[321].

Although CSPGs activate a number of receptors, the intracellular signalling cascade that they initiate is thought to be common to all receptors. The Rho A signalling pathway controls actin dynamics and CSPG-mediated receptor activation is thought to activate Rho A and ultimately its downstream effector, Rho A-associated kinase (ROCK)[39]. Activation of this signalling cascade results in growth cone collapse and repulsion of axon guidance. Many mechanisms of neural regeneration focus on inhibition of the downstream targets (Rho A and ROCK)[23,25–27,30,204,322] as opposed to targeting receptor activation, as multiple receptors are involved in the induction of CSPG-mediated neurite inhibition, whereas Rho A activation is a common inhibitory mechanism.

4.1.2.2.2 Myelin Inhibitors

Inhibitory molecules can also be found on the myelin debris from damaged neurons within the glial scar. The myelin inhibitors include Nogo, which is a member of the reticulon family of membrane proteins of which there are three isoforms (Nogo-A, -B and –C) generated by alternative splicing[39]. Nogo-A is the best characterised of the Nogo isoforms and contains an amino-terminal domain (amino-Nogo) specific to the Nogo-A isoform, along with a 66 amino acid loop domain (Nogo-66) that is common to all three isoforms[39]. Although Nogo-66 is thought to be the extracellular domain whilst amino-Nogo remains intracellular, some amino-Nogo has been detected on cell surfaces and both domains are known to inhibit neurite outgrowth[39].

Myelin inhibitors also include myelin-associated glycoprotein (MAG), a transmembrane protein with five immunoglobulin-like domains in its extracellular region that is both expressed as a cell surface protein and is thought to be released as soluble factor upon injury[39,323]. Oligodendrocyte myelin glycoprotein (OMGP) is also an inhibitor of neurite outgrowth found on myelin debris and is a GPI-anchored protein containing a leucine-rich repeat (LRR) domain[39,323].

Many studies have focused on elucidating the receptor and downstream signalling events that result in myelin-mediated neurite inhibition, with the view to intervene in the

pathway and induce neurite recovery. The Nogo receptor (NgR) is a GPI-linked protein expressed on many types of neuron that is known to interact with the Nogo-66 domain of Nogo-A[324] along with both MAG[325] and OMGP[326], which are structurally different from Nogo. NgR lacks an intracellular domain, therefore, acts through co-receptors including p75[327,328], TROY[329] and LINGO1[330].

Binding of the myelin ligands to NgR results in the formation of a receptor complex consisting of NgR and its co-receptor. This induces a rapid rise in intracellular Ca^{2+}, which in turn results in Rho A and ROCK activation, similarly to CSPG-mediated signalling, inducing growth cone collapse[331]. Furthermore, it also thought that the receptor complex is then internalised and transported to the cell body in signalling endosomes, where a decrease in the levels of phosphorylated cyclic AMP response element-binding (CREB) is observed[332]. This is associated with a downregulation in the transcription of growth promoting genes and transcription factors[332]. Understanding the complexities of NgR signalling has resulted in the design of blocking antibodies[333–335], receptor antagonists[336,337] and soluble receptors[338] that have induced functional recovery in animal models of SCI, highlighting the importance of elucidating the underlying signalling mechanisms.

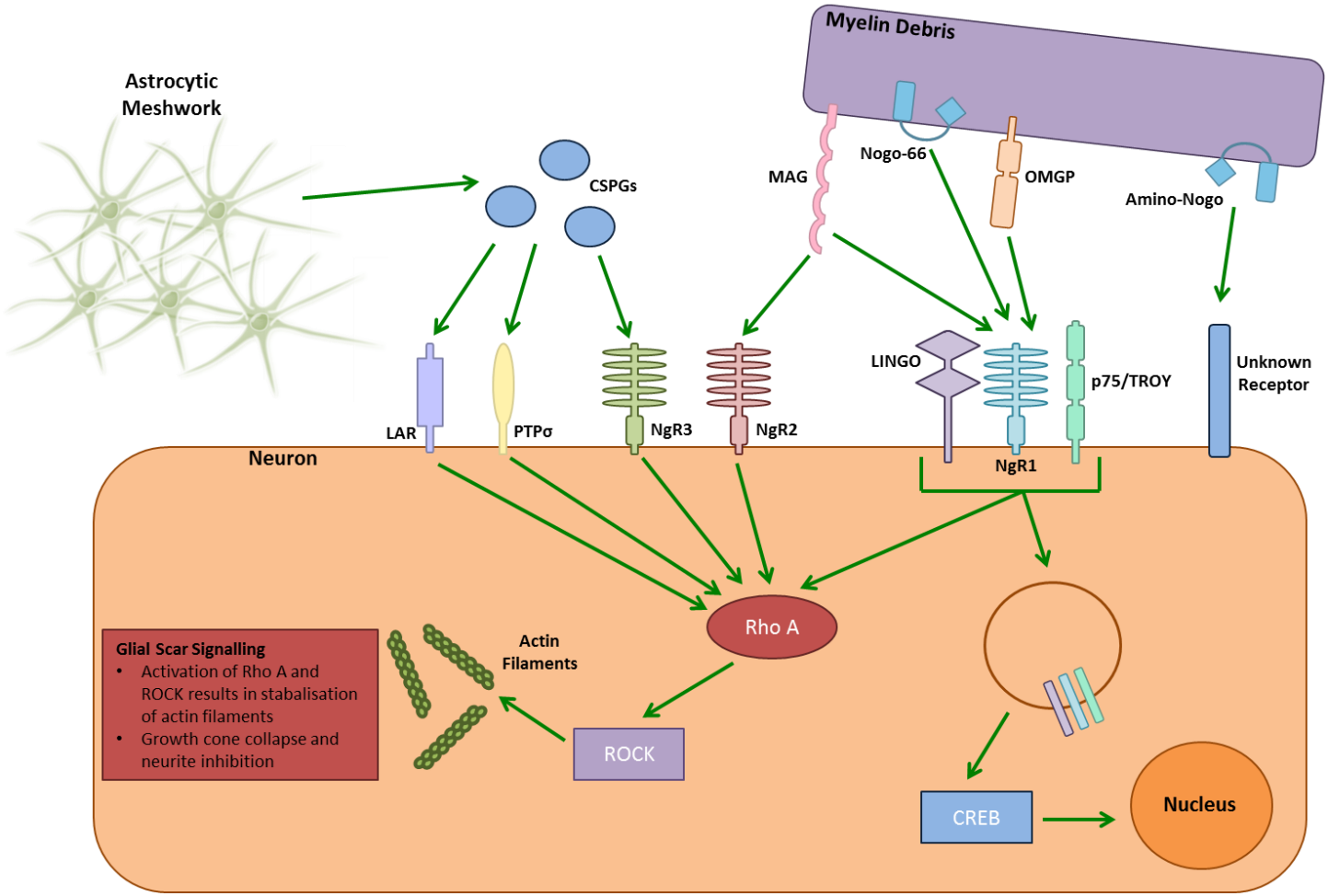

Fig 4-4: Molecular signalling events that lead to neurite inhibition in the glial scar.
Upon injury astrocytes become reactive, up regulate the intermediate filament protein GFAP and form long processes that interweave, resulting in a tightly woven meshwork that mechanically blocks the outgrowth of resident neurites. Reactive astrocytes also secrete CSPG molecules that act through receptors including: LAR, PTPσ, NgR1 and NgR3 to activate Rho A and ROCK signalling events. Similarly, myelin associated inhibitors of neurite outgrowth found on myelin debris from damaged nerves, include: MAG, Nogo-66, OMGP and Amino-Nogo. With the exception of Amino-Nogo, which binds to an unknown receptor, all of the myelin inhibitors bind to and activate NgR1, which along with its co-receptors LINGO, P75 and TROY, activates the Rho A signalling pathway. The NgR1 receptor complex is also internalised and through activating CREB is associated with the down regulation of growth promoting gene transcription. Activation of Rho A and downstream ROCK, results in the stabalisation of actin filaments which leads to growth cone collapse and neurite retraction.

4.1.3 Disease Modelling of the Glial Scar

Disease models of the glial scar provide a tool to enable the investigation into the pathological mechanisms by which neurite inhibition is achieved. This can be useful to uncover both the cellular and molecular processes that contribute toward neurite inhibition, increasing our understanding of the process. Furthermore, both *in vivo* and *in vitro* based models of the glial scar can be useful in the screening of potential compounds and substances to overcome inhibition in this context.

There are advantages and disadvantages to both *in vitro* and *in vivo* based disease models, such as *in vitro* models are generally far removed from the complex setting of the *in vivo* injury and may only include a limited number of cell types. However, this may be an advantage depending upon the hypothesis being tested, as it offers a reductionist approach whereby individual mechanisms can be tested without the impact of complex interacting pathways. Although *in vivo* glial scar models recreate the large number of events that occur following injury, generally they are based on either rat or mouse models, therefore the relevance when comparing to human SCI may be questionable. It is therefore important to fully evaluate the available options in terms of disease modelling when deciding upon the most appropriate model to apply to a particular research question.

4.1.3.1 Current in Vivo Models of the Glial Scar

Most *in vivo* models of the glial scar involve the induction of SCI in mouse or rat-based systems. Under anaesthesia, the spinal cord of mice and rats is cut or damaged and the resultant symptoms studied for functional abnormalities such as motor function deficits[339,340]. This provides a complex physiological setting to study the interaction between different cell types and biological systems, such as the invasion of immune cells and the inflammatory response evoked upon injury[341,342], which would not usually be able to be studied in basic cell-based *in vitro* systems.

Animal based models of SCI are essential in the testing and identification of potential therapeutic compounds, as *in vitro* models are able to identify compounds that have a positive effect on neurite outgrowth but this may not necessarily translate into a functional recovery *in vivo*. Bradbury *et al* first describe the beneficial effects of chondroitinase ABC (Ch'ase) treatment following lesions to the dorsal column of adult rats[312]. This study observes a functional recovery of locomotor and proprioceptive behaviour in injured rats, suggesting that Ch'ase treatment may provide a useful treatment strategy in human SCI[312,343]. This initial study has since been built upon by

further groups who have identified the optimal time post-injury for Ch'ase delivery[344] and also combination therapies[345] that can enhance the recovery effects.

A distinct advantage to mouse-based *in vivo* models is the ability to create transgenic animals to study the up or downregulation of particular genes and proteins. This allows for the identification of key elements involved in signalling pathways and responses. For example, Menet *et al* describe functional recovery in double knockout, vimentin and GFAP deficient mice, two cytoskeletal components of reactive astrocytes[346]. Functional recovery in this study was found to correlate with reduced glial reactivity, thus, highlighting the important role of the reactive astrocyte in the formation of the inhibitory environment that arises post-SCI[346,347]. Furthermore, the role of the receptor, LAR, in CSPG-mediated neurite inhibition was first identified in transgenic, knockout mice[348]. Injured LAR knockout mice were observed to undergo significant locomotor functional recovery, along with axonal regrowth, therefore, highlighting the important role of the receptor in neurite inhibition[348].

Although animal models provide complex, physiological systems to study the events that surround SCI, they are animal based models as oppose to human, and there may be subtle differences in the way in which mice or rat neurons react to stimuli compared with human neurons. This can pose problems in the translation of potential therapeutic approaches, as compounds that have had favourable effects in animal models may not have the desired effects in humans due to their inherent physiological differences. Similarly, the ethical use of animals in scientific research is continually under question[349], particularly in terms of wastage of animals, therefore *in vitro* cell-based models provide an attractive alternative.

4.1.3.2 Current in Vitro Models of the Glial Scar

Cell-based *in vitro* models of neurite outgrowth, as discussed in Chapter I, can often be adapted to study the process of neurite inhibition through several methods including the treatment of growth substrates with inhibitory molecules such as CSPGs. Cell-based models offer advantages over *in vivo* models in that human-derived cell lines can be used, avoiding the physiological discrepancies associated with animal models. Similarly, cell-based models are amenable to high-throughput screening and have applications in drug screening and discovery to identify possible compounds that are able to overcome neurite inhibition within particular systems. With emerging 3D cell culture technology, *in vitro* cell-based models are becoming more physiologically relevant and reliable for drug screening purposes.

Vahidi *et al* describe the development of a microfluidic strip system to test the ability of molecules to inhibit neurite outgrowth[350]. This comprised of alternating strips of

permissive and non-permissive substrates with a solution of CSPGs being applied to a series of strips to produce the non-permissive sites[350]. Neurons were then cultured on the surfaces and were only able to develop along the permissive stripes due to CSPG-mediated inhibition[350]. This allows the alignment of neurons in culture and can provide a screening tool to test the ability of compounds to overcome CSPG-mediated inhibition. For example, compounds such as Ch'ase can be applied in the culture medium, resulting in neurons no longer developing in aligned columns within the permissive strips, as inhibition has been overcome and neurons can now migrate onto the previously non-permissive strips[350]. A similar strip-based neurite outgrowth assay was employed by Monnier *et al* to determine the ability of an inhibitor of Rho A (C3 transferase) and an inhibitor of ROCK (Y-27632) to overcome CSPG-mediated neurite inhibition chick retina ganglion cells[26].

Other methods of modelling aspects of the glial scar *in vitro* involve the co-culture of neurons and astrocytes to study their interactions. However, the *in vitro* culture of astrocytes generally results in their activation[351], resulting in a reactive phenotype. Depending upon the application of the *in vitro* model, this may or may not be desired. Studies have revealed that the culture of astrocytes in a 3D environment using hydrogel[351] or scaffold-based systems[192] allows them to retain their native, non-reactive phenotype. East *et al* demonstrate an application of this technology by using non-reactive astrocytes cultured within a hydrogel as an assay of reactivity[352]. This system was used to investigate the effect of potential stem cell therapies such as, neural stem cells, adipose-derived stem cells and mesenchymal stem cells on the induction of astrogliosis[352]. This is important, as repairing spinal cord damage via stem cell therapy should not contribute toward glial scarring, as this would have adverse effects upon recovery. This system was also used in another study by East *et al* to investigate the role of astrocyte-mediated neurite inhibition in rat DRG neurons[353].

Therefore, *in vitro* models can be used to model specific aspects as the glial scar such as CSPG-mediated inhibition or neuronal-glial interactions, this provides a more simplified system to study the underlying molecular mechanisms without interference from other cell types or systems. However, when developing therapeutic strategies to intervene in the events that follow SCI, one must consider all the complexities of the *in vivo* situation in which case the use of *in vivo* models may be more appropriate.

4.1.4 Neurite Regeneration Beyond the Glial Scar

The major obstacle in the treatment of SCI is the inability of neurons to regenerate and restore lost neuronal conenctions[220]. The main barrier in the regeneration of neurons is the glial scar, which is an inhibitory environment composed of several components

including reactive astrocytes, CSPGs and myelin inhibitors. For this reason, there has been a great effort in the development of mechanisms to overcome the inhibitory factors that contribute to glial scarring, with the aim of restoring functional recovery following injury.

4.1.4.1 Chondroitinase ABC

Chondroitinase ABC (Ch'ase) is an enzyme purified from *Proteus vulgaris* that cleaves GAG side chains from CSPG molecules[354], rendering them inactive and leaving a protein core with a carbohydrate stub[220]. Cleavage of the GAG chains from the CSPG molecule prevents receptor activation along with activation of the downstream signalling pathway including Rho and ROCK activation that leads to growth cone collapse. Therefore, this enzyme has potential therapeutic applications in overcoming CSPG-mediated inhibition of neurite outgrowth in the glial scar and restoring lost neuronal connections.

The therapeutic benefits of Ch'ase treatment have been demonstrated by many studies. Most notably a study by Bradbury *et al* established the ability of intrathecal Ch'ase treatment to upregulate regeneration-associated proteins and promote functional locomotor recovery in adult rats with lesioned dorsal columns[312]. This was further observed by Huang *et al* who demonstrate the ability of Ch'ase to induce the outgrowth of new fibres in a rat-based model of SCI[355].

However, the use of Ch'ase in this regenerative context is thought to be limited, as aggrecan digested by Ch;ase has been found to still induce neurite inhibition[220]. This is thought to be due to the remaining protein and sugar stub post-digestion, as although its inhibitory potency is lost, it has still has been demonstrated to inhibit neurite outgrowth in DRG cultures[220].

4.1.4.2 Blocking Nogo Receptor Signalling

The Nogo-66 receptor (NgR1) is activated by many inhibitory molecules found within the glial scar, including, Nogo, MAG, OMGP and CSPGs. For this reason, it is an attractive target in the pursuit of neurite recovery and there are many strategies that have been explored to reduce NgR-mediated neurite inhibition including blocking antibodies[333,334,356], receptor antagonists[336,337,357] and soluble receptors[338,358].

IN-1 is a monoclonal antibody specific to the Nogo-A molecule, that has been shown to have positive effects when administered post-SCI to rats[334] and primates[333]. Both Merkler *et al*[356] and Leibscher *et al*[334] demonstrate the ability of IN-1 to restore locomotion function in rat models of SCI, however through differing antibody delivery techniques. Liebsher *et al*[334] delivered the antibody through an intrathecal catheter whereas Merkler

et al[356] implanted IN-1 secreting hybridoma cells into the injury site. In both cases animals that received the antibody treatment recovered to a greater degree than control animals, both in terms of function and histology.

Another approach at hindering NgR mediated signalling is through the use of a receptor antagonist peptide such as Nogo-A extracellular peptide residues 1-40 (NEP 1-40)[332]. NEP 1-40 is a soluble peptide that contains the first 40 amino acids of Nogo-66 and competitively binds NgR, preventing receptor activation[332]. This has been shown to have positive effects on neurite outgrowth both *in vitro* and *in vivo*, providing a potential therapeutic target. NEP 1-40 has been reported to have beneficial effects in rat-based models of SCI when administered both at the time of injury[337,357] and on a delayed timescale[336] and in both cases resulted in functional recovery and axon sprouting.

Similarly, a soluble Nogo-66 receptor has been shown to bind Nogo, MAG and OMGP, mopping them up and preventing them from activating NgR and its downstream signalling cascade. This has been demonstrated *in vivo* following delivery of the purified, soluble receptor intrathecally after midthoracic dorsal over-hemisection in rats[358]. Delivery of the receptor resulted in axonal sprouting and improved electrical conductivity along with improved locomotion[358]. A soluble, truncated, Nogo-66 receptor has also been used *in vitro* to recover neurite outgrowth on myelin and Nogo, non-permissive substrates[338].

4.1.4.3 Enhancement of Intrinsic Growth Cues

Most of the commonly used approaches to promote neurite regeneration in the injured spinal cord, focus on the reduction of inhibitory cues, however, enhancing the intrinsic growth stimuli within the CNS can also have positive regenerative effects. For example, there have been several reports that the neurite promoting effects of nerve growth factor (NGF)[274] may restore functionality and improve connectivity following SCI[359–363]. A study by Oudega *et al* demonstrates the ability of NGF infusion post-spinal cord injury in rats to promote regeneration of fibres that bridge the glial scar[363]. In a later study by Oudega *et al,* other neurotrophins such as brain-derived neurotrophic factor (BDNF) were found to have little impact on NGF-induced enhancement of neural connectivity[362]. Other neurotrophins such as glial-derived neurotrophic factor (GDNF), neurotrophin-3 and BDNF, have also been shown to have neurite enhancing capabilities[361].

Other approaches have focused on enhancing neurite promoting effects of the ECM and promoting cellular-ECM interactions. Only as neurons mature, do they lose their ability to regenerate and embryonic neurons are known to have a higher capacity for regeneration than adult neurons. This was demonstrated by Maureen Condic, who determined that

postnatal neurons could be cultured on non-permissive, CSPG-coated surfaces with no adverse effect to neurite outgrowth[364]. However, this was not the case with adult-derived neurons whose neurite outgrowth was significantly inhibited on CSPG surfaces[364]. This finding led to a comparison of cell-adhesion markers on both postnatal and adult neurons, which found that integrin expression was significantly lower in adult neurons[364]. This study then focused on the role of integrin-mediated neurite outgrowth in terms of inhibition and found that when integrin-binding was blocked using an antibody, neurons could not adhere to the growth substrate and develop neurites[364]. This was complemented by an overexpression study that found when mature, adult neurons overexpress integrins, their neurite outgrowth can be enhanced and rescued within an inhibitory environment[364].

Reducing the inhibitory cues that mediate neurite inhibition within the glial scar by Nogo receptor blocking or Ch'ase treatment can promote functional recovery, as discussed previously. However, this is not the only mechanism by which inhibition can be overcome, and enhancing the intrinsic capacity for neurite growth can recover the inhibitory phenotype in much the same way. Therefore, the outcome of neurite growth is dependent upon a balance between both inhibitory and growth cues, both of which should be taken into account when designing a potential therapeutic intervention.

4.1.4.4 Manipulation of Rho A/ROCK Signalling

Many efforts have been made to intervene in the downstream signalling events that occur following receptor activation within the glial scar. Particularly the focus has been on the Rho A signaling cascade, which is a mechanism common to many receptors implicated in glial scar signalling including those which respond to CSPGs and those which respond to myelin inhibitors. Inhibition of Rho A and downstream ROCK, are common strategies employed to recover neurite inhibition in the context of the glial scar[220].

Multiple mechanisms of Rho A inhibition have been shown to enhance neurite outgrowth in the presence of inhibitory stimuli, such as the bacterial enzyme C3 transferase[220]. C3 transferase is an enzyme produced by the bacterium *Clostridium botulinum* that covalently attaches an ADP-ribose moiety to Rho A, inactivating the molcule[365]. The ability of C3 transferase to overcome neurite inhibition *in vitro* was demonstrated by Dergham *et al*[366]. This study involved the culturing of primary cortical neurons on inhibitory substrates including those composed of myelin, CSPGs and a mixture of myelin and CSPGs alone[366]. Treatment with C3 transferase resulted in recovery of neurite outgrowth on the inhibitory surfaces[366] and this effect has further been evidenced by a number of studies[28,287,367].

Non-steroidal anti-inflammatory drugs (NSAIDs) such as ibuprofen relieve pain and inflammation through the inhibition of cylcooxygenases, however, ibuprofen has also been found to be an intracellular inhibitor of Rho A[30,368]. Ibuprofen is thought to inhibit Rho A signalling through a peroxisome proliferator-activated receptor γ (PPARγ) dependent mechanism[31] and has previously been shown to enhance neurite outgrowth in human model neurons[21]. Wang *et al* demonstrate the ability of ibuprofen to overcome neurite inhibition both *in vitro* and *in vivo*[369]. This study found that subcutaneous administration of ibuprofen following spinal cord contusion resulted in functional recovery in rats with twice as many rats achieving a hind limb weight-bearing status[369]. This functional recovery was also accompanied by an increase axonal sprouting following SCI[369].

Inhibition of ROCK, an enzyme downstream of Rho A, is another commonly employed strategy to reduce neurite inhibition in the glial scar. There is a large body of evidence in the literature that documents the ability of the selective ROCK inhibitor, Y-27632, to overcome neurite inhibition, and its effects have been demonstrated both *in vitro* an *in vivo*[26,27,204,209,366,370,371]. Gopalakrishnan *et al* demonstrate the ability of Y-27632 to overcome neurite inhibition on non-permissive CSPG-coated substrates in a PC12 model of neurite outgrowth[27]. Chan *et al* found a similar result in a rat-based *in vivo* model of SCI, in that high-dose Y-27632 treatment resulted in a functional recovery and increased axonal sprouting[209].

Fasudil is another inhibitor of ROCK commonly used to restore neurite following SCI[372,373]. An *in vivo* study by Nishio *et al* revealed that immediate local delivery of fasudil to the injured spinal cord of rats, resulted in recovery of hind limb function and enhanced axonal sprouting[374]. However, when fasudil treatment was delayed and began only four weeks post-operatively, no functional or histological effects were observed[374]. This suggests that the method and timeframe for treatment may result in a difficult translation of these molecules into clinical practice. However, BA-210, a drug which blocks the activation of Rho A, has shown promising results in initial clinical trials through improvement of motor function in patients with pre-existing SCI[375].

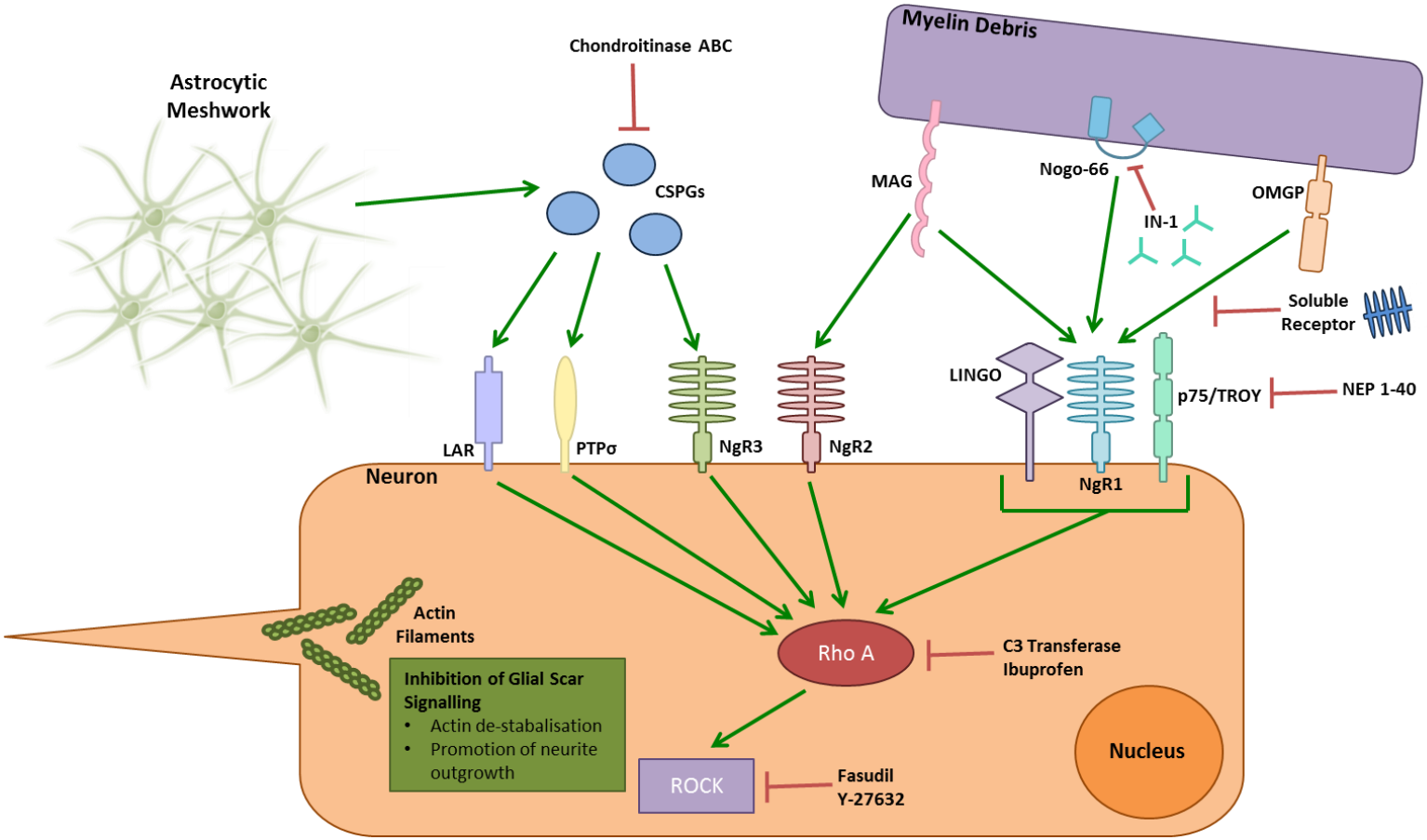

Fig 4-5: Targets for intervention in the glial scar signalling pathway that can restore neurite outgrowth within the inhibitory environment. There are several approaches that have been used throughout the literature to promote the growth of neurites in the non-permissive environment that forms post-SCI. One of which is the digestion of CSPGs by Chondroitinase ABC, which cleaves GAG chains from the molecules leaving the CSPGs unable to interact with their receptors. IN-1 is a monoclonal antibody targeted to Nogo-66 that binds to the inhibitory molecule, blocking ligand-receptor binding. Similarly, a soluble Nogo receptor has been developed that sequesters MAG, Nogo-66 and OMGP, again preventing ligand-receptor binding. The NgR1 receptor antagonist peptide NEP 1-40 mimics the extracellular loop domain of the Nogo molecule and competitively binds to the receptor, preventing signal transduction. Methods to inhibit the intracellular signalling events focus on the inhibition of Rho A by molecules such as C3 transferase and ibuprofen or inhibition of ROCK by fasudil or Y-27632. Inhibition of these signalling events leads to actin de-stabalisation and promotion of neurite outgrowth.

4.1.5 Conclusions

SCI is a debilitating condition that is difficult to treat due to the inhibitory glial scar that forms following injury that prevents the regeneration of resident neurons. There are many inhibitory pathways that contribute to the glial scar including the activation of receptors by inhibitory molecules, leading to a Rho A and ROCK dependent signalling and growth cone collapse. Many attempts have been made to elucidate the molecular mechanisms that underpin neurite inhibition in the glial scar and this has given rise to the development of potential treatments such as Ch'ase, Nogo receptor blockage and inhibition of Rho A/ROCK signalling, that have all shown promising effects *in vitro* and *in vivo*. This chapter describes the application of a novel, 3D, human-derived, *in vitro* model of neurite outgrowth, to investigate the process of neurite inhibition in terms of the glial scar. We also describe mechanisms, by which neurite outgrowth can be restored in the presence of inhibitory stimuli, demonstrating the potential use for this *in vitro* system in drug screening and discovery.

4.1.5.1 Chapter Aims

This chapter aims to investigate the role of CSPG-mediated signalling in the process of neurite inhibition that occurs within the glial scar. This Chapter discusses several different methodologies in the pursuit of CSPG-mediated inhibition including, the coating of growth substrates with inhibitory molecules and various investigations into the release of CSPGs from glioma cells that resemble the reactive astrocytes from the glial scar, with the aim of developing a novel co-culture model with which to study neurite inhibition.

Furthermore, this chapter aims to further elucidate the molecular mechanisms that underpin CSPG-mediated neurite inhibition along with the identification of small molecules that may be able to overcome such inhibition. This chapter aims to demonstrate the potential application of this novel model of human neuritogenesis as a screening tool, able to identify novel molecules that may be of therapeutic value. This chapter also evaluates the role of inhibitors of Rho A/ROCK signalling in overcoming CSPG-mediated neurite inhibition, enhancing our understanding of the signalling mechanisms involved in this process.

We hypothesise that incorporating CSPG molecules into our novel neurite outgrowth model, either in the form of coatings or secreted from glioma cells, will result in inhibition of neurite growth from stem cell-derived human neurites. We also hypothesise that application of small molecules, will be able to overcome this inhibitory response, through intervention in the downstream signalling response to CSPG-receptor activation. This provides an application of the novel human-derived 3D model of human neuritogenesis

described in Chapter III, and evidences the use of this model as an assay for neurite outgrowth that can be used to measure inhibition and regeneration.

4.1.5.2 Chapter Objectives

- Investigate the ability of aggrecan coating of 2D and 3D growth substrates to induce neurite inhibition in human-derived neurites.

- Investigate the ability of Rho A (ibuprofen) and ROCK (Y-27632) inhibition to overcome aggrecan mediated neurite inhibition, on non-permissive 2D and 3D growth substrates.

- Evaluate the suitability of glioma cell lines for use in a co-culture model of neurite inhibition to recapitulate reactive astrocytes found within the glial scar.

- Assess the effect of confluency and growth rate on expression of reactive astrocyte markers in glioma cells.

- Develop a 2D co-culture methodology to study the process of astrocyte-induced neurite inhibition and methods of recovery.

- Investigate the effect of Rho A (ibuprofen) and ROCK (Y-27632) inhibition on glioma cell proliferation and phenotype.

- Investigate the impact of medium conditioned by glioma cells cultured in 2D or 3D on neurite outgrowth and the effect of Rho A and ROCK inhibition in this system.

- Develop a novel 2D/3D co-culture system whereby neurites and glioma cells are not in contact with one another to study the effects of glioma cell conditioned medium on neurite outgrowth.

4.2 Materials & Methods

4.2.1 Aggrecan Coating of Growth Substrates for Neurite Inhibition Studies

For neurite inhibition studies, substrates were coated with aggrecan in addition to standard poly-D-lysine and laminin coating solution, to provide an inhibitory substrate for neurite outgrowth. Neurospheres were formed as described in section *2.2.5 Formation of Neurospheres from Human Pluripotent Stem Cells* and seeded as in section *2.2.6.2 Seeding of Neurospheres for Neurite Outgrowth Assays*, however the coating of 2D and 3D growth substrates differs from that of the standard neurite outgrowth assay. Aggrecan from bovine articular cartilage (Sigma-Aldrich) was reconstituted in PBS without Ca++ and Mg++ at 1 $mgmL^{-1}$. The desired volume of aggrecan solution was then added to the standard coating solution of 10 μgmL^{-1} poly-D-lysine and laminin. For example, to achieve a final concentration of 50 μgmL^{-1} aggrecan, 1 mL of 1 $mgmL^{-1}$ aggrecan solution was added to 19 mL of 10 μgmL^{-1} poly-D-lysine and laminin coating solution. Throughout this study a range of 0.5 – 50 μgmL^{-1} aggrecan coating was used. Both 2D and 3D growth substrates were then coated overnight at room temperature and washed twice in PBS prior to neurosphere seeding.

4.2.2 3D Culture of Glioma Cells

Both U-118MG and U-251MG glioma cell lines were cultured in 3D using Alvetex® Scaffold using the following methodology. Alvetex® Scaffold 12-well format inserts were prepared by plasma treatment using the K1050X Plasma Asher at a power level of 40 W, for 5 mins to render the scaffolds hydrophilic. The scaffolds were then washed in PBS twice before being washed in culture medium. Scaffolds were then placed in a standard 12-well tissue culture plate and unless otherwise stated, 0.5 million glioma cells were seeded per 12-well Alvetex® insert. Cells were seeded using a concentrated method of seeding, whereby cells were seeded in a volume of 50 µL growth medium, which was added directly to the centre of the scaffold. Scaffolds were then incubated at 37 °C and 5 % CO_2 in a humidified environment for one hour before the wells were topped up with 4 mL culture medium. Cells were incubated for 24 hours to allow them to adhere before the culture medium and tissue culture plate were replaced. This removes any cells that may have passed through the 3D material and adhered to the bottom of each well i.e be growing in 2D within the well, as these cells may release paracrine factors that may interfere with the growth of the cells within the 3D material. Cells were then cultured in 3D for up to 10 days (unless otherwise stated) with a 50 % media change on day 5 of culture.

4.2.3 MTT Cell Viability Assay

The MTT tetrazolium reduction assay was used to measure viable cells with active metabolism. The assay involves the application of the MTT reagent to cells that metabolise the substrate forming a purple coloured formazan product that accumulates as an insoluble precipitate in and around cells. The product can be solubilised using organic solvents and measured using a spectrophotometer to produce data that represent the number of viable cells and metabolic activity.

Monolayer cultures were washed in sterile PBS prior to the addition of 1 $mgmL^{-1}$ thiazolyl blue tetrazolium bromide (Sigma-Aldrich) dissolved in phenol red free DMEM-HG (Gibco) and incubated for 1 hour at 37 °C, 5 % CO_2 in a humidified environment. MTT solution was then aspirated from cultures and cells were incubated with acidified isopropanol for 10 minutes at room temperature on a shaking platform. To each well of a flat-bottomed 96-well plate, 200 µL isopropanol and 20 µL of sample were added to each well. Absorbance was then measured at 570 nm using a BioTek, ELx800 microplate reader.

4.2.4 TUNEL Assay

The DeadEnd™ Fluorometric TUNEL System (Promega, Southampton, UK) was used to detect apoptotic cells in cultures of U-251MG cells treated with modulators of Rho/ROCK signaling. Cells were seeded onto 16 mm diameter sterile glass coverslips in a 12-well tissue culture plate at a density of 50,000 cells per well. Cells were then incubated at 37 °C, 5 % CO_2 in a humidified environment for 24 hours in 4 mL maintenance medium before medium was replaced with 4 mL DMEM with 2mM L-glutamine, 10 % heat treated FBS, 20 active units of Penicillin and Streptomycin supplemented with the small molecule of interest. Cultures were then maintained for 10 days with a 50 % media change on day 5 of culture. Following 10 days the coverslips were fixed in 4 % PFA at room temperature for 20 minutes prior to analysis.

Samples were permeabilised in 0.2 % Triton X-100 in PBS for 5 minutes before being washed twice in PBS for 5 minutes. A positive control coverslip was prepared by incubating the sample with 100 µL of DNase I buffer containing 5 UmL^{-1} of DNase I for 10 minutes at room temperature. All samples were then incubated with 100 µL equilibration buffer and were allowed to equilibrate at room temperature for 10 minutes. Samples were then protected from light and incubated for 60 minutes at 37 °C in a humidified environment with 50 µL of reaction mixture containing: 45 µL of equilibration buffer, 5 µL nucleotide mix and 1 µL rTdT enzyme. A negative control was also prepared, however the reaction mixture for this coverslip contained 1 µL of dionized H_2O replacing the 1 µL rTdT enzyme. Cells were then incubated with 2X SSC for 15 minutes at room temperature to

stop the reaction. Finally, coverslips were washed twice in PBS for 5 minutes and were mounted using Hardset Vectasheild containing DAPI (Vecta Laboratories).

4.2.5 Chondroitin Sulphate ELISA

To determine the CSPG content of glioma cell conditioned medium, an enzyme-linked immunosorbent assay (ELISA) was used to detect the chondroitin sulphate (CS) motif present on the CSPG molecule. The human chondroitin sulphate ELISA kit (Abbexa, Cambridge, UK) was used and manufacturer's instructions were followed.

Conditioned medium collected from glioma cell cultures was prepared for analysis by centrifugation at 2000 x g for 20 minutes to remove any precipitate. A standard curve of known CS concentration was prepared as described in manufacturer's instructions initially, 5 tubes were labelled 1500, 1000, 500, 250 and 125 $pgmL^{-1}$. Standard diluent buffer was added to each tube in the following volumes: 200 µL in 1500 and 1000 $pgmL^{-1}$ tubes and 300 µL in each remaining tube. To the 1500 $pgmL^{-1}$ tube 400 µL of 2250 $pgmL^{-1}$ standard solution was added and then 400 µL was taken from the 1500 $pgmL^{-1}$ tube and added to the 1000 $pgmL^{-1}$ tube and 300 µL was then taken from each tube and added to the following tube in a serial dilution to achieve the final concentrations.

Each diluted standard and sample was then added in triplicate to wells within the pre-coated ELISA plate, provided with the kit (50 µL per well), along with standard diluent buffer to provide a zero well. The plate was then sealed and incubated at 37 °C for 30 minutes before being washed 5 times in wash buffer. HRP conjugant reagent was then added to each well (50 µL) excluding the zero well and incubated for a further 30 minutes at 37 °C. The plate was then washed 5 times in wash buffer prior to the addition of 50 µL TMB substrate A and 50 µL TMB substrate B was then added to each well and the plate was incubated for 15 minutes at 37 °C. Following this final incubation 50 µL of stop solution was added to each well and he colour changed to yellow. Absorbance was then measured at 450 nm using a BioTek, ELx800 microplate reader.

A standard curve of corrected absorbance against chondroitin sulphate concentration was plotted using GraphPad Prism 6 and linear regression was fitted through the points, as shown in Figure 4-6. The equation of the regression was obtained and rearranged to make x the subject, y (absorbance of the test value) was then substituted into the equation. This results in the calculation of the chondroitin sulphate concentration of each known absorbance. An example is shown below:

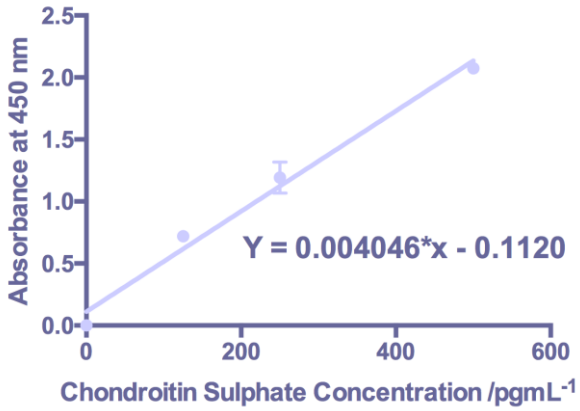

Fig 4-6: Typical standard curve of chondroitin sulphate quantification obtained from an ELISA.
A typical standard curve plotted from absorbance at 450 nm for a series of standard solutions of known chondroitin sulphate concentration. A linear regression was plotted through the data set and an R^2 value obtained (0.971 for this data set) which demonstrates the relationship between the two variables, the closer to 1, the more correlated the variables are. Plotting a linear regression determines the equation of the line, which can then be rearranged and the absorbance of conditioned medium of unknown chondroitin sulphate content can be substituted into the equation to determine their concentration.

Calculation:

$$y = 0.004046x - 0.1120$$

$$x = \frac{y + 0.1120}{0.004046}$$

e.g For an absorbance at 450 nm of 0.119, substitute *y*:

$$x = \frac{0.119 + 0.1120}{0.004046}$$

$$x = 57 \text{ pgmL}^{-1}$$

4.2.6 Co-culture of U-251MG cells and Neurospheres in 2D

For 2D co-culture of U-251MG cells and human pluripotent stem cell derived neurospheres, 48-well tissue culture plates were coated overnight with 10 μgmL^{-1} poly-D-lysine and laminin solution, as described in section *2.1.6.1 Coating of Growth Substrates for Neurite Outgrowth Studies*. However, whereas for mono-culture experiments, substrates were coated 24 hours prior to the end of differentiation of stem cell aggregates, for co-culture experiments tissue culture plates were coated 48 hours prior to the end of differentiation. Following overnight coating of tissue culture plates, U-251MG cells were seeded in each well at a density of 40,000 cells per well of a 48-well tissue culture plate (unless otherwise stated). Cells were incubated overnight at 37 °C and 5 % CO_2 in a humidified environment to allow cells to adhere to the substrate. For neurosphere seeding, maintenance medium was removed from each well containing glioma cells and 0.5 mL TERA2.cl.SP12 maintenance medium containing mitotic inhibitors (1 μM cytosine arabinose, 10 μM 5'fluoro 2'deoxyuridine and 10 μM uridine) was added to each well and 1 – 2 neurospheres were then placed into each well. Neurosphere and glioma cell co-cultures were then incubated for the standard 10 day neurite outgrowth period and received a 50 % media change on day 5 of culture, before being fixed in 4 % PFA for fluorescent analysis.

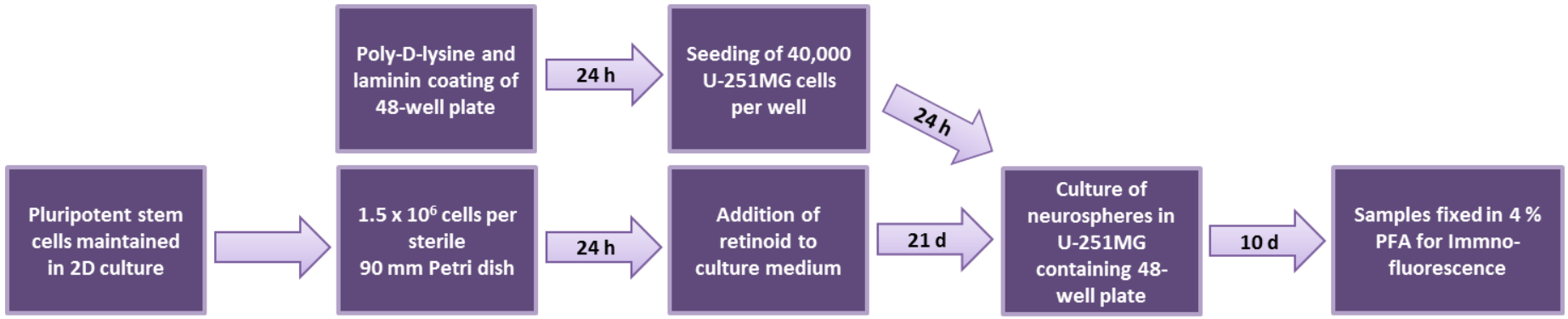

Fig 4-7: A flow chart summarising the stages of a co-culture model combining neurospheres and glioblastoma cells in 2D culture.
Human pluripotent stem cells were seeded in suspension culture at a density of 1.5 x 10^6 cells per sterile 90 mm Petri dish and allowed to aggregate for 24 hours. EC23 was then added to the culture following 24 hours, at a concentration of 0.01 µM and cell aggregates were further maintained for 21 days. 48 hours prior to the end of the differentiation period, 48-well culture plates were coated with poly-D-lysine and laminin solution overnight before U-251MG glioma cells were seeded into them. The cells were allowed 24 hours to adhere to the coated surface before neurospheres were seeded onto the monolayer of glioma cells and incubated with mitotic inhibitors for 10 days. Co-cultures were then fixed in 4 % PFA for immunofluorescent processing.

4.2.7 Conditioning of Growth Medium

4.2.7.1 Conditioning of Growth Medium by 2D and 3D Cultured U-251MG Cells

To study the paracrine effects of inhibitory molecules secreted from U-251MG cells, medium was taken from 2D and 3D cultures of U-251MG cells and was used during the neurite outgrowth phase of culture of human stem cell derived neurospheres. For 2D media conditioning, U-251MG cells were seeded in 175 cm^2 culture flasks at density of 1 million cells per flask in 30 mL of maintenance medium. Cells were then incubated overnight at 37 °C and 5 % CO_2 in a humidified environment to allow cell attachment, before media was replaced with 30 mL of TERA2.cl.SP12 maintenance medium. Cells were then incubated for a further 10 days with a 50 % media change on the 5^{th} day of culture.

Similarly for 3D conditioning of media, cells were seeded at a density of 0.5 million cells per scaffold using the concentrated seeding method on 12-well format Alvetex® scaffolds that were prepared by plasma treatment (as described in section *4.2.2 3D Culture of Glioma Cells*). Scaffolds were incubated overnight at 37 °C and 5 % CO_2 in a humidified environment to allow cell attachment before being transferred into a new 12-well tissue culture plate with 4 mL of TERA2.cl.SP12 maintenance medium. Scaffolds were incubated for a further 10 days with a 50 % media change on the 5^{th} day of culture.

Following 10 days of culture, media was taken from 2D and 3D cultures of U-251MG for use in the neurite outgrowth assay described in section *2.1.6 Induction of Neurite Outgrowth from Stem Cell Derived Neurospheres*.

4.2.7.2 Conditioning of Growth Medium in a 2D/3D Co-culture System

To study the direct effect of U-251MG conditioned medium on neurite outgrowth from human pluripotent stem cell derived neurospheres, glioma cells and neurospheres were cultured within the same well of a tissue culture plate, however not within direct contact of one another. U-251MG cells were seeded at a density of 0.05 million cells per well of a 12-well tissue culture plate in 4 mL of U-251MG maintenance medium, 24 hours prior to the end of differentiation of stem cell aggregates. Cells were incubated overnight at 37 °C and 5 % CO_2 in a humidified environment to allow cell attachment. Medium was then removed and 4 mL of TERA2.cl.SP12 maintenance medium containing mitotic inhibitors (1 μM cytosine arabinose, 10 μM 5'fluoro 2'deoxyuridine and 10 μM uridine) was added to each well. Poly-D-lysine and laminin coated Alvetex® scaffolds (see section *2.1.6.1 Coating of Growth Substrates for Neurite Outgrowth Studies* for coating of scaffolds) were then placed in each U-251MG containing well and 5 – 10 neurospheres were seeded onto each

scaffold. Cultures were then further maintained for 10 days with a 50 % media change on the 5th day of culture before being fixed in 4 % PFA for immunofluorescent analysis.

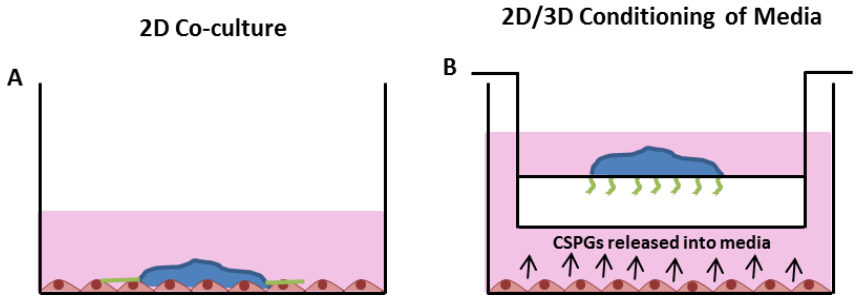

Fig 4-8: A schematic depicting different methods of co-culture of glioma cells and neurospheres.
Glioma cells (U-251MG, red) were cultured in 2D in the bottom of a 48-well tissue culture plate and allowed to adhere for 24 hours prior to the addition of a neurosphere (blue), which was then subsequently cultured on top of the glioma cell monolayer (A) during which time neurites (green) radiate from the aggregate, this is described as 2D co-culture. To investigate the paracrine effect of secreted factors from U-251MG cells on neurite outgrowth, glioma cells were cultured in 2D within the well of a tissue culture plate, whilst the neurosphere was cultured on top of Alvetex® scaffold within the same well, this is described as 2D/3D conditioning of media (B), as the glioma cells and neurosphere are not in contact with one another.

4.3 Results

4.3.1 Inhibition of Neurite Outgrowth by Aggrecan

A number of methodologies were used throughout this chapter to induce neurite inhibition, by recapitulating certain aspects of glial scar signalling. The first of which involves the coating of 2D and 3D growth substrates with the CSPG aggrecan. This provides a non-permissive, inhibitory growth surface to study neurite inhibition along with mechanisms of recovery. Aggrecan induced neurite inhibition is evident in 2D culture, as demonstrated by Figure 4-9. A reduction in TUJ-1 positive (green) extensions can be observed from immunofluorescence images (Figure 4-9A) with increasing concentration of aggrecan coating (0.05 – 50 μgmL^{-1}). This reduction in visible neurites is particularly apparent at high aggrecan concentrations such as 5 μgmL^{-1} (Figure 4-9Ae,f) and 50 μgmL^{-1} (Figure 4-9Ag,h).

Quantification reveals that both the number of neurites per neurosphere (Figure 4-9B) and neurite density of each neurosphere (Figure 4-9C), decline in a dose dependant fashion with increasing aggrecan concentration. Similarly, neurite length shown in Figure 4-9D, also appears to share a negative relationship with aggrecan concentration, however,

there appears to be an anomaly between points 0.5 μgmL^{-1} and 5 μgmL^{-1}. Generally though, increasing concentration of aggrecan appears to have a negative effect upon neurite length and growth in 2D culture.

To investigate the ability of aggrecan coatings to provide a non-permissive environment for neurite growth in 3D culture, Alvetex® Scaffold was coated with a range of concentrations (0.05 – 50 μgmL^{-1}) of aggrecan. Neurospheres can be seen to remain on the top of the scaffold (Figure 4-10Aa,c,e,g) whilst TUJ-1 positive (green) neurites can be seen to have penetrated the depth of the 3D material (Figure 4-10Ab,d,f,h). Increasing aggrecan concentration resulted in a decrease in the number of neurites that are visible from the bottom view of the scaffold and at 50 μgmL^{-1} there are almost no visible neurites penetrating the depth of the scaffold. This observation is complemented by quantification (Figure 4-10B), which reveals that the number of neurites penetrating the scaffold decreases in dose dependent relationship with increasing aggrecan concentration.

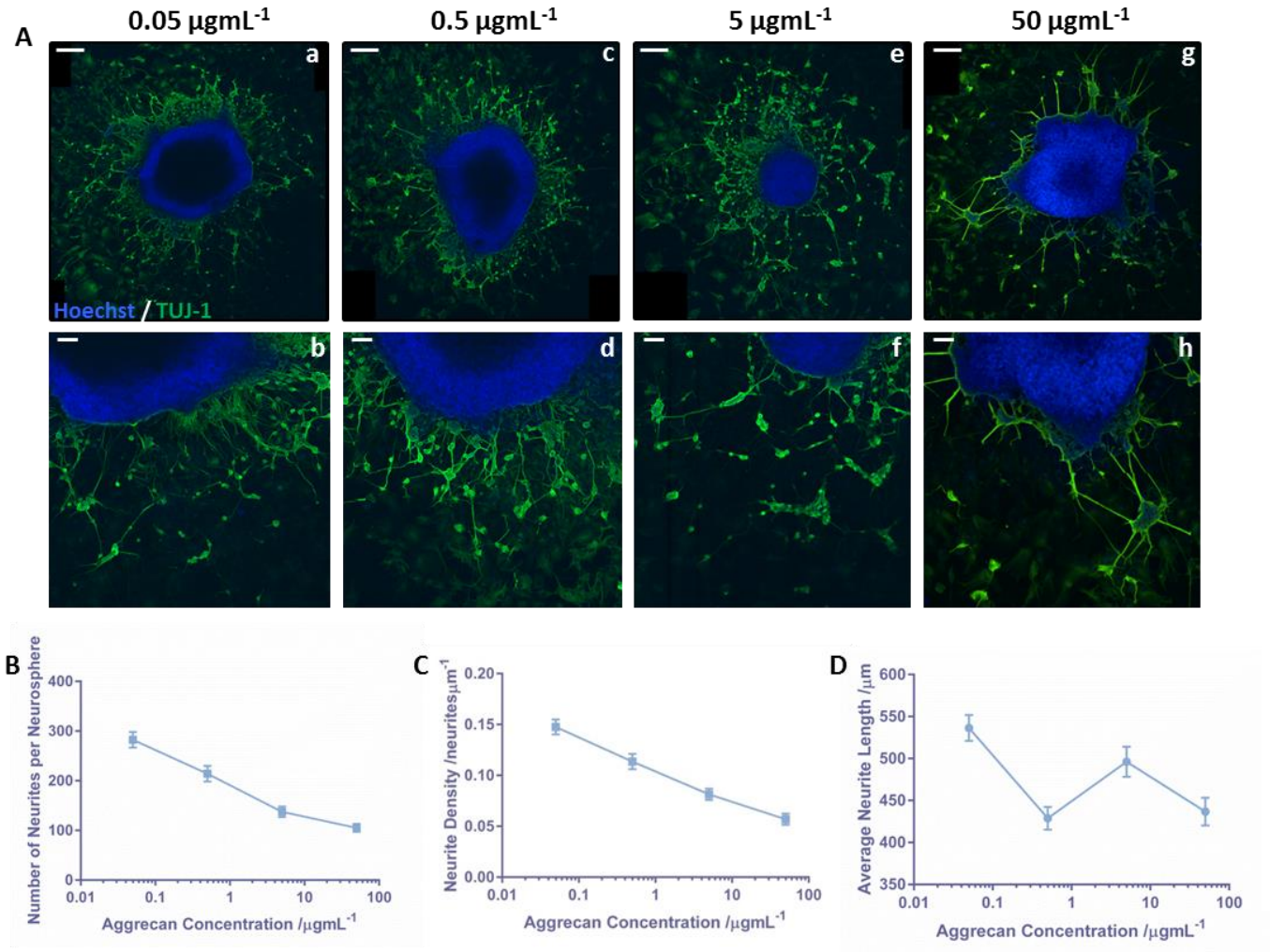

Fig 4-9: Culture of neurospheres on 2D inhibitory substrates, coated with the CSPG, aggrecan, inhibits neurite outgrowth. Representative confocal images of neurospheres cultured on an inhibitory substrate in 2D (A) stained for the pan-neuronal marker TUJ-1 (green) and nuclei are stained blue. Scale bars: Aa,c,e,g: 200 µm Ab,d,f,h: 50 µm. Substrates were coated with a range of concentrations (0.05 – 50 µgmL^{-1}) of aggrecan, a CSPG molecule, in addition to standard poly-D-lysine and laminin coating solution. The number of neurites per neurosphere (B) (data represent mean ± SEM, n=21-27; between 7-9 neurospheres were analysed from each of 3 independently differentiated populations of neurospheres) decreases in a dose-dependent manner with increasing concentrations of aggrecan, as does neurite density (C) (data represent mean ± SEM, n=21-27; between 7-9 neurospheres were analysed from each of 3 independently differentiated populations of neurospheres) and the average length of neurites (D) (data represent mean ± SEM, n=130; a total of 130 neurites were measured from 7-9 neurospheres analysed from 3 independently differentiated populations of neurospheres) also generally decreases with increasing aggrecan concentration.

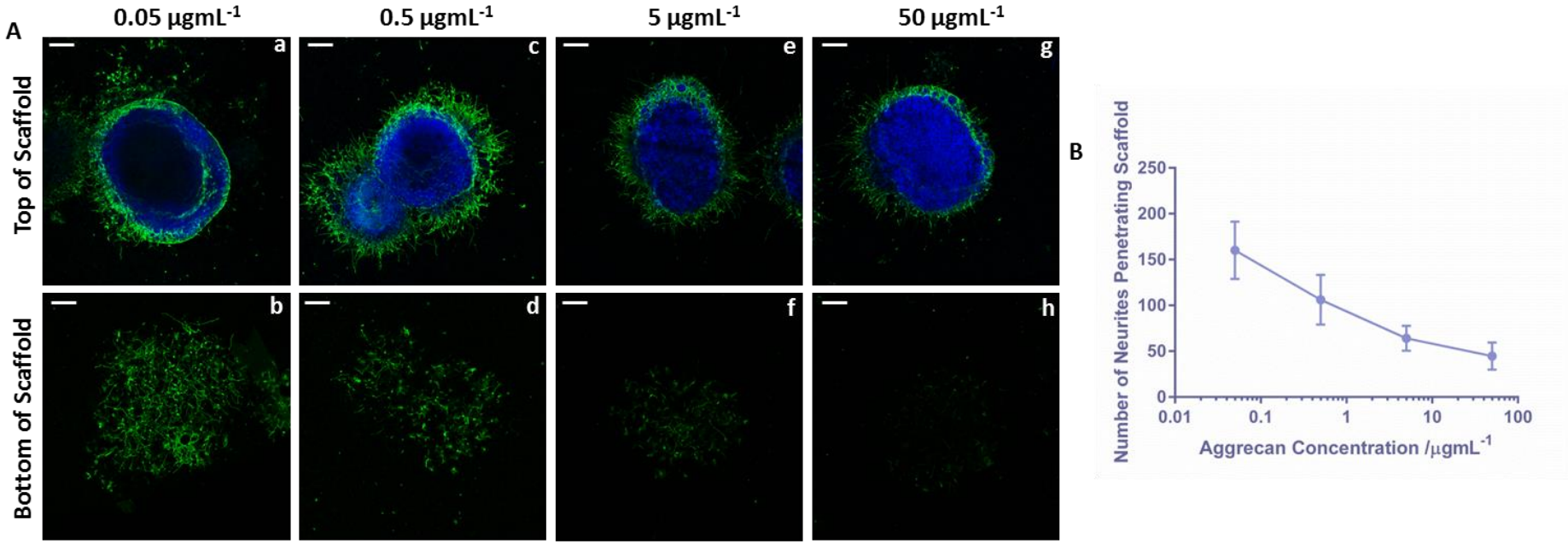

Fig 4-10: Culture of neurospheres on 3D inhibitory substrates, coated with the CSPG, aggrecan, inhibits neurite outgrowth.
Representative confocal images of neurospheres cultured on an inhibitory 3D surface (A) stained for the pan-neuronal marker TUJ-1 (green) and nuclei are stained blue. Neurospheres can be observed from the top view of the scaffold (Aa,c,e,g) and neurites have visibly penetrated the 3D material, as seen from the bottom view (Ab,d,f,h). Scale bars: 200 µm. Substrates were coated with a range of concentrations (0.05 – 50 µgmL^{-1}) of aggrecan, a CSPG molecule, in addition to standard poly-D-lysine and laminin coating solution, and fewer neurites visibly penetrate the scaffold with increasing aggrecan concentration. Quantification of the number of neurites penetrating the scaffold (B) (data represent mean ± SEM, n=7-10; between 2-3 neurospheres were quantified per repeat within each independent cellular population tested, of which there were 3) reveals that neurite outgrowth is inhibited in a dose dependent manner with increasing aggrecan concentration.

4.3.1.1 Recovery of Aggrecan Induced Neurite Inhibition through Modulation of Rho A/ROCK Signaling

As outlined in detail earlier within this chapter, CSPGs such as aggrecan are thought to induce a series of intracellular signalling events following receptor activation. This is thought to include activation of Rho A and ROCK, ultimately leading to cytoskeletal changes that induce growth cone collapse and neurite retraction[26,33,39]. To investigate the role of this signalling pathway in aggrecan-mediated neurite inhibition, Y-27632 an inhibitor of ROCK, and ibuprofen an inhibitor of Rho A, were added to the culture medium of neurospheres cultured on non-permissive aggrecan-coated growth substrates.

4.3.1.1.1 Inhibition of ROCK by Y-27632

In 2D culture conditions, neurospheres were either cultured without aggrecan coating (Figure 4-11Aa,b) or upon non-permissive growth substrates coated with 50 μgmL^{-1} aggrecan solution (Figure 4-11Ac-j). In addition to this, neurospheres were also cultured with growth medium containing a range of concentrations (0.5 – 15 μM) of Y-27632 (Figure 4-11Ae-j). Significant neurite outgrowth can be observed from neurospheres cultured on permissive surfaces without aggrecan coating (Figure 4-11Aa,b), whereas those cultured on the non-permissive aggrecan coated surfaces (Figure 4-11Ac,d) generate a significantly reduced number of neurites. The addition of Y-27632 to the culture medium appears to rescue aggrecan-induced neurite inhibition in a dose dependant manner with the induction of extremely dense neurite outgrowth from neurospheres cultured with 15 μM Y-27632 (Figure 4-11Ai,j). However, neurites from 15 μM Y-27632 treated neurospheres also appear extremely short compared those generated in the presence of lower concentrations of the molecule.

The culture of neurospheres on substrates coated with 50 μgmL^{-1} aggrecan was found to significantly inhibit the number of neurites extended per neurosphere (Figure 4-11B) and addition of Y-27632 was found to rescue this inhibitory response. The addition of 0.5 μM Y-27632 to the culture medium was found to significantly enhance neurite outgrowth on aggrecan coated surfaces, restoring the number of neurites per neurosphere to control levels. Higher concentrations of Y-27632 (10 – 15 μM) actually resulted in an enhancement of neurite outgrowth, with the number of neurites per neurosphere surpassing the control levels.

A similar trend is also observed in quantification of neurite density (Figure 4-11C), with aggrecan coating resulting in a significant inhibition in the neurite density of the neurospheres. This again, was rescued by Y-27632 treatment with 0.5 μM resulting in restoration of neurite density to control levels, whereas 10 – 15 μM treatment resulted in

an enhancement of neurite density. Neurite length (Figure 4-11D) is also significantly inhibited by 50 μgmL^{-1} aggrecan coating, and 0.5 μM Y-27632 also restores this inhibitory effect. However, as Y-27632 concentration increases from 0.5 μM to 15 μM, a dose dependent decrease in neurite length is observed. This has also been observed in the absence of an inhibitory stimulus as described in Chapter III. Therefore, although all concentrations of Y-27632 rescue aggrecan-induced inhibition of neurite length, a secondary relationship between Y-27632 and inhibition of neurite length is also evident from this quantification.

Neurospheres cultured in 3D, were either cultured upon Alvetex® Scaffold alone (Figure 4-12Aa,b) or coated with 50 μgmL^{-1} aggrecan (Figure 4-12Ac-j) with Y-27632 medium supplementation (Figure 4-12Ae-j). Neurospheres remain on top of the scaffold (Figure 4-12Aa,c,e,g,i) with few TUJ-1 positive (green) neurites visibly radiating from the central neurosphere, as neurites penetrate the 3D material. However, addition of Y-27632 to the culture medium results in observation that more neurites appear to radiate from the neurosphere and traverse the surface of the scaffold itself. The bottom view of the scaffold (Figure 4-12Ab,d,f,h,j) highlights neurite penetration, as a number of TUJ-1 positive (green) neurites can be seen to have completely penetrated the 3D material. In the absence of aggrecan coating (Figure 4-12Aa,b) significant neurite outgrowth is visible from the bottom view of the scaffold, whereas very few neurites can be seen to have penetrated scaffolds coated with 50 μgmL^{-1} aggrecan. Addition of Y-27632 at a range of concentrations (0.5 – 15 μM) results in a large amount of neurite outgrowth visible from the underside of the scaffold (Figure 4-12Ae-j).

Quantification further evidenced the findings observed from the immunofluorescence images, as the number of neurites penetrating each scaffold (Figure 4-12B) was reduced by aggrecan coating and enhanced by Y-27632 treatment. Y-27632 even at the lowest concentration tested (0.5 μM) was found to enhance neurite penetration to levels that surpass that of the control, with both 10 μM and 15 μM significantly enhancing the number of neurites that penetrate aggrecan-coated scaffold scaffolds.

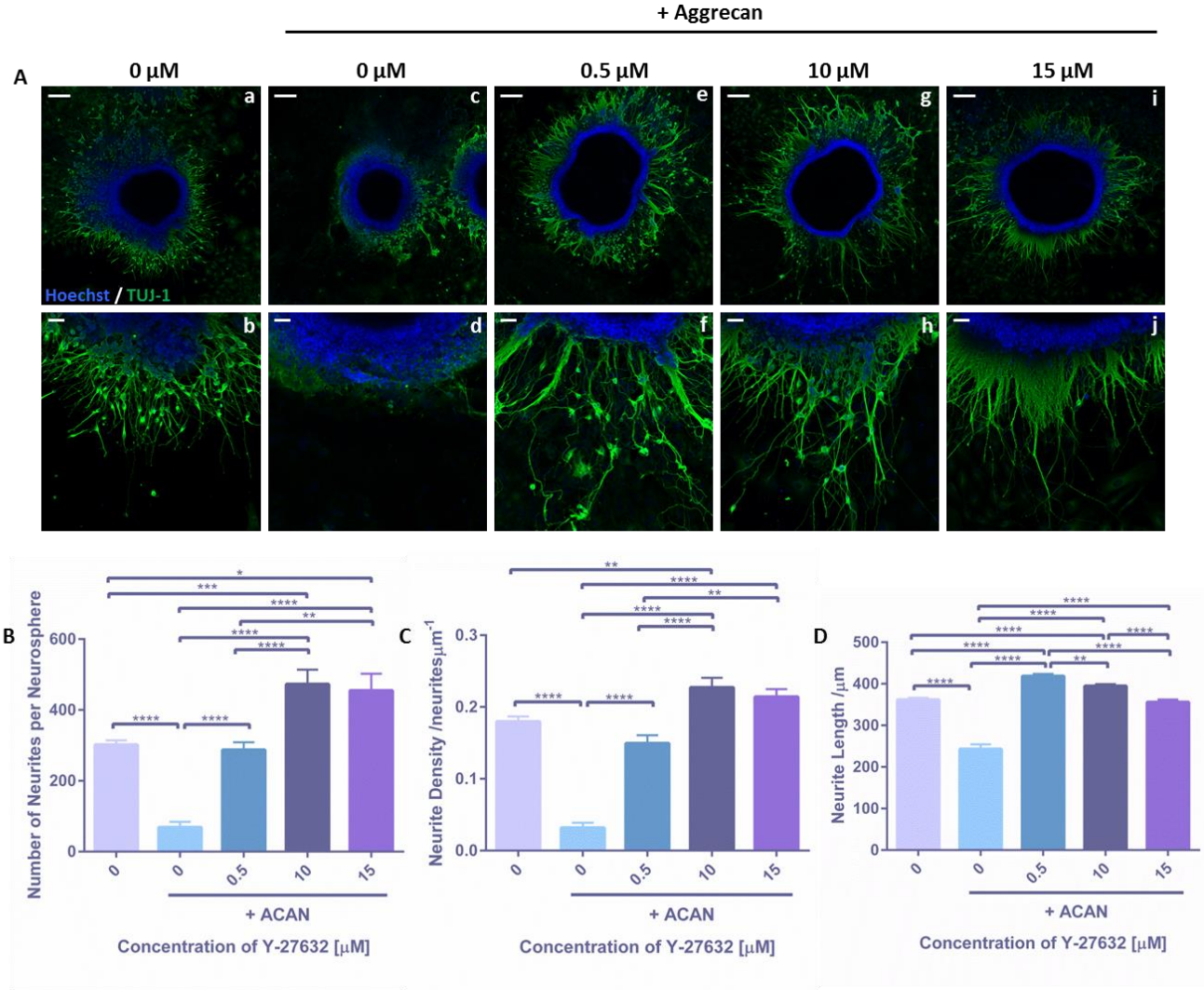

Fig 4-11: Inhibition of ROCK by Y-27632 can overcome aggrecan-mediated neurite inhibition in 2D culture.

Representative confocal images of neurospheres cultured on an inhibitory 2D substrate coated with 50 µgmL^{-1} aggrecan (ACAN) (A). Neurite outgrowth is highlighted by the pan neuronal marker TUJ-1 (green) and nuclei are stained in blue. Neurospheres cultured without aggrecan (Aa,b) have extensive neurite outgrowth radiating from the central aggregate, however neurospheres cultured on 2D plastic coated with aggrecan (Ac,d) have very few neurites protruding from the cell aggregate. The addition of Y-27632, a selective ROCK inhibitor (Ae-j) recovers neurite outgrowth on aggrecan coated 2D surfaces. Scale bars: (Aa,c,e,g,i): 200 µm (Ab,d,f,h,j): 50 µm. The number of neurites per neurosphere (B) (data represent mean ± SEM, n=9-18; between 3-6 neurospheres were quantified per independent replicate, of which there were 3) was significantly decreased in the presence of aggrecan and addition of Y-27632 was able to overcome this inhibition, restoring neurite outgrowth to control levels and even enhancing neurite outgrowth at higher concentrations. Y-27632 was also able to restore neurite density (C) (data represent mean ± SEM, n=9-18; between 3-6 neurospheres were quantified per independent replicate, of which there were 3) on aggrecan coated surfaces and neurite length (D) (data represent mean ± SEM, n=110-784; in total between 110-784 individual neurites were measured from 3 replicates of neurospheres derived from independent pools of cells) was enhanced to greater than control levels with low concentrations (0.5 µM) of Y-27632, however this effect decreased with increasing concentrations of the molecule. One-way ANOVA with Tukey's multiple comparisons: * = $p \leq 0.05$, ** = $p \leq 0.01$, *** = $p \leq 0.001$, **** = $p \leq$

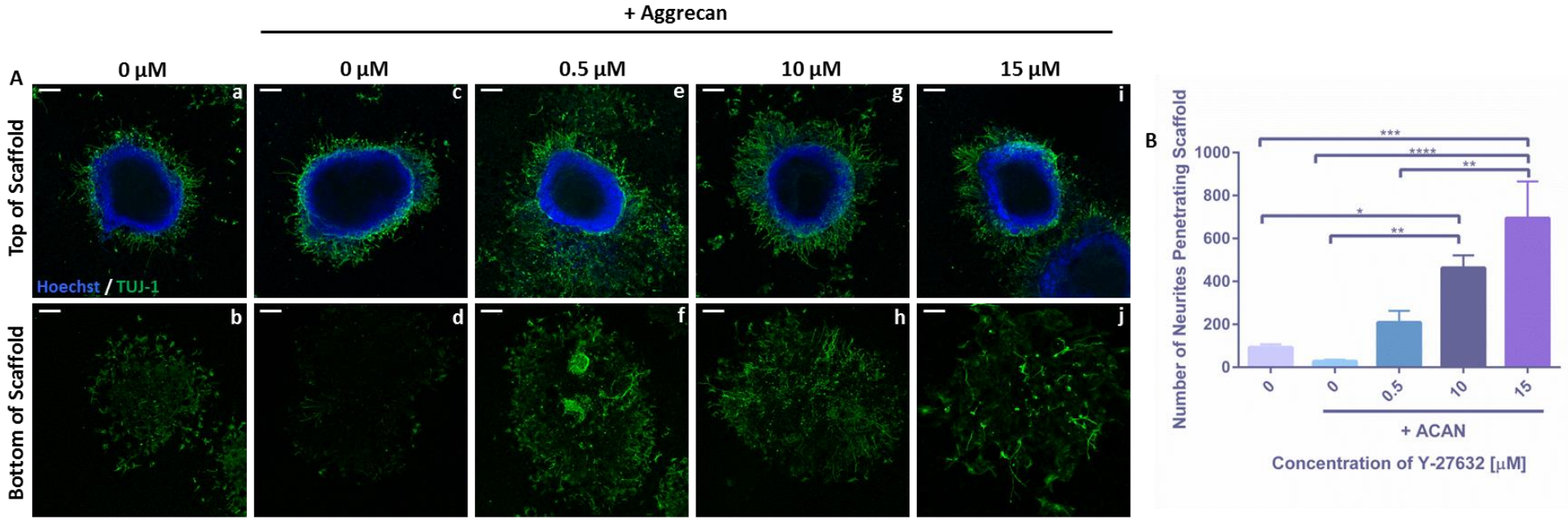

Fig 4-12: Inhibition of ROCK by Y-27632 can overcome aggrecan-mediated inhibition of neurite outgrowth in 3D culture.
Representative confocal images of neurospheres cultured on Alvetex® scaffold coated with 50 µgmL^{-1} aggrecan (ACAN). Neurospheres are visible from the top view of the scaffold (Aa,c,e,g,i) and TUJ-1 (green) positive neurites can be seen penetrating the scaffold depth from the bottom view of the scaffold (Ab,d,f,h,j). Scale bars: 200 µm. The number of neurites penetrating the scaffold (B) (data represent mean ± SEM, n=6-7; 2-3 neurospheres were quantified from 3 independent replicates) is greatly inhibited in the presence of aggrecan and with the addition of 0.05 µM Y-27632, is recovered levels similar to that of the control. However when Y-27632 concentration is increased, the number of neurites penetrating the scaffold increases to levels that surpass that of the control. One-way ANOVA with Tukey's multiple comparisons: * = $p \leq 0.05$, ** = $p \leq 0.01$, *** = $p \leq 0.001$, **** = $p \leq 0.0001$.

4.3.1.1.2 Inhibition of Rho A by Ibuprofen

To investigate the role of Rho A in CSPG-induced neurite inhibition, neurospheres were cultured on 2D surfaces coated with aggrecan and a range of concentrations of ibuprofen (10 – 500 μM) were added to the culture medium. Neurospheres were cultured on control substrates (Figure 4-13Aa,b) or non-permissive substrates coated with 50 μgmL^{-1} aggrecan (Figure 4-13Ac-j). Neurospheres cultured upon aggrecan-coated surfaces (Figure 4-13Ac,d) appear to produce far fewer neurites than those cultured on control surfaces (Figure 4-13Aa,b). The addition of ibuprofen to the culture medium (Figure 4-14Ae-j), resulted in the generation of more visible neurites than aggrecan-coating alone, with higher concentrations 100 μM – 500 μM of ibuprofen appearing to generate the most neurites.

Neurospheres cultured on 50 μgmL^{-1} aggrecan coated surfaces produced significantly fewer neurites per neurosphere (Figure 4-13B) than those cultured on control surfaces. This effect was rescued by ibuprofen treatment with the number of neurites per neurosphere increasing in a dose dependent manner with ibuprofen concentration. Ibuprofen treatment of 100 μM and 500 μM resulted in the generation of a similar number of neurites as control cultures.

The same effect is also observed in terms of neurite density (Figure 4-13C) with aggrecan coating significantly inhibiting neurite density compared with controls. Neurite density is partially restored with 10 μM ibuprofen treatment and higher concentrations of ibuprofen (100 μM – 500 μM) restores neurite density to similar levels as neurospheres cultured without aggrecan coating. Neurite length (Figure 4-13D) is slightly reduced by aggrecan coating, however, this is not statistically significant and 10 μM ibuprofen treatment has no effect upon neurite legnth. Higher concentrations of ibuprofen such as 100 μM and 500 μM, enhance neurite length significantly compared to neurites generate on both permissive and non-permissive substrates alone.

Neurospheres cultured in 3D remain on top of the scaffold (Figure 4-14Aa,c,e,g,i) whereas neurites penetrate the scaffold and are visible from below (Figure 4-14Ab,d,f,h,j). A large volume of neurites can be seen to have penetrated scaffolds coated with permissive, control proteins (Figure 4-14Aa,b), however, this is significantly reduced when scaffolds are coated with aggrecan (Figure 4-14Ac,d) and very few neurites are visible from the bottom view of the scaffold. More neurites have visibly penetrated aggrecan-coated scaffolds with increasing concentration of ibuprofen treatment.

This is reflected in the quantification of the number of neurites that have penetrated the scaffold (Figure 4-14B) with each treatment condition. In the absence of aggrecan, a large

number of neurites penetrate the scaffold, however in the presence of aggrecan coating, this number is significantly reduced. Ibuprofen medium treatment increases neurite outgrowth within aggrecan-coated 3D scaffolds, however even the highest concentration (500 μM) of ibuprofen tested does not fully restore neurite growth. Treatment with 500 μM ibuprofen results in a significant increase in neurite penetration compared with aggrecan coating without ibuprofen medium supplementation, however the number of neurites penetrating the scaffold is still significantly reduced compared with control cultures. Therefore ibuprofen partially restores aggrecan-induced inhibition of neurite growth in a 3D culture environment.

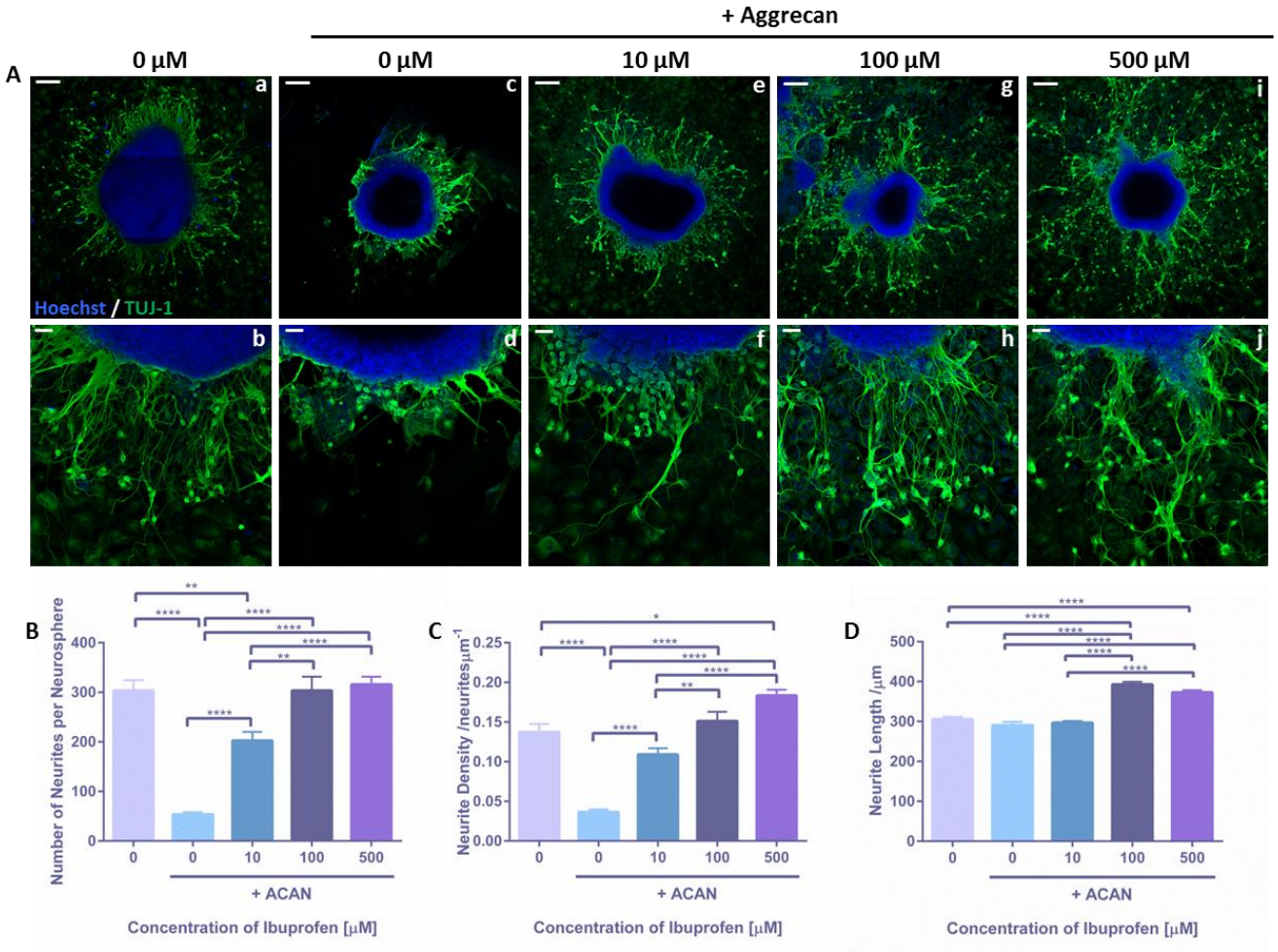

Fig 4-13: Ibuprofen overcomes aggrecan-mediated inhibition of neurite outgrowth in 2D culture.

Representative confocal images of neurospheres cultured on inhibitory 2D growth substrates coated with 50 µgmL^{-1} aggrecan (ACAN) and treated with ibuprofen (A). Scale bars: (Aa,c,e,g,i): 200 µm (Ab,d,f,h,j): 50 µm. Neurites are highlighted by staining for the pan-neuronal marker TUJ-1 (green) and nuclei are stained in blue. Neurospheres cultured without aggrecan (Aa,b) have a large amount of neurites radiating from the central cell aggregate, whereas those cultured on the inhibitory substrate have very few neurites protruding from the aggregate body (Ac,d). The number of neurites per neurosphere (B) (data represent mean ± SEM, n=9-27; between 3-9 neurospheres were quantified per independent replicate, of which there were 3) is greatly inhibited when neurospheres are cultured on inhibitory substrates, and the addition of ibuprofen is able to overcome such inhibition, restoring neurite outgrowth to levels similar to that of the control. Similarly, the density of neurites (C) (data represent mean ± SEM, n=9-27; between 3-9 neurospheres were quantified per independent replicate, of which there were 3) is restored by ibuprofen in the presence of aggrecan and even enhanced to levels greater than the control by high concentrations of ibuprofen. Neurite length (D) (data represent mean ± SEM, n=154-845; in total between 154-845 individual neurites were measured from 3 replicates of neurospheres derived from independent pools of cells) however, is only enhanced by high concentrations of ibuprofen. One-way ANOVA with Tukey's multiple comparisons: * = $p \leq 0.05$, ** = $p \leq 0.01$, *** = $p \leq 0.001$, **** = $p \leq 0.0001$.

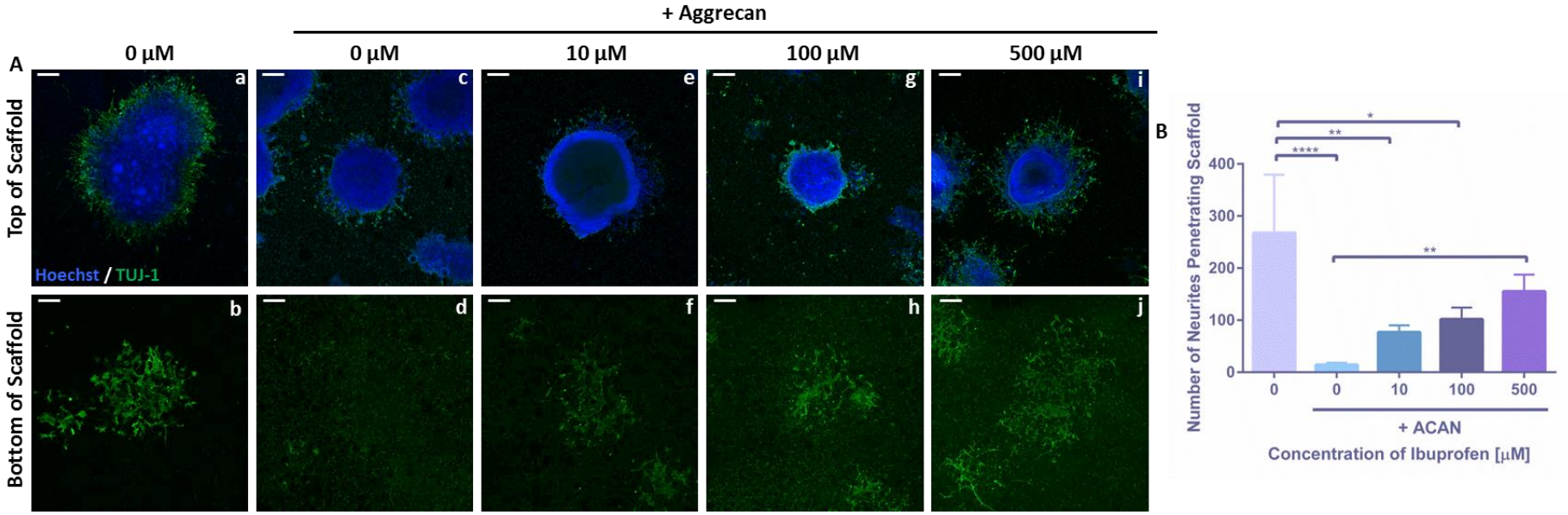

Fig 4-14: Ibuprofen overcomes aggrecan-mediated inhibition of neurite outgrowth in 3D culture.
Representative confocal images of neurospheres cultured on 3D inhibitory growth substrates coated with 50 µgmL^{-1} aggrecan (ACAN) and treated with ibuprofen (A). Neurospheres can be visualised from the top view of the scaffold (Aa,c,e,g,i) and TUJ-1 (green) positive neurites can be observed to have penetrated the 3D material and are visible from the bottom view of the scaffold (Ab,d,f,h,j). Scale bars: 200 µm. The number of neurites penetrating the scaffold (B) (data represent mean ± SEM, n=3-9; 2-3 neurospheres were quantified from 3 independent replicates) is greatly inhibited when neurospheres are cultured on aggrecan-coated scaffolds and this effect is rescued in a dose dependent manner with increasing ibuprofen concentration. However, the number of neurites penetrating the scaffold, even at the highest concentration of ibuprofen tested, still does not reach the same level as those neurospheres cultured without aggrecan. One-way ANOVA with Tukey's multiple comparisons: * = $p \leq 0.05$, ** = $p \leq 0.01$, *** = $p \leq 0.001$, **** = $p \leq 0.0001$.

4.3.2 Development of a Co-culture Model to More Accurately Reflect the in Vivo Environment of the Glial Scar

Reactive astrocytes are the major cell type involved in neurite inhibition within the glial scar. They express GFAP and secrete CSPGs, which act through receptors to induce growth cone collapse and inhibition of neurite growth. To more accurately reflect the cellular interactions that occur in the glial scar, and provide an alternative system to investigate the process of CSPG-induced inhibition, a co-culture model was developed.

This first required the characterisation and selection of a cell line that most accurately recapitulates the important aspects of reactive astrocytes that are involved in neurite inhibition i.e CSPG secretion. The chosen cell line was then carefully characterised to ensure the optimal set of growth conditions were used throughout the co-culture methodology and that expression of desired proteins remained constant when cultured in these conditions. A 2D co-culture model was then developed and applied to study the process neurite inhibition and inhibitors of CSPG-induced signalling were used to promote neurite recovery.

4.3.2.1 Characterisation and Selection of Glioma Cell Lines

To select an appropriate glioma cell line that best reflects the characteristics of the reactive astrocytes found in the glial scar, two commonly used cell lines were characterised. U-118MG cells are a human glioblastoma cell line with mixed morphology, Figure 4-15A is a phase contrast micrograph of U-118MG cells cultured at confluence in 2D. In 3D conditions, as shown by H&E staining (Figure 4-15B) U-118MG line the edges of the scaffold with cell layers visible on the top and bottom of the scaffold, and a small number of cells populate the centre of the scaffold.

U-251MG cells are also a human glioblastoma cell line, however they are known to contain GFAP positive cells. Figure 4-15C is a phase contrast image that depicts the morphology of U-251MG cells at confluence in 2D culture. Unlike U-118MG cells, in 3D culture U-251MG cells do not form cell layers on the top and bottom of the scaffold, as the majority of cells populate the centre of the 3D material.

Immunofluorescence staining highlights GFAP immunoreactivity (Figure 4-15E-H) in U-251MG cells cultured in 2D (Figure 4-15G) but not in U-118MG cultured in any condition (as expected) or in 3D cultured U-251MG cells (Figure 4-15H). A small amount of positive immunostaining for the chondroitin sulphate (CS) epitope (Figure 4-15I-L), which is an epitope present on CSPG molecules, can be observed in 2D (Figure 4-15I) and 3D (Figure 4-15J) cultures of U-118MG cells. However, there is no visibly apparent staining in 2D

cultures of U-251MG cells (Figure 4-15K) but perhaps the strongest staining is visible in 3D cultures (Figure 4-15L) of U-251MG cells.

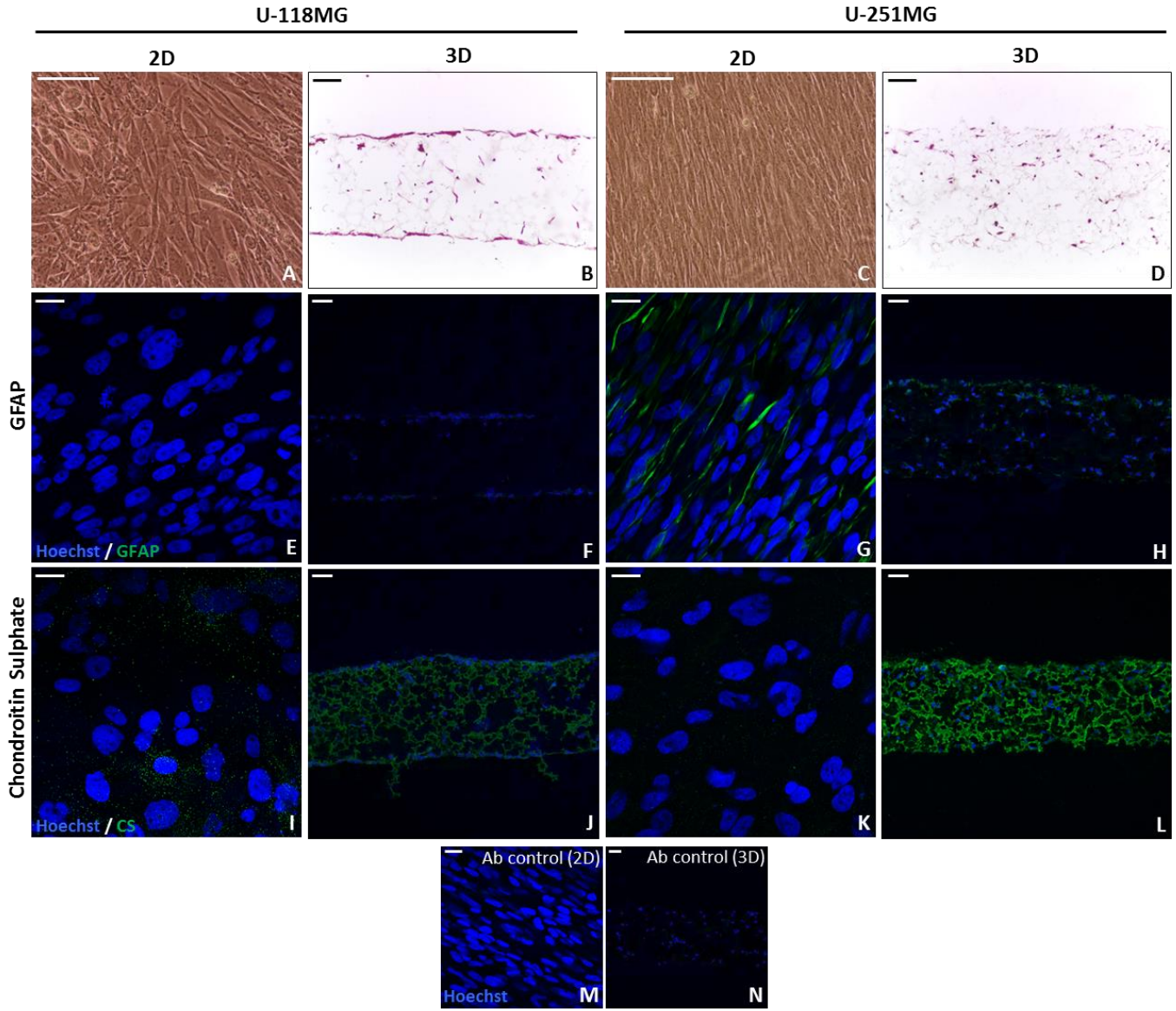

Fig 4-15: Characterisation and reactive marker expression in glioma cell lines cultured in 2D and 3D.
Representative phase contrast images of confluent cultures of the glioma cell lines, U-118MG (A) and U-251MG (C) cultured in 2D conditions. Representative H&E staining of U-118MG and (B) U-251MG (D) cell lines cultured in 3D for 10 days within Alvetex® scaffold. Representative confocal images of U-118MG and U-251MG cells cultured in 2D and 3D with the reactive astrocyte marker, GFAP being highlighted in green and nuclei stained blue (E-H). Representative confocal images of chondroitin sulphate expression in U-118MG and U-251MG cells cultured in 2D and 3D (I-L). U-251MG cells appear to express markers of reactive astrocytes found in the glial scar to a greater extent than U-118MG cells in 2D and 3D culture conditions. 2D (M) and 3D (N) antibody controls show no positive staining. Scale bars: (A-D): 100 µm, (E,G,I,K,M): 20 µm, (F,H,J,L,N): 50 µm.

Immunofluorescence staining of the CSPG marker, chondroitin sulphate, highlights positive expression of CSPGs within cells. However as CSPGs are secreted molecules, this does not necessarily give an accurate reflection of the CSPG-content of the culture medium. For this reason an ELISA assay was used to determine the CSPG concentration of the culture medium from 2D and 3D cultures of each glioma cell line. Figure 4-16 describes the data obtained from this assay, and although the results are not statistically significant, slight variances in the CSPG concentration of the culture medium can be noted. For example 2D cultures of U-118MG cells appear to contain a higher concentration of CSPGs than 2D cultures of U-251MG; however due to the lack of statistical support, little can be drawn from this. Similarly, 3D cultures of U-251MG appear to produce medium with a higher CSPG content than their 2D counterpart, which is supported by the immunofluorescence data described in Figure 4-15, however, again this is not statistically significant. The main observation made from this assay, therefore, is that both 2D and 3D cultures of U-118MG and U-251MG cells generate CSPG-containing medium.

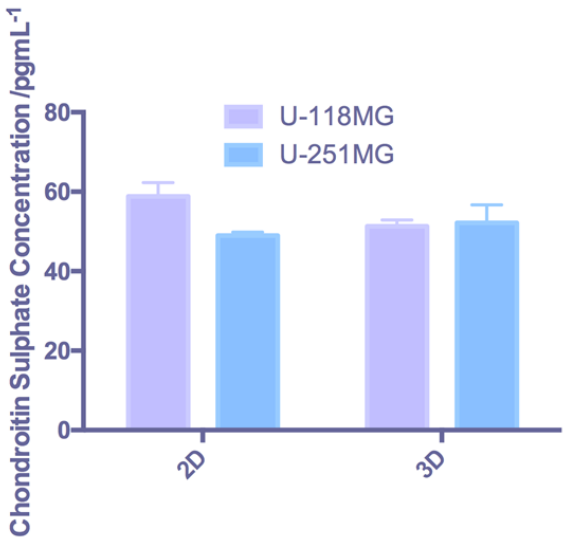

Fig 4-16: Characterisation of CSPG secretion from glioma cell lines cultured in 2D and 3D conditions.
An ELISA analysis of the CSPG content of medium conditioned by the glioma cell lines U-118MG and U-251MG for 10 days in 2D and 3D culture (data represent mean ± SEM, n=3; 3 samples individual cell cultures were tested). Medium conditioned by U-118MG cells cultured in 2D was found to have a higher CSPG content than U-251MG conditioned medium. However, in 3D culture, medium conditioned by U-251MG cells, was found to contain a slightly higher concentration of CSPG molecules than U-118MG conditioned medium.

Therefore from both the immunofluorescence and ELISA data it was decided that the U-251MG glioblastoma cell line was the most suitable to recapitulate aspects of reactive astrocyte signalling from the glial scar. U-251MG cells were found to positively stain for GFAP, a hallmark of reactive gliosis, whereas U-118MG cells do not express this marker. In addition to this, U-251MG cells were also found to highly express CSPGs in 3D culture. This is particularly important, as the main application of the co-culture model is to study the molecular signalling events that lead to CSPG-induced neurite inhibition.

4.3.2.2 Analysis of Optimal Growth Conditions for U-251MG Glioma Cells

4.3.2.2.1 Optimisation of Growth Medium

The guidelines outlined by the European collection of cell cultures (ECACC) for the culture of U-251MG cells describe the suitable culture medium as: Earle's Minimum Essential Medium supplemented with 2 mM L-glutamine, 1 % non-essential amino acids, 1 mM sodium pyruvate and 10 % FBS (EMEM). However, the human pluripotent stem cell line, TERA2.cl.SP12, which the neurite outgrowth model is based upon, require culture medium of Dulbecco's Modified Eagle's Medium supplemented with 2 mM L-glutamine, 1 mM sodium pyruvate and 10 % FBS (DMEM). Therefore, to combine both cell types in a co-culture model of neurite inhibition, one culture medium must be selected in which both cell types can be cultured without adverse effects upon protein expression and cellular phenotype. As the neurite outgrowth model had previously been optimised and developed using DMEM, it was decided to analyse the effect of this medium upon the glioma cell line.

Figure 4-17 outlines the effect of each medium composition on U-251MG cellular growth and morphology over a 10-day time frame, which is the normal timescale of a neurite outgrowth study. Phase contrast images of U-251MG cells cultured in EMEM in 2D over time (Figure 4-17Aa-c) show cell density increasing over the culture period, with cells appearing extremely sparse at day 2 post-seeing (Figure 4-17Aa) and extremely confluent at day 10 (Figure 4-17Ac). Phase contrast images of cells cultured in 2D in DMEM (Figure 4-17Ag-i) however, appear less confluent compared with their EMEM counterpart. Cells cultured in 2D with DMEM at day 6 appear only 80 – 90 % confluent rather than the extremely dense 100 % confluent monolayer observed in EMEM cultures.

A similar effect is noted in H&E stained 3D cultures (Figure 4-17Ad-f,j-l) with cell density appearing to increase over the culture period. However at day 10, cells cultured in EMEM (Figure 4-17Af) appear to change in morphology, with cells appearing more rounded and darkly stained, perhaps indicative of cellular death. This morphological change is not

noted in 3D DMEM cultures, with cells maintaining their healthy morphology even at day 10 in culture. This apparent cell death could be induced as maximal confluency or competition for nutrients is reached in cell dense cultures, as cell proliferation appears to be enhanced in EMEM as oppose to DMEM.

This effect upon cellular proliferation was further investigated by use of an MTT cell viability assay, that utilises precipitate formation measured as absorbance, as an indirect measure of cell viability. In 2D cultures (Figure 4-17B) grown in EMEM, absorbance, thus cell viability was found to increase over the 10-day culture period, however at day 10, absorbance was found to decrease slightly. This suggests a loss of cell viability toward the end of the culture period in 2D conditions with EMEM. However, when cells were cultured in 2D with DMEM, MTT absorbance increased steadily over the period, with no evident decrease in viability apparent over the course of the culture. Interestingly, MTT absorbance was found to be consistently higher in EMEM cultures than DMEM in 2D conditions, prior to the EMEM-induced reduction in cell viability. This consolidates the observations made based upon the phase contrast micrographs, that cells proliferate more quickly in EMEM, which perhaps also explains the reduction in viability noted at day 10, as cells become over confluent and begin to die.

MTT viability of cells cultured in 3D (Figure 4-17C) with EMEM decreases initially, before slowly beginning to increase and decreasing once again toward the end of the culture period. Again this reduction in viability is also evidenced in the H&E image of a representative day 10 culture, as morphological changes consistent with cellular death were apparent. Similarly, the viability of 3D-DMEM cultures was found to remain mostly constant throughout the culture period with an increase in viability around day 6. Generally the viability of 3D-DMEM-based cultures was good and consistently higher than EMEM cultures.

Immunostaining highlights expression of GFAP (Figure 4-18A) and chondroitin sulphate (Figure 4-18B) in each culture medium and within 2D and 3D cultures. This reveals that less confluent 2D cultures maintained in DMEM (Figure 4-18Ab) express GFAP to a much greater extent than those fully confluent cultures maintained in EMEM (Figure 4-18Aa). This is similar to chondroitin sulphate expression, which appears enhanced in DMEM (Figure 4-18Bb) 2D cultures as opposed to EMEM (Figure 4-18Ba) cultures. However expression of GFAP is not evident in 3D cultures maintained with both media (Figure 4-18Ac,d) and very little positive chondroitin sulphate staining is apparent with either medium type (Figure 4-18Bc,d). The chondroitin sulphate content of medium collected from each culture condition was analysed by ELISA (Figure 4-18D) and although the results obtained were not statistically significant, a slight increase in CSPG expression in 3D DMEM-based cultures was noted.

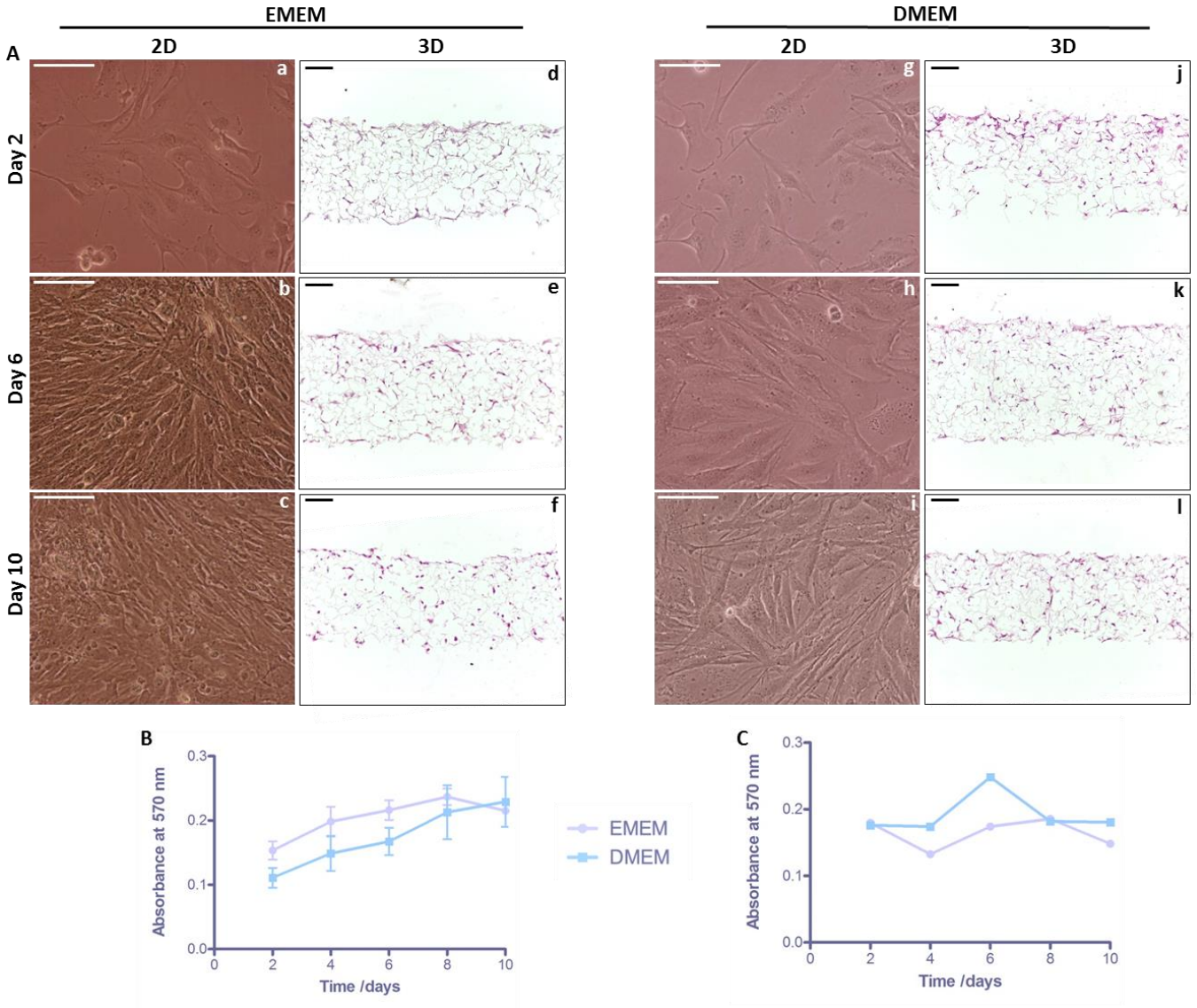

Fig 4-17: The effect of different media conditions on the growth of U-251MG glioma cells.
U-251MG glioma cells were cultured for 10 days either in the recommended maintenance medium of EMEM (supplemented with 10 % FBS, 2 mM L-glutamine, 1 % NEAA, 1 mM sodium pyruvate and 20 active units of penicillin and streptomycin) or DMEM (supplemented with 10 % FBS, 2 mM L-glutamine, and 20 active units of penicillin and streptomycin). Representative phase contrast images (Aa-c, g-i) of U-251MG cultured in 2D and haematoxylin and eosin staining (Ad-f, j-l) of U-251MG cells grown in 3D within Alvetex® scaffold in both EMEM and DMEM. Scale bars: 100 µm. Cells cultured in EMEM appear to reach confluency earlier in culture than those cultured in DMEM. MTT cell viability analysis of cells cultured in 2D (B) and 3D (C) in both types of medium (data represent mean ± SEM, n=3; repeated with 3 independent cultures).

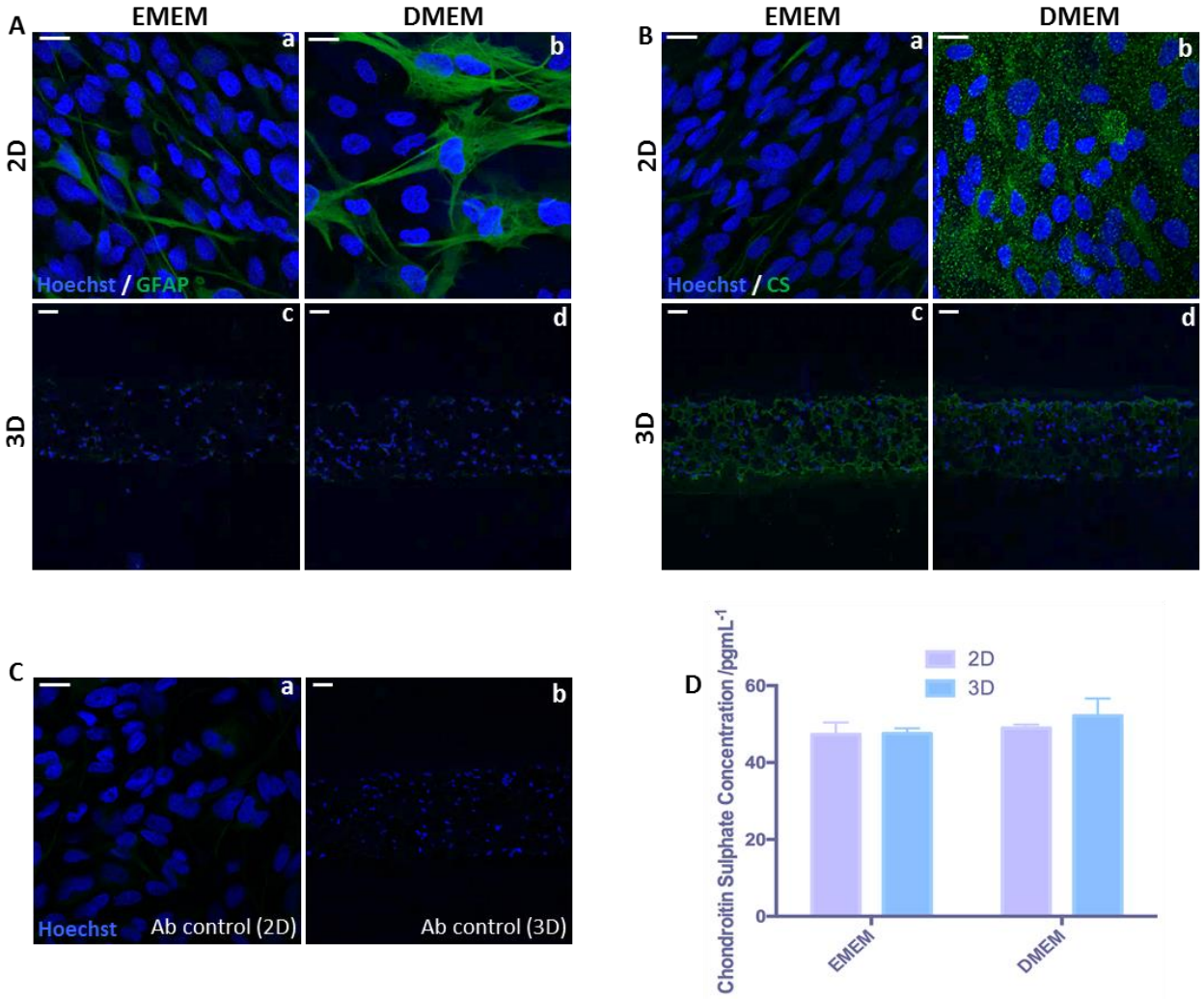

Fig 4-18: The expression of reactive astrocyte markers in U-251MG glioma cells is dependent upon culture medium.
Representative confocal images of U-251MG cells cultured in EMEM or DMEM for 10 days in both 2D and 3D culture environments. Expression of GFAP (A, green) appears increased in 2D (Aa,b) cells cultured in DMEM rather than EMEM, whereas 3D cultures (Ac,d) do not appear to express GFAP in levels similar to 2D. Expression of chondroitin sulphate (B, green), a motif common to CSPGs, appears increased in cells cultured in 2D (Ba,b) in DMEM, rather than EMEM medium. 3D cultures (Ba,d) appear to express chondroitin sulphate (CS) to a slightly greater extent when cultured in EMEM rather than DMEM. Hoechst stains nuclei blue and 2D (Ca) and 3D (Cb) antibody controls show no positive staining. Scale bars: 20 µm. ELISA analysis (D) of the chondroitin sulphate content of culture medium from cells cultured in each growth medium (EMEM/DMEM) suggests that cells cultured, particularly in 3D, in DMEM secrete more CS containing molecules into the culture medium than cells cultured in EMEM (data represent mean ± SEM, n=3; medium from 3 independent cultures per condition).

Therefore, EMEM was found to enhance proliferation of U-251MG cultures in comparison to DMEM, which is not suitable for this co-culture application as cells become over confluent and lose viability over the 10-day duration of a neurite outgrowth assay. However, the slower growth and enhanced viability in 3D culture of DMEM cultured cells, is more favourable for maintenance of U-251MG cells over the course of an assay and allows for the easy incorporation of the cells into the existing neurite outgrowth methodology. In addition to this, the enhanced expression of GFAP and CS observed in DMEM 2D cultures, suggests that when cultured at a lower cell density in DMEM, cells express more of the desired characteristics of native reactive astrocytes.

4.3.2.2.2 Optimisation of Cell Seeding Density

As U-251MG cells were found to express both GFAP and CS to a greater degree in DMEM-based cultures that were less densely populated than their EMEM-based counterparts, it was hypothesised that cellular density (confluency) may play a role in the regulation of expression of these key proteins. For this reason, the expression of both GFAP and CS was measured by immunofluorescence in 2D and 3D cultures of varying densities (Figure 4-19).

Phase contrast micrographs reveal the morphology of U-251MG cells in 2D culture at sub-confluency (Figure 4-19A) where large areas of unpopulated space can be seen and confluent cultures of densely packed cells (Figure 4-19B). There appears to be increased immunoreactivity to both GFAP (Figure 4-19G,H) and CS (Figure 4-19M,N) in sub-confluent 2D cultures compared with their confluent counterpart. This suggests that in 2D culture U-251MG cells express both GFAP and CSPGs to a greater extent when cells are less densely packed together. This further supports the use of DMEM to reduce cellular proliferation and maintain cells in a sub-confluent state, expressing GFAP and CS throughout the 10-day culture period.

Furthermore, a variety of cell seeding densities (0.5 million – 3 million cells per scaffold) in 3D culture were also trialed, and expression of GFAP and CS was analysed. H&E images demonstrate increasing density of cells populating the scaffold in 3D culture (Figure 4-19C-F) with increasing cell seeding density. There appears to be a thick cell-dense layer on top of scaffolds seeded with 3 million cells (Figure 4-19F), as not all cells penetrate and populate the 3D material. Little GFAP-positive staining is noted in 3D cultures, however, a small amount of positive staining is identifiable in cultures seeded with the lowest cell densities (0.5 – 1 million cells per scaffold) (Figure 4-19I-J), whereas no positive staining is evident in scaffolds seeded with 2 and 3 million cells (Figure 4-19K-L). Interestingly, the strongest, positive staining for CS expression is observed in cultures seeded with 0.5 million cells (Figure 4-19O) and little positive staining is present in cultures seeded with a

larger number of cells (Figure 4-19P-R). However, expression of CS in cultures seeded with 3 million cells (Figure 4-19R) appears to form a gradient, with highest expression at the bottom of the scaffold and as cell density increases toward the top of the scaffold, where the thick cell layer is located, expression of CS becomes reduced.

This proposed relationship between confluency and CSPG/GFAP expression was further evidenced by western blot analysis of protein expression from cells cultured in each 2D and 3D condition (Figure 4-20A). Versican is a CSPG known to be expressed by the glioma cell line U-251MG and due to alternative splicing, several isoforms of varying molecular weight exist (V_0 – V_4)[376]. Through western blotting it was determined that most versican isoforms (V_1 – V_4) are expressed much more highly in 3D culture than in 2D, and expression is maximal at lower seeding densities, decreasing with as cell density increases. However, the expression of V_0 increased with seeding density, opposing the expression profile of the other isoforms and perhaps suggesting some reciprocal control mechanism. Similarly to versican, expression of GFAP was also found to decline with increasing cell density and expression was greater in 3D cultures, further confirming the immunofluorescence findings. β-actin was used as a loading control and little variation between lanes is evident.

ELISA analysis of the CSPG content (Figure 4-20B) of medium generated from 3D cultures seeded with increasing cell densities (0.5 – 3 million cells per scaffold) reveals little difference in concentration between the conditions. However, it does appear that there may be a dose-dependent decrease in CSPG-content of the culture medium with increasing cell seeding density, but this is not statistically significant.

Therefore, it appears that at low cell density U-251MG cells express protein markers consistent with reactive astrocytes found in the glial scar to a greater degree. This has been evidenced by a number of techniques including immunofluorescence, western blotting and ELISA and the outcome remains consistent. This is a consideration that must be taken into account during the development of a co-culture model, as a seeding density should be selected that allows for maximal expression of proteins of interest. In addition to this, the enhanced expression of GFAP and CSPGs observed in 3D culture, is also an interesting finding. This could be due to the increased surface area provided by the 3D scaffold, resulting in fewer cell-cell interactions and a reduced cellular density, in turn leading to enhanced expression of GFAP and CSPGs. This finding also supports the use of 3D cell culture technology throughout this study to enhance the expression of such proteins in U-251MG cultures.

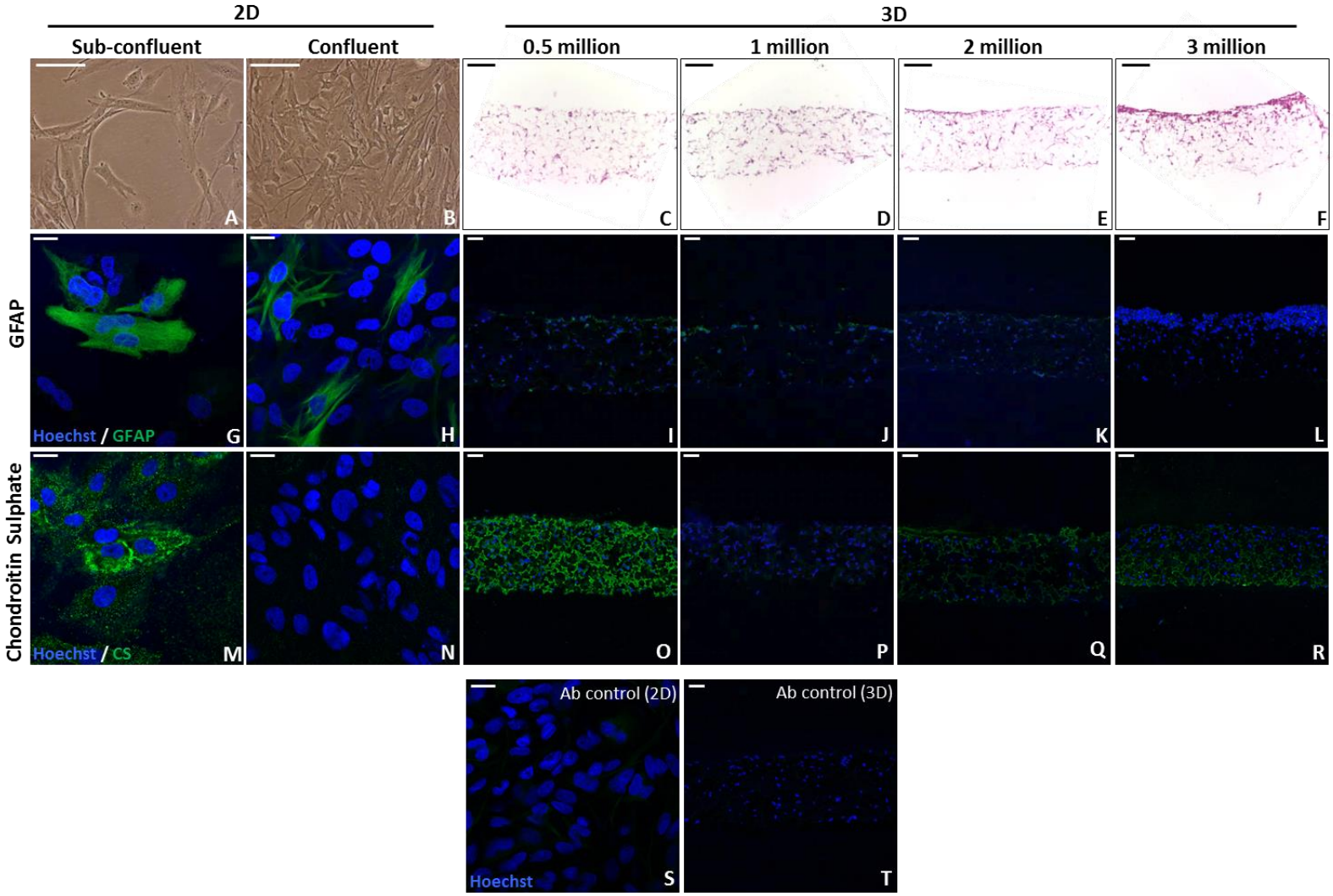

Fig 4-19: Immunostaining of reactive astrocyte markers in U-251MG glioma cells is confluency dependent. Representative phase contrast images of U-251MG cells cultured at low confluency (A) and high confluency in 2D (B). Representative haematoxylin and eosin staining of U-251MG cells cultured in 3D within Alvetex® Scaffold for 10 days at varying seeding densities (C-F). Representative confocal images of GFAP expression of U-251MG cells cultured in 2D (G,H) and 3D (I-L) culture at different levels of confluency. Representative confocal images of chondroitin sulphate (CS) expression, a motif common to CSPGs, in glioma cells cultured in 2D (M,N) and 3D (O-R). Nuclei are stained by hoechst in blue and antibody controls (S,T) are negative for staining. Cells appear to express both GFAP and chondroitin sulphate more at lower confluency. Scale bars: (A-D): 100 µm, (G,H,M,N): 20 µm, (I-L,O-R): 50 µm.

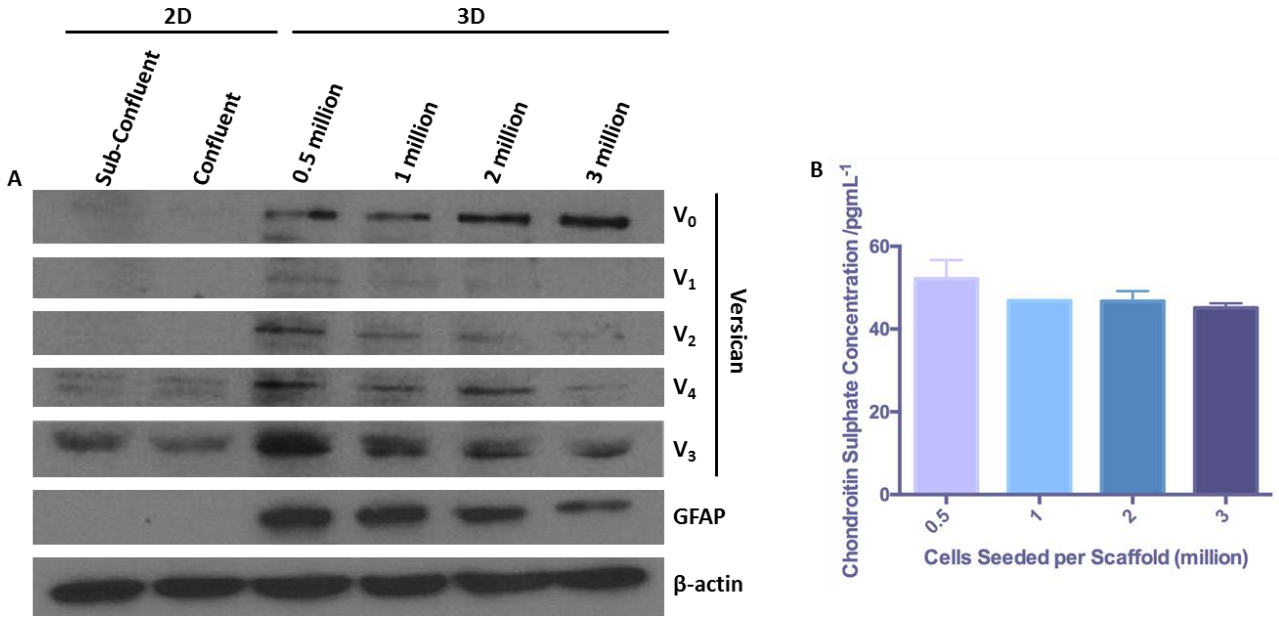

Fig 4-20: The expression of reactive astrocyte markers in 2D and 3D cultured U-251MG cells is dependent upon cellular confluency.
Representative western blot analysis (A) of versican and GFAP expression with increasing confluency in 2D and 3D cultured U-251MG cells. Versican is a CSPG molecule and its isoforms (V_{1-4}) along with GFAP are expressed more in 3D cultures that are seeded with less cells and expression decreases with increasing cell-seeding density. These molecules are also expressed much less in 2D cultures than 3D cultures. However, the V_0 isoform is expressed much more at higher seeding densities in a pattern that opposes the expression of V_{1-4}. ELISA analysis (B) (data represent mean ± SEM, n=3; conditioned medium from 3 independent cultures) of the chondroitin sulphate content of medium conditioned by U-251MG cells cultured in 3D at a range (0.5 – 3 million) of seeding densities. Chondroitin sulphate secretion appears to be dependent upon confluency and its expression appears enhanced at lower seeding densities.

4.3.2.3 Application of a 2D Co-culture Glioma/Neurosphere Model to Investigate Neurite Inhibition

Following the optimsation of each of the U-251MG growth parameters, a 2D co-culture model to study the process of CSPG-mediated neurite inhibition could finally be developed. This involved the seeding of U-251MG cells in 2D wells of standard tissue culture plates coated with poly-D-lysine and laminin as per the neurite outgrowth protocol. Glioma cells were allowed to adhere for 24 hours prior to the seeing of fully differentiated neurospheres for neurite outgrowth studies. Initially a variety of glioma cell seeding densities (10,000 – 40,000 cells per well of a 48-well tissue culture plate) were trialed to identify the optimal set of conditions to study neurite outgrowth (Figure 4-21A).

Neurite outgrowth (TUJ-1 positive staining – green) can be seen to radiate from neurospheres cultured on glioma cell monolayers (GFAP positive staining – red) (Figure 4-21A). Neurite outgrowth appears reduced with increasing U-251MG seeding density and neurites become extremely short and barely able to extend from the neurosphere at the maximum seeding density of 40,000 glioma cells per well (Figure 4-21Ai,j). This could either be due to CSPG-induced inhibition or mechanical blockage of neurites by the physical presence of glioma cells.

Quantification of neurite outgrowth reveals a dose dependent inhibition in the number of neurites per neurosphere (Figure 4-21B) with increasing glioma cell seeding density. However, this is not statistically significant and there appears to be a potential anomalous point at 20,000 cells per well. This anomaly disappears when neurite growth is normalised to neurosphere size and expressed as neurite density (Figure 4-21C), in addition to this, differences between the glioma cell seeding densities also become statistically significant. Therefore the co-culture of neurospheres and glioma cells results in a statistically significant inhibition of neurite density. Neurite length (Figure 4-12D) however, is a lot more variable amongst the seeding densities tested with significant inhibition only observed with 20,000 and 40,000 cells per well and an apparent increase in neurite legnth with 10,000 U-251MG cells per well.

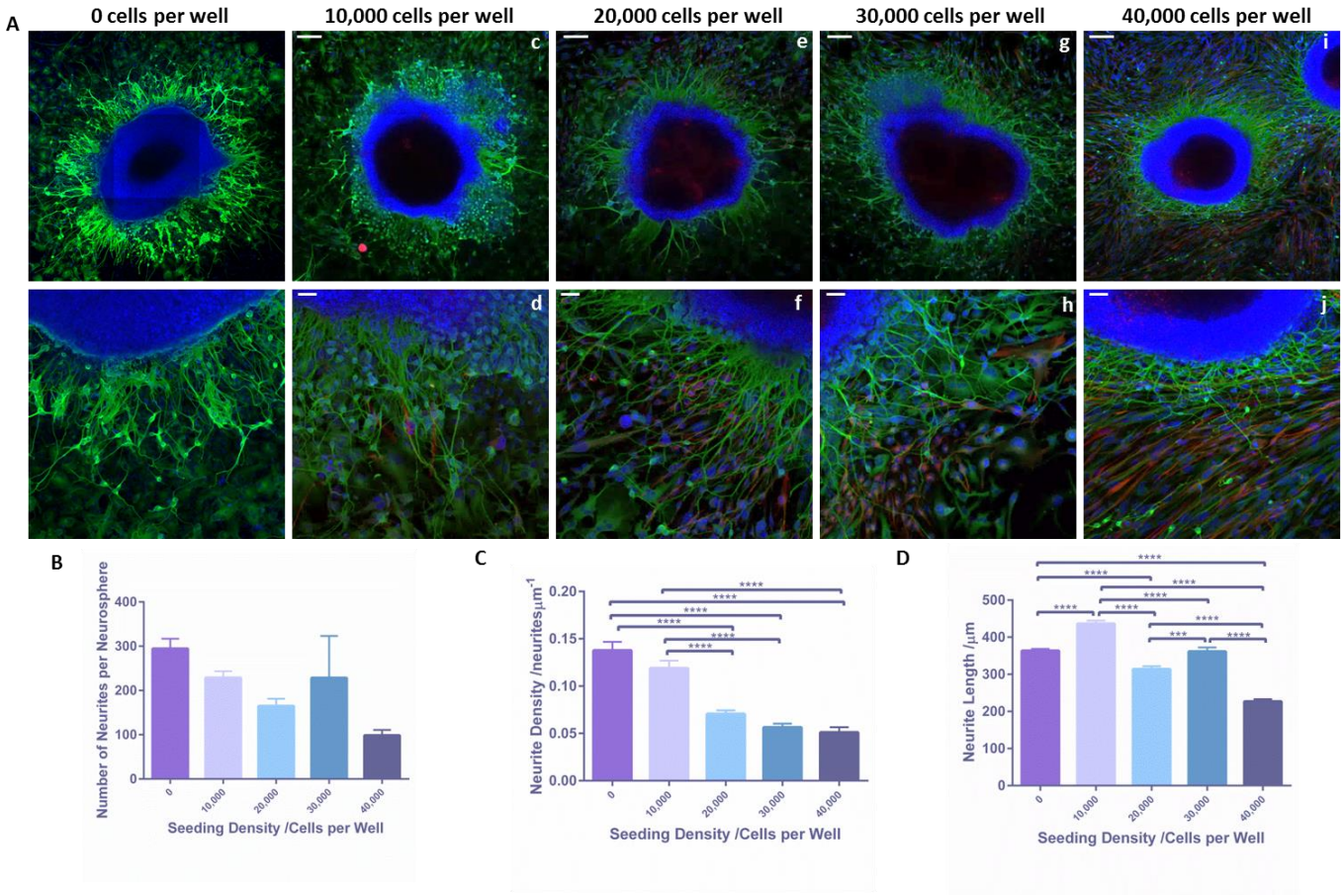

Fig 4-21: Co-culture of neurospheres with U-251MG glioma cells in 2D is inhibitory to neurite outgrowth.
Representative confocal images of neurospheres co-cultured with U-251MG cells at varying seeding densities (A). Glioma cells were seeded at varying seeding densities 24 hours prior to the addition of neurospheres to the culture, to allow glioma cells to adhere and form a monolayer of cells. The pan-neuronal marker, TUJ-1 (green), highlights neurite outgrowth, while U-251MG can be distinguished due to their positive expression of the intermediate filament protein, GFAP (red) and nuclei are highlighted in blue. Scale bars: (Aa,c,e,g,i): 200 µm (Ab,d,f,h,j): 50 µm. Quantification of the number of neurites per neurosphere (B) (data represent mean ± SEM, n=15-27; between 5-9 neurospheres were quantified from 3 independent replicates) at each seeding density indicates that increasing seeding density of glioma cells is gradually more inhibitory to neurite outgrowth. Neurite density (C) (data represent mean ± SEM, n=15-27; between 5-9 neurospheres were quantified from 3 independent replicates), also gradually declines with increasing glioma cell seeding density and reaches a maximal state of inhibition at 30,000 cells per well of a 48-well culture plate, as increasing the seeding density further does not impact neurite outgrowth. However, the average length of neurites (D) (data represent mean ± SEM, n=256-461; in total between 154-845 individual neurites were measured from 3 replicates of neurospheres derived from independent pools of cells) was only found to be inhibited in the presence of 20,000 or 40,000 glioma cells per well. One-way ANOVA with Tukey's multiple comparisons: * = $p \leq 0.05$, ** = $p \leq 0.01$, *** = $p \leq 0.001$, **** = $p \leq 0.0001$.

Several approaches were then used to potentially recover neurite outgrowth in this 2D co-culture model. This included growth medium supplementation with chondroitinase (Ch'ase), an enzyme known to break down CSPGs rendering them inactive, along with inhibitors of the downstream signalling pathway induced by CSPG-mediated receptor activation that leads to neurite inhibition. Y-27632 is a selective inhibitor of ROCK and ibuprofen is an inhibitor of Rho A both of which are known to be involved in CSPG-mediated signalling downstream of receptor activation, and lead to changes in the actin cytoskeleton associated with neurite retraction. For this reason, Ch'ase, Y-27632 and ibuprofen were all added to the culture medium of 2D co-culture models to potentially induce neurite outgrowth within this inhibitory environment (Figure 4-22).

A significant volume of neurites can be observed to radiate from neurospheres cultured in the absence of U-251MG cells (Figure 4-22Aa,b) whereas neurites become much shorter and struggle to develop and fully extend in the presence of glioma cells (Figure 4-11Ac,d). Although neurite outgrowth does not appear comparable with the monoculture control, the addition of Ch'ase (Figure 4-22Ae,f) to co-cultures does perhaps seem beneficial to neurite legnth. The addition of 10 μM Y-27632 (Figure 4-22Ag,h) to co-cultures appears to rescue the inhibitory phenotype induced by the glioma cells, as neurite outgrowth appears dense and neurites appear long. A similar result is noted with 500 μM ibuprofen treatment (Figure 4-22Ai,j), as again neurite outgrowth appears dense, although neurite legnth still appears to be impaired. Interestingly, in both Y-27632 and ibuprofen treated samples, it appears that the number of GFAP positive (red) glioma cells is reduced and their morphology appears unusual. This could suggest that inhibition of such an essential cellular pathway has adverse effects upon glioma cell structure and function.

The number of neurites per neurosphere (Figure 4-22B) is significantly inhibited in co-cultures with glioma cells. Ch'ase treatment was found to significantly enhance neurite number in co-cultures, restoring neurite outgrowth to a similar level as the monoculture control. Y-27632 treatment was not only found to restore the number of neurites per neurosphere to control levels, but also significantly enhance neurite outgrowth compared with control cultures. Ibuprofen treatment has a similar effect upon neurite number as Y-27632, in that neurite outgrowth in co-cultures is enhanced to a level greater than that of monoculture, however this enhancement is not statistically significant in the case of ibuprofen treatment.

Neurite density (Figure 4-22C) is similarly, significantly inhibited by glioma cell co-culture, and restored to a level reminiscent of the control with Ch'ase treatment. Y-27632 and ibuprofen were both found to not only recover neurite density but to significantly enhance neurite density in co-culture models compared with their monoculture control

counterpart. This action of Y-27632 and ibuprofen to restore neurite outgrowth could arise due to their apparent detrimental effect upon U-251MG glioma cells. There appears to be a reduced number of GFAP positive U-251MG cells visible in Y-27632 and ibuprofen treated cultures which could be due to cell-death, induced by inhibition of Rho A and ROCK signalling. This could give rise to reduced inhibitory action which could mediate the recovery in neurite outgrowth observed in these cultures, as oppose to a reduction in inhibitory signalling. However, this would not explain the increase in neurite density observed with both Y-27632 and ibuprofen treatment, which has also been observed in the absence of inhibitory stimulus as described in Chapter III.

Neurite length (Figure 4-22D) is significantly inhibited by the presence of U-251MG cells. A partial, but significant recovery in neurite length is observed with Ch'ase treatment, and Y-27632 also partially restores neurite legnth, to a greater extent than Ch'ase. Ibuprofen treatment, however, further inhibits neurite legnth to a greater degree than co-culture alone. This perhaps is not surprising if the effect of ibuprofen upon neurite length in the absence of an inhibitory stimulus (as described in Chapter III) is considered.

One criticism of this co-culture model is, perhaps, that direct contact between the glioma cells and neurites may lead to physical inhibition of neurite growth as oppose to solely CSPG-mediated inhibition, which is the interest of this study. This is true, and physical interactions between the glioma cells and neurites will impact neurite outgrowth. However, the ability of Ch'ase to restore neurite outgrowth to control levels in this system indicates that at least one component of the inhibition observed here is mediated by CSPGs.

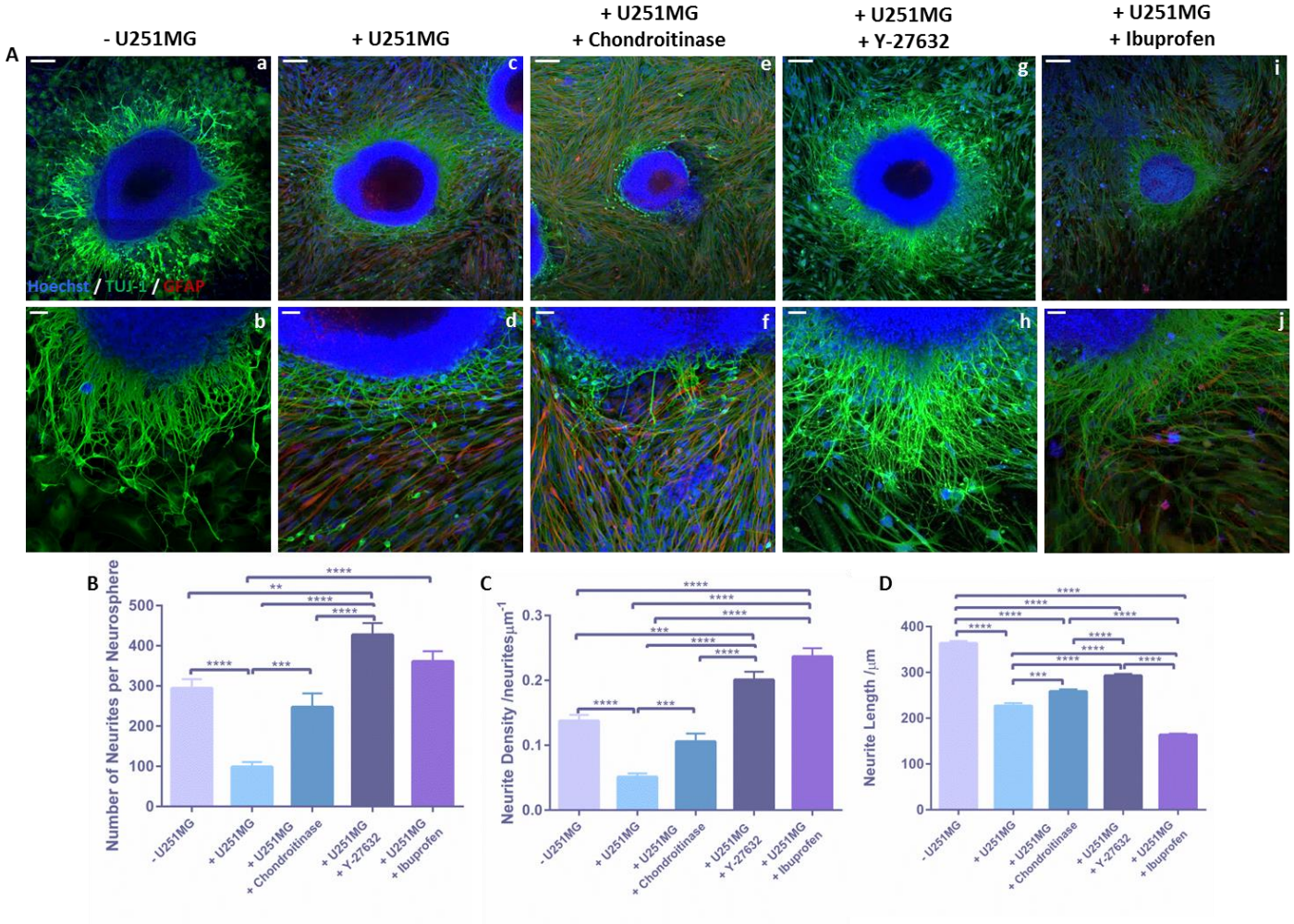

Fig 4-22: Recovery of neurite outgrowth through inhibition of Rho A/ROCK signalling in a 2D co-culture system. Representative confocal images of neurospheres co-cultured with U-251MG cells (40,000 cells per well of a 48-well tissue culture plate) with the addition of chondroitinase, Y-27632 or ibuprofen to the culture medium (A). The pan-neuronal marker TUJ-1 highlights neurite outgrowth in green, while U-251MG cells are highlighted in red due to their GFAP expression and nuclei are stained blue. Scale bars: (Aa,c,e,g,i): 200 µm (Ab,d,f,h,j): 50 µm. Number of neurites per neurosphere (B) (data represent mean ± SEM, n=9-27; between 5-9 neurospheres were quantified from 3 independent replicates) and neurite density (C) (data represent mean ± SEM, n=9-27; between 5-9 neurospheres were quantified from 3 independent replicates) are significantly inhibited in the presence of U-251MG cells which is recovered to a level similar to that of the control with the addition of chondroitinase and significantly enhanced with the addition of Y-27632 and ibuprofen to the culture medium. Neurite length (D) (data represent mean ± SEM, n=256-707; in total between 256-707 individual neurites were measured from 3 replicates of neurospheres derived from independent pools of cells) is significantly inhibited by the glioma cells, and although medium supplementation increases neurite length, under none of the conditions tested does it reach the same level as the control, in the absence of glioma cells. One-way ANOVA with Tukey's multiple comparisons: * = $p \leq 0.05$, ** = $p \leq 0.01$, *** = $p \leq 0.001$, **** = $p \leq 0.0001$.

4.3.3 Investigation into the Effect of Rho A/ROCK Signaling on U-251MG Glioma Cells

Unusual observations were made in reference to the morphology and confluency of glioma cells within the 2D co-culture system when treated with Y-27632 and ibuprofen. These treatments resulted in glioma cells losing their characteristic morphology and adopting a more stellate shape. In addition to this glioma cell monolayers appeared less dense, and fewer cells were observed. To investigate the cytotoxic effects of inhibition of Rho A and ROCK upon U-251MG dose responses with each molecule were conducted throughout a 10-day culture period.

Confluency of U-251MG 2D monolayers incubated with a range of concentrations (0.5 – 50 μM) of Y-27632 can be observed within the phase contrast micrographs (Figure 4-23Aa-d). Monolayers cultured without Y-27632 medium supplementation (Figure 4-23Aa) appear fully confluent and very densely packed together, whereas 50 μM treatment results in a less densely packed monolayer of cells that appear to extend long cytoplasmic processes. Apoptotic cell death was detected by use of a TUNEL assay (Figure 4-23Ae-i) which stains double stranded breaks in DNA, resulting in green staining within the nuclei of apoptotic cells (Figure 4-23Ai). Apoptotic cell death was not detectable within the range of Y-27632 concentrations tested, as no positive staining was detected (Figure 4-23Ae-h). This suggests that the reduction in cell density observed within Y-27632 treated cultures is due to a reduction in cellular proliferation as oppose to an increase in cell death.

To test this hypothesis, MTT cell viability assays were used to determine the effect of Y-27632 concentration upon cellular viability (Figure 4-23B). Absorbance was found to decrease in a linear fashion with increasing Y-27632 concentration suggesting that at high concentrations, less metabolically active cells are present. This further evidences the observation made upon analysis of the phase contrast images, that at high concentrations of Y-27632, cultures contain fewer cells. To determine that this effect is due to slower proliferation over the course of the culture, rather than a loss of viability, MTT cell viability was coducted over the 10-day culture period (Figure 4-23C). Monolayers treated with 50 μM Y-27632 consistently produced an absorbance reading much less than that of their untreated counterpart, indirectly suggesting that less viable cells are present in Y-27632 treated cultures. Furthermore, the absorbance reading of both treated and untreated cultures increases over the 10-day time frame. This suggests that within the limits of this assay, both treated and untreated cells have proliferated over the course of the culture period, however Y-27632 treated cells have proliferated more slowly.

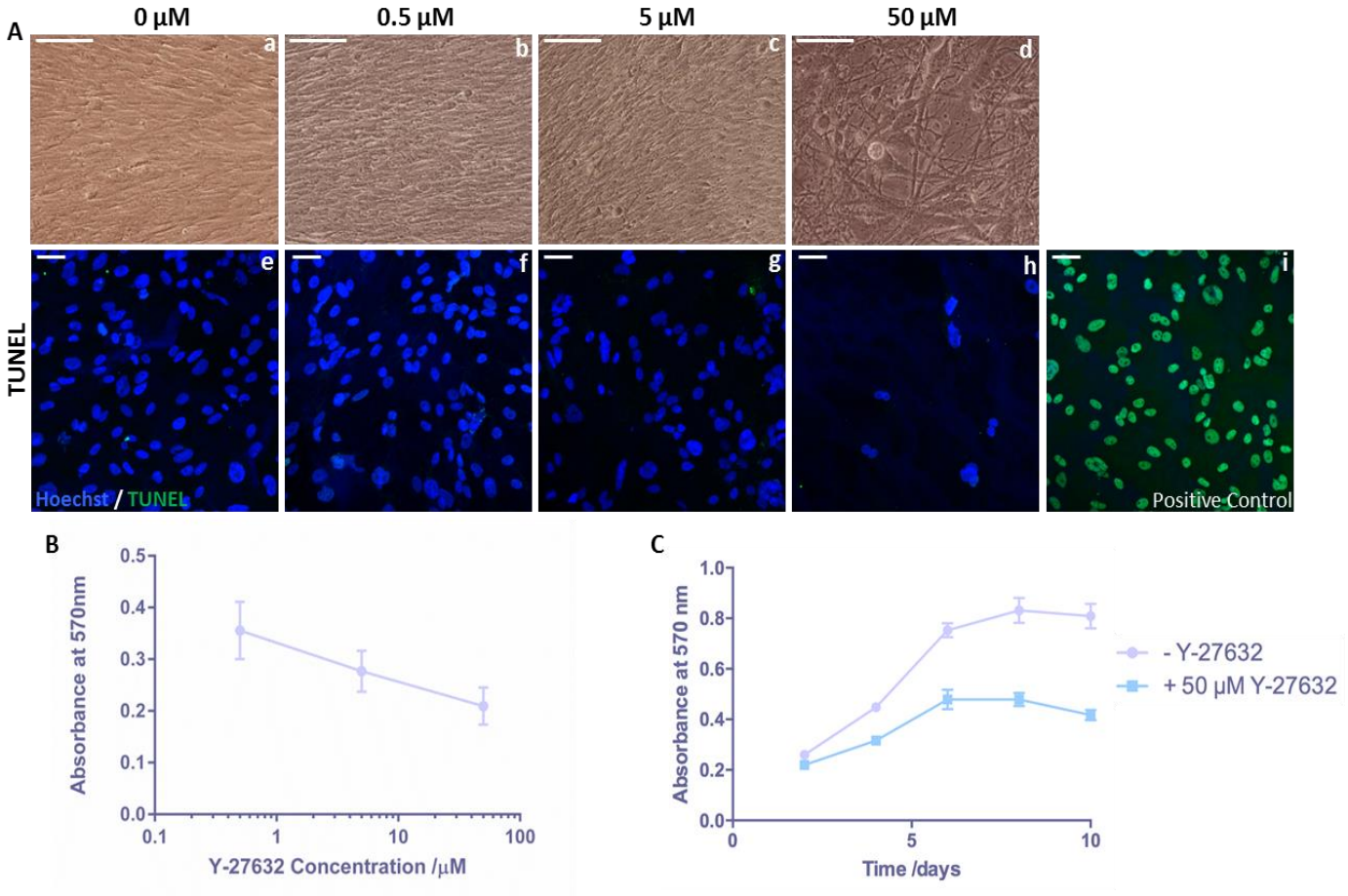

Fig 4-23: Inhibition of ROCK reduces cell density, in the glioma cell line U-251MG.

Representative phase contrast images of U-251MG glioma cells cultured for 10 days in the presence of a range of concentrations (0 – 50 µM) of the selective ROCK inhibitor, Y-27632 (Aa-d). Cells appear extremely confluent at lower concentrations of the molecule; however, at higher concentrations cell density appears much less. Representative confocal images of TUNEL staining (Ae-h), indicate the presence of apoptotic cells by staining fragmented DNA green, as can be seen in the positive control (Ai). There is no evidence of apoptotic cell death with any concentration of Y-27632 tested. Scale bars: (Aa-d): 100 µm, (Ae-i): 50 µm. MTT cell viability data for U-251MG cells cultured with a range of concentrations (0 – 50 µM) Y-27632 for 10 days (B) shows that with increasing concentration, cell viability decreases. MTT cell viability over the 10-day culture period (C) with and without 50 µM Y-27632 treatment, shows that under both conditions cell viability increases over the culture period indicating that the cells are proliferating and not dying, however with Y-27632 treatment, they appear to proliferate at a much slower rate.

Monolayers of U-251MG cells treated with a variety of concentrations of ibuprofen (50 – 750 μM), also appear less confluent following a 10-day culture period. This effect can be observed in the phase contrast micrographs (Figure 4-24Aa-e) as untreated cultures appear extremely densely packed and confluent whereas cultures treated with high concentrations of ibuprofen (500 – 750 μM) appear significantly less confluent. Cultures treated with 500 μM (Figure 4-24Ad) ibuprofen appear significantly less dense compared with untreated monolayers and cultures treated with 750 μM (Figure 4-24Ae) ibuprofen appear sparsely populated with cells.

As with Y-27632 treatment, a TUNEL assay (Figure 4-24Af-j) was used to determine the presence of apoptotic cells within the cultures and as with Y-27632, there was no evidence of cell death at any concentration of ibuprofen tested. To determine if the reduction in confluency was a reflection of reduced cellular proliferation, an MTT cell viability assay was used to determine the effect of ibuprofen concentration upon cellular behaviour (Figure 4-24B). Absorbance, and therefore viability, was found to decrease with increasing ibuprofen concentration in a dose dependent fashion. This suggests that a reduced number of cells are metabolically active in cultures treated with ibuprofen, confirming the phase contrast-based observations. As with Y-27632 treatment, an MTT measured time course (Figure 4-24C) was conducted on untreated and ibuprofen treated cultures, to determine if this effect was due to reduced proliferation. Although the viability of both populations of cells increases over the course of the culture period, suggesting cells are not actively proliferating, viability for ibuprofen treated cultures remains reduced in comparison to untreated cells. This suggests that ibuprofen reduces cellular proliferation as oppose to inducing cell death.

There is no evidence of apoptotic cell death in cultures treated with both Y-27632 and ibuprofen even at high concentrations. This suggests that inhibition of Rho A and ROCK does not have a cytotoxic effect upon on the cells. Reduced confluency as observed through microscopy and reduced cell viability as measured by MTT assay, suggests that cellular proliferation is reduced with Y-27632 and ibuprofen treatment.

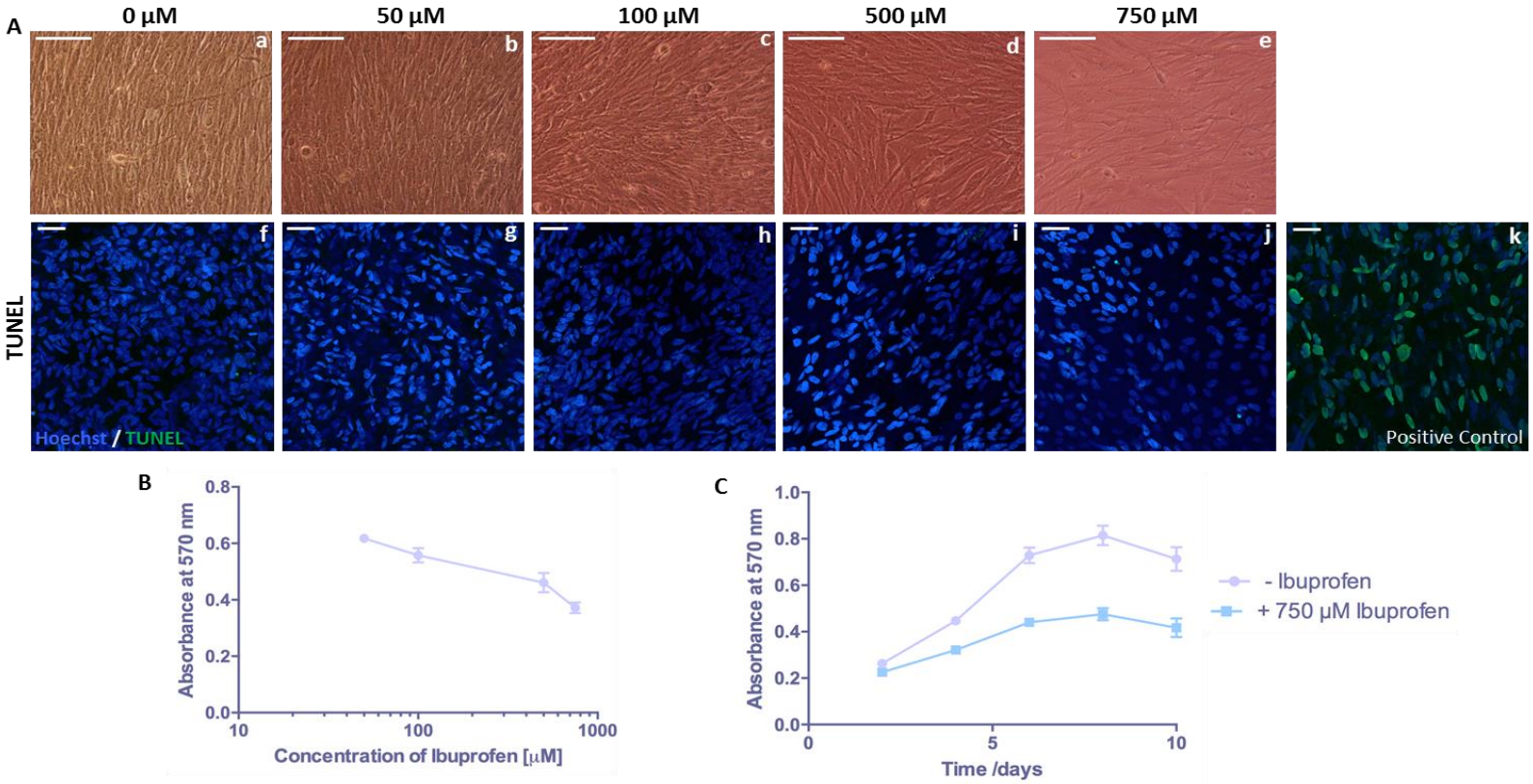

Fig 4-24: Inhibition of Rho A decreases proliferation of the glioma cell line, U-251MG.
Representative phase contrast images of U-251MG glioma cells cultured for 10 days with a range of concentrations of the drug ibuprofen (0 – 750 µM), an inhibitor of Rho A signalling (Aa-e). Cells appear confluent at lower concentrations of ibuprofen and cell density appears to decrease at higher concentrations of the drug (500 – 750 µM). Representative confocal images of TUNEL staining (Af-j), hilights fragmented DNA (a result of apoptosis) in green, as can be seen in the positive control (Ak). There is no evidence of apoptotic cell death with any concentration of ibuprofen tested. Scale bars: (Aa-e): 100 µm, (Af-k): 50 µm. MTT cell viability data (B) suggests that as ibuprofen concentration increases, cell viability decreases, and as there is no evidence of cell death, this may be due to a decrease in proliferation. MTT cell viability over the 10 day culture period (C) with and without 750 µM ibuprofen treatment, shows that under both conditions cell viability increases, indicating that cells are proliferating rather than dying, however with ibuprofen treatment, they appear to proliferate at a much slower rate.

Expression of GFAP and CSPGs was analysed via immunofluorescence in U-251MG monolayers treated with Y-27632 and ibuprofen. Cultures were treated with a range of concentrations (0.5 – 50 μM) of Y-27632 (Figure 4-25A) for 10 days with GFAP positive staining (Figure 4-25Aa-d) appearing increased in cultures treated with 50 μM Y-27632. Monolayers treated with 50 μM Y-27632 appear much less confluent than their untreated counterpart and both staining for GFAP and CS appear enhanced in these treated cultures. Furthermore, treatment with a range of concentrations (50 – 750 μM) of ibuprofen (Figure 4-25B) resulted in little variations in GFAP (Figure 4-25Ba-e) and CS (Figure 4-25Bf-j) expression. However, potentially more GFAP staining may be visible in cultures treated with 750 μM ibuprofen.

This evidence suggests that inhibition of Rho A and ROCK, results in reduced proliferation of U-251MG as oppose to cytotoxicity, which leads to reduced confluency of cultures. As the effects of confluency upon GFAP and CS expression were explored in the previous section, it was evident that immunoreactivity of GFAP and CS appeared enhanced in sub-confluent cultures. Reduced confluency of Y-27632 and ibuprofen treated cultures therefore could explain any enhanced GFAP and CS immunostaining observed.

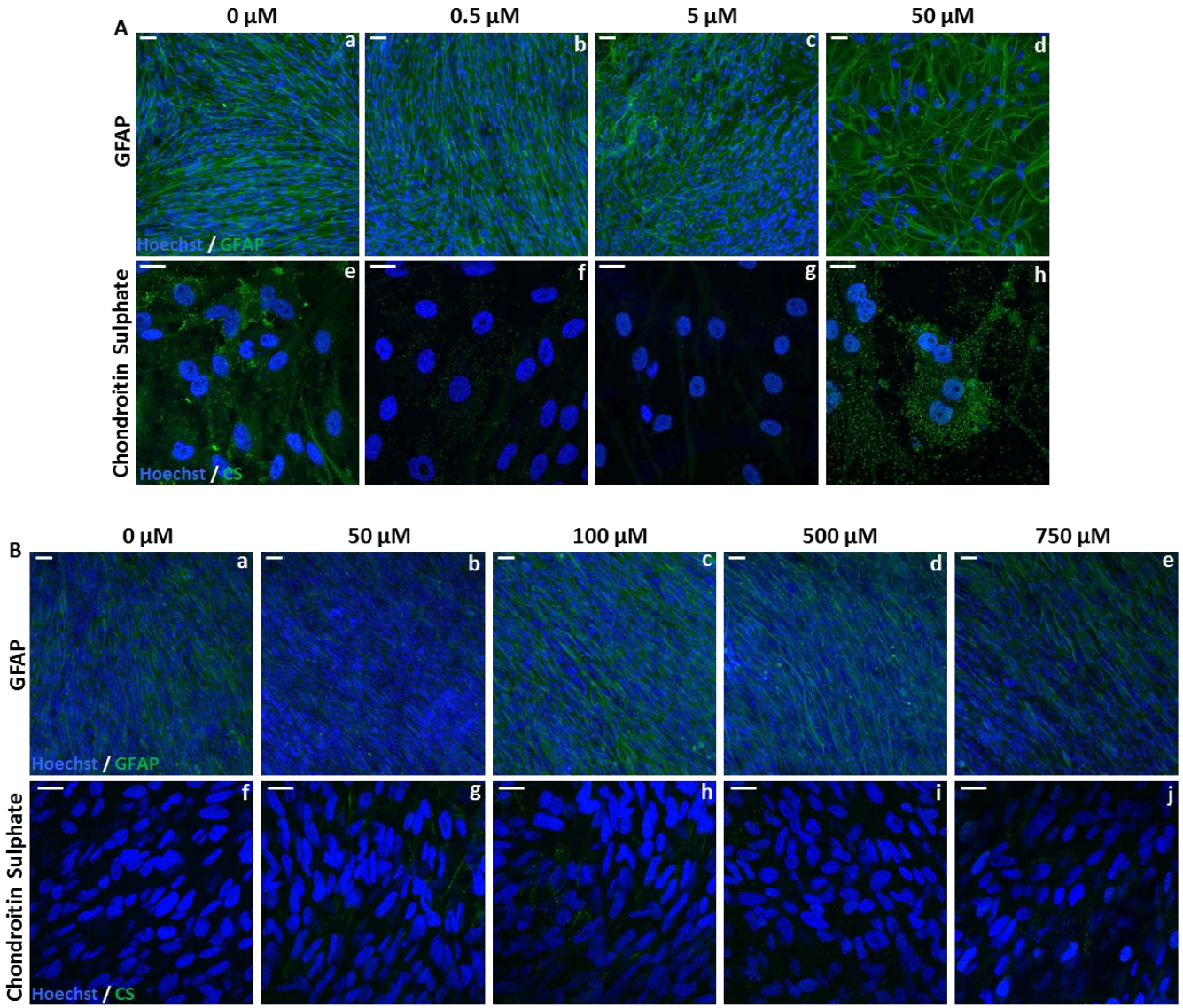

Fig 4-25: Inhibition of Rho A/ROCK signalling in U-251MG glioma cells promotes expression of markers of reactivity.
Representative confocal images of U-251MG cells cultured for 10 days with a range of concentrations of the selective ROCK inhibitor, Y-27632 (A) or the inhibitor of Rho A, ibuprofen (B). Expression of the intermediate filament protein, GFAP (Aa-d, Ba-e), stained in green, appears to increase at higher concentrations of each molecule (5 – 50 µM Y-27632, 100 – 750 µM ibuprofen). Similarly expression of chondroitin sulphate (Ae-h, Bf-j), a marker for the inhibitory molecules, CSPGs, secreted by reactive astrocytes and stained in green, again appears to increase at the higher concentrations of each molecule, and expression appears to be greatest with 50 µM Y-27632. This increase in expression of GFAP and chondroitin sulphate could be due to the decreased cell density of cultures treated with each molecule. Scale bars: (Aa-d, Ba-e): 50 µm, (Ae-h, Bf-j): 20 µm.

4.3.4 Investigation into the Paracrine Effect of Glioma Cell Secreted Soluble Inhibitory Factors upon Neurite Outgrowth

4.3.4.1 Conditioned Medium

To overcome the restriction of physical neurite blockage observed in 2D co-culture, a conditioned medium experiment was devised to determine the effect on neurite outgrowth of soluble inhibitory molecules secreted by the glioma cells. To achieve this, U-251MG cells were cultured in 2D (Figure 4-26Aa) or 3D (Figure 4-26Ba) conditions for 10 days, before their culture medium was harvested. Conditioned medium was then mixed in a 50:50 ratio with fresh growth medium (Figure 4-26Ab,Bb) for use in 2D (Figure 4-26Ac,Bc) and 3D neurite outgrowth assays (Figure 4-26Ad,Bd). This ensures that the pH and condition of the medium is suitable for neurosphere growth, as medium harvested from 10-day old glioma cell cultures, may contain too many metabolites and insufficient nutrients.

Neurospheres were cultured in 2D or 3D with medium conditioned by 2D cultures of U-251MG cells (Figure 4-27A). In the absence of conditioned medium, significant TUJ-1 positive (green) neurite outgrowth visibly radiates from the central neurosphere in 2D cultures (Figure 4-27Ba,b), however neurite outgrowth appears reduced from neurospheres cultured in the presence of glioma cell conditioned medium (Figure 4-27Bc,d). Ch'ase supplementation of conditioned medium (Figure 4-27Be,f) results in a similar level of neurite outgrowth as control cultures in 2D. Whilst addition of Y-27632 to the conditioned medium (Figure 4-27Bg,h) results in 2D neurite outgrowth that appears denser than control cultures and ibuprofen treatment (Figure 4-27Bi,j) also appears to restore neurite outgrowth to control levels.

Neurospheres cultured in 3D with 2D glioma cell conditioned medium (Figure 4-27Bk-t) all remain on top of the scaffold (Figure 4-27Bk,m,o,q,s), whereas TUJ-1 positive (green) neurites penetrate the depth of the 3D material (Figure 4-27Bl,n,p,r,t). Significant neurite outgrowth can be seen to have penetrated the scaffold in control cultures (Figure 4-27Bl), whereas there is no evidence of neurite outgrowth from the underside of scaffolds cultured in 2D glioma cell conditioned medium (Figure 4-27Bn). Few TUJ-1 positive (green) neurites are visible from the bottom view of Ch'ase treated cultures (Figure 4-27Bp) and a large number of neurites can be seen to have penetrated scaffolds treated with Y-27632 (Figure 4-27Br). Ibuprofen treatment (Figure 4-27Bt) also resulted in a small number of neurites that had visibly penetrated the 3D material.

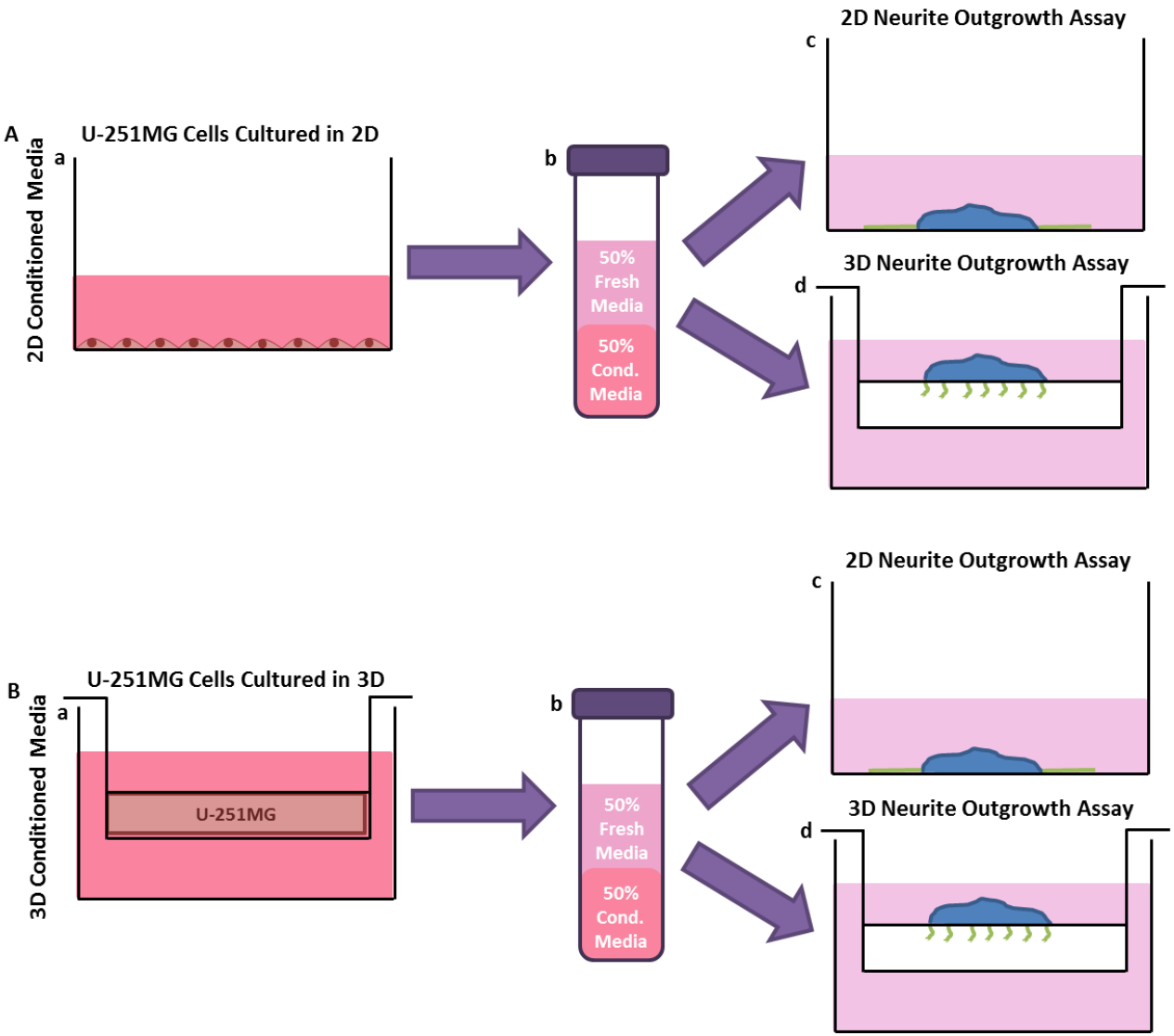

Fig 4-26: A schematic depicting the use of U-251MG glioma cell conditioned medium in both 2D and 3D neurite outgrowth assays.
To investigate the effect of paracrine factors such as CSPGs secreted from U-251MG glioma cells, medium conditioned by glioma cells was used in both 2D and 3D neurite outgrowth assays. U-251MG glioma cells were either cultured in 2D (A) or 3D (B) for 10 days in DMEM (supplemented with 10 % FBS, 2 mM L-glutamine, and 20 active units of penicillin and streptomycin) with a 50 % media change on day 5 of culture. Following the 10 day culture period, media was removed from U-251MG cultures and mixed in a 1:1 ratio with fresh DMEM medium (b). This conditioned medium was then used in both 2D (c) and 3D (d) neurite outgrowth assays, with neurospheres being cultured in this medium for the 10 day neurite outgrowth period of culture.

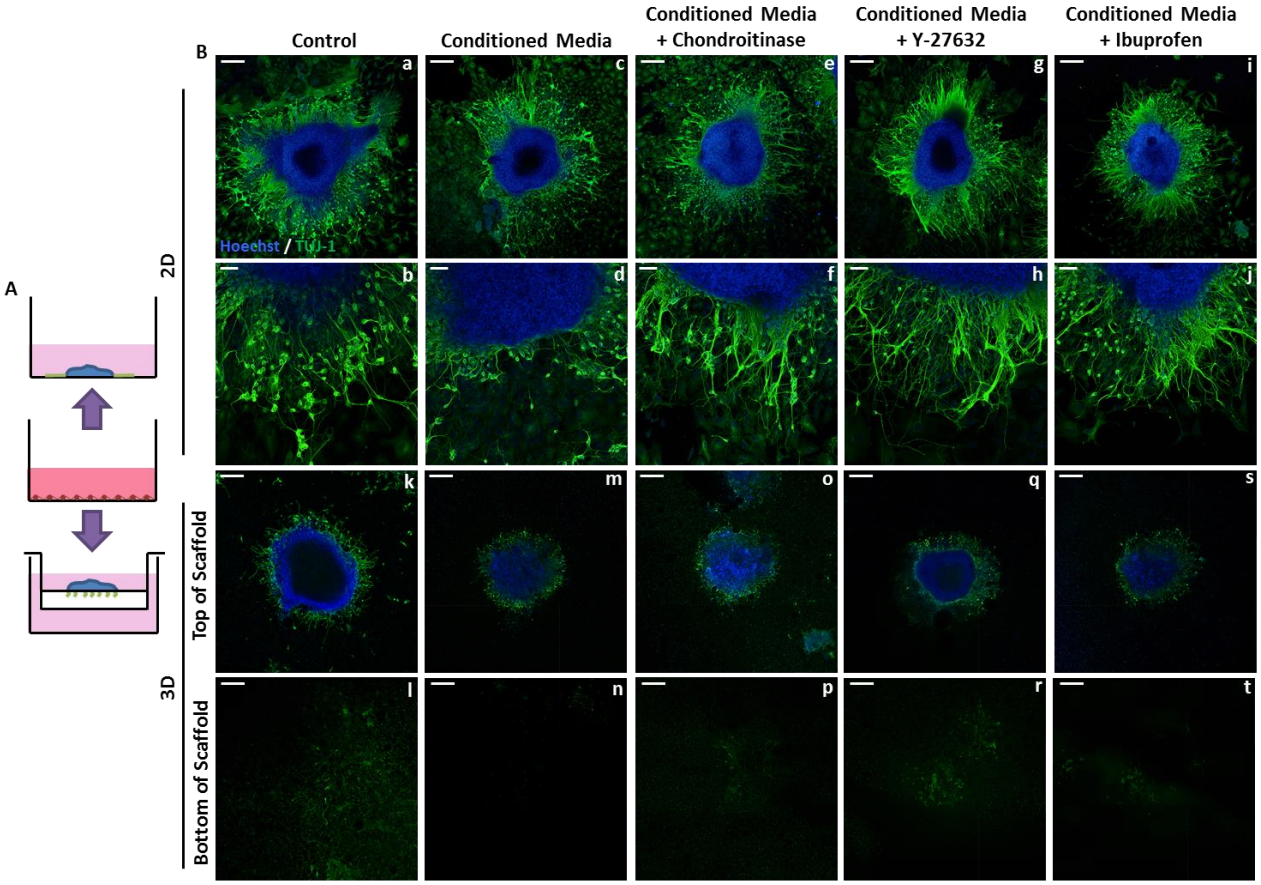

Fig 4-27: Culture of neurospheres in medium conditioned by 2D cultured glioma cells is inhibitory to neurite outgrowth and can be overcome by modulation of Rho A/ROCK signalling.
Conditioned medium was obtained from U-251MG glioma cells cultured in 2D conditions for 10 days, as depicted in schematic (A) for use in 2D and 3D neurite outgrowth assays. Representative confocal images of neurospheres cultured in 2D (Ba-j) or 3D (Bk-t) conditions with 2D glioma cell conditioned medium and medium supplementation with chondroitinase, Y-27632 or ibuprofen. Neurite outgrowth is highlighted in green by the pan neuronal marker; TUJ-1 and nuclei remain within the central body of the neurosphere and are stained in blue. Neurospheres cultured without conditioned medium have extensive neurite outgrowth radiating from the neurosphere in 2D (Ba,b) and penetrating the scaffold in 3D culture (Bk,l). Whereas with 2D conditioned medium, neurite outgrowth is visibly reduced in 2D culture (Bc,d) and no neurites can be seen to have penetrated the 3D material in 3D culture (Bm,n). Chondroitinase supplementation, an enzyme that breaks down inhibitory CSPGs in addition to conditioned medium treatment, appears to restore neurite outgrowth in 2D culture (Be,f) and more neurites can be seen to once again penetrate the scaffold in 3D culture (Bo,p). Similarly treatment with the selective ROCK inhibitor, Y-27632, appears to restore neurite outgrowth in 2D culture (Bg,h) and a significant amount of neurites can be seen penetrating the scaffold in 3D culture (Bq,r). Ibuprofen, an inhibitor of Rho A signalling, has a similar effect to Y-27632 in 2D (Bi,j) and 3D (Bs,t) culture conditions. Scale bars: (Ba,c,e,g,i,k-t): 200 μm, (B,b,d,f,h,j): 50 μm.

Medium conditioned by 3D cultured U-251MG cells (Figure 4-28A) was applied to 2D and 3D cultured neurospheres during induction of neurite outgrowth. Neurospheres cultured in 2D without glioma cell conditioned medium (Figure 4-28Ba,b) project a large quantity of TUJ-1 (green) positive neurites; whilst neurites generated in conditioned medium (Figure 4-28Bc,d) appear extremely short and reduced in size. Treatment of neurospheres cultured in conditioned medium with the enzyme Ch'ase (Figure 4-28Be,f) results in neurite growth comparable to that of control cultures. Treatment of 2D neurospheres cultured in conditioned medium with Y-27632 (Figure 4-28Bg,h), results in extremely dense neurite outgrowth and ibuprofen treatment (Figure 4-28Bi,j) also restores neurite outgrowth to a level that is comparable to the control.

Neurospheres cultured in 3D with 3D glioma cell conditioned medium, remain on top of the scaffold (Figure 4-28Bk,m,o,q,s) whilst TUJ-1 positive (green) neurites penetrate the depth of the 3D material, as visible from the underside of the scaffold (Figure 4-28Bl,n,p,r,s,t). A significant number of neurites are visible from the underside of cultures maintained without conditioned medium (Figure 4-28Bl), whereas no neurites visibly penetrate scaffolds cultured in glioma cell conditioned medium (Figure 4-28Bn). A small number of neurites visibly penetrate scaffolds in the presence of Ch'ase (Figure 4-28Bp). A large number of neurites are visible from the underside of scaffolds treated with Y-27632 (Figure 4-28Br), perhaps even more than control cultures. Ibuprofen treatment (Figure 4-28Bt), however, results in few neurites visibly penetrating the 3D material.

Quantification of the number of neurites generated per neurosphere (Figure 4-29A) from neurospheres cultured in 2D with conditioned medium and each treatment condition, reveals that neurite number is inhibited by both 2D and 3D glioma cell conditioned medium. Furthermore, 3D glioma cell conditioned medium inhibits neurite number to a greater degree than 2D conditioned medium albeit not statistically significantly. Ch'ase treatment partially restores the number of neurites per neurosphere in cultures treated with both 2D and 3D conditioned medium and Y-27632 treatment enhances neurite outgrowth in both cases, to a level that is greater than that of the control. Ibuprofen however, restores neurite outgrowth in the prescence of both 2D and 3D glioma cell conditioned medium to levels reminiscent of the control.

A similar outcome is evident in terms of the neurite density of each neurosphere (Figure 4-29B) cultured in 2D. Neurite density is inhibited in both 2D and 3D glioma cell conditioned medium and 3D conditioned medium inhibits neurite outgrowth in 2D to a greater extent than 2D conditioned medium. Ch'ase treatment restores neurite outgrowth in both cases to a level that is similar to the control and both Y-27632 and ibuprofen enhance neurite density in the presence of 2D and 3D conditioned medium to a level that surpasses that of the control.

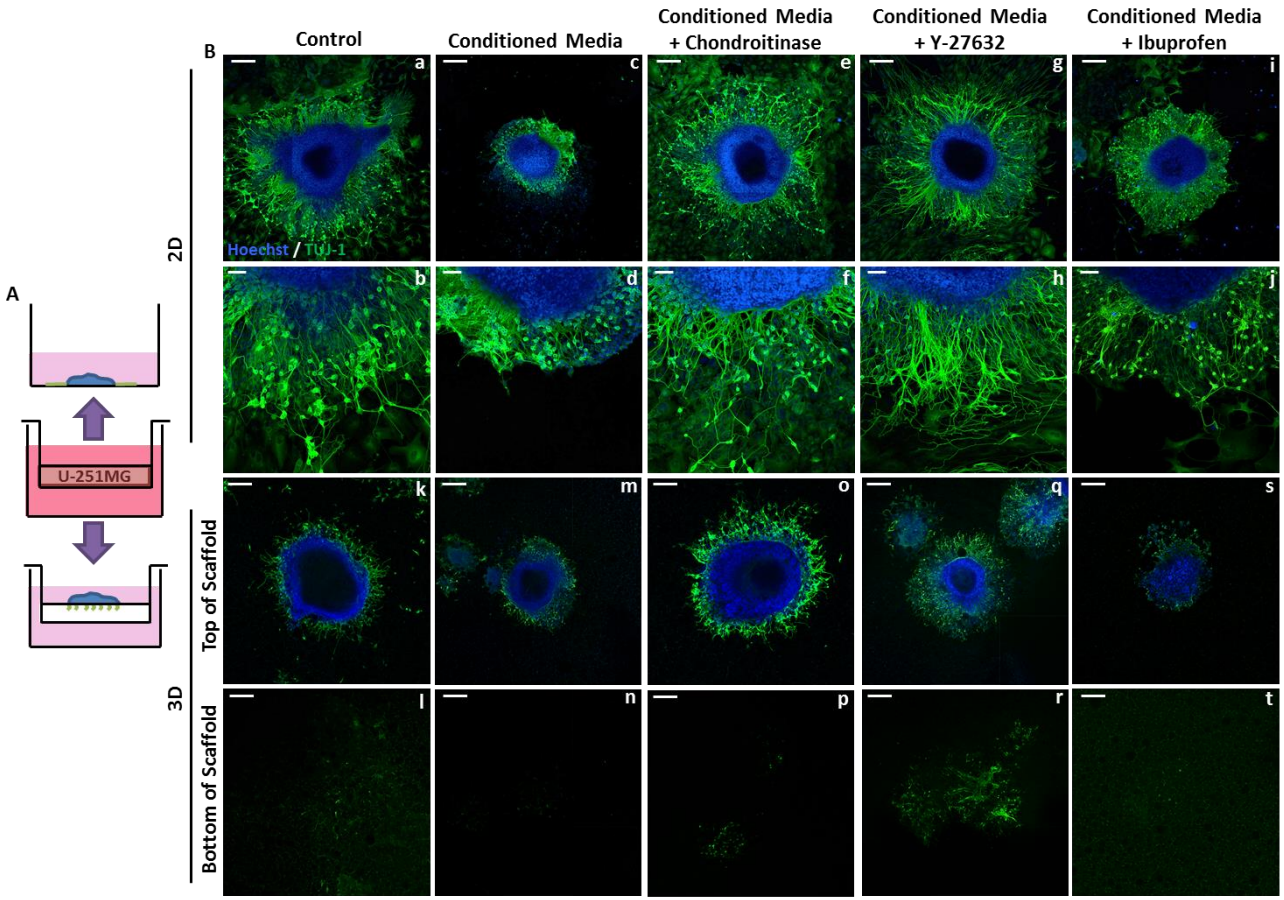

Fig 4-28: Culture of neurospheres in medium conditioned by 3D cultured glioma cells is inhibitory to neurite outgrowth and can be overcome by modulation of Rho A/ROCK signalling.

Conditioned medium was obtained from U-251MG glioma cells culture in 3D conditions for 10 days for use in 2D and 3D neurite outgrowth assays, as depicted in schematic (A). Representative confocal images of neurospheres cultured in 2D (Ba-j) or 3D (Bk-t) culture conditions with 3D glioma cell conditioned medium and supplementation with chondroitinase, Y-27632 or ibuprofen. Staining for the pan-neuronal marker TUJ-1 in green highlights neurite outgrowth and nuclei are highlighted in blue. Neurospheres cultured without conditioned medium have extensive neurite outgrowth radiating from the neurosphere in 2D (Ba,b) and penetrating the scaffold in 3D culture (Bk,l). However, in the presence of conditioned medium, neurospheres cultured in 2D (Bc,d), appear to produce reduced neurite outgrowth. In 3D conditions (Bm,n) no neurites are visible from the bottom view of the scaffold. However, treatment with chondroitinase in addition to conditioned medium, appears to restore neurite outgrowth in 2D culture (Be,f) and more neurites can be seen to penetrate the scaffold in 3D culture (Bo,p). Similarly treatment with the selective ROCK inhibitor, Y-27632, appears to restore neurite outgrowth in 2D culture (Bg,h) and a significant number of TUJ-1 positive neurites can be seen to penetrate the scaffold in 3D culture (Bq,r). Ibuprofen, an inhibitor of Rho A signalling, has a similar effect an appears to restore neurite outgrowth in 2D (Bi,j) and 3D (Bs,t) culture conditions. Scale bars: (Ba,c,e,g,i,k-t): 200 μm, (B,b,d,f,h,j): 50 μm.

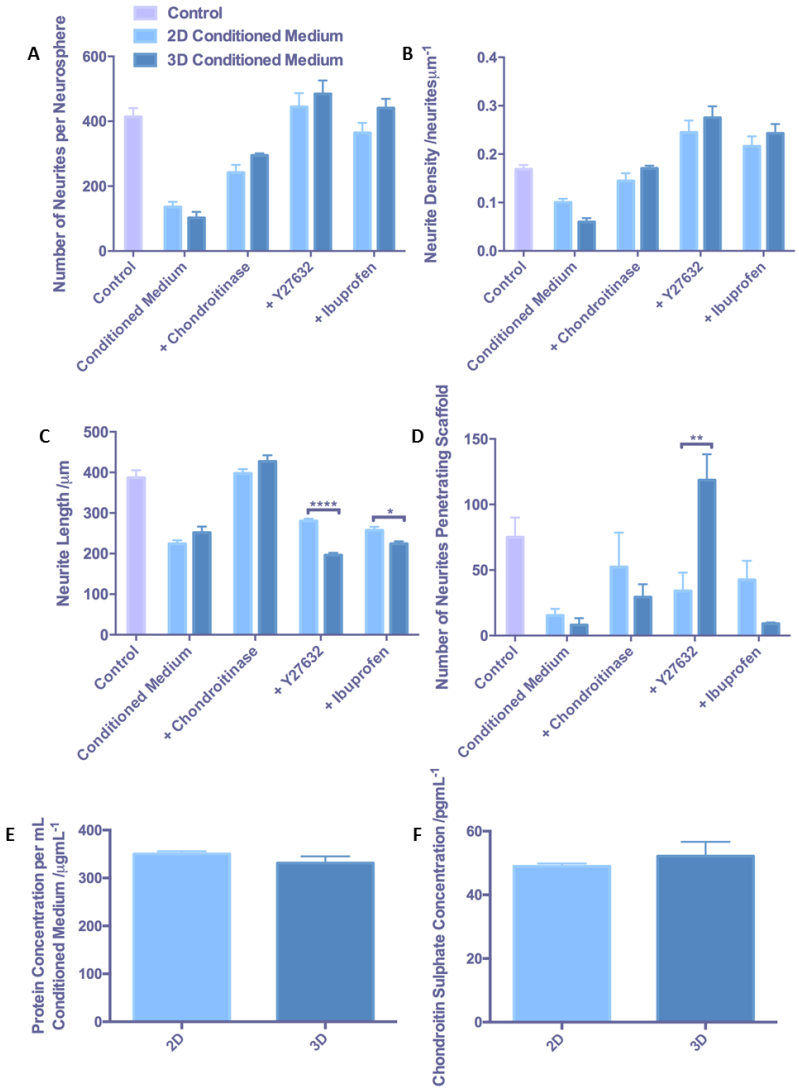

Fig 4-29: Inhibition of neurite outgrowth from neurospheres cultured in U-251MG conditioned medium in 2D and 3D culture systems.
Quantification of neurite number (A) (data represent mean ± SEM, n=9-18; between 3-6 neurospheres were quantified per independent replicate, of which there were 3) and density (B) (data represent mean ± SEM, n=9-18; between 3-6 neurospheres were quantified per independent replicate, of which there were 3) from neurospheres cultured in 2D in medium conditioned by glioma cells cultured in 2D or 3D. Neurite length (C) (data represent mean ± SEM, n=52-100; in total between 52-100 individual neurites were measured from 3 replicates of neurospheres derived from independent pools of cells) is inhibited in neurospheres cultured in 2D with glioma cell conditioned medium. Quantification of neurite penetration through Alvetex® scaffold (D) (data represent mean ± SEM, n=3-6; between 1-2 neurospheres were quantified from 3 independent replicates) from neurospheres cultured in 3D with glioma cell conditioned medium reveals that less neurites penetrate the scaffold in the presence of conditioned medium.. The protein concentration of 2D and 3D glioma cell cultures was determined by Bradford assay (E) (data represent mean ± SEM, n=3; lysates from 3 independent cultures) and normalised to the volume of conditioned medium generated by the cultures. ELISA analysis (F) (data represent mean ± SEM, n=3; conditioned medium generated from 3 independent cultures) of the chondroitin sulphate content of 2D and 3D glioma cell conditioned medium reveals that 3D cultures generate containing a slightly higher concentration of chondroitin sulphate. Two-way ANOVA with Tukey's multiple comparisons (A-D) and unpaired T-test (E-F). * = $p \leq 0.05$, ** = $p \leq 0.01$, *** = $p \leq 0.001$, **** = $p \leq 0.0001$.

The length of neurites (Figure 4-29C) generated from 2D cultured neurospheres is severely impaired from neurospheres cultured in glioma cell conditioned medium. This reduction in neurite length is restored upon treatment with Ch'ase, however both Y-27632 and ibuprofen have little effect upon neurite length and in both cases 3D conditioned medium significantly impairs neurite length to a greater degree.

Neurospheres cultured in 3D in the presence of glioma cell conditioned medium generate fewer neurites capable of traversing the depth of the 3D material (Figure 4-29D). Ch'ase treatment partially restores neurite penetration by 3D culture, whilst Y-27632 was found to have little effect upon 2D glioma cell conditioned medium samples, however significantly enhanced neurite penetration in the presence of 3D glioma cell conditioned medium. Ibuprofen treatment partially restored 3D neurite outgrowth from 2D conditioned medium samples and had little effect upon neurite penetration from neurospheres cultured with 3D conditioned medium.

In terms of neurite number and density in 2D culture, and penetration in 3D culture, it appears that neurite growth is impaired to a greater degree in 3D glioma cell conditioned medium as oppose to 2D conditioned medium. This could be due to differences in cell number and density of the cultures, as 3D cultures may contain a larger number of CSPG secreting cells. To account for this a Bradford assay was used to determine the total protein concentration of both 2D and 3D cultures (Figure 4-29E), and as 2D and 3D cultures require different volumes of growth medium, total protein concentration was normalised to the volume of conditioned medium generated by each culture condition.

This analysis resulted in a similar protein concentration per mL of conditioned medium for both 2D and 3D cultures, with slightly reduced (not statistically significant) protein content in 3D cultures. This suggests that both 2D and 3D cultures contain a similar number of cells, once normalised, and that 3D cultures perhaps contain slightly fewer cells, which may explain the enhanced inhibition as CSPG expression may be enhanced by reduced cell density in 3D cultures. To confirm this, an ELISA was used to determine the absolute CSPG concentration of 2D and 3D glioma cell conditioned medium samples and found that 3D conditioned medium contained a slightly higher concentration of CSPGs than 2D conditioned medium, however this was not statistically significant.

4.3.4.2 2D/3D Glioma Cell-Neurosphere Co-culture Model

To further study the effects of soluble inhibitory factors secreted from glioma cells in a dynamic system, 3D culture technology was utilised to develop a co-culture model whereby each cell type is not in contact with the other. This culture system consisted of a monolayer of glioma cells cultured at the bottom of a well within a standard tissue culture plate whilst a neurosphere is cultured on top of Alvetex® scaffold suspended within the same well (Figure 4-30C). Any soluble inhibitory factors secreted by the glioma cell monolayer will enter the culture medium and interact with the neurites within the scaffold. This reduces the difficulties associated 2D co-culture and mechanical blockage of neurite outgrowth due to contact between the two cell types.

Immunofluorescence analysis reveals that whilst neurospheres remain on top of the scaffold in each case (Figure 4-30Aa,d,g,j,m) neurites can be seen to have penetrated the entire 200 μm depth of the 3D material and are visible from the bottom view of the scaffold (Figure 4-30Ab,e,h,k,n) in some cases. Extensive neurite outgrowth can be seen to have penetrated scaffolds from neurospheres cultured in the absence of glioma cells (Figure 4-30Aa-c). The presence of U-251MG GFAP (green) positive glioma cells (Figure 4-30Af) resulted in a lack of visible neurite outgrowth from the underside of the scaffold (Figure 4-30Ae).

Treatment with Ch'ase resulted the generation of a significant number of neurites capable of penetrating the scaffold (Figure 4-30Ah) despite the presence of U-251MG cells (Figure 4-30Ai). Treatment of cultures with Y-27632 resulted in significant neurite outgrowth as visible from the bottom view of the scaffold (Figure 4-30Ak) along with a detrimental effect upon U-251MG cell density (Figure 4-30Al) with monolayers appearing less confluent and cell morphology altered. Few neurites are visible from the underside of scaffolds treated with ibuprofen (Figure 4-30n), however more neurites are visible than in co-culture samples with no treatment (Figure 4-30e). Ibuprofen also has a similar effect upon U-251MG morphology and confluency (Figure 4-30o), as discussed earlier within this chapter. The recovery effect of Y-27632 and partial recovery effect of ibuprofen, is unlikely to be due to the reduced confluency of glioma cell monolayers in these cultures, as it has been identified earlier in this chapter that sub-confluent glioma cells express CSPGs to a greater degree than confluent monolayers.

The number of neurites that penetrate the scaffold (Figure 4-30B) was quantified in each case and the incorporation of U-251MG cells into the model was found to reduce neurite inhibition by a large degree. Medium supplementation with Ch'ase was found to restore neurite penetration to a similar level as the control and Y-27632 treatment was found to significantly enhance neurite outgrowth compared with the control. Ibuprofen medium

treatment was found to partially restore neurite penetration. This quantification supports the observations made upon analysis of the immunofluorescent images.

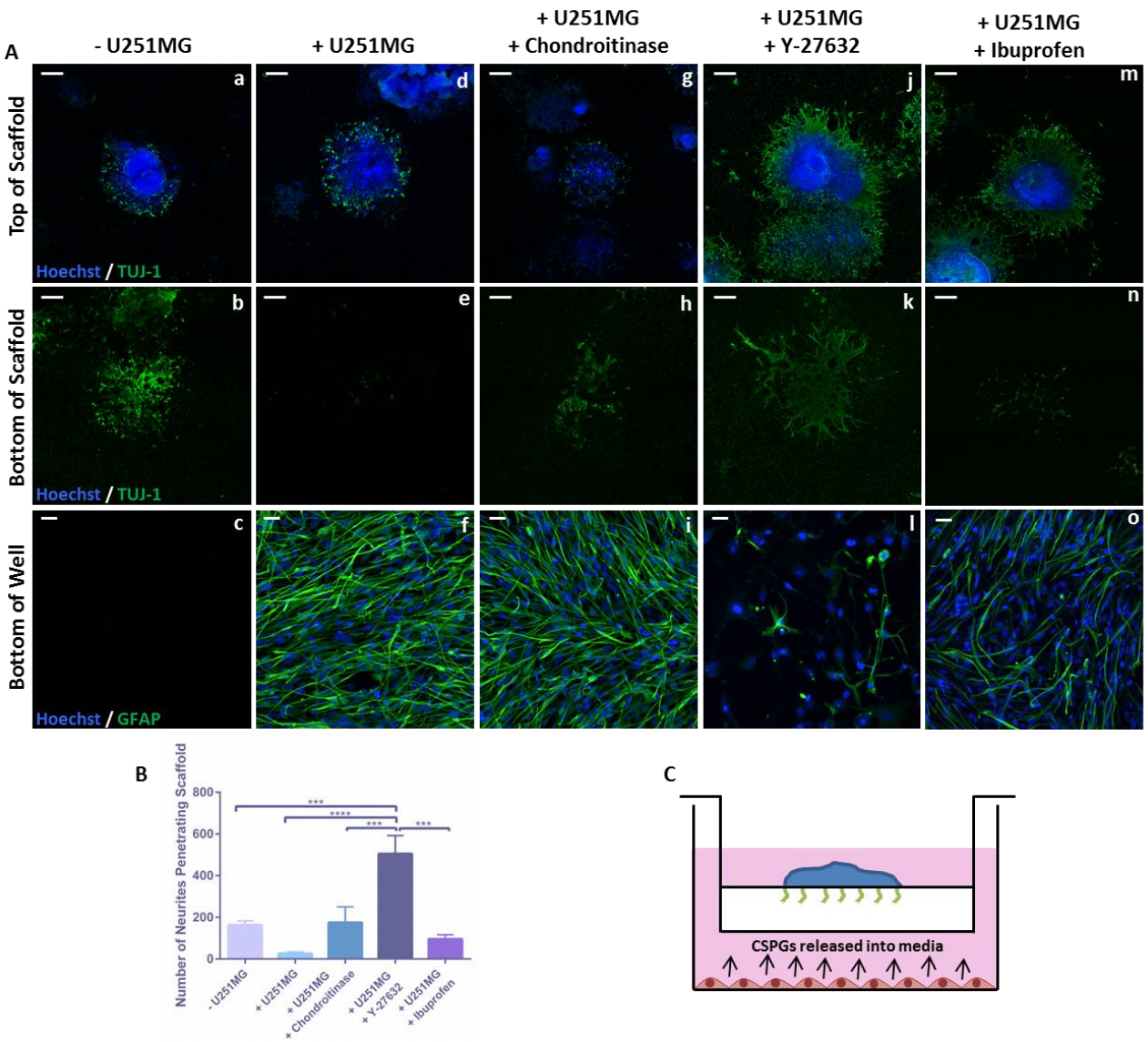

Fig 4-30: Co-culture of U-251MG glioma cells and neurospheres that are not in contact is inhibitory to neurite outgrowth and can be overcome by modulation of the Rho A/ROCK pathway.
Representative confocal images (A) of neurospheres cultured in 3D on top of Alvetex® scaffold and glioma cells cultured in 2D at the bottom of each well. Neurospheres can be observed from the top view of the scaffold (Aa,d,g,j,m) with neurites penetrating the depth of the 3D material and are visible from the underside of the scaffold (Ab,e,h,k,n). GFAP positive U-251MG (Ac,f,i,l,o) are visible within each culture well. The pan-neuronal marker TUJ-1 is highlighted in green (Aa,b,d,e,g,h,j,k,m,n) as is the intermediate filament protein GFAP (Ac,f,i,l,o) and nuclei are highlighted in blue. Scale bars: (Aa,b,d,e,g,h,j,k,m,n): 200 µm, (Ac,f,i,l,o): 50 µm. Quantification of the number of the number neurites that have penetrated the scaffold (B) (data represent mean ± SEM, n=3-9; 1-3 neurospheres were quantified per independent replicate, of which there were 3) indicates that in the presence of U-251MG glioma cells, neurite outgrowth is greatly inhibited and with the addition of chondroitinase, an enzyme known to render CSPGs inactive, neurites penetrating the scaffold is restored to a similar level as the control. Addition of small molecule modulators of the Rho/ROCK pathway into this system also has a recovery effect on neurite outgrowth, with Y-27632 enhancing neurite outgrowth to a level that surpasses the control and ibuprofen restoring neurite levels to a similar level as the control. A schematic depicting U-251MG cells cultured in 2D at the bottom of the culture well and a neurosphere being cultured in 3D within Alvetex® scaffold in the same well (C). One-way ANOVA with Tukey's multiple comparisons: * = $p \leq 0.05$, ** = $p \leq 0.01$, *** = $p \leq 0.001$, **** = $p \leq 0.0001$.

4.4 Discussion

Unlike other biological systems, the CNS has limited capacity for regeneration; therefore trauma to the brain and spinal cord can result in catastrophic injury[220,306]. The inability of neurons to regenerate and restore lost neuronal connections, particularly following traumatic spinal cord injury, forms a major obstacle in the treatment and restoration of function[33,34,39,206,220]. This occurs due to the formation of a glial scar that consists of multiple, interconnecting inhibitory pathways that act to impair the regeneration of lost neuronal circuitry[33,34,39,206,220]. This chapter outlines the application of a novel human pluripotent stem cell based model to study the molecular mechanisms that underpin neurite inhibition within the glial scar and describes several distinct methodologies used to induce neurite inhibition and promote recovery of neurite growth.

4.4.1 Aggrecan-Induced Neurite Inhibition

The culture of neurons on non-permissive growth substrates coated with inhibitory molecules such as astrocyte-secreted CSPGs, is a strategy commonly used to induce neurite inhibition[25,26,377–380]. Aggrecan is a member of the CSPG family that is also found in cartilage[220,381–383] and is commonly used *in vitro* to induce neurite inhibition[384,385]. This chapter describes several methodologies used to induce and subsequently investigate the underlying mechanisms involved in CSPG-mediated neurite inhibition, the first of which involves a simple system of aggrecan coating. Both 2D and 3D growth substrates were coated with aggrecan to provide non-permissive growth environments for neurite development. This methodology successfully induced neurite inhibition in human stem cell derived neurites in a dose-dependent manner in both 2D and 3D culture systems.

Furthermore, the signalling pathway by which CSPGs are thought to induce neurite inhibition, has previously been described to involve Rho A and ROCK activation downstream of receptor binding[26,27,209,372]. To investigate this in the context of specifically aggrecan-induced neurite inhibition, ibuprofen an inhibitor of Rho A and Y-27632 a ROCK inhibitor, were both shown to recover neurite growth on non-permissive aggrecan coated growth substrates. This supports evidence outlined in the literature that implicates Rho A and ROCK signalling in downstream CSPG induced signal transduction.

However, although aggrecan coating of growth substrates is a simple and effective methodology that can be used to study CSPG-induced neurite inhibition, it is not necessarily physiologically representative in terms of neurite inhibition within the glial scar. Aggrecan is a CSPG, and does induce neurite inhibition *in vitro*, however, there is little evidence that aggrecan is secreted or over-expressed following spinal cord injury

and Lemons *et al* even describe a significant reduction in aggrecan levels in the spinal cord post-injury[386].

This aggrecan-based model of neurite inhibition is also extremely simple, which may be an advantage for some applications, but does not provide an accurate representation of the cocktail of CSPGs secreted by reactive astrocytes following injury[387,388]. A simplified model of inhibition such as this may be beneficial in some circumstances such as investigations into generic CSPG signalling mechanisms or screening of compounds for the ability to overcome CSPG-mediated inhibition in an industrial or academic setting. However, to better recreate the complex nature of CSPG-mediated inhibition in the context of the glial scar, a co-culture model was developed to incorporate CSPG secreting cells into the culture system.

4.4.2 Co-culture of Glioma Cells and Neurospheres in 2D Culture

To better recapitulate the complex cellular microenvironment encountered by damaged neurons in the injured spinal cord, a co-culture model was developed to incorporate cells that express similar CSPGs to the reactive astrocytes of the glial scar. Reactive astrocytes are the major cellular component of the glial scar and upon injury to the spinal cord, astrocytes upregulate the intermediate filament protein GFAP and secrete significant quantities of CSPGs that inhibit neurite extesion[33,39,220]. *In vivo* following injury, evidence suggests that reactive astrocytes secrete a number of CSPGs including: NG2, neurocan, brevican, phosphacan and versican, which form an inhibitory matrix following SCI[387,388].

In the interest of developing a fully human-based model of neurite inhibition and to maintain medical relevance, human glioma cell lines were characterised and considered for use in this model. Alternatively, to avoid the use of neoplastic cells, primary animal derived reactive astrocytes could have been considered for use in this model, however introducing cells from a different species may have consequences in terms of cross-species reactivity of CSPGs.

The human gliomablastoma cell line U-251MG was selected for use in this co-culture model as there is an abundance of evidence throughout the literature that describes the expression of CSPGs from this cell line including versican and phosphacan[389–392], and it is also well documented that this cell line contains GFAP positive cells[393–396]. Unlike aggrecan, both versican and phosphacan are known to be upregulated and actively secreted in the injured spinal cord[387], therefore U-251MG cells both secrete CSPGs and express GFAP similarly to the reactive astrocytes found in the glial scar. Characterisation described throughout this chapter also confirms that U-251MG cultures express both GFAP and CSPGs, and specific expression of all versican isoforms was confirmed by

western blot. Therefore it was determined that U-251MG cells have similar properties to the reactive astrocytes of the glial scar making them a suitable candidate for use in this co-culture model.

The co-culture model described in this chapter involved the seeding of U-251MG cells in 2D as a monolayer culture, allowing the cells to populate the microenvironment for 24 hours before seeding a mature neurosphere on top of the monolayer for neurite outgrowth studies. However, neurite inhibition within this system may not be solely mediated by chemical factors such as CSPGs and their downstream signalling pathways, because the glioma cells and neurites are in contact with one another which may result in a physical inhibition of neurite extension. Reactive astrocytes in the glial scar *in vivo* form long cytoskeletal processes that interweave, resulting in a meshwork that mechanically blocks the growth of neurites[33,39,220,293]. Although this aspect of the co-culture model represents a mechanism of neurite inhibition that occurs *in vivo*, this is not the objective of this study. The objective of this study is to identify the molecular signalling events involved in CSPG-mediated inhibition, which may be masked or complicated by the physical interactions involved between the cell types in this co-culture model.

However, chondroitinase, an enzyme that degrades CSPGs reducing their function[312–314,343,344,355], was found to restore neurite outgrowth in this 2D co-culture model to a level comparable with that of neurospheres cultured alone. This suggests that actually a large proportion of the neurite inhibition observed in this model, is mediated by CSPGs and the physical interaction of the glioma cells and neurons has little impact on neurite outgrowth. Similarly, both inhibitors of Rho A and ROCK signalling were also found to restore some aspects of neurite outgrowth in this co-culture system. This again, could suggest that physical inhibition may play only a minor role in inhibition within this model or perhaps the neurite enhancing effects of Y-27632 and ibuprofen, as discussed in Chapter III, may drive neurite growth despite the nature of the physical interactions between cell types.

Although mechanical inhibition of neurite outgrowth by reactive astrocytes is an important component of the glial scar, the main focus of this study is chemical induced neurite inhibition mediated by CSPGs. This co-culture model is perhaps suitable for the study of physical cellular interactions between neurites and reactive astrocytes; however, its application to study CSPG-mediated inhibition is limited. For this reason, other culture methodologies were explored such as the use of glioma cell conditioned medium to investigate the effect of soluble inhibitors of neurite outgrowth only, removing any inhibitory effect mediated by cellular physical interaction.

4.4.3 Effect of Glioma Cell Conditioned Medium on Neurite Outgrowth

In order to further improve and build upon the 2D co-culture model developed within this chapter, several methodologies were implemented to examine glioma cell-induced neurite inhibition-mediated by soluble, secreted molecules only. U-251MG cells have previously been described to secrete CSPGs such as versican into their growth medium[389,390], which in addition to the ELISA analysis of glioma cell conditioned medium described within this chapter, suggests that U-251MG cells secrete soluble CSPG molecules just as reactive astrocytes secrete CSPGs into the extracellular space within the glial scar. Therefore, a number of experiments were devised to investigate the inhibitory ability of glioma cell conditioned medium in terms of neurite outgrowth, reducing the limitations of the previously described 2D co-culture model.

The effect of conditioned medium harvested from 2D and 3D cultures of U-251MG cells upon neurite outgrowth was determined, as 3D cultures had been demonstrated to more positively stain for the CSPG motif CS, than 2D cultures. Therefore, it was hypothesised that 3D cultures of U-251MG cells secrete CSPGs to a greater extent than 2D cultures, and potentially may induce neurite inhibition to a greater extent. Both 2D and 3D glioma cell conditioned medium was found to be inhibitory to 2D and 3D cultured neurites and in some aspects of neurite outgrowth, 3D conditioned medium was found to induce neurite inhibition to a greater extent. ELISA analysis confirmed that CSPGs were present in the conditioned medium, however a full analysis of the CSPG content of the conditioned medium would be beneficial, to determine the content and ratio of a variety of CSPG molecules within the medium.

In addition to the use of previously conditioned medium, a dynamic co-culture model was also developed that allowed U-251MG cells to simultaneously condition medium whilst neurites develop. This involved the culture of U-251MG cells as a monolayer at the bottom of a culture well, whilst neurospheres were cultured on Alvetex® scaffold suspended within the same well. This allowed U-251MG to gradually condition the growth medium throughout the course of the culture period, exposing neurites to a time-dependent gradient of CSPG secretion, similar to the *in vivo* environment that forms post-spinal cord injury.

This methodology avoids the problem that arises during the conditioning of growth medium, in that U-251MG culture depletes nutrients from the medium whilst also generating metabolites that may be toxic and reducing the pH of the medium. This may have detrimental effects upon neuronal survival and neurite generation, whereas if U-251MG and neurospheres are cultured in the same system, medium quality can be better managed. However, this system also has the disadvantage of glioma cell death when

screening potential drugs that may be cytotoxic. This chapter describes the ability of particular molecules to restore neurite growth in the presence of inhibitory stimuli (ibuprofen and Y-27632), however such molecules were also found to impact glioma cell growth and morphology. The combination of both neurospheres and glioma cells within the same culture system may reduce the ability of the model to screen cytotoxic compounds, as they may induce glioma cell death reducing CSPG secretion within the model. In this case pre-conditioned medium may be a more useful tool to study the ability of compounds to overcome CSPG-mediated inhibition without impacting CSPG secretion and viability of the glioma cells themselves. Therefore, the suitability of each conditioned medium model for the desired application should be considered prior to use.

4.4.4 Methods of Recovery of Neurite Outgrowth

The main aim of this chapter was to induce neurite inhibition in human derived neurites, to then identify methods that are able to recover neurite growth. This is important to identify key signalling pathways involved in CSPG-mediated inhibition in the glial scar and this also demonstrates the potential screening application of inhibition models, to help identify molecules that may be beneficial in the treatment of SCI.

CSPGs are secreted by reactive astrocytes in the glial scar; they then induce neurite inhibition in neighbouring neurons through the activation of cell surface receptors including LAR and PTPσ[318–320]. Receptor activation is thought to induce a signalling cascade that leads to activation of Rho A and ROCK, resulting in actin filament stabalisation and growth cone collapse[27,365,366,372,373]. The use of many small molecules to intervene and inhibit this signalling pathway has been examined within this chapter, as summarised in Figure 4-31. This has particularly focused on the inhibition of Rho A and downstream ROCK to prevent neurite collapse through destabilisation of the actin cytoskeleton.

Chondroitinase (Ch'ase) is an enzyme that cleaves GAG side chains from CSPG molecules, preventing their structural interaction with cell surface receptors, subsequently inhibiting signal transduction at the ligand-receptor binding stage[343]. Ch'ase has been well characterised in terms of promoting functional recovery in animal models[312,313,344,345,355] of SCI and is also known to promote axonal regeneration *in vitro*[397]. For this reason Ch'ase was added to the culture medium of both 2D co-culture and conditioned medium systems with the view to promote neurite growth in the presence of inhibitory CSPGs. In most systems Ch'ase was found to restore neurite outgrowth to control levels, which suggests that Ch'ase may reduce the function of CSPGs in culture supporting evidence outlined in the primary literature. Furthermore, this also suggests that the neurite inhibition observed both in 2D co-culture and conditioned medium models, is induced by CSPG-

action, as recovery is demonstrated with Ch'ase supplementation. Therefore, neurite regeneration-induced by Ch'ase treatment, not only demonstrates a potential recovery mechanism but also contributes toward model validation.

CSPG-mediated receptor activation is thought to lead to the activation of Rho A, which has consequences upon the actin cytoskeletal leading to neurite inhibition[365]. Ibuprofen is an NSAID and also an inhibitor of Rho A that has been documented to promote functional recovery following SCI[28,30,31,372]. Although there is a large body of evidence that ibuprofen treatment leads to recovery in functional deficit post-SCI[368,369], there are only a small number of studies that identify the ability of ibuprofen to induce axonal regeneration *in vitro*[31]. This chapter describes the use of ibuprofen treatment to consistently promote neurite outgrowth both in 2D and 3D models of neurite inhibition. Ibuprofen was found to either partially or fully restore neurite outgrowth in all the models of inhibition described in this chapter including aggrecan-coating, 2D co-culture and conditioned medium systems. This, along with evidence outlined in literature, supports the role of Rho A in CSPG-mediated inhibition of neurite outgrowth and identifies the neuroregenerative properties of ibuprofen.

The proposed pathway by which CSPGs elicit neurite inhibition states that Rho A activation leads to activation of downstream ROCK which in turn determines actin dynamics resulting in neurite inhibition[26,27]. Y-27632 is a selective inhibitor of ROCK and has been used to promote neurite growth in many systems, both without the presence of an inhibitory stimulus and in neurite inhibition studies. Numerous studies, both *in vivo*[209,398–400] and *in vitro*[23,27,204], identify the beneficial effects of Y-27632 following spinal cord injury in terms of neurite sprouting and functional recovery. This chapter documents the ability of Y-27632 to not only overcome neurite inhibition in the many models described herein, but also to enhance neurite outgrowth regardless of the inhibitory stimulus. In all models of inhibition described in this chapter, and in both 2D and 3D culture systems, Y-27623 was found to consistently enhance neurite growth to levels greater than the control. Very impressive neurite outgrowth was observed both in 2D and 3D neurite outgrowth assays that incorporate this molecule. The enhanced potency of Y-27632 compared with ibuprofen, is perhaps due to the efficiency at which each molecule inhibits its target.

Therefore, Ch'ase, Y-27632 and ibuprofen have all been demonstrated to overcome neurite inhibition in the models described within this chapter. This suggests a pivotal role for Rho A and ROCK signalling in CSPG-mediated signal transduction which is supported by a large body of primary literature. Furthermore, this has been demonstrated in an aggrecan-based model of neurite inhibition in addition to several more complex glioma

cell-based models of neurite inhibition, which demonstrates the reliability and reproducibility of these findings.

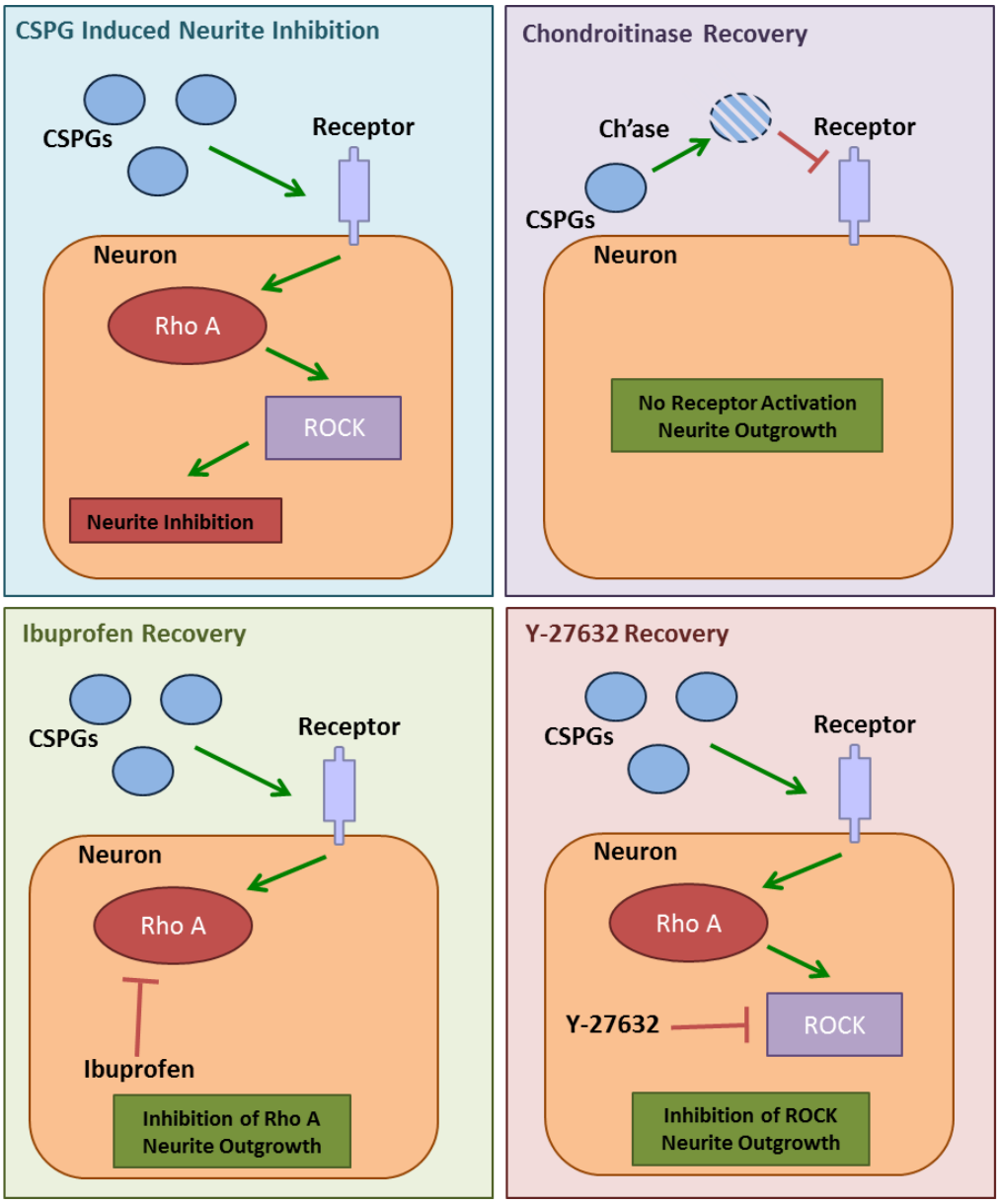

Fig 4-31: Overview of CSPPG-mediated neurite inhibition and methods of recovery. Schematics depicting the molecular mechanisms that underpin CSPG-mediated inhibition in the glial scar and mechanisms to inhibit the process and restore neurite growth. Chondroitinase breaks down CSPGs rendering them unable to activate their receptors, ibuprofen inhibits Rho A downstream of receptor activation and Y-27632 inhibits ROCK, all of which are capable of restoring neurite growth in the inhibitor glial scar.

4.4.5 Expression of Reactive Astrocyte Markers by Glioma Cells is Confluency Dependent

Primary astrocytes, when harvested from animal models and cultured *in vitro* generally adopt a reactive phenotype, upregulate GFAP and form complex cytoplasmic projections[192,351,401] . This may be the desirable astrocytic phenotype for studies that require astrocytes to become reactive, such as glial scar interactions, however methods to maintain a more non-reactive astrocyte phenotype have been developed[192,351]. Particularly, more physiologically relevant 3D cell culture technology has been used to maintain primary astrocytes *in vitro* in a less-reactive state. Solid scaffolds such as Alvetex® scaffold[192], hydrogels[351] and nanofiber scaffolds[401] have all been demonstrated to promote a non-reactive phenotype in primary astrocytes cultured *in vitro.* This led to the hypothesis that cell-cell interactions and culture confluency may regulate the expression of reactive astrocyte markers in cultured cells *in vitro*.

The majority of studies focus on the reactive phenotype of primary astrocyte cultures, and little characterisation as to the expression of GFAP and CSPGs has been carried out in established glioma cell lines. However, due to the effect of 3D cell culture technology on primary cultures, it may be hypothesised that 3D cell culture technology may possibly reduce the expression of GFAP and CSPGs in glioma cell lines also. Data outlined in this chapter actually describes enhanced expression of CSPGs and GFAP, when U-251MG cells are cultured in Alvetex® scaffold, particularly at lower seeding densities. Expression of reactive astrocyte markers is enhanced in 3D culture compared with 2D and is also enhanced in sub-confluent rather than confluent cultures.

Therefore, this suggests that expression of GFAP and CS is confluency dependent, implicating the role of cell-cell contacts in the phenotype of glial cells *in vitro*. However, expression of such markers in glioma cells opposes the expression profiles documented in primary cell cultures, suggesting that the neoplastic nature of glioma cell lines impacts cellular phenotype.

4.4.6 Inhibition of Rho A and ROCK Signalling Reduces Glioma Cell Proliferation

Inhibition of Rho A and ROCK through small molecule modulators was used to restore neurite growth in the presence of inhibitory U-251MG glioma cells. However, the effect of such molecules on the glioma cells themselves resulted in some interesting observations. Application of both Y-27632 and ibuprofen resulted in morphological changes in the glioma cells, which was particularly apparent in Y-27632 cultures, as cells adopted a clearly more stellate morphology. This has also been observed in primary astrocytes, which adopt a flat polygonal morphology upon *in vitro* culture but can be induced by Y-

27632 to form stellate structures with complex cellular processes[402–405]. The effect of Y-27632 induction of astrocytic process formation has been utilised by Holtje *et al* to promote wound closure following injury[404]. This highlights the importance of understanding such basic, fundamental processes including control of actin dynamics in detail, and devising innovative, novel applications of such knowledge.

Treatment of U-251MG cells with ibuprofen and Y-27632 to inhibit Rho A and ROCK respectively, appeared to result in a reduction of cellular proliferation. This was measured by MTT assay, which is a metabolic assay that indirectly measures cellular viability through metabolic behaviour. It therefore does not give an accurate representation of cellular proliferation and to confirm this effect, more direct studies are required.

However, the effects of Rho A/ROCK inhibition in primary astrocyte cultures, partocicularly Y-27632 treatment has previously been documented by Yu *et al* to promote proliferation of spinal cord-derived astrocytes[406]. Although Y-27632-mediated inhibition of ROCK has been documented to promote proliferation of primary astrocytes, inhibition of ROCK has been well documented in other cell types to reduce cellular proliferation[406]. In particular, proliferation of glioblastoma cell lines including the U-251MG line as discussed in this chapter, has previously been described to be inhibited by the selective ROCK inhibitor, Y-27632[407,408]. These findings have even led to the consideration of inhibition of Rho A and ROCK as a suitable therapeutic strategy in the treatment of malignant glioblastomas, particularly to reduce tissue invasion and prevent cancer progression. This supports the findings outlined in this chapter that suggest inhibition of Rho A and ROCK may reduce cell proliferation in U-251MG cells.

Furthermore, increased expression of both GFAP and CS was documented upon induction by Y-27632 and ibuprofen. This was thought to be a consequence of the reduced proliferative capacity of the cells, leading to less confluent cultures and as described earlier U-251MG cells were found to express these markers to a greater extent at reduced cell density. However, a study by Chan *et al* does document the ability of Y-27632-induced inhibition of ROCK to induce a reactive phenotype, resulting in enhanced expression of these markers in primary astrocyte cultures[409].

4.5 Key Findings

- Growth substrates coated with CSPGs (aggrecan) were inhibitory to neurite outgrowth in 2D and 3D culture.

- Aggrecan-mediated neurite inhibition was overcome by inhibition of Rho A (ibuprofen) or inhibition of ROCK (Y-27632) in 2D and 3D culture systems.

- The glioma cell line, U-251MG, was found to express GFAP and CSPGs reminiscent of the reactive astrocytes that contribute toward glial scarring post-SCI.

- Expression of GFAP and CSPGs in U-251MG cells was found to be dependent upon cellular density and culture parameters. Inhibition of Rho A (ibuprofen) or ROCK (Y-27632) enhanced expression of both GFAP and CSPGs, and also reduced cellular proliferation.

- A 2D co-culture model combining U-251MG cells and human stem cell-derived neurospheres was developed. However, this method of co-culture had significant limitations, although recovery of neurite growth was evident when treated with Ch'ase, Y-27632 or ibuprofen.

- Glioma cell conditioned medium containing secreted CSPG molecules, was used to successfully induce neurite inhibition from human-derived neurospheres. This inhibitory response was overcome by Ch'ase, Y-27632 and ibuprofen treatment.

- A dynamic co-culture model was developed whereby; glioma cells were cultured at the bottom of the culture well, whilst neurospheres were cultured in 3D in the same well. This resulted in inhibition of neurite outgrowth that was overcome by Ch'ase, Y-27632 and ibuprofen treatment.

4.6 Conclusions

This chapter has involved the development of several different methodologies used to induce neurite inhibition and study the interactions in the glial scar. These range from simple CSPG coatings, to complex co-culture models, the suitability of which depends upon the application for which it is intended. More simple models such as the aggrecan-induced model of inhibition described within this chapter are useful to give insight into specific CSPG-mediated signalling pathways, however do not accurately reflect the complex environment that forms post-SCI. More complex models such as the conditioned medium and co-culture models described in this chapter are helpful in the study of complex interactions that occur following injury to the spinal cord, however their complexity may impede the successful dissection of clear molecular signalling.

In addition to models of inhibition, this chapter also discusses the signalling mechanisms involved in CSPG-mediated neurite inhibition with particular focus on Rho A and ROCK signalling. Inhibitors of Rho A and ROCK signalling can be used to overcome CSPG-mediated inhibition and provide not only a potential therapeutic target but also help provide a more detailed view of the signalling pathway that leads to growth cone collapse and neurite inhibition.

Understanding the Rho A signalling pathway is not only important in the development of neural regeneration strategies but also in the development of therapeutic applications in the context of other pathologies. This chapter describes the ability of the selective ROCK inhibitor, Y-27632 to reduce cellular proliferation of the glioma cell line U-251MG, this in turn has implications in the treatment of malignant gliomas, as such molecules could be used to reduce cell proliferation and thus cancer progression. Inhibition of ROCK can potentially provide a strategy to reduce tumour progression and invasion, along with identifying key signalling pathways involved in this process.

Furthermore, this chapter describes an application of the novel human stem cell derived model of neuritogenesis described in Chapter III to study the process of neurite inhibition that occurs following spinal cord injury. In addition to this, applications such as investigations into the signalling pathways involved in CSPG-mediated neurite inhibition and screening of molecules to overcome inhibitory stimulation have also been described. Therefore this model could provide a 3D and therefore more physiologically relevant *in vitro* model of neurite growth and inhibition that may be beneficial in the screening of drugs, to identify candidate compounds that promote neurite regeneration.

4.7 Future Directions

Future work building upon the data described in this chapter could include the following:

- The inhibitory effects of glioma cell-deposited ECM could be investigated by culturing U-251MG cells in Alvetex® scaffold for a desired culture period. Cells could then be lysed leaving only the secreted ECM that coats the remaining scaffold. Neurospheres cultured on top of the scaffold to determine the effect of the deposited ECM on neurite growth.

- Other modulators of Rho A and ROCK signalling could be used to potentially achieve neurite recovery in the inhibitory models outlined in this chapter. These could include fasudil and C3 transferase, which have been well documented in by many studies to promote neurite regeneration.

- A complex analysis of U-251MG conditioned medium could be conducted to identify both neurite promoting and inhibitory constituents of the medium. This could be achieved through mass spectroscopy and additional ELISA assays to determine the composition of the conditioned medium.

- The co-culture model described in this chapter that separates glioma cells from neurospheres and was used to assess the effect of soluble inhibitory molecules upon neurite outgrowth could be further enhanced. The glioma cells in this model are cultured in 2D at the bottom of the culture well, however to further improve the model, glioma cells could be cultured in 3D within an Alvetex® membrane at the bottom of the well to further enhance the secretion of CSPGs.

Chapter V: Investigation into the Role of β-amyloid in Neurite Inhibition within Alzheimer's Disease

5.1 Introduction

Neurodegenerative diseases including Alzheimer's and Parkinson's disease are characterised by a loss of neuronal connectivity. Inhibition of neurite development is one of multiple pathogenic mechanisms that lead to a reduction in connectivity in these diseases. Therefore, the example of neurodegeneration, highlights the need for reliable, physiologically relevant and robust *in vitro* models to both study the complex molecular signalling pathways involved in neurite inhibition, and to screen the ability of molecules to overcome inhibitory influences.

5.1.1 Alzheimer's Disease

Alzheimer's disease (AD) is the most common age-related neurodegenerative disease and perhaps one of the most devastating diagnoses a patient and their family can receive[410]. The incidence of AD is increasing, reflecting an ageing population and in 2009 there were 35.6 million cases of AD recorded world wide with this number expected to more than double by 2050[411]. As of yet there is no complete cure for AD and other forms of dementia, however, there has been a great deal of research in this area with a focus on understanding the molecular pathophysiology of the disease subsequently leading to rational therapeutic design[412–418].

The main clinical characteristics of AD involve the decline of memory initially as a loss of episodic memory[411]. This results in the inability of a patient to recall recent events such as autobiographical activities[411]. Understanding the molecular events that lead to disease progression and pathogenesis, can help discover points at which treatments can intervene, preventing this episodic memory loss and relieving the symptoms of the disease.

5.1.2 Pathophysiology of Alzheimer's Disease

In 1907, Alois Alzheimer first identified two pathological anomalies in the brain of a female dementia patient[410]. These two lesions represent the hallmark features of the disease and their observation postmortem is still required for a confirmed AD diagnosis today[410]. Generation of proteinaceous aggregates is common to the pathogenesis of many neurodegenerative diseases including AD[264]. The brains of AD patients in addition to

displaying synapse loss, include two hallmark lesions, extracellular senile plaques containing aggregated β-amyloid peptides and intracellular neurofibrillary tangles (NFTs) composed of hyperphosphorylated forms of the microtubule-associated protein Tau[264].

There is a growing body of evidence that implicates these protein aggregates in the onset and progression of AD and understanding their development and interactions may be essential in the identification of successful drug candidates[264]. However, AD is a multi-faceted disease with many contributing pathogenic mechanisms, including synapse loss, inflammatory responses and oxidative stress which along with proteinaceous aggregate deposition all play a role in the development and progression of the disease[410]. Therefore, the development of successful drug candidates to treat AD has been difficult, as all of the aforementioned mechanisms should be taken into consideration during the development of such therapeutics.

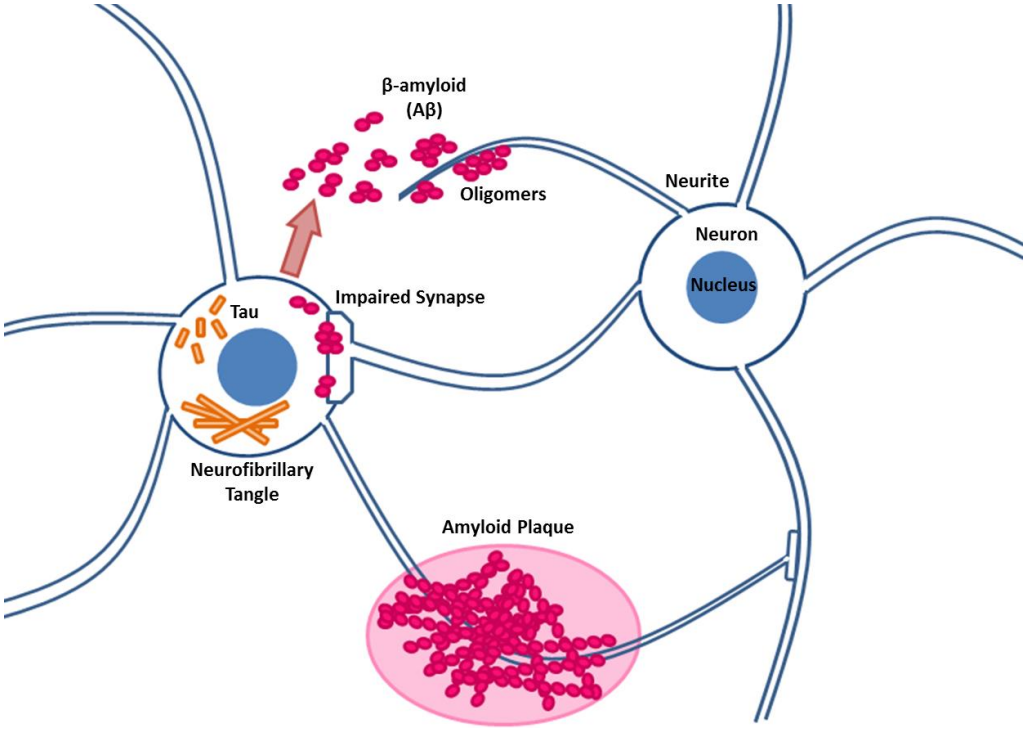

Fig 5-1: Pathological hallmarks of Alzheimer's disease.
The two major, most well characterised hallmarks of AD include the extracellular accumulation of β-amyloid as plaques and the intracellular accumulation of hyperphosphorylated tau as neurofibrillary tangles.

5.1.2.1 β-amyloid Generation and Senile Plaque Formation

β-amyloid (Aβ) is produced by the proteolytic cleavage of the parental amyloid precursor protein (APP) via the sequential action of secretase enzymes[410]. There are three families of secretase enzymes: α-, β- and γ-secretases all of which contain proteolytic enzymes. For example, ADAM9, ADAM10 and ADAM17 are metalloproteinase enzymes that have α-secretase activity[419,420]. Similarly β-site APP-cleaving enzyme 1 (BACE1) is an integral membrane protein that belongs to the β-secretase category[421,422] and γ-secretase exists as a complex of enzymes including presenilin 1 and 2 (PS1 and PS2), nicastrin, anterior pharynx defective and presenilin enhancer 2[262,423].

The cleavage and enzymatic processing of APP can be separated into amyloidgenic and non-amyloidgenic processing (see Figure 5-2). The non-amyloidgenic pathway is the most prevalent method of APP processing and involves the cleavage of APP 83 amino acids from the C-terminus by α-secretase[410]. This produces a large N-terminal ectodomain (sAPPα) that is secreted into the ECM along with an 83 amino acid long C-terminal fragment (C83) that is retained in the membrane[410,424]. C83 is then cleaved by γ-secretase producing a short p3 fragment. Cleavage by α-secretase occurs within the Aβ region; therefore prevents the formation of Aβ specieis[410,424].

Alternatively the amyloidgenic pathway of APP cleavage leads to the generation of Aβ species associated with AD pathogenesis. The initial proteolysis within this pathway is mediated by β-secretase, as oppose to α-secretase at a location 99 amino acids from the C-terminus[410,424,425]. This results in the release of sAPPβ into the ECM whilst a 99 amino acid C-terminal stub (C99) remains within the membrane. Subsequent cleavage of C99 by γ-secretase between residues 39 and 43, results in the generation of Aβ species, of which the 40-residue length peptide ($A\beta_{40}$) is the most prevelant[410,424,425]. A small proportion (~ 10 %) of total Aβ is made up of the 42-residue variant ($A\beta_{42}$), which is more hydrophobic and more readily forms insoluble fibrils and aggregates compared with $A\beta_{40}$[410,426]. For this reason $A\beta_{42}$ is the predominant Aβ species associated with senile plaque formation and AD pathogenesis is associated with an increase in the ratio $A\beta_{42}$ relative to $A\beta_{40}$, which is even used as a diagnostic biomarker in CSF analysis[426–434].

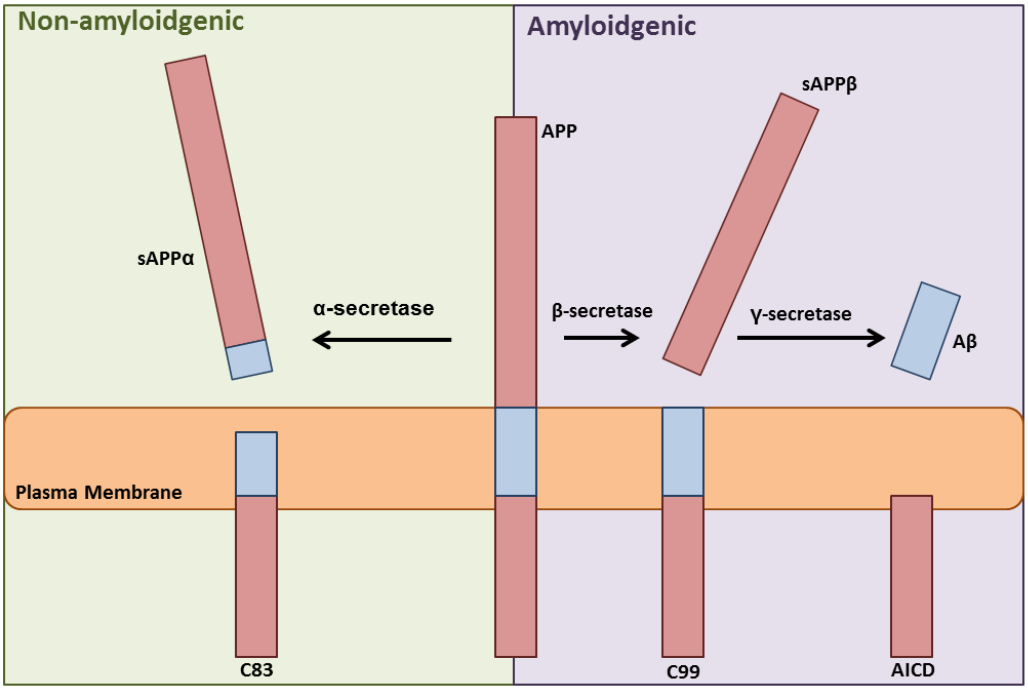

Fig 5-2: Proteolytic processing of amyloid precursor protein (APP).
A schematic that depicts two forms of APP proteolytic cleavage including the abundant non-amyloidgenic pathway and Aβ generation through the amyloidgenic pathway. Non-amyloidgenic cleavage involves the action of α-secretase that cleaves APP within the Aβ domain, giving rise to soluble sAPPα and membrane bound C83. Amyloidgenic processing however, first involves the action of β-secretase that releases soluble sAPPβ whilst C99 remains within the plasma membrane. γ-secretase then acts upon the remaining C99 liberating Aβ species. AD is associated with an increase in amyloidgenic processing of APP and the buildup of Aβ deposits.

Familial forms of AD are generally associated with mutations involved in the processing of APP for example mutations in *APP*[435–437], *PS1* and *PS2*[438] are associated with autosomal dominant early-onset AD[439]. One mutation in APP known as the Swedish mutation (APP_{Swe}) is the result of a double amino-acid change that leads to increased cleavage of APP by β-secretase[440]. Mutations in the presenilins such as PS1M146V result in increased levels of $Aβ_{42}$ therefore enhanced aggregation and incidence of senile plaques[410]. Increased dosage of APP is also associated with dementia as patients with Down's syndrome often experience Aβ accumulation early in life. This is because the APP gene resides on chromosome 21, which Down syndrome patients have three copies of[441–443].

The central role of Aβ formation in the pathophysiology of AD has resulted in numerous attempts at therapeutic intervention[444]. Inhibition of the secretase enzymes thus prevention of Aβ formation has been a common strategy in the design of AD drugs. However, inhibition of γ-secretase resulted in reduced Aβ levels in the brain[445] but was associated with a cognitive decline at clinical trial in the treatment group[263]. This was

later thought to be due to the wide range of protein targets of γ-secretase with over 100 targets having now being identified[446–450]. β-secretase inhibition has been regarded with more success, as reduction in Aβ concentration within the CSF of patients was noted without any obvious detrimental effects[418]. However, one β-secretase inhibitor clinical trial was halted due to hepatotoxicity[444,451–453]. Other therapeutic strategies that target Aβ accumulation include stimulation of the non-amyloidgenic pathway[444], aggregation inhibitors[454,455], immunotherapy[456] and promotion of Aβ clearance[457,458].

Although Aβ appears to play a central role in the pathogenic molecular mechanisms involved in AD progression, early thoughts that Aβ deposits were the driving force of the disease are now beginning to be rejected[459]. In the early 1990s the amyloid cascade hypothesis was first suggested and involves the theory that Aβ formation and aggregation occurs in a linear pathway resulting in the gradual accumulation and aggregation of the peptide in the brain[460]. Amyloid deposition was thought to drive inflammation and oxidative stress, leading to neuronal injury and loss[460]. However, recently many experts in the field openly dismiss the amyloid cascade hypothesis, as emerging studies reveal that AD is a complex disease involving many interacting cellular imbalances in processes such as autophagy, lysosomes, mitochondria, DNA damage etc[459,461]. Nevertheless, Aβ production is still thought to be an important factor in the development of the disease but must be considered in conjunction with other factors as oppose to a single driving force.

5.1.2.2 Abnormal Phosphorylation of Tau

Tau is a microtubule associated protein (MAP) found in the axons of neurons and is involved in the stabalisation of microtubules (MTs)[264]. There are six major isoforms of tau found within the human brain, all of which are derived from a single gene by alternative splicing and contain a MT-binding domain comprised of repeats of a highly conserved tubulin-binding motif[462]. Each tau isoform differs in terms of the number of tubulin-binding repeats and in the presence of either one or two 29 amino acid long inserts at the N-terminal domain, however this is not instrumental in MT-binding[463]. Although the primary function of tau is known to be stabalisation of MTs, other binding partners such as RNA[464] and PS1[465] have been identified suggesting that tau may be prone to heterogenous interactions and may even play a role in protein misfolding and aggregation[264].

The role of tau in MT-binding is regulated post-translationally by serine/threonin-directed phosphorylation that modulates MT-binding affinity in a dynamic equilibirum[264,466–468], as shown in Figure 5-3. This is thought to be important during development, as phosphorylation of tau during development is much higher than in the adult brain, which is usually characterised by a considerably lower tau phosphorylation

state[264,469–471]. The role of tau in the stabalisation of MT is essential to the normal functioning of the neuron as the MT network is involved in maintaining the correct morphology of the cell, which is particularly important in neurons as their morphology is essential to their function and connectivity particularly as neurons span large distances in the body[264]. The MT-network, thus tau, is also essential in the transport of cellular cargo including signalling molecules, trophic factors, organelles and other essential cellular components[264]. Therefore, correct functioning of tau is essential to ensure proper axonal transport, which in turn impacts the function and viability of neurons along with their highly extended processes.

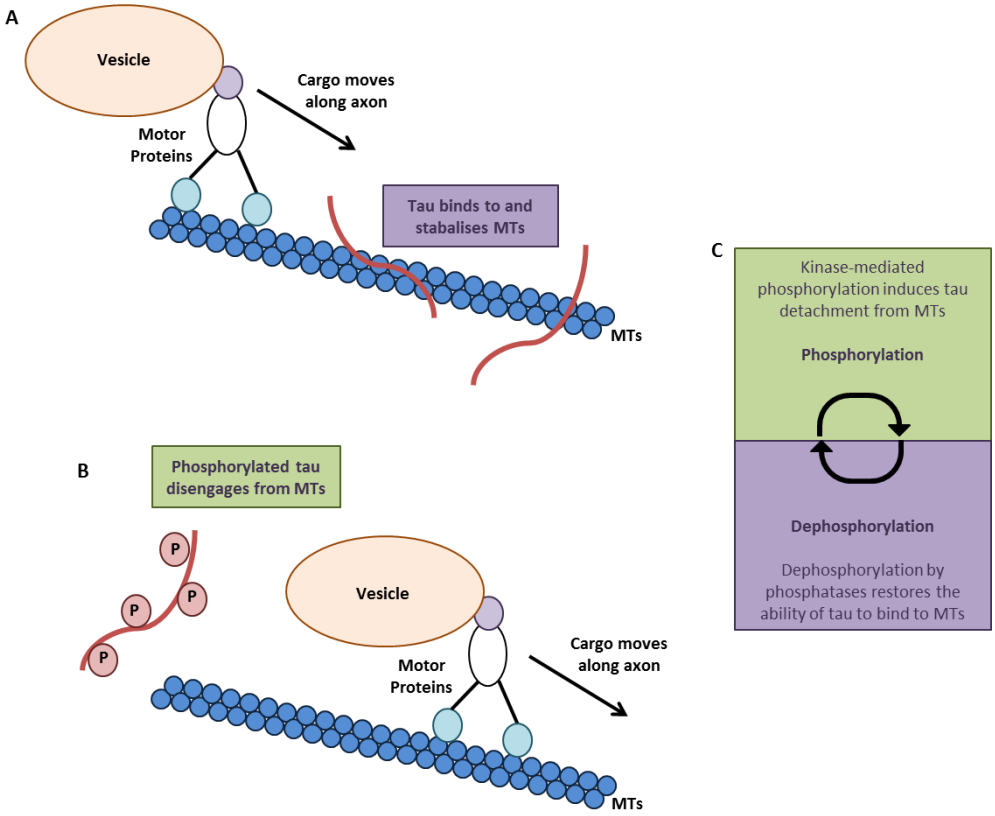

Fig 5-3: Dynamic equilibrium of tau phosphorylation in microtubule homeostasis. A schematic representation of tau (red) binding to microtubules (MTs, blue) in its unphosphorylated state (A) which is essential for MT integrity, although hinders the movement of cargo along MTs. Phosphorylation of tau (B) results in MT detachment and a dynamic equilibrium of tau phosphorylation (C) ensures effective axonal transport is maintained.

In AD and other taupathies the equilibrium of tau binding to MTs is disrupted resulting in high levels of unbound tau, which increases the likelihood of pathogenic conformational changes resulting in tau aggregation and fibrillisation[264]. Aggregation of tau first begins with the abnormal disengagement of tau from MTs that can be a result of many factors, including hyperphosphorylation[264,472–475]. This results in a high cytosolic concentration of unbound tau, increasing the likelihood of misfolding and rendering tau more likely to undergo aggregation[264]. Small intracellular deposits of tau then form, known as pre-tangles that are non-fibrillary and do not contain β-sheets[264]. A structural rearrangement of pre-tangles is then required for the formation of paired helical filaments that self-assemble to form neurofibrillary tangles (NFTs): intracellular inclusions associated with neurodegeneration[264].

In AD the highest concentration of aggregated tau (~ 95 % of total tau) is found within the dystrophic neurites of the neuron[264]. Therefore it is though that tau pathology can lead to abnormal cytoskeletal structure and function that can compromise axonal transport leading to synaptic dysfunction, neurodegeneration and loss of functional neurites[264]. In addition to this, tau is also thought to contribute to AD pathology through interactions with Aβ, which remain poorly understood and of which there are three proposed models of interaction[411], as summarised in Figure 5-4. One model suggests that Aβ is the driving force that stimulates hyperphosphorylation of tau[411]. This is supported by the fact that Aβ deposition in APP transgenic mice was observed to lead to hyperphorphorylation of tau, whereas in tau transgenic mice Aβ aggregation was not noted[476,477]. Furthermore intracranial injection of synthetic Aβ into tau transgenic mice was found to enhance NFT formation[478].

Another model of tau/Aβ driven pathology suggests that both Aβ and tau act through different mechanisms to have a synergistic, complimentary effect[411]. For example, mitochondrial dysfunction and oxidative stress are thought to play an important role in AD progression and tau is known to impair complex I of the respiratory chain, whilst Aβ is known to block complex IV-dependent respiration[479–482]. Therefore, both Aβ and tau impair mitochondrial function but through distinct mechanisms. The final school of thought states that tau may play a secondary role in Aβ-mediated toxicity[411]. This theory was founded on the evidence that in the tau knockout, transgenic neurons were protected from Aβ induced cell death in culture[483], therefore it was hypothesised that tau was simply a mediator of the negative effects of Aβ.

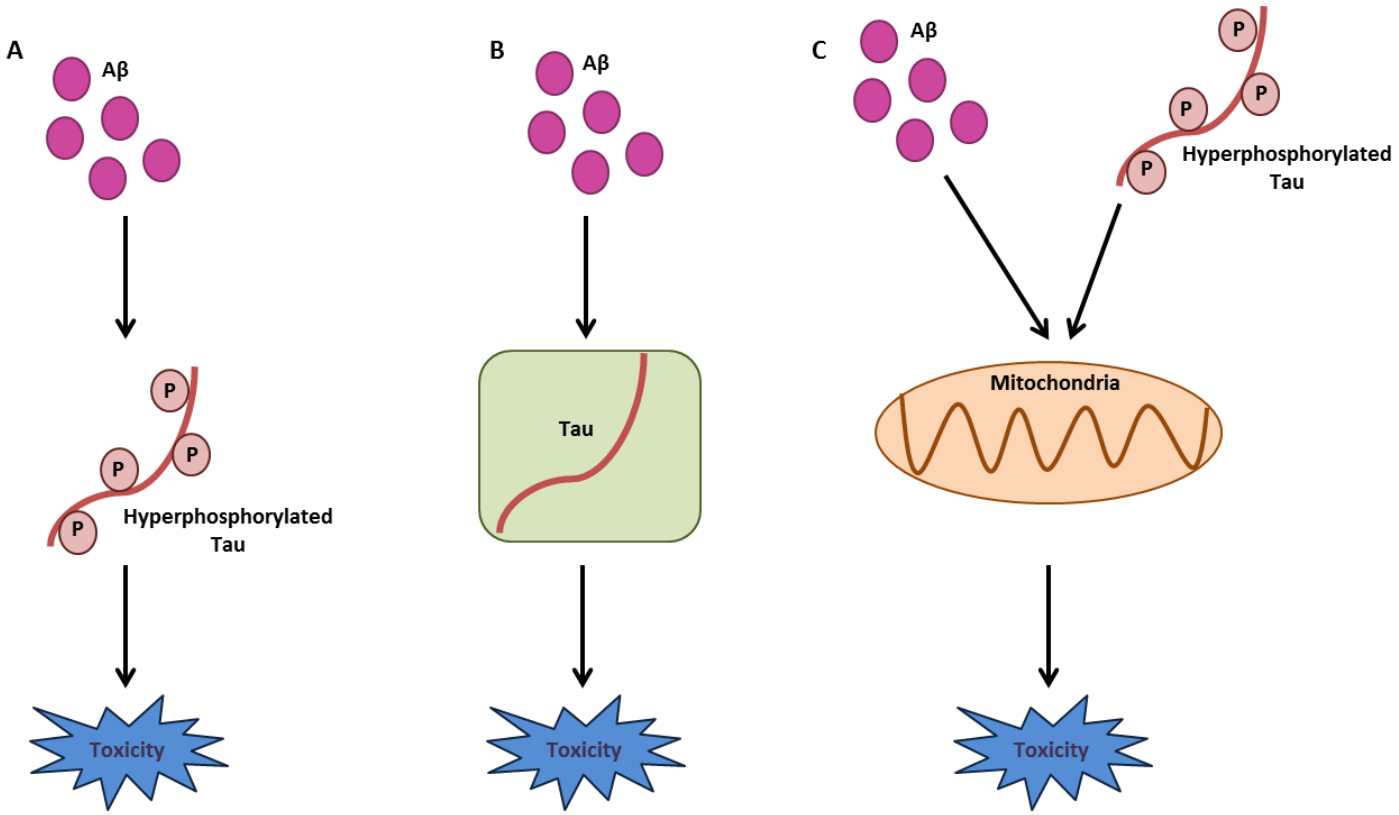

Fig 5-4: Proposed models of tau and β-amyloid interaction in Alzheimer's disease pathogenesis.
A schematic describing three potential modes of Aβ and tau interactions in the development of AD pathology. Aβ deposition may drive hyperphosphorylation of tau resulting in neurotoxicity (A) or tau may mediate the toxic effects of Aβ, therefore disease progression is dependent upon tau presence (B). Alternatively tau and Aβ may independently target cellular processes amplifying the toxic effect of the other (C).

There is an abundance of contradictory evidence as to the role of Aβ and tau aggregation in the onset and progression of AD, however both are thought to play a central role in the development of the disease. This highlights the complex nature of neurodegenerative diseases involving interplay between multiple pathogenic mechanisms that should always be considered in the development of disease models and potential therapeutics.

5.1.3 Neurite Outgrowth and Alzheimer's Disease

One of the major hallmarks of AD, other than the accumulation of proteinaceous aggregates, is the loss of neuronal connectivity. This occurs due to synaptic loss[484–488] and the inhibition of neurite growth[411], which are essential in the formation of neuronal connections. The molecular mechanisms that underpin neurite inhibition within the brain of AD patients remain relatively unknown. However *in vitro* studies have interestingly revealed opposing functions of APP and Aβ in neurite outgrowth and survival. APP has been found by many studies to enhance neurite development[489–491] whereas Aβ has been found to have inhibitory effects upon neurite growth[36,40]. Understanding the molecular signalling events that underpin these processes may be essential in revealing the underlying pathogenic mechanisms involves in AD progression and in the development of novel therapeutics with the aim of restoring lost neuronal connections in the brain of patients with AD.

5.1.3.1 APP and Neurite Outgrowth

The amyloid precursor protein (APP) is perhaps one of the most studied proteins to date, due to its central role in the generation of Aβ and the significance of this in AD pathology. However, its role in many biological processes appears complex as APP has been found to exhibit both neurotoxic and neuroprotective effects with functions including cell adhesion, acting as a cell surface receptor, synapse formation and cell division[492]. However, many studies have struggled with identifying the exact functions of APP, as many experimental models involving over- or under-expression of APP result in varied expression of many proteolytic products, which may impact experimental outcomes[492].

One of the most widely studied functions of full length-APP is its ability to induce neurite outgrowth and synaptogenesis, particularly in the developing brain. Expression of APP in the developing chick brain is thought to coincide with the developmental period associated with maximal neurite outgrowth and synaptogenesis, suggesting a potential role of APP in nervous system development[493]. Many *in vitro* cell-based neuronal models have been used to identify the neurite promoting properties of APP, which were first identified in the 1990s[490,494]. However, since the identification of the role of APP in

stimulation of neurite outgrowth, little has been uncovered of the underlying molecular mechanisms that drive this function.

Proposed mechanisms by which APP may enhance neurite generation include: enhancement of cellular adhesion[495], interactions with integrins[496] and ECM components[497] along with mediation of the effects of NGF[498]. Although the specific mechanisms of APP induction of neurite outgrowth remain undetermined, studies such as that of Allinquant *et al* highlight the importance of APP function in this key developmental process[499]. Alliquant *et al* demonstrate the ability of anti-sense oligonucleotides to block APP expression in embryonic cortical neurons *in vitro* resulting in a reduction in axonal and dendritic outgrowth[499].

Therefore although the exact molecular mechanisms remain largely unknown, APP is thought to play an integral role in neurite outgrowth during development. This raises interesting questions in the loss of neuronal connectivity associated with AD such as a potential link between increased amyloidgenic processing and a reduction in neuritogenesis and synaptogenesis. In addition to this the opposing effects of Aβ upon neurite outgrowth further implicate impaired neuritogenesis in the pathophysiology of AD.

5.1.3.2 β-amyloid Peptides and Neurite Outgrowth

The role of Aβ species in neurite outgrowth, unlike that of APP, is thought to be negative with many studies evidencing the inhibitory qualities of Aβ[36,40]. Several *in vitro* cell-based models have analysed the effects of Aβ upon neurite outgrowth, which provide the advantage of a simplified system to study the impact of Aβ alone as opposed to, the complex interacting pathways involved in AD pathogenesis that may also impact neuronal connectivity.

Petratos *et al* describe the exogenous addition of Aβ species to the culture medium of SH-SY5Y cells with the resultant neurite outgrowth being inhibited by both $A\beta_{40}$ and $A\beta_{42}$ supplementation compared with controls[36]. Interestingly, this study found that neurite outgrowth was inhibited to a greater degree by $A\beta_{40}$ than the more insoluble and aggregate-prone $A\beta_{42}$[36]. In a similar study Postuma *et al* examined the ability of Aβ species to induce neurite inhibition in primary neuronal cultures with Aβ presented to cells bound to the growth substrate[40]. This study determined that substrate-bound Aβ inhibited neurite outgrowth to a greater extent than soluble Aβ supplementation of culture medium and that when bound to the growth substrate $A\beta_{42}$ inhibited neurite outgrowth to a greater extent than $A\beta_{40}$[40].

The inhibitory function of Aβ is supported by observations of dystrophic growth cones within the brain of patients with AD. As neurites pass through Aβ-rich deposits such as senile plaques, they adopt a curvature and their morphology becomes dystrophic[500,501]. Furthermore, transgenic animal models of AD have been used to observe dendritic abnormalities associated with Aβ deposition and in a comparison with human postmortem AD brain, several dendritic abnormalities were identified[502]. These morphological abnormalities include spine loss, shaft atrophy, bending, branch breaking and sprouting[502]. A study by Jin *et al* identifies the ability of soluble Aβ dimers isolated from AD brain tissue to induce neurite degeneration[503]. This study has the advantage of applying naturally occurring Aβ peptides to primary cell cultures as opposed to synthetic forms of the peptides used in other studies and similarly it evidences abnormal neurite development in the presence of Aβ.

Therefore, many techniques both *in vitro* and *in vivo* have been used to evidence the role of Aβ in neurite inhibition and dysfunction. This change in morphology associated with Aβ deposition and inhibition of growth has a striking impact on neuronal connectivity and signal transduction along with synapse formation[500]. Such changes in neuronal connectivity may have a negative impact on memory function and may be involved in the clinical onset of symptoms in conjunction with other pathogenic factors. Therefore, although there is a large body of evidence to support the role of Aβ in inhibition of neurite outgrowth, the molecular mechanisms that drive this process must now be uncovered to aid in the development of therapeutics and to further our understanding of the process.

5.1.3.2.1 Interactions Between β-amyloid and the Nogo Receptor

Inhibitory molecule-mediated signal transduction plays a huge role in the inability of neurons to regenerate following traumatic injury to the CNS (as reviewed in Chapter IV). The Nogo receptor (NgR) present on neurons, initiates an intracellular signalling cascade upon ligand binding that results in neurite dystrophy and growth cone collapse[39]. In the injured spinal cord NgR ligands include myelin inhibitors such as Nogo, OMGP and MAG along with CSPGs secreted from reactive astrocytes[39]. Interestingly there is emerging evidence to suggest NgR plays a role in AD pathophysiology as both APP and Aβ have been found to bind to the receptor[504–506].

Numerous studies have determined the ability of both APP and Aβ to bind to the NgR, however the ability of Aβ to activate this receptor and its downstream signalling events is still remains unclear. It has been reported by Park *et al* that whilst Aβ binds to NgR, disruption of NgR expression in transgenic mouse models results in increased Aβ deposition and dystrophic neurites[504]. Similarly, this study also discusses that overexpression of NgR results in decreased Aβ production in cultured cells[504]. This

evidence may suggest that Aβ binds to but does not activate NgR, and NgR simply sequesters Aβ preventing it from performing its neurodegenerative functions.

However, a study by Knowles *et al* describes the role of p75, which is a constituent of the NgR complex, in Aβ mediated neuritic dystrophy[507,508]. This study determined that primary neuronal cultures obtained from p75 knockout transgenic mice, were protected against the deleterious effects of Aβ on neurite growth[507]. Similarly, transgenic knockout mice exhibited a significant reduction in neuritic dystrophy and a complete reversal of cholinergic neurite degeneration compared to wild type[507]. This evidence supports the role of p75, thus the NgR signalling complex in Aβ-mediated inhibition of neurite outgrowth.

An interesting treatment approach has been developed based upon the finding of Aβ-NgR binding. This is explored in another study by Park *et al* that utilises subcutaneous delivery of NgR to improve spatial memory in a transgenic mouse model of AD[509]. This is thought to improve the clinical symptoms of AD through both sequestering of Aβ and blocking the function of secretase enzymes involved in amyloidgenic processing, therefore overexpression of NgR has also been associated with a decreased production of Aβ species[505,506]. This highlights the necessity of understanding the molecular mechanisms that underpin such processes to identify potential therapeutic interventions aimed at restoring normal physiological functions.

5.1.3.2.2 The Role of Rho A & ROCK Signaling in β-amyloid-mediated Neurite Inhibition

The common neurite inhibitory signalling pathway, as discussed in Chapter IV in the context of spinal cord injury, involves receptor activation that leads to activation of Rho A and downstream ROCK that impacts the actin cytoskeleton resulting in growth cone collapse and neurite inhibition. This signalling pathway is also thought to mediate the inhibitory effects of Aβ, however whether it is initiated by NgR activation still remains unclear. Petratos *et al* describe the role of Rho A signalling in Aβ-mediated inhibition using a cell-based *in vitro* neurite outgrowth model[36]. Aβ induction of neurite inhibition was found to result in an increase in GTP-bound active Rho A and the selective ROCK inhibitor, Y-27632 was found to restore neurite outgrowth in the presence of $A\beta_{40}$ to control levels[36].

However, this study also suggests that other mechanisms may be involved in Aβ-mediated inhibition, including microtubule involvement[36]. Collapsin response mediator protein-2 (CRMP-2) phosphorylation is activated by ROCK and associated with inhibition of tubulin polymerisation and therefore microtubule elongation. Petratos *et al* also describe the

increased expression of CRMP-2 upon Aβ treatment in SH-SY5Y model neurons along with *in vivo* observations of increased CRMP-2 and GTP-Rho A in the region of amyloid deposits[36]. This suggests that Aβ induces inhibition of neurite outgrowth through multiple mechanisms including activation of Rho A leading to actin stabalisation and neurite retraction along with activation of CRMP-2 and inhibition of microtubule polymerisation[510].

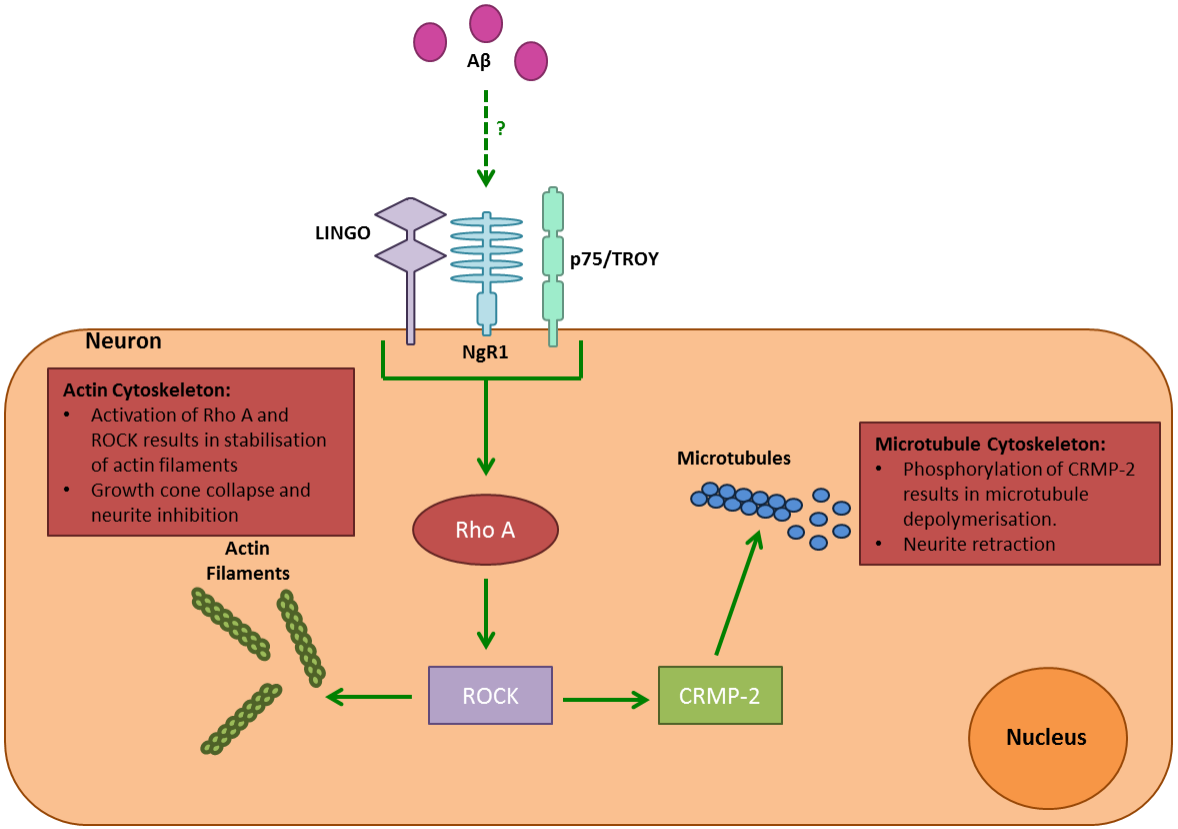

Fig 5-5: Proposed mechanism of Aβ-mediated neurite inhibition in Alzheimer's disease.
A schematic depicting the events that may lead to Aβ-induced inhibition of neurite outgrowth and decreased neuronal connectivity in AD. Aβ is known to bind to the NgR receptor, however, it is not known whether or not it activates the receptor. Rho A and ROCK activation have been implicated in the inhibition of neurite growth via Aβ as they have in many other inhibitory mechanisms. It is therefore hypothesised that Aβ acts through the NgR to activate Rho A and downstream ROCK which results in stabalisation of the actin cytoskeleton resulting in growth cone collapse and neurite retraction. Activation of ROCK is also thought to lead to phosphorylation of CRMP-2 that induces depolymerisation of microtubules and also contributes toward inhibition of neurite outgrowth.

5.1.4 iPSC Technology and Alzheimer's Disease Modelling

The underlying pathophysiological mechanisms that are involved in onset of AD and its clinical symptoms are extremely complex. The clinical manifestations of AD are thought to be driven by a number of interacting mechanisms including: abnormal protein homeostasis and accumulation, oxidative stress, mitochondrial dysfunction, inflammation, and loss of neuronal connectivity[511–514]. For this reason the development of accurate *in vitro* disease models is extremely challenging, as many factors should be considered in the development of such models.

Advancements in induced pluripotent stem cell (iPSC) technology offer novel opportunities to study cellular responses and establish therapeutic strategies against complex, multi-faceted diseases such as AD. Takuya *et al* initially describe the isolation of AD-patient specific iPSCs along with their use in modelling neurodegeneration in 2011[157]. This study describes the isolation of fibroblasts from autosomal-dominant early-onset familial AD patients with mutations in PS1 (A246E) and PS2 (N141I) along with their subsequent reprogramming to form a population of disease-specific iPSCs[157]. The patient-specific iPSCs were then induced to differentiate toward a neural lineage and the subsequent neurons were characterised as expressing a higher ratio of $A\beta_{42}$:$A\beta_{40}$ representative of the diseased state[157].

Since the first isolation of AD-patient derived iPSCs by Takuya *et al* in 2011, many other groups have developed similar lines with APP[236,237,515] and PS1 mutations[235] along with lines from patients with sporadic forms of AD[237,515]. In depth characterisation of such cell lines has revealed that *in vitro* models can replicate the increased levels of $A\beta_{42}$, hyperphosphorylated tau[236] and oxidative stress[237], associated with AD-progression. Applications of such unique models have also been demonstrated. For example Sproul *et al* used iPSC-derived neural progenitors from a patient with a mutation in PS1 to identify novel candidate genes that may be implicated in sporadic AD[235].

Patient specific *in vitro* models such as these offer novel systems to study the complex pathophysiological mechanisms that underpin neurodegenerative diseases, whilst also offering more a more physiologically relevant platform with which to screen potential drugs. This technology also has implications in terms of personalised medicine, as patient-specific *in vitro* models can be developed for the purpose of drug screening, with better predicative value in order to determine if a specific treatment regime may be suitable on an individual basis.

5.1.5 Conclusions

AD is the commonest form of dementia and is a growing burden associated with an ageing population. It is a complex, multi-faceted degenerative disease that results in a loss of neuronal connectivity associated with synaptic dysfunction and neurite inhibition. Accumulation of Aβ as extra-cellular senile plaques is a hallmark of AD that is associated with neurite dystrophy and growth cone collapse *in vivo*. Similarly, many studies have used *in vitro* cell-based models to dissect the molecular signalling involved in Aβ-mediated neurite inhibition and have determined the involvement of Rho A, ROCK and CRMP-2 along with the actin and microtubule components of the cytoskeleton. Aβ-mediated neurite inhibition in AD is thought to share similarities with neurite inhibition that occurs following SCI with the NgR receptor and its downstream signalling cascade being implicated in both pathologies.

Understanding the molecular mechanisms that underpin Aβ-mediated inhibition may help elucidate potential therapeutic targets, therefore reliable *in vitro* neuronal models are essential to uncover the signalling pathways involved in such complex diseases. This chapter describes the application of a novel, 3D human-derived *in vitro* model of neurite outgrowth and its application to study the process of Aβ-mediated neurite inhibition along with methods of recovery through inhibition of Aβ-mediated signalling. This chapter also highlights the use of iPSC-based patient-derived models of neuritogenesis AD-specific neuritic abnormalities and signalling.

5.1.5.1 Chapter Aims

This chapter aims to investigate the role of Aβ-mediated signalling in the process of neurite inhibition that occurs within AD, through the use of a novel 3D model of human neuritogenesis. Several different methodologies were applied to study this process including the use of synthetic Aβ-peptides to coat growth substrates or supplement culture medium along with AD-patient specific iPSC-derived neuroprogenitor cells. Furthermore, this chapter examines the role of the NgR along with downstream Rho A and ROCK in the inhibition of human model neurites along with the application of inhibitors of each of these molecules to the *in vitro* system with the aim of overcoming Aβ-mediated inhibition. This demonstrates the ability of such *in vitro* models to be used as drug screening tools or to help identify modulators of specific signalling pathways to overcome the inhibitory properties of Aβ, along with the development of a patient-specific model that may have implications in the field of personalised medicine.

We hypothesise that adding Aβ species to our current EC cell-based models (2D/3D) of neurite outgrowth will result in a reduction in neurite outgrowth, based upon evidence

described throughout the literature. We also hypothesise that inhibition of Rho A (ibuprofen) and inhibition of ROCK (Y-27632) will overcome Aβ-mediated inhibition, in a similar manner as CSPG-mediated inhibition discussed in Chapter IV. This hypothesis, again, is based upon evidence previously discussed in the primary literature that suggests Aβ-mediated inhibition is controlled through a RhoA/ROCK dependent mechanism. In this chapter, we will also discuss the ability of AD-model neurons to form neurites in a novel iPSC-based *in vitro* model, and we hypothesise that due to an increased ratio of $A\beta_{42}$:$A\beta_{40}$, their ability to form neurites will be reduced.

5.1.5.2 Chapter Objectives

- Investigate the ability of substrate bound Aβ peptides to inhibit neurite outgrowth in human-derived neurons.
- Investigate the ability of soluble Aβ peptides presented in culture medium to inhibit neurite outgrowth from human stem cell-derived neurons.
- Characterise the effects of "ageing" Aβ peptides upon peptide aggregation.
- Determine the effect of a variety of $A\beta_{40}$:$A\beta_{40}$ ratios upon neurite outgrowth in 2D culture.
- Assess the ability of ROCK inhibition (Y-27632) in overcoming Aβ-mediated neurite inhibition in 2D and 3D culture.
- Analyse the ability of Rho A inhibition by ibuprofen to overcome Aβ-mediated neurite inhibition in 2D and 3D culture.
- Determine the role of NgR in Aβ signalling by the use of NEP 1-40 to potentially overcome Aβ-mediated neurite inhibition in 2D and 3D culture.
- Investigate the ability of soluble Aβ to inhibit neurite outgrowth in WT iPSC-derived neurons in 2D and 3D culture.
- Characterise WT and AD-patient obtained iPSC-derived neuroprogenitor cells in 2D culture.
- Determine the ability of AD-patient derived neuroprogenitor cells to form neurites in 2D and 3D culture systems.

- Investigate the effect of Rho A (Y-27632) and ROCK (ibuprofen) inhibition upon AD-patient derived neurites.

5.2 Materials & Methods

5.2.1 Ageing of β-amyloid Peptides

A well-established technique of ageing β-amyloid peptides ($A\beta_{40}$ and $A\beta_{42}$) was employed to promote aggregation of the peptides, so that in culture they are presented to neurites as aggregated masses similar to the senile plaques of AD. Peptides were incubated at 37 °C for 24 hours to promote aggregation prior to use in a neurite outgrowth assay.

5.2.2 Protein Aggregation Assay

The PROTEOSTAT® Protein Aggregation Assay (Enzo, Exeter, UK) was used to measure aggregation of β-amyloid peptides. Manufacturer's instructions were followed; briefly, $A\beta_{40}$ and $A\beta_{42}$ peptides were diluted in their respective vehicles to a stock concentration of 50 μgmL^{-1}. Proteostat detection solution was then prepared by adding 1.5 µL of detection reagent to 3 µL of 10 x assay buffer and 25.5 µL of DMSO to give a final volume of 30 µL. To each well of a black walled microtitre plate (ThermoFisher), 2 µL of protoestat detection solution was added, along with 98 µL of 50 μgmL^{-1} protein solution. The plate was then incubated at room temperature for 15 mins before being analysed using the Biotek Synergy H4 fluorescent plate reader with excitation of 550 nm and emission of 600 nm.

5.2.3 Coating of Growth Substrates with β-amyloid Peptides for Neurite Outgrowth Studies

Growth substrates were coated with Aβ peptides prior to seeding of neurospheres. 24 hours preceding the end of differentiation of human pluripotent stem cell aggregates, 48-well tissue culture plates were coated with poly-D-lysine and laminin coating solution containing Aβ peptides. $A\beta_{40}$ and $A\beta_{42}$ were reconstituted in their respective vehicles at a concentration of 1 $mgmL^{-1}$ and the desired volume of peptide was added to 10 μgmL^{-1} poly-D-lysine and laminin coating solution to achieve a final concentration of 0.05 – 50 μgmL^{-1}. For example, for a final concentration of 50 μgmL^{-1}, 1 mL of 1 $mgmL^{-1}$ Aβ stock solution would be added to 19 mL of 10 μgmL^{-1} poly-D-lysine and laminin coating solution. Aβ containing coating solution was then added at a volume of 150 µL per well to

a 48-well tissue culture plate and incubated overnight at room temperature before being washed twice in PBS prior to neurosphere seeding for neurite outgrowth.

5.2.4 Addition of Ratios of β-amyloid Peptides to Neurite Outgrowth Cultures

To investigate the effect of varying ratios of $A\beta_{42}$:$A\beta_{40}$ on neurite outgrowth from stem cell derived neurospheres, both peptides were added to the culture medium for the duration of the neurite outgrowth period. The final concentration of both peptides remained constant at 1 µM, so that any effect observed was not that of varying total peptide concentration. The amount of $A\beta_{40}$ and $A\beta_{42}$ making up the final concentration of 1 µM changed relative to each other. Table 5–1 contains the volume of each peptide for the respective ratios of $A\beta_{42}$:$A\beta_{40}$.

Ratio of $A\beta_{42}$:$A\beta_{40}$	$A\beta_{42}$ Concentration [µM]	$A\beta_{40}$ Concentration [µM]
1:10	0.1	0.9
1:5	0.17	0.83
1:1	0.5	0.5
5:1	0.83	0.17
10:1	0.9	0.1

Table 5-1: Concentrations of Aβ Peptides per $A\beta_{42}$:$A\beta_{40}$ Ratio.
Varying ratios of $A\beta_{42}$ and $A\beta_{40}$ were added to neurosphere culture medium for the 10-day neurite outgrowth period, resulting in a total concentration of 1 µM.

5.2.5 Culture of Alzheimer's Phenotype Cells

ReproNeuro AD-mutation cells (ReproCELL) are neural progenitors derived from iPSCs transfected with a mutation in the presenilin 1 (PS1) gene. PS1 is one of the core proteins of the γ-secretase enzyme that is involved in amyloidgenic processing of APP and production of Aβ species. ReproNeuro AD-mutation cells have a mutation (P117L) in the PS1 gene and exhibit an increased ratio of $A\beta_{42}$:$A\beta_{40}$.

ReproNeuro AD-Patient 1 cells (ReproCELL) are neural progenitors differentiated from iPSCs derived from a patient with AD. These cells have a mutation in the presenilin 2 (PS2) gene (R62H), another of the core proteins that make up the γ-secretase enzyme and mutations in both PS1 and PS2 have been identified as pathogenic loci involved in early onset, autosomal dominant AD.

Both ReproNeuro AD-mutation and ReproNeuro AD-patient 1 cells were cultured as 2D monolayers and spheroids for use in 2D and 3D neurite outgrowth assays. They were cultured in the same manner as ReproNeuro cells described in section *2.2.10 Culture of ReproNeuro Cells,* and ReproNeuro cells acted as a wild type control.

5.3 Results

5.3.1 The Role of β-amyloid peptides in Inhibition of Neurite Outgrowth

To explore the ability of Aβ species to induce neurite inhibition in human pluripotent stem cell-derived model neurites, 2D growth substrates were coated with a range of concentrations (0.05 – 50 μgmL^{-1}) of peptides ($A\beta_{40}$, $A\beta_{42}$, aged $A\beta_{40}$ and aged $A\beta_{42}$). Peptides were aged at 37 °C to promote their aggregation, and produce peptide aggregates similar to the hallmark senile plaques of AD[36,40,516]. Immunofluorescence images (Figure 5-6A) depict TUJ-1 positive (green) neurite outgrowth from neurospheres cultured on each of the Aβ coated substrates. Most notably perhaps, neurospheres cultured on 5 μgmL^{-1} $A\beta_{40}$ (Figure 5-6Ac) appear to produce significantly shorter neurites than other conditions tested. Similarly, increasing the peptide concentration of the coating solution to 50 μgmL^{-1} $A\beta_{40}$ (Figure 5-6Ad) resulted in neurite outgrowth appearing less uniform around the neurosphere. High concentrations (5 – 50 μgmL^{-1}) of $A\beta_{42}$ and aged $A\beta_{40}$ coating also result in a reduction in neurite length.

Quantification of the average number of neurites generated per neurosphere (Figure 5-6B) revealed a dose dependent inhibition induced by all peptides tested. Interestingly, $A\beta_{42}$ induced inhibition to the greatest degree, followed by $A\beta_{40}$, with the aged peptides having the least effect upon neurite outgrowth. A similar trend is evident from quantification depicting the neurite density of the neurospheres (Figure 5-6C), as coatings containing all peptides tested resulted in a dose dependent inhibition in neurite growth. Again, $A\beta_{42}$ induced neurite inhibition to the greatest degree, closely followed by $A\beta_{40}$ and the aged peptides had the least effect upon neurite density.

Generally neurite length (Figure 5-6D) was inhibited by all Aβ species with $A\beta_{42}$ coating resulting in a large reduction in neurite length. The length of neurites generated from those neurospheres cultured on $A\beta_{40}$ coated substrates appeared a lot more variable and whilst both aged peptides induced a clear inhibition of neurite length, their effect was not as significant as fresh $A\beta_{42}$ coating.

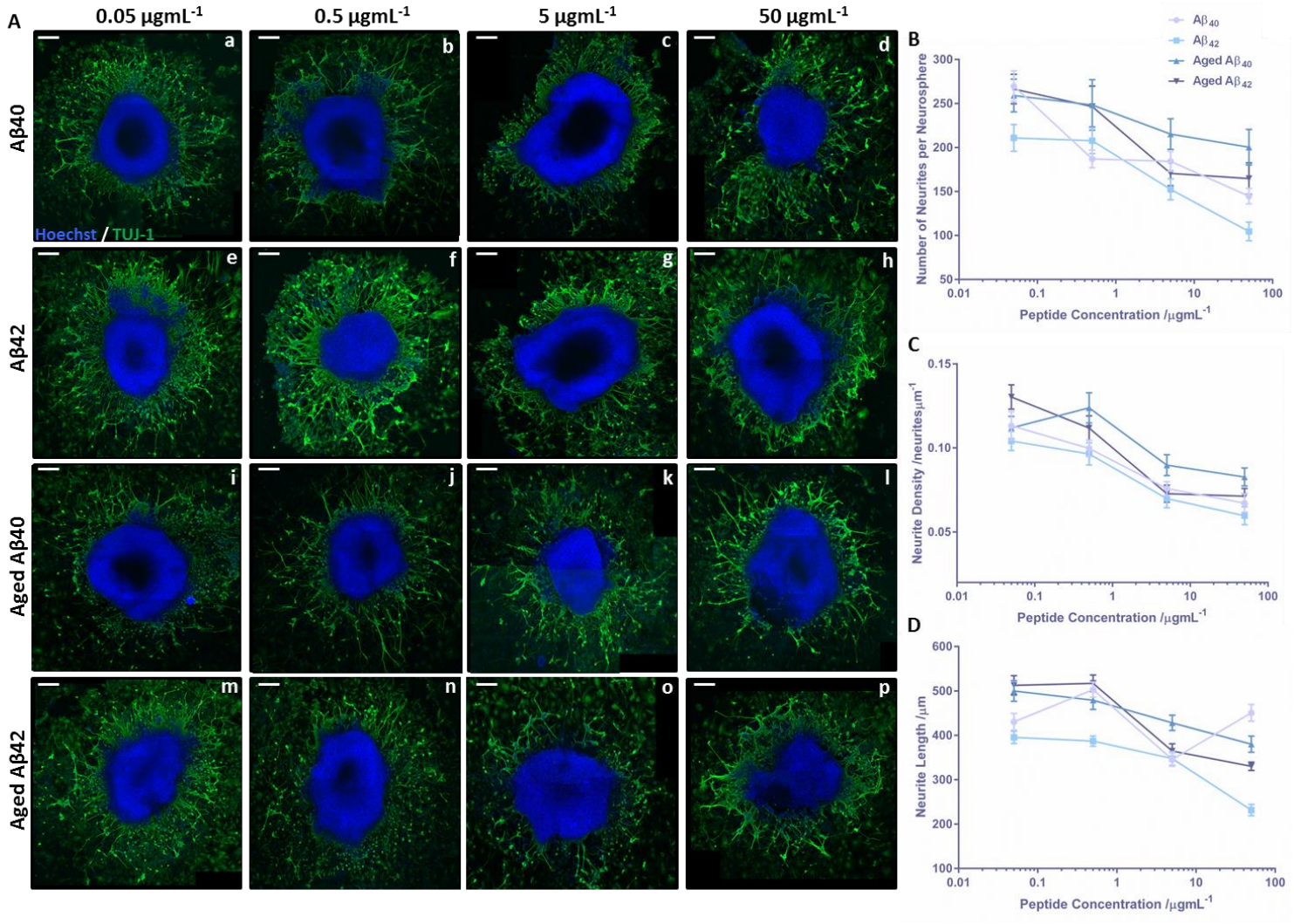

Fig 5-6: Substrate bound β-amyloid peptides are inhibitory to 2D neurite outgrowth.
Representative confocal images of neurospheres cultured on 2D growth substrates coated with Aβ peptides (A). Neurites are highlighted in green, stained for the pan-neuronal marker TUJ-1 and nuclei are stained in blue. Scale bars: 200 µm. The number of neurites per neurosphere (B) (data represent mean ± SEM, n=8; neurite outgrowth from a total of 8 neurospheres was quantified from 3 independent replicates) and neurite density (C) (data represent mean ± SEM, n=8; neurite outgrowth from a total of 8 neurospheres was quantified from 3 independent replicates) both decline with Aβ concentration for all peptides tested, including peptides that were aged at 37 °C to promote aggregation. Neurite length (D) (data represent mean ± SEM, n=60; a total of 20 neurites were quantified from 1-2 neurospheres per independent replicate, of which there were 3) is similarly inhibited with increasing Aβ concentration with $A\beta_{40}$ and aged $A\beta_{42}$ having the greatest inhibitory effect.

The effect upon neurite outgrowth of the soluble addition of Aβ species to the culture medium was also analysed by supplementing culture medium with 1 μM of each peptide ($A\beta_{40}$, $A\beta_{42}$, aged $A\beta_{40}$ and aged $A\beta_{42}$). Immunofluorescence images (Figure 5-7A) highlighting TUJ-1 positive (green) neurite outgrowth show that neurospheres cultured with exogenous Aβ species (Figure 5-7Ab-e) appear to generate less neurites than the vehicle matched control (Figure 5-7Aa). Particularly, $A\beta_{40}$ treated neurospheres (Figure 5-7Ab) appear to produce fewer neurites, whilst $A\beta_{42}$ treated neurospheres (Figure 5-7Ac) appear to produce much shorter neurites than the control. Aged peptides (Figure 5-7Ad,e) appear to have less effect on neurite outgrowth than their fresh counterparts; however, neurite outgrowth surrounding aged $A\beta_{40}$ treated neurospheres (Figure 5-7Ad) appears less uniform.

The number of neurites per neurosphere (Figure 5-7B) is significantly inhibited by the addition of all Aβ species to the culture medium. However, $A\beta_{40}$ was found to have the largest impact on neurite number, significantly reducing neurite number to a greater degree compared with $A\beta_{42}$. Fresh $A\beta_{42}$, along with both aged $A\beta_{40}$ and aged $A\beta_{42}$ were found to have a similar effect upon neurite number. A similar effect was observed when this was normalised to neurosphere size and expressed as neurite density (Figure 5-7C). All Aβ species were found to significantly reduce neurite density, with $A\beta_{40}$ inducing neurite inhibition to the greatest degree. $A\beta_{42}$ was found to not be as inhibitory as $A\beta_{40}$ when presented to cells as soluble mediators in the culture medium and both aged peptides had the least effect upon neurite density.

Interestingly the action of Aβ species upon neurite length (Figure 5-7D) differs from that of both neurite number and density. Although all peptides were found to significantly inhibit neurite length, $A\beta_{42}$ was actually found to induce inhibition to the greatest degree, unlike its effects upon neurite number and density. Aged $A\beta_{40}$ had a similar effect upon neurite length as the fresh $A\beta_{40}$ peptide and aged $A\beta_{42}$ also had a similar effect to the fresh $A\beta_{42}$ peptide and in both cases $A\beta_{42}$ was found to significantly induce neurite inhibition to a greater degree than its $A\beta_{40}$ counterpart.

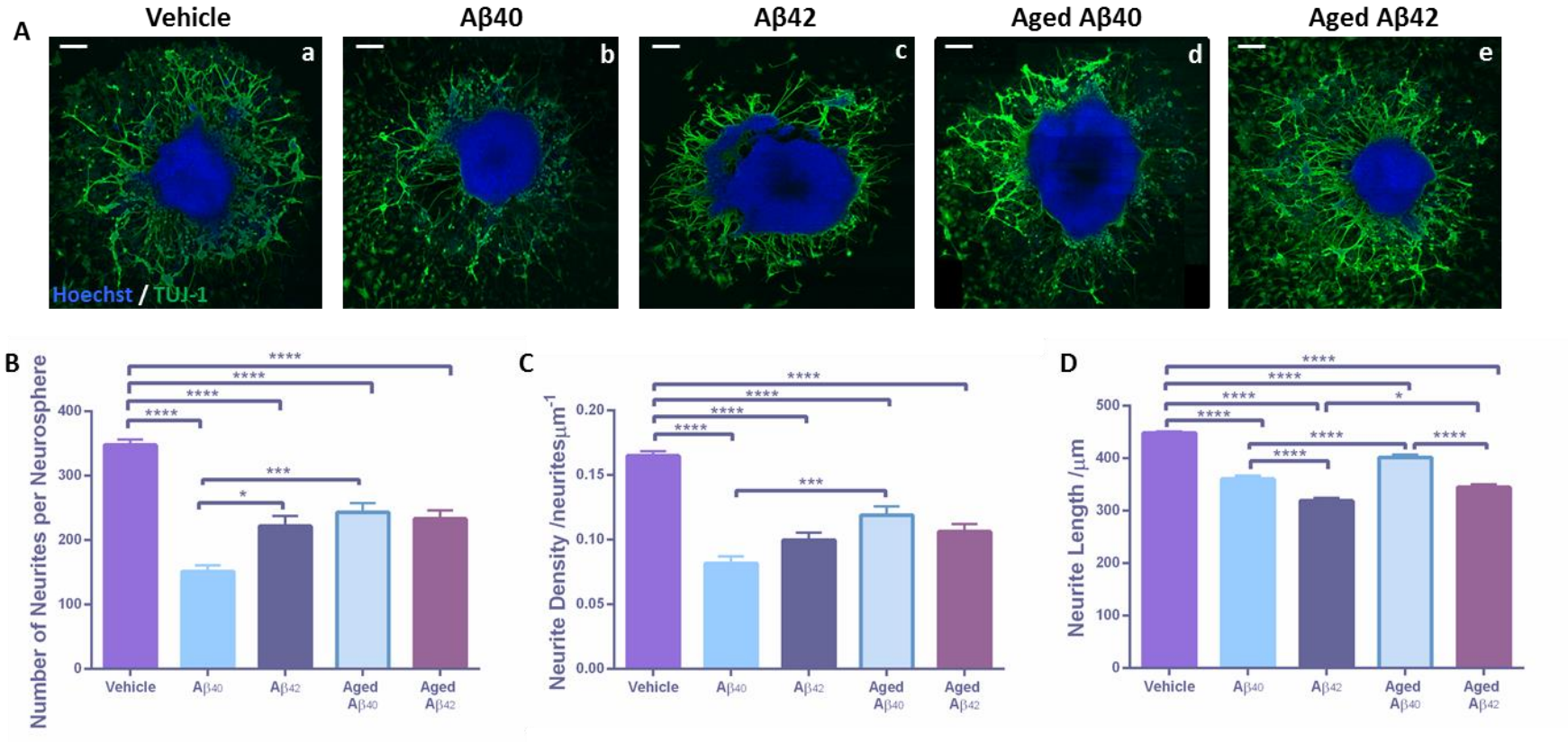

Fig 5-7: Media soluble β-amyloid peptides are inhibitory to neurite outgrowth in 2D culture.
Representative confocal images of neurospheres cultured in 2D in medium supplemented with 1 µM Aβ peptides (A). TUJ-1 (green) positive neurites can be seen extending from the central aggregate, where nuclei (blue) remain. Scale bars: 200 µm. Quantification of the number of neurites per neurosphere (B) (data represent mean ± SEM, n=9; 3 individual neurospheres were quantified from 3 independent replicates) and neurite density (C) (data represent mean ± SEM, n=9; 3 individual neurospheres were quantified from 3 independent replicates) are inhibited in the presence of all Aβ peptides, with $Aβ_{40}$ having the greatest inhibitory effect. Similarly, all Aβ peptides were found to be inhibitory to neurite length (data represent mean ± SEM, n=23-104; between 23-104 neurites were measured from 3 neurospheres per independent replicate, of which there were 3), with the greatest inhibitory effect being observed with $Aβ_{42}$ and aged $Aβ_{42}$. One-way ANOVA with Tukey's multiple comparisons: * = $p \leq 0.05$, ** = $p \leq 0.01$, *** = $p \leq 0.001$, **** = $p \leq 0.0001$.

Ageing Aβ peptides at 37 °C is a well-documented methodology to promote their aggregation[36,40,516]. This is often used to present the peptides to cells as protein aggregates, reminiscent of the peptide plaques that are a hallmark of AD. To characterise the effect of the ageing process upon the peptides, a protein aggregation assay (Figure 5-8) was conducted to measure the level of peptide aggregation in both fresh and aged peptides. The basis of this assay was to fluorescently label protein aggregates, therefore net fluorescence intensity correlates with protein aggregation[517–519]. Little aggregation was observed in both fresh and aged $A\beta_{40}$ samples, whilst aggregation noted in $A\beta_{42}$ samples exceeds that of the positive control and assay limits. Although both aged $A\beta_{42}$ and fresh $A\beta_{42}$ peptides exhibited large amounts of peptide aggregation, ageing of the peptide at 37 °C did enhance this process, albeit not statistically significantly.

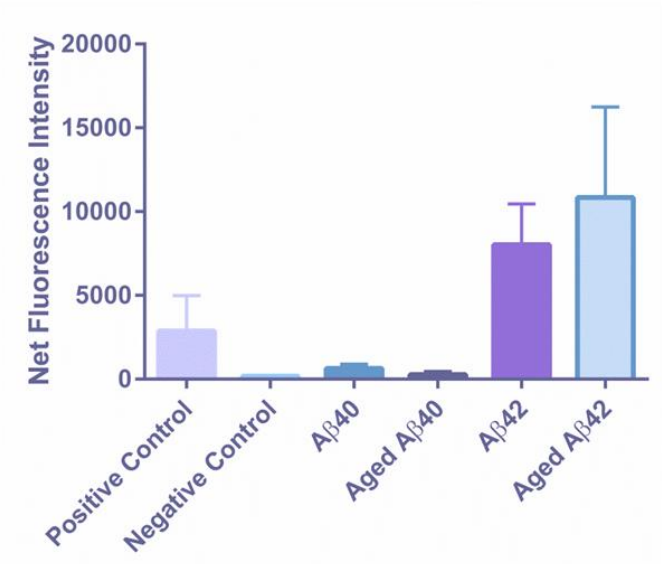

Fig 5-8: Characterisation of the ability of 37 °C incubation to promote Aβ aggregation.
The PROTEOSTAT® protein aggregation assay was used to characterise the effects of a well-established "ageing" procedure used to promote peptide aggregation. Aβ peptides were incubated at 37 °C to promote aggregation for 24 hours and then analysed using the PROTEOSTAT® assay, which detects peptide aggregation as fluorescent signal. Net fluorescence intensity is a measure of peptide aggregation, and very little aggregation was observed in $A\beta_{40}$ samples. A large amount of aggregation was observed in the longer, more insoluble, $A\beta_{42}$ peptide and which was enhanced by the "ageing" procedure (data represent mean ± SEM, n=3, repeated 3 times with different samples of peptide).

To better recreate physiological conditions, several $A\beta_{42}$:$A\beta_{40}$ ratios were tested (Figure 5-9), as a defining characteristic of AD is an increase in the ratio of $A\beta_{42}$ to $A\beta_{40}$[438,444]. A range of ratios were tested including those high in $A\beta_{40}$ (1:10) and those high in $A\beta_{42}$ (10:1) with 1:10 simulating the Aβ mix of healthy brain[426] and Aβ peptides were added to the culture medium of 2D models at a concentration of 1 μM.

Neurite outgrowth visible from neurospheres via immunofluorescence analysis (Figure 5-9A) appears to be reduced in those cultures treated with ratios higher in $A\beta_{42}$ than $A\beta_{40}$ (Figure 5-9Ak-n) with $A\beta_{42}$ supplementation alone (Figure 5-9Ao,p) resulting in sparse neurite outgrowth and neurites that appear extremely short. All peptides tested appear to reduce neurite outgrowth compared with the control (Figure 5-9Aa,b), however those treated with higher ratios of $A\beta_{42}$ appear to generate the least neurites.

Supplementation of the culture medium with all peptide mixes tested resulted in a significant reduction in the number of neurites generated per neurosphere (Figure 5-9B), with variable results between the ratios tested. There was not a clear relationship between neurite number and $A\beta_{42}$ content of the peptide mixes tested, although, all Aβ conditions were inhibitory. A similar result was obtained in terms of neurite density (Figure 5-9C), as all peptide mixes induced a significant reduction in the density of neurite outgrowth. However, no clear relationship between the $A\beta_{42}$ content of the culture medium and inhibition of neurite density was identified.

Medium supplementation with all peptide mixes resulted in a significant reduction in neurite length (Figure 5-9C), with the exception of $A\beta_{40}$ supplementation alone, which resulted in a slight, insignificant increase in neurite length compared with the control. All ratios of peptides tested resulted in a significant reduction in neurite length, however ratios higher in $A\beta_{42}$ inhibited neurite length to the greatest degree and were even found to be more inhibitory than $A\beta_{42}$ treatment alone.

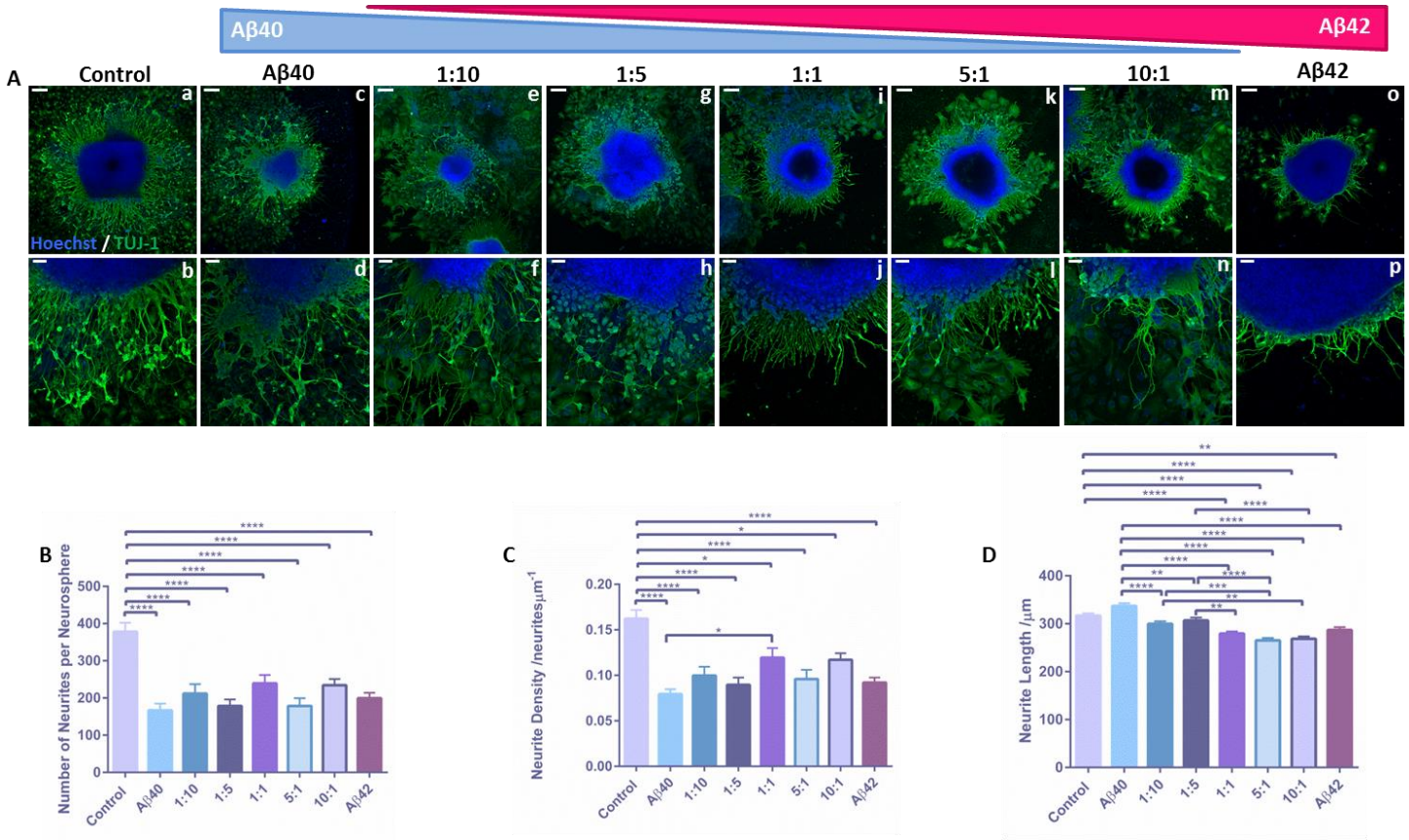

Fig 5-9: Ratio of $A\beta_{40}$ to $A\beta_{42}$ in culture medium impacts neurite outgrowth in 2D culture.
Representative confocal images of neurospheres cultured in 2D (A) in media supplemented with $A\beta_{40}$ and $A\beta_{42}$ at varying ratios making up a total concentration of 1 µM. Neurites are highlighted by positive TUJ-1 (green) staining and Hoechst stains nuclei blue. Scale bars: (Aa,c,e,g,i,k,m,o): 200 µm (Ab,d,f,h,j,l,n,p): 50 µm. The number of neurites per neurosphere (B) (data represent mean ± SEM, n=18-32; 6-11 individual neurospheres were quantified from 3 independent replicates) and the average neurite density of the neurospheres (C) (data represent mean ± SEM, n=18-32; 6-11 individual neurospheres were quantified from 3 independent replicates) both are significantly inhibited with the addition of all Aβ conditions. The average length of neurites (D) (data represent mean ± SEM, n=369-615; between 369-615 neurites were measured from 6-11 neurospheres per independent replicate, of which there were 3) is significantly decreased with the addition of increased $A\beta_{42}$:$A\beta_{40}$ (5:1, 10:1), a phenotype of Alzheimer's disease. One-way ANOVA with Tukey's multiple comparisons: * = $p \leq 0.05$, ** = $p \leq 0.01$, *** = $p \leq 0.001$, **** = $p \leq 0.0001$.

5.3.2 Modulation of the Rho A/ROCK Pathway to overcome β-amyloid Mediated Neurite Inhibition

Activation of the Rho A/ROCK signalling cascade is thought to be responsible for the effects mediated by Aβ upon neurite growth[510]. For this reason the ROCK inhibitor Y-27632 and ibuprofen an inhibitor of Rho A, were both added to the culture medium of 2D and 3D neurite outgrowth assays with the aim of providing recovery from the Aβ-mediated effects upon neurite growth.

5.3.2.1 Inhibition of ROCK by Y-27632

The culture medium of 2D neurite outgrowth models was supplemented with $A\beta_{40}$ to induce neurite inhibition or $A\beta_{40}$ in combination with 10 μM Y-27632 to potentially restore neurite growth in the presence of inhibitory Aβ species. Extensive neurite growth can be seen to radiate from vehicle treated neurospheres (Figure 5-10Aa,b), whereas fewer TUJ-1 positive projections visibly extend from neurospheres treated with 1 μM $A\beta_{40}$ (Figure 5-10Ac,d). Neurospheres cultured in medium supplemented with both 1 μM $A\beta_{40}$ and 10 μM Y-27632 (Figure 5-10Ae,f) appear to generate a large number of densely packed neurites that perhaps seem a little short compared with the control neurites.

Treatment with $A\beta_{40}$ alone resulted in a significant inhibition in the average number of neurites (Figure 5-10B) generated by each neurosphere. The addition of Y-27632 to the culture medium, however did not just result in a recovery of neurite number, but significantly enhanced the number of neurites generated by each neurosphere even compared with control cultures. This was supported by quantification of neurite density (Figure 5-10C) that also revealed a significant inhibition in neurite growth when neurospheres were treated with $A\beta_{40}$ and significant enhancement of neurite density with Y-27632 supplementation.

No significant inhibition in neurite length (Figure 5-10D) was detectable with $A\beta_{40}$ treatment alone, however combination treatment with $A\beta_{40}$ and Y-27632 resulted in a significant reduction in neurite length compared with both control and $A\beta_{40}$ treated neurites. This effect is similar to Y-27632 treatment in the absence of an inhibitory stimulus as described in Chapter III.

In 3D culture, neurospheres remained on top of the scaffold (Figure 5-11Aa,c,e) whereas TUJ-1 positive (green) neurites can be visualised from the bottom view of the scaffold (Figure 5-11Ab,d,f) having penetrated the entire 200 μm depth of the 3D material. Extensive neurite outgrowth can be seen from the underside of control scaffolds (Figure

5-11Ab), whereas, significantly fewer neurites can be seen to have penetrated the scaffold with $A\beta_{40}$ treatment (Figure 5-11Ad). Combination treatment with Y-27632 and $A\beta_{40}$ resulted in a large number of neurites visible from the bottom of the scaffold (Figure 5-11Af), which actually appears greater that the neurite outgrowth visible from control cultures.

Quantification of neurite penetration (Figure 5-11B) confirms this, as neurite penetration is significantly reduced with $A\beta_{40}$ treatment alone, in comparison to control cultures. Treatment with both $A\beta_{40}$ and Y-27632 resulted in a significant increase in neurite penetration compared with both control cultures and $A\beta_{40}$ supplementation alone. This supports the 2D culture findings that Y-27632 treatment not only recovers $A\beta_{40}$-mediated inhibition of neurite growth, but also enhances neurite outgrowth to levels that are greater than the control.

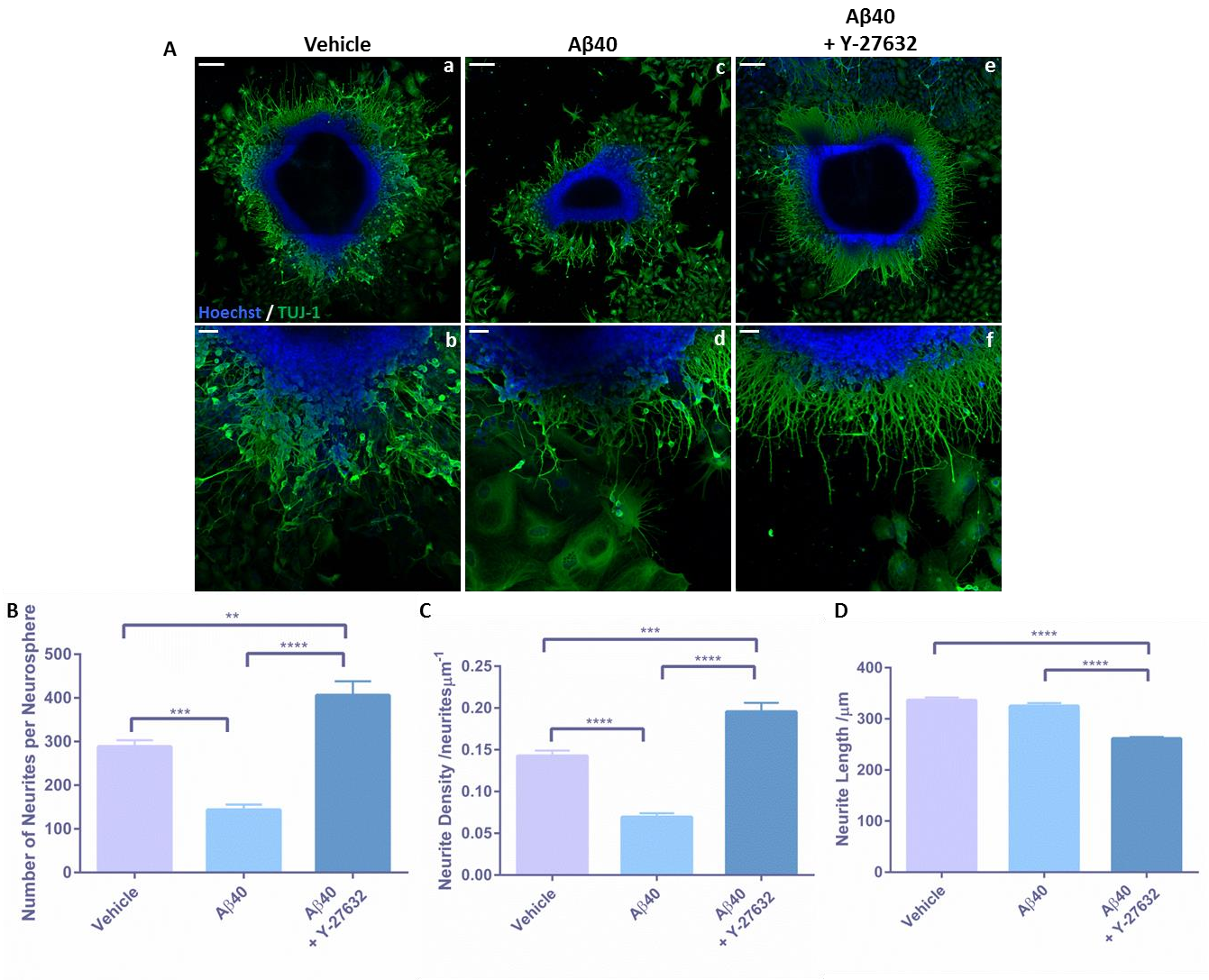

Fig 5-10: Inhibition of ROCK by the small molecule inhibitor, Y-27632, can recover Aβ mediated inhibition of neurite outgrowth in 2D culture.

Representative confocal images of neurospheres cultured in 2D (A) without medium supplementation (Aa,b), with the addition of 1 µM $A\beta_{40}$ (Ac,d) and with the addition of 1 µM $A\beta_{40}$ and 15 µM Y-27632 (Ae,f). TUJ-1 (green) positive neurites extend from the central neurosphere where nuclei (blue) remain. Scale bars: Aa,c,e: 200 µm Ab,d: 50 µm. Quantification of the number of neurites per neurosphere (B) (data represent mean ± SEM, n=9-18; 3-6 individual neurospheres were quantified from 3 independent replicates.) show neurite inhibition in the presence of $A\beta_{40}$ alone and with the addition of Y-27632 the number of neurites is enhanced, even surpassing that of the control. A similar response is observed with neurite density (C) (data represent mean ± SEM, n=9-18; 3-6 individual neurospheres were quantified from 3 independent replicates) with Y-27632 not only recovering neurite density, but enhancing it to levels greater than the control. Neurite length however (D) (data represent mean ± SEM, n=200-605; between 200-605 neurites were measured from 3-6 neurospheres per independent replicate, of which there were 3) is not found to be significantly inhibited with the addition of $A\beta_{40}$, however, when Y-27632 is added to the culture, neurite length is significantly reduced. One-way ANOVA with Tukey's multiple comparisons: * = $p \leq 0.05$, ** = $p \leq 0.01$, *** = $p \leq 0.001$, **** = $p \leq 0.0001$.

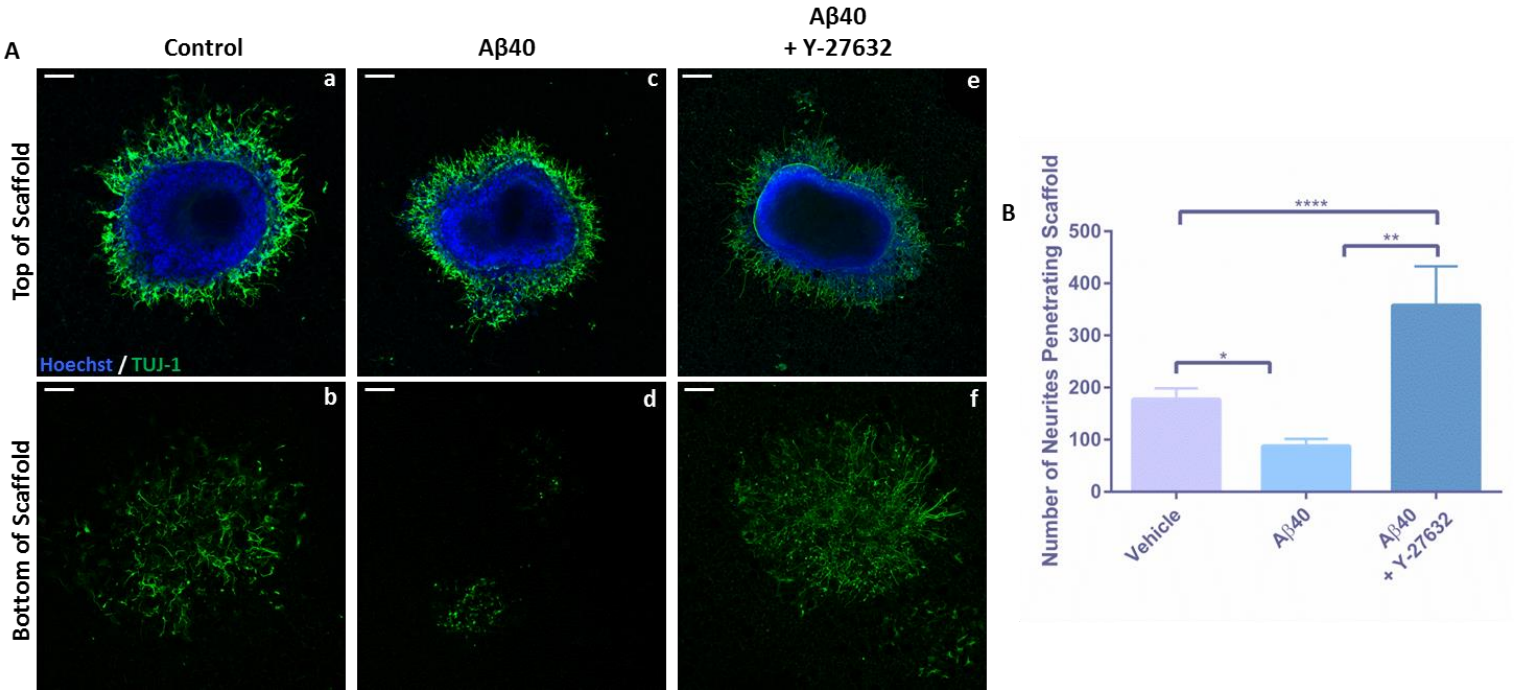

Fig 5-11: Inhibition of ROCK by the small molecule inhibitor, Y-27632, can recover Aβ mediated neurite inhibition in 3D culture.
Representative confocal images of neurospheres on top of Alvetex® scaffold (Aa,c,e) and TUJ-1 (green) positive neurites penetrating the depth of the 3D material, as visible from below (Ab,d,f) with nuclei being highlighted in blue. Neurospheres were cultured without medium supplementation (Aa,b), with the addition of 1 μM $A\beta_{40}$ to the culture medium (Ac,d) or with the addition of 1 μM $A\beta_{40}$ and 15 μM Y-27632 (Ae,f) to the culture medium. Scale bars: 200 μm. The number of neurites penetrating the 3D material (B) (data represent mean ± SEM, n=5-16; between 2-5 neurospheres were quantified per independent replicate, of which there were 3) is significantly inhibited by the addition of $A\beta_{40}$ to the culture medium and this effect is not only recovered by Y-27632, but neurite outgrowth is enhanced to levels greater than the control. One-way ANOVA with Tukey's multiple comparisons: * = $p \leq 0.05$, ** = $p \leq 0.01$, *** = $p \leq 0.001$, **** = $p \leq 0.0001$.

5.3.2.2 Inhibition of Rho A by Ibuprofen

To investigate the role of Rho A in Aβ-mediated inhibition of neurite outgrowth, neurosphere cultures were supplemented with $A\beta_{40}$ in combination with a range of concentrations of ibuprofen (10 – 500 μM). Neurite outgrowth can be seen to radiate from neurospheres cultured in 2D (Figure 5-12A) with significant neurite outgrowth visible from neurospheres cultured without $A\beta_{40}$ medium supplementation (Figure 5-12Aa,b). The addition of 1 μM $A\beta_{40}$ to the culture medium resulted in neurite outgrowth appearing less dense around the neurosphere (Figure 5-12Ac,d). Ibuprofen supplementation in addition to $A\beta_{40}$ treatment resulted in densely packed neurites more reminiscent of the control, with high concentrations of ibuprofen such as 100 μM (Figure 5-12Ag,h) and 500 μM (Figure 5-12Ai,j) resulting in extremely dense neurite outgrowth.

The average number of neurites (Figure 5-12B) generated per neurosphere was significantly inhibited by the addition of $A\beta_{40}$ to the culture medium. This inhibitory effect was rescued in a dose dependent manner with increasing ibuprofen concentration. High concentrations of ibuprofen including 100 μM and 500 μM also resulted in a significant increase in the number of neurites generated per neurosphere compared with the control. Similarly to neurite number, neurite density (Figure 5-12C) is also inhibited by $A\beta_{40}$ supplementation and rescued in a dose dependent manner with increasing ibuprofen concentration. Treatment with 100 μM ibuprofen in addition to $A\beta_{40}$ resulted in a similar neurite density as the control, however treatment with 500 μM ibuprofen resulted in a significant increase in neurite density, enhancing neurite outgrowth compared with control cultures.

Addition of $A\beta_{40}$ to the culture medium of 2D neurite outgrowth cultures resulted in a significant inhibition in neurite length (Figure 5-12D). This reduction in length was rescued by 10 μM ibuprofen treatment, restoring neurite length to a similar level as the control. Treatment with 100 μM ibuprofen also rescued $A\beta_{40}$-induced inhibition of neurite length and resulted in a slight increase in neurite length compared with 10 μM ibuprofen treatment. However, 500 μM ibuprofen treatment resulted in a significant reduction in neurite length compared with 100 μM. This ibuprofen-induced reduction in neurite length has also been noted in the absence of an inhibitory stimulus, as described in Chapter III.

In 3D culture, neurospheres remain on top of the scaffold (Figure 5-13Aa,c,e,g,i) whereas TUJ-1 positive (green) neurites can be seen from the bottom view of the scaffold (Figure 5-13Ab,d,f,h,j) having penetrated the entire depth of the 3D material. Significant neurite outgrowth can be observed on the underside of control scaffolds cultured without medium supplementation (Figure 5-13Ab), whereas fewer neurites have visibly penetrated the scaffold in cultures treated with $A\beta_{40}$ (Figure 5-13Ad). Few neurites are

visible on the underside of scaffolds treated with $A\beta_{40}$ and 10 μM ibuprofen (Figure 5-13Af), however 100 – 500 μM ibuprofen treated cultures (Figure 5-13Ah,j) appear to have generated a similar number of neurites as control cultures.

Significantly fewer neurites penetrated the scaffold (Figure 5-13B) with $A\beta_{40}$ medium supplementation compared with control cultures. Treatment of cultures with 10 – 100 μM ibuprofen resulted in a slight increase in neurite penetration, however, treatment with 500 μM ibuprofen resulted in a significant increase in neurite outgrowth, restoring neurite growth to a level similar to that of the control.

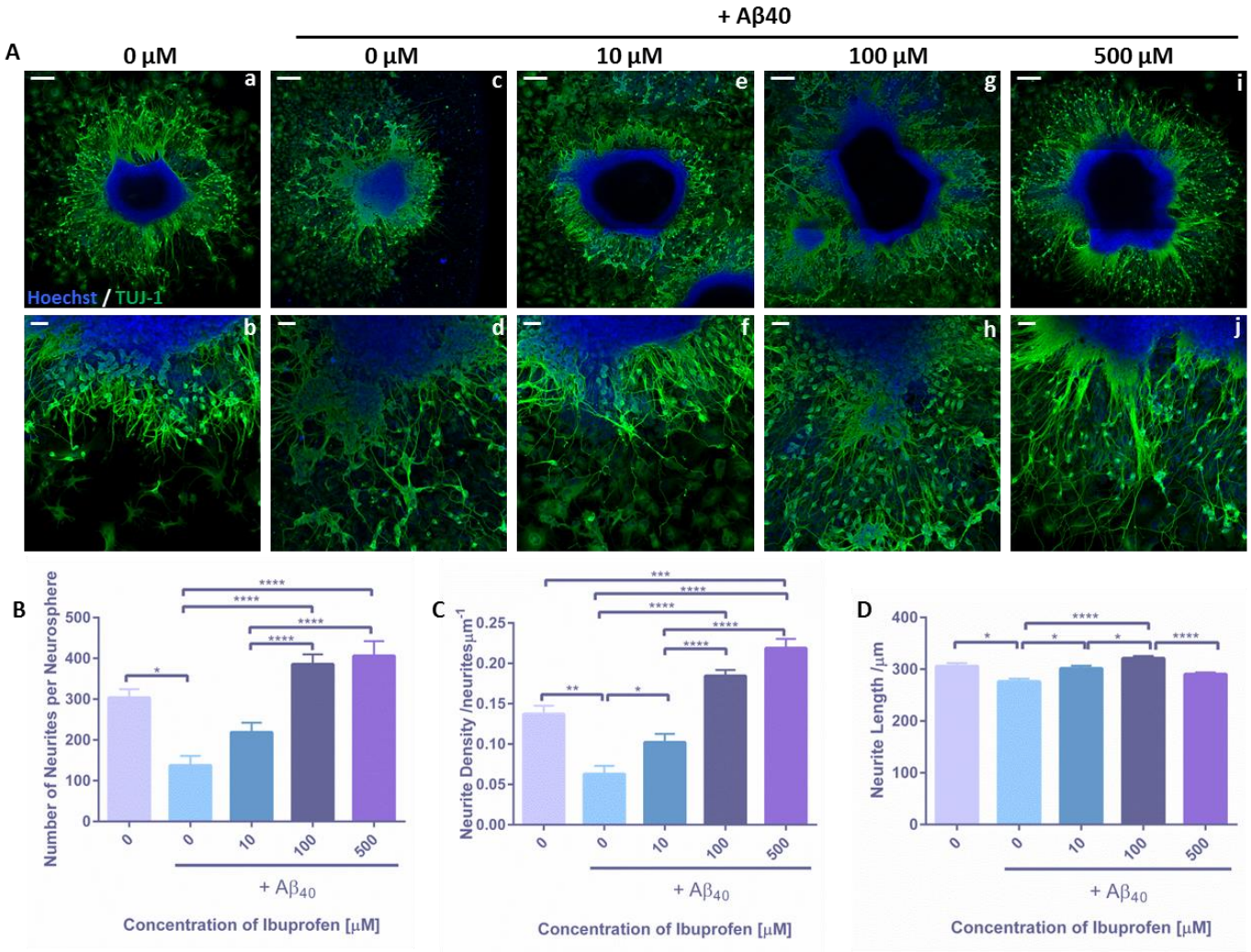

Fig 5-12: Recovery of Aβ mediated neurite inhibition in 2D culture by ibuprofen, an inhibitor of Rho A.
Representative confocal images of neurospheres (A) cultured without $A\beta_{40}$ (Aa,b) with the addition of 1 µM $A\beta_{40}$ to the culture medium and the addition of varying concentrations (0 – 500 µM) of ibuprofen (Ac-j). Neurites are TUJ-1 positive and highlighted in green with nuclei stained blue and restricted to the cell aggregate body. Scale bars: (Aa,c,e,g,i): 200 µm (Ab,d,f,h,j): 50 µm. Both the number of neurites per neurosphere (B) (data represent mean ± SEM, n=9-27; 3-9 individual neurospheres were quantified from 3 independent replicates) and neurite density (C) (data represent mean ± SEM, n=9-27; 3-9 individual neurospheres were quantified from 3 independent replicates) are significantly inhibited in the presence of $A\beta_{40}$, this inhibitory effect is rescued in a dose dependent manner with increasing ibuprofen concentration. Similarly, neurite length (D) (data represent mean ± SEM, n=232-938; between 232-938 neurites were measured from 3-9 neurospheres per independent replicate, of which there were 3) is inhibited with the addition of $A\beta_{40}$ and subsequently rescued by supplementation with ibuprofen in a dose dependent manner until 500 µM ibuprofen is reached and the effect is lost. One-way ANOVA with Tukey's multiple comparisons: * = $p \leq 0.05$, ** = $p \leq 0.01$, *** = $p \leq 0.001$, **** = $p \leq 0.0001$.

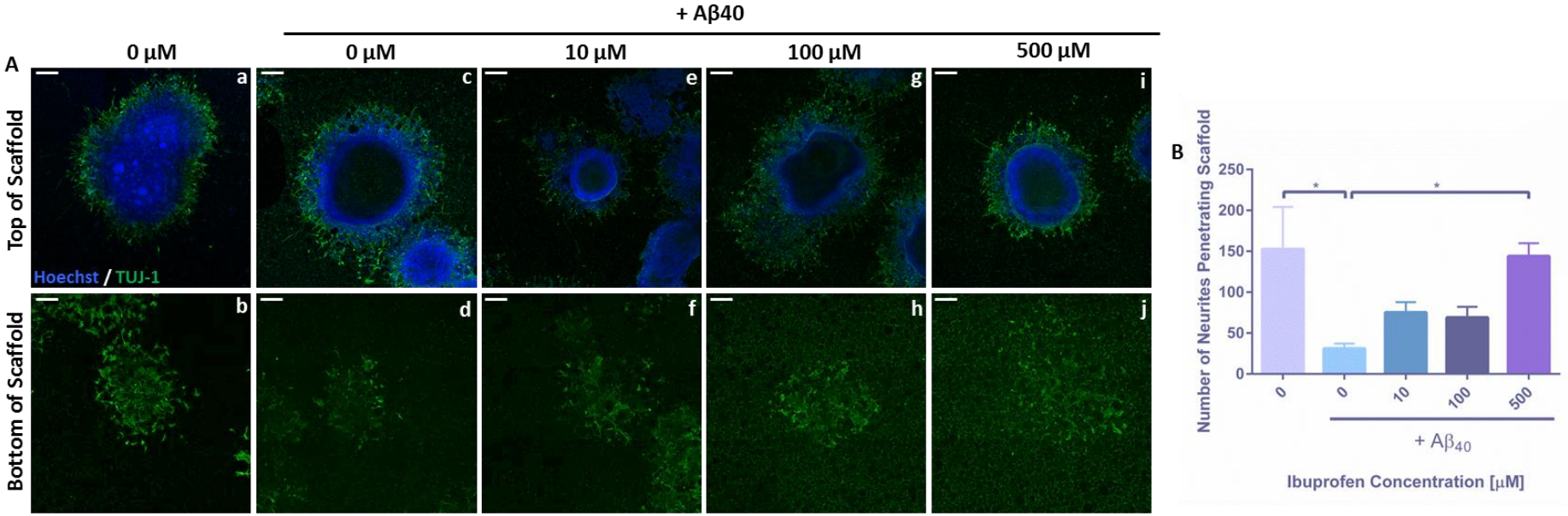

Fig 5-13: Recovery of Aβ mediated neurite inhibition in 3D culture by ibuprofen, an inhibitor of Rho A.
Representative confocal images (A) of neurospheres cultured on top of Alvetex® scaffold (Aa,c,e,g,i) with TUJ-1 (green) positive neurites penetrating the depth of the 3D material and are visible from below the scaffold (Ab,d,f,h,j). Nuclei are highlighted in blue. Neurospheres were cultured without media supplementation (Aa,b) or with the addition of 1 µM $A\beta_{40}$ in combination with varying concentrations (0 – 500 µM) of ibuprofen (Ac-j). Scale bars: 200 µm. Quantification of the number of neurites penetrating each scaffold (B) (data represent mean ± SEM, n=8-9; between 2-3 neurospheres were quantified per independent replicate, of which there were 3) demonstrates significant inhibition with the addition of $A\beta_{40}$ to the culture medium, an effect that is rescued in a dose dependent manner with addition of the drug ibuprofen. One-way ANOVA with Tukey's multiple comparisons: * = $p \leq 0.05$, ** = $p \leq 0.01$, *** = $p \leq 0.001$, **** = $p \leq 0.0001$.

5.3.3 Investigation into the Role of the Nogo Receptor in β-amyloid Mediated Inhibition of Neurite Outgrowth

A number of studies have identified the ability of Aβ to structurally interact with the Nogo receptor (NgR), however it is not yet known if Aβ actually activates the receptor[504–506]. Activation of NgR in the glial scar results in the activation of Rho A and ROCK, ultimately leading to actin filament stabalisation and neurite retraction[324,368,400]. The evidence previously described in this chapter suggests that both activation of Rho A and ROCK are involved in Aβ-mediated neurite inhibition, therefore, it can be hypothesised that activation of the signalling pathway may be induced by NgR-Aβ binding and subsequent activation of the receptor. To test this hypothesis an NgR antagonist (NEP 1-40) was added to both 2D and 3D neurite outgrowth culture systems to determine the ability of NgR antagonism to recover the neurite inhibitory effects of Aβ.

Neurospheres cultured in 2D conditions without Aβ supplementation (Figure 5-14Aa,b) generate a significant quantity of TUJ-1 positive (green) neurites that radiate from the central neurosphere. The number of neurites generated by neurospheres cultured with 1 μM $A\beta_{40}$ medium supplementation (Figure 5-14Ac,d), appears to be reduced in comparison to untreated neurospheres. Aβ treated neurospheres appear to generate fewer, shorter neurites than their untreated counterparts. Supplementation of the culture medium with 1 μM NEP 1-40 in addition to 1 μM $A\beta_{40}$ (Figure 5-14Ae,f) resulted in significant neurite outgrowth, with a large number of TUJ-1 positive (green) neurites extending from the central neurosphere in a similar manner to untreated neurospheres.

The average number of neurites per neurosphere (Figure 5-14B) is significantly inhibited by the addition of $A\beta_{40}$ to the culture medium. Supplementation of medium with $A\beta_{40}$ and NEP 1-40, resulted in a significant enhancement in neurite number compared with $A\beta_{40}$ treatment alone. However the number of neurites generated from $A\beta_{40}$ and NEP 1-40 treated neurospheres was still significantly reduced in comparison to control neurospheres. This is partial recovery of neurite outgrowth by NEP 1-40 treatment is further supported by quantification of neurite density (Figure 5-14C). Neurite density is significantly inhibited by $A\beta_{40}$ treatment, and significantly enhanced by NEP 1-40 treatment in comparison to $A\beta_{40}$ alone. However, again $A\beta_{40}$ and NEP 1-40 treatment still results in a significantly reduced neurite density compared with control neurospheres.

Similarly to the other aspects of neurite outgrowth measured, neurite length (Figure 5-14D) is also significantly inhibited by the presence of $A\beta_{40}$. However, interestingly NEP 1-40 supplementation actually enhanced the inhibitory effects of $A\beta_{40}$, resulting in further

inhibition of neurite length that was statistically significant compared with both control and $A\beta_{40}$-alone treated neurospheres.

In 3D culture, neurospheres are situated on top of the scaffold (Figure 5-15Aa,c,e), whereas neurites are visible from the bottom view (Figure 5-15Ab,d,f) of the scaffold, having completely penetrated and exited the 3D material. Extensive neurite outgrowth can be observed from the underside of scaffolds cultured without medium supplementation (Figure 5-15Ab), whereas few TUJ-1 positive (green) projections are visible from $A\beta_{40}$ treated cultures (Figure 5-15Ad). Treatment with both $A\beta_{40}$ and NEP 1-40 (Figure 5-15Af) resulted in a significant number of neurites visible from the underside of the scaffold, similar in number to control cultures. Significantly fewer neurites penetrated the scaffold (Figure 5-15B) and were found to exit the scaffold in $A\beta_{40}$ treated cultures. Although, NEP 1-40 treatment resulted in a slight increase in neurite penetration, this value did not differ significantly from either control of $A\beta_{40}$ treated cultures.

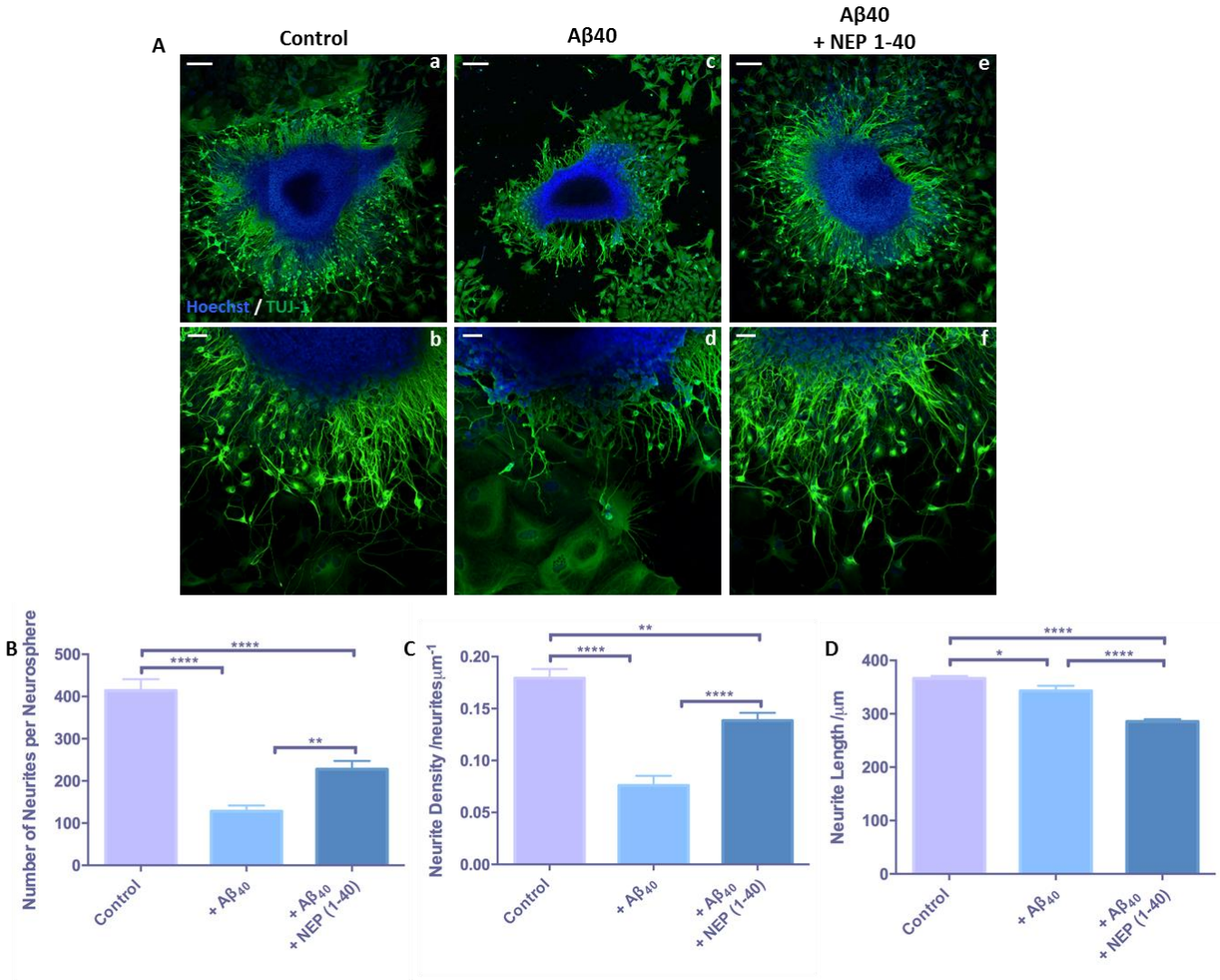

Fig 5-14: Partial recovery of Aβ mediated neurite inhibition in 2D culture by NEP 1-40, a Nogo receptor antagonist.

Representative confocal images (A) of neurospheres cultured in 2D without $A\beta_{40}$ (Aa,b) with the addition of 1 µM $A\beta_{40}$ alone (Ac,d) or in combination with 1 µM NEP (Ae,f) to the culture medium. Neurite outgrowth is highlighted in green by staining for the pan-neuronal marker TUJ-1 and nuclei are stained blue. Scale bars: 200 µm. Quantification of number of neurites per neurospheres (B) (data represent mean ± SEM, n=15-18; 5-9 individual neurospheres were quantified from 3 independent replicates) and neurite density (C) (data represent mean ± SEM, n=15-18; 5-9 individual neurospheres were quantified from 3 independent replicates) demonstrate the ability of $A\beta_{40}$ to inhibit neurite outgrowth. The Nogo receptor antagonist peptide, NEP 1-40, is able to partially overcome $A\beta_{40}$ mediated inhibition, however, NEP does not recover neurite outgrowth to control levels. Neurite length (D) (data represent mean ± SEM, n=213-653; between 213-653 neurites were measured from 5-9 neurospheres per independent replicate, of which there were 3), however, is inhibited by the presence of $A\beta_{40}$ and NEP. One-way ANOVA with Tukey's multiple comparisons: * = $p \leq 0.05$, ** = $p \leq 0.01$, *** = $p \leq 0.001$, **** = $p \leq 0.0001$.

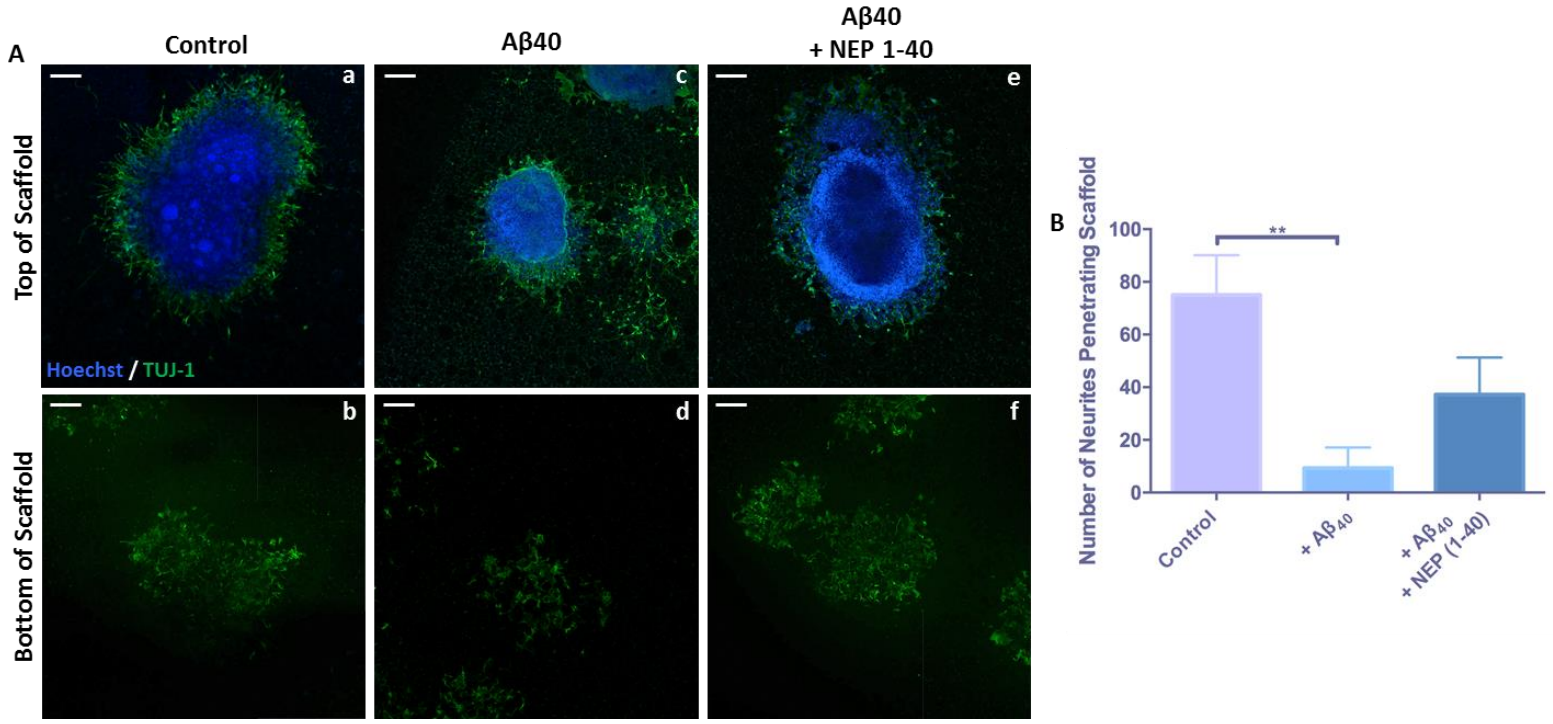

Fig 5-15: Partial recovery of Aβ mediated neurite inhibition by NEP 1-40, a Nogo receptor antagonist, in 3D culture.
Representative confocal images (A) of neurospheres cultured on top of Alvetex® scaffold (Aa,c,e) with TUJ-1 (green) positive neurites penetrating the depth of the scaffold and are visible from below the scaffold (Ab,d,f). Nuclei are highlighted in blue. Neurospheres were cultured without supplementation (Aa,b) or with the addition of 1 µM $A\beta_{40}$ alone (Ac,d) or in combination with 1 µM NEP (Ae,f) to the culture medium. Scale bars: (Aa,c,e): 200 µm (Ab,d,f): 50 µm. Quantification of the number of neurites penetrating the 3D material (B) (data represent mean ± SEM, n=4-6; between 1-2 neurospheres were quantified per independent replicate, of which there were 3) reveals that $A\beta_{40}$ significantly inhibits the number of neurites penetrating the material and NEP partially restores this, however not to the same levels as the control. One-way ANOVA with Tukey's multiple comparisons: * = $p \leq 0.05$, ** = $p \leq 0.01$, *** = $p \leq 0.001$, **** = $p \leq 0.0001$.

5.3.4 Investigation the Inhibitory Effects of Exogenous β-amyloid in an iPSC-based Model of Neurite Outgrowth

To further investigate the role of Aβ in neurite inhibition, the iPSC ReproNeuro model system was also applied to examine the ability of exogenous addition of Aβ to inhibit neurite outgrowth. Conducting the same experiments in another model system helps to confirm the previous findings and provide robust and reproducible data.

ReproNeuro-derived neurospheres were cultured in 2D without treatment (Figure 5-16Aa,b) with 1 μM $A\beta_{40}$ alone (Figure 5-15Ac,d), or in combination with 10 μM Y-27632 (Figure 5-15Ae,f) or 100 μM ibuprofen (Figure 5-15Ag,h). Neurite outgrowth from $A\beta_{40}$-treated neurospheres appears less dense and less consistent compared with untreated neurite outgrowth. Treatment with Y-27632 in addition to $A\beta_{40}$ results in significant neurite generation with neurite growth appearing more dense that in control cultures. Similarly, neurospheres treated with $A\beta_{40}$ in combination with ibuprofen also appear to generate a large number of neurites comparable to control cultures.

Although the number of neurites generated per neurosphere (Figure 5-16B) was reduced by $A\beta_{40}$ treatment, this inhibition was not statistically significant. Both Y-27632 and ibuprofen treatment resulted in a significant enhancement in neurite number compared with $A\beta_{40}$ treatment alone, and even resulted in the production of a greater number of neurites compared with control cultures. However, when this was normalised to neurosphere size and expressed as neurite density (Figure 5-16C), the inhibitory action of $A\beta_{40}$ became statistically significant. Both Y-27632 and ibuprofen treatment significantly enhanced neurite density compared with $A\beta_{40}$ treatment alone, restoring neurite density to a similar, slightly enhanced level compared with the control.

Neurite length (Figure 5-16D) was significantly inhibited by $A\beta_{40}$ treatment in comparison to the vehicle treated control. This inhibition of neurite length was successfully recovered by Y-27632 treatment, which resulted in a significant enhancement in neurite length compared with $A\beta_{40}$ treatment alone. However, ibuprofen treatment resulted in a further significant inhibition in neurite length compared with all conditions tested.

ReproNeuro-derived neurospheres cultured in 3D remained on top of the scaffold (Figure 5-17Aa,c,e,g), with penetration of neurites visible from the bottom view of the scaffold (Figure 5-17Ab,d,f,h). Vehicle treated control neurospheres (Figure 5-17Aa,b) resulted in complete penetration of the 3D material with a large number of neurites can visible from the bottom of the scaffold. Treatment with $A\beta_{40}$ (Figure 5-17Ac,d) however, resulted in few visible neurites radiating from the neurosphere on top of the scaffold, and no neurites

had visibly penetrated the depth of the scaffold itself. Treatment with Y-27632 in addition to $A\beta_{40}$ (Figure 5-17Ae,f) resulted in restoration of neurite outgrowth from the neurosphere situated on top of the scaffold, and few neurites had visibly penetrated the scaffold, however this neurite growth was still reduced in comparison to the control. Treatment with ibuprofen and $A\beta_{40}$ (Figure 5-17Ag,h), resulted in penetration of neurites as visible from the bottom view of the scaffold. All test conditions induced a significant inhibition in the number of neurites that penetrated the scaffold (Figure 5-17B), with Y-27632 and ibuprofen treatment only partially enhancing neurite penetration compared with $A\beta_{40}$ alone.

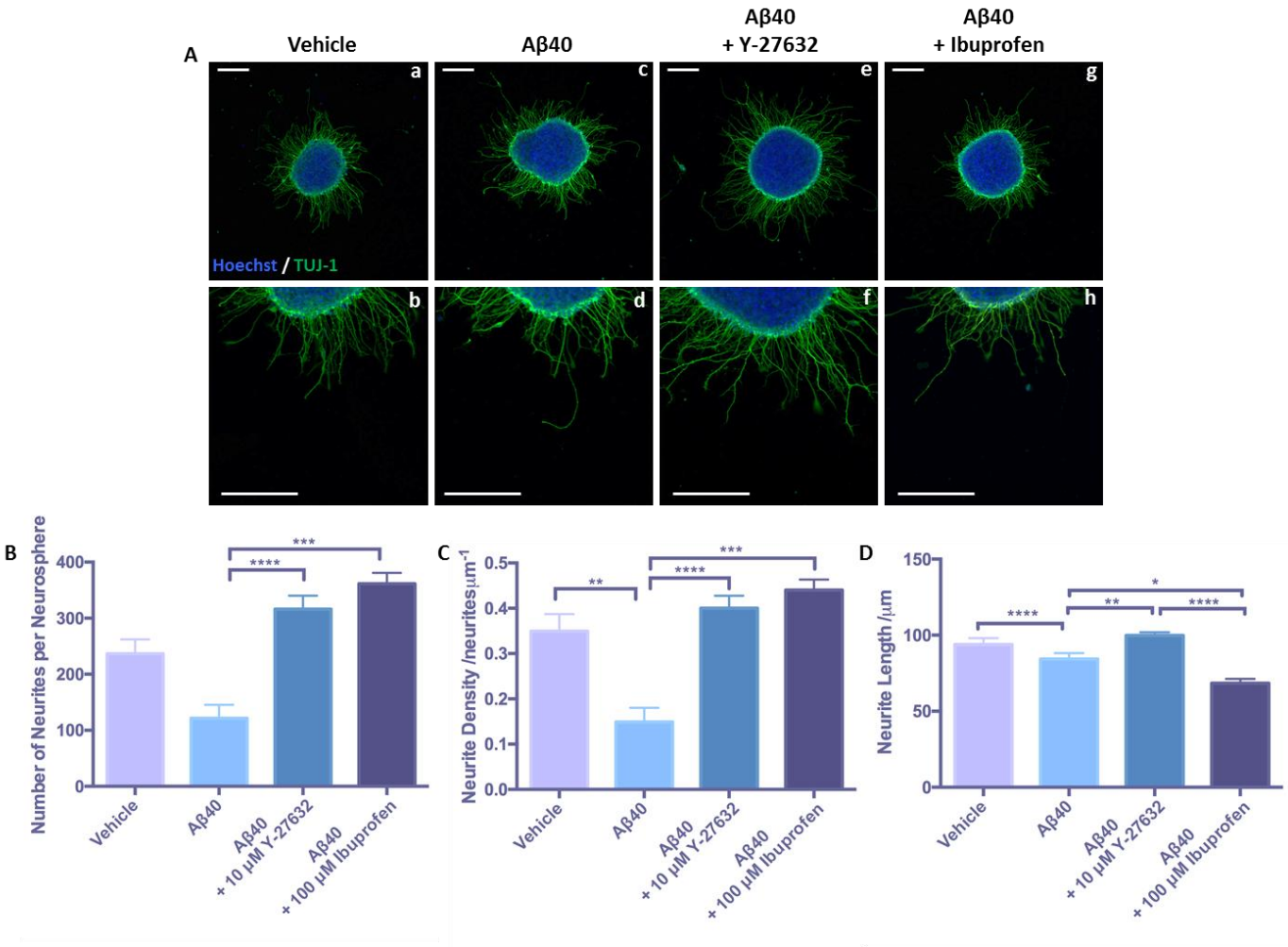

Fig 5-16: Exogenous addition of $A\beta_{40}$ is inhibitory to neurite outgrowth from iPSC-derived neurospheres in 2D culture.
Representative confocal images (A) of ReproNeuro derived neurospheres cultured in 2D (Aa,b) with the addition of 1 μM $A\beta_{40}$ to the culture medium (Ac,d) and with further supplementation of Y-27632 (Ae,f) and ibuprofen (Ag,h). Scale bars: 100 μm. Neurite outgrowth is highlighted by staining for the pan-neuronal marker TUJ-1 (green) and nuclei are stained in blue. Quantification of the number of neurites per neurosphere (B) (data represent mean ± SEM, n=3-9; 1-3 individual neurospheres were quantified from 3 independent replicates) and neurite density (C) (data represent mean ± SEM, n=3-9; 1-3 individual neurospheres were quantified from 3 independent replicates) reveal that addition of $A\beta_{40}$ to the culture medium is inhibitory to neurite outgrowth and both Y-27632 and ibuprofen can overcome this inhibition to control levels. Neurite length (D) (data represent mean ± SEM, n=57-213; between 57-213 neurites were measured from 1-3 neurospheres per independent replicate, of which there were 3) is inhibited with $A\beta_{40}$ supplementation and restored to normal levels by Y-27632 however, not by ibuprofen. One-way ANOVA with Tukey's multiple comparisons: * = $p \leq 0.05$, ** = $p \leq 0.01$, *** = $p \leq 0.001$, **** = $p \leq 0.0001$.

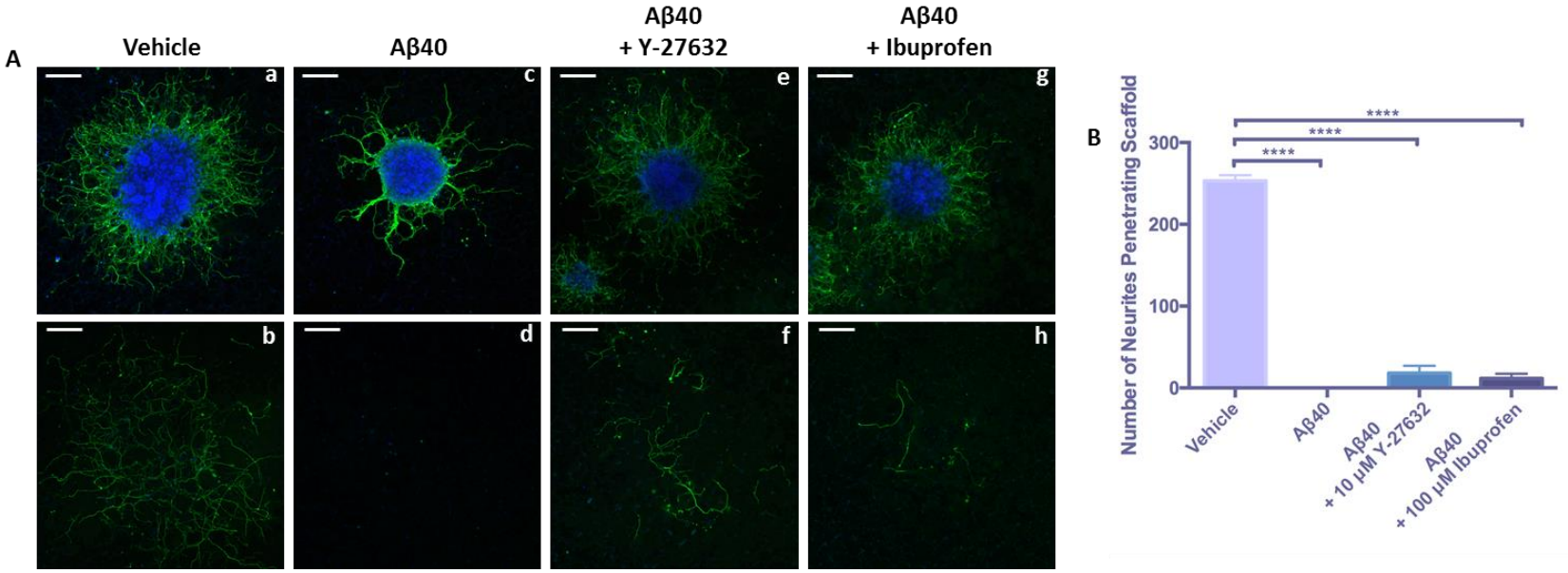

Fig 5-17: Exogenous addition of $A\beta_{40}$ is inhibitory to neurite outgrowth from iPSC-derived neurospheres in 3D culture.
Representative confocal images (A) of ReproNeuro derived neurospheres cultured in 3D (Aa,b) with the addition of 1 μM $A\beta_{40}$ to the culture medium (Ac,d) and with further supplementation of Y-27632 (Ae,f) and ibuprofen (Ag,h). Neurospheres remain on top of the scaffold (Aa,c,e,g) whilst TUJ-1 (green) positive neurites penetrate the depth of the scaffold, as visible from the bottom view of the scaffold (Ab,d,f,h). Nuclei are stained blue. Scale bars: 100 μm. Quantification of the number of neurites penetrating the 3D material (B) (data represent mean ± SEM, n=3; due to limited cell availability 3 neurospheres from 1 population of cells were quantified) demonstrates the ability of $A\beta_{40}$ to induce neurite inhibition in a 3D environment, with partial recovery induced by Y-27632 and ibuprofen. One-way ANOVA with Tukey's multiple comparisons: * = $p \leq 0.05$, ** = $p \leq 0.01$, *** = $p \leq 0.001$, **** = $p \leq 0.0001$.

5.3.5 Investigation into the Neurite Outgrowth Properties of Alzheimer's Disease Phenotype Cells

Alzheimer's disease model neuroprogenitor cells are available from the ReproNeuro range, and produce an increased ratio of $A\beta_{42}$:$A\beta_{40}$ consistent with pathological abnormalities found within the brain of Alzheimer's disease patients[212]. There are two types of AD phenotype cells, the first of which is termed *AD-patient 1*, and is derived from an iPSC line established from an AD patient. This cell line contains a mutation (R62H) in presenilin 2 (PS2) a component of the γ-secretase complex that is involved in APP processing and Aβ species generation[212]. The second AD-model cell type is known as *AD-mutation* and involved the derivation of an iPSC line from a healthy individual which was then transfected with a known AD-associated mutation (P117L) of presenilin 1 (PS1), another component of the γ-secretase complex[212]. A schematic depicting the derivation of each AD-phenotype ReproNeuro cell type is outlined in Figure 5-18.

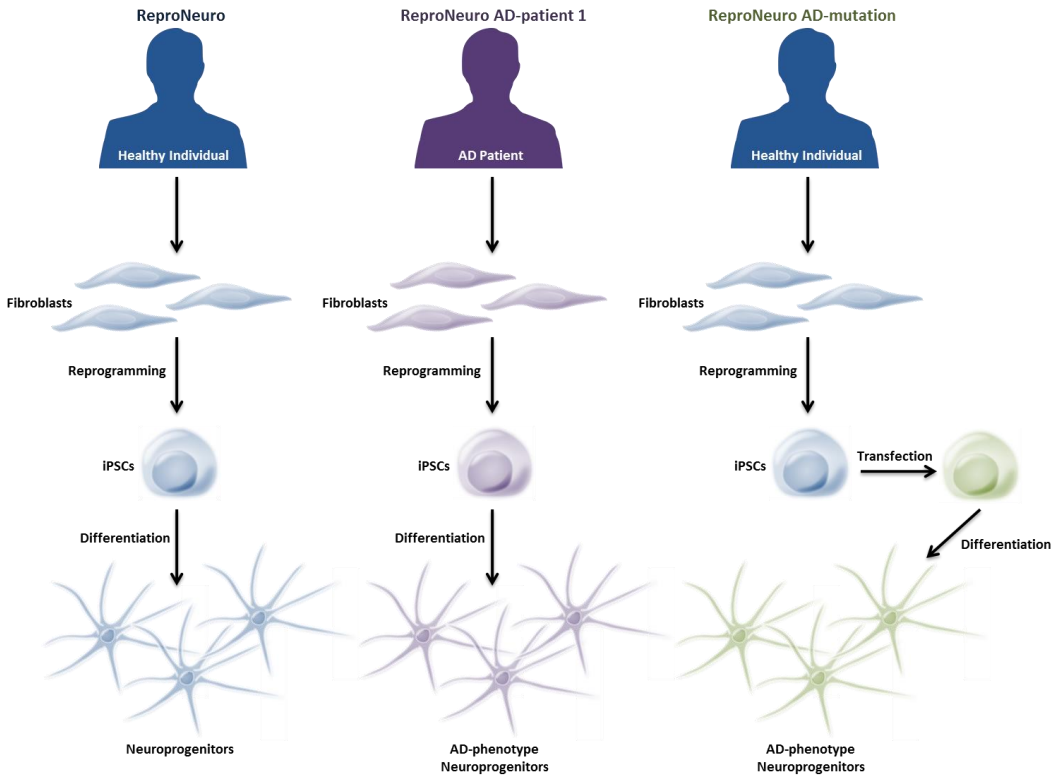

Fig 5-18: Schematic depicting the origin of each ReproNeuro AD-phenotype cell line. ReproNeuro cells act as the wild type control for each AD-phenotype cell line and are derived from a healthy individual. ReproNeuro AD-patient 1 are derived from somatic cells from an AD patient with a mutation in PS2 (R62H), reprogrammed into iPSCs and subsequently differentiated to generate disease-specific neuroprogenitor cells. ReproNeuro AD-mutation cells were formed from an iPSC line derived from a healthy individual and subsequently transfected with a mutation in PS1 (P117L) and differentiated into neuroprogenitor cells that express a higher ratio of $A\beta_{42}$:$A\beta_{40}$.

Initially, to characterise the growth of each ReproNeuro cell type, cells were cultured as 2D monolayers as per the manufacturer's instructions. Phase contrast images (Figure 5-19A-C) reveal that a significant number of cells in wild type cultures have not adhered to the growth substrate (Figure 5-19A), this could be due to a loss of viability upon cellular revival from cryopreservation. Patient-derived cells appear from phase contrast analysis (Figure 5-19B) to contain a mixed population of different cell types with most cells appearing to adopt a large, flattened glial-like morphology. Monolayer culture of the mutation cell line, however, resulted in the formation of a vast neuronal network with an array of projections and connections (Figure 5-19C).

Immunofluorescence analysis of these cultures, highlighting expression of the pan-neuronal marker TUJ-1 (green) revealed that wild type cultures generated few neurites (Figure 5-19D). Although patient cultures (Figure 5-19E) also resulted in the formation of a small number of neurites, cultures also contained a large number of other cell types appearing with varied morphology, suggesting that cultures are not pure. As observed via phase contrast microscopy, immunofluorescence staining of mutation monolayers (Figure 5-19F) reveals a large number of TUJ-1 positive processes that interconnect forming a large neuronal network.

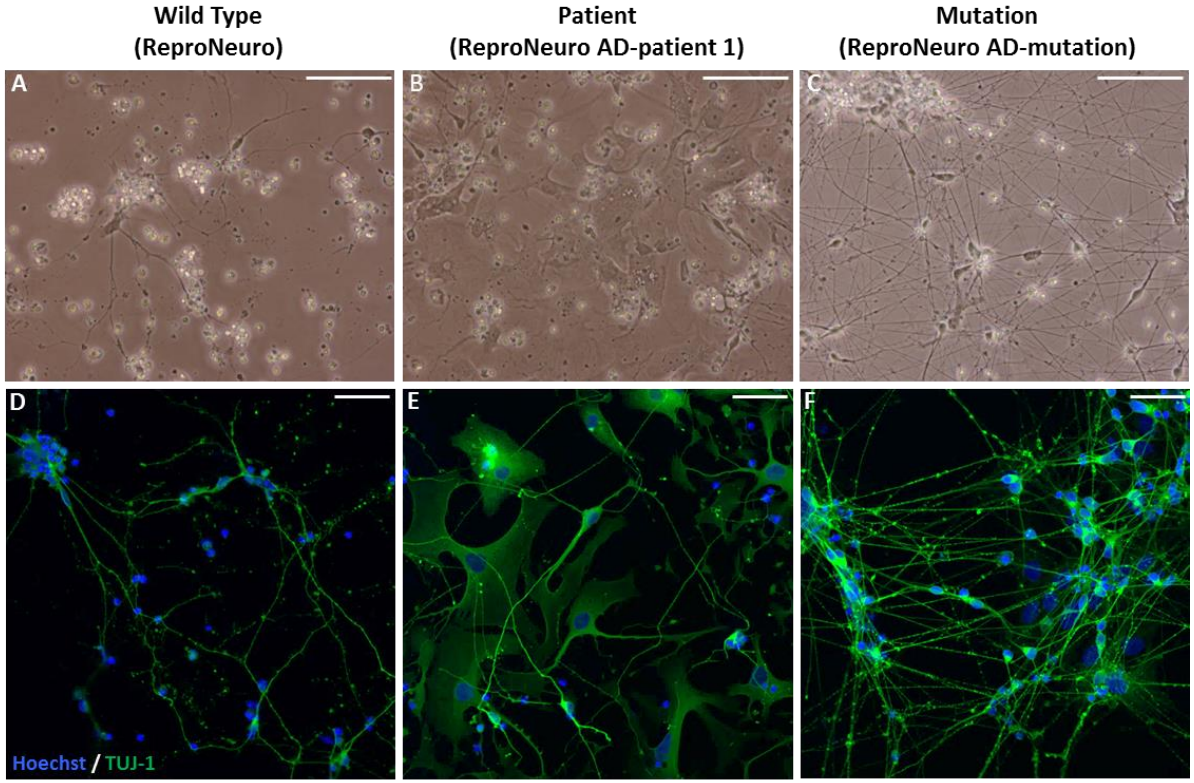

Fig 5-19: Neurite outgrowth from 2D monolayers of iPSC derived, Alzheimer's disease phenotype cells.
Representative phase contrast images (A-C) of ReproNeuro, iPSC derived neuroprogenitor cells, cultured for 14 days on ECM coated glass coverslips. ReproNeuro (A,D) cells are the isogenic control for the two Alzheimer's phenotype cell types (B-F). ReproNeuro AD-Patient 1 (B,E) are neuroprogenitor cells derived from iPSCs from an Alzheimer's disease patient with a mutation in presenilin 2. ReproNeuro AD-Mutation (C,F) are iPSC derived neuroprogenitor cells, transfected with a mutation in presenilin 1. Presinilin is a subunit of the γ-secretase enzyme involved in the amyloidgenic processing and generation of Aβ. Representative confocal images (D-F) of TUJ-1 (green) positive neurons in 14-day-old cultures of ReproNeuro cells. Nuclei are highlighted in blue. Scale bars: (A-C): 100 µm (D-F): 50 µm. Patient derived cells appear to be a more heterogeneous mix of cell types than the other two cellular populations, as under both phase contrast and immunofluorescence, larger cells are clearly visible in addition to neurons. A significant number of neurons and neuritic extensions are visible in mutation cultures with the formation of complex neuronal networks.

Each ReproNeuro cell type was then cultured as neurospheres in 2D to analyse the radial extension of neurites from the central cellular mass. Neurites from each cell type were visible under phase contrast (Figure 5-20Aa,c,e), however, similar to monolayer cultures, patient-derived neurospheres do not appear to contain a pure population of neuroprogenitor cells. Patient-derived neurospheres (Figure 5-20Ac), extend not only neurites, but cell bodies with varied morphology, from the central cellular mass.

Immunofluorescence staining (Figure 5-20Ab,d,f) highlighting TUJ-1 (green) positive neurite outgrowth, revealed significant neurite extension from wild type neurospheres (Figure 5-20Ab). Patient-derived neurospheres (Figure 5-20Ad), on the other hand, not only generate a significant number of neurites, but a mixture of cell types can be observed with TUJ-1 positive cell bodies appearing to migrate outward from the neurosphere. Mutation-derived neurospheres (Figure 5-20Af) produce significant neurite outgrowth with little evidence of cellular migration; however, neurite outgrowth around the perimeter of the neurosphere appears less consistent than wild type neurite outgrowth.

Both the number of neurites per neurosphere (Figure 5-20B) and neurite density (Figure 5-20C) reveal a similar trend in that both variables are significantly inhibited in patient and mutation cells. Neurite outgrowth was significantly inhibited in the patient-derived cell line compared with mutation and wild type cells. Neurite length (Figure 5-20D), however, exhibits a different correlation with cell type. Both patient and mutation cells produce significantly shorter neurites than wild type cells, with patient-derived cells producing the longest neurites. A similar correlation was observed in quantification of cellular migration (Figure 5-20E), as a large number of nuclei were found to lie outside of the cellular aggregate in patient-derived cultures, but not in wild type or mutation cultures.

In 3D culture, all neurosphere bodies remain on top of the scaffold (Figure 5-21Aa-c) whereas TUJ-1 positive (green) neurites grow into the 3D material and penetrate the entire depth to emerge from the bottom of the scaffold (Figure 5-21Ad-f). Few neurites can be observed from the bottom view of wild type neurospheres (Figure 5-21Ad), whereas a large number of neurites have visibly penetrated the scaffold in patient-derived cultures (Figure 5-21Ae), and again only a small amount of penetration is visible in mutation cultures (Figure 5-21Ag). This was confirmed by quantification of neurite penetration (Figure 5-21B), which established that a large number of neurites had penetrated the scaffold from patient-derived cultures compared with both wild type and mutation.

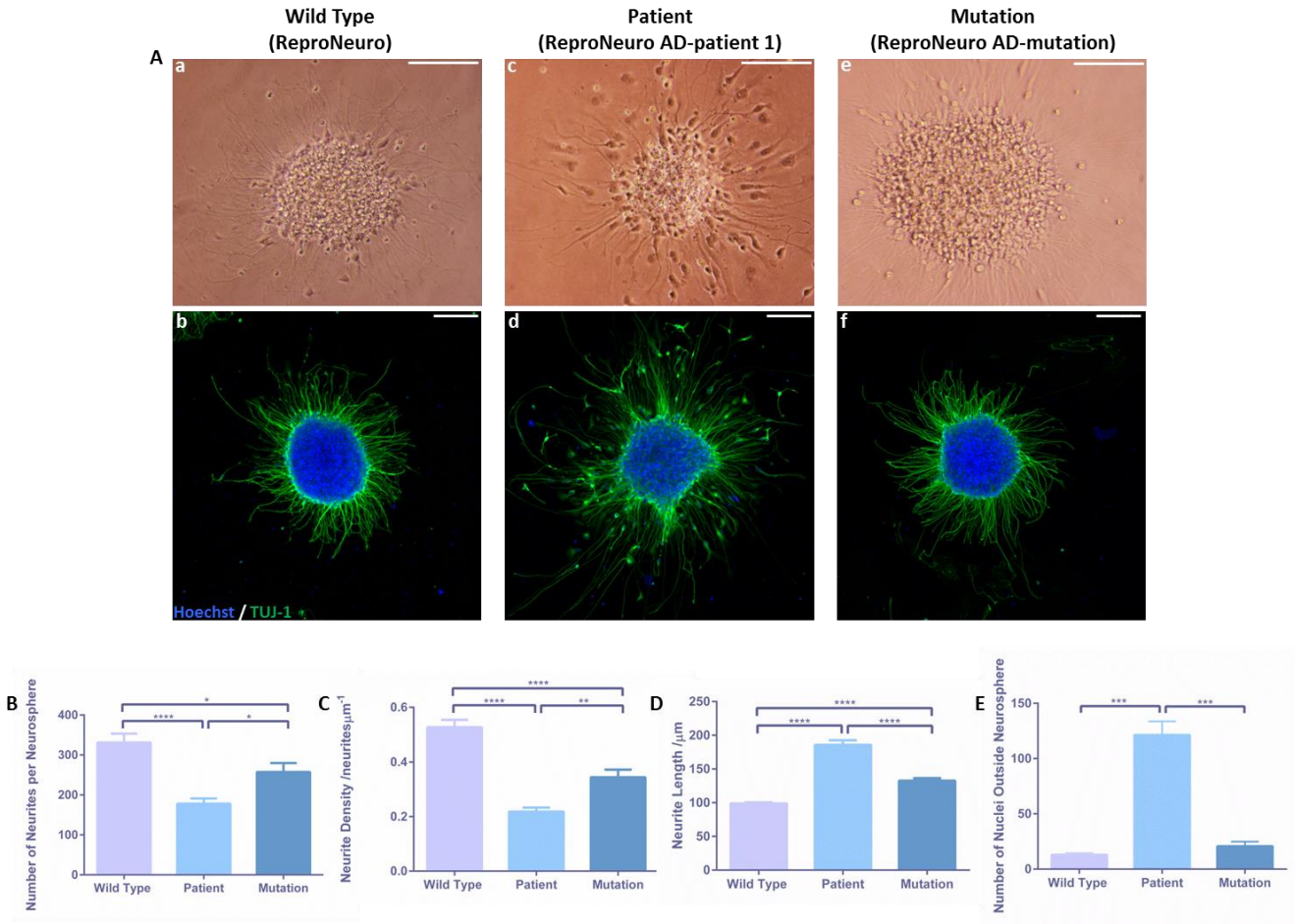

Fig 5-20: Reduced of 2D neurite outgrowth in neurospheres formed from Alzheimer's phenotype iPSC derived neuroprogenitor cells. Representative phase contrast (Aa,c,e) and confocal (Ab,d,f) images of neurospheres formed from ReproNeuro, iPSC derived neuroprogenitor cells. Both phase contrast and immunofluorescence (staining for the pan-neuronal marker TUJ-1, green and nuclei are highlighted in blue) analysis demonstrate significant neurite outgrowth from the central cellular aggregate. Many short neurites can be observed to radiate from wild type neurospheres (Aa,b), whereas patient derived neurospheres (Ac,d) appear to have a mixed population of cells protruding from the cellular aggregate. Neurospheres derived from mutation cells (Ae,f), also appear to have many short neurites, similar to wild type cultures. Scale bars: 100 µm. Quantification of the number of neurites per neurosphere (B) (data represent mean ± SEM, n=11-15; 3-5 individual neurospheres were quantified from 3 independent replicates) and neurite density (C) (data represent mean ± SEM, n=11-15; 3-5 individual neurospheres were quantified from 3 independent replicates) reveals that neurite outgrowth was significantly inhibited in neurospheres derived from both patient and mutation cells. However, the average neurite length (D) (data represent mean ± SEM, n=173-516; between 173-516 neurites were measured from 3-5 neurospheres per independent replicate, of which there were 3) was significantly enhanced in neurites from patient derived neurospheres and neurites from both patient and mutation neurospheres were significantly longer than from wild type neurospheres. Similarly, the number of nuclei that have appeared to migrate from the central cellular aggregate (E) (data represent mean ± SEM, n=3) is significantly greater in patient derived neurospheres than any other condition tested, similarly to neurite length. One-way ANOVA with Tukey's multiple comparisons: * = $p \leq 0.05$, ** = $p \leq 0.01$, *** = $p \leq 0.001$, **** = $p \leq 0.0001$.

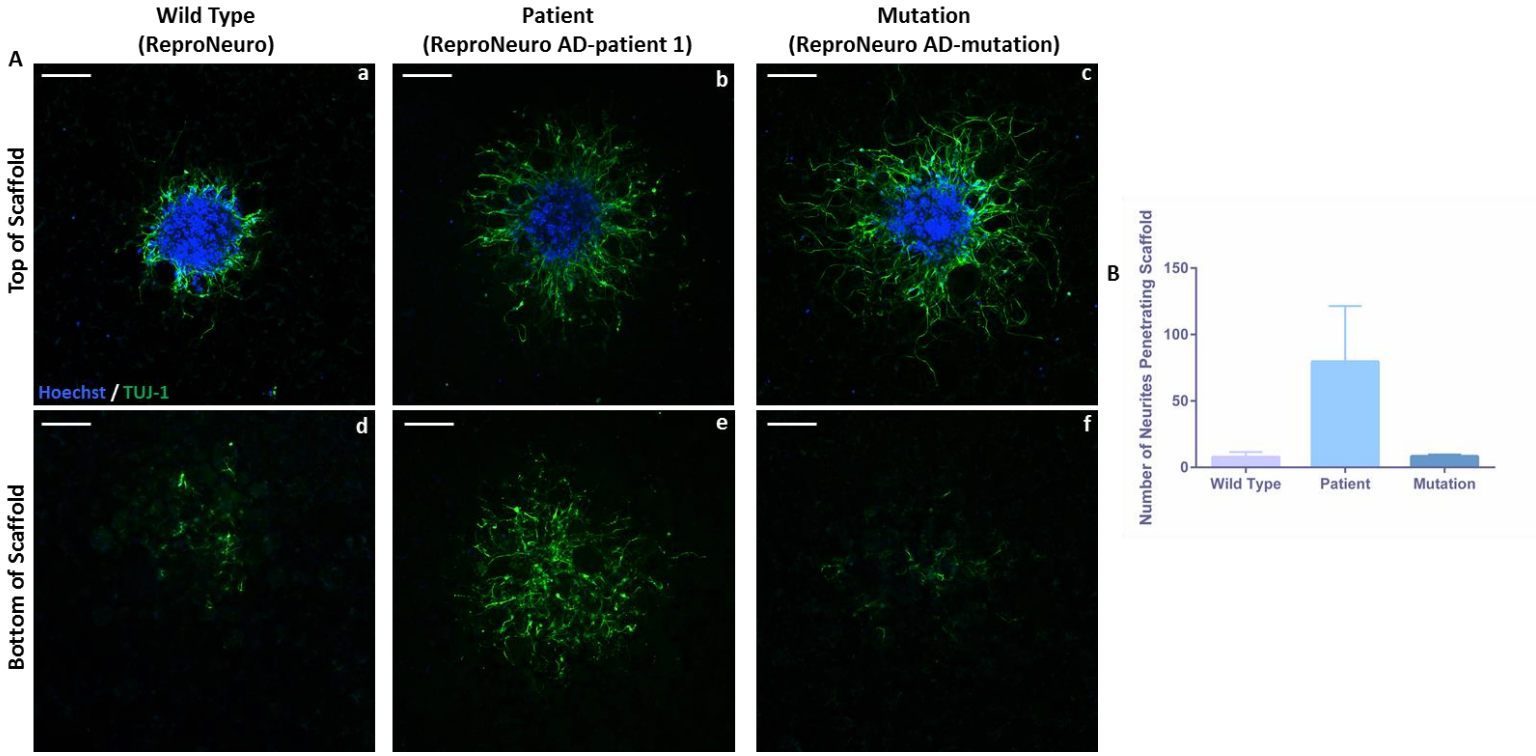

Fig 5-21: Increase of neurite outgrowth in 3D culture by neurospheres formed from iPSC derived Alzheimer's phenotype neuroprogenitor cells.
Representative confocal images of neurospheres formed from ReproNeuro, iPSC derived neuroprogenitor cells and subsequently cultured in 3D (A). Neurite outgrowth is highlighted by staining for the pan-neuronal marker TUJ-1 (green) and nuclei are stained blue. Nuclei generally remain within the cellular aggregate as visible from the top view of the scaffold (Aa-c), whereas neurites are visible from the bottom view of the scaffold (Ad-f), as they have penetrated the entire depth of the 3D material. Scale bars: 100 µm. Quantification of the number of neurites that have penetrated the scaffold for each cell type (B) (data represent mean ± SEM, n=3-6; due to limited cell availability 1-2 neurospheres from 1 population of cells were quantified) reveals that a much larger number of neurites penetrate the scaffold from neurospheres derived from patient cells rather than the wild type or mutation cells. One-way ANOVA with Tukey's multiple comparisons: * = $p \leq 0.05$, ** = $p \leq 0.01$, *** = $p \leq 0.001$, **** = $p \leq 0.0001$

5.3.6 The Effect of Rho A/ROCK Inhibition on Neurite Outgrowth From Alzheimer's Disease Phenotype Cells

To further understand the mechanisms governing Aβ-mediated inhibition of neurite growth, the effect of Rho A inhibition by ibuprofen and ROCK inhibition by Y-27632 was investigated in these AD-phenotype cell lines.

5.3.6.1 ReproNeuro AD-Patient 1

ReproNeuro patient-derived cells were cultured as neurospheres in 2D with a range of concentrations (0.5 – 15 μM) of Y-27632 (Figure 5-22Ac-k). Significant neurite outgrowth can be observed from wild type derived cultures (Figure 5-22Aa,b), along with patient-derived cultures (Figure 5-22Ac,d). However patient-derived neurospheres appear to produce fewer neurites and contain a more heterogenous population of cell types. Addition of Y-27632 to the culture medium of patient-derived cells resulted in a slight increase in visible neurite outgrowth, and a reduction of visible cell bodies outside of the neurosphere was particularly evident at 15 μM Y-27632 treatment (Figure 5-22Aj,k).

The number of neurites per neurosphere (Figure 5-22B) was reduced in patient-derived cells compared with wild type. This inhibition was rescued with 0.5 μM Y-27632 treatment, which restored neurite number to control levels. Treatment with higher concentrations of Y-27632, however, resulted in a significant enhancement in the number of neurites generated per neurosphere compared with control, wild type cultures. Neurite number was also enhanced by 15 μM Y-27632 treatment, however the number of neurites generated by 15 μM treated neurospheres was reduced compared with those treated with 10 μM Y-27362.

A similar result was obtained from quantification of neurite density (Figure 5-22C), as neurite outgrowth from patient-derived neurospheres was significantly reduced compared with wild type neurospheres. This inhibitory effect was recovered by treatment with 0.5 μM Y-27632, whilst higher concentrations of Y-27632 such as 10 μM and 15 μM significantly enhanced neurite density compared with the wild type, control.

Neurite length (Figure 5-22D) was significantly enhanced in patient-derived cultures compared with wild type, and inhibited in a dose dependent manner by Y-27632 treatment. Although all treatment conditions produced significantly longer neurites than wild type cultures, Y-27632 treatment did have an inhibitory effect upon neurite length with 15 μM treatment resulting in significantly shorter neurites than 0.5 μM treatment. A similar effect is noted in terms of cellular migration (Figure 5-22E) from each

neurosphere. Significantly more nuclei were located outside of each neurosphere in patient-derived cultures than wild type, and Y-27632 treatment induced a dose dependent decrease in the number of nuclei that lie outside of each neurosphere, with both 10 μM and 15 μM Y-27632 resulting in a statistically significant inhibition of migration.

In 3D culture, all neurospheres remained on top of the scaffold (Figure 5-23Aa,c,e,g,i) and more neurites visibly radiated from the central cellular point in patient-derived cultures. A similar number of neurites appear visible from the underside of wild type (Figure 5-23b) and patient-derived cultures (Figure 5-23Ad) with Y-27632 treatment (Figure 5-23Af,h,j) appearing to enhance the number of neurites visible from the bottom view of each scaffold. Quantification of neurite penetration (Figure 5-23B) confirms this observation, as slightly more (but not statistically significant) neurites penetrate the scaffold in patient-derived cultures as oppose to wild type cultures. Y-27632 treatment was also found to enhance neurite penetration and 0.5 μM and 15 μM Y-27632 significantly enhanced neurite penetration compared with wild type cultures.

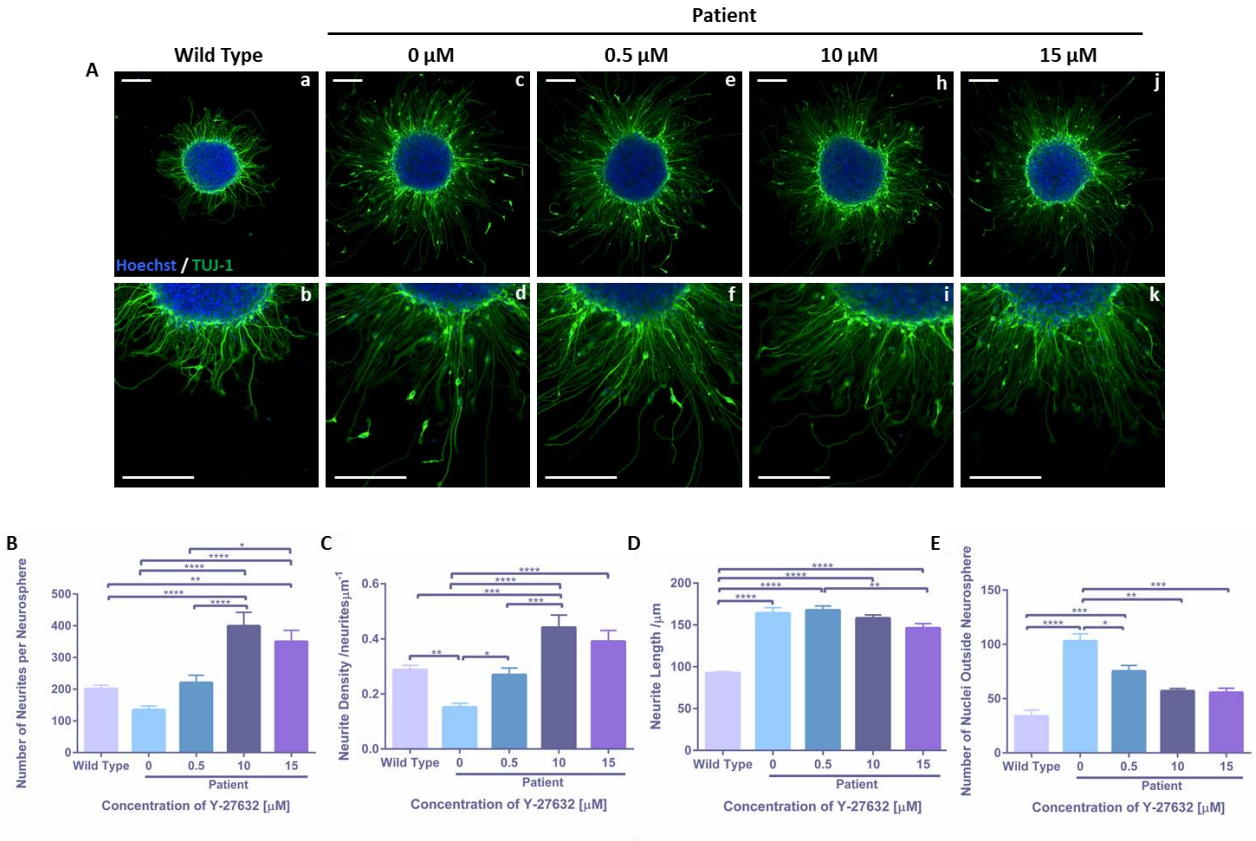

Fig 5-22: Restoration of neurite outgrowth from Alzheimer's disease patient derived neurospheres cultured in 2D with treatment with the ROCK inhibitor, Y-27632.

Representative confocal images of ReproNeuro derived neurospheres cultured in 2D for 24 hours to induce neurite outgrowth (A) with a range of concentrations (0 – 15 µM) of Y-27632. Staining for the pan-neuronal marker TUJ-1 in green highlights neurite outgrowth and nuclei are highlighted in blue. Significant neurite outgrowth can be observed from wild type neurospheres (Aa,b), whereas patient derived neurospheres (Ac,d) appear to produce a reduced number of neurites that are longer, which appears to be enhanced and restored to normal levels with Y-27632 treatment (Ae-k). Scale bars: 100 µm. Quantification of the number of neurites per neurosphere (B) (data represent mean ± SEM, n=6-18; 2-6 individual neurospheres were quantified from 3 independent replicates) and the neurite density (C) (data represent mean ± SEM, n=6-18; 2-6 individual neurospheres were quantified from 3 independent replicates) show that neurite outgrowth is inhibited in patient derived neurospheres and can be enhanced by treatment with Y-27632. 0.5 µM Y-27632 treatment restored neurite outgrowth to a similar level as wild type and 10 – 15 µM enhanced neurite outgrowth to a level that surpasses that of the wild type. However, neurite length (D) (data represent mean ± SEM, n=81-319; between 81-319 neurites were measured from 3-6 neurospheres per independent replicate, of which there were 3.) is significantly enhanced in patient derived neurospheres compared with the control, and increasing Y-27632 concentration acts to inhibit neurite length. However, even at 15 µM Y-27632 length is still significantly enhanced compared with wild type. Similarly to length, cellular migration (E) (data represent mean ± SEM, n=3-6) is enhanced in patient derived neurospheres compared with wild type and is inhibited with increasing Y-27632 concentration. One-way ANOVA with Tukey's multiple comparisons: * = $p \leq 0.05$, ** = $p \leq 0.01$, *** = $p \leq 0.001$, **** = $p \leq 0.0001$.

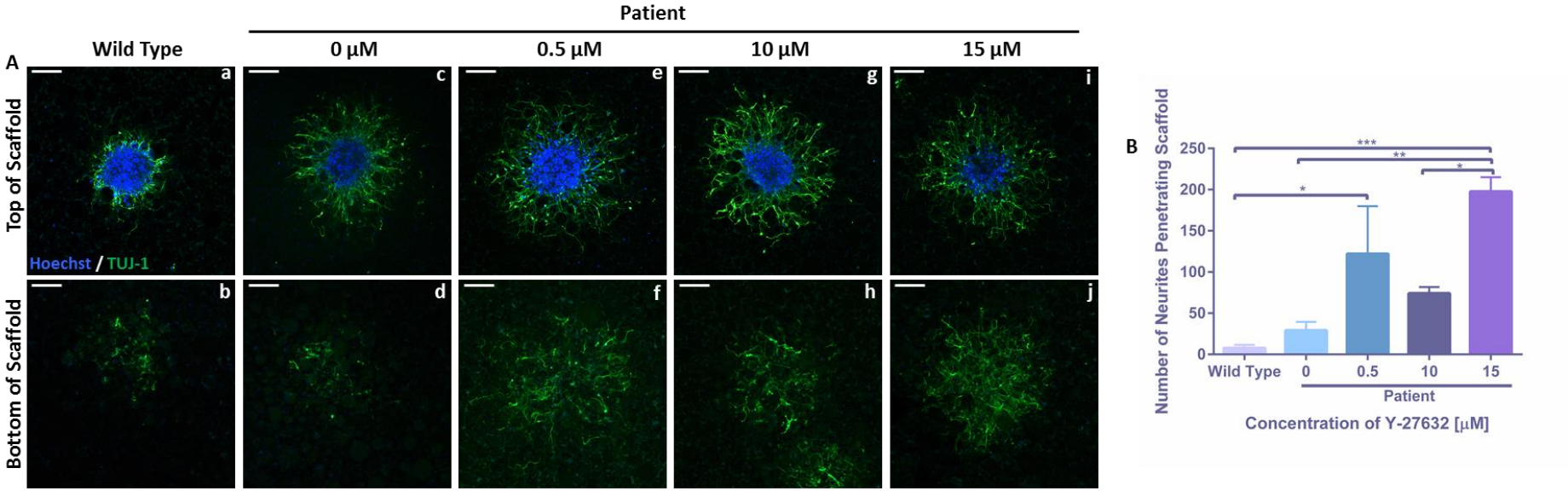

Fig 5-23: Enhancement of neurite outgrowth from Alzheimer's disease patient derived neurospheres cultured in 3D with ROCK inhibitor, Y-27632. Representative confocal images of ReproNeuro derived neurospheres cultured in 3D for 10 days to induce neurite outgrowth (A) with a range of concentrations (0 – 15 µM) of the ROCK inhibitor, Y-27632. Neurospheres can be seen from the top view of the scaffold, with neurite outgrowth highlighted by green staining for the pan-neuronal marker TUJ-1 and nuclei are stained blue (Aa,c,e,g,i), significant neurite outgrowth can be observed from the underside of the scaffold (Ab,d,f,g,j) and appears to be enhanced in patient derived samples with Y-27632 treatment. Scale bars: 100 µm. Quantification of the number of neurites penetrating the scaffold (B) (data represent mean ± SEM, n=3-6; due to limited cell availability 3-6 neurospheres from 1 population of cells were quantified) reveals that more neurites penetrate the 3D material from AD patient rather than WT-derived neurospehres. Neurite outgrowth from patient derived neurospheres was also further enhanced by addition of Y-27632 to the culture medium with the highest concentration (15 µM) Y-27632 producing significantly more neurites that have penetrated the 3D material compared with untreated patient derived samples. One-way ANOVA with Tukey's multiple comparisons: * = $p \leq 0.05$, ** = $p \leq 0.01$, *** = $p \leq 0.001$, **** = $p \leq 0.0001$.

To identify the role of Rho A in Aβ-mediated inhibition, 2D ReproNeuro cultures were treated with a range of concentrations (10 – 500 μM) of ibuprofen. Less visible neurites were evident in cultures of patient-derived cells (Figure 5-24Ac,d) compared with wild type cultures (Figure 5-24Aa,b), although neurites did appear longer. Treatment with high concentrations (100 – 500 μM) of ibuprofen appear to enhance the number of TUJ-1 positive (green) neurites radiating from patient-derived neurospheres, with the generation of particularly dense neurite outgrowth from neurospheres treated with 500 μM ibuprofen (Figure 5-24Ai,j).

The number of neurites per neurosphere (Figure 5-24B) was significantly inhibited in patient-derived cultures compared with wild type cultures. This inhibitory effect was rescued by ibuprofen treatment, with 10 μM ibuprofen restoring neurite number to a similar level as the wild type control. Treatment with 100 μM ibuprofen significantly enhanced neurite number compared with untreated patient-derived samples and 500 μM ibuprofen significantly enhanced the number of neurites generated from patient-derived neurosphere in comparison with wild type neurite outgrowth.

A similar result was obtained in terms of neurite density (Figure 5-24C), as neurite density was significantly reduced in patient-derived cultures compared with wild type. Ibuprofen treatment induced a dose dependent increase in neurite density, with 100 μM ibuprofen treatment resulting in a neurite density similar to that of the wild type control. Treatment with 500 μM ibuprofen also significantly enhanced neurite density from patient-derived cells.

Neurite length (Figure 5-24D) was significantly enhanced in patient-derived cultures, and ibuprofen treatment had little effect upon neurite length. However, cellular migration from the central neurosphere (Figure 5-24E) was significantly enhanced in patient-derived cultures compared with wild type cells. Ibuprofen treatment reduced cellular migration in a dose dependent manner and treatment with 500 μM ibuprofen significantly reduced cellular migration compared with untreated patient-derived neurospheres.

In 3D culture, neurospheres remain on top of the scaffold (Figure 5-25Aa,c,e,g,i) and more neurites visibly radiate from the neurosphere itself in patient-derived cultures. The bottom view of the scaffold (Figure 5-25Ab,d,f,h,j) reveals neurite penetration and it can be seen that more neurites penetrate the depth of the 3D material in patient-derived cultures (Figure 5-25Ad,f,h,j) as oppose to wild type (Figure 5-25Ab). It also appears that particularly high concentrations of ibuprofen such as 500 μM may enhance neurite penetration in 3D culture (Figure 5-15Aj). Quantification of neurite penetration (Figure 5-25B) confirms this observation, and reveals that a large number of neurites penetrate the scaffold from patient-derived neurospheres as oppose to wild type. It also appears that

ibuprofen increases neurite penetration in a dose dependent manner, however this is not statistically significant.

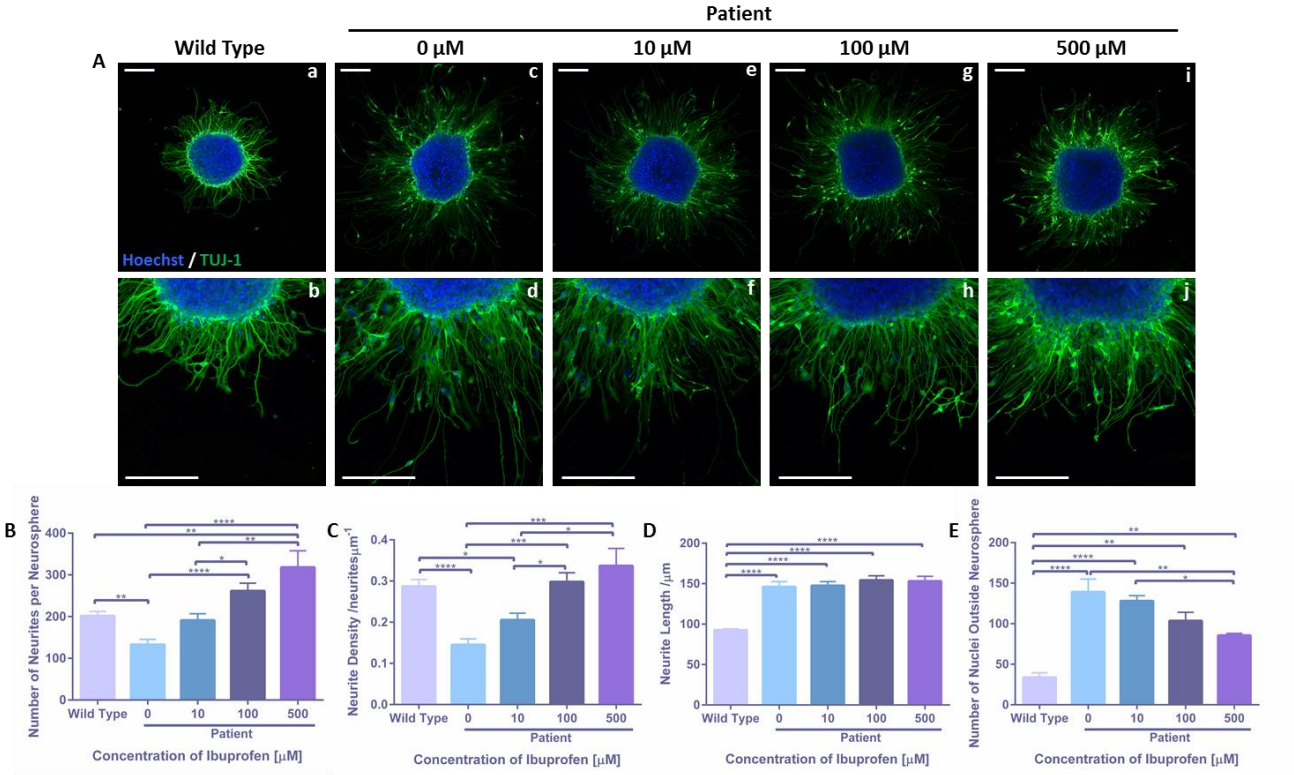

Fig 5-24: Recovery of neurite outgrowth from Alzheimer's disease patient derived neurospheres cultured in 2D through inhibition of Rho A by ibuprofen.
Representative confocal images (A) of ReproNeuro Alzheimer's disease patient derived neurospheres cultured in 2D for 24 hours with a range of concentrations (0 – 500 µM) of ibuprofen. TUJ-1 (green) positive neurites can be seen radiating from the central cellular aggregate with nuclei (blue) generally remaining within the cell mass of the neurosphere. Scale bars: 100 µm. Quantification of the number of neurites per neurosphere (B) (data represent mean ± SEM, n=3-18; 1-6 individual neurospheres were quantified from 3 independent replicates) and neurite density (C) (data represent mean ± SEM, n=3-18; 1-6 individual neurospheres were quantified from 3 independent replicates) reveals that neurite outgrowth is inhibited in Alzheimer's disease patient derived cells compared with wild type, and this is rescued in a dose dependent manner by increasing ibuprofen concentration, with the highest concentration tested (500 µM) enhancing neurite outgrowth to levels greater than that of the wild type. However, neurite length (D) (data represent mean ± SEM, n=62-319; between 62-319 neurites were measured from 1-6 neurospheres per independent replicate, of which there were 3) is significantly greater in those neurites produced from patient derived neurospheres than wild type, and this is not affected by ibuprofen concentration. Migration of cells from the neurosphere body (E) (data represent mean ± SEM, n=3-6; 1-6 individual neurospheres were quantified from 3 independent replicates) is significantly greater in patient derived samples compared with wild type and this is inhibited in a dose dependent fashion with increasing ibuprofen concentration. One-way ANOVA with Tukey's multiple comparisons: * = $p \leq 0.05$, ** = $p \leq 0.01$, *** = $p \leq 0.001$, **** = $p \leq 0.0001$.

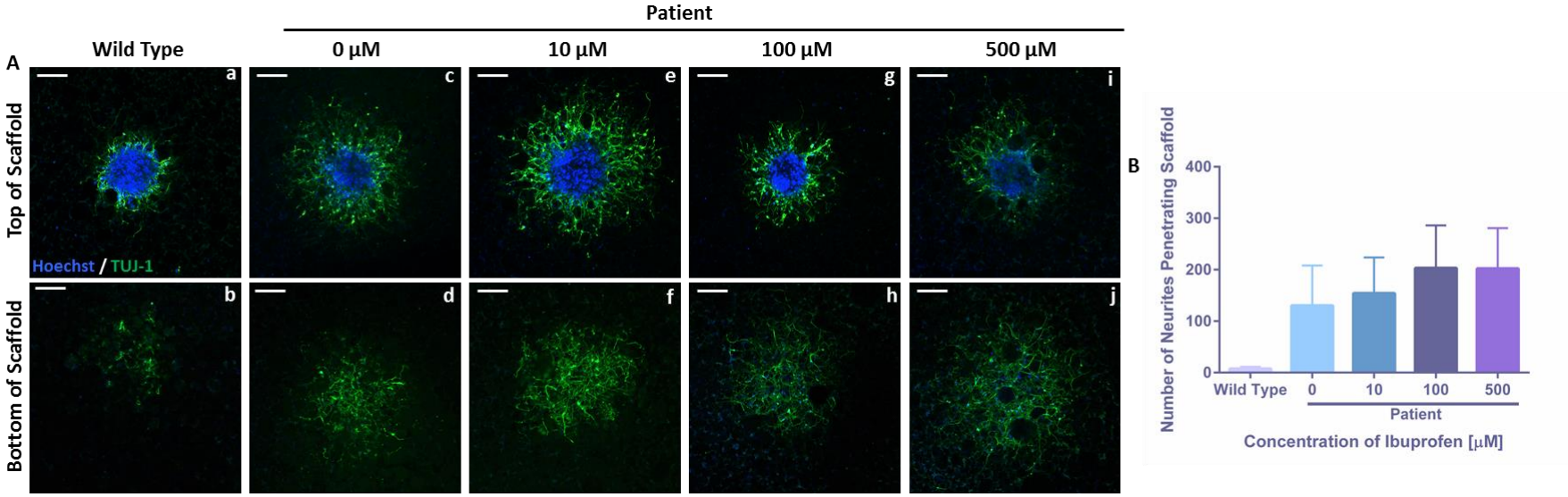

Fig 5-25: Recovery of neurite outgrowth from Alzheimer's disease patient derived neurospheres cultured in 3D through inhibition of Rho A by ibuprofen.

Representative confocal images (A) of ReproNeuro Alzheimer's disease patient derived neurospheres cultured in 3D for 10 days with a range of concentrations (0 – 500 µM) of ibuprofen. Neurospheres can be seen from the top view of the scaffold (Aa,c,e,g,i) with neurites stained green and nuclei stained blue. TUJ-1 positive neurites can be seen from the bottom view of the scaffold (Ab,d,f,h,j) having penetrated the entire depth of the 3D material. Scale bars: 100 µm. Quantification of the number of neurites penetrating the scaffold (B) (data represent mean ± SEM, n=3-6; due to limited cell availability 1-2 neurospheres from 1 population of cells were quantified) reveals that more neurites penetrate the scaffold from patient derived neurospheres than wild type, and this is slightly enhanced by high concentrations (100 – 500 µM) of ibuprofen. One-way ANOVA with Tukey's multiple comparisons: * = $p \leq 0.05$, ** = $p \leq 0.01$, *** = $p \leq 0.001$, **** = $p \leq 0.0001$.

5.3.6.2 ReproNeuro AD-Mutation

ReproNeuro mutation-derived neurospheres were cultured in 2D with a range of concentrations (0.5 - 15 μM) of Y-27632. Significant neurite growth developed from wild type-derived neurospheres (Figure 5-26Aa,b). However, neurite outgrowth from mutation-derived neurospheres (Figure 5-26Ac,d) appears less dense and uniform around the neurosphere compared with wild type control. Treatment with increasing concentrations of Y-27632 (Figure 5-26Ac-j) appears to enhance visible neurite growth from mutation-derived neurospheres, and neurites appear particularly long with 0.5 μM Y-27632 treatment (Figure 5-26Ae,f).

The number of neurites generated per neurosphere (Figure 5-26B) was significantly reduced in mutation cultures compared with wild type. Y-27632 treatment enhanced neurite number in a dose dependent manner with the lowest concentration tested, 0.5 μM Y-27632, leading to a significant enhancement in neurite number compared with mutation alone. Treatment with the highest concentration of Y-27632 tested, 15 μM, led to a significant increase in neurite number from mutation-derived neurospheres compared with wild type-derived neurospheres.

Neurite density (Figure 5-26C) is also significantly reduced in mutation-derived cultures in comparison with wild type cultures. Y-27632 treatment enhances neurite density in a dose dependent manner and 15 μM Y-27632 enhances neurite density even compared to wild type cultures. Neurite length (Figure 5-26D) is significantly enhanced in mutation-derived cultures and Y-27632 treatment results in an inhibition in length. However, even with Y-27632-induced inhibition of length, all mutation-derived neurospheres generate neurites that are significantly longer than wild type-derived neurites. Migration of cells from the central body of the neurosphere (Figure 5-26E) is reduced in mutation cultures compared with wild type cells and Y-27632 inhibits cellular migration in a dose dependent fashion.

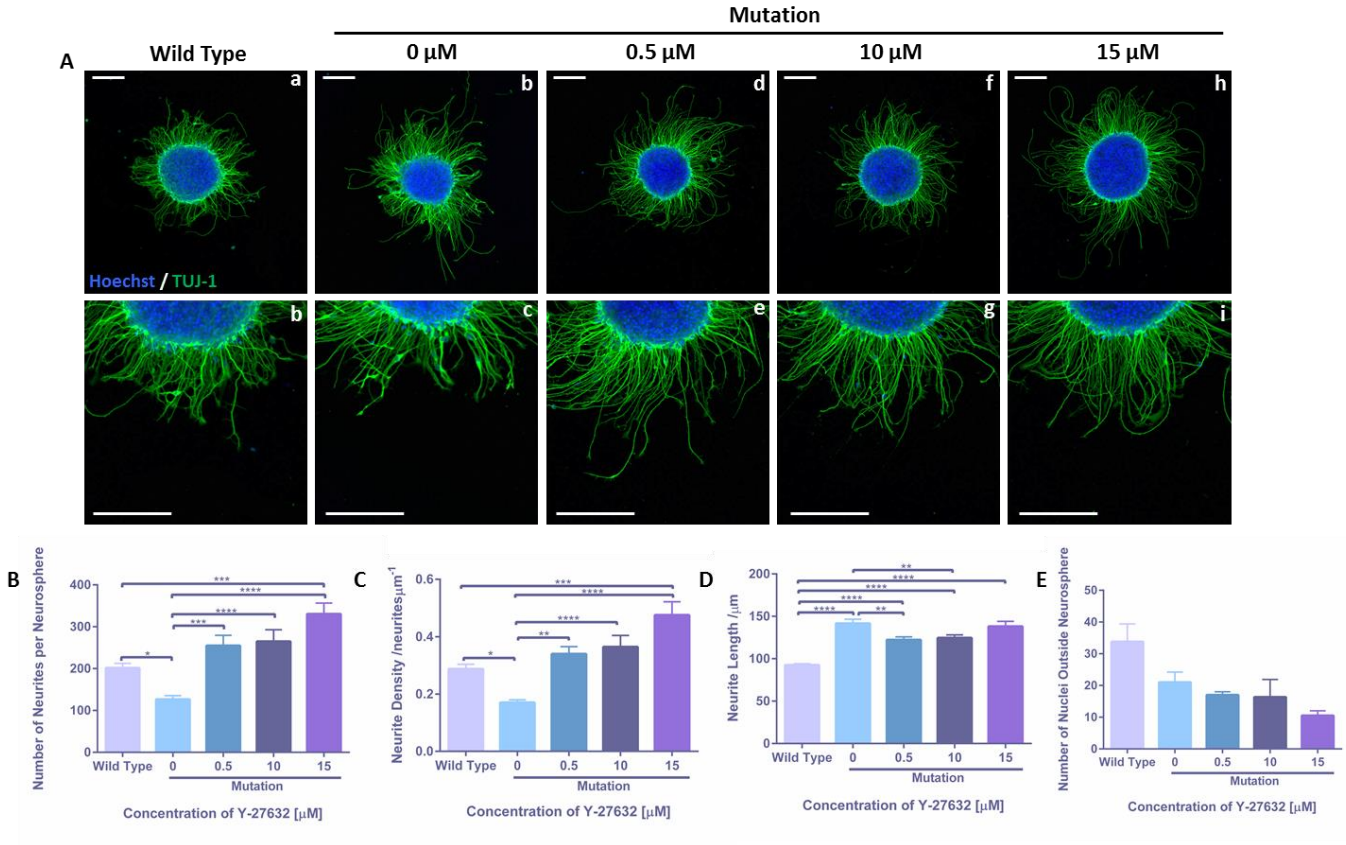

Fig 5-26: Recovery of neurite outgrowth from Alzheimer's disease mutation neurospheres cultured in 2D through inhibition of ROCK by Y-27632.

Representative confocal images (A) of neurospheres derived from ReproNeuro mutation Alzheimer's disease phenotype cells, cultured in 2D for 24 hours with a range of concentrations (0 – 15 µM) of the selective ROCK inhibitor Y-27632. Neurites are stained for the pan-neuronal marker TUJ-1 in green and nuclei are stained blue and generally remain within the cellular aggregate. Scale bars: 100 µm. The number of neurites per neurosphere (B) (data represent mean ± SEM, n=6-18; 2-6 individual neurospheres were quantified from 3 independent replicates) and neurite density (C) (data represent mean ± SEM, n=6-18; 2-6 individual neurospheres were quantified from 3 independent replicates) are both inhibited in mutation derived neurospheres compared with wild type, an effect that is rescued with increasing Y-27632 concentration and even enhanced to levels greater than that of the wild type. Neurite length (D) (data represent mean ± SEM, n=84-319; between 84-319 neurites were measured from 2-6 neurospheres per independent replicate, of which there were 3) however, is enhanced in mutation derived neurospheres compared with wild type, an effect that is reduced by Y-27632 treatment. Migration of cells from the neurosphere (E) (data represent mean ± SEM, n=3-6; 2-6 individual neurospheres were quantified from 3 independent replicates) is reduced in neurospheres derived from mutation cells compared with wild type, and migration is inhibited further by treatment with Y-27632. One-way ANOVA with Tukey's multiple comparisons: * = $p \leq 0.05$, ** = $p \leq 0.01$, *** = $p \leq 0.001$, **** = $p \leq 0.0001$.

Mutation-derived neurospheres were also cultured in 2D with a range of concentrations of ibuprofen (10 – 500 μM). Immunofluorescence analysis of the pan-neuronal marker TUJ-1 (green) reveals that mutation-derived neurospheres (Figure 5-27Ac,d) clearly produce fewer neurites that are less densely packed than wild type control cultures (Figure 5-27Aa,b). Ibuprofen treatment appears to enhance neurite growth producing more a uniform extension of neurites from the body of the neurosphere with neurite outgrowth also appearing denser. This is particularly apparent with 500 μM ibuprofen treatment (Figure 2-27Ai,j).

The number of neurites produced per neurosphere (Figure 5-27B) is reduced in mutation-derived cultures and enhanced in a dose dependent manner with ibuprofen treatment. Treatment with 10 μM ibuprofen resulted in the generation of a similar number of neurites as the wild type control, whereas treatment with 500 μM ibuprofen resulted in a significant enhancement in neurite growth compared with the wild type control. Neurite density (Figure 5-17C) is also reduced in mutation-derived cultures compared with wild type and is enhanced by ibuprofen in a dose dependent manner. Treatment with 10 μM ibuprofen significantly increased neurite density compared with untreated mutation control cultures and treatment with 500 μM ibuprofen treatment significantly enhanced neurite density compared with the wild type control.

Neurite length (Figure 5-27D) is significantly enhanced in mutation-derived cultures compared with wild type control and ibuprofen treatment consistently reduced neurite length. Although, ibuprofen treatment resulted in a reduction in neurite length, all mutation samples both untreated and ibuprofen treated resulted in significantly enhanced neurite length compared with the wild type control. Cellular migration (Figure 5-17E) was reduced in mutation cells and further inhibited by ibuprofen treatment in a dose dependent manner as 500 μM ibuprofen resulted in a significant reduction in cellular migration compared with wild type cultures.

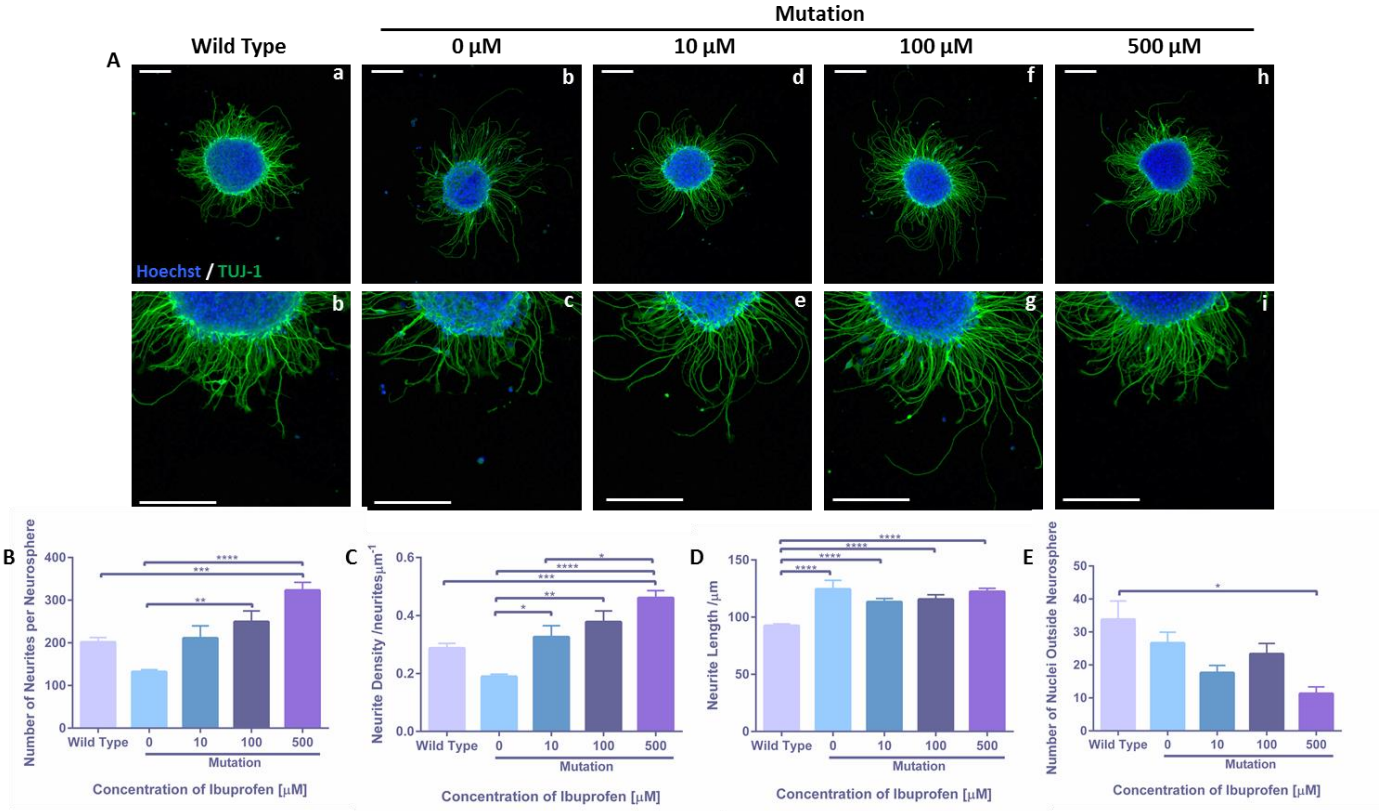

Fig 5-27: Recovery of neurite outgrowth from Alzheimer's disease mutation neurospheres cultured in 2D through inhibition of Rho A by ibuprofen.
Representative confocal images (A) of neurospheres derived from ReproNeuro mutation, Alzheimer's phenotype cells, cultured in 2D for 24 hours with a range of concentrations (0 – 500 µM) of ibuprofen, an inhibitor of Rho A. Neurites are highlighted in green by staining for the pan-neuronal marker, TUJ-1 and nuclei are stained blue. Scale bars: 100 µm. The number of neurites per neurosphere (B) (data represent mean ± SEM, n=6-18; 2-6 individual neurospheres were quantified from 3 independent replicates) and neurite density (C) (data represent mean ± SEM, n=6-18; 2-6 individual neurospheres were quantified from 3 independent replicates) are both decreased in mutation derived neurospheres compared with wild type, however this effect is rescued by treatment with ibuprofen and at 500 µM, is even enhanced to a level that is greater than wild type. Neurite length (D) (data represent mean ± SEM, n=79-319; between 79-319 neurites were measured from 2-6 neurospheres per independent replicate, of which there were 3.) is enhanced in mutation-derived neurospheres compared with wild type, however this is slightly inhibited by the addition of ibuprofen to the culture medium. Migration of cells from the neurosphere (E) (data represent mean ± SEM, n=3-6; 2-6 individual neurospheres were quantified from 3 independent replicates) is inhibited in mutation derived neurospheres compared with wild type, and is further inhibited by ibuprofen, particularly at high concentrations (500 µM). One-way ANOVA with Tukey's multiple comparisons: * = $p \leq 0.05$, ** = $p \leq 0.01$, *** = $p \leq 0.001$, **** = $p \leq 0.0001$.

In 3D culture neurospheres remain situated on top of the scaffold (Figure 5-28Aa,c,e,g) whilst TUJ-1 positive (green) neurites are visible from the bottom view of the scaffold (Figure 5-18Ab,d,f,h) having completely penetrated the 3D material. A significant number of neurites can be visualised from the underside of both wild type (Figure 5-28Ab) and mutation (Figure 5-28Ad) cultures and Y-27632 treatment appears to result in an increase in the number of neurites visible from the bottom of the scaffold (Figure 5-18Af).

The number of neurites that had penetrated the scaffold (Figure 5-28B) from both wild type and mutation cultures were similar. However Y-27632 and ibuprofen treatment both enhanced the number of neurites that penetrated the scaffold from mutation cultures, resulting in an increased level of 3D neuritogenesis compared with wild type control cultures.

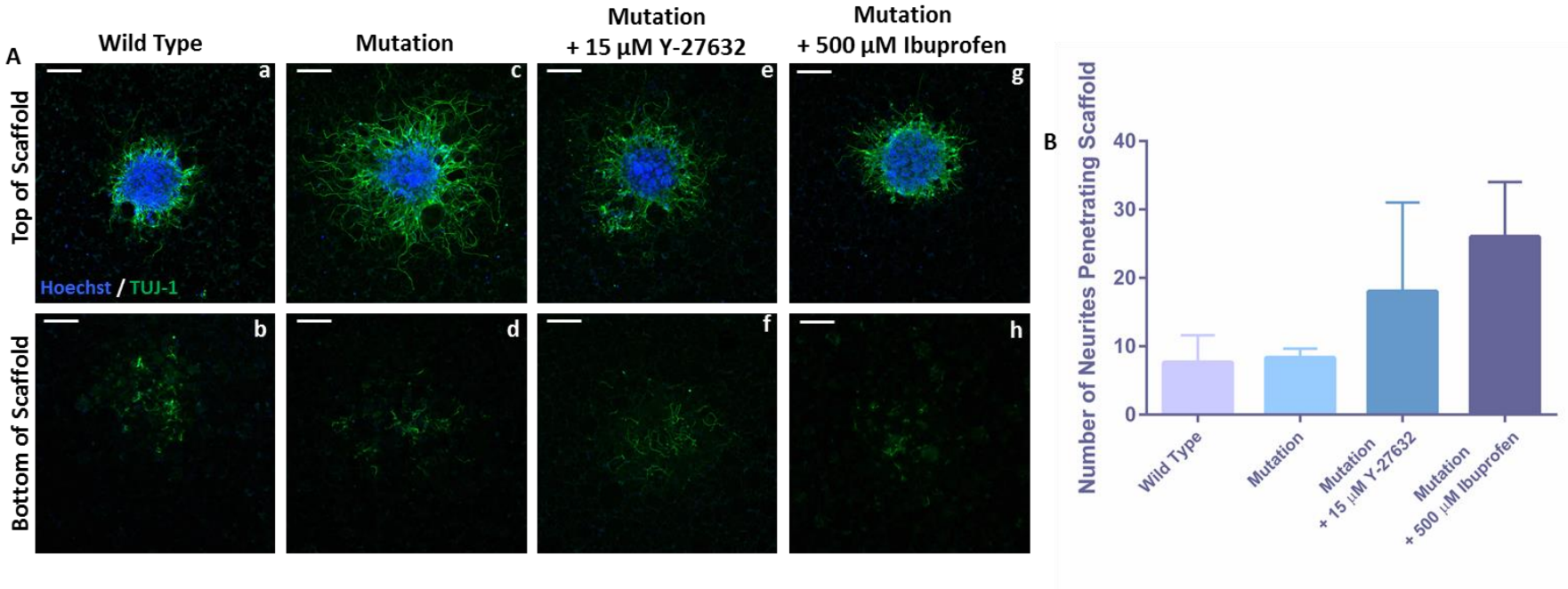

Fig 5-28: Enhancement of neurite outgrowth from Alzheimer's disease mutation derived neurospheres cultured in 3D by inhibition of Rho A and ROCK signalling.

Representative confocal images (A) of neurospheres derived from ReproNeuro mutation, Alzheimer's phenotype cells, cultured in 3D for 10 days with 15 µM Y-27632, a selective ROCK inhibitor or 500 µM ibuprofen, an inhibitor of Rho A. Neurospheres remain on top of the scaffold, as can be seen from the top view (Aa,c,e,g) while TUJ-1 positive (green) neurites penetrate the entire depth of the scaffold, visible from the bottom view of the scaffold (Ab,d,f,h), with nuclei being stained blue. Scale bars: 100 µm. Quantification of the number of neurites penetrating the scaffold (B) (data represent mean ± SEM, n=3-6; due to limited cell availability 3-6 neurospheres from 1 population of cells were quantified) reveals little difference between wild type and mutation derived neurospheres with both Y-27632 and ibuprofen supplementation enhancing the number of neurites penetrating the scaffold from mutation derived neurospheres. One-way ANOVA with Tukey's multiple comparisons: * = $p \leq 0.05$, ** = $p \leq 0.01$, *** = $p \leq 0.001$, **** = $p \leq 0.0001$.

5.3.6.3 Summary

A further comparison of each ReproNeuro cell type with each medium supplementation regime was conducted. Analysis of the number of neurites generated per neurosphere (Figure 5-29A) in 2D culture found that neurite number was reduced in patient and mutation samples compared with wild type. Y-27632 treatment was found to enhance neurite number from all cell types and restored neurite number to a level that was similar to wild type in patient-derived cells. Similarly, ibuprofen treatment resulted in similar number of neurites per neurosphere from all cell types. Neurite density (Figure 5-29B) of 2D cultures was significantly reduced in both patient and mutation-derived cells compared with control. This significant difference was reduced by both Y-27632 and ibuprofen treatment, restoring neurite density to a similar level as the wild type.

The length (Figure 5-29C) of neurites generated in 2D was significantly enhanced in patient-derived compared with wild type cells and mutation-derived cells also produced significantly longer neurites than their wild type counterparts, however mutation-derived neurites were significantly shorter than patient-derived neurites. Y-27632 and ibuprofen treatment had little effect upon neurite length. Similarly, the migration of cells from neurospheres (Figure 5-29D) in 2D culture was also significantly enhanced in patient-derived cultures with all medium supplementation. However, Y-27632 treatment did reduced migration in all cell types.

Neurite outgrowth in 3D culture (Figure 5-29E) varies little between the cell lines with Y-27632 treatment inducing a slight increase in neurite penetration whereas; ibuprofen treatment only induces an increase in patient-derived neurites.

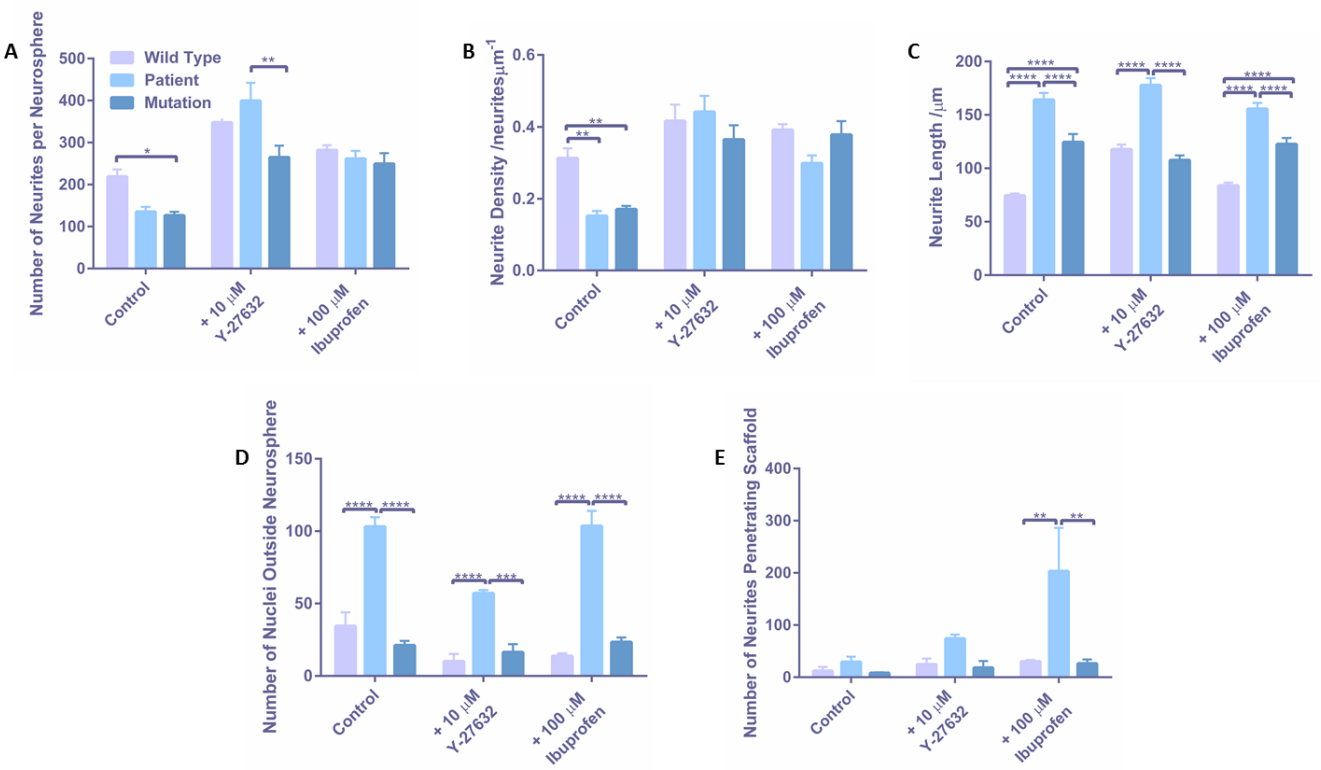

Fig 5-29: Comparison of the effect of ROCK and Rho A inhibition on Alzheimer's phenotype and wild type derived neurospheres cultured in 2D and 3D.
Quantification of neurite outgrowth from wild type, Alzheimer's disease patient and mutation derived neurospheres treated with an inhibitor of ROCK, Y-27632 and an inhibitor of Rho A, ibuprofen. Number of neurites per neurosphere (A) (data represent mean ± SEM, n=9; 3 individual neurospheres were quantified from 3 independent replicates) cultured in 2D and treated with Y-27632 and ibuprofen. The neurite density (B) (data represent mean ± SEM, n=9; 3 individual neurospheres were quantified from 3 independent replicates) of neurospheres cultured in 2D for 24 hours is inhibited in patient and mutation derived neurospheres compared with wild type, an effect that is rescued with both Y-27632 and ibuprofen treatment, aThe length (C) (data represent mean ± SEM, n=100; 100 neurites were measured from 3 neurospheres per independent replicate, of which there were 3) of neurites generated from 2D cultured neurospheres for 24 hours is greatly enhanced in patient derived neurospheres followed by mutation and wild type, a trend that is conserved with Y-27632 and ibuprofen treatment. Migration of cells (D) (data represent mean ± SEM, n=3; 1 individual neurosphere was quantified per independent repeat) from neurospheres cultured in 2D, is significantly enhanced in patient derived neurospheres than wild type or mutation, an effect that is maintained with both Y-27632 and ibuprofen treatment. The number of neurites penetrating the scaffold (E) (data represent mean ± SEM, n=3; due to limited cell availability 1-2 neurospheres from 1 population of cells were quantified) of neurospheres cultured in 3D is greater in patient derived neurospheres than wild type or mutation, an effect that is enhanced by Y-27632 and ibuprofen treatment. Two-way ANOVA with Tukey's multiple comparisons: * = $p \leq 0.05$, ** = $p \leq 0.01$, *** = $p \leq 0.001$, **** = $p \leq 0.0001$.

5.4 Discussion

5.4.1 β-amyloid-mediated Neurite Inhibition In Vitro

This chapter explores the role of Aβ in neurite inhibition through the use of several *in vitro* systems. The first of which involved the coating of growth substrates with Aβ peptides, which has previously been demonstrated to induce neurite inhibition in primary neurons by Postuma *et al*[40]. However, Postuma *et al* only analysed the effect of Aβ species upon neurite length, whereas data outlined in this chapter addresses the impact of Aβ-coating upon many aspects of neurite outgrowth including number, density and length. The data described in this chapter outlines an inhibitory relationship between all Aβ-species and neurite growth; however, it was found that the coating of growth substrates with the $A\beta_{42}$ peptide resulted in the largest reduction in neurite length. This finding is supported by Postuma *et al* who demonstrate the ability of $A\beta_{42}$ coatings to induce inhibition of neurite of neurite length to a greater degree than $A\beta_{40}$[40].

A study by Petratos *et al* also describes the ability of Aβ species to inhibit neurite growth in a SH-SY5Y model of neuritogenesis, when added exogenously to the culture medium[36]. This was further evidenced by data presented in this chapter as culture medium supplementation with both $A\beta_{40}$ and $A\beta_{42}$ resulted in significant reductions in neurite growth. Interestingly, Petratos *et al* found that $A\beta_{40}$, which is less prone to fibril formation and senile plaque generation, actually resulted in the largest reduction in neurite outgrowth within this model[36]. The data outlined in this chapter supports this finding as $A\beta_{40}$ was found to induce the largest reductions in neurite number and density. However $A\beta_{42}$ was found to have the largest impact on neurite length. This highlights an advantage of this stem cell-derived, neurosphere-based model of neurite outgrowth, as multiple variables and aspects of neurite outgrowth can be quantified. This gives a better indication as to the effect of a molecule upon neurite outgrowth because several aspects of neurite growth can be quantified including number, density and length, rather than relying on quantification of one variable alone.

Ageing of Aβ peptides through incubation at 37 °C is a common strategy to promote peptide aggregation and to present the peptides to cell cultures in a manner more befitting of the senile plaques encountered by cells in the brain of Alzheimer's disease patients[516,520,521]. However, throughout this chapter it was found that aged Aβ species impacted neurite growth the least, with fresh peptides actually inducing inhibition to a greater extent than their aged counterparts. This was also the case in Petratos *et al*'s study, which found that the aged $A\beta_{42}$ peptide was a less potent inhibitor of neurite growth than its fresh peptide counterpart[36]. This study hypothesised that the reduction in potency of aged peptides could be due to over aggregation, as large insoluble aggregates

may be generated that are unable to interact with cells. The level of peptide aggregation was then characterised by atomic force microscopy (AFM), which confirmed this hypothesis[36]. A similar finding is outlined in the protein aggregation assay data detailed in this chapter, as ageing of the $A\beta_{42}$ peptide resulted in such a high result that it exceeded the assay range. Therefore, it could be hypothesised that the reduced effects of aged peptides upon neurite outgrowth may be due to over aggregation of $A\beta_{42}$.

The substrate bound and medium supplementation approaches used to investigate Aβ-induced neurite inhibition in this chapter, provide simple, robust models of Aβ-cellular interaction. However, in the brain of both healthy individuals and AD-patients, a variety of different Aβ species exist, whereas, these models only involve the presentation of one type of Aβ peptide to neurites. Therefore to better recapitulate the *in vivo* environment, a variety of $A\beta_{42}$:$A\beta_{40}$ ratios were added to the culture medium of neurite outgrowth assays, as an increased level of $A\beta_{42}$ in comparison to $A\beta_{40}$ is a hallmark of AD[426–428]. In the healthy adult brain the Aβ composition is thought to be 10 parts $A\beta_{40}$ for every 1 part $A\beta_{42}$, whereas this ratio can differ up to 10-fold in the brains of AD-patients[426]. For this reason a variety of Aβ ratios ranging from 1:10 to 10:1 were tested to investigate the ability of neurites to grow in these culture conditions. Although there was little correlation between Aβ ratio and neurite number or density, neurite legnth was significantly inhibited by ratios higher in $A\beta_{42}$ than $A\beta_{40}$, consistent with the AD-phenotype.

A number of methodologies have been used to determine the role of Aβ species in neurite growth and development, all of which consistently provide evidence that $A\beta_{42}$ has a significant impact upon neurite length. Although $A\beta_{40}$ is less closely linked to senile plaque development and protein aggregation as $A\beta_{42}$ the data outlined in this chapter still found a correlation between neurite inhibition and $A\beta_{40}$ treatment through a number of model systems.

5.4.2 Neurite Inhibition in Alzheimer's Disease Phenotype Cells

iPSC technology offers the ability to develop physiologically relevant *in vitro* models of complex diseases that otherwise would be studied in much more simplified systems. AD model cells were first isolated in 2011 by Yagi *et al* from patients with early-onset familial AD and mutations in the genes for PS1 and PS2[157]. PS1 and PS2 form the γ-secretase complex involved in Aβ generation from APP, mutations of which lead to increased production of amyloidgenic species[411,461]. The iPSC AD-model line derived by Yagi *et al* was differentiated to form neuronal cultures that express higher ratios of $A\beta_{42}$:$A\beta_{40}$ indicative of AD[157]. The ReproNeuro AD-model neurons described in this chapter are similar to those described by Yagi *et al* in that they were derived from iPSC lines

developed from an AD-patient with a mutation in PS2 (R62H) or transfected with a similar mutation in PS1 (P117L)[212], resulting in an increased $A\beta_{42}$:$A\beta_{40}$ ratio[438].

ReproNeuro patient and mutation derived AD-model cells provide a more physiologically relevant *in vitro* system to investigate the process of Aβ-mediated inhibition compared with the more simple models described in this chapter that rely upon synthetic peptides. Both AD patient and mutation lines were found to produce fewer neurites with less dense neurite outgrowth than the wild type ReproNeuro line. However, cultures of patient cells produced significantly longer neurites than wild type cultures. One reason for this, could be that, as observed in 2D monolayer cultures patient-derived cells were a mixed population containing other cell types, which was also evident in neurosphere cultures.

Excessive cellular migration was observed in 2D neurosphere cultures of patient-derived cells, perhaps a result of the heterogenous cell population, which may provide a more permissive substrate for neurite development. One hypothesis is that neurites may grow over other cell types more easily than the plastic growth substrate resulting in their increased length, or that the population of cells may contain glial cells that provide neurotrophic support to the developing neurites[522–524]. However, it does appear that patient-derived cells are inherently different from wild type perhaps in more ways than just Aβ secretion and a thorough characterisation and evaluation of the cell types is required.

When patient and mutation-derived neurospheres were cultured in the 3D neurite outgrowth model using Alvetex® scaffold, it appeared that ReproNeuro AD-Patient cells generated more neurites capable of traversing the depth of the scaffold. If this result is considered alone, it might be thought that neurite outgrowth from patient-derived cells is enhanced, however, when taken into consideration with the 2D data, a more reliable picture of the neurite generating capability of patient-derived cells forms. Neurite length was enhanced from patient derived cells in 2D culture; therefore more neurites were capable of spanning the 200 μm depth of the scaffold. This may not be a true reflection of the neurite outgrowth capabilities of each cell type and highlights a limitation of the 3D model system in that only those neurites that are longer than 200 μm are quantified. Therefore, although a 3D culture environment provides a more physiologically representative model of neurite development, 3D and 2D obtained data should be closely considered together, as the 2D outgrowth model measures more variables and may be more sensitive to changes in neurite outgrowth between experimental conditions.

5.4.3 Proposed Mechanism of β-amyloid-mediated Neurite Inhibition

Petratos *et al*'s study into the neurite inhibitory properties of Aβ, implicates Rho A and ROCK signalling in this process and found that the selective ROCK inhibitor, Y-27632 was able to overcome Aβ-induced inhibition[36]. For this reason, ibuprofen an inhibitor of Rho A and Y-27632 an inhibitor of ROCK, were both used with the aim of reducing the inhibitory effect of Aβ upon neurite outgrowth. Various concentrations of Y-27632 and ibuprofen were used to overcome Aβ-induced inhibition in both the exogenous addition of Aβ to the culture medium, and AD phenotype cell models of neurite inhibition described throughout this chapter.

On the whole both Y-27632 and ibuprofen treatment was able to overcome Aβ-induced neurite inhibition in both 2D and 3D culture systems. However, Y-27632 and ibuprofen treatment often has unusual effects upon neurite legnth both in the presence and absence of an inhibitory stimulus, as described in Chapter III. This could be due to some kind of reciprocal control of neurite number and length, perhaps as inhibition of Rho A and ROCK results in the destabilisation of actin filaments, this may restrict filament length and therefore neurite elongation. Variable results in terms of neurite length in 2D often transcend into unexpected results in 3D culture due to the aforementioned limitations of the 3D-culture assay.

The ability of Y-27632 and ibuprofen to overcome Aβ-mediated neurite inhibition in these systems, suggests that Rho A and ROCK activation are integral signalling pathways involved in this process. In addition to this, Aβ is also known to bind to the NgR[504–506,509], activation of which leads to Rho A and ROCK stimulation, although it is not confirmed that Aβ binding results in receptor activation[324,325,331,332]. Therefore, one proposed mechanism of action is that, Aβ-binding activates NgR leading to Rho A and ROCK activation resulting in neurite inhibition and growth cone collapse, similar to the signalling pathway evoked by inhibitory molecules within the glial scar (outlined in Figure 5-30).

To test this hypothesis, the NgR antagonist Nogo extracellular peptide (NEP 1-40), was added to inhibition models to potentially overcome Aβ-mediated inhibition, implicating receptor activation in the downstream signalling pathway. NEP 1-40 is an NgR competitive antagonist comprised of the first 40 amino acids of the Nogo-66 molecule, which binds to the leucine-rich region of the receptor blocking the inhibitory effects of Nogo-66. Therefore if NEP 1-40 was able to promote recovery of neurite outgrowth in the presence of Aβ, it might suggest that receptor activation is involved in the molecular pathway stimulated by Aβ that leads to neurite inhibition. However, the data only demonstrates a partial recovery of Aβ-induced inhibition with NEP 1-40 supplementation

in all model systems, suggesting that NgR activation may be one of multiple pathways involved.

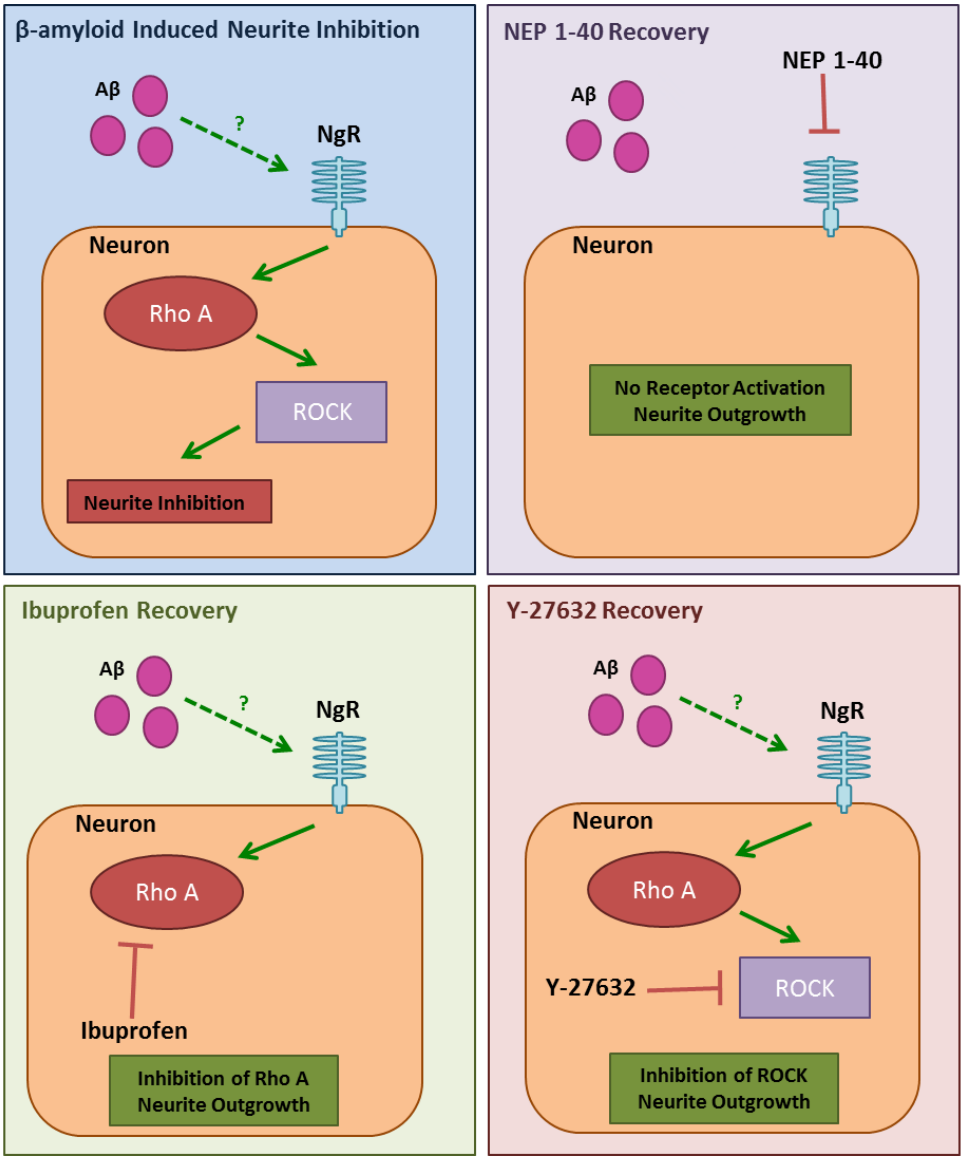

Fig 5-30: A schematic summary describing the molecular mechanisms of Aβ-induced neurite inhibition with mechanisms of recovery.
Aβ is thought to bind to the NgR resulting in activation of Rho A and ROCK signalling that ultimately results in changes in actin dynamics leading to growth cone collapse and neurite inhibition. NEP 1-40 is a receptor antagonist peptide thought to block NgR signalling, providing recovery and restoring neurite outgrowth in the presence of Aβ. Ibuprofen inhibits Rho A downstream of NgR signalling and Y-7632 inhibits ROCK downstream of Rho A, both of which lead to inhibition of NgR-mediated intracellular signalling and restoration of neurite outgrowth.

5.5 Key Findings

- Aβ species were inhibitory to neurite outgrowth both in substrate bound and soluble forms.

- High ratios of $A\beta_{42}$:$A\beta_{40}$ reminiscent of AD were particularly inhibitory to neurite length in 2D culture.

- Inhibition of Rho A (ibuprofen) and ROCK (Y-27632), was able to overcome Aβ-mediated inhibition in 2D and 3D culture.

- The NgR antagonist NEP 1-40 was able to partially restore neurite outgrowth, despite the presence of inhibitory Aβ.

- AD model iPSC-derived neurons produced fewer, longer neurites than their WT counterparts.

- AD patient-derived neurons appeared to be a heterogenous mix of neurons and glial cells.

- Inhibition of Rho A and ROCK was able to restore neurite outgrowth to WT levels in AD phenotype cell lines.

5.6 Conclusion

This chapter has involved the evaluation of the role of Aβ in neurite outgrowth in several different *in vitro* systems. These range from simple Aβ coating of growth substrates to complex iPSC-based diseased models, the suitability of which depends upon the application for which it is intended. More simple models of inhibition such as Aβ medium supplementation are useful to provide insight into specific underlying molecular mechanisms, however do not accurately reflect the complex *in vivo* environment. More complex models such as Aβ ratio administration and the use of disease model cells described within this chapter have useful applications in the understanding of complex pathways involved in AD pathogenesis, however their complexity may inhibit the successful identification of key signalling pathways.

In addition to the identification of the neurite inhibitory properties of Aβ, this chapter also discusses the potential signalling mechanisms that result in neurite inhibition as stimulated by Aβ. In particular, this has focussed on the Rho A and ROCK signalling pathway, inhibitors of which have been used to restore neurite growth in the presence of inhibitory Aβ species. This provides a therapeutic target in that attenuation of Rho A/ROCK signalling could provide a potential strategy to induce neural regeneration within neurodegenerative diseases. Furthermore, this chapter also identifies NgR as a potential receptor through which Aβ elicits it neurite inhibitory signalling, in addition to other potential pathways.

This chapter has also describes the development of a novel neurosphere-based neurite outgrowth model utilising AD disease model neuroprogenitor cells. This methodology could also be adapted for use with other disease model cell types including Parkinson's disease, to provide more information as to the development of neurites within these complex diseases. There are also personalised medicine implications as iPSC lines could be generated on a patient-specific basis and used within this neurite outgrowth assay with the application of screening potential drugs for the promotion of regeneration.

5.7 Future Directions

Future work building upon the data described in this chapter could include the following:

- Receptor-binding studies could be conducted to determine the ability of Aβ to bind and activate NgR within this model.

- AFM analysis could be used to further characterise the aggregation properties of each Aβ species.

- To further validate the proposed mechanism of Rho A and ROCK activation leading to growth cone collapse, other modulators of Rho A and ROCK signalling could be used to potentially recover neurite growth in the presence of Aβ. These might include C3 transferase and fasudil, which have been well documented to promote neurite regeneration.

- Other signalling mechanisms involving other aspects of the cytoskeleton could be explored including the involvement of the microtubule and intermediate filament-based cytoskeletal components.

- Genotypic analyses could be used to determine any differences between the wild type, patient and mutation-derived ReproNeuro cell types other than mutation in PS1 and PS2.

- The fundamental methodology developed within this chapter involving iPSC-derived AD model neurons could be applied to study the process of neurite development in other neurodegenerative diseases such as Parkinson's disease.

Chapter VI: Application of Biomimetic Surfaces to Study the Role of Extracellular Molecules in Neurite Outgrowth and Inhibition

6.1. Introduction

Previously, we have described how 3D technology can be used to enhance current *in vitro* models of neurite outgrowth (Chapter III), providing a more physiologically relevant situation to study developing neurites. In this chapter, we build on this, by using protein surface technology to recapitulate the native biochemical environment which developing neurites are exposed to *in vivo*. This not only helps to better represent the developmental process of neurite generation but also helps standardise this model of neurite outgrowth, providing a more reliable screening tool for the identification of degeneration/regeneration-promoting molecules. This combination of technologies helps to further enhance the novel model of human neurite outgrowth described in Chapter III.

6.1.1 The Role of the Extra-Cellular Matrix in Neurite Outgrowth

During neuritogenesis the ECM plays a pivotal role in providing adhesion points to maturing neurons and neurites whilst also providing neuritic growth cues along with forming a permissive environment for neuron maturation[525]. Guidance cues such as those provided by the ECM are essential for the correct development of a functional neural network[526]. Cues from the ECM are transmitted to the developing neuron by integrin receptors found at the developing growth cone and provide specific binding sites for ECM components and modulate cellular responses to guidance cues[526]. Interactions between integrins and specific biochemical signatures within the ECM results in axonal outgrowth and pathfinding behaviour essential for the correct assembly of the nervous system.

The ECM consists of a heterogenous mix of glycoproteins and proteoglycans that from the external microenvironment which a cell is exposed to[526]. The ECM often includes components such as laminin, fibronectin, collagen, tenascin and heparan sulphate proteoglycans (HSPGs), which are secreted by neurons and their supporting cells into the interstitial space. Large ECM proteins often form an immobilised, self-assembled, rigid scaffold that physically supports cellular adhesion and provides traction forces[526]. Both the mechanical and biochemical properties of the ECM influence cellular behaviour and this should be taken into consideration in the development of *in vitro* models.

Different constituents of the ECM have been reported to positively and negatively effect axonal growth *in vitro* and *in vivo* and some ECM proteins also work cooperatively with soluble growth factors to impact axonal outgrowth[11]. Collagens are expressed throughout the nervous system and have been demonstrated to play essential roles in axon guidance, pathfinding, target recognition and sprouting[526–532]. Interestingly, a C. *elegans* collagen type XV/XVIII mutant model results in disruption of normal motoneuron migration and motor axon guidance[533], highlighting the important role of collagens in neurite outgrowth. Laminins are perhaps the most widely studied ECM component in terms of neurite outgrowth promoting properties that include regulation of neuron adhesion, motility and differentiation[526], which will be discussed in detail in *6.1.2 Laminin Promotes Neurite Generation*.

Tenascins are a family of oligomeric glycoproteins that mediate neuronal-glial interactions and can be both inhibitory to neurite outgrowth or neurite promoting[534–539]. Tenascins consist of varying numbers of functional domains that have differential effects upon neurite outgrowth[540]. The EGF-like region of TN-R is inhibitory to neurite outgrowth and exhibits anti-adhesive properties, whereas, FN-II domains of TN promote adhesion and neurite outgrowth[541]. The role of fibronectin in neurite development, however, is thought to be more simple than that of tenascin and supportive in nature[526]. The functions of fibronectin within the nervous system involve promotion of neuronal survival, differentiation and morphogenesis, which have been evidenced in a number of *in vitro* cell-based studies[273,274,542–547].

6.1.1.1 Integrin Receptors and Neurite Outgrowth

Integrins are a family of receptors that are heterodimeric and consist of an α and β subunit, of which there are known to be eighteen different α subunits and eight different β subunits with 24 combinations of integrin complexes[526]. The role of integrin receptors is to promote cellular-ECM interactions. In the nervous system high integrin expression is observed during development[548–551] whilst in the mature nervous system progenitor and stem cells express high levels of integrins[552,553]. This is due to the integral role of integrins in mediation of the effects of the ECM upon neurite outgrowth, promoting neuronal migration and axonal generation during development[526].

Within the neuronal growth cone, integrins interact with the ECM to form adhesion complexes that form within filopodial and lamellipodial protrusions and remain in a fixed position during neurite elongation[554–557]. Adhesion complexes contain components such as integrins, paxillin and viniculin similarly to fibroblast focal adhesion complexes. Viniculin and paxillin are adaptor proteins that form a link between the actin cytoskeleton, one of the driving forces in neurite growth, and the extracellular

environment in the form of integrin-generated signals[557]. Adhesions have been observed by Robles and Gomez to cluster along bundles of actin filaments suggesting that external stimuli from the ECM via integrin mediated signalling, impacts neuritogenesis through an actin dependent mechanism[557].

Other signalling molecules found within adhesion complexes at the neuronal growth cone include non-receptor tyrosine kinases (NTKs), focal adhesion kinase (FAK) and Src[207,557–560]. These kinases modulate the downstream signalling of a number of receptors and interact with several signalling pathways to control cellular motility and neurite elongation. Downstream signalling of integrin activation includes the Rho family of GTPases such as Rac 1 and Rho A. Integrin activation and its downstream events result in Rac 1 activation and Rho A inhibition, which promotes actin polymerisation and growth cone advancement[284,561]. However, this signalling pathway exists in a balance with Rho A and ROCK activation leading to increased actomyosin contractility and growth cone collapse, as shown in Figure 6-1, which is important during development to promote growth cone stalling or turning[526]. This balance may exist through the binding of growth promoting or inhibitory ligands to integrins or as a result of re-association of FAK-associated protein complexes[526].

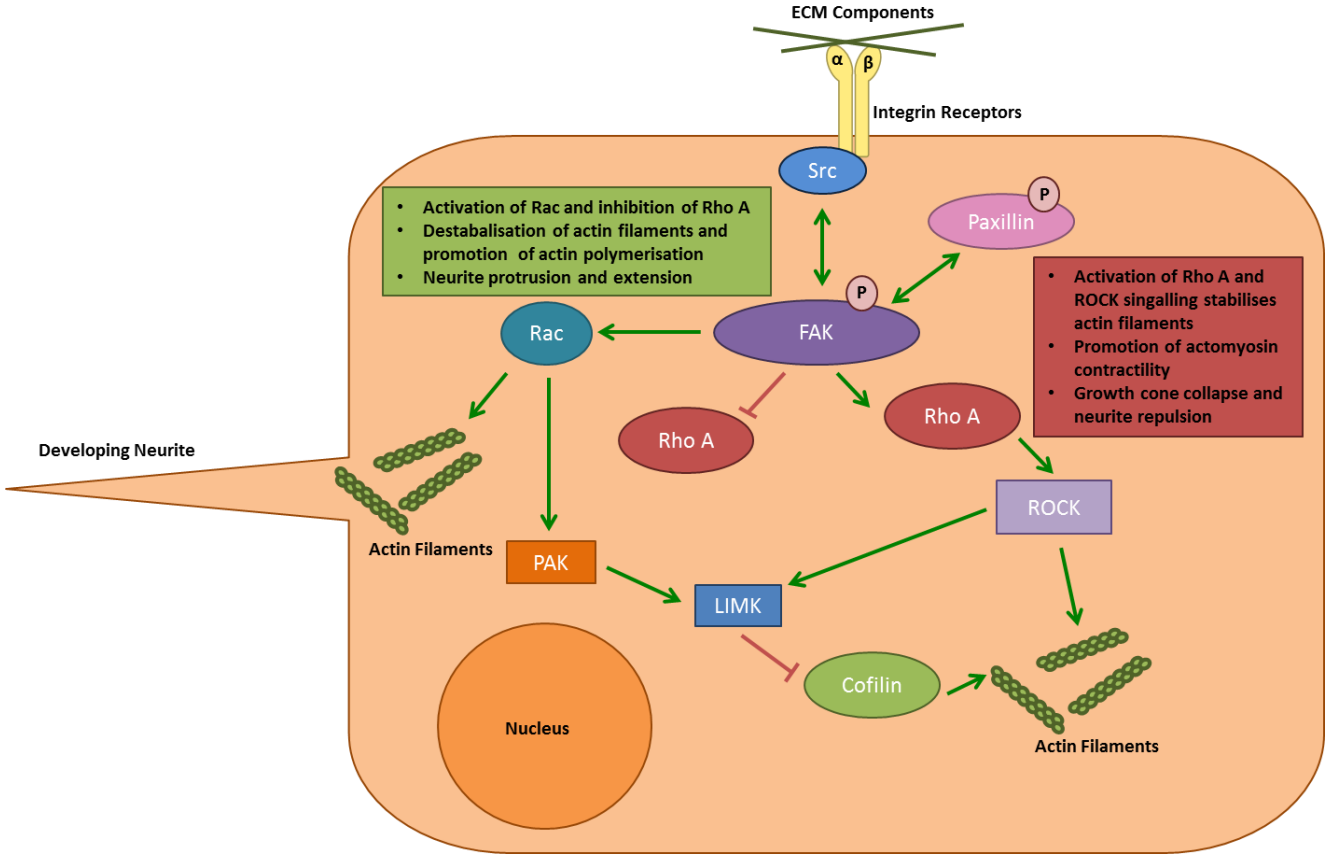

Fig 6-1: Integrin mediated control of neurite outgrowth.
A schematic depicting the role of ECM-integrin interactions and their role in neurite development and inhibition. Integrin signalling is mediated by a Src-FAK complex that promotes neurite extension through activation of Rac 1 and inhibition of Rho A. However, shifting the balance toward Rho A activation and away from Rac 1 activity results in a reduction in actin polymerisation and enhancement of actomyosin contractility resulting in growth cone collapse and axon retraction.

6.1.2 Laminin Promotes Neurite Generation

Laminin is a major component of the ECM in most physiological systems. It particularly is abundant in both the mature and developing nervous system. Laminins are heterotrimeric glycoproteins and consist of α, β and γ chains that are organised in a characteristic cruciform structure (Figure 6-2)[526]. At the moment, five different α, three β and three γ chains have been identified that combine to give over 15 different combinations of laminin isoforms[526,530,531]. Plantman *et al* determined in DRG model neurons that specific integrin complexes are responsible for the neurite outgrowth promoting effects of each laminin isoform[562]. This study identified the role of integrins α3β1 and α7β1 in mediating neurite growth on laminin-1 and -2 substrates and integrin α6β1 was found to be responsible for induction of neurite growth on substrates of laminin-8 and -10[562].

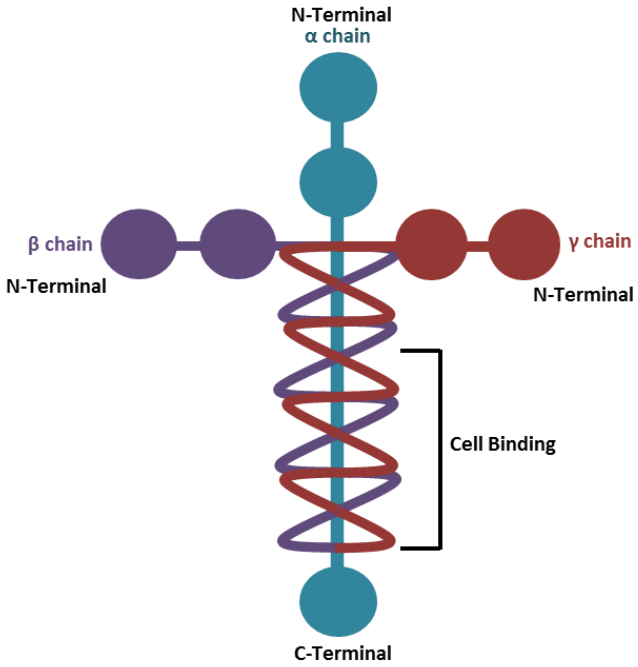

Fig 6-2: Cruciform structure of laminin.
A schematic depicting the molecular structure of laminin, consisting of three interweaving chains: α, β and γ.

Many *in vitro* neuronal culture models have documented the neurite enhancing effects of laminin, with identification of specific neurite promoting domains. Specifically the "IKVAV" domain of the α1-chain has been well documented to have neurite induction qualites[271,272,563,564], as demonstrated by Nomizu *et al* who use a synthetic peptide analogue to investigate the neurite promoting effects of the "IKVAV" domain[564]. Similarly, Adams *et al* describe the role of "IKVAV" as a guidance cue and observed growth cone turning with neurites preferentially extending along a gradient of the substrate bound peptide[271]. The domain "IKVSV" similar to the widely studied "IKVAV" motif has also been described to promote cell attachment and neurite outgrowth by Nomizu *et al*[564]. This suggests that a subtle change of one amino acid to the sequence does not greatly affect the biological function of the molecule in terms of neurite outgrowth at the concentrations tested within this investigation.

Previously "IKVAV" was thought to be the active site of laminin, and the sequence responsible for its neurite induction qualities, however, it was then discovered that a range of amino acid sequences were capable of neurite induction. Liesi *et al* identified the "RNIAEIIKDI" motif as playing an important role in neurite elongation and cell adhesion[275]. This was investigated through a competition assay whereby primary rat cerebellar neurons were cultured on a substrate coated with laminin and a synthetic peptide containing the "RNIAEIIKDI" sequence was added to the culture medium[275]. This resulted in the synthetic peptide competing for cellular binding against the laminin coating; therefore, fewer cells adhered to the growth substrate and developed neurites[275]. In addition to this Liesi *et al* also demonstrate the neurite promoting properties of "RNIAEIIKDI" in a traditional neurite outgrowth assay on growth substrates coated with the synthetic peptide[275].

Therefore, laminin has been well documented to enhance neurite outgrowth, playing an important role *in vivo* during neuronal development and also forming the basis of many *in vitro* cell culture substrates to enhance neuronal cultures. Specific neurite-promoting domains of laminin have been identified with "IKVAV" perhaps being the most widely studied, however more amino acid sequences are being uncovered to determine the specific molecular events that lead to laminin induction of neurite outgrowth. This is important as inhibition of laminin attachment and signalling is thought to be one of the mechanisms by which neurite outgrowth is inhibited in the injured spinal cord.

6.1.3 The Role of Laminin in Neurite Inhibition

The neurite enhancing properties of laminin are thought to be impaired in the glial scar that arises following spinal cord injury resulting in inhibition of neurite growth (for a comprehensive review of glial scar signalling see Chapter IV). Inhibitory molecules such

as those found on damaged myelin and CSPGs secreted from reactive astrocytes are thought to impair laminin-receptor binding, reducing the sensitivity of neurons to laminin-induced neurite generation.

McKeon *et al* describe the culture of neurons upon glial scar tissue containing CSPGs, derived from injured rats[317]. Treatment with chondroitinase ABC, led to an increase in neurite outgrowth upon the inhibitory substrate, however this recovery effect was reversed when blocking antibodies to the laminin β2 chain were applied[317]. This suggests that recovery and growth of neurites within the injured spinal cord is dependent upon the presence of laminin and that CSPGs may act as inhibitors of laminin mediated growth. Similarly, Friedlander *et al* discuss the ability of CSPGs to inhibit ECM-neuronal interactions through binding to N-CAM adhesion molecules[261]. N-CAM and Ng-CAM are adhesion molecules with important roles in neuronal development and are known to bind laminin[565,566]. Friedlander *et al* identify the ability of CSPGs to bind to both N-CAM and Ng-CAM inhibiting the ECM-neuronal interactions and resulting in neurite inhibition[261,315].

Similarly, the regenerative capacity of the PNS compared with the CNS is thought to be attributed to the laminin content of the ECM. Myelin inhibitors of neurite growth found in the injured central nervous system such as MAG have also been identified in the PNS, which was initially thought of as unusual due to the regenerative capacity of the PNS[567–569]. However, a study by David *et al* describes the ability of laminin to overcome MAG mediated neurite inhibition and the differences between the ECM content of the PNS and CNS, resulted in the observation that the inability of CNS neurons to regenerate may be due to an absence of laminin in the ECM[570].

Understanding the interactions between the ECM and developing neurons is important to help unveil the developmental events that result in neuronal maturation. Due to its role in neurite inhibition, understanding the specific role of laminin in neurite outgrowth may be an important factor in the development of therapeutics and to increase our understanding of the events that occur following injury to the nervous system.

6.1.4 In Vitro ECM Coatings

As discussed previously (Chapter I), to create *in vitro* models that best reflect the *in vivo* system, each aspect of the cellular microenvironment should be considered[161]. This includes the biochemical composition of the ECM and is the reason why many cell-based models include the coating of growth substrates with ECM components[161]. ECM coating procedures usually require incubation of growth substrates with solutions containing the desired molecule, which then adsorb onto the growth surface[571,572].

Most neuronal-based culture models require coating of growth substrates with laminin prior to cellular seeding to ensure correct neuronal development and neuritogenesis[573–579]. For example, a neurite outgrowth assay described by Smit *et al* based on PC12 cells, requires different ECM coatings to promote either cellular proliferation or differentiation[580]. To induce neuritogenesis within this assay Transwell™ 3D culture inserts were coated with laminin to promote neurite growth, which can then be quantified. Protocols such as this harness the neurite promoting properties of laminin to enhance their models and provide a more physiologically relevant environment for neurite development by recapitulating the biochemical environment of the developing nervous system.

6.1.5 Biomimetic Surfaces

In vitro tissue and disease modelling is beginning to increase in popularity due to the ethical issuesand regularions associated with animal models. Therefore, there is a great deal of interest in recapitulating the native cellular microenvironment to produce the most physiologically relevant models possible. This includes recreating cellular-matrix interactions that are paramount to so many cellular functions. Presentation of ECM-molecules to cells within culture systems can be achieved in many ways, including the use of ECM-based hydrogels such as collagen gels, traditional ECM adsorption coating or the use of biomimetic surfaces[581].

Biomimetic surfaces mimic many aspects of the ECM in tissues and can provide biochemical cues and cell-matrix interactions to promote tissue growth and formation[581]. There are two design strategies usually employed to produce functional biomimetic biomaterials, one of which involves the incorporation of soluble bioactive molecules such as growth factors into the biomaterial that are released over time to modulate tissue formation[582–584]. Another methodology involves the incorporation of peptide motifs or whole molecules by chemical or physical modification to present the bioactive sequences to cells cultured on the surface of the material[585–588]. There are many factors to consider in the design of biomimetic surfaces such as, concentration and spatial distribution of modified bioactive molecules, which must be optimised to produce the best possible growth surface[581].

Identification of specific bioactive domains within ECM-molecules that are responsible for receptor interaction, has allowed the generation of biomaterials containing just the bioactive sequence. The use of short bioactive peptides as oppose to whole ECM molecules is beneficial, as native ECM proteins are able to randomly fold which may inhibit presentation of the receptor-binding domain[581]. Short peptide sequences however, are more stable during the modification and coating process therefore in most cases the

modified peptide is available for cell binding[581]. Furthermore, the large-scale production of short peptide chains is more economically favourable and results in the same biological effect, as the active sequence of the molecule is presented[581].

Perhaps the most commonly used peptide incorporated into such systems is the "RGD" domain derived from fibronectin and laminin[589–593]. "RGD" is a motif heavily involved in cell adhesion and is incorporated into many biological surfaces to render surfaces adhesive that are usually inherently non-adhesive to cells[594–596]. Similarly, specific domains from laminin have been identified and incorporated into biomaterials to produce permissive growth environments for neuronal development and neurite extension. These include the "IKVAV", "RNIAEIIKDI" and "YIGSR" laminin domains that induce neural differentiation and development in desired systems[597–599].

Peptides such as these have been immobilised on a series of materials including glass[600,601], quartz[602], metal oxide[603] and polymers[604,605], a number of coupling techniques have also been employed. One immobilisation technique involves the use of reactive moieties on the surface of the material (usually NH_2) that react with functional groups such as COOH on the bioactive peptide[581]. Another approach can be the use of bi-functional long spacer arm cross linkers that can immobilise the bioactive peptide to the growth surface whilst enabling the peptide to move flexibly within the culture enrionment[602]. A photochemical immobilisation method has been employed to couple peptides to polymer substrates that lack appropriate functional groups[606].

Biomimetic materials such as these provide a more physiological relevant microenvironment for the culture of cells, which has application purposes in the field of tissue engineering for both transplantation or *in vitro* tissue modelling[581]. Modified bioactive growth surfaces can also be used to elucidate cellular responses to specific biochemical cues, to help gain understanding into the downstream signalling events initiated by cell-matrix interactions[607]. Similarly, surfaces such as these provide opportunities to study cellular behaviour in a defined manner such as the effect upon cellular function of density and spatial distribution of bioactive domains[581].

6.1.5.1 OrlaSURF Platform

The OrlaSURF platform is a method of peptide immobilisation to provide biomimetic surfaces for cell culture and tissue engineering purposes. Initially optimised on gold surfaces the technology involves the use of an engineered N-terminal transmembrane domain from *Esherichia coli* outer membrane protein, Omp A[608–610]. Specific bioactive ECM motifs are then engineered into the flexible outer loops of Omp A and the protein attaches to the biomaterial through a single cysteine residue[608–610]. This results in the formation of

an orientated peptide monolayer. The space between the peptide motifs can then be filled using thiolipids or thioalkanes to ensure the active motifs are exposed. This technology results in stable, orientated monolayers of peptides, displaying the motifs of interest in a functional conformation and alleviating the many problems associated with adsorption coating[608–610].

OrlaSURF technology is now used to produce commercially available functionalised cell culture growth substrates that overcome some of the problems associated with other coating methods[611]. Orla surfaces contain peptide motifs displayed in the precise orientation for cellular engagement resulting in high levels of reproducibility and functionality, as shown in Figure 6-3[612]. The technology is based on the combination of robust bacterial proteins and thiliolipids, involving a surface-binding unit (SBU) that connects target proteins/motifs to growth surfaces.[612] This allows for flexible engineering, as target peptides can be presented in a number of orientations such as loops, linear motifs or full-length peptides[611]. This technology can be used to functionalise a range of surfaces including gold, plastics, glass, polymers and metal oxides, along with offering the ability to produce heterogenous multi-protein surfaces or homogenous single-protein surfaces[611].

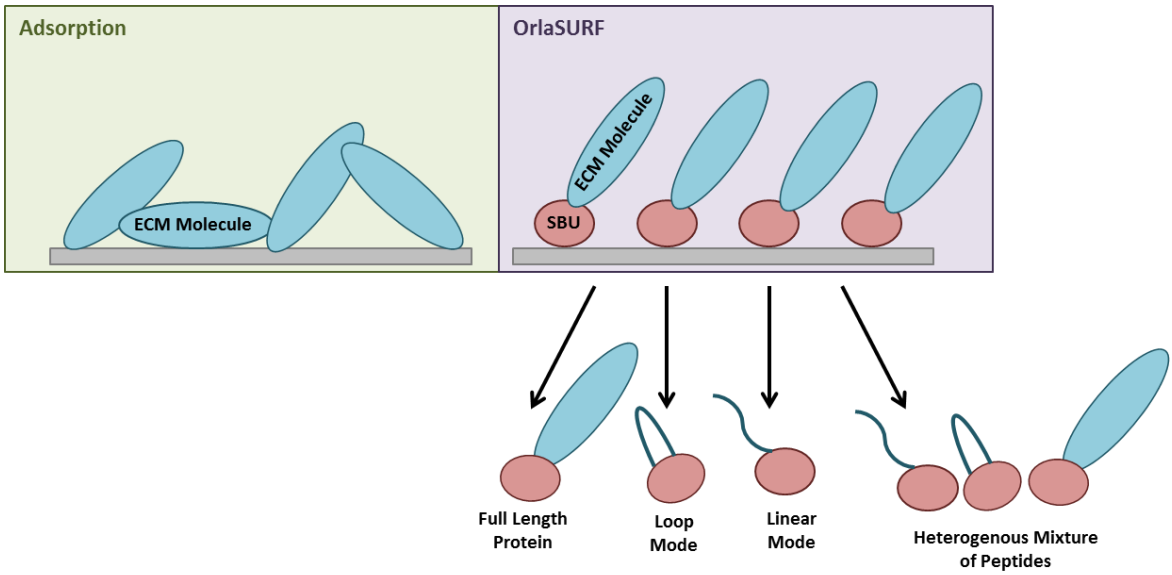

Fig 6-3: Comparison of traditional adsorption coating of growth substrates with the OrlaSURF platform.
A schematic depicting the differences between traditional adsorption coating of growth substrates with ECM molecules and application of OrlaSURF, which immobilises peptide sequences in the correct orientation to interact with cells. OrlaSURF also allows for the presentation of whole ECM-proteins or smaller peptide motifs displayed in a loop or linear fashion.

Adsorption	OrlaSURF
Lack of orientation	Precise orientation
Denaturation	Structurally intact
Poor functionality	Functionality retained
Inaccessible active sites	Accessible active sites
Poor reproducibility	Excellent reproducibility

Table 6-1: Advantages of OrlaSURF platform over traditional adsorption coating. OrlaSURF immobilies specific peptide domains onto cell culture growth substrates in the correct orientation to interact with cells. This has advantages over traditional adsorption coating of growth substrates including enhanced reproducibility and functionality.

This technology has previously been used to enhance cell adhesion upon substrates coated with various ECM-molecules. Cooke *et al* describe the culture of PC12 cells upon growth substrates coated by adsorption technique with collagens, fibronectin and laminin in comparison to substrates coated using an Omp A immobilisation technique[610]. It was found that cells were able to attach to growth substrates coated via Omp A and that each ECM molecule had varying effects upon cellular adhesion[610].

Another study by Cooke *et al* describes an application of this technology to investigate the ability of ECM-derived motifs to induce neuronal differentiation and neurite outgrowth in PC12 cells[613]. This study was able to identify specific neurite enhancing motifs and compare the ability of several ECM-derived amino acid sequences to induce neuritogenesis[613]. Sequences derived from collagen I and IV were found to enhance the number of neurites per cell and mean neurite length whereas a laminin motif "YIGSR" was found to enhance branching[613]. This demonstrates the application of such technology to study the important role of specific ECM-constituents in neuronal and neurite development.

6.1.6 Conclusions

The ECM provides biochemical cues that contribute toward the cellular microenvironment and recreating such cues is an important factor in the development of tissues and cell based models *in vitro*. Recapitulating aspects of the cellular microenvironment is important in ensuring that cellular behaviour is as similar to their *in vivo* counterpart as possible, therefore producing physiologically relevant and reliable *in vitro* models. The role of the ECM is particularly important in neuronal development, as integrin-ECM mediated signal transduction is important in the stimulation of neurite extension and guidance. Understanding the role of specific ECM-components in neurite

development such as laminin and its active domains has implications in the development of potential therapeutic interventions. For example, CSPG-mediated glial scar signalling may be targeted, as one mechanism of action of CSPGs is thought to be inhibition of laminin signalling. Furthermore, biomimetic surfaces offer novel, robust and reproducible bioactive growth substrates that enable investigations into the role of ECM-specific peptide domains in cellular processes. Initial studies have shown the application of OrlaSURF technology to study the role of ECM-derived motifs in the process of neuronal and neurite development. This caims to address the role of the ECM, with particular focus on the role of laminin, in neurite development and the application of OrlaSURF to study the process of neurite inhibition and recovery.

6.1.6.1 Chapter Aims

This chapter aims to investigate the role of the ECM in the process of neurite development, along with the specific role of laminin in neuritogenesis. This chapter discusses the ability of several ECM-derived peptide motifs from collagen, laminin and fibronectin to induce neuritogenesis, along with identifying specific laminin domains that actively in the induce neuritogenesis. A comparison of traditional laminin adsorption coating and OrlaSURF laminin coating is also discussed within this chapter along with multiple analytical methodologies to compare the different coating techniques. Additionally this chapter also aims to provide a potential application of biomimetic surfaces in the study of myelin-induced neurite inhibition, a component of the glial scar that follows spinal cord injury.

To investigate this process, this chapter describes the coating of surfaces via OrlaSURF with known inhibitors of neurite outgrowth including OMGP and Nogo (for a detailed review of Nogo and OMGP induced signalling see Chapter IV), and the ability of modulators of Rho A and ROCK to overcome myelin-induced inhibition. The aim of this is to help elucidate the molecular mechanisms that underpin myelin-mediated neurite inhibition and to provide a potential application of this technology as a screening tool to identify the ability of compounds to overcome inhibitory stimuli.

We hypothesise that growth substrate coated laminin-derived domains will enhance neurite outgrowth in this model, as there is a wealth of evidence described in the literature that support the role of laminin in neurite development. We also hypothesise that coating of growth substrates with Nogo and OMGP found in the glial scar will negatively impact neurite outgrowth. This inhibition should be recovered through application of NEP 1-40, ibuprofen and Y-27632, to intervene at each stage of the downstream signalling cascade, activated by Nogo and OMGP. This will provide a potential application of the model to be used as a screening tool, either to detect

compounds capable of induction of inhibition or recovery of neurite outgrowth. Overall this chapter aims to functionalise Alvetex® scaffold to provide a biochemically favourable environment for the development of neurons and to produce a physiologically relevant model of neurite development and inhibition.

6.1.6.2 Chapter Objectives

- Investigate the role of collagen, fibronectin and laminin-derived sequences in the induction of neurite outgrowth in 2D and 3D culture.

- Determine the ability of Orla poly-D-lysine and laminin coating to induce neurite outgrowth compared with the standard coating solution of poly-D-lysine and laminin used to develop this human stem cell-derived model of neurite outgrowth.

- Investigate the potential of laminin to enhance neurite outgrowth in a dose-dependent manner.

- Compare the effect of whole molecule laminin adsorption and Orla laminin coating on neurite outgrowth in 2D and 3D culture.

- Determine the ability of a range of laminin-derived domains to induce neurite outgrowth in 2D and 3D culture.

- Analyse the ability of OMGP and Nogo coatings to induce neurite inhibition in 2D and 3D culture.

- Determine the ability of Rho A (ibuprofen) and ROCK inhibition (Y-27632) to overcome inhibition of neurite outgrowth mediated by the myelin inhibitors found in the glial scar (OMGP, Nogo).

6.2 Materials & Methods

6.2.1 Seeding of Neurospheres on Orla Surfaces

Cell culture growth surfaces coated using OrlaSURF technology (Orla Protein Technologies, Newcastle, UK) were used to culture neurospheres and to assess the impact of varying extracellular molecules on neurite outgrowth, including those found in the ECM. For 2D neurite outgrowth studies, neurospheres were seeded into 6-well tissue culture plates (Orla Protein Technologies) coated with a peptide of interest, which do not require any additional treatment. For 3D neurite outgrowth studies, neurospheres were seeded onto 6-well Alvetex® Scaffold (ReproCELL Europe) coated with a peptide of interest (Orla Protein Technologies). Coated Alvetex® Scaffolds were prepared by ethanol washing to ensure a hydrophilic surface for cell attachment and media permeation; this was achieved through briefly dipping the scaffold in 70 % ethanol for 10 seconds, followed by 2 washes in PBS. Neurospheres were seeded onto both 2D and 3D surfaces as described in *2.2.6.2 Seeding of Neurospheres for Neurite Outgrowth Assays.*

6.2.2 Coating of Growth Substrates with Laminin from Engelberth-Holm-Swarm Murine Sarcoma Basement Membrane

Alvetex® Scaffold 12-well format inserts (Reinnervate) were prepared by plasma treatment using the K1050X Plasma Asher at a power level of 40 W, for 5 mins. Treated scaffolds and conventional 48-well tissue culture treated plates were coated overnight at room temperature with varying concentrations (0.05 – 50 μgmL^{-1}) laminin coating solution. Coating solution was prepared by adding the desired volume of 1 $mgmL^{-1}$ Laminin from Engelberth-Holm-Swarm murine sarcoma basement membrane to PBS without Ca^{++}, Mg^{++} to achieve the preferred concentration of coating. For example, to achieve a coating concentration of 50 μgmL^{-1}, 0.5 mL of 1 $mgmL^{-1}$ Laminin from Engelberth-Holm-Swarm murine sarcoma basement membrane was added to 9.5 mL PBS. To each well of a 48 well tissue culture plate, 150 µL coating solution was added and 300 µL coating solution was added to each Alvetex® Scaffold. Following overnight incubation at room temperature, coating solution was removed and growth substrates were washed three times with PBS and stored in PBS prior to neurosphere seeding.

Sequence	Molecule	Product Code
MNYYSNS	Collagen IV	ORLA165
RGDS	Fibronectin	ORLA153
YIGSR	Laminin β1	ORLA163
IKVAV	Laminin α1	ORLA162
IKVSV	Laminin α2	ORLA189
VRWGMQQIQLVV	Laminin α5	ORLA230
DITYVRLKF	Laminin γ1	ORLA236
RNAIAEIIKDI	Laminin γ1	ORLA239
-	Nogo (Loop Configuration)	ORLA51
-	Nogo (Linear Configuration)	ORLA53
-	OMGP	ORLA52

Table 6-2: Orla motifs used to study the process of neurite development and inhibition.
A range of peptide sequence domains used throughout this project from extracellular proteins. The OrlaSURF platform was used to coat growth substrates with these domains and present them to cells. This includes domains derived from components of the ECM such as laminins and also inhibitory molecules found on myelin debris of particular importance in glial scar signalling, such as OMGP and Nogo.

6.3 Results

6.3.1 Examining the Role of the Extra-Cellular Matrix in Neurite Outgrowth

To investigate the role of particular ECM-derived amino acid sequences in neurite development, fully matured neurospheres were cultured on 2D surfaces coated using Orla technology with a selection of domains. Immunofluorescence images highlighting TUJ-1 expression (green) reveal neurite outgrowth radiating from the central neurosphere (Figure 6-4Aa-d). Few neurites radiate from neurospheres cultured on the FLAG, control substrate (Figure 6-4Aa) whereas significant neurite outgrowth is visible from neurospheres cultured on ECM-coated surfaces (Figure 6-4Ab-d). Neurites generated from neurospheres cultured on collagen IV coated substrates appear shorter in length than those cultured on surfaces coated with the laminin YIGSR domain.

The number of neurites per neurosphere (Figure 6-4B) was enhanced by all ECM-derived domains tested; however, only fibronectin and laminin-derived domains induced a significant enhancement in neurite number compared to FLAG. Fibronectin coating resulted in the generation of significantly more neurites than collagen IV and a laminin-derived coating resulted in significantly more neurites than fibronectin. Similarly, neurite

density (Figure 6-4C) was significantly enhanced by all ECM domains tested, with again the laminin-derived YIGSR being responsible for the greatest generation of neurites. A similar trend was apparent in terms of neurite length (Figure 6-4D), as all ECM-derived domains induced a significant enhancement in neurite length and the laminin-derived YIGSR domain was responsible for the greatest enhancement in neurite length.

Neurospheres were also cultured in 3D on Alvetex® Scaffold coated using Orla technology with each ECM-derived domain. Neurospheres remain on top of the scaffold (Figure 6-5Aa,c,e,g,i) and TUJ-1 positive (green) neurites penetrate the depth of the 3D material and are visible from the bottom view of the scaffold (Figure 6-5Ab,d,f,h,j). Uncoated Alvetex® Scaffold (Figure 6-5Aa,b) from the same batch as those coated with Orla domains, was tested and few neurites were visible from the underside of the scaffold. Similarly, scaffolds coated with control FLAG peptide (Figure 6-5Ac,d), also generated few neurites as visible from the bottom view of the scaffold. Orla coating with all the ECM-domains tested (Figure 6-5Ae-j) resulted in a greater number of neurites that were visible from the bottom view of the scaffold, with the laminin YIGSR domain in particular appearing to have the most positive effect upon neurite penetration.

A similar number of neurites were found to penetrate the scaffold (Figure 6-5B) in cultures based on uncoated scaffolds and control FLAG coated scaffolds. Coating of 3D growth substrates with ECM-derived sequences, resulted in a significant increase in neurite penetration compared with both the uncoated and FLAG controls. Similarly to 2D culture, the fibronectin-derived domain induced neurite growth to a significantly greater degree than collagen IV and the laminin-derived motif induced neurite outgrowth to a significantly greater extent than fibronectin.

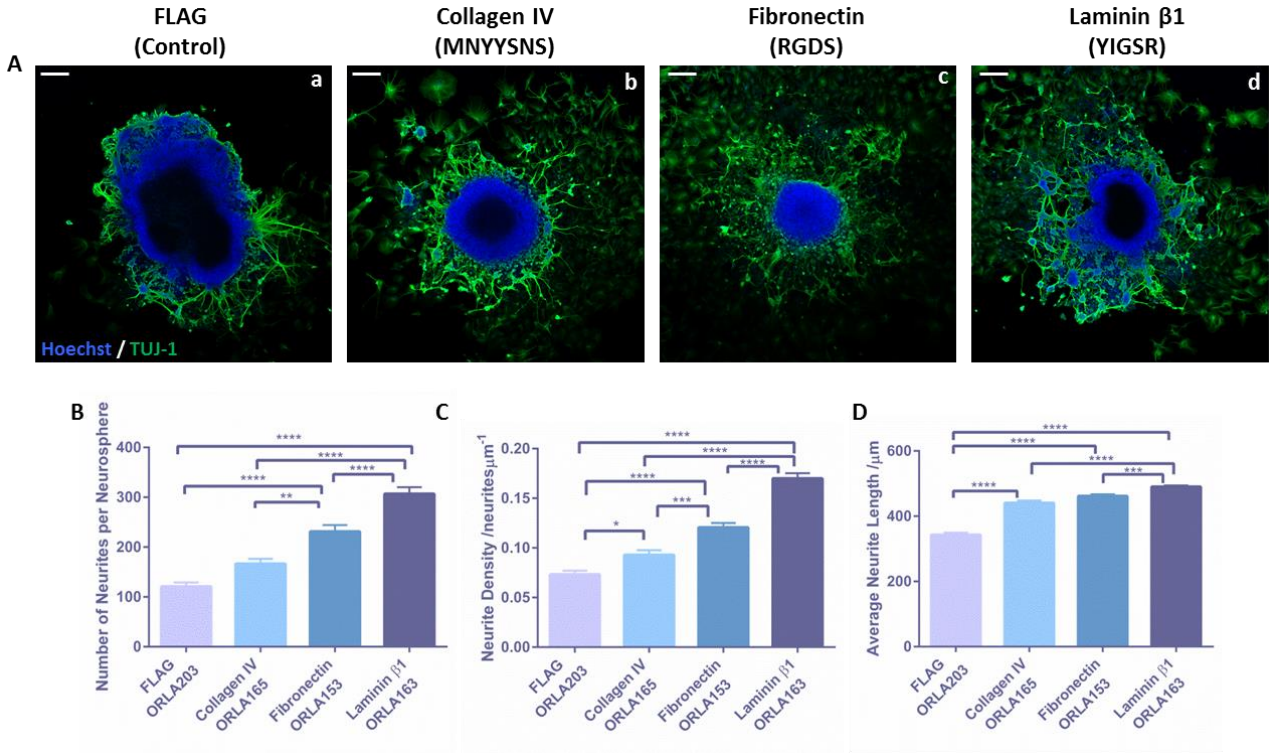

Fig 6-4: The ECM component, laminin β-1 has neurite enhancing effects in 2D culture.
Representative confocal images (A) of 2D neurite outgrowth from neurospheres cultured on Orla surfaces coated with either the control peptide Flag (Aa), a collagen IV motif (Ab), a fibronectin motif (Ac) or a laminin motif (Ad). Neurites are highlighted by expression of the pan-neuronal marker TUJ-1 (green) and nuclei are stained blue. Scale bars: 200 µm. The number of neurites per neurosphere (B) (data represent mean ± SEM, n=33-45; 11-15 individual neurospheres were quantified from 3 independent replicates) is significantly enhanced by the coating of growth substrates with Orla ECM motifs compared with the control peptide and the Orla laminin β-1 motif was found to enhance the number of neurites per neurosphere to the greatest extent. A similar pattern is observed in the neurites density (C) (data represent mean ± SEM, n=33-45; 11-15 individual neurospheres were quantified from 3 independent replicates) of the aggregates, with the coating of growth substrates with ECM molecules enhancing nerite outgrowth, and laminin β-1 having the largest effect. Neurite length (D) (data represent mean ± SEM, n=476-1340; between 476-1340 neurites were measured from 11-15 neurospheres per independent replicate, of which there were 3) is also enhanced by ECM coating, again being enhanced to the highest degree by the laminin β-1 motif. One-way ANOVA with Tukey's multiple comparisons: * = $p \leq 0.05$, ** = $p \leq 0.01$, *** = $p \leq 0.001$, **** = $p \leq 0.0001$.

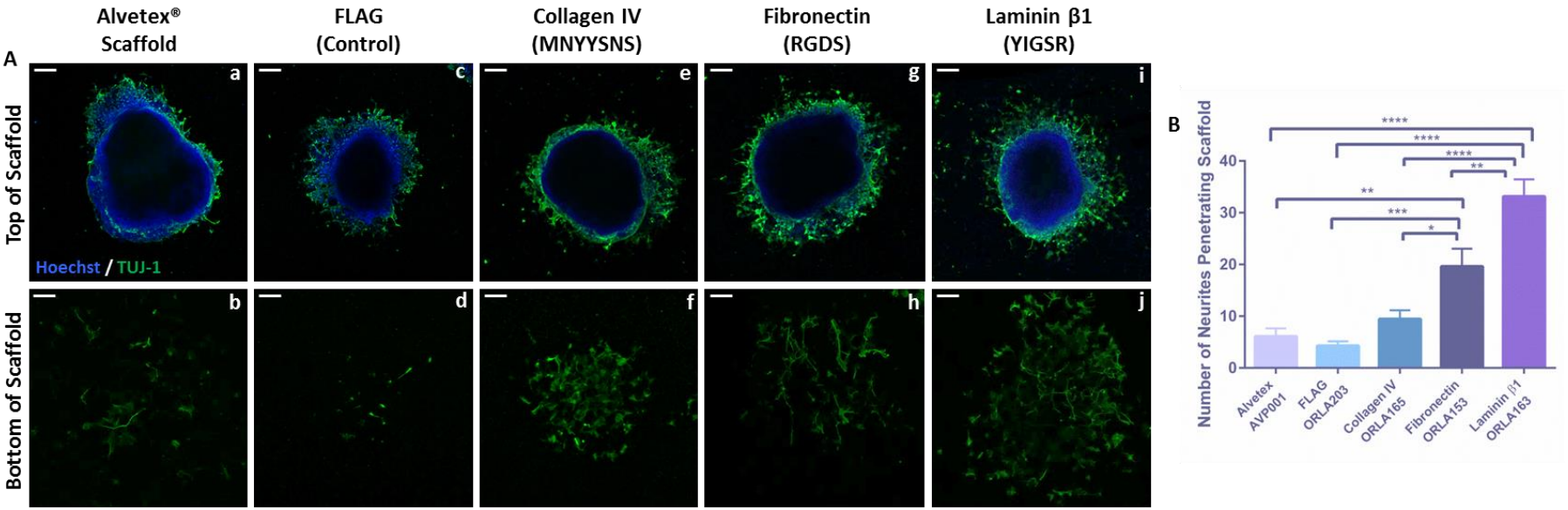

Fig 6-5: The ECM component, laminin β-1 has neurite enhancing effects in 3D culture.
Representative confocal images (A) of neurospheres cultured on top of Alvetex® scaffold (Aa,c,e,g,i) coated with Orla ECM motifs. TUJ-1 (green) positive neurites have penetrated the entire depth of the 3D material (Ab,d,f,h,j) whereas nuclei (blue) are restricted to the cellular aggregate. Neurospheres were cultured on Alvetex® scaffold without protein coating (Aa,b), coated with the control peptide (Flag Ac,d) or coated with motifs from collagen IV (Ae,f), fibronectin (Ag,h) or laminin β-1 (Ai,j). Scale bars: 200 μm. The number of neurites penetrating each scaffold (B) (data represent mean ± SEM, n=13-15, 4-5 individual neurospheres were quantified from 3 independent replicates) is significantly enhanced with Orla protein coating and enhanced to the greatest degree by coating with the laminin β-1 motif. One-way ANOVA with Tukey's multiple comparisons: * = $p \leq 0.05$, ** = $p \leq 0.01$, *** = $p \leq 0.001$, **** = $p \leq 0.0001$.

The ReproNeuro, iPSC-derived model of neuritogenesis, as described in Chapter III, is based upon the coating of growth substrates with particular ECM-derived products. It is recommended that ReproNeuro Glu cells are cultured on substrates coated with "*ReproCoat"* a coating mixture containing an unknown concentration of both laminin and fibronectin; however, the TERA2.cl.SP12 model of neuritogenesis involves the coating of growth substrates with 10 μgmL^{-1} laminin and poly-D-lysine. To compare the ability of each coating solution to induce neurite extension, ReproNeuro Glu-derived neurospheres were cultured on 2D substrates coated with each ECM-derived mixture using the traditional adsorption coating technique.

Immunofluorescence analysis (Figure 6-6A) reveals significant neurite outgrowth from neurospheres cultured on substrates coated with each solution. However, neurites appear longer and more curved when cultured on substrates coated with ReproCoat (Figure 6-6Aa) compared with poly-D-lysine and laminin coating (Figure 6-6Ab). Both the number of neurites (Figure 6-6B) and neurite density (Figure 6-6C) are similar from neurospheres cultured on each coating. However, neurite length (Figure 6-6D) is significantly enhanced on surfaces coated with ReproCoat as opposed to poly-D-lysine and laminin, perhaps suggesting a role for fibronectin in neurite elongation and extension.

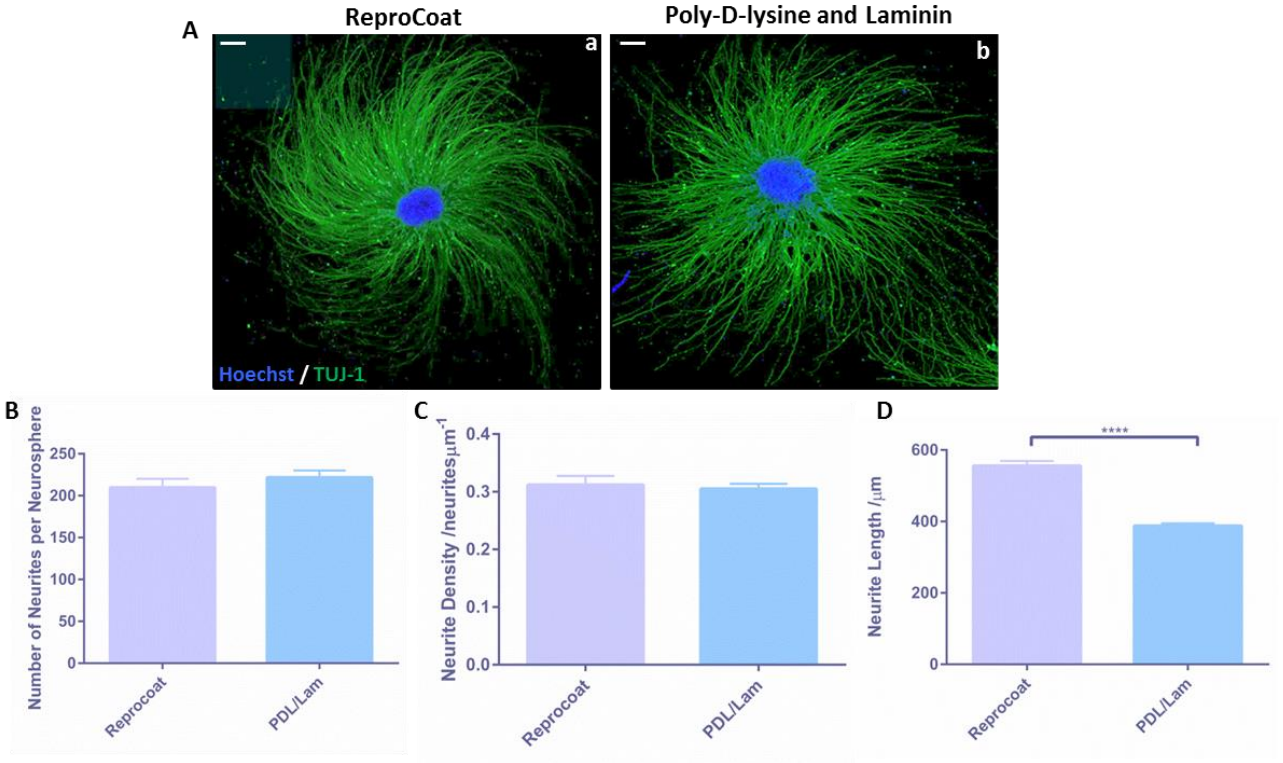

Fig 6-6: ECM coating impacts neurite outgrowth from neurospheres formed from iPSC derived neuroprogenitor cells in 2D culture.
Representative confocal images (A) of ReproNeuro Glu derived neurospheres cultured on 2D substrates coated with either ReproCoat (Aa) – a mixture of fibronectin and laminin coating solution, or 10 µgmL^{-1} poly-D-lysine and laminin coating solution (Ab) for 10 days. TUJ-1 (green) positive neurites radiate from the central cellular aggregate and nuclei are stained in blue. Scale bars: 200 µm. Quantification of the number of neurites (B) and neurite density (C) (data represent mean ± SEM, n=3; due to limited cell availability 3 neurospheres from 1 population of cells were quantified) reveals little difference between the two coating solutions, however ReproCoat significantly enhances neurite length (D) (data represent mean ± SEM, n=3) when compared to poly-D-lysine and laminin coating solution. Unpaired T-test: *** = $p \leq 0.001$

The original TERA2.cl.SP12 model of neurite outgrowth developed in Chapter III involves the adsorption coating of 2D and 3D growth substrates with 10 μgmL^{-1} laminin and poly-D-lysine solution. To test the ability of Orla technology to enhance neurite outgrowth compared with this standard model, neurospheres were cultured on 2D growth surfaces coated with various combinations of the laminin YIGSR domain and poly-D-lysine. Significant TUJ-1 positive (green) neurite outgrowth is evident from neurospheres cultured on surfaces coated with the conventional coating solution (10 μgmL^{-1} laminin and poly-D-lysine) (Figure 6-7Aa,b). Whereas, neurospheres cultured on Orla surfaces coated with either a mixture of 50 % YIGSR – 50 % Flag (Figure 6-7Ac,d) or 50 % poly-D-lysine – 50 % Flag (Figure 6-7Ae,f) resulted in fewer, shorter neurites and neurite outgrowth was less uniform. However, the coating of growth substrates with an Orla 50 % YIGSR – 50 % poly-D-lysine mix (Figure 6-7Ag,h), resulted in significant neurite outgrowth, which appeared dense and neurites appeared longer than those generated from neurospheres on traditional adsorption coated surfaces.

The number of neurites per neurosphere (Figure 6-7B) generated from neurospheres cultured on adsorption-coated poly-D-lysine and laminin surfaces was significantly enhanced compared with both 50 % Flag Orla mixes. Similarly, the number of neurites generated on Orla poly-D-lysine and laminin coating was significantly enhanced compared with both 50 % Flag Orla mixes. Both adsorption and Orla poly-D-lysine and laminin coatings generated a similar number of neurites per neurosphere that did not differ significantly.

The neurite density (Figure 6-7C) of neurospheres cultured on adsorption-coated poly-D-lysine and laminin-coated surfaces was significantly enhanced compared with all other conditions tested. Orla poly-D-lysine and laminin coating resulted in a significantly enhanced neurite density compared with either 50 % Flag Orla mixes. Neurite length (Figure 6-7D) was also enhanced by surfaces adsorption-coated with poly-D-lysine and laminin compared to both 50 % Flag Orla mixes. However, Orla laminin and poly-D-lysine coating resulted in significantly longer neurites than any other condition tested, including adsorption coating.

Neurospheres were also cultured in 3D on Alvetex® scaffolds coated with poly-D-lysine and laminin, adsorption and Orla coatings. Neurospheres remain on top of the scaffold (Figure 6-8Aa,c,e,f), whereas TUJ-1 positive (green) neurites are visible from the underside of the scaffold (Figure 6-8Ab,d,f,h). Significant neurite outgrowth can be observed from adsorption-coated cultures (Figure 6-8Aa,b) whereas few neurites are visible from the underside of 50 % Flag Orla mix-coated scaffolds (Figure 8-6c-f). Significant neurite outgrowth is also visible from the underside of scaffolds coated with Orla poly-D-lysine and laminin (Figure 6-8Ag,h).

The number of neurites penetrating the scaffold (Figure 6-8B) is significantly enhanced in cultures coated with Orla poly-D-lysine and laminin compared with any other condition tested. Adsorption poly-D-lysine and laminin coating results in increased neurite penetration compared with both 50 % Flag Orla mixes, however Orla poly-D-lysine and laminin coating results in the greatest number of neurites having penetrated the scaffold.

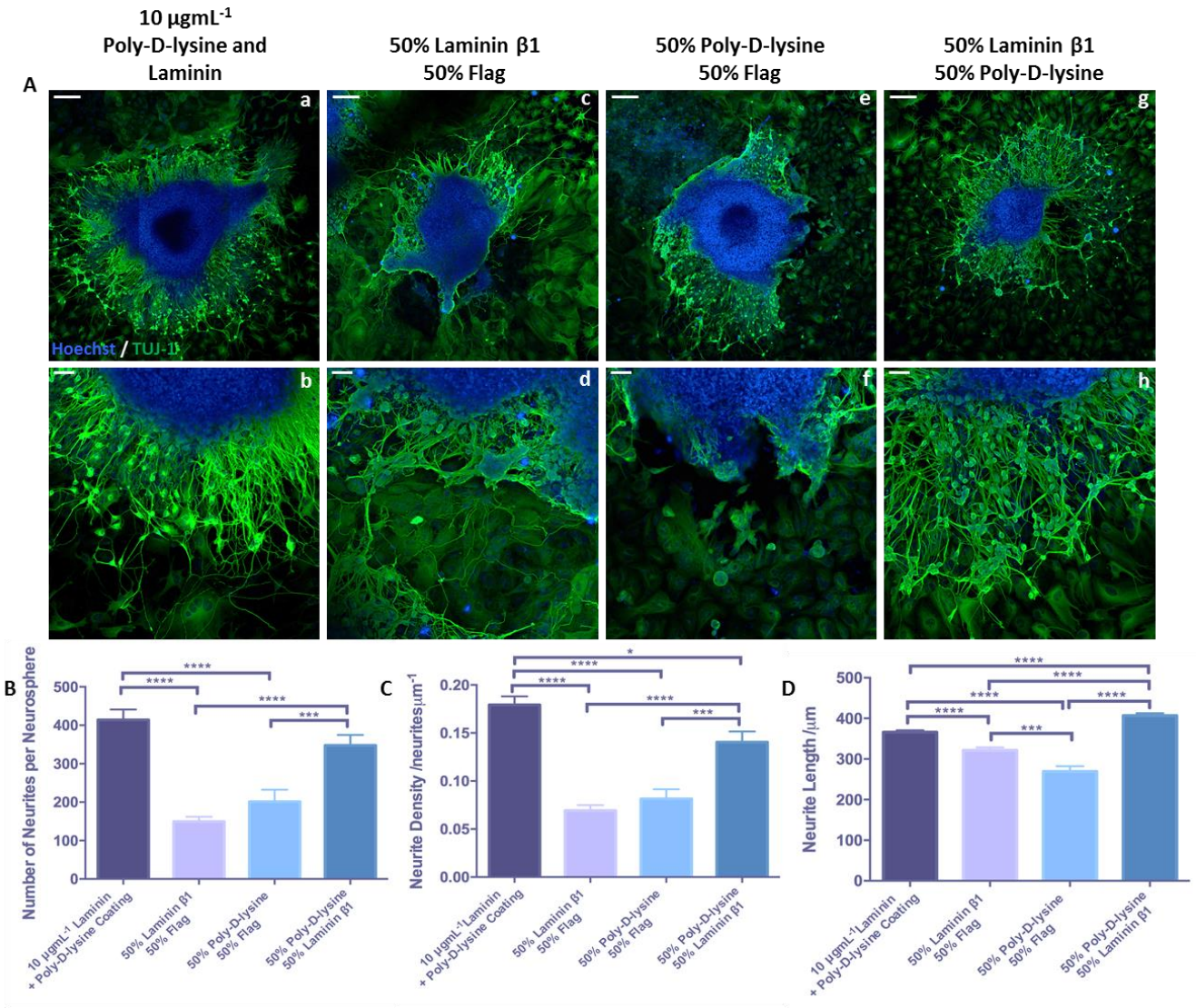

Fig 6-7: Coating of 2D growth substrates with Orla laminin β-1 and poly-D-lysine motifs enhances neurite length compared with adsorption coating.

Representative confocal images (A) of neurospheres cultured on 2D surfaces coated in the traditional adsorption manner with 10 µgmL^{-1} poly-D-lysine and laminin coating solution (Aa,b) or with laminin β-1 (Ac,d), poly-D-lysine (Ae,f) or a combination of laminin and poly-D-lysine (Ag,h) Orla motifs. Neurite outgrowth is highlighted in green through staining for the pan-neuronal marker, TUJ-1 and nuclei are highlighted in blue. Scale bars: 200 µm. The number of neurites per neurosphere (B) (data represent mean ± SEM, n=17-18; 5-6 individual neurospheres were quantified from 3 independent replicates) and neurite density (C) (data represent mean ± SEM, n=17-18; 5-6 individual neurospheres were quantified from 3 independent replicates) are both enhanced by the combination of Orla motifs as oppose to each motif displayed separately. However neurite outgrowth is not induced to the same level as that of the traditional adsorption coating. Neurite length (D) (data represent mean ± SEM, n=118-492; between 118-492 neurites were measured from 5-6 neurospheres per independent replicate, of which there were 3), is significantly enhanced by the mixture or Orla laminin and poly-D-lysine motifs compared with each motif-displayed separately and compared with traditional adsorption coating. One-way ANOVA with Tukey's multiple comparisons: * = $p \leq 0.05$, ** = $p \leq 0.01$, *** = $p \leq 0.001$, **** = $p \leq 0.0001$.

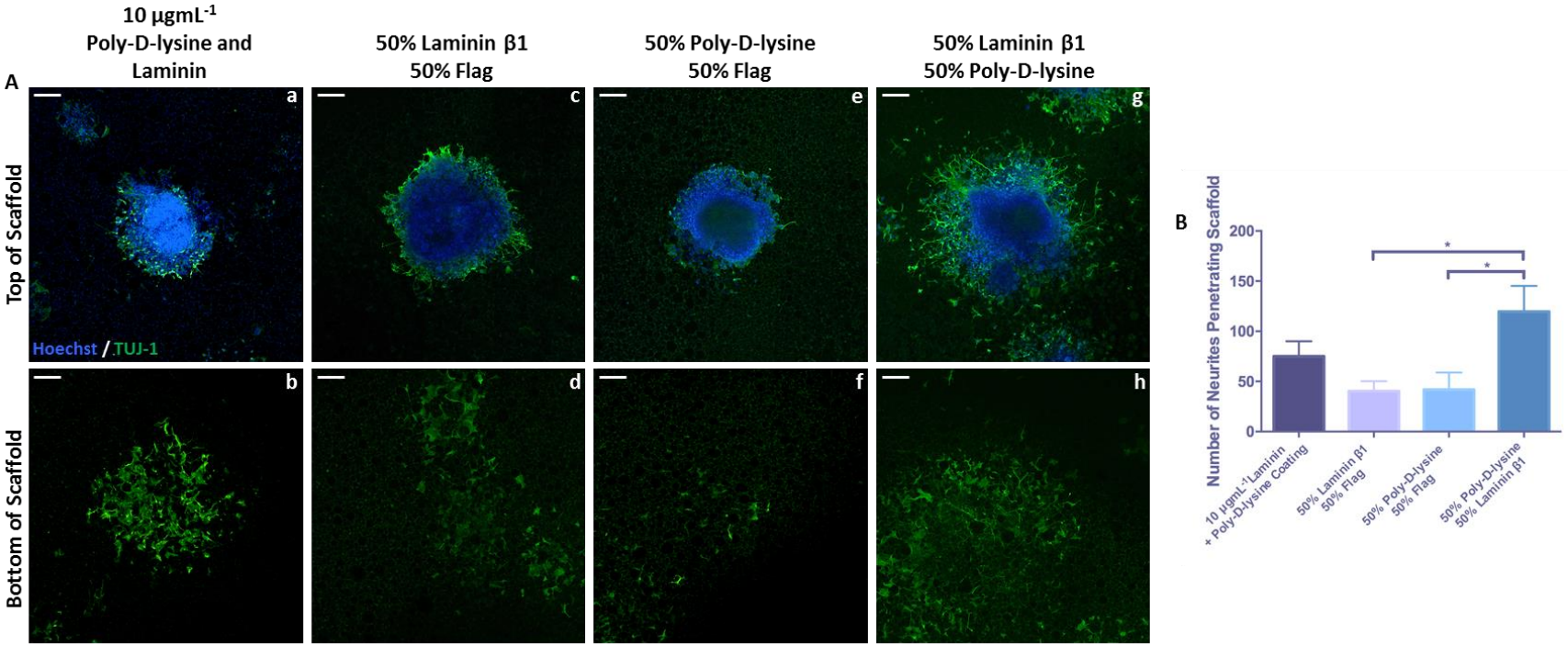

Fig 6-8: Coating of 3D growth substrates with Orla laminin β-1 and poly-D-lysine motifs enhances neurite outgrowth compared with adsorption coating
Representative confocal images (A) of neurospheres cultured on Alvetex® scaffold coated in the traditional adsorption manner with 10 µgmL^{-1} poly-D-lysine and laminin coating solution (Aa,b) or with laminin β-1 (Ac,d), poly-D-lysine (Ae,f) or a combination of laminin and poly-D-lysine (Ag,h) Orla motifs. Neurospheres remain on top of the scaffold (Aa,c,e,g) whilst TUJ-1 (green) positive neurites penetrate the 3D material and are visible from below (Ab,d,f,h). Nuclei are stained blue. Scale bars: 200 µm. Quantification of the number of neurites penetrating the scaffold (B) (data represent mean ± SEM, n=5-6; 1-2 individual neurospheres were quantified from 3 independent replicates) reveals that neurite outgrowth from scaffolds coated with the mixture of Orla laminin and poly-D-lysine motifs is enhanced compared with each motif displaced separately and compared with traditional adsorption coating. One-way ANOVA with Tukey's multiple comparisons: * = $p \leq 0.05$, ** = $p \leq 0.01$, *** = $p \leq 0.001$, **** = $p \leq 0.0001$.

6.3.1.1 Investigation into the Neurite Enhancing Properties of Laminin

To focus on the specific neurite enhancing properties of laminin and its specific domains, a dose response was conducted on 2D Orla-coated surfaces. Growth substrates were coated with various combinations of the "YIGSR" domain and control, Flag peptide to investigate the nature of laminin-induced neurite outgrowth. Few neurites radiated from neurospheres cultured on Flag control surfaces (Figure 6-9Aa,b), with a slight increase in visible neuritogenesis from 25 % and 50 % laminin mixes (Figure 6-9Ac-f). Neurite outgrowth from 75 % laminin "YIGSR" (Figure 6-9Ag,h) coated surfaces appears more uniform and dense compared with Flag control coating alone and neurite outgrowth appears the most uniform from neurospheres cultured on substrates coated with 100 % "YIGSR" (Figure 6-9Ai,j).

The number of neurites generated per neurosphere (Figure 6-9B) was enhanced in a dose dependent manner with increasing YIGSR content of the growth substrate coating 75 % and 100 % "YIGSR" coatings induced a significant increase in the number of neurites generated from neurospheres, compared with control and 25 % "YIGSR" coatings. Similarly, neurite density (Figure 6-9C) is also enhanced in a dose dependent manner with increasing YIGSR content of the Orla coating. Both 75 % and 100 % "YIGSR" coatings were found to enhance neurite density significantly compared with FLAG.

Neurite length (Figure 6-9D) again, was enhanced by the laminin "YIGSR" domain content of the growth substrate coating in a dose dependent manner. Orla coatings containing the highest content of the "YIGSR" domain (75 – 100 %) resulted in the growth of neurites with significantly enhanced length compared with FLAG and other conditions tested such as 25 % laminin coating.

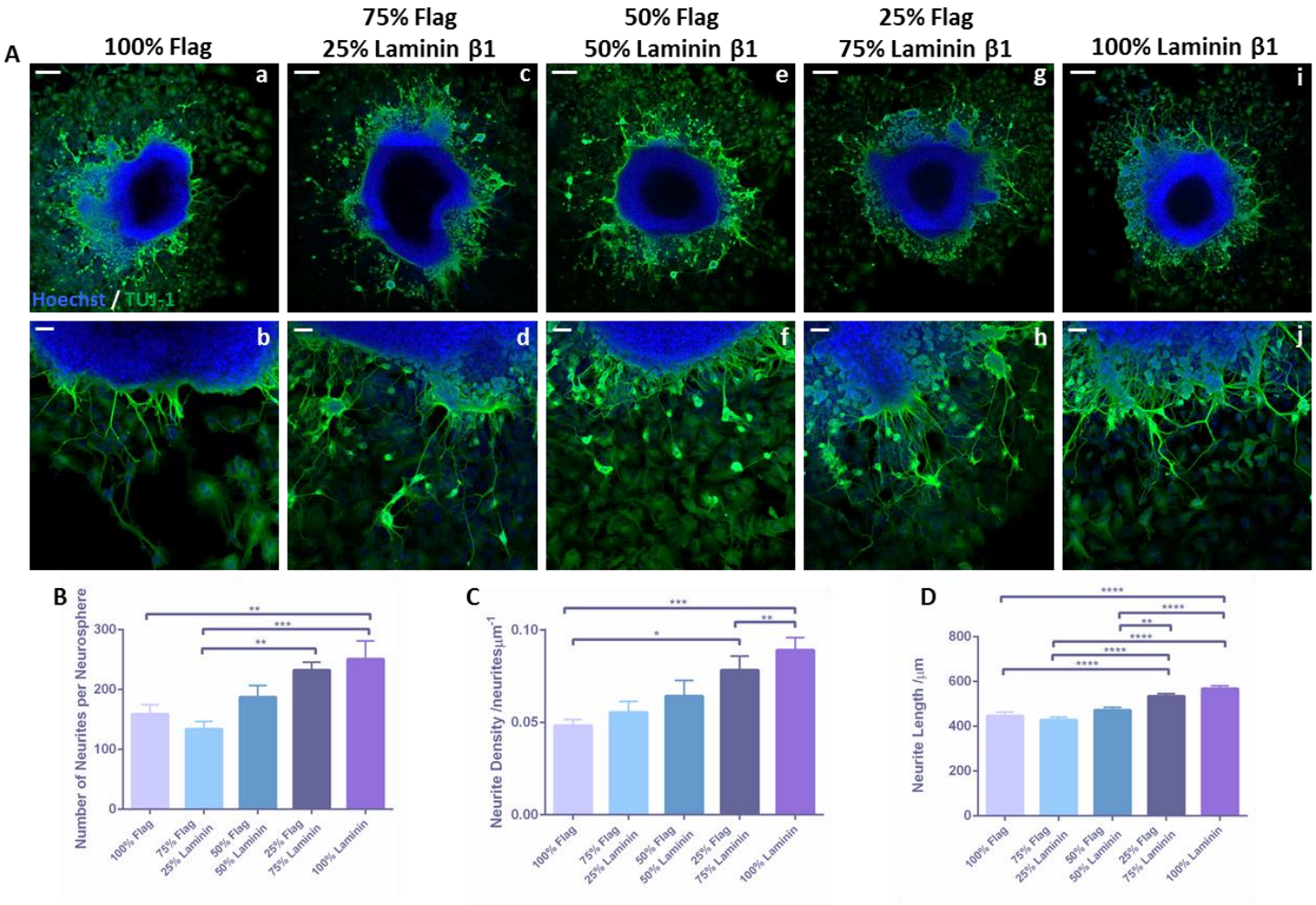

Fig 6-9: Coating of 2D growth substrates with the Orla laminin β-1 motif enhances neurite outgrowth in a dose dependent manner.

Representative confocal images (A) of neurospheres cultured on 2D substrates coated with an increasing content of the Orla laminin β-1 motif mixed with the control peptide, flag. Neurites are positive for TUJ-1 (green) and nuclei are stained blue and remain in the central body of the cellular aggregate. Scale bars: 200 µm. Both the number of neurites per neurosphere (B) (data represent mean ± SEM, n=18; 6 individual neurospheres were quantified from 3 independent replicates) and the neurite density (C) (data represent mean ± SEM, n=18; 6 individual neurospheres were quantified from 3 independent replicates) are enhanced in a dose dependent manner with increasing laminin β-1 coating content. Similarly, the average length of neurites (D) (data represent mean ± SEM, n=224-419; between 224-419 neurites were measured from 6 neurospheres per independent replicate, of which there were 3) is also enhanced by increasing laminin β-1 content of the substrate coating. Therefore, the Orla laminin β-1 motif has neurite enhancing properties in 2D culture. One-way ANOVA with Tukey's multiple comparisons: * = $p \leq 0.05$, ** = $p \leq 0.01$, *** = $p \leq 0.001$, **** = $p \leq 0.0001$.

In order to compare Orla laminin coatings directly with traditional adsorption coatings, a 2D laminin adsorption dose response was carried out. This involved the culture of neurospheres on 2D growth substrates coated with laminin from Engelberth-holm-swarm murine sarcoma basement membrane, in a traditional adsorption fashion. A range of concentrations of laminin coatings (0.5 – 50 μgmL^{-1}) were tested and at the lowest concentrations 0.5 – 1 μgmL^{-1} (Figure 6-10Aa-d), neurite outgrowth was not very uniform, with whole areas of the neurosphere free from outgrowth. This improved with increasing laminin concentration with 50 μgmL^{-1} (Figure 6-10Ak,l) laminin coating resulting in more uniform neurite outgrowth and neurites appeared longer.

Both the number of neurites per neurosphere (Figure 6-10B) and neurite density (Figure 6-10C) increased in a dose dependent manner with increasing laminin concentration. Similarly, neurite length (Figure 6-10D) also generally increased with increasing laminin coating concentration, however the data point at 10 μgmL^{-1} perhaps appears to be unusually high and could be anomalous.

To compare the Orla "YIGSR" laminin motif with the laminin adsorption coating, two distinct methods of comparison were employed. The first of which involves the plotting of the Orla YIGSR dose response side-by-side with the adsorption dose response (Figure 6-11A-C) for each variable measured within the 2D neurite outgrowth assay (i.e neurite number (Figure 6-11A), neurite density (Figure 6-11B) and neurite length (Figure 6-11C)). This method of comparison was termed the "*Estimated Method*", as the two dose responses can be compared by reading from the graph the laminin concentration that each Orla coating is equivalent to. This produces an equivalent range of laminin concentrations for each Orla substrate, for example 100 % Orla "YIGSR" coating produces a response in terms of neurite number that lies between 10 – 20 μgmL^{-1} laminin adsorption coating.

Another method of comparison employed to compare Orla and adsorption laminin coatings involved the use of the laminin adsorption dose response as a standard curve (Figure 6-11D-F). A linear regression was fitted through each data set (blue line) and the equation of the line of best fitted was calculated. From this the unknown laminin concentration (x) could be calculated for each Orla "YIGSR" dose, from the known response (y) in terms of neurite number (Figure 6-11D), neurite density (Figure 6-11E) and neurite length (Figure 6-11F). This method of comparison was termed the "*Numerical Method*" and a range of equivalent laminin concentrations were also obtained from the analysis of each measure of 2D neurite outgrowth.

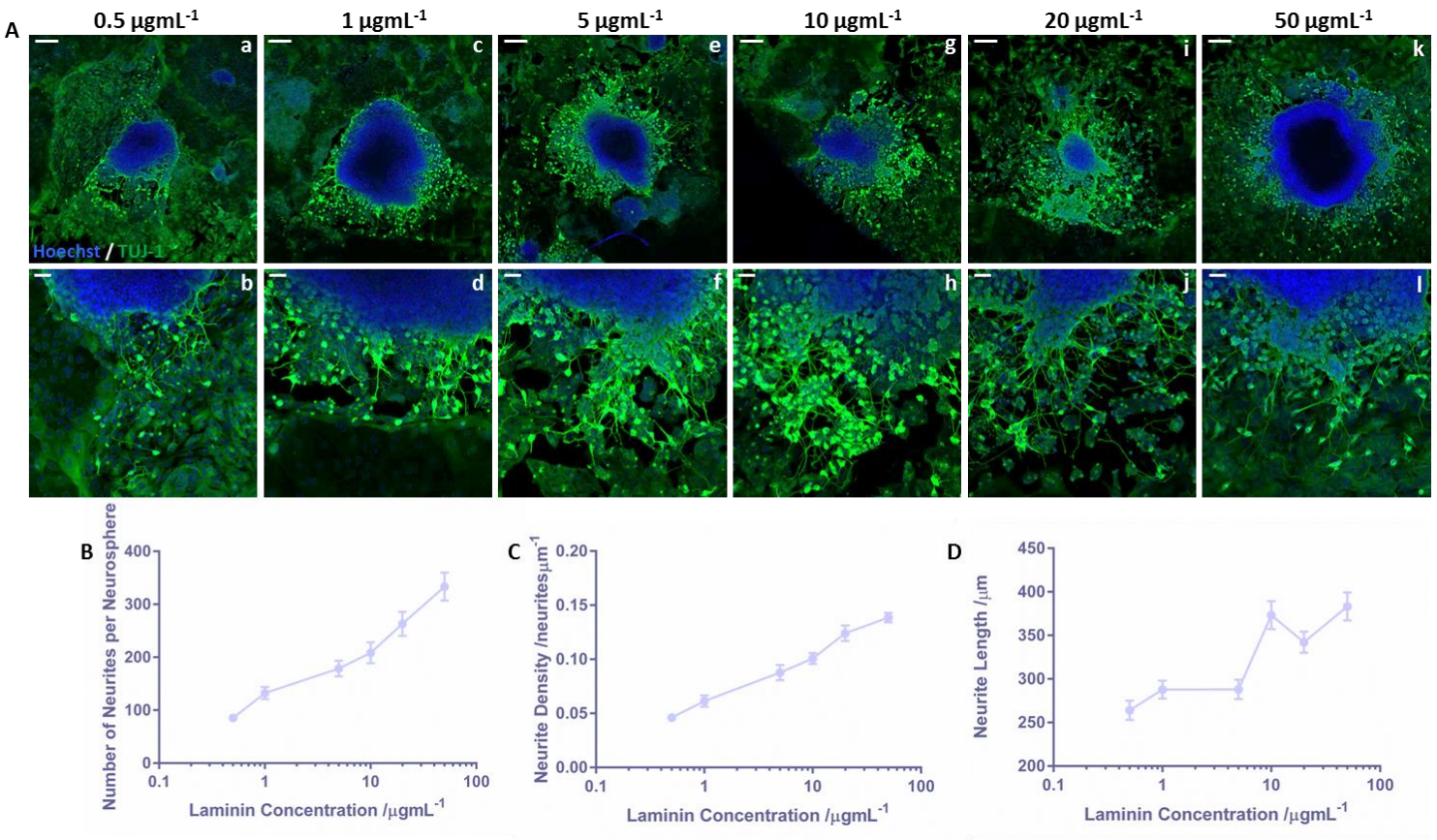

Fig 6-10: Conventional laminin coating of 2D growth substrates enhances neurite outgrowth in a dose dependent manner.
Representative confocal images (A) of neurospheres cultured on 2D substrates coated with a range of concentrations (0.5 – 50 µgmL^{-1}) of laminin from Engelbreth-Holm-Swarm murine sarcoma basement membrane. TUJ-1 (green) positive neurites can be seen to extend radially from the central cellular aggregate with nuclei (blue) remaining within the body of cellular mass. Scale bars: (Aa,c,e,g,i,k): 200 µm (Ab,d,f,h,j,l): 50 µm. The number of neurites per neurosphere (B) (data represent mean ± SEM, n=18-27; 6-9 individual neurospheres were quantified from 3 independent replicates) and the neurite density (C) (data represent mean ± SEM, n=18-27; 6-9 individual neurospheres were quantified from 3 independent replicates) gradually increases in a dose dependent fashion with increasing laminin coating concentration. Neurite length (D) (data represent mean ± SEM, n=66-100; between 66-100 neurites were measured from 6-9 neurospheres per independent replicate, of which there were 3) also has a positive correlation with laminin coating concentration.

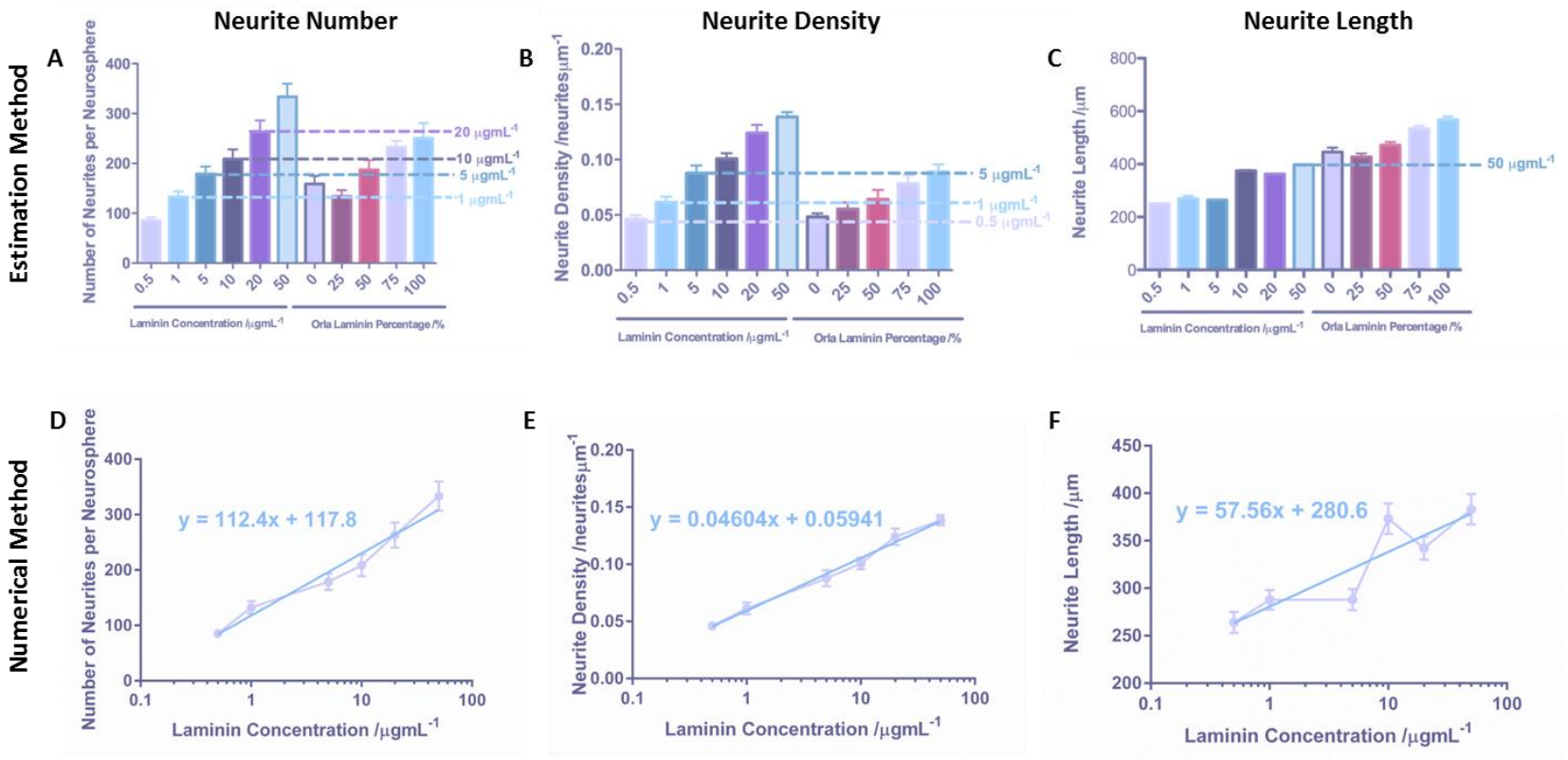

Fig 6-11: Comparison of Orla laminin β-1 coating with conventional laminin coating in 2D culture.
Neurite outgrowth from neurospheres cultured on 2D substrates coated with either the Orla laminin β-1 motif or with laminin from Engelbreth-Holm-Swarm murine sarcoma basement membrane was compared using two different methodologies. Neurite number, density and length were all compared either using an estimation method (A,B,C) or numerical method (D,E,F) of comparison. The estimation method of comparison involved plotting the Orla and conventional coating data side by side on the same graph, enabling the concentration of laminin coating solution that each Orla value was equivalent to, to be read from the graph. The numerical method of comparison involved using a dose response of neurite outgrowth against conventional laminin coating concentration (taken from Fig 6-7) as a standard curve. A linear regression was then fit to the standard curve and the linear equation could then be derived. Each equation was then rearranged to make x the subject and y (the average neurite number, density or length for each Orla laminin condition) could then be substituted into the equation to find the laminin concentration that each Orla condition was equivalent to.

Therefore, from each method of comparison, a range of laminin concentrations was obtained based on the analysis of each variable measured in 2D culture (Table 6-3). One limitation of the "*estimated method*" of comparison was that neurite length from the Orla surfaces surpassed the maximal concentration of adsorption laminin tested (50 μgmL^{-1}), whereas the numerical method allows for extrapolation, providing a more accurate representation of each concentration.

Percentage Laminin Motif /%	Range of [Laminin] from Estimated Method /μgmL^{-1}	Range of [Laminin] from Numerical Method /μgmL^{-1}
25	1 – 50	0.476 – 0.603
50	1 – 50	1.795 – 2.877
75	3 – 50	4.447 – 33.963
100	5 – 50	6.577 – 128.529

Table 6-3: Summary of Orla laminin β-1 coating and conventional laminin coating comparison in 2D.
The laminin concentration that each Orla laminin β-1 condition is equivalent to in 2D as derived from both the estimated method and numerical method of comparison.

A laminin adsorption dose-response was also carried out in 3D culture, again to allow for a comparison between Orla "YIGSR" and traditional whole molecule adsorption coating. As in all 3D neurite outgrowth assays, neurospheres remained on top of the scaffold (Figure 6-12Aa,c,e,g,i,k), whereas TUJ-1 positive (green) neurites penetrate the depth of the 3D material as visible from the underside of the scaffold (Figure 6-12Ab,d,f,h,j,l). Few neurites are visible from the bottom view of scaffolds coated with low concentrations of laminin (0.5 – 10 μgmL^{-1}), whereas significant neurite outgrowth can be observed in 3D cultures coated with 20 – 50 μgmL^{-1}. Quantification of the number of neurites penetrating each scaffold (Figure 6-12B) reveals that neurite penetration increases in a dose dependent manner with increasing laminin concentration, with 5 – 50 μgmL^{-1} laminin coating evoking the largest response in neurite growth in 3D culture.

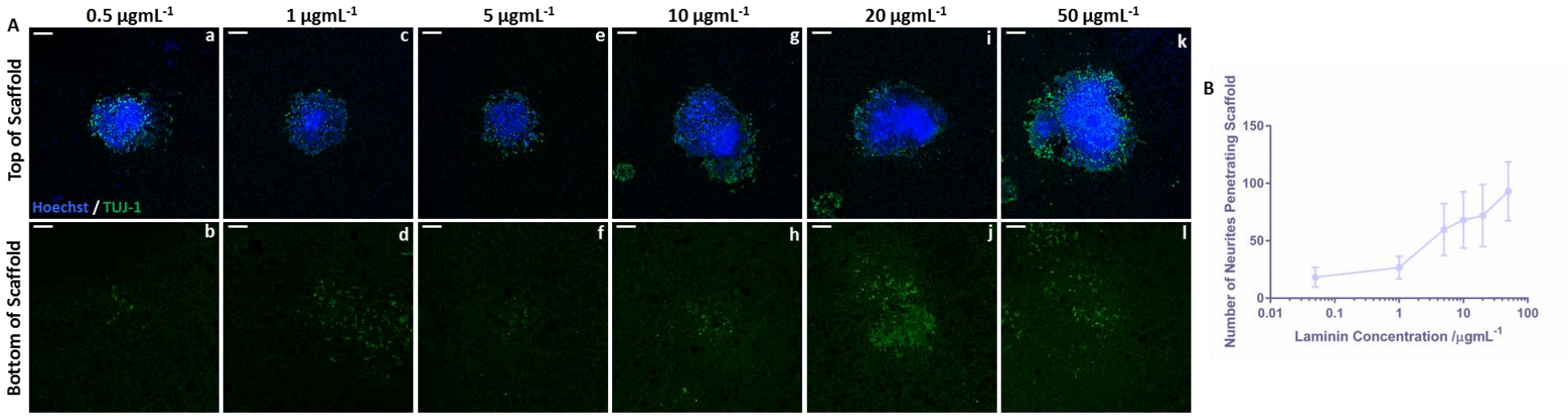

Fig 6-12: Conventional laminin coating of 3D growth substrates enhances neurite outgrowth in a dose dependent manner.
Representative confocal images (A) of neurospheres cultured on top of Alvetex® scaffold (Aa,c,e,g,i,k) coated in a range of concentrations (0.5 – 50 µgmL^{-1}) of laminin from Engelbreth-Holm-Swarm murine sarcoma basement membrane. TUJ-1 (green) positive neurites can be seen to have penetrated the scaffold depth and are visible from the underside of the scaffold (Ab,d,f,h,j,l) while nuclei (blue) remain within the central body of the neurosphere. Scale bars: 200 µm. The number of neurites penetrating the scaffold (B) (data represent mean ± SEM, n=9; 3 individual neurospheres were quantified from 3 independent replicates) increases in a dose dependent manner with increasing laminin concentration.

Similarly to 2D culture, both the "*Estimated*" (Figure 6-13A) and "*Numerical*" (Figure 6-13B) methods of comparison were employed to compare 3D neurite outgrowth on scaffolds coated with Orla "YIGSR" and traditional laminin adsorption coating. From the estimation method of comparison it was determined that the "YIGSR" domain resulted in a neurite outgrowth response similar to 1 – 5 μgmL^{-1} laminin adsorption coating (Table 6-4), and from the numerical method, it was calculated that 3D neurite outgrowth on scaffolds coated with "YIGSR" was equivalent to 5.33 μgmL^{-1} laminin coating (Table 6-4). Therefore, a similar result was obtained from both methods of comparison, suggesting that results obtained from this comparison of laminin coatings, are reliable and robust.

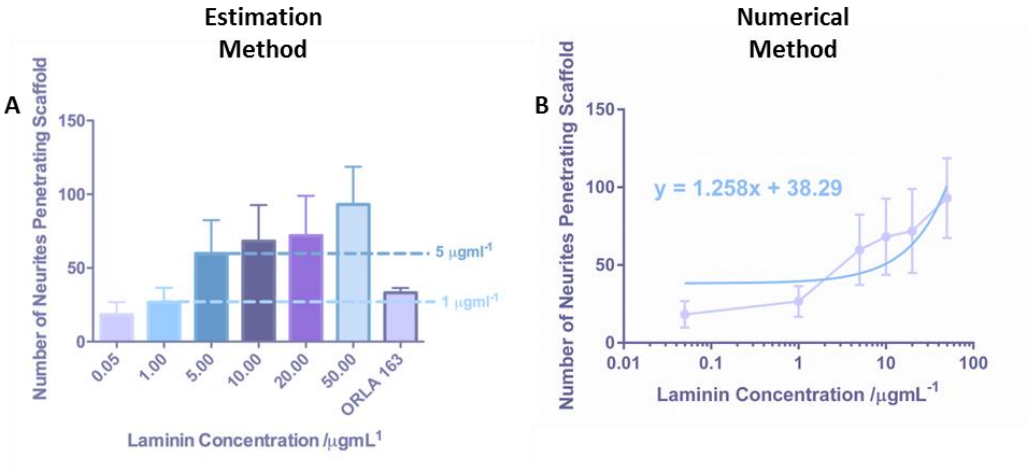

Fig 6-13: Comparison of Orla laminin β-1 coating with conventional laminin coating in 3D culture.
Neurite outgrowth from neurospheres cultured on Alvetex® scaffold coated either with Orla laminin β-1 or with laminin from Engelbreth-Holm-Swarm murine sarcoma basement membrane was compared using two different methodologies. The number of neurites penetrating the scaffold for each concentration of conventional laminin coating solution was plotted side by side with the number of neurites penetrating the scaffold when coated with Orla laminin β-1. The concentration of laminin coating solution equivalent to the same level of neurite outgrowth as the Orla laminin β-1 motif was then read from the graph, this is the estimation method of comparison (A). However, in the numerical method of comparison, a line of best fit was fitted through the points of the dose response between conventional laminin coating concentration and the number of neurites penetrating the scaffold (taken from Fig 6-10), an equation for the line was then derived. This equation was then rearranged to make x the subject and y (the average number of neurites penetrating the scaffold for Orla laminin β-1) was then substituted into the equation to calculate the equivalent concentration of laminin coating solution.

Method of Comparison	[Laminin] /μgmL^{-1}
Estimated	1 – 5
Numerical	5.33

Table 6-4: Summary of Orla laminin β-1 coating and conventional laminin coating comparison in 3D.
The laminin concentration that the Orla laminin β-1 coating is equivalent to in 3D as derived from both the estimated method and numerical method of comparison.

The impact of several other Orla laminin-derived domains on neurite outgrowth was tested in 2D culture, including the "IKVAV" motif of laminin α1 that has been well documented to promote neurite outgrowth. Neurospheres were cultured on 2D tissue culture plastic coated with each Orla laminin-derived domain and significant neurite outgrowth can be seen to radiate from neurospheres cultured on most laminin-coated substrates (Figure 6-14A). However, some laminin-derived domains such as "VRWGMQQIQLVV" (Figure 6-14Ag,h) and "DITYVRLKF" (Figure 6-14k,l) appear to produce less neurites than the control FLAG coating (Figure 6-14Aa,b).

The number of neurites generated per neurosphere (Figure 6-14B) is enhanced by most laminin-derived amino acid sequences, with the exception of "VRWGMQQIQLVV" and "DITYVRLKF" which resulted in a reduction in neurite number compared with control FLAG. However, only the "IKVAV" motif resulted in a signficiant increase in neurite outgrowth compared with the control coating. The impact of each laminin-derived domain on neurite density (Figure 6-14C) was similar to the impact of each domain upon neurite number. Most laminin-derived domains resulted in a small increase in neurite density; however, both "VRWGMQQIQLVV" and "DITYVRLKF" resulted in a reduction in neurite density compared with FLAG.

Furthermore, neurite length (Figure 6-14D) differs little between each laminin coating with only the "YIGSR" domain resulting in a massive enhancement of neurite length. "IKVAV" also results in a smaller enhancement of neurite length, which is significant compared with control neurites.

Neurospheres were also cultured in 3D upon Alvetex® Scaffold coated with the same Orla laminin-derived motifs that were used for 2D neurite outgrowth assays. Neurospheres remained on top of each scaffold (Figure 6-15Aa,c,e,g,i,k,m), whereas TUJ-1 positive neurites (green) can be seen to have penetrated and exited each scaffold, as visible from the bottom view of the scaffold (Figure 6-15Ab,d,f,h,j,l,n). Fewer neurites are visible from the bottom view of scaffolds coated with "DITVRLKF" (Figure 6-15Ak,l) than the other

conditions tested, with “IKVAV” (Figure 6-15Ac,d) and “IKVSV” (Figure 6-15Ae,f) coatings resulting in a large number of visible neurites from the bottom view of each scaffold.

The number of neurites penetrating the scaffold (Figure 6-15B) in the case of each Orla coating was significantly enhanced compared with FLAG by the “RNAIAEIIKDI” motif only. Both “IKVAV” and “IKVSV” motifs resulted in a slight increase in neurite outgrowth within 3D culture, however, “VRWGMQQIQLVV”, “YIGSR” and “DITYVRLKF” motifs induced neurite outgrowth to a similar level as the control FLAG surface.

A comparison between each Orla laminin-derived motif and whole molecule laminin adsorption coating for 2D and 3D neurite outgrowth was carried out. This involved the use of both “*Estimated*” (Figure 6-16) and “*Numerical*” methods of comparison to produce a range of equivalent laminin concentrations based on the variety of aspects of 2D and 3D neurite outgrowth measured (i.e number of neurites per neurosphere (Figure 6-16A), neurite density (Figure 6-16B), neurite length (Figure 6-16C) and 3D neurite outgrowth (Figure 6-16D)). The “YIGSR” and “RNAIAEIIKDI” domains performed particularly well in terms of most aspects of neurite outgrowth, resulting in a similar level of neurite outgrowth as high concentrations of laminin adsorption coating (Table 6-5). Again, the “*Numerical*” method of comparison resulted in a more accurate range of laminin concentrations; however, both methodologies produce similar numerical values.

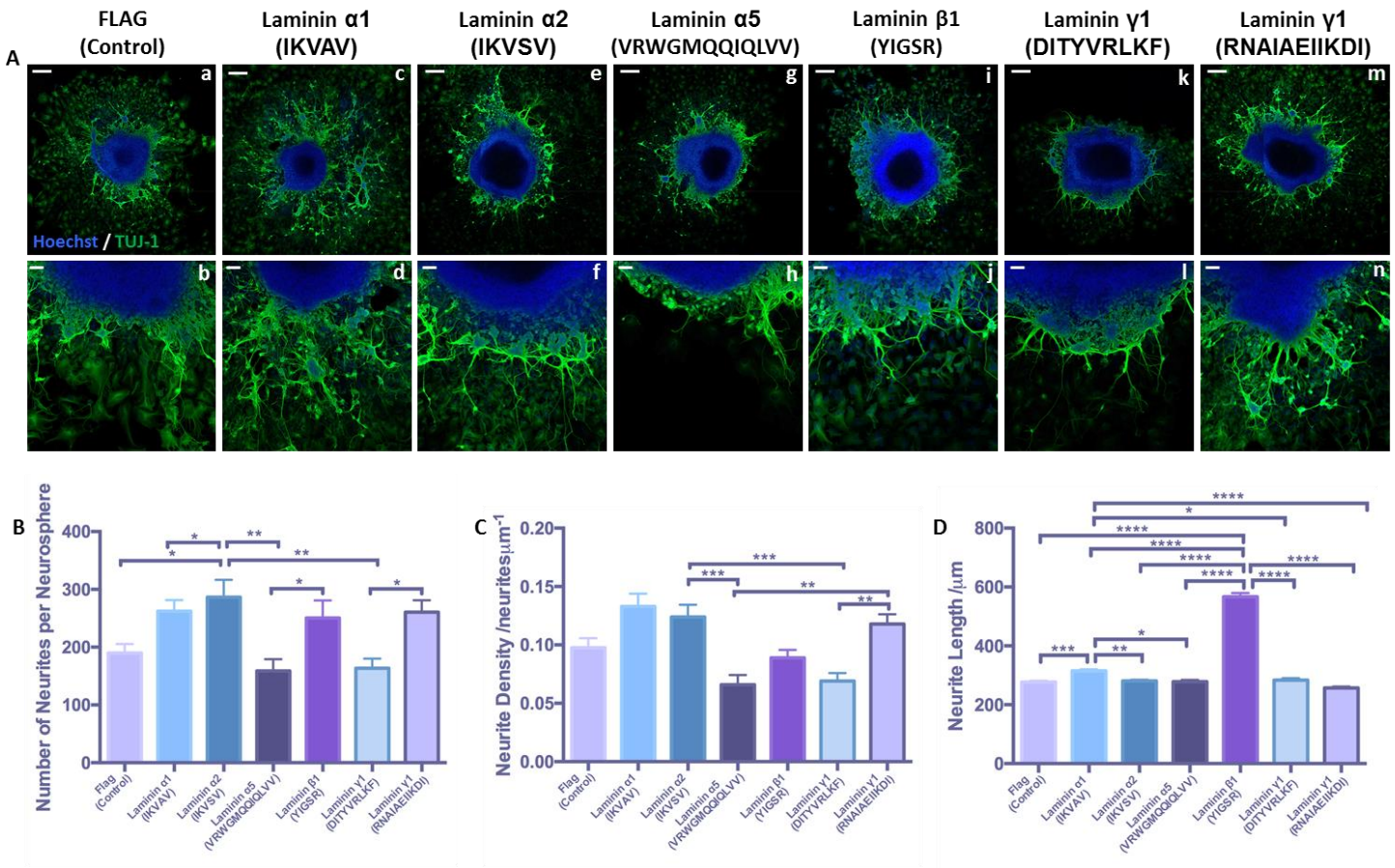

Fig 6-14: Identification of neurite promoting domains of laminin in 2D culture.
Representative confocal images of neurospheres cultured on 2D Orla substrates coated with a range of laminin domains (A). Neurite outgrowth is highlighted by positive staining for TUJ-1 (green) and nuclei are stained in blue. Scale bars: (Aa,c,e,g,i,k,m): 200 μm (Ab,d,f,h,j,l,n): 50 μm Quantification of the number of neurites per neurosphere (B) (data represent mean ± SEM, n=15; 5 individual neurospheres were quantified from 3 independent replicates) and neurite density (C) (data represent mean ± SEM, n=15; 5 individual neurospheres were quantified from 3 independent replicate) reveals that some motifs such as "IKVAV" and "IKVSV" enhance neurite outgrowth, whereas others such as "VRWGMQQIQLVV" and "DITYVRLKF" are inhibitory to neurite outgrowth. Similarly, the average length of neurites (D) (data represent mean ± SEM, n=184-354; between 184-354 neurites were measured from 5 neurospheres per independent replicate, of which there were 3) reveals that "YIGSR" clearly impacts neurite length to a greater degree than the other motifs tested. One-way ANOVA with Tukey's multiple comparisons: * = $p \leq 0.05$, ** = $p \leq 0.01$, *** = $p \leq 0.001$, **** = $p \leq 0.0001$.

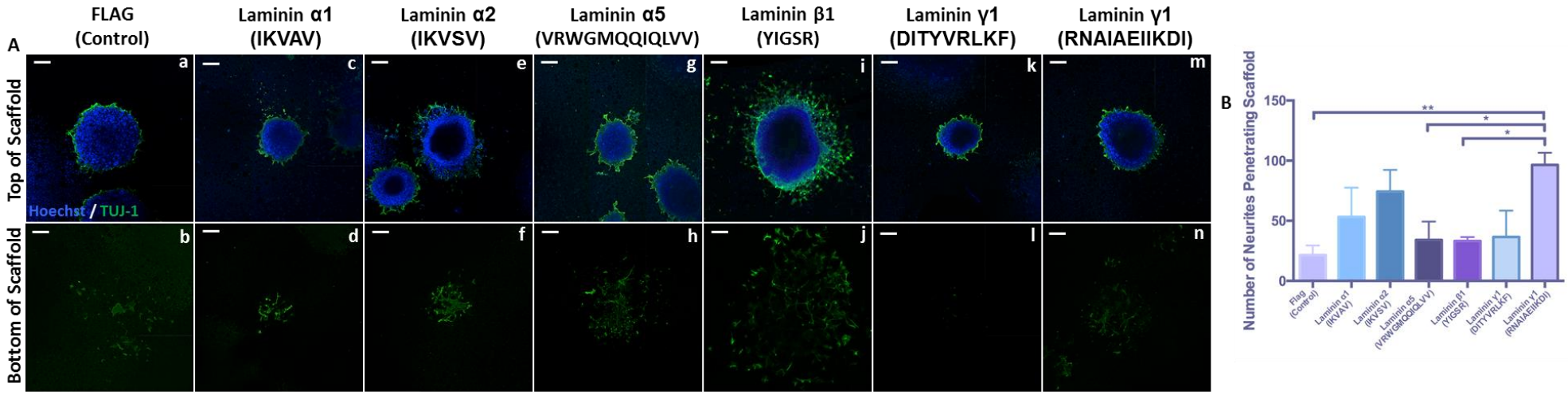

Fig 6-15: Identification of neurite promoting domains of laminin in 3D culture.
Representative confocal images of neurospheres cultured on top of Alvetex® scaffold coated using Orla technology with a range of laminin domains (A). Neurospheres reside on top of the scaffold (Aa,c,e,g,i,k,m) whilst TUJ-1 positive neurites (green) penetrate the depth of the scaffold and are visible from the underside (Ab,d,f,h,j,l,n). Scale bars: 200 µm. Quantification of the number of neurites penetrating the scaffold (B) (data represent mean ± SEM, n=9; 3 individual neurospheres were quantified from 3 independent replicates) reveals enhancement of neurite outgrowth by "IKVAV", "IKVSV" and "RNAIAEIIKDI" motifs. . One-way ANOVA with Tukey's multiple comparisons: * = $p \leq 0.05$, ** = $p \leq 0.01$, *** = $p \leq 0.001$, **** = $p \leq 0.0001$.

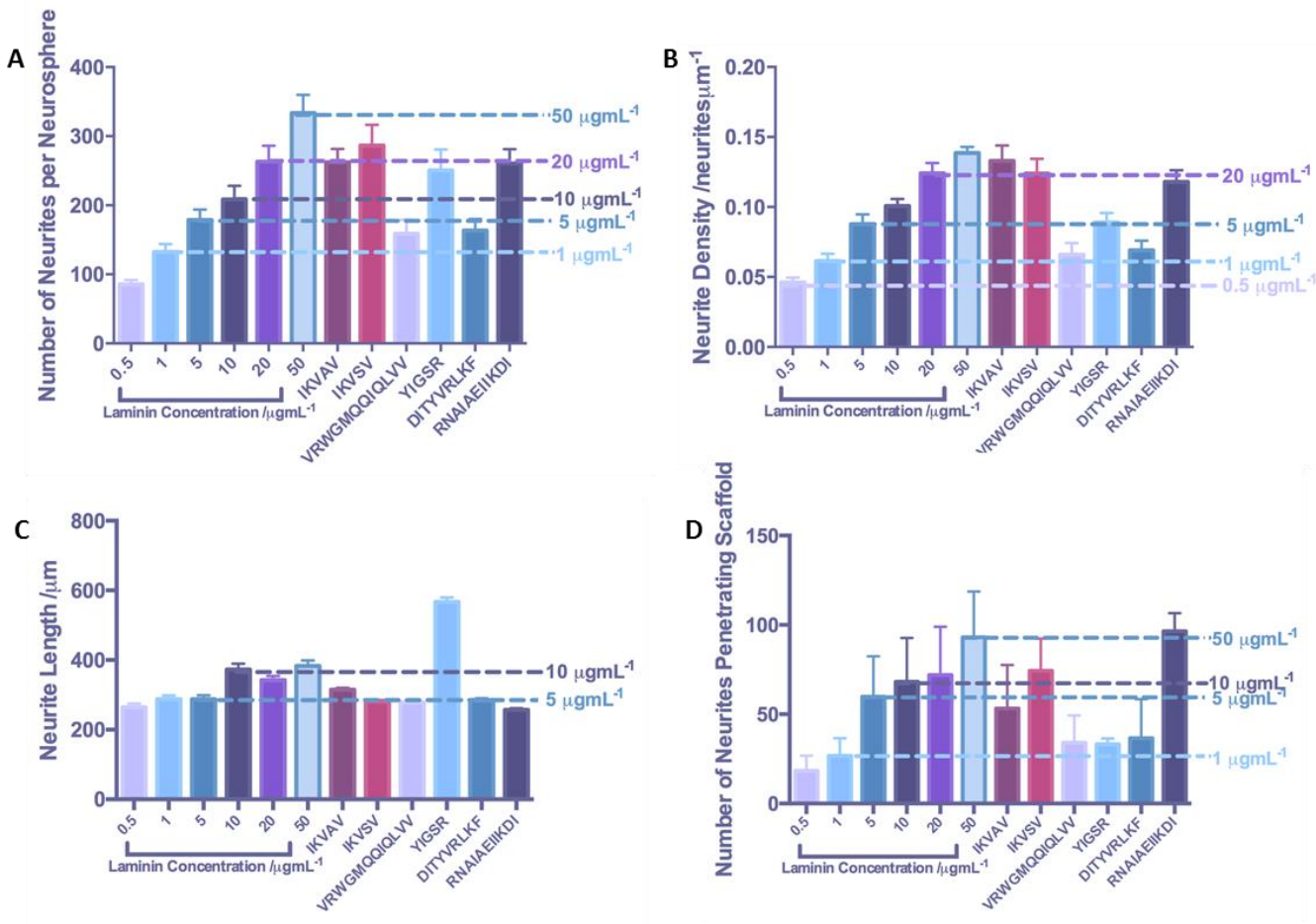

Fig 6-16: Comparison of Orla laminin motifs with laminin coated dose response using the estimated method of comparison. A side-by-side comparison of traditional laminin adsorption coating and each Orla laminin motif to determine the range of laminin coating that each motif is equivalent to in terms of number of neurites per neurosphere (A), neurite density (B), neurite length (C) and the number of neurites penetrating the scaffold in 3D culture (D).

Orla Laminin Motif	Range of [Laminin] from Estimated Method /μgmL^{-1}	Range of [Laminin] from Numerical Method /μgmL^{-1}
IKVAV	5 - 20	0.593 - 11.86
IKVSV	5 - 50	0.0059 - 28.65
VRWGMQQIQLVV	1 - 5	0 - 0.356
YIGSR	5 – 50	6.577 - 128.529
DITYVRLKF	1 - 5	0 - 0.407
RNAIAEIIKDI	1 - 20	0 - 46.2

Table 6-5: Comparison of Orla laminin motifs with traditional adsorption coating of laminin using the estimated and numerical methods of comparison.
A table comparing the range of laminin concentrations which each motif is equivalent to in terms of neurite number, density, length and penetration in 3D culture. The estimated method involves the side-by-side plotting of each data set adjacently (Figure 6-16) whereas the numerical method involves the analysis of a regression plotted through a laminin standard curve (Figure 6-11).

6.3.2 Inhibition of Neurite Outgrowth by Myelin Inhibitors found in the Glial Scar

To further investigate the molecular mechanisms that underpin neurite inhibition in the glial scar that forms following spinal cord injury, in addition to investigations outlined in Chapter IV, Orla surface technology was also used to functionalise 2D and 3D growth substrates with inhibitory molecules found in the glial scar. The myelin inhibitors of neurite outgrowth such as Nogo and OMGP, are found on myelin debris in the glial scar and activate NgRs to induce activation of Rho A and ROCK which ultimately leads to remodelling of the actin cytoskeleton along with inhibition of neurite growth and extension (reviewed by Figure 6-17)[32,309,323–325,327,331,614].

Therefore, to produce a more standardised model of neurite inhibition, to investigate the potential downstream signalling mechanisms involved in myelin-induced inhibition, 2D growth substrates were coated with OMGP and Nogo motifs to assess their effects upon neurite outgrowth. Neurospheres cultured on control surfaces (Figure 6-18Aa,b) generate a significant number of neurites that radiate from the central neurosphere, whereas, those cultured on OMGP (Figure 6-18Ac,d) coated 2D surfaces generate very few neurites. Similarly, neurite outgrowth from neurospheres cultured on substrates coated with Nogo in its traditional loop configuration (Figure 6-18Ae,f) is much less uniform with whole areas of the neurosphere free from neurite outgrowth. The Nogo sequence was also presented to cells in a linear configuration to determine if the loop structure is essential

for function, the linear Nogo sequence (Figure 6-18Ah,g) resulted in extension of few TUJ-1 positive (green) extensions. Similarly, a 50:50 coating mix of the two Nogo configurations (Figure 6-18Ai,j) resulted in the extension of few; short neurites compared with neurospheres cultured on FLAG coated surfaces.

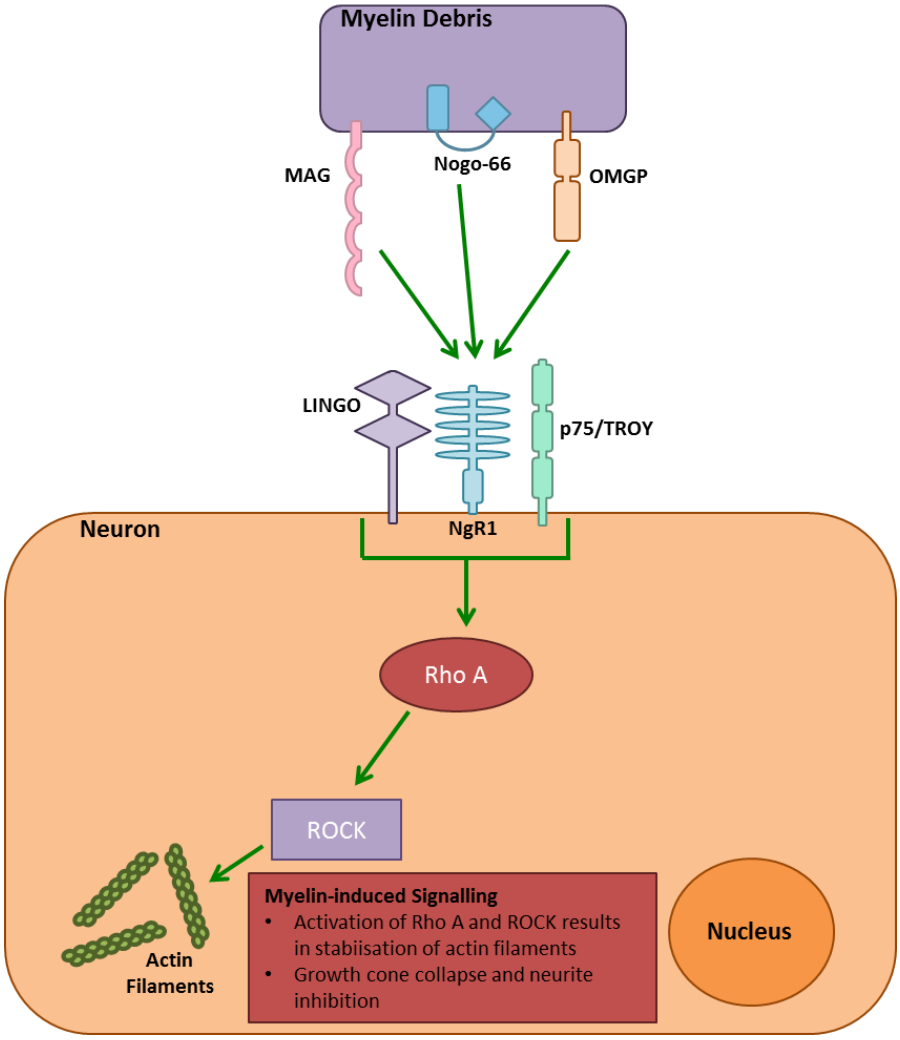

Fig 6-17: Myelin-induced inhibition of neurite outgrowth in the glial scar.
Inhibitory molecules such as Nogo-66, MAG and OMGP present on myelin debris released from damaged neurons induce growth cone collapse and neurite retraction in the glial scar. This is achieved through activation of the Nogo receptor (NgR) which leads to activation of the Rho A and ROCK signalling pathway. Activation of ROCK results in stabalisation of actin filaments and growth cone collapse, leading to the inability of neurons to regenerate neuritic processes.

The number of neurites per neurosphere (Figure 6-18B) was significantly reduced by the coating of growth substrates with each inhibitory motif compared with the control, FLAG coating. The Nogo linear configuration was also found to significantly reduce the number of neurites generated per neurosphere compared with both OMGP and Nogo loop motifs. Neurite density (Figure 6-18C) was also significantly reduced by all inhibitory coatings, with the Nogo linear domain inducing neurite inhibition to the greatest extent and significantly reducing neurite outgrowth further than OMGP.

Similarly to neurite number and density, neurite length (Figure 6-18D) was also significantly inhibited compared with control FLAG, by all inhibitory coated surfaces. The Nogo loop domain also significantly inhibited neurite length to a greater degree than OMGP or the 50:50 Nogo Mix coatings.

In 3D culture, neurospheres remained on top of Alvetex® scaffold (Figure 6-19Aa,c,e,g,i) with TUJ-1 positive (green) neurites penetrating the scaffold and exiting from the bottom of the 3D material (Figure 6-19Abd,f,h,j). Significant neurite penetration can be observed from the underside of FLAG-coated (Figure 6-19Aa,b) scaffolds whereas few neurites visibly penetrate the inhibitory-coated materials (Figure 6-19c-j). Quantification reveals that neurite penetration (Figure 6-19B) is reduced by coating of the 3D growth environment with each myelin inhibitory molecule, with only the 50:50 mix of each Nogo configuration inducing a significant reduction in neurite outgrowth compared with FLAG.

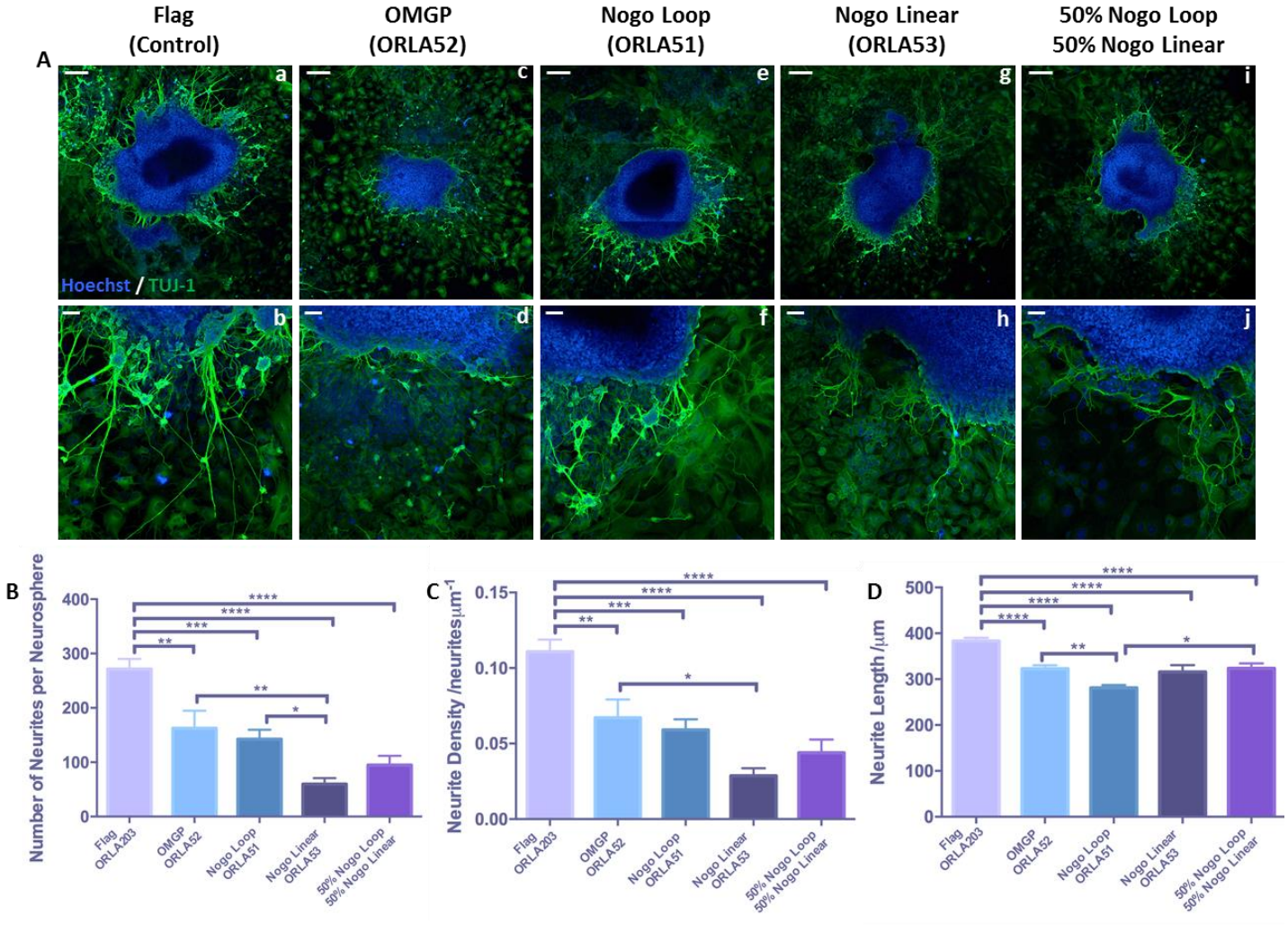

Fig 6-18: Orla motifs found on inhibitory molecules within the glial scar, induce neurite inhibition in 2D culture.
Representative confocal images (A) of neurospheres cultured on 2D surfaces coated with a control motif (Aa,b), an OMGP motif (Ac,d), a Nogo motif in a loop (Ae,f) or linear configuration (Ag,h) and a mixture of the two Nogo configurations (Ai,j). Neurite outgrowth is highlighted in green by positive expression of the pan-neuronal marker TUJ-1 and nuclei are stained in blue. Scale bars: (Aa,c,e,g,i): 200 µm (Ab,d,f,h,j): 50 µm. Neurite number (B) (data represent mean ± SEM, n=9; 3 individual neurospheres were quantified from 3 independent replicates), density (C) (data represent mean ± SEM, n=9; 3 individual neurospheres were quantified from 3 independent replicates) and length (D) (data represent mean ± SEM, n=118-492; between 118-492 neurites were measured from 3 neurospheres per independent replicate, of which there were 3) are all inhibited by the inhibitory motifs with length being inhibited to a greater degree by the Nogo loop configuration and number/density being inhibited a greater degree by the Nogo linear configuration. One-way ANOVA with Tukey's multiple comparisons: * = $p \leq 0.05$, ** = $p \leq 0.01$, *** = $p \leq 0.001$, **** = $p \leq 0.0001$.

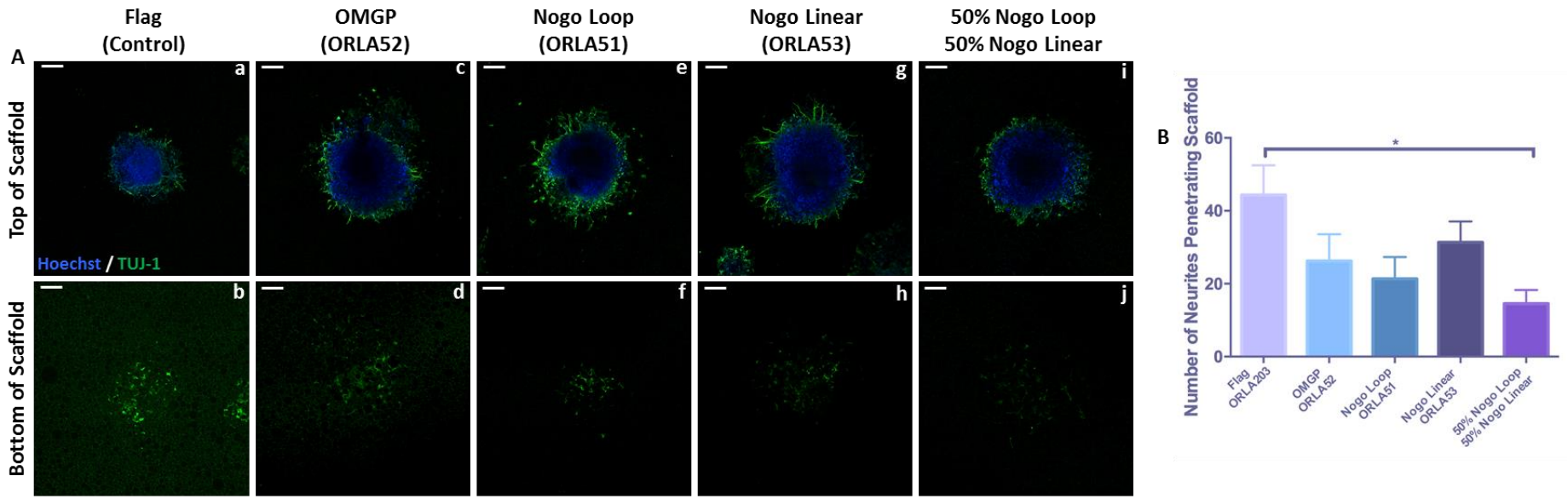

Fig 6-19: Orla motifs found on inhibitory molecules within the glial scar, induce neurite inhibition in 3D culture.
Representative confocal images (A) of neurospheres cultured on Alvetex® scaffold coated with a control motif (Aa,b), an OMGP motif (Ac,d), a Nogo motif in a loop (Ae,f) or linear configuration (Ag,h) and a mixture of the two Nogo configurations (Ai,j). Neurospheres remain on top of the scaffold (Aa,c,e,g,i) and TUJ-1 (green) positive neurites penetrate the 3D material and are visible from below (Ab,d,f,h,j). Nuclei are stained blue. Scale bars: 200 µm. Quantification of the number of neurites penetrating the 3D material (B) (data represent mean ± SEM, n=5-6; 1-2 individual neurospheres were quantified from 3 independent replicates) reveals that all motifs inhibit neurite outgrowth compared with the control flag peptide and the mixture of the two Nogo domains inhibits neurite outgrowth to the greatest degree. One-way ANOVA with Tukey's multiple comparisons: * = $p \leq 0.05$, ** = $p \leq 0.01$, *** = $p \leq 0.001$, **** = $p \leq 0.0001$.

6.3.2.1 Recovery of Myelin-induced Neurite Inhibition through Modulation Nogo Receptor Signalling

Inhibition of several aspects of NgR signalling has been demonstrated to restore functional recovery in animal models of SCI. For this reason, small molecule inhibitors have been added to the culture medium of 2D and 3D neurite outgrowth assays based on growth substrates coated with Orla inhibitory motifs (Nogo/OMGP). This demonstrates the potential application of this model to be used a screening tool to investigate the ability of small molecules to overcome myelin-induced neurite inhibition. The small molecules tested in this chapter include the selective ROCK inhibitor – Y-27632, inhibitor of Rho A – ibuprofen and an NgR antagonist – NEP 1-40. All of which inhibit either NgR signalling directly (NEP 1-40)[336,357] or downstream signal transduction (Y-27632[23,204,209,366] and ibuprofen[30,284,365,368,372]) with the aim of restoring normal neurite outgrowth.

6.3.2.1.1 Recovery of Nogo-mediated Inhibition

Neurospheres cultured in 2D on control FLAG-coated substrates (Figure 6-20Aa,b) generate a significant volume of TUJ-1 positive (green) neurites. However, neurospheres cultured on Nogo-coated substrates (Figure 6-20Ac,d) generate very few visible neurites. Supplementation of the culture medium with 10 μM Y-17632 (Figure 6-20Ae,f) resulted in the generation of a large number of neurites with neurite outgrowth appearing enhanced compared to that generated from the control surface. Treatment with 100 μM ibuprofen (Figure 6-20Ag,h) resulted in the generation of a similar number of neurites as the control surface, as did treatment with 1 μM NEP 1-40 (Figure 6-20Ai,j).

The number of neurites per neurosphere (Figure 6-20B) was reduced by Nogo coating alone and with the addition of Y-27632 to the culture medium; neurite number was significantly enhanced compared with both Nogo coating and FLAG coating without medium supplementation. Similarly, ibuprofen treatment significantly enhanced neurite number compared with Nogo coating alone, and slightly enhanced neurite outgrowth compared with the control FLAG substrate. NEP 1-40 supplementation restored neurite number to a similar level as the control FLAG-coated surface.

A similar trend was observed in terms of the density of neurite outgrowth (Figure 6-20C), which was significantly inhibited by Nogo coating. Neurite density was also significantly enhanced by the addition of Y-27632 to the culture medium both compared to FLAG and Nogo-coated substrates. Ibuprofen treatment significantly enhanced neurite density compared with Nogo and restored neurite density to a similar level as the control FLAG coating. Similarly, NEP 1-40 treatment also restored neurite density to a similar level as the control.

Neurite length (Figure 6-20D) was also reduced by Nogo coating and was significantly enhanced by Y-27632 treatment compared with FLAG coating alone. Ibuprofen treatment however, further inhibited neurite length compared with Nogo coating alone and NEP 1-40 treatment had little effect upon neurite length.

Neurospheres were also cultured in 3D on Alvetex® scaffold coated with Flag (Figure 6-21Aa,b) or Nogo (Figure 6-21Ac,d) and supplemented with Y-27632 (Figure 6-21Ae,f), ibuprofen (Figure 6-21Ag,h) or NEP 1-40 (Figure 6-21i,j). Neurite outgrowth is visible from the underside of scaffolds coated with the control FLAG peptide, whereas, little to no neurite outgrowth is visible from the bottom view of scaffolds coated with the Orla Nogo motif. Treatment with 10 μM Y-27632 resulted in a large enhancement of neurite outgrowth, with a huge network of intertwining neurites becoming visible from the bottom view of the scaffold. Both ibuprofen and NEP 1-40 treatment resulted in neurite penetration through the inhibitory 3D growth matrix; however, enhancement comparable to that of Y-27632 was not observed.

Quantification of the number of neurites penetrating each scaffold (Figure 6-21B) reveals that neurite penetration in 3D culture was inhibited by Nogo coating of Alvetex® scaffold. Treatment with Y-27632 significantly enhanced neurite penetration compared with both FLAG and Nogo coatings alone, whilst, ibuprofen and NEP 1-40 treatment restores neurite penetration in the inhibitory growth environment, to a similar level as control FLAG.

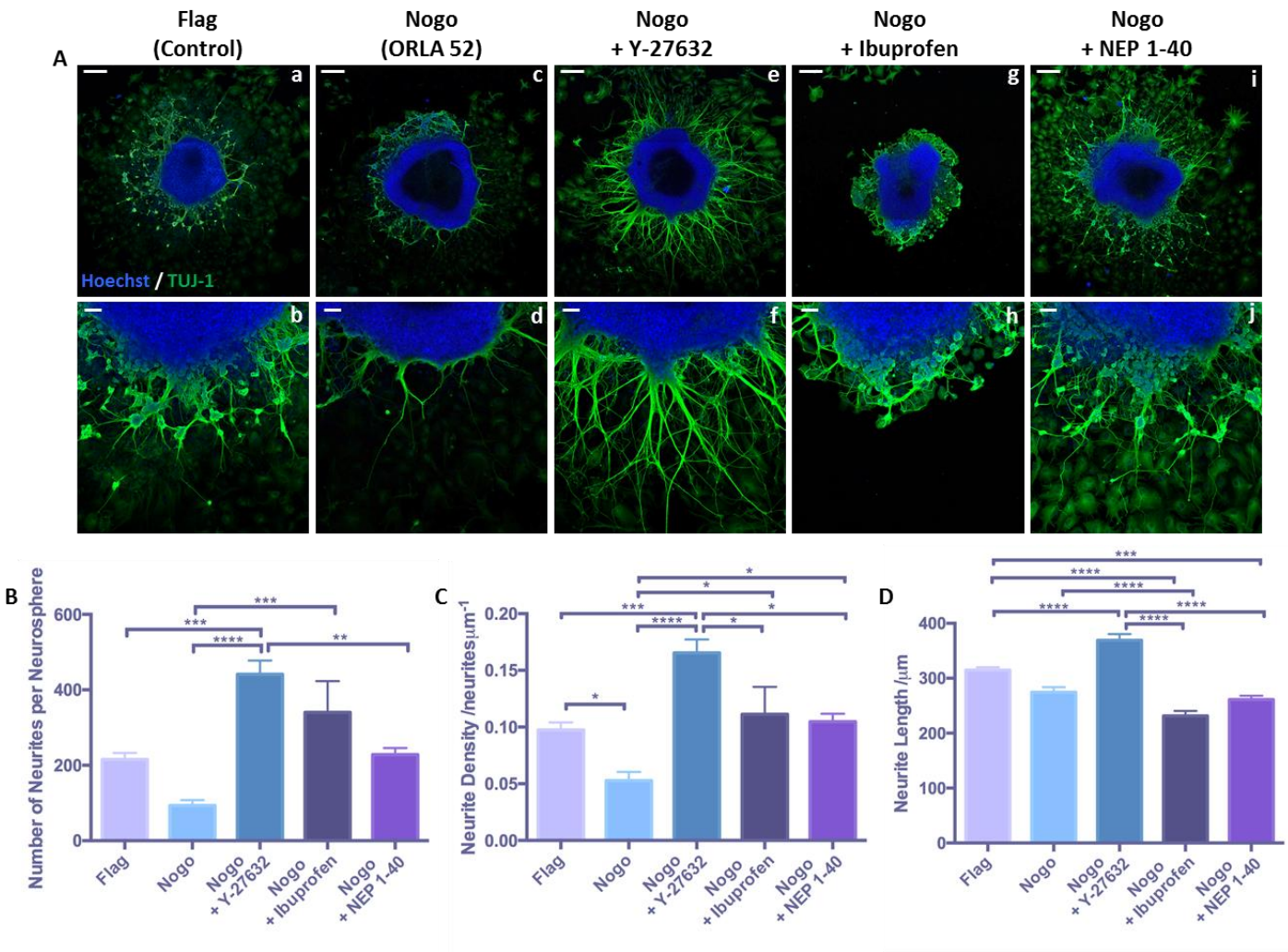

Fig 6-20: Recovery of Orla Nogo mediated neurite inhibition through inhibition of Nogo receptor signalling and its downstream pathway in 2D culture.

Representative confocal images of neurospheres cultured on Orla inhibitory surfaces coated with Nogo (A) and media supplementation with 15 µM Y-27632 (a selective ROCK inhibitor) (Ae,f), 500 µM ibuprofen (inhibitor of Rho A) (Ag,h) or 1 µM NEP 1-40 (Nogo receptor antagonist peptide) (Ai,j). Scale bars: (Aa,c,e,g,i): 200 µm (Ab,d,f,h,j): 50 µm. Quantification of the number of neurites per neurosphere (B) (data represent mean ± SEM, n=15; 5 individual neurospheres were quantified from 3 independent replicates) and neurite density (C) (data represent mean ± SEM, n=15; 5 individual neurospheres were quantified from 3 independent replicates) demonstrates the ability of Nogo to induce neurite inhibition, which is recovered by each media supplement. Neurite length (D) (data represent mean ± SEM, n=45-391; between 45-391 neurites were measured from 5 neurospheres per independent replicate, of which there were 3) is enhanced by Y-27632 and inhibited in all other conditions. One-way ANOVA with Tukey's multiple comparisons: * = $p \leq 0.05$, ** = $p \leq 0.01$, *** = $p \leq 0.001$, **** = $p \leq 0.0001$.

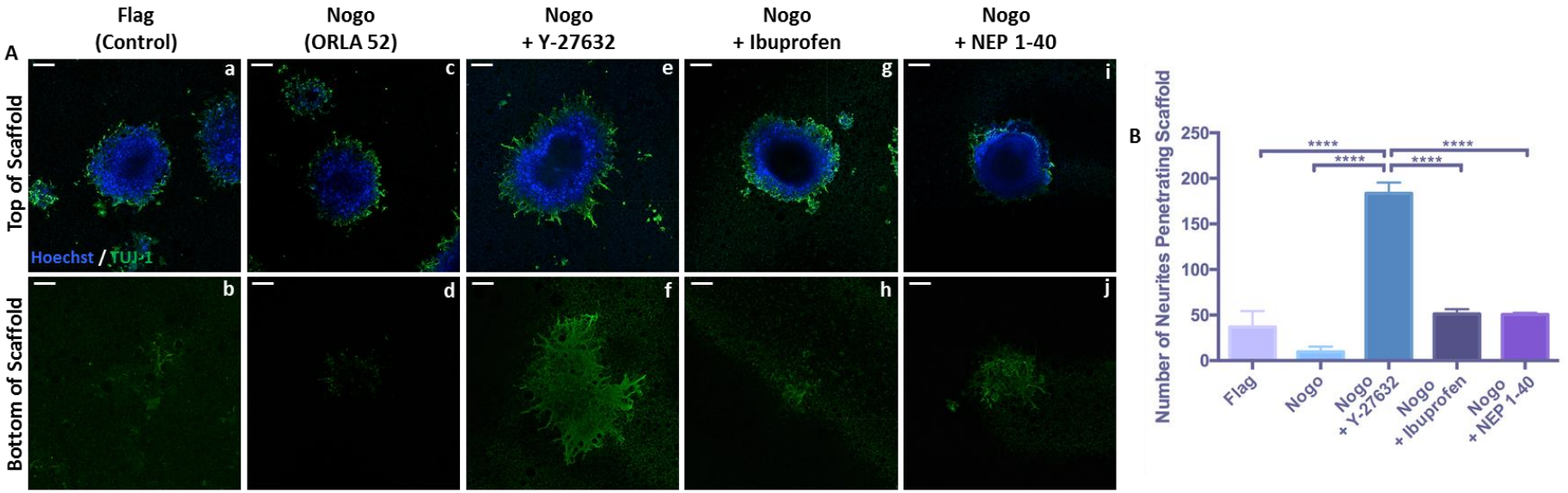

Fig 6-21: Recovery of Orla Nogo mediated neurite inhibition through inhibition of Nogo receptor signalling and its downstream pathway in 3D culture. Representative confocal images (A) of neurospheres cultured on top of Alvetex® scaffold coated with an Orla Nogo motif and culture medium supplemented with 15 µM Y-27632 (a selective ROCK inhibitor) (Ae,f), 500 µM ibuprofen (inhibitor of Rho A) (Ag,h) or 1 µM NEP 1-40 (Nogo receptor antagonist peptide) (Ai,j). Neurospheres remain on top of the scaffold with nuclei being stained blue (Aa,c,e,g,i) whereas TUJ-1 positive neurites (green) penetrate the depth of the 3D material (Ab,d,f,h,j). Scale bars: 200 µm. Quantification of the number of neurites penetrating the 3D material (B) (data represent mean ± SEM, n=9; 3 individual neurospheres were quantified from 3 independent replicates) reveals that ibuprofen and NEP 1-40 recover Nogo-mediated inhibition to a level that is similar to the control and Y-27632 enhances neurite outgrowth to a level greater than the control. One-way ANOVA with Tukey's multiple comparisons: * = $p \leq 0.05$, ** = $p \leq 0.01$, *** = $p \leq 0.001$, **** = $p \leq 0.0001$.

6.3.2.1.2 Recovery of OMGP-mediated Inhibition

Neurospheres were also cultured in 2D on growth substrates coated with the control FLAG (Figure 6-22Aa,b) and inhibitory OMGP (Figure 6-22Ac,d) sequences with Y-27632 (Figure 6-22Ae,f), ibuprofen (Figure 6-22Ag,h) or NEP 1-40 (Figure 6-22Ai,j) supplementation. Significant neurite outgrowth visibly radiated from neurospheres cultured on FLAG control substrates, whereas very little neurite outgrowth was visible from neurospheres cultured on OMGP coated surfaces. Supplementation with 10 μM Y-27632 resulted in a significant enhancement in neurite generation compared with both FLAG and OMGP coatings. Treatment with 100 μM ibuprofen or 1 μM NEP 1-40 resulted in neurite outgrowth that appeared similar to that obtained from FLAG coatings.

The number of neurites generated per neurosphere (Figure 6-22B) was significantly inhibited by OMGP coating. This was also significantly enhanced by Y-27632 culture medium supplementation compared with all other conditions tested. Ibuprofen treatment resulted in a slight enhancement of neurite number on the inhibitory coating and NEP 1-40 treatment resulted in the generation of a similar number of neurites to the control FLAG coating. Neurite density (Figure 6-22C) quantification revealed a similar trend in that OMGP coating significantly inhibited neurite density compared with FLAG. Y-27632 treatment also significantly enhanced neurite density compared with all other conditions tested, whilst ibuprofen and NEP 1-40 treatment rescued neurite density to a similar level as the FLAG control.

Similarly, neurite length (Figure 6-22D) was also significantly reduced when neurospheres were cultured on OMGP coated surfaces, compared with FLAG. This reduction in neurite length was rescued to a similar level as the control by Y-27632 treatment, however ibuprofen and NEP 1-40 had little beneficial effect upon rescue of neurite length on OMGP coated surfaces.

Neurospheres cultured in 3D on Alvetex® scaffold coated with the control FLAG sequence (Figure 6-23Aa,b) generate significant neurite outgrowth as visible from the underside of the scaffold, as the neurites have penetrated the entire depth of the 3D material. However, few neurites are visible from the underside of OMGP coated scaffolds (Figure 6-23Ac,d) and 10 μM Y-27632 resulted in a large volume of neurites visible from the underside of the scaffold (Figure 6-23Ae,f). Treatment with both 100 μM ibuprofen (Figure 6-23Ag,h) and 1 μM NEP 1-40 (Figure 6-23i,j) resulted in more neurites that had visibly penetrated the scaffold than OMGP coating alone.

The number of neurites that penetrated the 3D material (Figure 6-23B) was reduced by OMGP coating of the scaffold, and significantly enhanced by Y-27632 treatment compared

with all other conditions tested. Treatment with ibuprofen had little effect on neurite penetration within this inhibitory 3D microenvironment, whereas, NEP 1-40 treatment resulted in a similar level of neurite penetration as FLAG cultures.

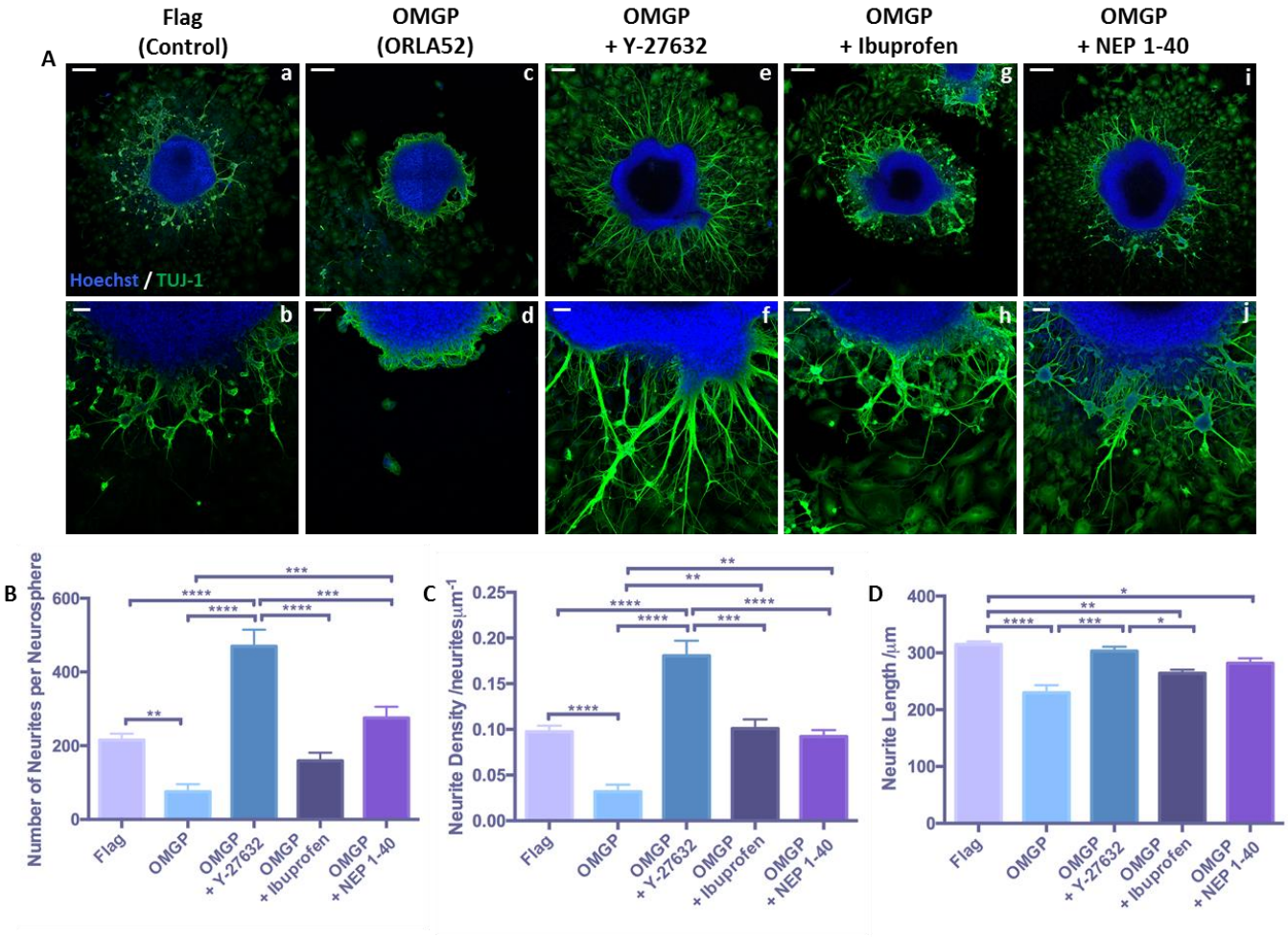

Fig 6-22: Recovery of Orla OMGP mediated neurite inhibition through inhibition of Nogo receptor signalling and its downstream pathway in 2D culture.
Representative confocal images of neurospheres cultured on Orla inhibitory surfaces coated with OMGP (A) and media supplementation with 15 µM Y-27632 (a selective ROCK inhibitor) (Ae,f), 500 µM ibuprofen (inhibitor of Rho A) (Ag,h) or 1 µM NEP 1-40 (Nogo receptor antagonist peptide) (Ai,j). Scale bars: (Aa,c,e,g,i): 200 µm (Ab,d,f,h,j): 50 µm. Quantification of the number of neurites per neurosphere (B) (data represent mean ± SEM, n=15; 5 individual neurospheres were quantified from 3 independent replicates) and neurite density (C) (data represent mean ± SEM, n=15; 5 individual neurospheres were quantified from 3 independent replicates) demonstrates the ability of OMGP to induce neurite inhibition, which is recovered by Y-27632 and partially recovered by ibuprofen and NEP 1-40. Neurite length (D) (data represent mean ± SEM, n=36-425; between 36-425 neurites were measured from 5 neurospheres per independent replicate, of which there were 3) is enhanced by Y-27632 and partially recovered by ibuprofen and NEP 1-40. One-way ANOVA with Tukey's multiple comparisons: * = $p \leq 0.05$, ** = $p \leq 0.01$, *** = $p \leq 0.001$, **** = $p \leq 0.0001$.

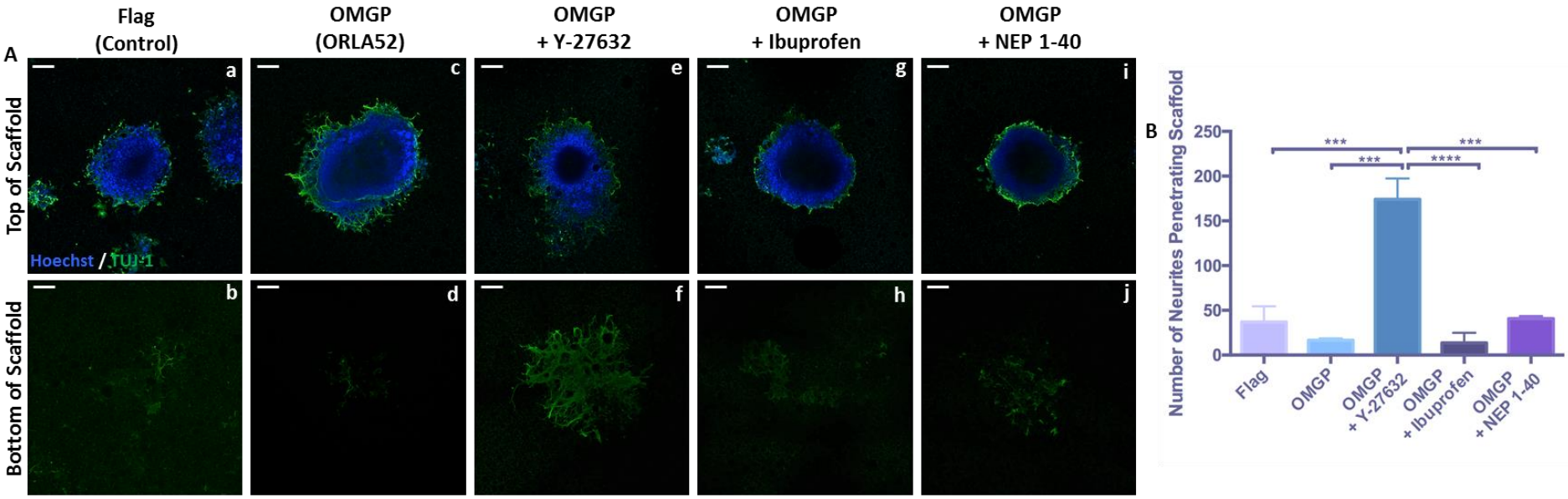

Fig 6-23: Recovery of Orla OMGP mediated neurite inhibition through inhibition of nogo receptor signalling and its downstream pathway in 3D culture. Representative confocal images (A) of neurospheres cultured on top of Alvetex® scaffold coated with an Orla OMGP motif and culture medium supplemented with 15 μM Y-27632 (a selective ROCK inhibitor) (Ae,f), 500 μM ibuprofen (inhibitor of Rho A) (Ag,h) or 1 μM NEP 1-40 (Nogo receptor antagonist peptide) (Ai,j). Neurospheres remain on top of the scaffold with nuclei being stained blue (Aa,c,e,g,i) whereas TUJ-1 positive neurites (green) penetrate the depth of the 3D material (Ab,d,f,h,j). Scale bars: 200 μm. Quantification of the number of neurites penetrating the 3D material (B) (data represent mean ± SEM, n=9; 3 individual neurospheres were quantified from 3 independent replicates) reveals that ibuprofen has no effect on neurite outgrowth whereas NEP 1-40 recovers OMGP-mediated inhibition to a level that is similar to the control and Y-27632 enhances neurite outgrowth to a level greater than the control. One-way ANOVA with Tukey's multiple comparisons: * = $p \leq 0.05$, ** = $p \leq 0.01$, *** = $p \leq 0.001$, **** = $p \leq 0.0001$.

6.3.2.1.3 Recovery of OMGP/Nogo-mediated Inhibition

In addition to this, the effect of 2D and 3D growth substrates coated with a 50:50 mixture of Nogo and OMGP inhibitory motifs upon neurite outgrowth was also examined. In 2D culture neurospheres were cultured on FLAG control coated substrates (Figure 6-24Aa,b) and significant neurite outgrowth was observed. Neurospheres were also cultured on growth substrates coated with a mixture of both OMGP and Nogo motifs (Figure 6-24Ac,d), which resulted in the generation of neurites that appeared shorter and neurite outgrowth that appeared less dense compared with control FLAG coating. Cultures were also treated with 10 μM Y-27632 (Figure 6-24Ae,f), which resulted in extremely dense neurite outgrowth with neurites appearing much longer than from any other culture condition. Furthermore, cultures were also treated with 100 μM ibuprofen (Figure 6-24Ag,h) and 1 μM NEP 1-40 (Figure 6-24Ai,j) which resulted in neurite outgrowth similar to that of neurospheres cultured on FLAG control substrates.

The number of neurites generated per neurosphere (Figure 6-24B) was significantly inhibited by the OMGP and Nogo coating mixture. This inhibitory effect was recovered by medium supplementation with ibuprofen and NEP 1-40, restoring neurite outgrowth to a similar level as the control FLAG substrate. However, as with the other inhibitory coatings tested, Y-27632 treatment resulted in an enhancement of neurite number of OMGP and Nogo coated surfaces. Y-27632 significantly enhanced neurite number compared with both FLAG and Nogo/OMGP coated substrates alone. A similar effect was also observed in terms of neurite density (Figure 6-24C), as Nogo/OMGP coating resulted in a significant inhibition in neurite density, which was recovered by both ibuprofen and NEP 1-40 and enhanced by Y-27632 treatment.

Neurite length (Figure 6-24D) was also significantly inhibited compared to FLAG by OMGP and Nogo coating. This effect was partially restored by Y-27632 treatment, and completely restored by NEP 1-40 treatment. However, ibuprofen treatment had little effect upon neurite length in this model of neurite inhibition.

Neurospheres were also cultured in 3D on scaffolds coated with Nogo and OMGP. In all cases neurospheres remained on top of the scaffold (Figure 6-25Aa,c,e,g,i), whilst TUJ-1 positive (green) neurites were visible from the bottom view of the scaffold (Figure 6-25Ab,d,f,h,j) having penetrated the depth of the 3D material. Significant neurite outgrowth can be visualised from the underside of scaffolds coated with the control FLAG sequence (Figure 6-25Aa,b), whereas no neurites have visibly penetrated the scaffold coated with the inhibitory Nogo and OMGP mixture (Figure 6-25Ac,d). Treatment with 10 μM Y-27632 (Figure 6-25Ae,f) resulted in significant neurite outgrowth, with a large interconnecting network of neurites visible from the bottom of the scaffold. Both 100 μM ibuprofen

(Figure 6-25Ag,h) and 1 μM NEP 1-40 (Figure 6-25Ai,j) treatment resulted in a significant amount of neurite penetration into the 3D scaffold.

The number of neurites penetrating the scaffold (Figure 6-25B) was quantified in each case, and it was found that Nogo and OMGP coating reduced neurite penetration compared with the FLAG coating alone. Treatment with Y-27632 significantly enhanced neurite penetration compared with all other conditions tested. Ibuprofen treatment resulted in a partial recovery of neurite outgrowth within the inhibitory 3D growth environment, whereas, NEP 1-40 treatment restored neurite outgrowth to a similar level as the control.

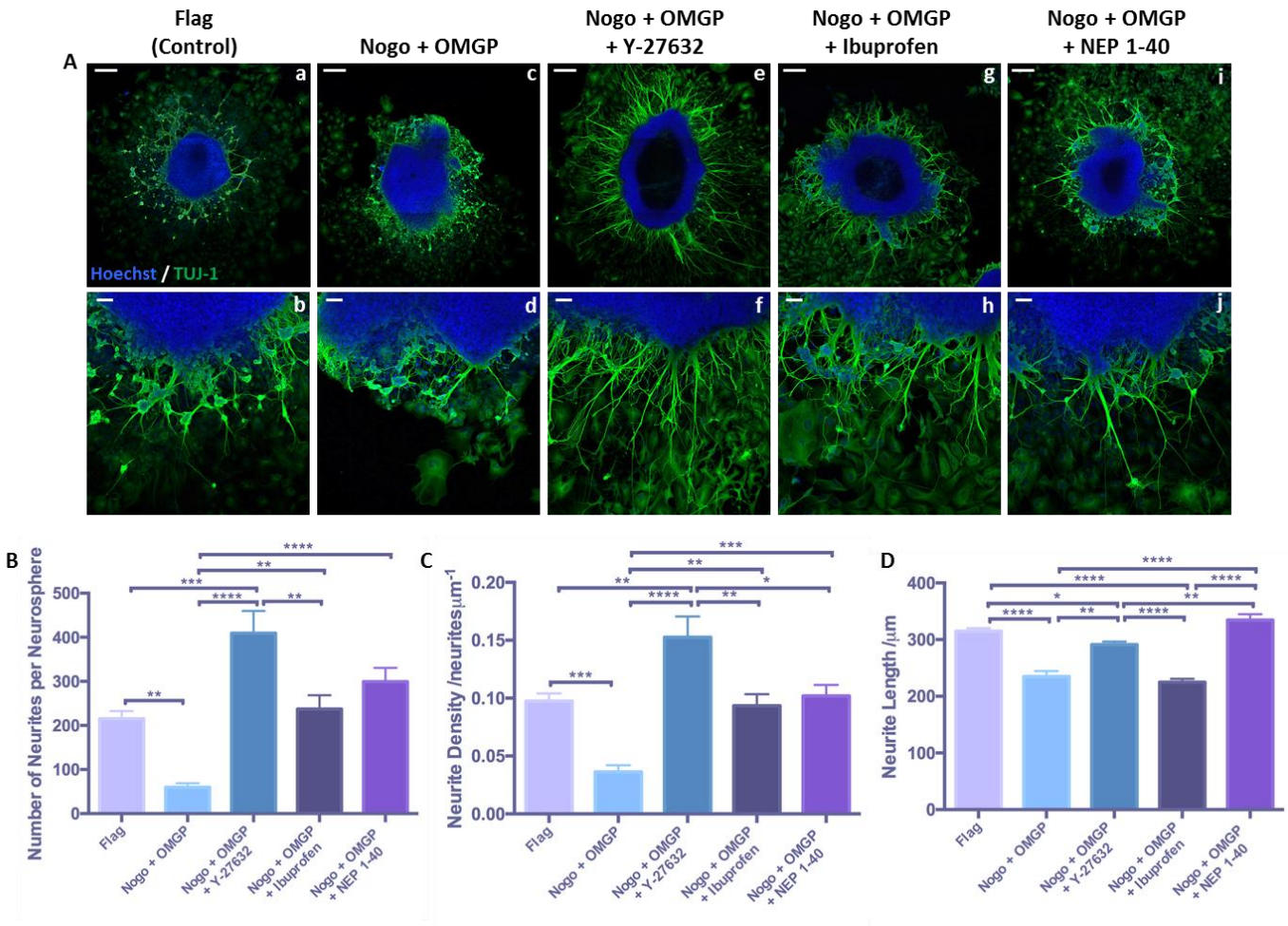

Fig 6-24: Recovery of Orla OMGP:Nogo mediated neurite inhibition through inhibition of Nogo receptor signalling and its downstream pathway in 2D culture.
Representative confocal images of neurospheres cultured on Orla inhibitory surfaces coated with a 50:50 mixture of nogo and OMGP motifs (A) along with media supplementation of 15 µM Y-27632 (a selective ROCK inhibitor) (Ae,f), 500 µM ibuprofen (inhibitor of Rho A) (Ag,h) or 1 µM NEP 1-40 (nogo receptor antagonist peptide) (Ai,j). Scale bars: (Aa,c,e,g,i): 200 µm (Ab,d,f,h,j): 50 µm. Quantification of the number of neurites per neurosphere (B) (data represent mean ± SEM, n=15; 5 individual neurospheres were quantified from 3 independent replicates) and neurite density (C) (data represent mean ± SEM, n=15; 5 individual neurospheres were quantified from 3 independent replicates) demonstrates the ability of the inhibitory substrate induced neurite inhibition, which is recovered by all media supplements tested. Neurite length (D) (data represent mean ± SEM, n=74-426; between 74-426 neurites were measured from 3 neurospheres per independent replicate, of which there were 3) from neurospheres cultured upon the inhibitory substrate is enhanced by Y-27632 and NEP 1-40. One-way ANOVA with Tukey's multiple comparisons: * = $p \leq 0.05$, ** = $p \leq 0.01$, *** = $p \leq 0.001$, **** = $p \leq 0.0001$.

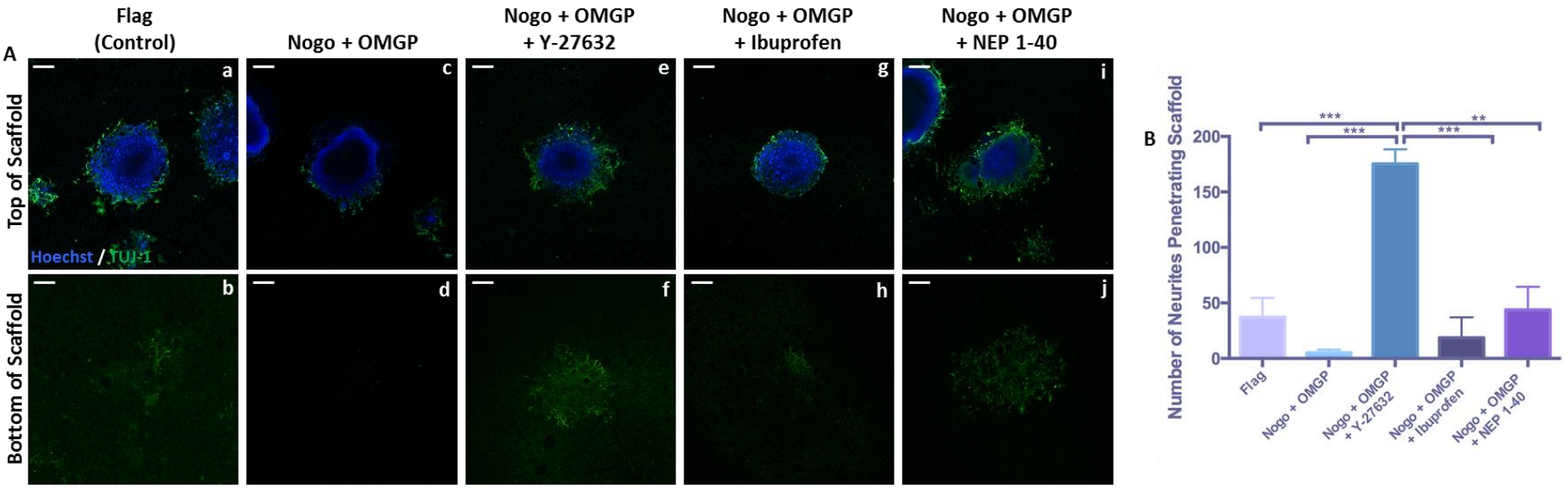

Fig 6-25: Recovery of Orla OMGP:Nogo mediated neurite inhibition through inhibition of Nogo receptor signalling and its downstream pathway in 3D culture.

Representative confocal images (A) of neurospheres cultured on top of Alvetex® scaffold coated with an 50:50 mixture of Orla OMGP and Nogo motifs with culture medium supplemented of 15 μM Y-27632 (a selective ROCK inhibitor) (Ae,f), 500 μM ibuprofen (inhibitor of Rho A) (Ag,h) or 1 μM NEP 1-40 (Nogo receptor antagonist peptide) (Ai,j). Neurospheres remain on top of the scaffold with nuclei being stained blue (Aa,c,e,g,i) whereas TUJ-1 positive neurites (green) penetrate the depth of the 3D material (Ab,d,f,h,j). Scale bars: 200 μm. Quantification of the number of neurites penetrating the 3D material (B) (data represent mean ± SEM, n=9; 3 individual neurospheres were quantified from 3 independent replicates) reveals that ibuprofen has no effect on neurite outgrowth whereas NEP 1-40 recovers OMGP-mediated inhibition to a level that is similar to the control and Y-27632 enhances neurite outgrowth to a level greater than the control. One-way ANOVA with Tukey's multiple comparisons: * = $p \leq 0.05$, ** = $p \leq 0.01$, *** = $p \leq 0.001$, **** = $p \leq 0.0001$.

6.3.2.1.4 Summary

In order to ensure a fair comparison between all of the inhibitory and recovery conditions tested, each data set obtained from each inhibitory condition was plotted together to give an overall summary as to the data collected. The number of neurites generated per neurosphere in 2D culture (Figure 6-26A) was inhibited by all inhibitory coatings compared with FLAG and both OMGP and OMGP/Nogo significantly inhibited neurite number compared to FLAG. All supplementation with small molecule inhibitors of the NgR signalling pathway resulted in a reduction in variation between the inhibitory coatings, with no significant difference between each coating and FLAG. Therefore, it can be determined that each small molecule inhibitor (Y-27632, ibuprofen and NEP 1-40) successfully restored neurite number on each inhibitory substrate.

Similarly to neurite number, neurite density (Figure 6-26B) from 2D cultures was also reduced by all inhibitory coatings and significantly reduced by both OMGP and Nogo/OMGP coatings. Supplementation with Y-27632 resulted in less variation between the growth substrates, therefore Y-27632 treatment can be said to restore neurite density in the presence of these inhibitory stimuli. Although ibuprofen treatment in some cases did not restore neurite density to the same level as that of FLAG, there was found to be no statistically significant difference between each substrate. NEP 1-40 treatment also resulted in no statistically significant difference between each growth substrate except for the Nogo/OMGP coating, which resulted in significantly reduced neurite density compared to FLAG coating supplemented with NEP 1-40.

The length (Figure 6-26C) of neurites generated in 2D culture was always significantly inhibited on surfaces coated with Nogo and OMGP compared with the control FLAG growth substrate. Y-27632 treatment enhanced neurite length on Nogo-coated 2D surfaces, however even Y-27632 treatment did not rescue neurite length on OMGP and OMPG/Nogo coated surfaces. Ibuprofen and NEP 1-40 treatment also did not rescue neurite length on inhibitory-coated 2D surfaces.

In 3D culture, neurite penetration (Figure 6-26D) was inhibited by coating with all inhibitory molecules compared to control FLAG coating. Y-27632 treatment restored neurite penetration to a similar level within scaffolds coated with all molecules tested. Ibuprofen treatment resulted in restoration in neurite penetration with Nogo coating but not with OMGP or Nogo/OMGP coatings. NEP 1-40 treatment restored neurite penetration to control levels with all coatings.

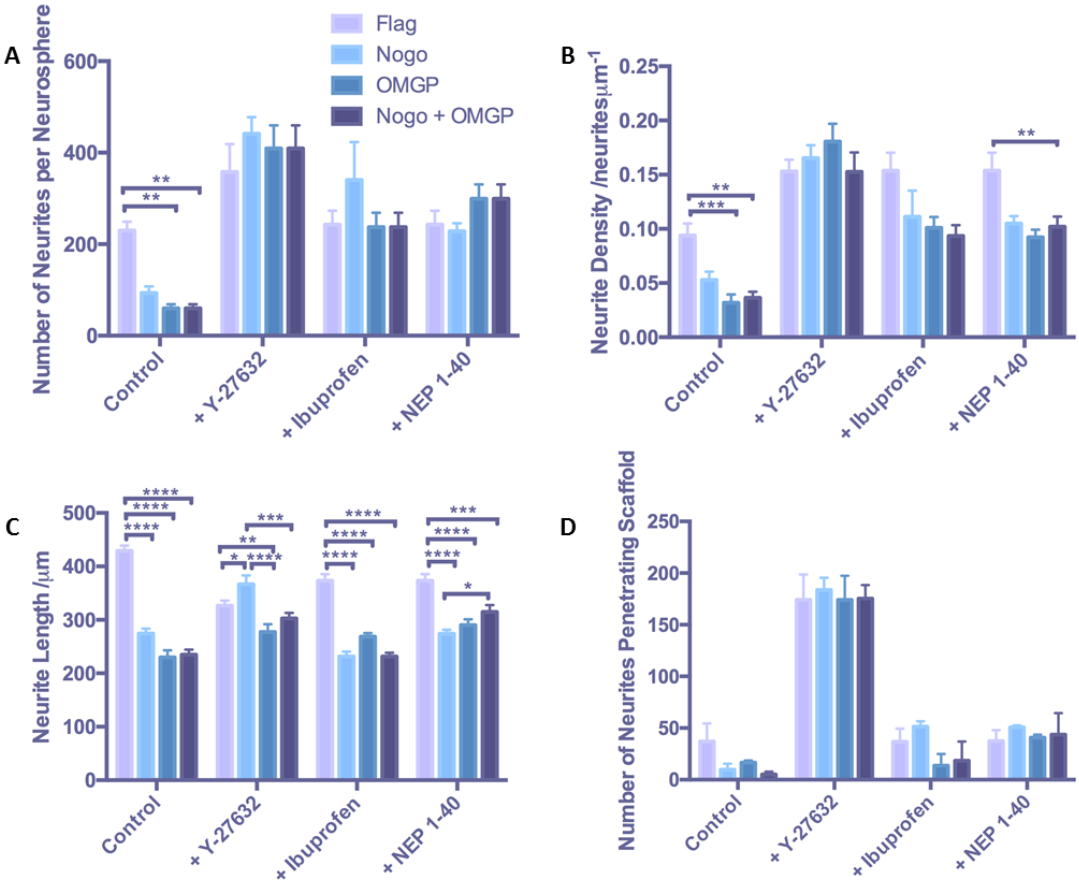

Fig 6-26: Comparison of Orla inhibitory motifs and methods of recovery.
Quantification of the number of neurites per neurosphere (A) (data represent mean ± SEM, n=15; 5 individual neurospheres were quantified from 3 independent replicates), neurite density (B) (data represent mean ± SEM, n=15; 5 individual neurospheres were quantified from 3 independent replicates), neurite length (C) (data represent mean ± SEM, n=36-426; between 36-426 neurites were measured from 5 neurospheres per independent replicate, of which there were 3) and neurite penetration in 3D (D) (data represent mean ± SEM, n=9; 3 individual neurospheres were quantified from 3 independent replicates) from neurospheres cultured on each Orla inhibitory surface. Two-way ANOVA with Tukey's multiple comparisons: * = $p \leq 0.05$, ** = $p \leq 0.01$, *** = $p \leq 0.001$, **** = $p \leq 0.0001$.

6.4 Discussion

6.4.1 The Role of the ECM in Neurite Development

The extracellular microenvironment has a large impact on cellular behaviour, for example the biochemical composition of the ECM influences many biological functions. This is the case in terms of neurite outgrowth, as ECM composition and integrin receptor expression both vary throughout development and have been linked to the reduced regenerative capacity of the adult CNS. The main aim of this chapter was to utilise novel protein surface

technology in collaboration with Orla Protein Technologies to further enhance the human pluripotent stem cell derived model of neuritogenesis described in Chapter III.

The ability of various ECM-derived amino acid sequences to induce neuritogenesis was tested in both 2D and 3D culture systems. This included the "MNYYSNS" domain of collagen IV, which was found to slightly enhance neurite outgrowth but its effects were limited compared with other ECM-derived motifs tested. This is consistent with other primary studies that have described the ability of "MNYYSNS" to promote neurite outgrowth in a PC12 model of neurite outgrowth but reduce neural differentiation and TUJ-1 expression in stem cell/neuroprogenitor derived models of neuritogenesis[613]. Here, we describe that this collagen IV-derived motif has a subtle yet significant impact on neurite outgrowth that could be due to the promotion of cellular adhesion[610]. Some *in vitro* models of neurite outgrowth incorporate collagen IV to biochemically promote neuritogenesis[529], however, the data detailed in this chapter suggest that other ECM-derived motifs may be more suitable for this purpose.

Similarly, the "RGDS" sequence derived from fibronectin was also found to have a positive effect upon neurite outgrowth. Again, this is consistent with published data, as this fibronectin-derived domain has also been previously documented to promote enhancement of neurite length[613]. The "RGD" motif itself has also been widely documented to promote neurite outgrowth from cultured neurons *in vitro* and is often incorporated into culture systems to promote neurite generation[547,615]. "RGD" is also a component of the laminin α chain and has been implicated in the neurite promoting effects of laminin in addition to fibronectin[615]; however, laminin has also been found to induce neurite outgrowth through a non-RGD-dependent mechanism, suggesting a role for other domains in neurite generation[616,617].

The primary function of the "YIGSR" domain of laminin is thought to be cell adhesion rather than neurite stimulation[598,618,619]. However, cellular adhesion and neurite generation are closely linked *in vitro*[620,621] and use of the "YIGSR" domain has been demonstrated to guide neurite outgrowth in 3D cultures[622,623]. The "YIGSR" motif of the laminin-β1 chain acts through the non-integrin receptor 67LR and has been implicated in axonal guidance and chemoattraction[624]. Previous studies have demonstrated that the "YIGSR" domain enhances both neurite length and branching *in vitro* which supports the evidence outlined in this chapter, that "YIGSR" can promote neuritogenesis in 2D and 3D culture and to a greater extent than collagen IV and fibronectin derived domains. This data suggests that laminin may play a more integral role in the developmental process of neuritogenesis than other ECM-derived components.

Both fibronectin and laminin-derived domains were found to enhance neurite outgrowth through a study that involved the combination of a novel EC cell-based model of neuritogenesis and Orla protein surface technology. However, the effect of both fibronectin and laminin on neurite outgrowth was also investigated using a novel iPSC-based model of neuritogenesis. This involved the assessment of the effect of adsorption coatings on neurite development. ReproCoat is the recommended coating solution for this cell type and includes fibronectin and laminin at unknown concentrations, and the effect of this coating solution upon neurite outgrowth was compared with the standard poly-D-lysine and laminin coating used throughout this project. ReproCoat resulted in significantly longer neurites that radiate and appeared to curve from the central neurosphere. This data may suggest that fibronectin has some involvement in neurite guidance and extension.

The EC cell-based model of neuritogenesis described and characterised in detail in Chapter III involved the coating of 2D and 3D growth substrates with 10 μgmL^{-1} poly-D-lysine and laminin solution. To further improve this model and enhance its robust and reproducible nature, Orla technology was utilised to produce 2D and 3D functionalised growth substrates containing a 50:50 mix of poly-D-lysine and laminin (YIGSR). This resulted in a significant enhancement of neurite length in 2D culture and neurite penetration in 3D culture.

Incorporating Orla coated growth substrates into the standard methodology of this model not only enhances neurite growth in 2D and 3D but also is advantageous in terms of reducing the use of animal-derived products within the model. Laminin from Engelbreth-Holm-Swarm murine sarcoma basement membrane is usually used for adsorption coating of growth substrates in the model, however, as this is an animal-derived product there are disadvantages associated with its use. Animal derived products can introduce unwanted variability into a model system[625], and the elimination of the use of murine-derived laminin in this system, produces a more standardised model for use in industrial applications including drug screening.

Furthermore, this chapter describes the use of Orla Protein Technology to coat 2D and 3D growth substrates with specific peptide sequences, in an active configuration to promote cellular interaction. This helps to recreate the biochemical microenvironment that a cell is exposed to *in vitro* and in combination with 3D cell culture technology is able to produce a more physiologically relevant model of neuritogenesis, producing data that more accurately reflects the *in vitro* process of neurite development.

6.4.2 Specific Laminin Domains Promote Neurite Outgrowth

The Laminin-I domain "YIGSR" was found to enhance neurite outgrowth to the greatest degree in 2D and 3D culture, compared with both fibronectin and collagen IV domains. For this reason, it was decided to focus investigations on the neurite promoting effects of laminin, particularly as laminin is commonly used in neuroscience research[626–629]. This initially involved assessing the effect of varying doses of "YIGSR" upon neurite outgrowth in 2D culture. From this, it became apparent that "YIGSR" had a dose-dependent effect upon all variables: neurite number, density and length, enhancing each aspect of neurite outgrowth with increasing "YIGSR" content of the growth substrate coating.

To further investigate the role of laminin in neurite development, the ability of other motifs to induce neuritogenesis in 2D and 3D culture was also evaluated. This study found that the "IKVAV" motif of the α1 chain and the similar "IKVSV" motif of the α2 chain successfully induced a greater number of neurites than other laminin-derived sequences tested. This is supported by evidence described throughout the literature, as "IKVAV" and "IKVSV" have both been shown to induce neurite development in several model systems[271,563,564,599], potentially through a β1 integrin dependent mechanism[630–632].

Other laminin-derived domains tested include the larger "VRWGMQQIQLVV" sequence of the α5 chain, which was found to inhibit some aspects of neurite outgrowth and have no effect upon others. This sequence is from the LG4 domain of α5, which has previously been shown to enhance neurite outgrowth *in vitro*[633]. However the α5 laminin chain is expressed only at low levels in the adult brain and is mostly expressed in tissues including: bone marrow, pancreas, lung and heart[634]. This could suggest that the α5 chain is not involved in neuritogenesis or neuronal homeostasis to the same extent as other laminin components.

In addition to this, sequences from the laminin γ1 chain including "DITYVRLKF" and "RNAIAEIIKDI" were also screened. Both sequences have been implicated in cell adhesion and neurite outgrowth *in vitro* previously[635], however the data described in this chapter reveals that neither sequence impacts neurite length significantly; however "RNAIAEIIKDI" does enhance neurite number and density in 2D culture and penetration into the scaffold in 3D culture. The distinct effects upon neurite density and length of "RNAIAEIIKDI" could support the hypothesis that neurite protrusion and elongation are supported by different signalling events. This was first hypothesised in Chapter III, due to the effects of the selective ROCK inhibitory, Y-27632, enhancing neurite number and density but inhibiting neurite length.

The Orla SURF platform offers several advantages over conventional adsorption coating including, reduction in the use of animal-derived products, excellent reproducibility, good availability of active sites and precise orientation of peptide motifs. Each laminin-derived Orla motif was compared with a standard dose-response of conventional adsorption coating with laminin from engelbreth-holm-swarm (EHS) murine sarcoma basement membrane. This comparison allowed for the determination of a concentration of EHS laminin coating equivalent to each Orla motif, which evokes the same response in terms of neurite generation. This comparison was achieved for all variables (neurite number, density, length and 3D penetration), resulting in an equivalent range of laminin concentrations.

Laminin from EHS contains laminin-1 ($\alpha1\beta1\gamma1$)[636]; therefore all of the sequences investigated in this study, apart from "IKVSV" and "VRWGMQQIQLVV" are present in the coating. This offers a direct comparison between whole molecule adsorption and Orla coating of the specific active sequence for most motifs assessed. Two methods of comparison were employed, the *"Estimated"* method involving side-by-side plotting to compare each data set and the *"Numerical"* method involving the use of the adsorption dose-response as a standard curve for each variable. This comparison resulted in a range of equivalent laminin concentrations for each motif from each method of comparison. The ranges obtained from the *"Estimated"* method of comparison are much broader than those obtained from the *"Numerical"* method, for example, for "DITYVRLKF" the "*Estimated*" method of comparison resulted in 1 – 5 μgmL^{-1} whereas the *"Numerical*" method of comparison resulted in 0 – 0.407 μgmL^{-1}.

Generally, comparison of most Orla motifs resulted in quite a vast range of laminin concentrations; however, the "YIGSR" motif resulted in neurites as long as those produced by 129 μgmL^{-1} EHS adsorption coating in 2D culture. This suggests that the same response in terms of neurite outgrowth, as extremely high concentrations of EHS adsorption coating, can be obtained by Orla coating with an active domain. This has many advantages such as standardising a model for industrial applications along with a reduction in coating time and reduction in the use of expensive coatings.

6.4.3 Modelling Myelin-Induced Neurite Inhibition in the Glial Scar In Vitro

The glial scar is an inhibitory environment that arises following SCI and prevents the regeneration of neurons and restoration of neural networks. One of the inhibitory mechanisms that contributes to the inability of neurites to grow and restore lost neural connections, involves the release of inhibitory molecules present on myelin debris from damaged neurons. These include the Nogo molecule consisting of an amino-terminal domain (amino-Nogo) and a 66 amino acid loop domain (Nogo-66), both known to elicit

neurite inhibition[33,34,39,220]. Oligodendrocyte myelin glycoprotein (OMGP) is also an inhibitor of neurite outgrowth found on myelin debris[33,34,39,220], and along with Nogo-66 activates the Nogo receptor (NgR), which acts through co-receptors (p75[324,327,328,331,508], TROY[329,637] and LINGO1[329,330,638]) to induce growth cone collapse and neurite retraction. Activation of NgR results in activation of Rho A and ROCK, which impacts actin dynamics resulting in neurite inhibition[32,309,322,366,368,400].

This chapter evaluated the use of Orla functionalised surfaces to study the molecular signalling events that underpin myelin-induced inhibition in the glial scar. To achieve this, 2D and 3D growth substrates were coated with Orla Nogo-66 and OMGP proteins. The 66-amino acid sequence of Nogo, known to interact with the NgR, was exposed to cells either as a loop structure (Nogo Loop) or as a linear sequence (Nogo Linear), as previous reports suggest that the loop configuration is essential for function[639–641]. Here we demonstrate that both Nogo configurations along with OMGP coatings inhibit neurite outgrowth in 2D and 3D culture systems with little difference in the level of inhibition between each motif. However, we do demonstrate that the Nogo-66 linear sequence, can elicit an inhibitory response contrary to popular opinion.

Orla functionalised inhibitory surfaces such as these provide opportunities to model and study the process of neurite inhibition that occurs following injury to the CNS. Applications for such a standardised model include the screening of small molecules to overcome inhibitory responses or a tool to investigate the molecular signalling events that drive the inhibitory response. Orla functionalised inhibitory surfaces offer a simplistic model of myelin-inhibition that can be used to dissect the underlying signalling pathways involved in this process.

6.4.3.1 Inhibition of NgR Receptor Signalling can Restore Neurite Outgrowth in the Presence of Myelin Inhibitors

Both OMGP and Nogo-66 are known to induce inhibition through the binding and activation of the Nogo receptor (NgR)[310,328,639,640]. This results in activation of Rho A and ROCK signalling, which ultimately impacts actin dynamics resulting in growth cone collapse and neurite retraction[32,322,331]. For this reason, several compounds that inhibit each stage of this signalling cascade were added to the model system with the aim of overcoming myelin-induced inhibition in each case (summarised in Figure 6-27). This not only demonstrates the potential application of this model as a drug screening system that could be used to identify regeneration-promoting compounds, but also provides more evidence building on existing knowledge as to the downstream signalling events that mediate inhibition.

The NgR antagonist peptide, NEP 1-40, mimics the first 40 amino acids of the Nogo-66 loop structure blocking receptor-ligand binding and has previously been shown to promote functional recovery in SCI models[336,357]. Data presented in this chapter describes the ability of NEP 1-40 to overcome OMGP and Nogo induced inhibition, restoring neurite outgrowth to control levels in 2D and 3D culture systems. This suggests that the neurite inhibition observed in this model is induced through the function of NgR, as expected. This helps to characterise the model, as NEP 1-40 treatment resulted in neurite recovery, as expected, suggesting that Nogo and OMGP are binding to NgR on the surfaces of developing neurites resulting in neurite inhibition, and when the function of this receptor is blocked, neurite growth is restored.

Activation of NgR is thought to lead to activation of Rho A and ibuprofen is a molecule known to inhibit Rho A and provide a beneficial response following SCI[30,368]. For this reason, ibuprofen was also tested in this model, to determine if Rho A activation was involved in myelin-induced inhibition and to determine the potential beneficial effect of ibuprofen upon neurite outgrowth in the presence of OMGP and Nogo. Ibuprofen treatment was found to have varying results depending on the variable measured, in some cases ibuprofen restored neurite outgrowth on the inhibitory substrates and in others only a partial restoration of neurite outgrowth was observed, but on the whole ibuprofen generally had a positive effect upon neurite outgrowth in this inhibitory system. This suggests that Rho A activation is an important event in the transmission of inhibitory signalling.

Rho A activation leads to activation of ROCK which ultimately results in the cytoskeletal changes associated with neurite inhibition. The selective ROCK inhibitor, Y-27632, is commonly used to overcome neurite inhibition and promote neurite outgrowth in other model systems[26,27,204,209], and was applied to this myelin-based model of inhibition to determine the role of ROCK in myelin-induced inhibition. The ROCK inhibitor was able to overcome and further enhance neurite outgrowth in all conditions and systems tested. This suggests that activation of ROCK is essential in the induction of neurite inhibition by OMGP and Nogo and also demonstrates a methodology that could be used to further enhance neurite outgrowth in this model.

Therefore, not only has neurite inhibition been achieved through the coating of 2D and 3D growth substrates with functional myelin-derived molecules, but recovery of neurite outgrowth has also been established through modulation of NgR and its downstream signalling. This provides a potential application for this model of inhibition as a drug screening tool that can be used to identify the ability of specific compounds to overcome myelin-induced inhibition or to further dissect the molecular signalling events involved in myelin-induced inhibition, building on data described within this chapter.

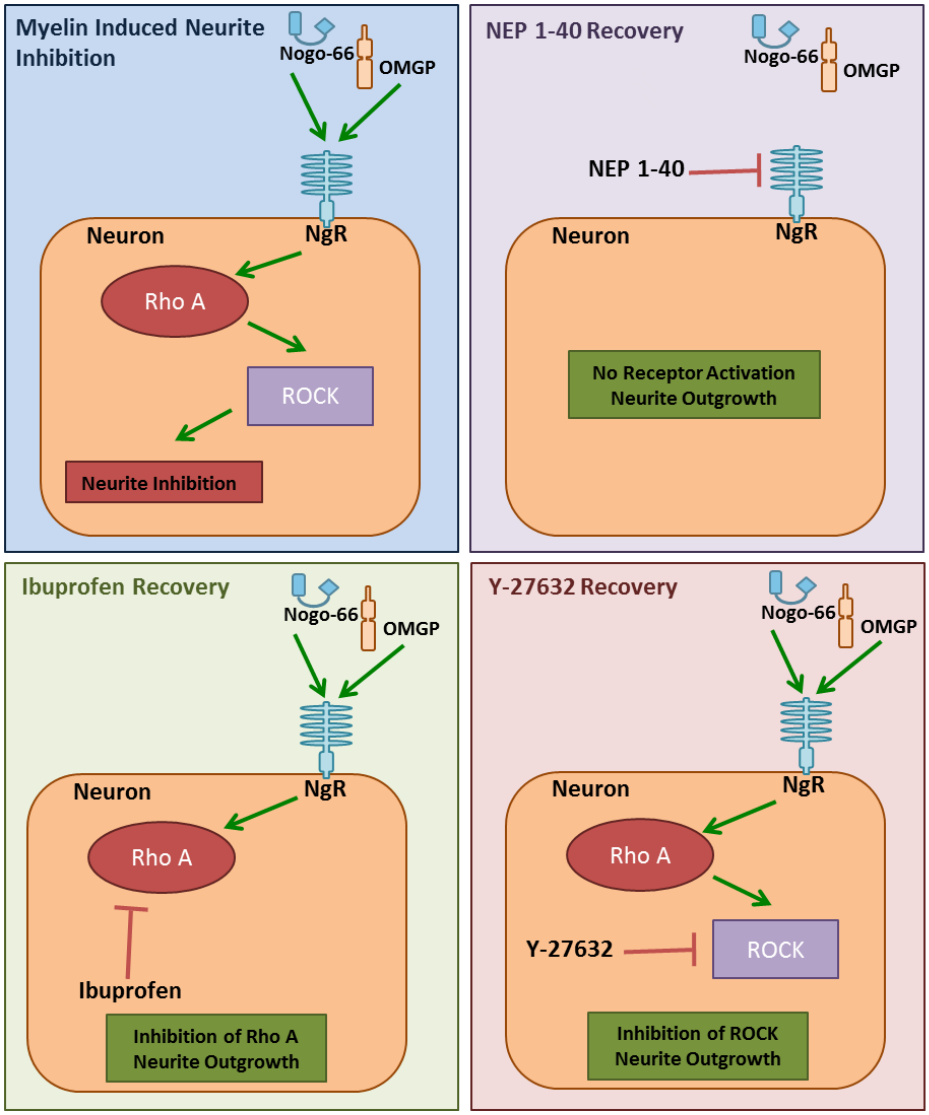

Fig 6-27: Schematic depicting mechanisms of recovery of myelin-induced neurite inhibition.
Myelin inhibitors of neurite outgrowth, including Nogo-66 and OMGP act through the NgR to induce Rho A and ROCK signalling events, leading to inhibition of neurite regeneration. This signalling process can be inhibited at various stages such as inhibition of receptor activation by the NgR antagonist peptide, NEP 1-40. Similarly, Rho A can be inhibited by ibuprofen and ROCK can be inhibited by Y-27632, all of which lead to recovery of neurite growth by reducing NgR activation and its downstream signalling cascade.

6.5 Key Findings

- ECM surface coatings enhanced neurite outgrowth in both 2D and 3D culture systems.

- Laminin-derived motifs enhanced neurite outgrowth to the greatest degree, compared with collagen and fibronectin-derived motifs.

- Orla poly-D-lysine and laminin coating, enhanced neurite length in 2D and penetration in 3D culture, compared with the traditional coating solution used in methodology.

- Laminin-derived motifs enhanced neurite outgrowth in a dose dependent manner.

- A variety of laminin-derived sequences induced neurite outgrowth ("IKVAV", "IKVSV"), whereas others reduced neurite outgrowth ("DITYVRLKF").

- Myelin-associated proteins expressed within the glial scar (Nogo, OMGP) inhibited neurite outgrowth in 2D and 3D culture.

- Inhibition of NgR activation (NEP 1-40), Rho A (ibuprofen) and ROCK (Y-27632), restored neurite outgrowth despite inhibitory coatings (Nogo, OMGP).

6.6 Conclusion

This chapter has involved the utilisation of Orla protein surface technology to identify extracellular protein domains involved in neurite growth and inhibition. This initially involved identification of ECM-derived sequences that were able to promote neurite growth, before focussing on the specific role of laminin in neurite generation. The specific role of laminin-derived amino acid sequences in neurite development was identified and compared with published data in other model systems. This suggests that specific laminin-receptor interactions are responsible for neurite induction and may be involved in the developmental process of neuritogenesis.

In addition to this, a comparison between traditional adsorption laminin coating and each Orla laminin-derived domain was conducted to determine the neurite promoting ability of each motif compared with established methodologies. This varied enormously depending upon the variable of interest and Orla surfaces were found to enhance neurite length to the greatest degree with the "YIGSR" domain inducing a similar length of neurite as 129 μgmL^{-1} laminin coating, which would be very expensive to replicate using the traditional adsorption technique. In addition to being a more economical basis for a model, the Orla coating procedure also offers a more standardised alternative to traditional coating methodologies. This is particularly important depending on the specific application of the model.

Furthermore, this chapter also describes the potential application of this model to study the process of neurite inhibition that occurs in the glial scar following SCI. This involved the coating of growth substrates with Orla inhibitory molecules including OMGP and Nogo. Not only is this useful in the study of the molecular processes that underpin myelin-induced neurite inhibition, but this inhibitory model is also suitable for the screening of potential compounds that are able to restore neurite regeneration in this inhibitory environment. Functionalisation of 2D and 3D growth substrates restores aspects of the *in vivo* biochemical environment, providing a more physiologically relevant microenvironment to study many aspects of cell biology.

6.7 Future Directions

Future work building upon the data described in this chapter could include the following:

- Investigate the ability of growth substrates coated with mixtures of each laminin domain to induce neurite outgrowth. A variety of combinations of laminin-derived amino acid sequences could be used to optimise the most effective Orla substrate in terms of neurite generation.

- A thorough analysis of the expression of specific integrins and laminin receptors in this EC cell-based model of neuritogenesis could be conducted. This could help support the fact that certain motifs had a large impact on neurite growth. This may help understand the receptor-based signalling pathways involved in neurite development and how the transmission of biochemical cues from the extracellular environment can induce intracellular changes that result in neurite generation.

- Laminin blocking antibodies could be added to cultures based on laminin coated growth substrates to confirm that laminin-receptor binding is responsible for neurite induction.

- In terms of neurite inhibition and the downstream signalling of NgR, expression analyses (such as Western Blot) of components in the Rho A and ROCK signalling cascade could be conducted. For example, the upregulation of Rho A in its active form within the inhibitory model may provide evidence of the downstream signalling events following NgR activation.

- Soluble NgR as a means of reducing receptor activation by sequestering inhibitory ligands has been demonstrated in other models of SCI and glial scarring. This could also be demonstrated to overcome inhibition in the model of myelin-induced inhibition to further evidence the role of NgR in Nogo and OMGP signal transduction within this model.

Chapter VII: Discussion

7.1 Introduction

This thesis has aimed to develop a novel human-derived model of neurite outgrowth, suitable for investigation into the molecular mechanisms that underpin neurite growth and inhibition, in a variety of neurological pathologies. This model was then used to investigate the molecular signalling events that govern inhibition of neurite outgrowth following SCI and in AD.

3D cell culture technology was employed in combination with protein surface technology to provide the most physiologically representative model of neuritogenesis. This system was then applied to study neurite inhibition using several inhibition models ranging from simple (growth substrate coating, exogenous peptide supplementation) to complex (co-culture, disease model cells).

In addition to this, several methods of recovery were employed, to determine the molecular signalling events involved in neurite inhibition, whilst also demonstrating a potential application of the model as a drug-screening tool. The model of neurite outgrowth described herein, has future applications ranging from academic interest including identification of specific signalling mechanisms involved in neurite growth and development, along with industrial applications including drug discovery, personalised medicine and neurotoxicity screening.

7.2 Development of Novel Human Models of Neurite Outgrowth

The initial stage of this project was to develop a robust and reproducible model of neurite outgrowth that could be applied to study neurite development and inhibition. Initially, an EC cell-based model of neuritogenesis was developed using TERA2.cl.SP12 human pluripotent stem cells. This cell type was selected, as neurite outgrowth from TERA2 EC cells has been well documented for many years[66,67,69,71,144,148]. In addition to this, the cell line is human derived, therefore its use in the study of human disease and medical applications, is more appropriate as it overcomes any physiological discrepancies associated with inter-species variation[71,146].

Retinoic acid is a potent morphogen involved in neuronal differentiation *in vitro* and has many applications *in vitro* to promote differentiation of human pluripotent stem cells[9,45,48,56]. However, its use *in vitro* is limited due to its ability to readily break down when exposed to light and heat[81]. For this reason, the stable, synthetic retinoid compound,

EC23[82,84] was used to induce singificant neuritogenesis within this model, producing a more reliable and reproducible model of neuritogenesis[149].

Furthermore, previous advances in induction of neurite outgrowth from TERA2.cl.SP12 spheroid structures[148], provided a solid foundation with which to begin development of the neurite outgrowth assay described within this thesis along with the development of a standard operating procedure outlining the methodology (Appendix I). Radial neurite outgrowth from a central cellular mass, allows for more accurate neurite quantification and a sampling method of quantification was developed to further enhance efficiency and accuracy of this process (Fig. 3-3). In addition to this, neurite outgrowth from this model was characterised and found to share similarities with neurite outgrowth during *in vitro* development (Fig. 3-4), suggesting that neurites generated in this manner have physiological relevance and can be used reliably to investigate the process of human neuritogenesis.

Therefore, the initial stage of this project was to develop a novel *in vitro* model of neurite outgrowth capable of applications including the investigation into inhibitory mechanisms. The EC-derived model of neuritogenesis described within Chapter III, is robust, reproducible and amenable to high-throughput screening, therefore suitable for both academic and industrial applications. This is particularly important as inability of neurites to regenerate is implicated in a wide variety of neurological conditions[33–36,38,39,42,43,220,441]. Therefore, there is need for a reliable *in vitro* model to investigate the molecular processes governing neurite inhibition and to screen compounds that may be able restore neurite growth in inhibitory situations.

In addition to this a novel iPSC-derived model of neuritogenesis was also developed, based upon the same spheroid culture and radial neurite outgrowth principles as the EC-derived model. Although the EC-derived model has advantages including that it is robust, reproducible, simple and cheap to maintain, this iPSC-derived model adds another dimension to neurite development. iPSC technology is more expensive and perhaps less robust due to problems with cellular viability, than the EC-derived model but has distinct advantages in other areas of interest. These include the use of disease model iPSC-derived cell types, as demonstrated with AD-model cells in Chapter V. iPSC-derived disease model cells exist for a number of other neurodegenerative diseases including Parkinson's disease Huntington's disease - neurodegenerative diseases where neurite growth and inhibition may be of particular interest[158,642–646].

Although the iPSC-derived model of neurite outgrowth lacks some of the advantages of the EC-derived model, it does possess its own range of distinct advantages. For example, personalised medicine is a rapidly growing field of research and this model could be used

to generate patient-specific neurite outgrowth models capable of screening drugs or other compounds for effectiveness[120,647–649].

7.2.1 Development of a Physiologically Relevant 3D Model of Neurite Outgrowth

To further improve these novel models of human neurite outgrowth, 3D cell culture technology was combined with both models to produce a more physiologically relevant model of human neuritogenesis. In embryonic development, developing neurites experience a 3D ECM environment and it is well established that the extracellular microenvironmental cues experienced by cells in culture impacts their structure and function[161,162,572]. For this reason Alvetex® scaffold, a 3D porous, polystyrene scaffold, was used to translate both EC and iPSC-derived models into a 3D culture environment.

A large number of drugs tested *in vitro* fail when their testing progresses into animal models[169,191]. One reason for this is that the 2D *in vitro* culture environment is so far removed from the *in vivo* physiological microenvironment, that cells behave differently in culture[169,191]. For this reason, many industrial assays are now being developed using 3D cell culture technology to provide a more reliable and physiologically relevant assay with better predictive value. The neurite outgrowth assays described in Chapter III were applied to 3D culture systems to further enhance their reliability and relevance.

To better re-create the geometry and topographical cues experienced by developing neurites *in vivo*, mature neurospheres (either EC or iPSC based) were cultured on top of Alvetex® scaffold and neurites penetrated the 3D material. This served as a method of quantification and the number of neurites per neurosphere was analysed in each assay. However, although 3D culture provides a more favourable environment, similar to the *in vivo* environment and it has even been evidenced that Alvetex® scaffold enhances neuritogenesis in a similar model[147,150], there are some disadvantages associated with this 3D model. For example, the method of quantification relies on neurites having penetrated the 200 μm depth of the 3D material, therefore is a reflection of both neurite length and number of neurites generated. However, this reduces assay sensitivity as many neurites may not reach the length of 200 μm required for quantification.

This particularly became apparent when investigating the induction of neurite outgrowth from AD-model cells in Chapter V. Neurite outgrowth from AD-patient neurospheres cultured in 2D revealed a significant impairment in neurite density and enhancement in neurite length, however, neurite penetration in 3D culture was enhanced, reflecting the 2D result of neurite length and not density. For this reason both 2D and 3D assays were carried out for each investigation detailed in this thesis, and the results of both were analysed and considered for each situation. In addition to this, 2D culture analyses more

variables including neurite length, number and density, therefore differential effects upon neurite length and number can be identified.

Other limitations of this model include the fact that the polystyrene scaffold described throughout this project recapitulates only the native geometry of developing neurites, as opposed to other aspects of the *in vivo* microenvironment. For example, to create a truly physiologically relevant model, all aspects of the cellular microenvironment need to be modeled including, substrate stiffness, oxygen and nutrient availability, cell-to-cell interations, and cell-to-matrix interactions. Therefore, this model improves on currently widely adopted techniques to provide a more physiologically relevant model of neuritogenesis, but itself is not a completely physiologically relevant model. However, despite these limitations, the 3D model of neurite outgrowth described herein, still is an advanced model compared with current techniques and as demonstrated throughout this thesis has a wide range of applications.

Applications of these 3D models have been outlined throughout this whole thesis, particularly to study the process of neurite inhibition in the glial scar (Chapter IV) and Alzheimer's disease (Chapter V). During the course of these studies neurite outgrowth was successfully inhibited and then recovered through the application of small molecules and use of inhibitory coatings. This provides potential applications for such models in terms of drug screening, by identifying the ability of molecules of interest to overcome inhibitory signalling and to screen molecules for neurotoxicity (summarised in Figure 7-1).

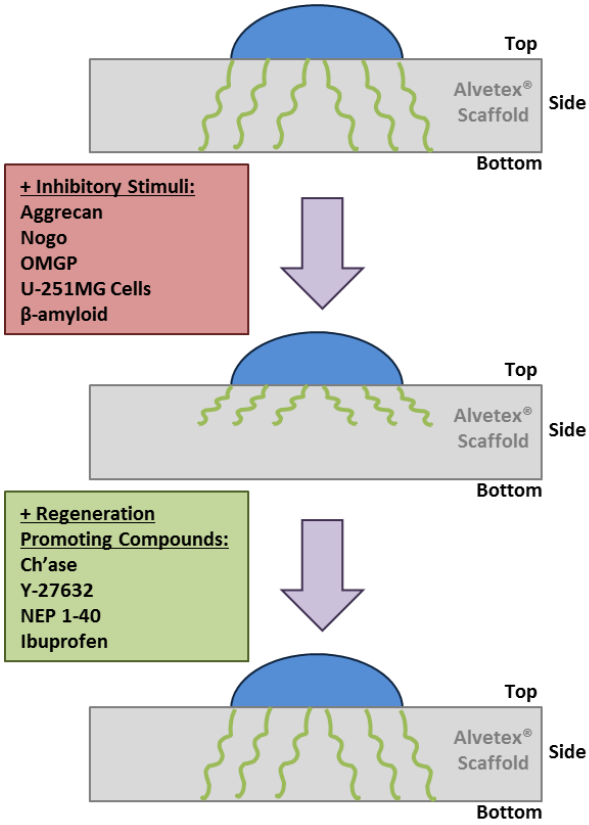

Fig 7-1: Application of 3D neurite outgrowth model to screen the ability of compounds to overcome inhibitory stimuli.
A schematic depicting the use of the novel 3D neurite outgrowth assay, developed within this thesis to study neurite inhibition and recovery. Neurospheres (blue) sit on top of Alvetex® scaffold (grey) whilst neurites (green) penetrate the 3D material. Upon addition of inhibitory molecules such as CSPGs (aggrecan), myelin inhibitors (Nogo, OMGP), glioma cells and β-amyloid peptides, neurites retract and no longer completely penetrate the 3D material. Molecules that reduce inhibitory signalling were then added to the model, such as Y-27632, ibuprofen, Ch'ase and NEP 1-40, to promote neurite regeneration, restoring neurite penetration into the 3D material, despite the presence of inhibitory stimuli.

7.3 Neurite Inhibition in the Glial Scar

Following SCI a series of events occur that lead to the formation of an inhibitory environment, preventing the growth of neurites and the restoration of lost neuronal connections leading to functional deficit[33,34,39,220]. These events include the release of CSPGs from reactive astrocytes and release of myelin debris from damaged neurons[33,34,39,220]. CSPGs and inhibitory molecules such as Nogo, MAG, and OMGP from myelin debris interact with receptor complexes to activate Rho A and ROCK signalling that ultimately impacts actin dynamics and results in growth cone collapse and neurite retraction[33,34,39,220].

Several methodologies to study the process of neurite inhibition in the context of the glial scar were employed, ranging from simple to more complex models of inhibition,

depending on its intended use. Simple, inhibitory coatings were employed such as the CSPG aggrecan (Chapter IV) and functionalisation of growth substrates with myelin inhibitors (Chapter VI) to provide non-permissive growth substrates that induce neurite inhibition. These novel 2D and 3D inhibitory growth surfaces provide basic models that can be used to study the process of neurite inhibition that occurs in the glial scar following SCI.

Signalling pathways involving both CSPG and myelin-induced inhibition are thought to be very similar. Although CSPGs act through receptors including LAR[319,348] and PTPσ[318–320] and NgR3[321], whilst myelin inhibitors act through the NgR1 receptor complex[32,324,329,331], signalling downstream of receptor activation is thought to be the same in each case. This includes Rho A activation that leads to activation of ROCK, resulting in stabalisation of actin filaments followed by growth cone collapse and neurite inhibition[25–27,31,366,368,372,398,636]. Therefore in each case, inhibitors of Rho A and ROCK were applied to these systems to overcome the inhibitory response. Both the inhibitor of Rho A, ibuprofen[30,368] and inhibitor of ROCK, Y-27632[23,286] were able to overcome both CSPG and myelin-induced inhibition, further evidencing the role of Rho A signalling in the inhibitory response and identifying the regeneration promoting properties of Y-27632 and ibuprofen. In addition to this, in the case of myelin-induced inhibition (described in Chapter VI) the NgR1 antagonist peptide NEP 1-40[336,357] was also used to restore neurite outgrowth in the presence of inhibitory stimuli.

Simple growth substrate inhibitory coatings such as aggrecan, Nogo and OMGP, provide basic, robust models to study the process of neurite inhibition and to screen molecules. Robust and standardised models (in the case of Orla inhibitory coatings) such as these are of particular value within the biotechnology industry, with particular applications of drug screening and molecular identification. However, they do not represent the complex inhibitory environment that cells experience within the glial scar. For this reason a more complex co-culture model of neurite inhibition was developed to better recapitulate the mixture of inhibitory molecules present within the *in vivo* glial scar.

To better re-create the complex mixture of inhibitory signals involved in glial scar signalling and to focus on CSPG-mediated inhibition, a co-culture model was developed that included a glioma cell line known to express similar proteins as reactive astrocytes involved in glial scar development[393–396]. Several approaches were used to combine neurosphere and glioma cell culture, including a traditional 2D co-culture model involving monolayer culture of glioma cells with a neurosphere cultured on top. This particular method of co-culture has the disadvantage of providing physical contact between the two cell types that could contribute toward the inhibitory response observed. The aim of this co-culture methodology was to study CSPG-induced neurite inhibition, therefore this 2D

co-culture was not suitable. However, physical inhibition of neurite outgrowth by a reactive astrocyte meshwork is a means of inhibition that contributes toward glial scarring[33,34,39,220], therefore, this co-culture model could be used to investigate this process.

To further build on this co-culture methodology and to eliminate physical contact between the cell types, glioma cell conditioned medium was focused upon. This involved either the application of growth medium-derived from glioma cell cultures or the culture of glioma cells as a monolayer and neurospheres cultured within the same environment suspended in Alvetex® scaffold. These experiments allowed the effects of soluble mediators on neurite outgrowth to be examined, eliminating the aspect of physical inhibition.

In all of the co-culture/conditioned medium experiments, Y-27632, ibuprofen and chondroitinase were able to rescue neurite growth (Chapter IV). This suggests that the neurite inhibition observed in these models is induced by CSPGs and further evidences the role of Rho A and ROCK signalling in CSPG-mediated inhibition. This, in combination with the recovery of neurite growth observed on inhibitory growth substrates (aggrecan and myelin-inhibitors) provides compelling evidence as to the role of Rho A and ROCK activation in neurite inhibition within the glial scar along with the potential use of ibuprofen and Y-27632 to overcome this inhibitory response.

7.4 Neurite Inhibition in Alzheimer's disease

One of the main hallmarks of Alzheimer's disease (AD) is the aberrant processing and extracellular accumulation of β-amyloid (Aβ) peptides in the form of senile plaques[410,422,444,460,461,482,510]. Neurites that pass through senile plaques lose their characteristic morphology, becoming dystrophic and abnormal[500,502]. This inhibition in neurite growth is thought to contribute toward a lack of neural connectivity associated with memory loss and disease progression[500,502]. For this reason, the ability of Aβ species to induce neurite inhibition was tested by he models of neurite outgrowth outlined in this project.

Consistent with primary literature, data outlined in this thesis found both $A\beta_{40}$ and $A\beta_{42}$ species to be inhibitory to neurite development when bound to growth substrates and soluble within culture medium[35,36]. These inhibitory models, similar to the aggrecan-based model of CSPG-mediated inhibition, are simple and provide modest systems to dissect the molecular signalling events involved in the inhibitory process. However, *in vivo* neurons are exposed to a number of Aβ peptides, therefore to better recapitulate the *in vivo* system, the effects of various ratios of $A\beta_{42}$:$A\beta_{40}$ upon neurite outgrowth was

examined. This also allows for the modelling of various stages of disease progression as the ratios tested range from healthy brain levels to advanced disease levels[426]. All ratios tested were found to be inhibitory to neurite outgrowth, further evidencing the neurite inhibitory effects of Aβ.

Although adding ratios of Aβ peptides to the culture medium better recreates the physiological environment experienced by neurons in the brain of patients with AD, it is still an extremely simple system aimed at modelling a multi-faceted exceptionally complex diseased state. Therefore to better model this complex neurodegenerative disease, the iPSC-derived model of neuritogenesis was applied to generate a disease-specific model of neurite outgrowth. ReproNeuro AD-model neuroprogenitor cells with mutations in PS1 and PS2 associated with aberrant Aβ production were used to develop an AD-specific model of neurite outgrowth[157,235,237]. These cell types endogenously produce a high ratio of $A\beta_{42}$:$A\beta_{40}$, characteristic of AD and provide a more complex, disease-specific model to study neurite inhibition and outgrowth.

This model was used to study the differences in neurite outgrowth between healthy individuals and those with an AD-associated mutations and found that neurite density was impaired in patient-derived samples. However, neurite length was enhanced in patient-derived samples, a result that was attributed to the heterogeneous nature of the cultures. This AD-specific model of neurite outgrowth based upon iPSC-technology has many potential applications, including personalised medicine, drug screening and identification of specific cellular signalling pathways involved in neurite development and inhibition.

Furthermore, in both simple and complex models of Aβ-mediated neurite inhibition, Rho A and ROCK inhibition restored neurite outgrowth to control levels. This suggests that Rho A and ROCK activation is involved in Aβ-mediated neurite inhibition, consistent with evidence throughout the literature[36,510]. Y-27632 and ibuprofen, inhibitors of ROCK and Rho A respectively were found to have a positive effect upon neurite outgrowth in the presence of inhibitory Aβ species and in AD-model neurites, which suggests that these compounds may have beneficial effects in restoring neural connectivity in AD. This *in vitro* finding is consistent with *in vivo* evidence provided by Lim *et al* that suggests that ibuprofen could be beneficial in restoring neurite growth and reducing inflammation in a mouse model of AD[650].

However, the mechanism by which Aβ activates Rho A and ROCK still remains unclear. Aβ is known to structurally interact with the NgR[504,505,509], a receptor heavily implicated in glial scar signalling activated by both CSPGs and myelin-associated inhibitory molecules, however it is not known if Aβ binding results in receptor activation. Therefore

experiments described within this thesis (Chapter V) aimed to identify the role of NgR in Aβ-mediated neurite inhibition by using the NgR receptor antagonist NEP 1-40[336,357] to rescue neurite outgrowth in the presence of inhibitory Aβ species. However, this was not the case, and neurite outgrowth was not fully restored by NEP 1-40 treatment, although partial recovery was evident. This suggests that Aβ induces neurite inhibition by multiple mechanisms, one of which may be NgR activation, however NgR activation is not the sole mechanism responsible for Aβ-mediated inhibition. Aβ-mediated neurite inhibition shares many similarities with glial scar signalling including the involvement of NgR in addition to Rho A and ROCK activation, a common pathway in CSPG and myelin-induced inhibition.

7.5 Similarities between the Glial Scar and Alzheimer's disease

The loss of neuronal connections leading to functional defects is involved in the pathogenic mechanisms that underpin many neurological disorders including trauma, in the form of SCI[33,34,39,220] and neurodegenerative diseases, including AD[36,40]. In both of these pathological states an inhibitory environment forms leading to the inability of neurites to restore lost neuronal connections resulting in functional deficits. Neurite inhibition can be triggered by a number of stimuli such as inhibitory proteoglycans[27,318,319,348] or peptides[36,40], but ultimately results in a reduction of neuronal connectivity.

In the glial scar, inhibitory molecules such as CSPGs secreted by reactive astrocytes and myelin inhibitors released from damaged neurons bind to receptors including the NgR, which leads to Rho A and ROCK activation, impacting the actin cytoskeleton and resulting in growth cone collapse[26,27,33,34,39,209,220,317,348,378], as evidenced throughout this thesis (Chapters IV & VI). However, in AD it is the amyloidgenic Aβ peptides that are thought to induce neurite inhibition and similarly to glial scar signalling, and are thought to induce activation of Rho A and ROCK[36,510], consistent with data outlined in this thesis (Chapter IV). Again, similarly to glial scar signalling, Aβ is known to interact with NgR, however it is not known if the peptide activates the receptor[504,505,509]. Delivery of soluble NgR has resulted in functional recovery in AD-animal models along with a reduction in Aβ deposition[509]; this suggests that the soluble NgR is capable of sequestering Aβ and reducing its inhibitory action. This is consistent with the role of Aβ as a ligand for NgR and in combination with data described in Chapter V, suggests that NgR may be one of multiple mechanisms implicated in the inhibitory action of Aβ.

In addition to receptor-mediated signalling and its downstream pathway, the inhibitory events that underpin neurite inhibition in the glial scar and AD also share similarities in other respects. Astrocyte activation is a major consequence of SCI and results in the

secretion of inhibitory molecules such as CSPGs in addition to providing mechanical inhibition in the form of an astrocytic meshwork that physically blocks neurite extension[33,34,39,220,293,347]. Astrocyte activation has also been identified in AD as a consequence of Aβ accumulation[651]. This again, suggests common pathological mechanisms that contribute toward the inhibitory environments in both glial scar and AD situations. This also suggests that CSPG-induced inhibition may contribute toward the reduction in neural connectivity associated with AD, as reactive astrocytes are known to secrete inhibitory molecules.

Therefore, the similarities and common signalling mechanisms involved in neurite inhibition in both AD and the glial scar highlight the importance of fully elucidating the molecular mechanisms that underpin neurite inhibition. Understanding the detailed inhibitory mechanisms that underpin the inability of neurites to grow in one diseased state may help improve understanding of the process in other pathological contexts, as this process appears to be common to many neurological disorders.

7.6 Biomimetic Growth Surfaces and Neurite Outgrowth

In addition to the development and application of neurite outgrowth models to understand the process of neurite inhibition following SCI and in AD, this thesis also examined the use of biomimetic growth substrates to further enhance the EC-derived model of neuritogenesis. The OrlaSURF platform has many distinct advantages compared to traditional adsorption coating of growth substrates, as specific biologically active domains are attached to growth surfaces in a precise and functional orientation[610,611,613]. This produces a more standardised culture environment, eliminating the use of more variable animal derived coatings[625]. In addition to this, coating 2D and 3D growth surfaces helps better re-create the biochemical physiological microenvironment[161].

This technology was used to study the role of ECM proteins in neurite development, as *in vivo* the ECM is thought to be an important factor in the development and elongation of neurites[526,530]. This process is particularly important, as inhibitory mechanisms, such as CSPG-mediated inhibition, are thought to block ECM-neurite binding, contributing to the inhibitory response[311,652] and variations in integrin expression are thought to be responsible for the reduction of regenerative capacity in the adult CNS[364,537,552,562]. The data outlined in this thesis found that the laminin β1 "YIGSR" domain, enhanced neurite outgrowth to a greater degree than collagen IV and fibronectin-derived domains. This is consistent with evidence throughout the literature, as the role of laminin in neurite development is well documented[187,562,624,626,627].

For this reason, the specific role of laminin in neurite generation was focused upon. This involved the screening of many laminin-derived motifs, including those from α1, α2, α5, β1, γ1 and γ1 chains. This allowed for the identification of specific neurite promoting domains and the data obtained was consistent with previous, documented literature as the "IKVAV" domain of laminin α1[271,563,564,598] generally enhanced neurite outgrowth to the greatest degree, however "YIGSR" of laminin β1 had the greatest impact on neurite length[279,598,622,624].

In addition to ECM focused investigations, this technology was also used to study the role of myelin-induced inhibition in the glial scar. Growth surfaces were functionalised with Nogo and OMGP, inhibitory molecules present on myelin debris[33,34,39,220], released from damaged neurons, to model the process of neurite inhibition, which impedes regeneration in the injured spinal cord. Inhibitors of down stream myelin-induced signalling such as Y-27632, an inhibitor of ROCK and ibuprofen an inhibitor of Rho A, in addition to NEP 1-40, a NgR antagonist, were able to recover neurite outgrowth on these inhibitory surfaces. This, in addition to data outlined in Chapters IV & V, provides strong evidence as to the role of Rho A and ROCK signalling as a common mechanism responsible for neurite inhibition in many systems. Furthermore, this also demonstrates an important application of this inhibitory model, as a potential screening tool that could be used to identify molecules capable of overcoming myelin-inhibitory signalling.

The OrlaSURF platform standardises growth substrate coating, compared with adsorption coating that limits the accessibility of active domains to the cells. This has distinct advantages, particularly in this model, as functionalisation with poly-D-lysine and laminin, replacing the standard ECM coating that this model relies on, not only enhances neurite outgrowth but also standardises the model itself[609,610,612,625]. This is beneficial in terms of industrial applications, and produces a more robust assay capable of screening potential neurotoxic compounds within an industrial setting. Furthermore, data outlined within this thesis also demonstrates the functionalisation of growth substrates with inhibitory molecules found within the glial scar following SCI, this provides the basis of an inhibitory model that has been successfully shown to induce neurite inhibition, which can be recovered through inhibition of NgR and its downstream signalling pathway. This standardised, inhibitory model could provide the basis for an assay capable of identifying regeneration promoting compounds (outlined in Figure 7-2).

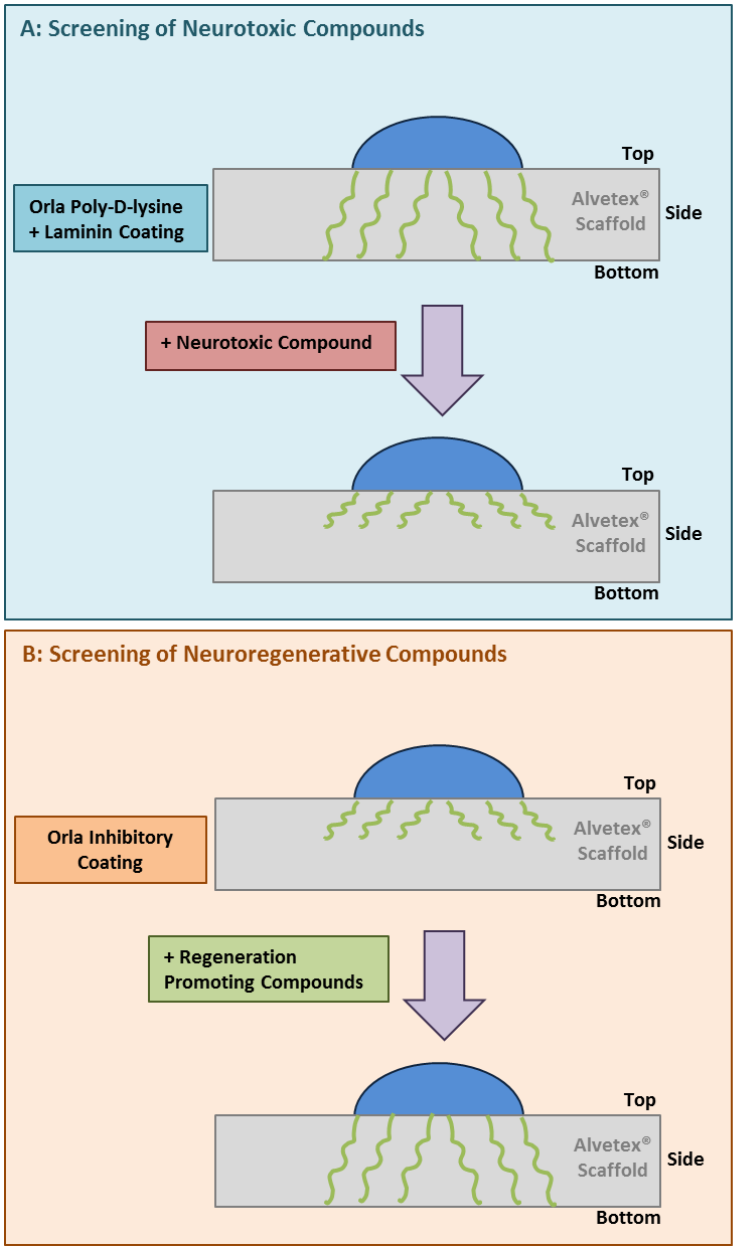

Fig 7-2: Potential application of 3D Orla-based models of neurite outgrowth and inhibition.
A schematic depicting the two main applications for the Orla coated 3D model of neuritogenesis. Neurospheres (blue) sit on top of Avetex® scaffold (grey) whilst neurites (green) penetrate the 3D material. Scaffolds coated with poly-D-lysine and laminin promote neurite generation (A), this model can be used to screen compounds for neurotoxicity effects, which would result in impaired neurite outgrowth. Scaffolds coated with inhibitory molecules such as Nogo and OMGP, inhibit neurite outgrowth (B), and can be used to screen the ability of compounds to promote neuroregeneration, despite the presence of an inhibitory stimulus. This could be used to identify compounds of interest that may provide a suitable basis for therapeutic design, aimed at restoring connectivity in the injured spinal cord.

7.7 Conclusions

In conclusion, this thesis has described the development of two novel, pluripotent human-derived models of neuritogenesis in 2D culture and the more physiologically relevant, 3D culture system. These models have combined synthetic retinoid technology with 3D cell culture systems and an efficient sampling method of quantification, to produce a robust and reliable model of neuritogenesis that can be used to study the process of neurite generation and inhibition.

This model, in addition to an iPSC-derived model of neuritogenesis also developed within this thesis, was used to study the process of neurite inhibition in the context of the glial scar that forms following spinal cord injury along with Alzheimer's disease. In addition to this the role of NgR, Rho A and ROCK-mediated signalling in each inhibitory setting was evaluated and Rho A/ROCK activation deemed a common process, responsible for mediating neurite inhibition in many inhibitory situations.

The data outlined in this thesis has provided a solid foundation for the investigation of neurite regeneration *in vitro* using a novel, physiologically relevant 3D model of neuritogenesis, based upon Alvetex® scaffold technology. In addition to this, the data contained within this thesis also demonstrates potential applications of such a model to study the process of neurite growth and inhibition in health and disease.

7.8 Future Directions

- Both models of neurite outgrowth described within this thesis have many potential future applications. For example, these models could be adopted to screen agents for potential neurotoxic properties or to identify regeneration promoting compounds. To further the identification of regeneration promoting compounds, the small molecules detailed within this thesis could be added to the model in combination. For example combination Ch'ase and Y-27632 treatment, to determine any beneficial additive effects that may help promote neurite regeneration in degenerative states.

- In this thesis, an Alzheimer's disease specific model of neurite outgrowth was developed. This has applications in many areas of neurodegeneration research, as this provides proof of concept, that models of neurite outgrowth can be developed from iPSC lines. In the future, this methodology could also be used to develop models of other neurodegernative diseases such as Parksinon's disease and Huntington's disease.

- Future work could focus on characterising the iPSC-derived model of neuritogenesis to the same level as the TERA2.cl.SP12-based model of neuritogenesis. Cytoskeletal markers were tracked over time in the EC-cell based model, this allowed for a comparison with *in vivo* neuritogenesis, to ensure neurite development was similar *in vitro*. This could be conducted for the ReproNeuro-based model and gene profiling could also enhance this characterisation.

- Rho A and ROCK activation has been implicated in neurite inhibition induced by many molecules (CSPGs, Aβ, Nogo, OMGP). Data described herein has used an inhibitory strategy to determine the role of Rho A and ROCK in neurite inhibition. To further provide evidence to this effect, techniques to analyse gene and protein expression such as Western Blotting and PCR could be employed to determine the availability and expression of pathway constituents such as, Rac, Cdc42 and ROCK and active Rho A.

Chapter VIII: Bibliography

1. Nógrádi & Vrbová. Anatomy and Physiology of the Spinal Cord BT - Transplantation of Neural Tissue into the Spinal Cord. In: Nógrádi A, editor. Boston, MA: Springer US; 2006. p. 1–23.
2. Silva, Sousa, Reis, & Salgado. From basics to clinical: A comprehensive review on spinal cord injury. Prog Neurobiol. 2014 Mar;25–57.
3. Bican, Minagar, & Pruitt. The Spinal Cord: A Review of Functional Neuroanatomy. Neurol Clin. 2013 Feb;1–18.
4. Pelvig, Pakkenberg, Stark, & Pakkenberg. Neocortical glial cell numbers in human brains. Neurobiol Aging. 2008 Nov;1754–62.
5. Stiles & Jernigan. The Basics of Brain Development. Neuropsychol Rev. 2010 Dec 3;327–48.
6. Wurst & Bally-Cuif. Neural plate patterning: Upstream and downstream of the isthmic organizer . Nat Rev Neurosci. 2001 Feb;99–108.
7. Blom, Shaw, den Heijer, & Finnell. Neural tube defects and folate: case far from closed. Nat Rev Neurosci. 2006 Sep;724–31.
8. Detrait, George, Etchevers, Gilbert, Vekemans, & Speer. Human neural tube defects: Developmental biology, epidemiology, and genetics. Neurotoxicol Teratol. 2005 May;515–24.
9. Maden. Retinoic acid in the development, regeneration and maintenance of the nervous system. Nat Rev Neurosci. 2007 Oct;755–65.
10. Da Silva & Dotti. Breaking the neuronal sphere: regulation of the actin cytoskeleton in neuritogenesis. Nat Rev Neurosci. 2002 Sep;694–704.
11. KIRYUSHKO, BEREZIN, & BOCK. Regulators of Neurite Outgrowth: Role of Cell Adhesion Molecules. Ann N Y Acad Sci. 2004 Apr 1;140–54.
12. Hansen, Berezin, & Bock. Signaling mechanisms of neurite outgrowth induced by the cell adhesion molecules NCAM and N-Cadherin. Cell Mol Life Sci. 2008;3809–21.
13. Dent, Gupton, & Gertler. The Growth Cone Cytoskeleton in Axon Outgrowth and Guidance. Cold Spring Harb Perspect Biol. 2011 Mar 1;a001800.
14. Jeon, Moon, Kim, Kim, Kim, Li, Jin, Kim, Kim, Meier, Kim, & Park. Control of neurite outgrowth by RhoA inactivation. J Neurochem. 2012;684–98.
15. Drubin, Feinstein, Shooter, & Kirschner. Nerve growth factor-induced neurite outgrowth in PC12 cells involves the coordinate induction of microtubule assembly and assembly-promoting factors. J Cell Biol. 1985 Nov;1799–807.
16. Liu, Lamb, Chou, Liu, & Li. Nerve Growth Factor-mediated Neurite Outgrowth via Regulation of Rab5. Barr F, editor. Mol Biol Cell. 2007 Apr 17;1375–84.
17. Govek, Newey, & Van Aelst. The role of the Rho GTPases in neuronal development. Genes Dev. 2005 Jan;1–49.
18. Sainath & Gallo. Cytoskeletal and Signaling Mechanisms of Neurite Formation. Cell Tissue Res. 2015 Jan 31;267–78.
19. Korobova & Svitkina. Arp2/3 Complex Is Important for Filopodia Formation, Growth Cone Motility, and Neuritogenesis in Neuronal Cells. Pollard T, editor. Mol Biol Cell. 2008 Apr 25;1561–74.
20. Pinyol, Haeckel, Ritter, Qualmann, & Kessels. Regulation of N-WASP and the Arp2/3 Complex by Abp1 Controls Neuronal Morphology. Heisenberg C-P, editor. PLoS One. 2007 May 2;e400.

21. Roloff, Scheiblich, Dewitz, Dempewolf, Stern, & Bicker. Enhanced neurite outgrowth of human model (NT2) neurons by small-molecule inhibitors of Rho/ROCK signaling. PLoS One. 2015;e0118536.

22. Jia, Ye, Wang, & Feng. ROCK inhibition enhances neurite outgrowth in neural stem cells by upregulating YAP expression in vitro. Neural Regen Res. 2016 Jun 1;983–7.

23. Nath, DeGuia, Akbar, Borosky, & Wang. Rho-associated kinase (ROCK) inhibitor, Y27632, promotes neurite outgrowth in PC12 cells in the absence of NGF. J Neurochem. 2002;92.

24. Minase, Ishima, Itoh, & Hashimoto. Potentiation of nerve growth factor-induced neurite outgrowth by the ROCK inhibitor Y-27632: A possible role of IP3 receptors. Eur J Pharmacol. 2010 Dec 1;67–73.

25. Lingor, Teusch, Schwarz, Mueller, Mack, Bahr, & Mueller. Inhibition of Rho kinase (ROCK) increases neurite outgrowth on chondroitin sulphate proteoglycan in vitro and axonal regeneration in the adult optic nerve in vivo. J Neurochem. 2007 Oct;181–9.

26. Monnier, Sierra, Schwab, Henke-Fahle, & Mueller. The Rho/ROCK pathway mediates neurite growth-inhibitory activity associated with the chondroitin sulfate proteoglycans of the CNS glial scar. Mol Cell Neurosci. 2003 Mar;319–30.

27. Gopalakrishnan, Teusch, Imhof, Bakker, Schurdak, Burns, & Warrior. Role of Rho kinase pathway in chondroitin sulfate proteoglycan-mediated inhibition of neurite outgrowth in PC12 cells. J Neurosci Res. 2008 Aug;2214–26.

28. Lehmann, Fournier, Selles-Navarro, Dergham, Sebok, Leclerc, Tigyi, & McKerracher. Inactivation of Rho Signaling Pathway Promotes CNS Axon Regeneration. J Neurosci. 1999 Sep 1;7537 LP-7547.

29. Gu, Yu, Gutekunst, Gross, & Wei. Inhibition of the Rho signaling pathway improves neurite outgrowth and neuronal differentiation of mouse neural stem cells. Int J Physiol Pathophysiol Pharmacol. 2013 Mar 8;11–20.

30. Fu, Hue, & Li. Nonsteroidal anti-inflammatory drugs promote axon regeneration via RhoA inhibition. J Neurosci. 2007 Apr;4154–64.

31. Dill, Patel, Yang, Bachoo, Powell, & Li. A Molecular Mechanism for Ibuprofen-Mediated RhoA Inhibition in Neurons. Vol. 30, The Journal of neuroscience : the official journal of the Society for Neuroscience. 2010.30(3) p. 963–72.

32. Niederost, Oertle, Fritsche, McKinney, & Bandtlow. Nogo-A and myelin-associated glycoprotein mediate neurite growth inhibition by antagonistic regulation of RhoA and Rac1. J Neurosci. 2002 Dec;10368–76.

33. Fawcett & Asher. The glial scar and central nervous system repair. Brain Res Bull. 1999 Aug;377–91.

34. Rolls, Shechter, & Schwartz. The bright side of the glial scar in CNS repair. Nat Rev Neurosci. 2009 Mar;235–41.

35. Postuma, He, Nunan, Beyreuther, Masters, Barrow, & Small. Substrate-bound beta-amyloid peptides inhibit cell adhesion and neurite outgrowth in primary neuronal cultures. J Neurochem. 2000 Mar;1122–30.

36. Petratos, Li, George, Hou, Kerr, Unabia, Hatzinisiriou, Maksel, Aguilar, & Small. The beta-amyloid protein of Alzheimer's disease increases neuronal CRMP-2 phosphorylation by a Rho-GTP mechanism. Brain. 2008 Jan;90–108.

37. Takenouchi, Hashimoto, Hsu, Mackowski, Rockenstein, Mallory, & Masliah. Reduced neuritic outgrowth and cell adhesion in neuronal cells transfected with human alpha-synuclein. Mol Cell Neurosci. 2001 Jan;141–50.

38. Winner, Melrose, Zhao, Hinkle, Yue, Kent, Braithwaite, Ogholikhan, Aigner, Winkler, Farrer, & Gage. Adult neurogenesis and neurite outgrowth are impaired in LRRK2 G2019S mice. Neurobiol Dis. 2011 Mar;706–16.

39. Yiu & He. Glial inhibition of CNS axon regeneration. Nat Rev Neurosci. 2006 Aug;617–27.

40. Postuma, He, Nunan, Beyreuther, Masters, Barrow, & Small. Substrate-Bound β-Amyloid Peptides Inhibit Cell Adhesion and Neurite Outgrowth in Primary Neuronal Cultures. J Neurochem. 2000 Mar 19;1122–30.

41. Miyoshi, Honda, Baba, Taniguchi, Oono, Fujita, Kuroda, Katayama, & Tohyama. Disrupted-In-Schizophrenia 1, a candidate gene for schizophrenia, participates in neurite outgrowth. Mol Psychiatry. :685–94.

42. Ozeki, Tomoda, Kleiderlein, Kamiya, Bord, Fujii, Okawa, Yamada, Hatten, Snyder, Ross, & Sawa. Disrupted-in-Schizophrenia-1 (DISC-1): Mutant truncation prevents binding to NudE-like (NUDEL) and inhibits neurite outgrowth. Proc Natl Acad Sci. 2003 Jan 7;289–94.

43. Murtomäki, Risteli, Risteli, Koivisto, Johansson, & Liesi. Laminin and its neurite outgrowth-promoting domain in the brain in Alzheimer's disease and Down's syndrome patients. J Neurosci Res. 1992;261–73.

44. Roizen & Patterson. Down's syndrome. Lancet. 2003 Apr 12;1281–9.

45. Janesick, Wu, & Blumberg. Retinoic acid signaling and neuronal differentiation. Cell Mol Life Sci. 2015 Apr;1559–76.

46. Maden. Retinoid signalling in the development of the central nervous system. Nat Rev Neurosci. 2002 Nov;843–53.

47. Clarke, Christie, Whiting, & Przyborski. Using Small Molecules to Control Stem Cell Growth and Differentiation. 2014.

48. Durston, Timmermans, Hage, Hendriks, de Vries, Heideveld, & Nieuwkoop. Retinoic acid causes an anteroposterior transformation in the developing central nervous system. Nature. 1989 Jul 13;140–4.

49. Cho & De Robertis. Differential activation of Xenopus homeo box genes by mesoderm-inducing growth factors and retinoic acid. Genes Dev. 1990 Nov;1910–6.

50. Dekker, Pannese, Houtzager, Timmermans, Boncinelli, & Durston. Xenopus Hox-2 genes are expressed sequentially after the onset of gastrulation and are differentially inducible by retinoic acid. Dev Suppl. 1992;195–202.

51. Verani, Cappuccio, Spinsanti, Gradini, Caruso, Magnotti, Motolese, Nicoletti, & Melchiorri. Expression of the Wnt inhibitor Dickkopf-1 is required for the induction of neural markers in mouse embryonic stem cells differentiating in response to retinoic acid. J Neurochem. 2007 Jan;242–50.

52. Papalopulu & Kintner. A posteriorising factor, retinoic acid, reveals that anteroposterior patterning controls the timing of neuronal differentiation in Xenopus neuroectoderm. Development. 1996 Nov;3409–18.

53. Sharpe & Goldstone. The control of Xenopus embryonic primary neurogenesis is mediated by retinoid signalling in the neurectoderm. Mech Dev. 2000 Mar;69–80.

54. Mey. New therapeutic target for CNS injury? The role of retinoic acid signaling after nerve lesions. J Neurobiol. 2006 Jun 1;757–79.

55. Wong, Yip, Battaglia, Grist, Corcoran, Maden, Azzouz, Kingsman, Kingsman, Mazarakis, & McMahon. Retinoic acid receptor [beta]2 promotes functional regeneration of sensory axons in the spinal cord. Nat Neurosci. 2006 Feb;243–50.

56. Maden & Hind. Retinoic acid, a regeneration-inducing molecule. Dev Dyn. 2003 Feb;237–44.

57. Cocco, Diaz, Stancampiano, Diana, Carta, Curreli, Sarais, & Fadda. Vitamin A deficiency produces spatial learning and memory impairment in rats. Neuroscience. 2002 Dec 2;475–82.

58. Etchamendy, Enderlin, Marighetto, Pallet, Higueret, & Jaffard. Vitamin A deficiency

and relational memory deficit in adult mice: relationships with changes in brain retinoid signalling. Behav Brain Res. 2003 Oct 17;37–49.

59. Bonnet, Touyarot, Alfos, Pallet, Higueret, & Abrous. Retinoic Acid Restores Adult Hippocampal Neurogenesis and Reverses Spatial Memory Deficit in Vitamin A Deprived Rats. PLoS One. 2008 Oct 22;e3487.

60. Mingaud, Mormede, Etchamendy, Mons, Niedergang, Wietrzych, Pallet, Jaffard, Krezel, Higueret, & Marighetto. Retinoid Hyposignaling Contributes to Aging-Related Decline in Hippocampal Function in Short-Term/Working Memory Organization and Long-Term Declarative Memory Encoding in Mice. J Neurosci. 2008 Jan 2;279 LP-291.

61. Etchamendy, Enderlin, Marighetto, Vouimba, Pallet, Jaffard, & Higueret. Alleviation of a Selective Age-Related Relational Memory Deficit in Mice by Pharmacologically Induced Normalization of Brain Retinoid Signaling. J Neurosci. 2001 Aug 15;6423 LP-6429.

62. Ding, Qiao, Wang, Goodwin, Lee, Block, Allsbrook, McDonald, & Fan. Retinoic Acid Attenuates β-Amyloid Deposition and Rescues Memory Deficits in an Alzheimer's Disease Transgenic Mouse Model. J Neurosci. 2008 Nov 5;11622 LP-11634.

63. Yeyeodu, Witherspoon, Gilyazova, & Ibeanu. A Rapid, Inexpensive High Throughput Screen Method for Neurite Outgrowth. Curr Chem Genomics. 2010 Dec 13;74–83.

64. Clagett-Dame, McNeill, & Muley. Role of all-trans retinoic acid in neurite outgrowth and axonal elongation. J Neurobiol. 2006 Jun;739–56.

65. Plum & Clagett-Dame. All-trans retinoic acid stimulates and maintains neurite outgrowth in nerve growth factor-supported developing chick embryonic sympathetic neurons. Dev Dyn. 1996;52–63.

66. Tegenge, Roloff, & Bicker. Rapid differentiation of human embryonal carcinoma stem cells (NT2) into neurons for neurite outgrowth analysis. Cell Mol Neurobiol. 2011 May;635–43.

67. Satoh, Yukitake, Kurohara, & Kuroda. Retinoic acid-induced neuronal differentiation regulates expression of mRNAs for neurotrophins and neurotrophin receptors in a human embryonal carcinoma cell line NTera2. Neuropathology. 1997;80–8.

68. Pewsey, Bruce, Tonge, Evans, Ow, Georgiou, Wright, Andrews, & Fazeli. Nuclear proteome dynamics in differentiating embryonic carcinoma (NTERA-2) cells. J Proteome Res. 2010 Jul;3412–26.

69. Przyborski, Christie, Hayman, Stewart, & Horrocks. Human embryonal carcinoma stem cells: models of embryonic development in humans. Stem Cells Dev. 2004 Aug;400–8.

70. Przyborski, Morton, Wood, & Andrews. Developmental regulation of neurogenesis in the pluripotent human embryonal carcinoma cell line NTERA-2. Eur J Neurosci. 2000 Oct;3521–8.

71. Przyborski, Smith, & Wood. Transcriptional profiling of neuronal differentiation by human embryonal carcinoma stem cells in vitro. Stem Cells. 2003;459–71.

72. Coyne, Shan, Przyborski, Hirakawa, & Halliwell. Neuropharmacological properties of neurons derived from human stem cells. Neurochem Int. 2011 Sep;404–12.

73. Encinas, Iglesias, Liu, Wang, Muhaisen, Ceña, Gallego, & Comella. Sequential Treatment of SH-SY5Y Cells with Retinoic Acid and Brain-Derived Neurotrophic Factor Gives Rise to Fully Differentiated, Neurotrophic Factor-Dependent, Human Neuron-Like Cells. J Neurochem. 2000;991–1003.

74. López-Carballo, Moreno, Masiá, Pérez, & Barettino. Activation of the Phosphatidylinositol 3-Kinase/Akt Signaling Pathway by Retinoic Acid Is Required

for Neural Differentiation of SH-SY5Y Human Neuroblastoma Cells. J Biol Chem. 2002 Jul 12;25297–304.

75. Påhlman, Ruusala, Abrahamsson, Mattsson, & Esscher. Retinoic acid-induced differentiation of cultured human neuroblastoma cells: a comparison with phorbolester-induced differentiation. Cell Differ. 1984;135–44.

76. Jämsä, Hasslund, Cowburn, Bäckström, & Vasänge. The retinoic acid and brain-derived neurotrophic factor differentiated SH-SY5Y cell line as a model for Alzheimer's disease-like tau phosphorylation. Biochem Biophys Res Commun. 2004 Jul 2;993–1000.

77. Xie, Hu, & Li. SH-SY5Y human neuroblastoma cell line: in vitro cell model of dopaminergic neurons in Parkinson's disease. Chin Med J (Engl). 2010 Apr;1086—1092.

78. Cheung, Lau, Yu, Lai, Yeung, So, & Chang. Effects of all-trans-retinoic acid on human SH-SY5Y neuroblastoma as in vitro model in neurotoxicity research. Neurotoxicology. 2009 Jan;127–35.

79. Sharow, Temkin, & Asson-Batres. Retinoic acid stability in stem cell cultures. Int J Dev Biol. 2012;273–8.

80. Bempong, Honigberg, & Meltzer. Normal phase LC-MS determination of retinoic acid degradation products. J Pharm Biomed Anal. 1995 Mar;285–91.

81. Clemens, Flower, Gardner, Henderson, Knowles, Marder, Whiting, & Przyborski. Design and biological evaluation of synthetic retinoids: probing length vs. stability vs. activity. Mol Biosyst. 2013 Dec;3124–34.

82. Christie, Maltman, Henderson, Whiting, Marder, Lako, & Przyborski. Retinoid supplementation of differentiating human neural progenitors and embryonic stem cells leads to enhanced neurogenesis in vitro. J Neurosci Methods. 2010 Nov 30;239–45.

83. Christie, Barnard, Batsanov, Bridgens, Cartmell, Collings, Maltman, Redfern, Marder, Przyborski, & Whiting. Synthesis and evaluation of synthetic retinoid derivatives as inducers of stem cell differentiation. Org Biomol Chem. 2008 Oct;3497–507.

84. Clemens, Flower, Henderson, Whiting, Przyborski, Jimenez-Hernandez, Ball, Bassan, Cinque, & Gardner. The action of all-trans-retinoic acid (ATRA) and synthetic retinoid analogues (EC19 and EC23) on human pluripotent stem cells differentiation investigated using single cell infrared microspectroscopy. Mol Biosyst. 2013;677–92.

85. Papka. Sensory Ganglia A2 - Squire, Larry R. BT - Encyclopedia of Neuroscience. In Oxford: Academic Press; 2009. p. 657–68.

86. Rush & Waxman. Dorsal Root Ganglion Neurons A2 - Squire, Larry R. BT - Encyclopedia of Neuroscience. In Oxford: Academic Press; 2009. p. 615–9.

87. He & Baas. Growing and Working with Peripheral Neurons. In: Biology BT-M in C, editor. Academic Press; 2003.Volume 71 p. 17–35.

88. Kumar, Adams, Harkins, Engeberg, & Willits. Stimulation Frequency Alters the Dorsal Root Ganglion Neurite Growth and Directionality In Vitro. IEEE Trans Biomed Eng. 2016 Jun;1257–68.

89. Haugen & Letourneau. Interleukin-2 enhances chick and rat sympathetic, but not sensory, neurite outgrowth. J Neurosci Res. 1990;443–52.

90. Corcoran, Shroot, Pizzey, & Maden. The role of retinoic acid receptors in neurite outgrowth from different populations of embryonic mouse dorsal root ganglia. J Cell Sci. 2000 Jul 15;2567 LP-2574.

91. Fields, Neale, & Nelson. Effects of patterned electrical activity on neurite outgrowth from mouse sensory neurons. J Neurosci. 1990 Sep 1;2950 LP-2964.

92. Jin, Kim, Shin, & Kim. Neurite outgrowth of dorsal root ganglia neurons is enhanced on aligned nanofibrous biopolymer scaffold with carbon nanotube coating. Neurosci Lett. 2011 Aug 21;10–4.

93. Corey, Lin, Mycek, Chen, Samuel, Feldman, & Martin. Aligned electrospun nanofibers specify the direction of dorsal root ganglia neurite growth. J Biomed Mater Res Part A. 2007 Dec 1;636–45. A

94. Hu-Tsai, Winter, Emson, & Woolf. Neurite outgrowth and GAP-43 mRNA expression in cultured adult rat dorsal root ganglion neurons: Effects of NGF or prior peripheral axotomy. J Neurosci Res. 1994;634–45.

95. Kaur & Dufour. Cell lines: Valuable tools or useless artifacts. Spermatogenesis. 2012 Jan 1;1–5.

96. Szpara, Vranizan, Tai, Goodman, Speed, & Ngai. Analysis of gene expression during neurite outgrowth and regeneration. BMC Neurosci. 2007;100.

97. Fudge & Mearow. Extracellular matrix-associated gene expression in adult sensory neuron populations cultured on a laminin substrate. BMC Neurosci. 2013;15.

98. Contestabile. Cerebellar granule cells as a model to study mechanisms of neuronal apoptosis or survival in vivo and in vitro. Cerebellum. 2002;41–55.

99. Bearer, Swick, O'Riordan, & Cheng. Ethanol Inhibits L1-mediated Neurite Outgrowth in Postnatal Rat Cerebellar Granule Cells. J Biol Chem. 1999

100. Borodinsky, O'Leary, Neale, Vicini, Coso, & Fiszman. GABA-induced neurite outgrowth of cerebellar granule cells is mediated by GABAA receptor activation, calcium influx and CaMKII and erk1/2 pathways. J Neurochem. 2003;1411–20.

101. Watanabe, Yamazaki, Miyazaki, Arikawa, Itoh, Sasaki, Maehama, Frohman, & Kanaho. Phospholipase D2 functions as a downstream signaling molecule of MAP kinase pathway in L1-stimulated neurite outgrowth of cerebellar granule neurons. J Neurochem. 2004;142–51.

102. Farwell, Dubord-Tomasetti, Pietrzykowski, Stachelek, & Leonard. Regulation of cerebellar neuronal migration and neurite outgrowth by thyroxine and 3,3′,5′-triiodothyronine. Dev Brain Res. 2005 Jan 1;121–35.

103. Taniwaki & Schwartz. Somatostatin enhances neurofilament expression and neurite outgrowth in cultured rat cerebellar granule cells. Dev Brain Res. 1995 Aug 28;109–16.

104. Ross, Spengler, & Biedler. Coordinate Morphological and Biochemical Interconversion of Human Neuroblastoma Cells2. JNCI J Natl Cancer Inst. 1983 Oct 1;741–7.

105. Tucholski, Lesort, & Johnson. Tissue transglutaminase is essential for neurite outgrowth in human neuroblastoma SH-SY5Y cells. Neuroscience. 2001 Jan 15;481–91.

106. Ferrari-Toninelli, Paccioretti, Francisconi, Uberti, & Memo. TorsinA negatively controls neurite outgrowth of SH-SY5Y human neuronal cell line. Brain Res. 2004 Jun 25;75–81.

107. Rogers, Buensuceso, Montague, & Mahadevan. Vanadate stimulates differentiation and neurite outgrowth in rat pheochromocytoma PC12 cells and neurite extension in human neuroblastoma SH-SY5Y cells. Neuroscience. 1994 May;479–94.

108. Fagerström, Påhlman, Gestblom, & Nånberg. Protein kinase C-epsilon is implicated in neurite outgrowth in differentiating human neuroblastoma cells. Cell Growth Differ. 1996;775–85.

109. Kovalevich & Langford. Considerations for the use of SH-SY5Y neuroblastoma cells in neurobiology. Methods Mol Biol. 2013;9–21.

110. Ciccarone, Spengler, Meyers, Biedler, & Ross. Phenotypic Diversification in Human Neuroblastoma Cells: Expression of Distinct Neural Crest Lineages. Cancer Res.

1989 Jan 1;219 LP-225.

111. Nicolini, Miloso, Zoia, Di Silvestro, Cavaletti, & Tredici. Retinoic acid differentiated SH-SY5Y human neuroblastoma cells: an in vitro model to assess drug neurotoxicity. Anticancer Res. 1998;2477–81.

112. Greene & Tischler. Establishment of a noradrenergic clonal line of rat adrenal pheochromocytoma cells which respond to nerve growth factor. Proc Natl Acad Sci . 1976 Jul 1;2424–8.

113. Harrill & Mundy. Quantitative Assessment of Neurite Outgrowth in PC12 Cells BT - In Vitro Neurotoxicology: Methods and Protocols. In: Costa LG, Giordano G, Guizzetti M, editors. Totowa, NJ: Humana Press; 2011. p. 331–48.

114. Greene. Nerve growth factor prevents the death and stimulates the neuronal differentiation of clonal PC12 pheochromocytoma cells in serum-free medium. J Cell Biol. 1978 Sep 1;747–55.

115. Chandler, Parsons, Hosang, & Shooter. A monoclonal antibody modulates the interaction of nerve growth factor with PC12 cells. J Biol Chem. 1984 Jun 10;6882–9.

116. Gunning, Landreth, Bothwell, & Shooter. Differential and synergistic actions of nerve growth factor and cyclic AMP in PC12 cells. J Cell Biol. 1981 May 1;240 LP-245.

117. The role of cAMP in nerve growth factor-promoted neurite outgrowth in PC12 cells. J Cell Biol. 1986 Mar 1;821–9.

118. Martinez-Morales, Revilla, Ocana, Gonzalez, Sainz, McGuire, & Liste. Progress in stem cell therapy for major human neurological disorders. Stem Cell Rev. 2013 Oct;685–99.

119. Martello & Smith. The nature of embryonic stem cells. Annu Rev Cell Dev Biol. 2014;647–75.

120. Tabar & Studer. Pluripotent stem cells in regenerative medicine: challenges and recent progress. Nat Rev Genet. 2014 Feb;82–92.

121. Takahashi, Tanabe, Ohnuki, Narita, Ichisaka, Tomoda, & Yamanaka. Induction of pluripotent stem cells from adult human fibroblasts by defined factors. Cell. 2007 Nov;861–72.

122. Takahashi & Yamanaka. A decade of transcription factor-mediated reprogramming to pluripotency. Nat Rev Mol Cell Biol. 2016 Mar;183–93.

123. Takahashi & Yamanaka. Induction of pluripotent stem cells from mouse embryonic and adult fibroblast cultures by defined factors. Cell. 2006 Aug;663–76.

124. Avior, Sagi, & Benvenisty. Pluripotent stem cells in disease modelling and drug discovery. Nat Rev Mol Cell Biol. 2016 Mar;170–82.

125. Trounson & DeWitt. Pluripotent stem cells progressing to the clinic. Nat Rev Mol Cell Biol. 2016 Mar;194–200.

126. Steinbeck & Studer. Moving stem cells to the clinic: potential and limitations for brain repair. Neuron. 2015 Apr;187–206.

127. Ganat, Calder, Kriks, Nelander, Tu, Jia, Battista, Harrison, Parmar, Tomishima, Rutishauser, & Studer. Identification of embryonic stem cell-derived midbrain dopaminergic neurons for engraftment. J Clin Invest. 2012 Aug;2928–39.

128. Grealish, Diguet, Kirkeby, Mattsson, Heuer, Bramoulle, Van Camp, Perrier, Hantraye, Bjorklund, & Parmar. Human ESC-derived dopamine neurons show similar preclinical efficacy and potency to fetal neurons when grafted in a rat model of Parkinson's disease. Cell Stem Cell. 2014 Nov;653–65.

129. Zhang, Stojkovic, Przyborski, Cooke, Armstrong, Lako, & Stojkovic. Derivation of Human Embryonic Stem Cells from Developing and Arrested Embryos. Stem Cells. 2006;2669–76.

130. Gertow, Przyborski, Loring, Auerbach, Epifano, Otonkoski, Damjanov, & Ährlund-Richter. Isolation of Human Embryonic Stem Cell–Derived Teratomas for the Assessment of Pluripotency. In: Current Protocols in Stem Cell Biology. John Wiley & Sons, Inc.; 2007.

131. Reubinoff, Pera, Fong, Trounson, & Bongso. Embryonic stem cell lines from human blastocysts: somatic differentiation in vitro. Nat Biotech. 2000 Apr;399–404.

132. Gaspard & Vanderhaeghen. Mechanisms of neural specification from embryonic stem cells. Curr Opin Neurobiol. 2010 Feb;37–43.

133. Li, Du, Zarnowska, Pankratz, Hansen, Pearce, & Zhang. Specification of motoneurons from human embryonic stem cells. Nat Biotech. 2005 Feb;215–21.

134. Harper, Krishnan, Darman, Deshpande, Peck, Shats, Backovic, Rothstein, & Kerr. Axonal growth of embryonic stem cell-derived motoneurons in vitro and in motoneuron-injured adult rats. Proc Natl Acad Sci United States Am. 2004

135. Bain, Kitchens, Yao, Huettner, & Gottlieb. Embryonic Stem Cells Express Neuronal Properties in Vitro. Dev Biol. 1995;342–57.

136. Chambers, Fasano, Papapetrou, Tomishima, Sadelain, & Studer. Highly efficient neural conversion of human ES and iPS cells by dual inhibition of SMAD signaling. Nat Biotech. 2009 Mar;275–80.

137. Zhang, Wernig, Duncan, Brustle, & Thomson. In vitro differentiation of transplantable neural precursors from human embryonic stem cells. Nat Biotech. 2001 Dec;1129–33.

138. Harrill, Freudenrich, Machacek, Stice, & Mundy. Quantitative assessment of neurite outgrowth in human embryonic stem cell-derived hN2™ cells using automated high-content image analysis. Neurotoxicology. 2010 Jun;277–90.

139. Berns, Sur, Pan, Goldberger, Suresh, Zhang, Kessler, & Stupp. Aligned neurite outgrowth and directed cell migration in self-assembled monodomain gels. Biomaterials. 2014 Jan;185–95.

140. Kotani, Osanai, Tajima, Kato, Imada, Kaneda, Kubo, & Sakuraba. Identification of neuronal cell lineage-specific molecules in the neuronal differentiation of P19 EC cells and mouse central nervous system. J Neurosci Res. 2002 Mar 1;595–606.

141. Yu, Chung, Deo, Thompson, & Turner. MicroRNA miR-124 regulates neurite outgrowth during neuronal differentiation. Exp Cell Res. 2008 Aug 15;2618–33.

142. Pearce, Cambray-Deakin, & Burgoyne. Glutamate acting on NMDA receptors stimulates neurite outgrowth from cerebellar granule cells. FEBS Lett. 1987;143–7.

143. Stipp & Hemler. Transmembrane-4-superfamily proteins CD151 and CD81 associate with alpha 3 beta 1 integrin, and selectively contribute to alpha 3 beta 1-dependent neurite outgrowth. J Cell Sci. 2000 Jun 1;1871 LP-1882.

144. Schwartz, Spivak, Baker, McDaniel, Loring, Nguyen, Chrest, Wersto, Arenas, Zeng, Freed, & Rao. NTera2: a model system to study dopaminergic differentiation of human embryonic stem cells. Stem Cells Dev. 2005 Oct;517–34.

145. Andrews. Retinoic acid induces neuronal differentiation of a cloned human embryonal carcinoma cell line in vitro. Dev Biol. 1984 Jun;285–93.

146. Przyborski. Isolation of human embryonal carcinoma stem cells by immunomagnetic sorting. Stem Cells. 2001;500–4.

147. Hayman, Smith, Cameron, & Przyborski. Enhanced neurite outgrowth by human neurons grown on solid three-dimensional scaffolds. Biochem Biophys Res Commun. 2004 Feb 6;483–8.

148. Stewart, Christie, & Przyborski. Manipulation of human pluripotent embryonal carcinoma stem cells and the development of neural subtypes. Stem Cells. 2003;248–56.

149. Clarke, Tams, Henderson, Roger, Whiting, & Przyborski. A robust and reproducible human pluripotent stem cell derived model of neurite outgrowth in a three-dimensional culture system and its application to study neurite inhibition. Neurochem Int.

150. Hayman, Smith, Cameron, & Przyborski. Growth of human stem cell-derived neurons on solid three-dimensional polymers. J Biochem Biophys Methods. 2005 Mar 31;231–40.

151. Yu, Vodyanik, Smuga-Otto, Antosiewicz-Bourget, Frane, Tian, Nie, Jonsdottir, Ruotti, Stewart, Slukvin, & Thomson. Induced pluripotent stem cell lines derived from human somatic cells. Science. 2007 Dec;1917–20.

152. Yamanaka. A Fresh Look at iPS Cells. Cell. 2017 Feb 24;13–7.

153. Yamanaka. Induced Pluripotent Stem Cells: Past, Present, and Future. Cell Stem Cell. 2017 Feb 24;678–84.

154. Takahashi & Yamanaka. Induction of Pluripotent Stem Cells from Mouse Embryonic and Adult Fibroblast Cultures by Defined Factors. Cell. 2017 Feb 24;663–76.

155. Dolmetsch & Geschwind. The Human Brain in a Dish: The Promise of iPSC-Derived Neurons. Cell. 2011 Jun 10;831–4.

156. Hu, Weick, Yu, Ma, Zhang, Thomson, & Zhang. Neural differentiation of human induced pluripotent stem cells follows developmental principles but with variable potency. Proc Natl Acad Sci. 2010 Mar 2;4335–40.

157. Yagi, Ito, Okada, Akamatsu, Nihei, Yoshizaki, Yamanaka, Okano, & Suzuki. Modeling familial Alzheimer's disease with induced pluripotent stem cells. Hum Mol Genet. 2011 Dec 1;4530–9.

158. Nguyen, Byers, Cord, Shcheglovitov, Byrne, Gujar, Kee, Schüle, Dolmetsch, Langston, Palmer, & Pera. LRRK2 Mutant iPSC-Derived DA Neurons Demonstrate Increased Susceptibility to Oxidative Stress. Cell Stem Cell. 2011 Mar 4;267–80. A

159. Byers, Cord, Nguyen, Schüle, Fenno, Lee, Deisseroth, Langston, Pera, & Palmer. SNCA Triplication Parkinson's Patient's iPSC-derived DA Neurons Accumulate α-Synuclein and Are Susceptible to Oxidative Stress. PLoS One. 2011 Nov 16;e26159.

160. Yahata, Asai, Kitaoka, Takahashi, Asaka, Hioki, Kaneko, Maruyama, Saido, Nakahata, Asada, Yamanaka, Iwata, & Inoue. Anti-Aβ Drug Screening Platform Using Human iPS Cell-Derived Neurons for the Treatment of Alzheimer's Disease. PLoS One. 2011 Sep 30;e25788.

161. Yamada & Cukierman. Modeling Tissue Morphogenesis and Cancer in 3D. Cell. 2007 Aug 24;601–10.

162. Knight & Przyborski. Advances in 3D cell culture technologies enabling tissue-like structures to be created in vitro. J Anat. 2015 Dec 1;746–56.

163. Takimoto. Why Drugs Fail: Of Mice and Men Revisited. Clin Cancer Res. 2001 Feb 1;229 LP-230.

164. Pritchard, Jurima-Romet, Reimer, Mortimer, Rolfe, & Cayen. Making Better Drugs: Decision Gates in Non-Clinical Drug Development. Nat Rev Drug Discov. 2003 Jul;542–53.

165. Kumar, Karnati, Reddy, & Chandramouli. Caco-2 cell lines in drug discovery- an updated perspective. J basic Clin Pharm. 2010 Mar;63–9.

166. Hubatsch, Ragnarsson, & Artursson. Determination of drug permeability and prediction of drug absorption in Caco-2 monolayers. Nat Protoc. 2007 Sep;2111–9.

167. Neuman, Koren, & Tiribelli. In vitro assessment of the ethanol-induced hepatotoxicity on HepG2 cell line. Biochem Biophys Res Commun. 1993 Dec;932–41.

168. Van Summeren, Renes, Bouwman, Noben, van Delft, Kleinjans, & Mariman.

Proteomics investigations of drug-induced hepatotoxicity in HepG2 cells. Toxicol Sci. 2011 Mar;109–22.

169. Huh, Hamilton, & Ingber. From 3D cell culture to organs-on-chips. Trends Cell Biol. 2011 Dec;745–54.

170. Griffith & Swartz. Capturing complex 3D tissue physiology in vitro. Nat Rev Mol Cell Biol. 2006 Mar;211–24.

171. Keller. In vitro differentiation of embryonic stem cells. Curr Opin Cell Biol. 1995 Dec;862–9.

172. Kurosawa. Methods for inducing embryoid body formation: in vitro differentiation system of embryonic stem cells. J Biosci Bioeng. 2007 May;389–98.

173. Antonchuk. Formation of embryoid bodies from human pluripotent stem cells using AggreWell plates. Methods Mol Biol. 2013;523–33.

174. Bratt-Leal, Carpenedo, & McDevitt. Engineering the Embryoid Body Microenvironment to Direct Embryonic Stem Cell Differentiation. Biotechnol Prog. 2009;43–51.

175. Takagi, Takahashi, Saiki, Morizane, Hayashi, Kishi, Fukuda, Okamoto, Koyanagi, Ideguchi, Hayashi, Imazato, Kawasaki, Suemori, Omachi, Iida, Itoh, Nakatsuji, Sasai et al. Dopaminergic neurons generated from monkey embryonic stem cells function in a Parkinson primate model. J Clin Invest. 2005 Jan 3;102–9.

176. Shim, Koh, Chang, Roh, Choi, Oh, Son, Lee, Studer, & Lee. Enhanced In Vitro Midbrain Dopamine Neuron Differentiation, Dopaminergic Function, Neurite Outgrowth, and 1-Methyl-4-Phenylpyridium Resistance in Mouse Embryonic Stem Cells Overexpressing Bcl-XL. J Neurosci. 2004 Jan 28;843 LP-852.

177. Marteyn, Maury, Gauthier, Lecuyer, Vernet, Denis, Pietu, Peschanski, & Martinat. Mutant human embryonic stem cells reveal neurite and synapse formation defects in type 1 myotonic dystrophy. Cell Stem Cell. 2011 Apr;434–44.

178. Doers, Musser, Nichol, Berndt, Baker, Gomez, Zhang, Abbeduto, & Bhattacharyya. iPSC-derived forebrain neurons from FXS individuals show defects in initial neurite outgrowth. Stem Cells Dev. 2014 Aug;1777–87.

179. Tibbitt & Anseth. Hydrogels as extracellular matrix mimics for 3D cell culture. Biotechnol Bioeng. 2009 Jul;655–63.

180. Nicodemus & Bryant. Cell encapsulation in biodegradable hydrogels for tissue engineering applications. Tissue Eng Part B Rev. 2008 Jun;149–65.

181. Salgado. Induction of neurite outgrowth in 3D hydrogel-based environments. Biomed Mater. 2015;51001.

182. Shepard, Stevans, Holland, Wang, Shikanov, & Shea. Hydrogel Design for Supporting Neurite Outgrowth and Promoting Gene Delivery to Maximize Neurite Extension. Biotechnol Bioeng. 2012 Mar 9;830–9.

183. Nisbet, Forsythe, Shen, Finkelstein, & Horne. Review paper: a review of the cellular response on electrospun nanofibers for tissue engineering. J Biomater Appl. 2009 Jul;7–29.

184. Swindle-Reilly, Paranjape, & Miller. Electrospun poly(caprolactone)-elastin scaffolds for peripheral nerve regeneration. Prog Biomater. 2014 Jun 21;20.

185. Quan, Chang, Meng, Liu, Wang, Lu, Peng, & Zhao. Use of electrospinning to construct biomaterials for peripheral nerve regeneration. Rev Neurosci. 2016 Oct;761–8.

186. Sivolella, Brunello, Ferrarese, Puppa, D'Avella, Bressan, & Zavan. Nanostructured Guidance for Peripheral Nerve Injuries: A Review with a Perspective in the Oral and Maxillofacial Area. Int J Mol Sci. 2014 Feb 20;3088–117.

187. Koh, Yong, Chan, & Ramakrishna. Enhancement of neurite outgrowth using nano-

structured scaffolds coupled with laminin. Biomaterials. 2008 Sep;3574–82.

188. Xie, Willerth, Li, Macewan, Rader, Sakiyama-Elbert, & Xia. The differentiation of embryonic stem cells seeded on electrospun nanofibers into neural lineages. Biomaterials. 2009 Jan;354–62.

189. Xie, MacEwan, Li, Sakiyama-Elbert, & Xia. Neurite Outgrowth on Nanofiber Scaffolds with Different Orders, Structures, and Surface Properties. ACS Nano. 2009 May 26;1151–9.

190. Wang, Mullins, Cregg, McCarthy, & Gilbert. Varying the diameter of aligned electrospun fibers alters neurite outgrowth and Schwann cell migration. Acta Biomater. 2010 Aug;2970–8.

191. Maltman & Przyborski. Developments in three-dimensional cell culture technology aimed at improving the accuracy of in vitro analyses. Biochem Soc Trans. 2010 Aug;1072–5.

192. Ugbode, Hirst, & Rattray. Astrocytes Grown in Alvetex® Three Dimensional Scaffolds Retain a Non-reactive Phenotype. Neurochem Res. 2016;1857–67.

193. Hayward, Sano, Przyborski, & Cameron. Acrylic-Acid-Functionalized PolyHIPE Scaffolds for Use in 3D Cell Culture. Macromol Rapid Commun. 2013;1844–9.

194. Barbetta, Cameron, & Cooper. High internal phase emulsions (HIPEs) containing divinylbenzene and 4-vinylbenzyl chloride and the morphology of the resulting PolyHIPE materials. Chem Commun. 2000;221–2.

195. Bokhari, Carnachan, Przyborski, & Cameron. Emulsion-templated porous polymers as scaffolds for three dimensional cell culture: effect of synthesis parameters on scaffold formation and homogeneity. J Mater Chem. 2007;4088–94.

196. Carnachan, Bokhari, Przyborski, & Cameron. Tailoring the morphology of emulsion-templated porous polymers. Soft Matter. 2006;608–16.

197. Smith, Haag, Ugbode, Tams, Rattray, Przyborski, Bithell, & Whalley. Neuronal-glial populations form functional networks in a biocompatible 3D scaffold. Neurosci Lett. 2015 Nov 16;198–202.

198. European Collection of Authenticated Cell Cultures (Public Health England). U-251MG ECACC Page.

199. Collection. U118MG ATCC Page.

200. Rønn, Ralets, Hartz, Bech, Berezin, Berezin, Møller, & Bock. A simple procedure for quantification of neurite outgrowth based on stereological principles. J Neurosci Methods. 2000 Jul 31;25–32.

201. Hill, Robinson, Caley, Chen, O'Toole, Armstrong, Przyborski, & Lovat. A novel fully-humanised 3D skin equivalent to model early melanoma invasion. Mol Cancer Ther. 2015 Nov 1;2665–73.

202. Schutte, Fox, Baradez, Devonshire, Minguez, Bokhari, Przyborski, & Marshall. Rat primary hepatocytes show enhanced performance and sensitivity to acetaminophen during three-dimensional culture on a polystyrene scaffold designed for routine use. Assay Drug Dev Technol. 2011 Oct;475–86.

203. Zhang, Ottens, Larner, Kobeissy, Williams, Hayes, & Wang. Direct Rho-associated kinase inhibiton induces cofilin dephosphorylation and neurite outgrowth in PC-12 cells. Cell Mol Biol Lett. 2006;12–29.

204. Ahmed, Berry, & Logan. ROCK inhibition promotes adult retinal ganglion cell neurite outgrowth only in the presence of growth promoting factors. Mol Cell Neurosci.2009 Sep;128–33.

205. da Silva & Dotti. Breaking the neuronal sphere: regulation of the actin cytoskeleton in neuritogenesis. Nat Rev Neurosci. 2002;694–704.

206. Varma, Das, Wallace, Barry, Vertegel, Ray, & Banik. Spinal cord injury: a review of current therapy, future treatments, and basic science frontiers. Neurochem Res.

2013 May;895–905.

207. Myers, Robles, Ducharme-Smith, & Gomez. Focal adhesion kinase modulates Cdc42 activity downstream of positive and negative axon guidance cues. J Cell Sci. 2012 Jun 15;2918–29.

208. Liao, Seto, & Noma. Rho Kinase (ROCK) Inhibitors. Vol. 50, Journal of cardiovascular pharmacology. 2007.50(1) p. 17–24.

209. Chan, Khodarahmi, Liu, Sutherland, Oschipok, Steeves, & Tetzlaff. Dose-dependent beneficial and detrimental effects of ROCK inhibitor Y27632 on axonal sprouting and functional recovery after rat spinal cord injury. Exp Neurol. 2005 Dec;352–64.

210. Bottiglieri, Arning, Wasek, Nunbhakdi-Craig, Sontag, & Sontag. Acute administration of L-DOPA induces changes in methylation metabolites, reduced protein phosphatase 2A methylation, and hyperphosphorylation of Tau protein in mouse brain. J Neurosci. 2012 Jul;9173–81.

211. Odawara, Gotoh, & Suzuki. A three-dimensional neuronal culture technique that controls the direction of neurite elongation and the position of soma to mimic the layered structure of the brain. RSC Adv. 2013;23620–30.

212. ReproCELL Website [Internet]. Available from: www.reprocell.com

213. Aschner. Neuron-astrocyte interactions: implications for cellular energetics and antioxidant levels. Neurotoxicology. 2000;1101–7.

214. Anderson & Swanson. Astrocyte glutamate transport: Review of properties, regulation, and physiological functions . Glia. 2000;1–14.

215. Turner & Adamson. Neuronal-Astrocyte Metabolic Interactions: Understanding the Transition Into Abnormal Astrocytoma Metabolism. J Neuropathol Exp Neurol. 2011 Mar 1;167–76.

216. Clarke & Barres. Emerging roles of astrocytes in neural circuit development. Nat Rev Neurosci. 2013 May;311–21.

217. Yoshida & Gage. Cooperative regulation of nerve growth factor synthesis and secretion in fibroblasts and astrocytes by fibroblast growth factor and other cytokines. Brain Res. 1992 Jan 8;14–25.

218. Gadient, Cron, & Otten. Interleukin-1 β and tumor necrosis factor-α synergistically stimulate nerve growth factor (NGF) release from cultured rat astrocytes. Neurosci Lett. 1990 Sep 18;335–40.

219. Yoshida & Gage. Fibroblast growth factors stimulate nerve growth factor synthesis and secretion by astrocytes. Brain Res. 1991 Jan 4;118–26.

220. Silver & Miller. Regeneration beyond the glial scar. Nat Rev Neurosci. 2004 Feb;146–56.

221. Bahn, Mimmack, Ryan, Caldwell, Jauniaux, Starkey, Svendsen, & Emson. Neuronal target genes of the neuron-restrictive silencer factor in neurospheres derived from fetuses with Down's syndrome: a gene expression study. Lancet. 2002 Jan 26;310–5.

222. Balgude, Yu, Szymanski, & Bellamkonda. Agarose gel stiffness determines rate of DRG neurite extension in 3D cultures. Biomaterials. 2001 May;1077–84.

223. Fitzgerald, Kwiat, Middleton, & Pini. Ventral spinal cord inhibition of neurite outgrowth from embryonic rat dorsal root ganglia. Development. 1993 Apr;1377–84.

224. Radio & Mundy. Developmental neurotoxicity testing in vitro: Models for assessing chemical effects on neurite outgrowth. Neurotoxicology. 2008 May;361–76.

225. Chan, Peng, & Chiu. Heterogeneous expression of neurofilament proteins in forebrain and cerebellum during development: clinical implications for spinocerebellar ataxia. Brain Res. 1997 Nov;107–18.

226. Grant, Tseng, Gould, Gainer, & Pant. Expression of neurofilament proteins during

development of the nervous system in the squid Loligo pealei. J Comp Neurol. 1995;311–26.

227. Wang, Wu, Zhan, Ma, Yang, Yang, & Li. Neurofilament proteins in axonal regeneration and neurodegenerative diseases. Neural Regen Res. 2012 Mar 15;620–6.

228. Shaw & Weber. Differential expression of neurofilament triplet proteins in brain development. Nature. 1982 Jul 15;277–9.

229. Escurat, Djabali, Gumpel, Gros, & Portier. Differential expression of two neuronal intermediate-filament proteins, peripherin and the low-molecular-mass neurofilament protein (NF-L), during the development of the rat. J Neurosci. 1990 Mar 1;764 LP-784.

230. Mignone, Kukekov, Chiang, Steindler, & Enikolopov. Neural stem and progenitor cells in nestin-GFP transgenic mice. J Comp Neurol. 2004;311–24.

231. Johansson, Momma, Clarke, Risling, Lendahl, & Frisén. Identification of a Neural Stem Cell in the Adult Mammalian Central Nervous System. Cell. 1999 Jan 8;25–34.

232. Alvarez-Buylla, Garcia-Verdugo, & Tramontin. A unified hypothesis on the lineage of neural stem cells. Nat Rev Neurosci. 2001 Apr;287–93.

233. Park, Xiang, Mao, Zhang, Di, Liu, Shao, Ma, Lee, Ha, Walton, & Lahn. Nestin Is Required for the Proper Self-Renewal of Neural Stem Cells. Stem Cells. 2010;2162–71.

234. Scott, Peters, & Dragan. Human induced pluripotent stem cells and their use in drug discovery for toxicity testing. Toxicol Lett. 2013 May 10;49–58.

235. Sproul, Jacob, Pre, Kim, Nestor, Navarro-Sobrino, Santa-Maria, Zimmer, Aubry, Steele, Kahler, Dranovsky, Arancio, Crary, Gandy, & Noggle. Characterization and Molecular Profiling of PSEN1 Familial Alzheimer's Disease iPSC-Derived Neural Progenitors. PLoS One. 2014 Jan 8;e84547.

236. Muratore, Rice, Srikanth, Callahan, Shin, Benjamin, Walsh, Selkoe, & Young-Pearse. The familial Alzheimer's disease APPV717I mutation alters APP processing and Tau expression in iPSC-derived neurons. Hum Mol Genet. 2014 Jul 1;3523–36.

237. Kondo, Asai, Tsukita, Kutoku, Ohsawa, Sunada, Imamura, Egawa, Yahata, Okita, Takahashi, Asaka, Aoi, Watanabe, Watanabe, Kadoya, Nakano, Watanabe, Maruyama et al. Modeling Alzheimer’s Disease with iPSCs Reveals Stress Phenotypes Associated with Intracellular Aβ and Differential Drug Responsiveness. Cell Stem Cell. 2017 Mar 21;487–96.

238. Honda, Kogami, Kitogo, & Inamura. ALZHEIMER'S DISEASE MODEL CELLS DERIVED FROM HUMAN IPS CELLS. Alzheimer's Dement. 2014 Jul;P441.

239. Murata, Takamatsu, Liu, Kataoka, Huh, & Sakaguchi. NRF2 Regulates PINK1 Expression under Oxidative Stress Conditions. PLoS One. 2015 Nov 10;e0142438.

240. Bratt-Leal, Carpenedo, Ungrin, Zandstra, & McDevitt. Incorporation of biomaterials in multicellular aggregates modulates pluripotent stem cell differentiation. Biomaterials. 2011 Jan;48–56.

241. Baraniak & McDevitt. Scaffold-free culture of mesenchymal stem cell spheroids in suspension preserves multilineage potential. Cell Tissue Res. 2012;701–11.

242. Kozhich, Hamilton, & Mallon. Standardized Generation and Differentiation of Neural Precursor Cells from Human Pluripotent Stem Cells. Stem Cell Rev Reports. 2013;531–6.

243. Antonchuk. Formation of Embryoid Bodies from Human Pluripotent Stem Cells Using AggreWell™ Plates BT - Basic Cell Culture Protocols. In: Helgason CD, Miller CL, editors. Totowa, NJ: Humana Press; 2013. p. 523–33.

244. Yanai, Laver, Joe, Viringipurampeer, Wang, Gregory-Evans, & Gregory-Evans. Differentiation of human embryonic stem cells using size-controlled embryoid

bodies and negative cell selection in the production of photoreceptor precursor cells. Tissue Eng Part C Methods. 2013 Oct;755–64.

245. Yang, Atkinson, Gu, Borneo, Roberts, Zheng, Pennington, & Williams. Rac and Cdc42 GTPases control hematopoietic stem cell shape, adhesion, migration, and mobilization. Proc Natl Acad Sci . 2001 May 8;5614–8.

246. Sander, van Delft, ten Klooster, Reid, van der Kammen, Michiels, & Collard. Matrix-dependent Tiam1/Rac Signaling in Epithelial Cells Promotes Either Cell–Cell Adhesion or Cell Migration and Is Regulated by Phosphatidylinositol 3-Kinase. J Cell Biol. 1998 Nov 30;1385 LP-1398.

247. Webb, Parsons, & Horwitz. Adhesion assembly, disassembly and turnover in migrating cells - over and over and over again. Nat Cell Biol. 2002 Apr;E97–100.

248. Ridley, Schwartz, Burridge, Firtel, Ginsberg, Borisy, Parsons, & Horwitz. Cell Migration: Integrating Signals from Front to Back. Science (80-). 2003 Dec 4;1704 LP-1709.

249. Ossowski & Aguirre-Ghiso. Urokinase receptor and integrin partnership: coordination of signaling for cell adhesion, migration and growth. Curr Opin Cell Biol. 2000 Oct 1;613–20.

250. Brakebusch & Fässler. β 1 integrin function in vivo: Adhesion, migration and more. Cancer Metastasis Rev. 2005;403–11.

251. Fukushima, Ohnishi, Arita, Hayakawa, & Sekiguchi. Integrin α3β1-mediated interaction with laminin-5 stimulates adhesion, migration and invasion of malignant glioma cells. Int J Cancer. 1998;63–72.

252. Hood & Cheresh. Role of integrins in cell invasion and migration. Nat Rev Cancer [Internet]. 2002 Feb;91–100. Available from: http://dx.doi.org/10.1038/nrc727

253. Tate, García, Keselowsky, Schumm, Archer, & LaPlaca. Specific β1 integrins mediate adhesion, migration, and differentiation of neural progenitors derived from the embryonic striatum. Mol Cell Neurosci. 2004 Sep;22–31.

254. Cary, Chang, & Guan. Stimulation of cell migration by overexpression of focal adhesion kinase and its association with Src and Fyn. J Cell Sci. 1996 Jul 1;1787 LP-1794.

255. Sieg, Hauck, & Schlaepfer. Required role of focal adhesion kinase (FAK) for integrin-stimulated cell migration. J Cell Sci. 1999 Aug 15;2677 LP-2691.

256. Cary, Han, Polte, Hanks, & Guan. Identification of p130^{Cas} as a Mediator of Focal Adhesion Kinase–promoted Cell Migration. J Cell Biol. 1998 Jan 12;211 LP-221.

257. Ilic, Furuta, Kanazawa, Takeda, Sobue, Nakatsuji, Nomura, Fujimoto, Okada, & Yamamoto. Reduced cell motility and enhanced focal adhesion contact formation in cells from FAK-deficient mice. Nature. 1995 Oct;539–44.

258. Gumbiner. Cell Adhesion: The Molecular Basis of Tissue Architecture and Morphogenesis. Cell. 1996 Feb 9;345–57.

259. Cole & McCabe. Identification of a developmentally regulated keratan sulfate proteoglycan that inhibits cell adhesion and neurite outgrowth. Neuron. 1991 Dec;1007–18.

260. Johnson, Abramow-Newerly, Seilheimer, Sadoul, Tropak, Arquint, Dunn, Schachner, & Roder. Recombinant myelin-associated glycoprotein confers neural adhesion and neurite outgrowth function. Neuron. 1989 Sep;377–85.

261. Friedlander, Milev, Karthikeyan, Margolis, Margolis, & Grumet. The neuronal chondroitin sulfate proteoglycan neurocan binds to the neural cell adhesion molecules Ng-CAM/L1/NILE and N-CAM, and inhibits neuronal adhesion and neurite outgrowth. J Cell Biol. 1994 May;669–80.

262. De Strooper, Vassar, & Golde. The secretases: enzymes with therapeutic potential

in Alzheimer disease. Nat Rev Neurol. 2010 Feb;99–107.

263. Hardy, Bogdanovic, Winblad, Portelius, Andreasen, Cedazo-Minguez, & Zetterberg. Pathways to Alzheimer's disease. J Intern Med. 2014;296–303.

264. Ballatore, Lee, & Trojanowski. Tau-mediated neurodegeneration in Alzheimer's disease and related disorders. Nat Rev Neurosci. 2007 Sep;663–72.

265. Kalia & Lang. Parkinson's disease. Lancet. 2017 Mar 31;896–912.

266. Beitz. Parkinson's disease: a review. Front Biosci (Schol Ed). 2014 Jan;65–74.

267. Schmidt, Shastri, Vacanti, & Langer. Stimulation of neurite outgrowth using an electrically conducting polymer. Proc Natl Acad Sci. 1997 Aug 19;8948–53.

268. Estrada, Uhlen, & Ehrlich. Ca²⁺ oscillations induced by testosterone enhance neurite outgrowth. J Cell Sci. 2006 Jan 31;733 LP-743.

269. Gomez & Schmidt. Nerve growth factor-immobilized polypyrrole: Bioactive electrically conducting polymer for enhanced neurite extension. J Biomed Mater Res Part A. 2007;135–49.

270. Zhang, Rouabhia, Wang, Roberge, Shi, Roche, Li, & Dao. Electrically Conductive Biodegradable Polymer Composite for Nerve Regeneration: Electricity-Stimulated Neurite Outgrowth and Axon Regeneration. Artif Organs. 2007;13–22.

271. Adams, Kao, Hypolite, Distefano, Hu, & Letourneau. Growth cones turn and migrate up an immobilized gradient of the laminin IKVAV peptide. J Neurobiol. 2005;134–47.

272. Sephel, Tashiro, Sasaki, Greatorex, Martin, Yamada, & Kleinman. Laminin a chain synthetic peptide which supports neurite outgrowth. Biochem Biophys Res Commun. 1989;821–9.

273. Gundersen. Response of sensory neurites and growth cones to patterned substrata of laminin and fibronectin in vitro. Dev Biol. 1987;423–31.

274. Baron-Van Evercooren, Kleinman, Ohno, Marangos, Schwartz, & Dubois-Dalcq. Nerve growth factor, laminin, and fibronectin promote neurite growth in human fetal sensory ganglia cultures. J Neurosci Res. 1982;179–93.

275. Liesi, Närvänen, Soos, Sariola, & Snounou. Identification of a neurite outgrowth-promoting domain of laminin using synthetic peptides. FEBS Lett. 1989;141–8.

276. Kingham, Kalbermatten, Mahay, Armstrong, Wiberg, & Terenghi. Adipose-derived stem cells differentiate into a Schwann cell phenotype and promote neurite outgrowth in vitro. Exp Neurol. 2007 Oct;267–74.

277. Armstrong, Wiberg, Terenghi, & Kingham. ECM molecules mediate both Schwann cell proliferation and activation to enhance neurite outgrowth. Tissue Eng. 2007 Dec;2863–70.

278. Meng, Chen, Dong, & Liu. Enhanced neural differentiation of neural stem cells and neurite growth by amniotic epithelial cell co-culture. Cell Biol Int. 2007 Jul;691–8.

279. Yu, Dillon, & Bellamkonda. A laminin and nerve growth factor-laden three-dimensional scaffold for enhanced neurite extension. Tissue Eng. 1999 Aug;291–304.

280. Recio-Pinto & Ishii. Effects of insulin, insulin-like growth factor-II and nerve growth factor on neurite outgrowth in cultured human neuroblastoma cells. Brain Res. 1984 Jun 8;323–34.

281. Walicke, Cowan, Ueno, Baird, & Guillemin. Fibroblast growth factor promotes survival of dissociated hippocampal neurons and enhances neurite extension. Proc Natl Acad Sci . 1986 May 1;3012–6.

282. Rydel & Greene. Acidic and basic fibroblast growth factors promote stable neurite outgrowth and neuronal differentiation in cultures of PC12 cells. J Neurosci. 1987 Nov 1;3639 LP-3653.

283. Hall & Lalli. Rho and Ras GTPases in axon growth, guidance, and branching. Cold Spring Harb Perspect Biol. 2010;

284. Luo, Jan, & Jan. Rho family small GTP-binding proteins in growth cone signalling. Curr Opin Neurobiol. 1997 Feb;81–6.

285. Giniger. How do Rho family GTPases direct axon growth and guidance? A proposal relating signaling pathways to growth cone mechanics. Differentiation. 2002 Oct;385–96.

286. Fuentes, Leemhuis, Stark, & Lang. Rho kinase inhibitors Y27632 and H1152 augment neurite extension in the presence of cultured Schwann cells. J Brachial Plex Peripher Nerve Inj. 2008 Sep 25;19.

287. Ellezam, Dubreuil, Winton, Loy, Dergham, Belles-Navarro, & McKerracher. Chapter 26 Inactivation of intracellular Rho to stimulate axon growth and regeneration. In: L. McKerracher GD and SRBT-P in BR, editor. Spinal Cord Trauma: Regeneration, Neural Repair and Functional Recovery. Elsevier; 2002.Volume 137 p. 371–80.

288. Raftopoulou & Hall. Cell migration: Rho GTPases lead the way. Dev Biol. 2004 Jan 1;23–32.

289. Ridley. Rho GTPases and cell migration. J Cell Sci. 2001 Aug 1;2713 LP-2722.

290. Schmitz, Govek, Böttner, & Van Aelst. Rho GTPases: Signaling, Migration, and Invasion. Exp Cell Res. 2000;1–12.

291. Wang, Yang, Liu, Liu, Ye, & Zhang. ROCK inhibitor Y-27632 inhibits the growth, migration, and invasion of Tca8113 and CAL-27 cells in tongue squamous cell carcinoma. Tumour Biol. 2016 Mar;3757–64.

292. Imamura, Mukai, Ayaki, & Akedo. Y-27632, an Inhibitor of Rho-associated Protein Kinase, Suppresses Tumor Cell Invasion via Regulation of Focal Adhesion and Focal Adhesion Kinase. Japanese J Cancer Res. 2000;811–6.

293. Sofroniew & Vinters. Astrocytes: biology and pathology. Acta Neuropathol. 2010 Jan 10;7–35.

294. Markiewicz & Lukomska. The role of astrocytes in the physiology and pathology of the central nervous system. Acta Neurobiol Exp (Wars). 2006;343–58.

295. Siddharthan, Kim, Liu, & Kim. Human astrocytes/astrocyte-conditioned medium and shear stress enhance the barrier properties of human brain microvascular endothelial cells. Brain Res. 2007 May 25;39–50.

296. Arthur, Shivers, & Bowman. Astrocyte-mediated induction of tight junctions in brain capillary endothelium: an efficient in vitro model. Dev Brain Res. 1987 Nov;155–9.

297. Shivers, Arthur, & Bowman. Induction of gap junctions and brain endothelium-like tight junctions in cultured bovine endothelial cells: local control of cell specialization. J Submicrosc Cytol Pathol. 1988;1–14.

298. Yamagata, Tagami, Nara, Mitani, Kubota, Fujino, Numano, Kato§, & Yamori. ASTROCYTE-CONDITIONED MEDIUM INDUCES BLOOD-BRAIN BARRIER PROPERTIES IN ENDOTHELIAL CELLS. Clin Exp Pharmacol Physiol. 1997;710–3. A

299. Raff, Lillien, Richardson, Burne, & Noble. Platelet-derived growth factor from astrocytes drives the clock that times oligodendrocyte development in culture. Nature. 1988 Jun 9;562–5.

300. O'Donnell, Martinez, & Sun. Cerebral microvascular endothelial cell Na-K-Cl cotransport: regulation by astrocyte-conditioned medium. Am J Physiol - Cell Physiol. 1995 Mar 1;C747 LP-C754.

301. Dou & Levine. Inhibition of neurite growth by the NG2 chondroitin sulfate proteoglycan. J Neurosci. 1994 Dec;7616–28.

302. Ji-wen, Tong-yan, & Qi-lin. Protective effect of astrocyte-conditioned medium on neurons following hypoxia and mechanical injury. Chinese J Traumatol. 2013;3–9.

303. Assouline, Bosch, Lim, Kim, Jensen, & Pantazis. Rat astrocytes and Schwann cells in culture synthesize nerve growth factor-like neurite-promoting factors. Dev Brain Res . 1987 Jan;103–18.

304. Kadle, Suksang, Roberson, & Fellows. Identification of an insulin-like factor in astrocyte conditioned medium. Brain Res. 1988 Sep 13;60–7.

305. Goss, O'Malley, Zou, Styren, Kochanek, & DeKosky. Astrocytes are the major source of nerve growth factor upregulation following traumatic brain injury in the rat. Exp Neurol. 1998 Feb;301–9.

306. McDonald & Sadowsky. Spinal-cord injury. Lancet. 2002 Feb 2;417–25.

307. Marino, Barros, Biering-Sorensen, Burns, Donovan, Graves, Haak, Hudson, & Priebe. International Standards For Neurological Classification Of Spinal Cord Injury. J Spinal Cord Med. 2003 Jan 1;S50–6.

308. Tian, Dong, Pan, He, Yu, Xie, & Wang. Attenuation of astrogliosis by suppressing of microglial proliferation with the cell cycle inhibitor olomoucine in rat spinal cord injury model. Brain Res. 2007 Jun;206–14.

309. Sandvig, Berry, Barrett, Butt, & Logan. Myelin-, reactive glia-, and scar-derived CNS axon growth inhibitors: Expression, receptor signaling, and correlation with axon regeneration. Glia. 2004 May 1;225–51.

310. Lee, Geoffroy, Chan, Tolentino, Crawford, Leal, Kang, & Zheng. Assessing Spinal Axon Regeneration and Sprouting in Nogo-, MAG-, and OMgp-Deficient Mice. Neuron. 2010 Jun 10;663–70.

311. Lau, Cua, Keough, Haylock-Jacobs, & Yong. Pathophysiology of the brain extracellular matrix: a new target for remyelination. Nat Rev Neurosci. 2013 Oct;722–9.

312. Bradbury, Moon, Popat, King, Bennett, Patel, Fawcett, & McMahon. Chondroitinase ABC promotes functional recovery after spinal cord injury. Nature. 2002 Apr 11;636–40.

313. Barritt, Davies, Marchand, Hartley, Grist, Yip, McMahon, & Bradbury. Chondroitinase ABC Promotes Sprouting of Intact and Injured Spinal Systems after Spinal Cord Injury. J Neurosci. 2006 Oct 18;10856 LP-10867.

314. Garcia-Alias, Barkhuysen, Buckle, & Fawcett. Chondroitinase ABC treatment opens a window of opportunity for task-specific rehabilitation. Nat Neurosci. 2009 Sep;1145–51.

315. Grumet, Flaccus, & Margolis. Functional characterization of chondroitin sulfate proteoglycans of brain: interactions with neurons and neural cell adhesion molecules. J Cell Biol. 1993 Feb;815–24.

316. Bovolenta & Fernaud-Espinosa. Nervous system proteoglycans as modulators of neurite outgrowth. Prog Neurobiol. 2000 Jun 1;113–32.

317. McKeon, Hoke, & Silver. Injury-induced proteoglycans inhibit the potential for laminin-mediated axon growth on astrocytic scars. Exp Neurol. 1995 Nov;32–43.

318. Sharma, Selzer, & Li. Scar-mediated inhibition and CSPG receptors in the CNS. Exp Neurol. 2012 Oct;370–8.

319. Xu, Park, Ohtake, Li, Hayat, Liu, Selzer, Longo, & Li. Role of CSPG receptor LAR phosphatase in restricting axon regeneration after CNS injury. Neurobiol Dis. 2015 Jan;36–48.

320. Shen, Tenney, Busch, Horn, Cuascut, Liu, He, Silver, & Flanagan. PTPσ Is a Receptor for Chondroitin Sulfate Proteoglycan, an Inhibitor of Neural Regeneration. Science (80-). 2009 Oct 22;592 LP-596.

321. Dickendesher, Baldwin, Mironova, Koriyama, Raiker, Askew, Wood, Geoffroy, Zheng, Liepmann, Katagiri, Benowitz, Geller, & Giger. NgR1 and NgR3 are receptors for chondroitin sulfate proteoglycans. Nat Neurosci. 2012 May;703–12.

322. Fujita & Yamashita. Axon growth inhibition by RhoA/ROCK in the central nervous system. Vol. 8, Frontiers in Neuroscience. 2014.8.

323. Yiu & He. Signaling mechanisms of the myelin inhibitors of axon regeneration. Curr Opin Neurobiol. 2003;

324. Hunt, Coffin, & Anderson. The Nogo receptor, its ligands and axonal regeneration in the spinal cord; A review. J Neurocytol. 2002;93–120.

325. Liu, Fournier, GrandPré, & Strittmatter. Myelin-Associated Glycoprotein as a Functional Ligand for the Nogo-66 Receptor. Science (80-). 2002 Aug 16;1190 LP-1193.

326. Wang, Koprivica, Kim, Sivasankaran, Guo, Neve, & He. Oligodendrocyte-myelin glycoprotein is a Nogo receptor ligand that inhibits neurite outgrowth. Nature. 2002 Jun 27;941–4.

327. Wong, Henley, Kanning, Huang, Bothwell, & Poo. A p75NTR and Nogo receptor complex mediates repulsive signaling by myelin-associated glycoprotein. Nat Neurosci. 2002 Dec;1302–8.

328. Wang, Kim, Sivasankaran, Segal, & He. p75 interacts with the Nogo receptor as a co-receptor for Nogo, MAG and OMgp. Nature. 2002 Nov 7;74–8.

329. Park, Yiu, Kaneko, Wang, Chang, & He. A TNF Receptor Family Member, TROY, Is a Coreceptor with Nogo Receptor in Mediating the Inhibitory Activity of Myelin Inhibitors. Neuron. 2005 Feb 3;345–51.

330. Mi, Lee, Shao, Thill, Ji, Relton, Levesque, Allaire, Perrin, Sands, Crowell, Cate, McCoy, & Pepinsky. LINGO-1 is a component of the Nogo-66 receptor/p75 signaling complex. Nat Neurosci. 2004 Mar;221–8.

331. McGee & Strittmatter. The Nogo-66 receptor: focusing myelin inhibition of axon regeneration. Trends Neurosci. 2003 Apr;193–8.

332. Schwab. Functions of Nogo proteins and their receptors in the nervous system. Nat Rev Neurosci. 2010 Dec;799–811.

333. Freund, Schmidlin, Wannier, Bloch, Mir, Schwab, & Rouiller. Anti-Nogo-A antibody treatment promotes recovery of manual dexterity after unilateral cervical lesion in adult primates – re-examination and extension of behavioral data. Eur J Neurosci. 2009 Mar 5;983–96.

334. Liebscher, Schnell, Schnell, Scholl, Schneider, Gullo, Fouad, Mir, Rausch, Kindler, Hamers, & Schwab. Nogo-A antibody improves regeneration and locomotion of spinal cord-injured rats. Ann Neurol. 2005 Nov;706–19.

335. Freund, Schmidlin, Wannier, Bloch, Mir, Schwab, & Rouiller. Nogo-A-specific antibody treatment enhances sprouting and functional recovery after cervical lesion in adult primates. Nat Med. 2006 Jul;790–2.

336. Li & Strittmatter. Delayed Systemic Nogo-66 Receptor Antagonist Promotes Recovery from Spinal Cord Injury. J Neurosci. 2003 May 15;4219 LP-4227.

337. GrandPre, Li, & Strittmatter. Nogo-66 receptor antagonist peptide promotes axonal regeneration. Nature. 2002 May 30;547–51.

338. Fournier, Gould, Liu, & Strittmatter. Truncated Soluble Nogo Receptor Binds Nogo-66 and Blocks Inhibition of Axon Growth by Myelin. J Neurosci. 2002 Oct 15;8876 LP-8883.

339. Rivlin & Tator. Objective clinical assessment of motor function after experimental spinal cord injury in the rat. J Neurosurg. 1977 Oct 1;577–81.

340. Gale, Kerasidis, & Wrathall. Spinal cord contusion in the rat: Behavioral analysis of functional neurologic impairment. Exp Neurol. 1985 Apr;123–34.

341. Dusart & Schwab. Secondary Cell Death and the Inflammatory Reaction After Dorsal Hemisection of the Rat Spinal Cord. Eur J Neurosci. 1994;712–24.

342. Popovich, Wei, & Stokes. Cellular inflammatory response after spinal cord injury in

sprague-dawley and lewis rats. J Comp Neurol. 1997;443–64.

343. Bradbury & Carter. Manipulating the glial scar: Chondroitinase ABC as a therapy for spinal cord injury. Brain Res Bull. 2011 Mar 10;306–16.

344. Cheng, Lin, Lee, Tsai, Huang, Huang, Lin, Chen, Huang, & Cheng. Local Delivery of High-Dose Chondroitinase ABC in the Sub-Acute Stage Promotes Axonal Outgrowth and Functional Recovery after Complete Spinal Cord Transection. PLoS One. 2015 Sep 22;e0138705.

345. Zhao & Fawcett. Combination treatment with chondroitinase ABC in spinal cord injury--breaking the barrier. Neurosci Bull. 2013 Aug;477–83.

346. Menet, Prieto, Privat, & Ribotta. Axonal plasticity and functional recovery after spinal cord injury in mice deficient in both glial fibrillary acidic protein and vimentin genes. Proc Natl Acad Sci . 2003 Jul 22;8999–9004.

347. Ribotta, Menet, & Privat. Glial scar and axonal regeneration in the CNS: lessons from GFAP and vimentin transgenic mice BT - Mechanisms of Secondary Brain Damage from Trauma and Ischemia: Recent Advances of our Understanding. In: Baethmann A, Eriskat J, Lehmberg J, Plesnila N, editors. Vienna: Springer Vienna; 2004. p. 87–92.

348. Fisher, Xing, Dill, Li, Hoang, Zhao, Yang, Bachoo, Cannon, Longo, Sheng, Silver, & Li. LAR is a functional receptor for CSPG axon growth inhibitors. J Neurosci. 2011 Oct 5;14051–66.

349. Festing & Wilkinson. The ethics of animal research. EMBO Rep. 2007 May 18;526 LP-530.

350. Vahidi, Park, Kim, & Jeon. Microfluidic-based strip assay for testing the effects of various surface-bound inhibitors in spinal cord injury. J Neurosci Methods. 2008 May 30;188–96.

351. East, Golding, & Phillips. A versatile 3D culture model facilitates monitoring of astrocytes undergoing reactive gliosis. J Tissue Eng Regen Med. 2009 Dec 28;634–46.

352. East, Johns, Georgiou, Golding, Loughlin, Kingham, & Phillips. A 3D in vitro model reveals differences in the astrocyte response elicited by potential stem cell therapies for CNS injury. Regen Med. 2013 Nov;10.2217/rme.13.61.

353. East, Golding, & Phillips. Engineering an integrated cellular interface in three-dimensional hydrogel cultures permits monitoring of reciprocal astrocyte and neuronal responses. Tissue Eng Part C Methods. 2012 Jul;526–36.

354. PRABHAKAR, CAPILA, BOSQUES, POJASEK, & SASISEKHARAN. Chondroitinase ABC I from Proteus vulgaris: cloning, recombinant expression and active site identification. Biochem J. 2005 Feb 8;103 LP-112.

355. Huang, Kuo, Cherng, Hsu, Chen, Huang, Huang, Liu, & Cheng. Chondroitinase ABC promotes axonal re-growth and behavior recovery in spinal cord injury. Biochem Biophys Res Commun. 2006 Oct 27;963–8.

356. Merkler, Metz, Raineteau, Dietz, Schwab, & Fouad. Locomotor Recovery in Spinal Cord-Injured Rats Treated with an Antibody Neutralizing the Myelin-Associated Neurite Growth Inhibitor Nogo-A. J Neurosci. 2001 May 15;3665 LP-3673.

357. Cao, Shumsky, Sabol, Kushner, Strittmatter, Hamers, Lee, Rabacchi, & Murray. Nogo-66 Receptor Antagonist Peptide (NEP1-40) Administration Promotes Functional Recovery and Axonal Growth After Lateral Funiculus Injury in the Adult Rat. Neurorehabil Neural Repair. 2008 May 1;262–78.

358. Li, Liu, Budel, Li, Ji, Walus, Li, Jirik, Rabacchi, Choi, Worley, Sah, Pepinsky, Lee, Relton, & Strittmatter. Blockade of Nogo-66, Myelin-Associated Glycoprotein, and Oligodendrocyte Myelin Glycoprotein by Soluble Nogo-66 Receptor Promotes Axonal Sprouting and Recovery after Spinal Injury. J Neurosci. 2004 Nov 17;10511 LP-10520.

359. CHEN, ZHANG, WANG, & LV. Combined treatment with FK506 and nerve growth factor for spinal cord injury in rats. Exp Ther Med. 2013 Oct 7;868–72.

360. Zhang, Wu, Kong, Yang, Chen, Deng, Cheng, Ye, Zhu, Zhang, Wang, Shi, Fu, Li, Xu, Lin, & Xiao. Nerve growth factor improves functional recovery by inhibiting endoplasmic reticulum stress-induced neuronal apoptosis in rats with spinal cord injury. J Transl Med. 2014 May;130.

361. Bradbury, Khemani, Von, King, Priestley, & McMahon. NT-3 promotes growth of lesioned adult rat sensory axons ascending in the dorsal columns of the spinal cord. Eur J Neurosci. 1999 Nov;3873–83.

362. Oudega & Hagg. Neurotrophins promote regeneration of sensory axons in the adult rat spinal cord. Brain Res. 1999 Feb;431–8.

363. Oudega & Hagg. Nerve growth factor promotes regeneration of sensory axons into adult rat spinal cord. Exp Neurol. 1996 Aug;218–29.

364. Condic. Adult neuronal regeneration induced by transgenic integrin expression. J Neurosci. 2001 Jul;4782–8.

365. Wu & Xu. RhoA/Rho kinase in spinal cord injury. Neural Regen Res. 2016 Jan 24;23–7.

366. Dergham, Ellezam, Essagian, Avedissian, Lubell, & McKerracher. Rho Signaling Pathway Targeted to Promote Spinal Cord Repair. J Neurosci. 2002 Aug 1;6570 LP-6577.

367. Jain, Brady-Kalnay, & Bellamkonda. Modulation of Rho GTPase activity alleviates chondroitin sulfate proteoglycan-dependent inhibition of neurite extension. J Neurosci Res. 2004;299–307. A

368. Kopp, Liebscher, Niedeggen, Laufer, Brommer, Jungehulsing, Strittmatter, Dirnagl, & Schwab. Small-molecule-induced Rho-inhibition: NSAIDs after spinal cord injury. Cell Tissue Res. 2012 Jul;119–32.

369. Wang, Budel, Baughman, Gould, Song, & Strittmatter. Ibuprofen enhances recovery from spinal cord injury by limiting tissue loss and stimulating axonal growth. J Neurotrauma. 2009 Jan;81–95.

370. Chiba, Kuroda, Shichinohe, Hokari, Osanai, Maruichi, Yano, Hida, & Iwasaki. Synergistic effects of bone marrow stromal cells and a Rho kinase (ROCK) inhibitor, Fasudil on axon regeneration in rat spinal cord injury. Neuropathology. 2010;241–50.

371. Boomkamp, Riehle, Wood, Olson, & Barnett. The development of a rat in vitro model of spinal cord injury demonstrating the additive effects of rho and ROCK inhibitors on neurite outgrowth and myelination. Glia. 2012;441–56.

372. Forgione & Fehlings. Rho-ROCK Inhibition in the Treatment of Spinal Cord Injury. World Neurosurg. 2014 Sep;e535–9.

373. Mueller, Mack, & Teusch. Rho kinase, a promising drug target for neurological disorders. Nat Rev Drug Discov. 2005 May;387–98. A

374. Nishio, Koda, Kitajo, Seto, Hata, Taniguchi, Moriya, Fujitani, Kubo, & Yamashita. Delayed treatment with Rho-kinase inhibitor does not enhance axonal regeneration or functional recovery after spinal cord injury in rats. Exp Neurol. 2006 Aug;392–7.

375. Fehlings, Theodore, Harrop, Maurais, Kuntz, Shaffrey, Kwon, Chapman, Yee, Tighe, & McKerracher. A phase I/IIa clinical trial of a recombinant Rho protein antagonist in acute spinal cord injury. J Neurotrauma. 2011 May;787–96.

376. Paulus, Baur, Dours-Zimmermann, & Zimmermann. Differential expression of versican isoforms in brain tumors. J Neuropathol Exp Neurol. 1996 May;528–33.

377. Kantor, Chivatakarn, Peer, Oster, Inatani, Hansen, Flanagan, Yamaguchi, Sretavan, Giger, & Kolodkin. Semaphorin 5A Is a Bifunctional Axon Guidance Cue Regulated

by Heparan and Chondroitin Sulfate Proteoglycans. Neuron. 2004 Dec 16;961–75.

378. Ketschek, Haas, Gallo, & Fischer. The roles of neuronal and glial precursors in overcoming chondroitin sulfate proteoglycan inhibition. Exp Neurol. 2012 Jun;627–37.

379. Siebert & Osterhout. The inhibitory effects of chondroitin sulfate proteoglycans on oligodendrocytes. J Neurochem. 2011;176–88.

380. Hur, Yang, Kim, Byun, Saijilafu, Xu, Nicovich, Cheong, Levchenko, Thakor, & Zhou. Engineering neuronal growth cones to promote axon regeneration over inhibitory molecules. Proc Natl Acad Sci . 2011 Mar 22;5057–62.

381. Kiani, Chen, Wu, Yee, & Yang. Structure and function of aggrecan. Cell Res. 2002 Mar;19–32.

382. Watanabe, Yamada, & Kimata. Roles of aggrecan, a large chondroitin sulfate proteoglycan, in cartilage structure and function. J Biochem. 1998 Oct;687–93.

383. Roughley & Mort. The role of aggrecan in normal and osteoarthritic cartilage. J Exp Orthop. 2014 Dec 16;8.

384. Canning, Höke, Malemud, & Silver. A POTENT INHIBITOR OF NEURITE OUTGROWTH THAT PREDOMINATES IN THE EXTRACELLULAR MATRIX OF REACTIVE ASTROCYTES. Int J Dev Neurosci. 1996 Jun;153–75.

385. Cua, Lau, Keough, Midha, Apte, & Yong. Overcoming neurite-inhibitory chondroitin sulfate proteoglycans in the astrocyte matrix. Glia. 2013;972–84.

386. Lemons, Sandy, Anderson, & Howland. Intact Aggrecan and Fragments Generated by Both Aggrecanse and Metalloproteinase-Like Activities Are Present in the Developing and Adult Rat Spinal Cord and Their Relative Abundance Is Altered by Injury. J Neurosci. 2001 Jul 1;4772 LP-4781.

387. Jones, Margolis, & Tuszynski. The chondroitin sulfate proteoglycans neurocan, brevican, phosphacan, and versican are differentially regulated following spinal cord injury. Exp Neurol. 2003 Aug;399–411.

388. Jones, Yamaguchi, Stallcup, & Tuszynski. NG2 Is a Major Chondroitin Sulfate Proteoglycan Produced after Spinal Cord Injury and Is Expressed by Macrophages and Oligodendrocyte Progenitors. J Neurosci. 2002 Apr 1;2792 LP-2803.

389. Dutt, Kleber, Matasci, Sommer, & Zimmermann. Versican V0 and V1 guide migratory neural crest cells. J Biol Chem. 2006 Apr;12123–31.

390. Dours-Zimmermann & Zimmermann. A novel glycosaminoglycan attachment domain identified in two alternative splice variants of human versican. J Biol Chem. 1994 Dec;32992–8.

391. Sim, Hu, & Viapiano. Reduced expression of the hyaluronan and proteoglycan link proteins in malignant gliomas. J Biol Chem. 2009 Sep;26547–56.

392. Touab, Villena, Barranco, Arumí-Uría, & Bassols. Versican Is Differentially Expressed in Human Melanoma and May Play a Role in Tumor Development. Vol. 160, The American Journal of Pathology. 2002.160(2) p. 549–57.

393. Lopes, Frankfurter, Zientek, & Herman. The presence of neuron-associated microtubule proteins in the human U-251 MG cell line. Mol Chem Neuropathol. 1992;273–87. A

394. Nishiyama, Onda, Washiyama, Kumanishi, Kuwano, Sakimura, & Takahashi. Differential expression of glial fibrillary acidic protein in human glioma cell lines. Acta Neuropathol. 1989;9–15.

395. Kumanishi, Usui, Ichikawa, Nishiyama, Katagiri, Abe, Yoshida, Washiyama, Kuwano, & Sakimura. Human glial fibrillary acidic protein (GFAP): molecular cloning of the complete cDNA sequence and chromosomal localization (chromosome 17) of the GFAP gene. Acta Neuropathol. 1992;569–78.

396. Lopes, Frankfurter, Zientek, & Herman. The presence of neuron-associated

microtubule proteins in the human U-251 MG cell line. A comparative immunoblot and immunohistochemical study. Mol Chem Neuropathol. 1992 Dec;273–87.

397. Jin, Ketschek, Jiang, Smith, & Fischer. Chondroitinase activity can be transduced by a lentiviral vector in vitro and in vivo. J Neurosci Methods. 2011 Aug;208–13.

398. Sung, Miao, Calvert, Huang, Louis Harkey, & Zhang. A possible role of RhoA/Rho-kinase in experimental spinal cord injury in rat. Brain Res. 2003 Jan 3;29–38.

399. Cadotte & Fehlings. Spinal Cord Injury: A Systematic Review of Current Treatment Options. Clin Orthop Relat Res. 2011;732–41.

400. Fournier, Takizawa, & Strittmatter. Rho Kinase Inhibition Enhances Axonal Regeneration in the Injured CNS. J Neurosci . 2003 Feb 15;1416–23.

401. Puschmann, Zandén, De Pablo, Kirchhoff, Pekna, Liu, & Pekny. Bioactive 3D cell culture system minimizes cellular stress and maintains the in vivo-like morphological complexity of astroglial cells. Glia. 2013;432–40.

402. Racchetti, D'Alessandro, & Meldolesi. Astrocyte stellation, a process dependent on Rac1 is sustained by the regulated exocytosis of enlargeosomes. Glia. 2012;465–75.

403. Abe & Misawa. Astrocyte stellation induced by Rho kinase inhibitors in culture. Dev Brain Res. 2003 Jun 12;99–104.

404. Höltje, Hoffmann, Hofmann, Mucke, Große, Van Rooijen, Kettenmann, Just, & Ahnert-Hilger. Role of Rho GTPase in astrocyte morphology and migratory response during in vitro wound healing. J Neurochem. 2005;1237–48.

405. Avalos, Arthur, Schneider, Quest, Burridge, & Leyton. Aggregation of integrins and RhoA activation are required for Thy-1-induced morphological changes in astrocytes. J Biol Chem. 2004 Sep;39139–45.

406. Yu, Liu, Fu, Xie, Wang, & Luo. ROCK inhibition with Y27632 promotes the proliferation and cell cycle progression of cultured astrocyte from spinal cord. Neurochem Int. 2012 Dec;1114–20.

407. ZOHRABIAN, FORZANI, CHAU, MURALI, & JHANWAR-UNIYAL. Rho/ROCK and MAPK Signaling Pathways Are Involved in Glioblastoma Cell Migration and Proliferation. Anticancer Res. 2009 Jan 1;119–23.

408. Deng, Li, Li, Liu, He, & Zhang. Rho-kinase inhibitor, fasudil, suppresses glioblastoma cell line progression in vitro and in vivo. Cancer Biol Ther. 2010 Jun 1;875–84.

409. Chan, Wong, Liu, Steeves, & Tetzlaff. ROCK inhibition with Y27632 activates astrocytes and increases their expression of neurite growth-inhibitory chondroitin sulfate proteoglycans. Glia. 2007;369–84.

410. LaFerla, Green, & Oddo. Intracellular amyloid-beta in Alzheimer's disease. Nat Rev Neurosci. 2007 Jul;499–509.

411. Ittner & Gotz. Amyloid-beta and tau--a toxic pas de deux in Alzheimer's disease. Nat Rev Neurosci. 2011 Feb;65–72.

412. Winblad, Jones, Wirth, Stöffler, & Möbius. Memantine in Moderate to Severe Alzheimer's Disease: a Meta-Analysis of Randomised Clinical Trials. Dement Geriatr Cogn Disord. 2007;20–7.

413. Kaduszkiewicz, Zimmermann, Beck-Bornholdt, & van den Bussche. Cholinesterase inhibitors for patients with Alzheimer's disease: systematic review of randomised clinical trials. BMJ. 2005 Aug 4;321 LP-327.

414. Mangialasche, Solomon, Winblad, Mecocci, & Kivipelto. Alzheimer's disease: clinical trials and drug development. Lancet Neurol. 2017 Mar 18;702–16.

415. Doody, Thomas, Farlow, Iwatsubo, Vellas, Joffe, Kieburtz, Raman, Sun, Aisen, Siemers, Liu-Seifert, & Mohs. Phase 3 Trials of Solanezumab for Mild-to-Moderate Alzheimer's Disease. N Engl J Med. 2014 Jan 22;311–21.

416. Doody, Raman, Farlow, Iwatsubo, Vellas, Joffe, Kieburtz, He, Sun, Thomas, Aisen, Siemers, Sethuraman, & Mohs. A Phase 3 Trial of Semagacestat for Treatment of Alzheimer's Disease. N Engl J Med. 2013 Jul 24;341–50.

417. Cummings, Morstorf, & Zhong. Alzheimer's disease drug-development pipeline: few candidates, frequent failures. Alzheimers Res Ther. 2014;37.

418. Vassar. BACE1 inhibitor drugs in clinical trials for Alzheimer's disease. Alzheimers Res Ther. 2014;89.

419. Lichtenthaler. Alpha-secretase in Alzheimer's disease: molecular identity, regulation and therapeutic potential. J Neurochem. 2011;10–21.

420. Lannfelt, Basun, Wahlund, Rowe, & Wagner. Decreased [alpha]-secretase-cleaved amyloid precursor protein as a diagnostic marker for Alzheimer's diseas. Nat Med. 1995 Aug;829–32.

421. Luo, Bolon, Kahn, Bennett, Babu-Khan, Denis, Fan, Kha, Zhang, Gong, Martin, Louis, Yan, Richards, Citron, & Vassar. Mice deficient in BACE1, the Alzheimer's [beta]-secretase, have normal phenotype and abolished [beta]-amyloid generation. Nat Neurosci. 2001 Mar;231–2.

422. Vassar, Bennett, Babu-Khan, Kahn, Mendiaz, Denis, Teplow, Ross, Amarante, Loeloff, Luo, Fisher, Fuller, Edenson, Lile, Jarosinski, Biere, Curran, Burgess et al. β-Secretase Cleavage of Alzheimer's Amyloid Precursor Protein by the Transmembrane Aspartic Protease BACE. Science (80-). 1999 Oct 22;735 LP-741.

423. Selkoe. The cell biology of β-amyloid precursor protein and presenilin in Alzheimer's disease. Trends Cell Biol. 1998 Nov 1;447–53.

424. Mattson. Pathways towards and away from Alzheimer's disease. Nature. 2004 Aug 5;631–9.

425. Thinakaran & Koo. Amyloid Precursor Protein Trafficking, Processing, and Function. J Biol Chem . 2008 Oct 31;29615–9. t

426. Näslund, Schierhorn, Hellman, Lannfelt, Roses, Tjernberg, Silberring, Gandy, Winblad, & Greengard. Relative abundance of Alzheimer A beta amyloid peptide variants in Alzheimer disease and normal aging. Proc Natl Acad Sci. 1994 Aug 30;8378–82.

427. Wiltfang, Esselmann, Bibl, Hüll, Hampel, & Kessler. Amyloid β peptide ratio 42/40 but not Aβ42 correlates with phospho-Tau in patients with low- and high-CSF Aβ40 load. J Neurochem. 2007;

428. Lewczuk, Esselmann, Otto, Maler, Henkel, Henkel, Eikenberg, Antz, Krause, Reulbach, Kornhuber, & Wiltfang. Neurochemical diagnosis of Alzheimer's dementia by CSF Aβ42, Aβ42/Aβ40 ratio and total tau. Neurobiol Aging. 2004 Mar;273–81.

429. Mattsson, Andreasson, Persson, Carrillo, Collins, & Chalbot. CSF biomarker variability in the Alzheimer's Association quality control program. Alzheimers Dement. 2013;

430. Verwey, Kester, Flier, Veerhuis, Berkhof, & Twaalfhoven. Additional value of CSF amyloid-β40 levels in the differentiation between FTLD and control subjects. J Alzheimers Dis. 2010;

431. Hansson, Zetterberg, Buchhave, Andreasson, Londos, & Minthon. Prediction of Alzheimer's disease using the CSF Aβ42/Aβ40 ratio in patients with mild cognitive impairment. Dement Geriatr Cogn Disord. 2007;

432. Bibl, Mollenhauer, Esselmann, Lewczuk, Trenkwalder, & Brechlin. CSF diagnosis of Alzheimer's disease and dementia with Lewy bodies. J Neural Transm. 2006;

433. Spies, Slats, Sjogren, Kremer, Verhey, Rikkert, & Verbeek. The cerebrospinal fluid amyloid beta42/40 ratio in the differentiation of Alzheimer's disease from non-Alzheimer's dementia. Curr Alzheimer Res. 2010 Aug;470–6.

434. Lewczuk, Lelental, Spitzer, Maler, & Kornhuber. Amyloid-beta 42/40 cerebrospinal fluid concentration ratio in the diagnostics of Alzheimer's disease: validation of two novel assays. J Alzheimers Dis. 2015;183–91.

435. Citron, Oltersdorf, Haass, McConlogue, Hung, Seubert, Vigo-Pelfrey, Lieberburg, & Selkoe. Mutation of the beta-amyloid precursor protein in familial Alzheimer's disease increases beta-protein production. Nature. 1992 Dec;672–4.

436. Giaccone, Morbin, Moda, Botta, Mazzoleni, Uggetti, Catania, Moro, Redaelli, Spagnoli, Rossi, Salmona, Di Fede, & Tagliavini. Neuropathology of the recessive A673V APP mutation: Alzheimer disease with distinctive features. Acta Neuropathol. 2010;803–12.

437. Nilsberth, Westlind-Danielsson, Eckman, Condron, Axelman, Forsell, Stenh, Luthman, Teplow, Younkin, Naslund, & Lannfelt. The "Arctic" APP mutation (E693G) causes Alzheimer's disease by enhanced A[beta] protofibril formation. Nat Neurosci. 2001 Sep;887–93.

438. Citron, Westaway, Xia, Carlson, Diehl, Levesque, Johnson-wood, Lee, Seubert, Davis, Kholodenko, Motter, Sherrington, Perry, Yao, Strome, Lieberburg, Rommens, Kim et al. Mutant presenilins of Alzheimer's disease increase production of 42-residue amyloid [beta]-protein in both transfected cells and transgenic mice. Nat Med. 1997 Jan;67–72.

439. Campion, Dumanchin, Hannequin, Dubois, Belliard, Puel, Thomas-Anterion, Michon, Martin, Charbonnier, Raux, Camuzat, Penet, Mesnage, Martinez, Clerget-Darpoux, Brice, & Frebourg. Early-Onset Autosomal Dominant Alzheimer Disease: Prevalence, Genetic Heterogeneity, and Mutation Spectrum. Am J Hum Genet 1999 Sep;664–70.

440. Haass, Lemere, Capell, Citron, Seubert, Schenk, Lannfelt, & Selkoe. The Swedish mutation causes early-onset Alzheimer's disease by [beta]-secretase cleavage within the secretory pathway. Nat Med. 1995 Dec;1291–6.

441. Mann. The pathological association between down syndrome and Alzheimer disease. Mech Ageing Dev. 1988 May;99–136.

442. Lai & RS. A prospective study of alzheimer disease in down syndrome. Arch Neurol. 1989 Aug 1;849–53.

443. Masters, Simms, Weinman, Multhaup, McDonald, & Beyreuther. Amyloid plaque core protein in Alzheimer disease and Down syndrome. Proc Natl Acad Sci. 1985 Jun 1;4245–9.

444. Gouras, Olsson, & Hansson. β-amyloid Peptides and Amyloid Plaques in Alzheimer's Disease. Neurotherapeutics. 2015;3–11.

445. Dovey, John, Anderson, Chen, De Saint Andrieu, Fang, Freedman, Folmer, Goldbach, Holsztynska, Hu, Johnson-Wood, Kennedy, Kholodenko, Knops, Latimer, Lee, Liao, Lieberburg et al. Functional gamma-secretase inhibitors reduce beta-amyloid peptide levels in brain. J Neurochem. 2001;173–81.

446. De Strooper, Annaert, Cupers, Saftig, Craessaerts, Mumm, Schroeter, Schrijvers, Wolfe, Ray, Goate, & Kopan. A presenilin-1-dependent [gamma]-secretase-like protease mediates release of Notch intracellular domain. Nature. 1999 Apr 8;518–22.

447. Haapasalo & Kovacs. The Many Substrates of Presenilin/γ-Secretase. J Alzheimer's Dis. 2011;3–28.

448. Rao, O'Neil, Liberator, Hardwick, Dai, Zhang, Tyminski, Yuan, Kohl, Richon, Van der Ploeg, Carroll, Draetta, Look, Strack, & Winter. Inhibition of NOTCH Signaling by Gamma Secretase Inhibitor Engages the RB Pathway and Elicits Cell Cycle Exit in T-Cell Acute Lymphoblastic Leukemia Cells. Cancer Res. 2009 Apr 1;3060 LP-3068.

449. Pollack & Lewis. Secretase inhibitors for Alzheimer's disease: challenges of a promiscuous protease. Curr Opin Investig Drugs. 2005;35–47.

450. Ni, Murphy, Golde, & Carpenter. γ-Secretase Cleavage and Nuclear Localization of ErbB-4 Receptor Tyrosine Kinase. Science (80-). 2001 Dec 7;2179 LP-2181.

451. May, Willis, Lowe, Dean, Monk, Cocke, Audia, Boggs, Borders, Brier, Calligaro, Day, Ereshefsky, Erickson, Gevorkyan, Gonzales, James, Jhee, Komjathy et al. The potent BACE1 inhibitor LY2886721 elicits robust central Abeta pharmacodynamic responses in mice, dogs, and humans. J Neurosci. 2015 Jan;1199–210.

452. Rajendran, Schneider, Schlechtingen, Weidlich, Ries, Braxmeier, Schwille, Schulz, Schroeder, Simons, Jennings, Knölker, & Simons. Efficient Inhibition of the Alzheimer's Disease β-Secretase by Membrane Targeting. Science (80-). 2008 Apr 25;520 LP-523.

453. Ghosh, Brindisi, & Tang. Developing β-secretase inhibitors for treatment of Alzheimer's disease. J Neurochem. 2012;71–83.

454. Aisen, Gauthier, Ferris, Saumier, Haine, Garceau, Duong, Suhy, Oh, Lau, & Sampalis. Tramiprosate in mild-to-moderate Alzheimer's disease - a randomized, double-blind, placebo-controlled, multi-centre study (the Alphase Study). Arch Med Sci. 2011 Feb;102–11.

455. Salloway, Sperling, Keren, Porsteinsson, van Dyck, Tariot, Gilman, Arnold, Abushakra, Hernandez, Crans, Liang, Quinn, Bairu, Pastrak, & Cedarbaum. A phase 2 randomized trial of ELND005, scyllo-inositol, in mild to moderate Alzheimer disease. Neurology. 2011 Sep;1253–62.

456. Holmes, Boche, Wilkinson, Yadegarfar, Hopkins, Bayer, Jones, Bullock, Love, Neal, Zotova, & Nicoll. Long-term effects of Abeta42 immunisation in Alzheimer's disease: follow-up of a randomised, placebo-controlled phase I trial. Lancet (London, England). 2008 Jul;216–23.

457. Ihara, Morishima-Kawashima, & Nixon. The ubiquitin-proteasome system and the autophagic-lysosomal system in Alzheimer disease. Cold Spring Harb Perspect Med. 2012 Aug;

458. Citron. Alzheimer's disease: treatments in discovery and development. Nat Neurosci. 2002 Oct 28;

459. Herrup. The case for rejecting the amyloid cascade hypothesis. Nat Neurosci. 2015 May 26;794–9.

460. Hardy & Higgins. Alzheimer's disease: the amyloid cascade hypothesis. Science (80-). 1992;184.

461. Hardy & Selkoe. The Amyloid Hypothesis of Alzheimer's Disease: Progress and Problems on the Road to Therapeutics. Science (80-). 2002 Jul 19;353 LP-356.

462. Buee, Bussiere, Buee-Scherrer, Delacourte, & Hof. Tau protein isoforms, phosphorylation and role in neurodegenerative disorders. Brain Res Brain Res Rev. 2000 Aug;95–130.

463. Goode, Chau, Denis, & Feinstein. Structural and functional differences between 3-repeat and 4-repeat tau isoforms. Implications for normal tau function and the onset of neurodegenetative disease. J Biol Chem. 2000 Dec;38182–9.

464. Dinkel, Holden, Matin, & Margittai. RNA Binds to Tau Fibrils and Sustains Template-Assisted Growth. Biochemistry. 2015 Aug 4;4731–40.

465. Takashima, Murayama, Murayama, Kohno, Honda, Yasutake, Nihonmatsu, Mercken, Yamaguchi, Sugihara, & Wolozin. Presenilin 1 associates with glycogen synthase kinase-3β and its substrate tau. Proc Natl Acad Sci . 1998 Aug 4;9637–41.

466. Wagner, Utton, Gallo, & Miller. Cellular phosphorylation of tau by GSK-3 beta influences tau binding to microtubules and microtubule organisation. J Cell Sci. 1996 Jun 1;1537 LP-1543.

467. Sontag, Nunbhakdi-Craig, Lee, Bloom, & Mumby. Regulation of the Phosphorylation State and Microtubule-Binding Activity of Tau by Protein Phosphatase 2A. Neuron. 1996 Dec;1201–7.

468. MANDELKOW, SCHWEERS, DREWES, BIERNAT, GUSTKE, TRINCZEK, & MANDELKOW. Structure, Microtubule Interactions, and Phosphorylation of Tau Proteina. Ann N Y Acad Sci. 1996;96–106.

469. Bramblett, Goedert, Jakes, Merrick, Trojanowski, & Lee. Abnormal tau phosphorylation at Ser396 in alzheimer's disease recapitulates development and contributes to reduced microtubule binding. Neuron. 1993 Jun;1089–99.

470. Goedert, Jakes, Crowther, Six, Lübke, Vandermeeren, Cras, Trojanowski, & Lee. The abnormal phosphorylation of tau protein at Ser-202 in Alzheimer disease recapitulates phosphorylation during development. Proc Natl Acad Sci. 1993 Jun 1;5066–70.

471. Wang & Liu. Microtubule-associated protein tau in development, degeneration and protection of neurons. Prog Neurobiol. 2008 Jun;148–75.

472. Bancher, Brunner, Lassmann, Budka, Jellinger, Wiche, Seitelberger, Grundke-Iqbal, Iqbal, & Wisniewski. Accumulation of abnormally phosphorylated τ precedes the formation of neurofibrillary tangles in Alzheimer's disease. Brain Res. 1989 Jan 16;90–9.

473. Iqbal, del C. Alonso, Gong, Khatoon, Pei, Wang, & Grundke-Iqbal. Mechanisms of neurofibrillary degeneration and the formation of neurofibrillary tangles BT - Ageing and Dementia. In: Jellinger K, Fazekas F, Windisch M, editors. Vienna: Springer Vienna; 1998. p. 169–80.

474. Braak, Braak, & Strothjohann. Abnormally phosphorylated tau protein related to the formation of neurofibrillary tangles and neuropil threads in the cerebral cortex of sheep and goat. Neurosci Lett. 1994 Apr 25;1–4.

475. Alonso, Grundke-Iqbal, & Iqbal. Alzheimer's disease hyperphosphorylated tau sequesters normal tau into tangles of filaments and disassembles microtubules. Nat Med. 1996 Jul;783–7.

476. Zheng, Bastianetto, Mennicken, Ma, & Kar. Amyloid β peptide induces tau phosphorylation and loss of cholinergic neurons in rat primary septal cultures. Neuroscience. 2002 Nov 15;201–11.

477. Gotz, Streffer, David, Schild, Hoerndli, Pennanen, Kurosinski, & Chen. Transgenic animal models of Alzheimer's disease and related disorders: histopathology, behavior and therapy. Mol Psychiatry. 2004 Jul;664–83.

478. Gotz, Chen, van Dorpe, & Nitsch. Formation of neurofibrillary tangles in P301l tau transgenic mice induced by Abeta 42 fibrils. Science. 2001 Aug;1491–5.

479. Schapira. Complex I: Inhibitors, inhibition and neurodegeneration. Exp Neurol. 2010 Aug;331–5.

480. Lin & Beal. Mitochondrial dysfunction and oxidative stress in neurodegenerative diseases. Nature. 2006 Oct 19;787–95.

481. Reddy & Beal. Amyloid beta, mitochondrial dysfunction and synaptic damage: implications for cognitive decline in aging and Alzheimer's disease. Trends Mol Med. 2008 Feb;45–53.

482. Rhein, Song, Wiesner, Ittner, Baysang, Meier, Ozmen, Bluethmann, Dröse, Brandt, Savaskan, Czech, Götz, & Eckert. Amyloid-β and tau synergistically impair the oxidative phosphorylation system in triple transgenic Alzheimer's disease mice. Proc Natl Acad Sci . 2009 Nov 24;20057–62.

483. Rapoport, Dawson, Binder, Vitek, & Ferreira. Tau is essential to beta -amyloid-induced neurotoxicity. Proc Natl Acad Sci U S A. 2002 Apr;6364–9.

484. Terry, Masliah, Salmon, Butters, DeTeresa, Hill, Hansen, & Katzman. Physical basis of cognitive alterations in alzheimer's disease: Synapse loss is the major correlate of cognitive impairment. Ann Neurol. 1991;572–80.

485. Hamos, DeGennaro, & Drachman. Synaptic loss in Alzheimer's disease and other dementias. Neurology. 1989 Mar;355–61.

486. Scheff, Neltner, & Nelson. Is synaptic loss a unique hallmark of Alzheimer's disease? Biochem Pharmacol. 2014 Apr 15;517–28.

487. Selkoe. Alzheimer's Disease Is a Synaptic Failure. Science (80-). 2002 Oct 25;789 LP-791.

488. Shankar, Li, Mehta, Garcia-Munoz, Shepardson, Smith, Brett, Farrell, Rowan, Lemere, Regan, Walsh, Sabatini, & Selkoe. Amyloid-[beta] protein dimers isolated directly from Alzheimer's brains impair synaptic plasticity and memory. Nat Med. 2008 Aug;837–42.

489. Gakhar-Koppole, Hundeshagen, Mandl, Weyer, Allinquant, Müller, & Ciccolini. Activity requires soluble amyloid precursor protein α to promote neurite outgrowth in neural stem cell-derived neurons via activation of the MAPK pathway. Eur J Neurosci. 2008;871–82.

490. Qiu, Ferreira, Miller, Koo, & Selkoe. Cell-surface beta-amyloid precursor protein stimulates neurite outgrowth of hippocampal neurons in an isoform-dependent manner. J Neurosci. 1995 Mar 1;2157 LP-2167.

491. Williamson, Mok, Henry, Cappai, Lander, Nurcombe, Beyreuther, Masters, & Small. Secreted Glypican Binds to the Amyloid Precursor Protein of Alzheimer's Disease (APP) and Inhibits APP-induced Neurite Outgrowth. J Biol Chem. 1996 Dec 6;31215–21.

492. Nhan, Chiang, & Koo. The multifaceted nature of amyloid precursor protein and its proteolytic fragments: friends and foes. Acta Neuropathol. 2015;1–19. A

493. Small, Nurcombe, Moir, Michaelson, Monard, Beyreuther, & Masters. Association and release of the amyloid protein precursor of Alzheimer's disease from chick brain extracellular matrix. J Neurosci. 1992 Nov;4143–50.

494. Small, Nurcombe, Reed, Clarris, Moir, Beyreuther, & Masters. A heparin-binding domain in the amyloid protein precursor of Alzheimer's disease is involved in the regulation of neurite outgrowth. J Neurosci. 1994 Apr;2117–27.

495. Breen, Bruce, & Anderton. Beta amyloid precursor protein mediates neuronal cell-cell and cell-surface adhesion. J Neurosci Res. 1991;90–100.

496. Young-Pearse, Chen, Chang, Marquez, & Selkoe. Secreted APP regulates the function of full-length APP in neurite outgrowth through interaction with integrin beta1. Neural Dev. 2008;15.

497. Kibbey, Jucker, Weeks, Neve, Van Nostrand, & Kleinman. beta-Amyloid precursor protein binds to the neurite-promoting IKVAV site of laminin. Proc Natl Acad Sci U S A. 1993 Nov 1;10150–3.

498. Milward, Papadopoulos, Fuller, Moir, Small, Beyreuther, & Masters. The amyloid protein precursor of Alzheimer's disease is a mediator of the effects of nerve growth factor on neurite outgrowth. Neuron. 1992 Jul;129–37.

499. Allinquant, Hantraye, Mailleux, Moya, Bouillot, & Prochiantz. Downregulation of amyloid precursor protein inhibits neurite outgrowth in vitro. J Cell Biol. 1995 Mar 1;919 LP-927.

500. Knowles, Wyart, Buldyrev, Cruz, Urbanc, Hasselmo, Stanley, & Hyman. Plaque-induced neurite abnormalities: Implications for disruption of neural networks in Alzheimer's disease. Proc Natl Acad Sci U S A. 1999 Apr 27;5274–9.

501. Serrano-Pozo, Frosch, Masliah, & Hyman. Neuropathological Alterations in Alzheimer Disease. Cold Spring Harb Perspect Med. 2011 Sep;a006189.

502. Grutzendler, Helmin, Tsai, & Gan. Various dendritic abnormalities are associated with fibrillar amyloid deposits in Alzheimer's disease. Ann N Y Acad Sci. 2007 Feb 1;30–9.

503. Jin, Shepardson, Yang, Chen, Walsh, & Selkoe. Soluble amyloid β-protein dimers isolated from Alzheimer cortex directly induce Tau hyperphosphorylation and neuritic degeneration. Proc Natl Acad Sci. 2011 Apr 5;5819–24.

504. Park & Strittmatter. Nogo Receptor Interacts with Brain APP and Aβ to Reduce Pathologic Changes in Alzheimer's Transgenic Mice. Curr Alzheimer Res. 2007 Dec;568–70.

505. Park, Gimbel, GrandPre, Lee, Kim, Li, Lee, & Strittmatter. Alzheimer Precursor Protein Interaction with the Nogo-66 Receptor Reduces Amyloid-β Plaque Deposition. J Neurosci. 2006 Feb 1;1386 LP-1395.

506. Zhou, Hu, He, Tang, Shi, Zhang, & Yan. Interaction between amyloid precursor protein and Nogo receptors regulates amyloid deposition. FASEB J. 2011 Sep 1;3146–56.

507. Knowles, Rajadas, Nguyen, Yang, LeMieux, Vander Griend, Ishikawa, Massa, Wyss-Coray, & Longo. The p75 Neurotrophin Receptor Promotes Amyloid-β(1-42)-Induced Neuritic Dystrophy In Vitro and In Vivo J Neurosci. 2009 Aug 26;10627 LP-10637.

508. Dechant & Barde. The neurotrophin receptor p75NTR: novel functions and implications for diseases of the nervous system. Nat Neurosci. 2002 Nov;1131–6.

509. Park, Widi, Gimbel, Harel, Lee, & Strittmatter. Subcutaneous Nogo Receptor Removes Brain Amyloid-β and Improves Spatial Memory in Alzheimer's Transgenic Mice. J Neurosci. 2006 Dec 20;13279–86.

510. Mokhtar, Bakhuraysah, Cram, & Petratos. The Beta-amyloid protein of Alzheimer's disease: communication breakdown by modifying the neuronal cytoskeleton. Int J Alzheimers Dis. 2013;910502.

511. Nixon & Yang. Autophagy failure in Alzheimer's disease—locating the primary defect. Neurobiol Dis. 2011 Jul;38–45.

512. Barnham, Masters, & Bush. Neurodegenerative diseases and oxidative stress. Nat Rev Drug Discov. 2004 Mar;205–14.

513. Pimplikar, Nixon, Robakis, Shen, & Tsai. Amyloid-Independent Mechanisms in Alzheimer's Disease Pathogenesis. J Neurosci. 2010 Nov 10;14946 LP-14954.

514. Pastorino & Lu. Pathogenic mechanisms in Alzheimer's disease. Eur J Pharmacol. 2006 Sep 1;29–38.

515. Israel, Yuan, Bardy, Reyna, Mu, Herrera, Hefferan, Van Gorp, Nazor, Boscolo, Carson, Laurent, Marsala, Gage, Remes, Koo, & Goldstein. Probing sporadic and familial Alzheimer/'s disease using induced pluripotent stem cells. Nature. 2012 Feb 9;216–20.

516. Pike, Walencewicz, Glabe, & Cotman. In vitro aging of ß-amyloid protein causes peptide aggregation and neurotoxicity. Brain Res. 1991 Nov 1;311–4.

517. Boivin, Kozak, & Meijers. Optimization of protein purification and characterization using Thermofluor screens. Protein Expr Purif. 2013 Oct;192–206.

518. Lebendiker, Maes, & Friedler. A screening methodology for purifying proteins with aggregation problems. Methods Mol Biol. 2015;261–81.

519. Pihlasalo, Kirjavainen, Hanninen, & Harma. High sensitivity luminescence nanoparticle assay for the detection of protein aggregation. Vol. 83, Analytical chemistry. United States; 2011.83(4) p. 1163–6.

520. Pike, Burdick, Walencewicz, Glabe, & Cotman. Neurodegeneration induced by beta-amyloid peptides in vitro: the role of peptide assembly state. J Neurosci. 1993 Apr 1;1676 LP-1687.

521. Howlett, Jennings, Lee, Clark, Brown, Wetzel, Wood, Camilleri, & Roberts. Aggregation State and Neurotoxic Properties of Alzheimer Beta-Amyloid Peptide. Neurodegeneration. 1995 Mar;23–32.

522. Bowenkamp, Hoffman, Gerhardt, Henry, Biddle, Hoffer, & Granholm. Glial cell line-derived neurotrophic factor supports survival of injured midbrain dopaminergic

neurons. J Comp Neurol. 1995;479–89.

523. Boyd & Gordon. Glial cell line-derived neurotrophic factor and brain-derived neurotrophic factor sustain the axonal regeneration of chronically axotomized motoneurons in vivo. Exp Neurol. 2003 Oct;610–9.

524. Müller & Seifert. A neurotrophic factor (NTF) released from primary glial cultures supports survival and fiber outgrowth of cultured hippocampal neurons. J Neurosci Res. 1982;195–204.

525. Yu, Leipzig, & Shoichet. Promoting neuron adhesion and growth. Mater Today. 2008 May;36–43.

526. Myers, Santiago-Medina, & Gomez. Regulation of axonal outgrowth and pathfinding by integrin-ECM interactions. Dev Neurobiol. 2011 Nov;901–23.

527. Turner, Flier, & Carbonetto. Identification of a cell-surface protein involved in PC12 cell-substratum adhesion and neurite outgrowth on laminin and collagen. J Neurosci. 1989 Sep;3287–96.

528. Tessier-Lavigne & Goodman. The molecular biology of axon guidance. Science (80-). 1996;

529. Cullen, Lessing, & LaPlaca. Collagen-Dependent Neurite Outgrowth and Response to Dynamic Deformation in Three-Dimensional Neuronal Cultures. Ann Biomed Eng. 2007;835–46.

530. Venstrom & Reichardt. Extracellular matrix. 2: Role of extracellular matrix molecules and their receptors in the nervous system. FASEB J. 1993 Aug 1;996–1003.

531. Letourneau, Condic, & Snow. Interactions of developing neurons with the extracellular matrix. J Neurosci. 1994 Mar;915–28.

532. Watanabe, Nakamura, Okano, & Toyama. Establishment of three-dimensional culture of neural stem/progenitor cells in collagen Type-1 Gel. Restor Neurol Neurosci. 2007;109–17.

533. Ackley, Crew, Elamaa, Pihlajaniemi, Kuo, & Kramer. The Nc1/Endostatin Domain of Caenorhabditis elegans Type Xviii Collagen Affects Cell Migration and Axon Guidance. J Cell Biol. 2001 Mar 19;1219 LP-1232.

534. Götz, Scholze, Clement, Joester, Schütte, Wigger, Frank, Spiess, Ekblom, & Faissner. Tenascin-C contains distinct adhesive, anti-adhesive, and neurite outgrowth promoting sites for neurons. J Cell Biol. 1996 Feb 15;681 LP-699.

535. Fischer, Brown-Ludi, Schulthess, & Chiquet-Ehrismann. Concerted action of tenascin-C domains in cell adhesion, anti-adhesion and promotion of neurite outgrowth. J Cell Sci. 1997 Jul 1;1513 LP-1522.

536. Husmann, Faissner, & Schachner. Tenascin promotes cerebellar granule cell migration and neurite outgrowth by different domains in the fibronectin type III repeats. J Cell Biol. 1992 Mar 15;1475 LP-1486.

537. Andrews, Czvitkovich, Dassie, Vogelaar, Faissner, Blits, Gage, ffrench-Constant, & Fawcett. α9 Integrin Promotes Neurite Outgrowth on Tenascin-C and Enhances Sensory Axon Regeneration. J Neurosci. 2009 Apr 29;5546 LP-5557.

538. J1/tenascin in substrate-bound and soluble form displays contrary effects on neurite outgrowth. J Cell Biol. 1991 Jun 1;1159–71.

539. Wehrle-Haller & Chiquet. Dual function of tenascin: simultaneous promotion of neurite growth and inhibition of glial migration. J Cell Sci. 1993 Oct;597–610.

540. Rigato, Garwood, Calco, Heck, Faivre-Sarrailh, & Faissner. Tenascin-C promotes neurite outgrowth of embryonic hippocampal neurons through the alternatively spliced fibronectin type III BD domains via activation of the cell adhesion molecule F3/contactin. J Neurosci. 2002 Aug;6596–609.

541. Meiners, Mercado, Nur-e-Kamal, & Geller. Tenascin-C contains domains that

independently regulate neurite outgrowth and neurite guidance. J Neurosci. 1999 Oct;8443–53.

542. Tonge, de Burgh, Docherty, Humphries, Craig, & Pizzey. Fibronectin supports neurite outgrowth and axonal regeneration of adult brain neurons in vitro. Brain Res. 2012 May;8–16.

543. Rogers, Letourneau, Palm, McCarthy, & Furcht. Neurite extension by peripheral and central nervous system neurons in response to substratum-bound fibronectin and laminin. Dev Biol. 1983;212–20.

544. Millaruelo, Nieto-Sampedro, & Cotman. Cooperation between nerve growth factor and laminin or fibronectin in promoting sensory neuron survival and neurite outgrowth. Dev Brain Res. 1988 Feb 1;219–28.

545. Akers, Mosher, & Lilien. Promotion of retinal neurite outgrowth by substratum-bound fibronectin. Dev Biol. 1981;179–88.

546. Müller, Bossy, Venstrom, & Reichardt. Integrin alpha 8 beta 1 promotes attachment, cell spreading, and neurite outgrowth on fibronectin. Mol Biol Cell. 1995 Apr 1;433–48.

547. Zhang, Yoo, Wells, Beebe Jr., Biran, & Tresco. Neurite outgrowth on well-characterized surfaces: preparation and characterization of chemically and spatially controlled fibronectin and RGD substrates with good bioactivity. Biomaterials. 2005 Jan;47–61.

548. Velling, Collo, Sorokin, Durbeej, Zhang, & Gullberg. Distinct α7Aβ1 and α7Bβ1 integrin expression patterns during mouse development: α7A is restricted to skeletal muscle but α7B is expressed in striated muscle, vasculature, and nervous system. Dev Dyn. 1996;355–71.

549. Lallier, Whittaker, & DeSimone. Integrin alpha 6 expression is required for early nervous system development in Xenopus laevis. Development. 1996 Aug 1;2539 LP-2554.

550. Harper, Ye, Blong, Jacobson, & Sakaguchi. Integrins contribute to initial morphological development and process outgrowth in rat adult hippocampal progenitor cells. J Mol Neurosci. 2010 Mar;269–83.

551. Marchetti, Escuin, van der Flier, De Arcangelis, Hynes, & Georges-Labouesse. Integrin alpha5beta1 is necessary for regulation of radial migration of cortical neurons during mouse brain development. Eur J Neurosci. 2010 Feb;399–409.

552. Jones. Integrins: possible functions in the adult CNS. Trends Neurosci. 1996 Feb;68–72.

553. Pinkstaff, Detterich, Lynch, & Gall. Integrin subunit gene expression is regionally differentiated in adult brain. J Neurosci. 1999 Mar;1541–56.

554. Lowery & Vactor. The trip of the tip: understanding the growth cone machinery. Nat Rev Mol Cell Biol. 2009 May;332–43.

555. Gomez, Roche, & Letourneau. Chick sensory neuronal growth cones distinguish fibronectin from laminin by making substratum contacts that resemble focal contacts. J Neurobiol. 1996 Jan;18–34.

556. Renaudin, Lehmann, Girault, & McKerracher. Organization of point contacts in neuronal growth cones. J Neurosci Res. 1999 Feb;458–71.

557. Robles & Gomez. Focal adhesion kinase signaling at sites of integrin-mediated adhesion controls axon pathfinding. Nat Neurosci. 2006 Oct;1274–83.

558. Woo, Rowan, & Gomez. Retinotopic mapping requires focal adhesion kinase-mediated regulation of growth cone adhesion. J Neurosci. 2009 Nov;13981–91.

559. Suter & Forscher. An emerging link between cytoskeletal dynamics and cell adhesion molecules in growth cone guidance. Curr Opin Neurobiol. 1998 Feb;106–16.

560. Myers & Gomez. Focal Adhesion Kinase Promotes Integrin Adhesion Dynamics Necessary for Chemotropic Turning of Nerve Growth Cones. J Neurosci. 2011 Sep 21;13585 LP-13595.

561. DeMali, Wennerberg, & Burridge. Integrin signaling to the actin cytoskeleton. Curr Opin Cell Biol. 2003 Oct;572–82.

562. Plantman, Patarroyo, Fried, Domogatskaya, Tryggvason, Hammarberg, & Cullheim. Integrin-laminin interactions controlling neurite outgrowth from adult DRG neurons in vitro. Mol Cell Neurosci. 2008 Sep;50–62.

563. Tashiro, Sephel, Weeks, Sasaki, Martin, Kleinman, & Yamada. A synthetic peptide containing the IKVAV sequence from the A chain of laminin mediates cell attachment, migration, and neurite outgrowth. J Biol Chem. 1989 Sep 25;16174–82.

564. Nomizu, Weeks, Weston, Kim, Kleinman, & Yamada. Structure-activity study of a laminin α1 chain active peptide segment Ile-Lys-Val-Ala-Val (IKVAV). FEBS Lett. 1995;227–31.

565. Grumet, Friedlander, & Edelman. Evidence for the binding of Ng-CAM to laminin. Cell Adhes Commun. 1993 Sep;177–90.

566. Amoureux, Cunningham, Edelman, & Crossin. N-CAM Binding Inhibits the Proliferation of Hippocampal Progenitor Cells and Promotes Their Differentiation to a Neuronal Phenotype. J Neurosci. 2000 May 15;3631 LP-3640.

567. Figlewicz, Quarles, Johnson, Barbarash, & Sternberger. Biochemical Demonstration of the Myelin-Associated Glycoprotein in the Peripheral Nervous System. J Neurochem. 1982;749–58.

568. Trapp & Quarles. Presence of the myelin-associated glycoprotein correlates with alterations in the periodicity of peripheral myelin. J Cell Biol. 1982 Mar 1;877 LP-882.

569. Bollensen, Steck, & Schachner. Reactivity with the peripheral myelin glycoprotein P0 in serum from patients with monoclonal IgM gammopathy and polyneuropathy. Neurology. 1988 Aug;1266–70.

570. David, Braun, Jackson, Kottis, & McKerracher. Laminin overrides the inhibitory effects of peripheral nervous system and central nervous system myelin-derived inhibitors of neurite growth. J Neurosci Res. 1995 Nov;594–602.

571. DeQuach, Mezzano, Miglani, Lange, Keller, Sheikh, & Christman. Simple and High Yielding Method for Preparing Tissue Specific Extracellular Matrix Coatings for Cell Culture. PLoS One. 2010 Sep 27;e13039.

572. Cukierman, Pankov, Stevens, & Yamada. Taking Cell-Matrix Adhesions to the Third Dimension. Science (80-). 2001 Nov 23;1708 LP-1712.

573. Longo, Hayman, Davis, Ruoslahti, Engvall, Manthorpe, & Varon. Neurite-promoting factors and extracellular matrix components accumulating in vivo within nerve regeneration chambers. Brain Res. 1984 Aug 20;105–17.

574. Calof, Campanero, O'Rear, Yurchenco, & Landert. Domain-specific activation of neuronal migration and neurite outgrowth-promoting activities of laminin. Neuron. 1994 Jul;117–30.

575. Buettner & Pittman. Quantitative effects of laminin concentration on neurite outgrowth in vitro. Dev Biol. 1991;266–76.

576. Hammarback, Palm, Furcht, & Letourneau. Guidance of neurite outgrowth by pathways of substratum-adsorbed laminin. J Neurosci Res. 1985;213–20.

577. Hantaz-Ambroise, Vigny, & Koenig. Heparan sulfate proteoglycan and laminin mediate two different types of neurite outgrowth. J Neurosci. 1987 Aug 1;2293 LP-2304.

578. Snow & Letourneau. Neurite outgrowth on a step gradient of chondroitin sulfate

proteoglycan (CS-PG). J Neurobiol. 1992;322–36.

579. Evans, Euteneuer, Chavez, Mullen, Hui, Bhatia, & Ryan. Laminin and fibronectin modulate inner ear spiral ganglion neurite outgrowth in an in vitro alternate choice assay. Dev Neurobiol. 2007;1721–30.

580. Smit, Leng, & Klemke. Assay for neurite outgrowth quantification. Biotechniques. 2003 Aug;254–6.

581. Shin, Jo, & Mikos. Biomimetic materials for tissue engineering. Biomaterials. 2003 Nov;4353–64.

582. Whitaker, Quirk, Howdle, & Shakesheff. Growth factor release from tissue engineering scaffolds. J Pharm Pharmacol. 2001 Nov;1427–37.

583. Jang, Rives, & Shea. Plasmid Delivery in Vivo from Porous Tissue-Engineering Scaffolds: Transgene Expression and Cellular Transfection. Mol Ther. 2005 Sep;475–83.

584. Lee, Silva, & Mooney. Growth factor delivery-based tissue engineering: general approaches and a review of recent developments. J R Soc Interface. 2011 Feb 6;153–70.

585. Costa, Carvalho, Montelaro, Gomes, & Martins. Covalent immobilization of antimicrobial peptides (AMPs) onto biomaterial surfaces. Acta Biomater. 2011 Apr;1431–40.

586. Massia & Stark. Immobilized RGD peptides on surface-grafted dextran promote biospecific cell attachment. J Biomed Mater Res. 2001;390–9.

587. Kam, Shain, Turner, & Bizios. Selective adhesion of astrocytes to surfaces modified with immobilized peptides. Biomaterials. 2002 Jan;511–5.

588. Shin, Jo, & Mikos. Modulation of marrow stromal osteoblast adhesion on biomimetic oligo[poly(ethylene glycol) fumarate] hydrogels modified with Arg-Gly-Asp peptides and a poly(ethyleneglycol) spacer. J Biomed Mater Res. 2002 Aug;169–79.

589. Chua, Neoh, Kang, & Wang. Surface functionalization of titanium with hyaluronic acid/chitosan polyelectrolyte multilayers and RGD for promoting osteoblast functions and inhibiting bacterial adhesion. Biomaterials. 2008 Apr;1412–21.

590. Davis, Giannoulis, Johnson, & Desai. Immobilization of RGD to 〈1 1 1〉 silicon surfaces for enhanced cell adhesion and proliferation. Biomaterials. 2002 Oct;4019–27.

591. Hersel, Dahmen, & Kessler. RGD modified polymers: biomaterials for stimulated cell adhesion and beyond. Biomaterials. 2003 Nov;4385–415.

592. Lopez, Gristina, Ceccone, Rossi, Favia, & d'Agostino. Immobilization of RGD peptides on stable plasma-deposited acrylic acid coatings for biomedical devices. Surf Coatings Technol. 2005 Oct 1;1000–4.

593. Jin Yoon, Ho Song, Sung Lee, & Park. Immobilization of cell adhesive RGD peptide onto the surface of highly porous biodegradable polymer scaffolds fabricated by a gas foaming/salt leaching method. Biomaterials. 2004 Nov;5613–20.

594. Ruoslahti & Pierschbacher. New perspectives in cell adhesion: RGD and integrins. Science. 1987 Oct;491–7.

595. Maheshwari, Brown, Lauffenburger, Wells, & Griffith. Cell adhesion and motility depend on nanoscale RGD clustering. J Cell Sci. 2000 May 15;1677 LP-1686.

596. D'Souza, Ginsberg, & Plow. Arginyl-glycyl-aspartic acid (RGD): a cell adhesion motif. Trends Biochem Sci. 1991;246–50.

597. Schense, Bloch, Aebischer, & Hubbell. Enzymatic incorporation of bioactive peptides into fibrin matrices enhances neurite extension. Nat Biotech. 2000 Apr;415–9.

598. Ranieri, Bellamkonda, Bekos, Vargo, Gardella, & Aebischer. Neuronal cell attachment to fluorinated ethylene propylene films with covalently immobilized laminin oligopeptides YIGSR and IKVAV. II. J Biomed Mater Res. 1995 Jun;779–85.

599. Bellamkonda, Ranieri, & Aebischer. Laminin oligopeptide derivatized agarose gels allow three-dimensional neurite extension in vitro. J Neurosci Res. 1995 Jul;501–9.

600. Dee, Andersen, & Bizios. Design and function of novel osteoblast-adhesive peptides for chemical modification of biomaterials. J Biomed Mater Res. 1998 Jun;371–7.

601. Dee, Andersen, & Bizios. Osteoblast population migration characteristics on substrates modified with immobilized adhesive peptides. Biomaterials. 1999;221–7.

602. Rezania, Johnson, Lefkow, & Healy. Bioactivation of Metal Oxide Surfaces. 1. Surface Characterization and Cell Response. Langmuir. 1999 Sep 1;6931–9.

603. Xiao, Textor, Spencer, & Sigrist. Covalent Attachment of Cell-Adhesive, (Arg-Gly-Asp)-Containing Peptides to Titanium Surfaces. Langmuir. 1998 Sep 1;5507–16.

604. Massia & Hubbell. Human endothelial cell interactions with surface-coupled adhesion peptides on a nonadhesive glass substrate and two polymeric biomaterials. J Biomed Mater Res. 1991;223–42.

605. Massia & Hubbell. Covalently attached GRGD on polymer surfaces promotes biospecific adhesion of mammalian cells. Ann N Y Acad Sci. 1990;261–70.

606. Sugawara & Matsuda. Photochemical surface derivatization of a peptide containing Arg-Gly-Asp (RGD). J Biomed Mater Res. 1995 Sep;1047–52.

607. Chen. 3D Biomimetic Cultures: The Next Platform for Cell Biology. Trends Cell Biol. 2016 Nov;798–800.

608. Terrettaz, Ulrich, Vogel, Hong, Dover, & Lakey. Stable self-assembly of a protein engineering scaffold on gold surfaces. Protein Sci. 2002 Aug 27;1917–25.

609. Shah, Thomas, Phillips, Cisneros, Le Brun, Holt, & Lakey. Self-assembling layers created by membrane proteins on gold. Biochem Soc Trans. 2007 Jun;522–6.

610. Cooke, Phillips, Shah, Athey, Lakey, & Przyborski. Enhanced cell attachment using a novel cell culture surface presenting functional domains from extracellular matrix proteins. Cytotechnology. 2008;71–9.

611. Orla Protein Technologies Website. Available from: http://www.orlaproteins.com

612. Athey, Shah, Phillips, & Lakey. A manufacturable surface-biology platform for nano applications; Cell culture, analyte detection, diagnostics sensors. Ind Biotechnol. 2005 Sep 1;185–9.

613. Cooke, Zahir, Phillips, Shah, Athey, Lakey, Shoichet, & Przyborski. Neural differentiation regulated by biomimetic surfaces presenting motifs of extracellular matrix proteins. J Biomed Mater Res A. 2010 Jun;824–32.

614. Filbin. Myelin-associated inhibitors of axonal regeneration in the adult mammalian CNS. Nat Rev Neurosci. 2003;

615. Tashiro, Sephel, Greatorex, Sasaki, Shirashi, Martin, Kleinman, & Yamada. The RGD containing site of the mouse laminin A chain is active for cell attachment, spreading, migration and neurite outgrowth. J Cell Physiol. 1991;451–9.

616. Wildering, Hermann, & Bulloch. Neurite outgrowth, RGD-dependent, and RGD-independent adhesion of identified molluscan motoneurons on selected substrates. J Neurobiol. 1998 Apr;37–52.

617. Tomaselli, Hall, Flier, Gehlsen, Turner, Carbonetto, & Reichardt. A neuronal cell line (PC12) expresses two β1-class integrins—α1β1, and α3β1—that recognize different neurite outgrowth-promoting domains in laminin. Neuron. 1990 Nov;651–62.

618. MATSUZAWA, WEIGHT, POTEMBER, & LIESI. DIRECTIONAL NEURITE

OUTGROWTH AND AXONAL DIFFERENTIATION OF EMBRYONIC HIPPOCAMPAL NEURONS ARE PROMOTED BY A NEURITE OUTGROWTH DOMAIN OF THE B2-CHAIN OF LAMININ. Int J Dev Neurosci. 1996 Jun;283–95.

619. Graf, Ogle, Robey, Sasaki, Martin, Yamada, & Kleinman. A pentapeptide from the laminin B1 chain mediates cell adhesion and binds the 67,000 laminin receptor. Biochemistry. 1987;6896–900.

620. Ignelzi Jr., Miller, Soriano, & Maness. Impaired neurite outgrowth of src-minus cerebellar neurons on the cell adhesion molecule L1. Neuron. 1994 Apr;873–84.

621. Doherty & Walsh. Signal transduction events underlying neurite outgrowth stimulated by cell adhesion molecules. Curr Opin Neurobiol. 1994;49–55.

622. Smith Callahan, Xie, Barker, Zheng, Reneker, Dove, & Becker. Directed differentiation and neurite extension of mouse embryonic stem cell on aligned poly(lactide) nanofibers functionalized with YIGSR peptide. Biomaterials. 2013 Dec;9089–95.

623. Dhoot, Tobias, Fischer, & Wheatley. Peptide-modified alginate surfaces as a growth permissive substrate for neurite outgrowth. J Biomed Mater Res Part A. 2004;191–200.

624. Masuda, Sakuma, Kobayashi, Kikuchi, Soda, Shiga, Kobayashi, & Yaginuma. Laminin peptide YIGSR and its receptor regulate sensory axonal response to the chemoattractive guidance cue in the chick embryo. J Neurosci Res. 2009 Feb;353–9.

625. Phillips. Animal-Free Surfaces for Cellular Research. Genet Eng Biotechnol NEWS. 2010;30–1.

626. Laminin promotes neuritic regeneration from cultured peripheral and central neurons. J Cell Biol. 1983 Dec 1;1882–90.

627. Lein, Banker, & Higgins. Laminin selectively enhances axonal growth and accelerates the development of polarity by hippocampal neurons in culture. Dev Brain Res. 1992 Oct 23;191–7.

628. Lander, Fujii, & Reichardt. Laminin is associated with the “neurite outgrowth-promoting factors” found in conditioned media. Proc Natl Acad Sci. 1985 Apr 1;2183–7.

629. Clark, Britland, & Connolly. Growth cone guidance and neuron morphology on micropatterned laminin surfaces. J Cell Sci. 1993 May 1;203 LP-212.

630. Agius, Sagot, Duprat, & Cochard. Antibodies directed against the β1-integrin subunit and peptides containing the IKVAV sequence of laminin perturb neurite outgrowth of peripheral neurons on immature spinal cord substrata. Neuroscience. 1996 Apr;773–86.

631. Muir, Johnson, Rojiani, Inglis, Rojiani, & Maria. Assessment of laminin-mediated glioma invasion in vitro and by glioma tumors engrafted within rat spinal cord. J Neurooncol. 1996;199–211.

632. Caniggia, Liu, Han, Wang, Tanswell, Laurie, & Post. Identification of receptors binding fibronectin and laminin on fetal rat lung cells. Am J Physiol. 1996 Mar;L459-68.

633. Makino, Okazaki, Kasai, Nishi, Bougaeva, Weeks, Otaka, Nielsen, Yamada, & Nomizu. Identification of cell binding sites in the laminin alpha5-chain G domain. Exp Cell Res. 2002 Jul;95–106.

634. Katagiri, Ishikawa, Yamada, Hozumi, Kikkawa, & Nomizu. Screening of integrin-binding peptides from the laminin α4 and α5 chain G domain peptide library. Arch Biochem Biophys. 2012 May;32–42.

635. Nomizu, Kuratomi, Song, Ponce, Hoffman, Powell, Miyoshi, Otaka, Kleinman, & Yamada. Identification of Cell Binding Sequences in Mouse Laminin γ1 Chain by Systematic Peptide Screening. J Biol Chem. 1997 Dec 19;32198–205.

636. Suh, Kim, & Han. Laminin-111 Stimulates Proliferation of Mouse Embryonic Stem Cells Through a Reduction of Gap Junctional Intercellular Communication via RhoA-Mediated Cx43 Phosphorylation and Dissociation of Cx43/ZO-1/Drebrin Complex. Stem Cells Dev. 2012 Jul 20;2058–70.

637. Park, Yiu, Kaneko, Wang, Chang, & He. A TNF Receptor Family Member, TROY, Is a Coreceptor with Nogo Receptor in Mediating the Inhibitory Activity of Myelin Inhibitors. Neuron. 2016 Sep 18;345–51.

638. Benson, Romero, Lush, Lu, Henkemeyer, & Parada. Ephrin-B3 is a myelin-based inhibitor of neurite outgrowth. Proc Natl Acad Sci United States Am. 2005 Jul 26;10694–9.

639. Barton, Liu, Tzvetkova, Jeffrey, Fournier, Sah, Cate, Strittmatter, & Nikolov. Structure and axon outgrowth inhibitor binding of the Nogo-66 receptor and related proteins. EMBO J. 2003 Jul 1;3291 LP-3302.

640. Laurén, Hu, Chin, Liao, Airaksinen, & Strittmatter. Characterization of Myelin Ligand Complexes with Neuronal Nogo-66 Receptor Family Members. J Biol Chem. 2007 Feb 23;5715–25.

641. Brittis & Flanagan. Nogo Domains and a Nogo Receptor:Implications for Axon Regeneration. Neuron. 2001 Apr;11–4.

642. Zhang, An, Montoro, & Ellerby. Characterization of Human Huntington's Disease Cell Model from Induced Pluripotent Stem Cells. PLoS Curr. 2010 Oct 28;RRN1193.

643. Soldner, Hockemeyer, Beard, Gao, Bell, Cook, Hargus, Blak, Cooper, Mitalipova, Isacson, & Jaenisch. Parkinson's Disease Patient-Derived Induced Pluripotent Stem Cells Free of Viral Reprogramming Factors. Cell. 2009 Mar 6;964–77.

644. Tousley & Kegel-Gleason. Induced Pluripotent Stem Cells in Huntington's Disease Research: Progress and Opportunity. J Huntingtons Dis. 2016 Jun 28;99–131.

645. Ren, Jiang, Hu, Fan, Wang, Janoschka, Wang, Ge, & Feng. Parkin Mutations Reduce the Complexity of Neuronal Processes in iPSC-derived Human Neurons. Stem Cells. 2015 Jan;68–78.

646. Cooper, Seo, Andrabi, Guardia-Laguarta, Graziotto, Sundberg, McLean, Carrillo-Reid, Xie, Osborn, Hargus, Deleidi, Lawson, Bogetofte, Perez-Torres, Clark, Moskowitz, Mazzulli, Chen et al. Pharmacological rescue of mitochondrial deficits in iPSC-derived neural cells from patients with familial Parkinson's disease. Sci Transl Med. 2012 Jul;141ra90.

647. Chun, Byun, & Lee. Induced pluripotent stem cells and personalized medicine: current progress and future perspectives. Anat Cell Biol. 2011 Dec 30;245–55.

648. Ferreira & Mostajo-Radji. How induced pluripotent stem cells are redefining personalized medicine. Gene. 2013 May 10;1–6.

649. Sharma. iPS Cells—The Triumphs and Tribulations. Dent J. 2016 Jun 6;19.

650. Lim, Yang, Chu, Chen, Beech, Teter, Tran, Ubeda, Ashe, Frautschy, & Cole. Ibuprofen Suppresses Plaque Pathology and Inflammation in a Mouse Model for Alzheimer's Disease. J Neurosci. 2000 Aug 1;5709 LP-5714.

651. Pike, Cummings, Monzavi, & Cotman. β-Amyloid-induced changes in cultured astrocytes parallel reactive astrocytosis associated with senile plaques in Alzheimer's disease. Neuroscience. 1994 Nov;517–31.

652. Costa, Planchenault, Charriere-Bertrand, Mouchel, Fages, Juliano, Lefrancois, Barlovatz-Meimon, & Tardy. Astroglial permissivity for neuritic outgrowth in neuron-astrocyte cocultures depends on regulation of laminin bioavailability. Glia. 2002 Feb;105–13.

Appendix I: Standard Operating Procedure for Induction of Neurite Outgrowth from Human Embryonal Carcinoma Cells

Introduction

Neuritogenesis is an important developmental process that occurs during the formation of the mature neuron[1]. This process is impaired in many nervous system disorders that range from trauma, such as spinal cord injury (SCI)[2–6] to neurodegenerative diseases including Alzheimer's disease[7,8]. In this unit, we describe the generation of a robust and reproducible human pluripotent stem cell-derived model of neurite outgrowth in a 3D culture system, which provides a more physiologically relevant geometry to study the development and inhibition of neurites[9]. This model of neurite outgrowth uses a commercially available polystyrene scaffold, Alvetex® scaffold that is available in formats compatible with high-throughput screening. This is beneficial as a potential application of this model could be to screen the ability of drug candidates to overcome inhibitory stimuli or to assess their neurotoxicity.

NOTE: All procedures in this unit require standard tissue culture facilities. All cell work should be conducted under sterile conditions in a Class II Biological biosafety cabinet.

NOTE: All cell cultures were incubated at 37 °C in a 5 % CO_2 humidified environment.

DIFFERENTIATION OF HUMAN PLURIPOTENT STEM CELLS IN SUSPENSION CULTURE

For the development of this neurite outgrowth model, the embryonal carcinoma (EC) cell line TERA2.cl.SP12 was used, which, is a sub-clone of the original TERA-2 line isolated based on its expression of the stem cell marker, SSEA-3 and exhibits enhanced differentiation when exposed to retinoic acid[15]. TERA2.cl.SP12 cells have formed the basis of many neuronal differentiation studies, and the neuronal subtypes that are formed following differentiation have been well characterised[9,16–18].

Materials

Dulbecco's Modified Eagle's Medium (DMEM; ThermoFisher Scientific, cat no. 21969-035)
Heat-treated Foetal Bovine Serum (HT-FBS; ThermoFisher Scientific, cat no. 10270-106)
200 mM L-glutamine (ThermoFisher Scientific, cat no. 11500-626)
10,000 U/mL Penicillin and Streptomycin (ThermoFisher Scientific, cat no. 11548-876)
0.25 % trypsin/2 mM EDTA solution (ThermoFisher Scientific, cat no. 11570-626)
0.1 mM EC23 Stock Solution (ReproCELL Europe, cat no. SRP002)
Dulbecco's Phosphate Buffered Saline (DPBS; Lonza, cat no. BE17-512F)
0.4 % Trypan Blue Solution (Sigma Aldrich, cat no. T8154)

75 cm^2 Culture Flasks (BD Flacon, cat no. 353136)
90 mm Sterile Biological Petri Dishes (ThermoFisher Scientific, cat no. FB51504)
Acid Washed Glass Beads (ThermoFisher Scientific, cat no. G8772)
50 mL Conical Tube (Sarstedt, cat no. 62.547.254)

Vacuum Aspirator
Haemocytometer
Bench Top Centrifuge

Generation of Neurospheres

1. Prepare growth medium by supplementing 500 mL DMEM with 5 mL L-glutamine (final concentration 2 mM), 50 mL HT-FBS and 1 mL Penicillin and Streptomycin (final concentration 20 active units).

2. TERA2.cl.SP12 cells should be maintained in 75 cm^2 culture flasks in 20 mL growth medium at high confluency as shown in Figure 1, and their medium should be replaced every 2-3 days or as needed.

Cells should be maintained at high confluence to ensure their pluripotent phenotype, as they can spontaneously differentiate at low confluence.

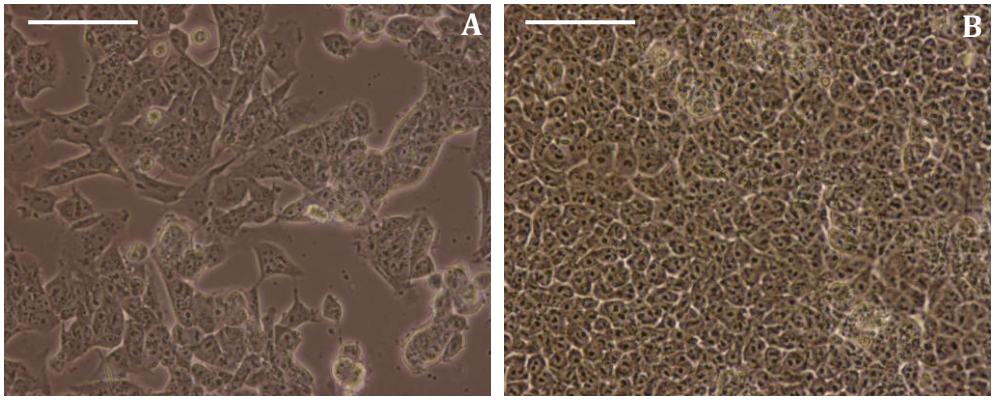

Fig 1. Phase contrast images of TERA2.cl.SP12 cells cultured as 2D monolayers at low (A) and high (B) confluence. Cells should be maintained at high confluence to reduce spontaneous differentiation. Scale bars: 100 µm

3. Monolayers of TERA2.cl.SP12 should be passaged every 3-4 days once 100 % confluence has been reached. This is achieved by aspirating the growth medium before adding 6 mL of fresh growth medium with 3-5 acid washed glass beads per flask. Cells can then be mechanically dislodged by the beads, this produces a cellular suspension that can then be split in a 1:3 ratio between new culture flasks and topped up to a total volume of 20 mL growth medium per flask.

4. To seed cells for neurosphere formation, a single cell suspension should be prepared by aspirating growth medium from cultures, and washing cells in 3 mL DPBS. Cells can then be dissociated by trypsinisation, achieved by incubation with 3 mL 0.25 % trypsin/2 mM EDTA at 37 °C in a 5 % CO_2 humidified environment until cells detach from the flask. Trypsin should then be neutralised by addition of 7 mL growth medium, and pipetted gently to break up any cellular clumps.

5. To determine the number of viable cells present in the cellular suspension, a trypan blue exclusion assay should be performed. A sample of the cell suspension (10 µL) should be diluted 1:1 with trypan blue solution and cells counted using a haemocytometer. From this, the total number of cells in the cellular suspension can be determined.

Usually 15-25 x 10^6 cells per 75 cm^2 culture flask are obtained.

6. Cells should then be centrifuged at 1,000 rpm for 3 minutes at room temperature and resuspended in growth medium prior to seeding. Cells should be seeded in suspension culture at a density of 1.5 x 10^6 cells per untreated 90 mm biological Petri dish to promote their aggregation and maintained with 20 mL growth medium.

7. Following 24 hours incubation, 20 µL of 0.01 mM EC23 stock solution (final concentration of 0.01 µM) should be added directly to the suspension culture to promote neuronal differentiation.

Growth medium should not be replaced after 24 hours, as this can result in disaggregation of the cells.

8. Cells should be maintained in suspension culture for a 21-day differentiation period with replacement of differentiation medium every 3-4 days. Differentiation medium should be replaced by transferring the contents of each Petri dish into a 50 mL conical tube and allowing the spheroids to settle at the bottom of the tube. The medium can then be aspirated, leaving a pellet of spheroids remaining, and 20 mL fresh differentiation medium can then be added to the spheroids. Cellular aggregates should then be seeded into a fresh 90 mm Petri dish for incubation.

Each time the medium is replaced, the Petri dish should also be replaced, as spheroids may begin to adhere to the plastic following a long incubation period.

INDUCTION OF NEURITE OUTGROWTH IN 2D/3D CULTURE

Following the initial differentiation phase of culture, mature neurospheres can be seeded onto a 3D polystyrene scaffold or a 2D tissue culture surface to promote the induction of neurite outgrowth over a 10-day culture period, figure 2 shows an overview of this two-step process.

Materials

Dulbecco's Modified Eagle's Medium (DMEM; ThermoFisher Scientific, cat no. 21969-035)
Heat-treated Foetal Bovine Serum (HT-FBS; ThermoFisher Scientific, cat no. 10270-106)
200 mM L-glutamine (ThermoFisher Scientific, cat no. 11500-626)
10,000 UmL^{-1} Penicillin and Streptomycin (ThermoFisher Scientific, cat no. 11548-876)
Dulbecco's Phosphate Buffered Saline (DPBS; Lonza, cat no. BE17-512F)
Engelberth-Holm-Swarm murine sarcoma basement membrane (Sigma-Aldrich, cat no. L2020)
1 $mgmL^{-1}$ Poly-D-lysine Stock Solution (Sigma-Aldrich, cat no. P6407)
1 mM cytosine β-D arabinofuranoside (Sigma-Aldrich, cat no. C1768)
10 mM 5'fluoro 2'deoxyuridine (Sigma-Aldrich, cat no. F0503)
10 mM Uridine (Sigma-Aldrich, cat no. U3003)
4 % Paraformaldehyde (PFA; Sigma-Aldrich, cat no. P6148)

12-well format Alvetex® Scaffold Inserts (ReproCELL Europe, cat no. AVP005-12)
12-well tissue culture plates (Greiner Bio-One, cat no. 665 180)
48-well tissue culture plates (Greiner Bio-One, cat no. 677 180)
6-well tissue culture plates (Greiner Bio-One, 657 160)
100 μm cell strainer (BD Falcon, cat no. 352360)
50 mL Conical Tube (Sarstedt, cat no. 62.547.254)
90 mm Sterile Biological Petri Dishes (ThermoFisher Scientific, cat no. FB51504)

K1050X Plasma Asher
Vacuum Aspirator
Haemocytometer
Bench Top Centrifuge

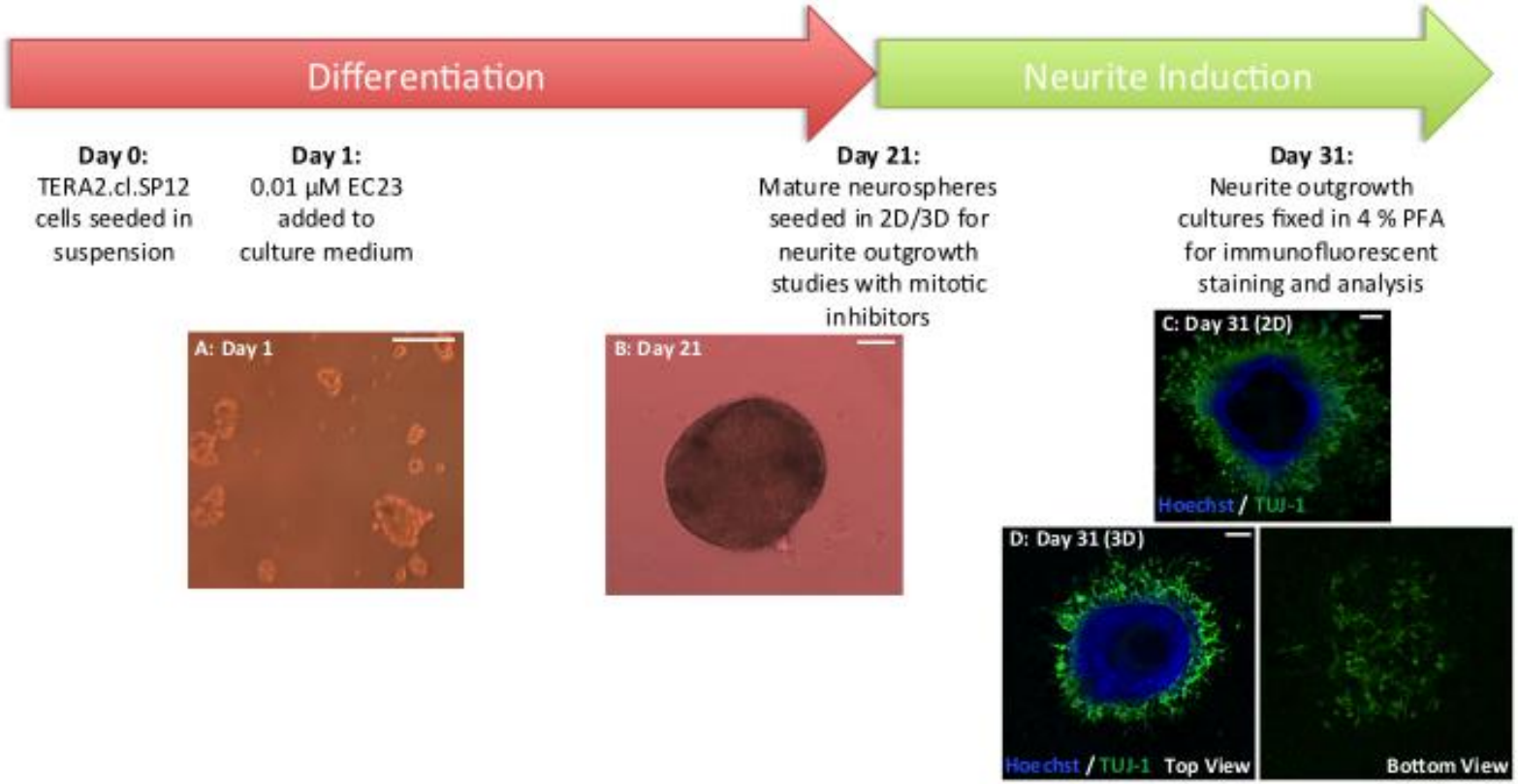

Fig 2. Schematic outlining the induction of 3D neurite outgrowth from human EC-cell derived neurospheres. TERA2.cl.SP12 cells are seeded in suspension, allowed to aggregate for 24 hours (A) and dosed with EC23 to promote neuronal differentiation. Spheroids are then maintained with EC23 for 21 days and mature neurospheres (B) are placed on 2D growth substrates or Alvetex® scaffolds coated with 10 $\mu g mL^{-1}$ poly-D-lysine and laminin. Neurites then begin to develop over the 10 day neurite outgrowth period and cultures can then be fixed with 4 % PFA for immunofluorescent analysis. The pan-neuronal marker TUJ-1 highlights neurite outgrowth (C/D) and neurites radiate from the central cellular mass in 2D (C) or to have penetrated the depth of the 3D material from the bottom view of the scaffold (D). Scale bars: (A,B) 100 µm, (C,D) 200 µm.

Preparation of Growth Surfaces for Neurite Outgrowth

1. Alvetex® Scaffold inserts should be prepared by plasma treatment using the K1050X Plasma Asher at a power of 40 W for 5 minutes. Scaffolds should then be washed twice in DPBS.

Plasma treatment renders the scaffolds hydrophilic promoting the perfusion of medium throughout the scaffold. Alternatively, scaffolds may be washed in 70 % ethanol to render them hydrophilic.

2. A coating solution of 10 μgmL^{-1} poly-D-lysine and laminin should be prepared by adding 500 µL of 1 $mgmL^{-1}$ poly-D-lysine and 500 µL of 1 $mgmL^{-1}$ laminin from Engelberth-Holm-Swarm murine sarcoma basement membrane to 49 mL DPBS. (Final concentration of 10 μgmL^{-1} laminin and poly-D-lysine).

3. For 2D neurite outgrowth assays, 150 µL of coating solution should be added to each well of a 48-well tissue culture plate. For 3D neurite outgrowth assays, each 12-well format Alvetex® Scaffold insert should be placed into a well of a 6-well tissue culture plate and 300 µL coating solution should be added to each scaffold.

4. Surfaces should be coated overnight, at room temperature prior to the seeding of fully differentiated neurospheres.

Seeding of Mature Neurospheres for Neurite Outgrowth

Following 21 days differentiation in suspension with 0.01 µM EC23, mature neurospheres are ready for use within a neurite outgrowth assay.

1. Pass suspension culture through a 100 µm cell strainer to remove any single cells and retinoid containing medium. Backwash neurospheres into a clean 90 mm Petri dish with fresh growth medium that has not been supplemented with EC23.

3. To prepare growth medium with mitotic inhibitors, add 500 µL of each mitotic inhibitor stock solution to a 500 mL bottle of culture medium.

Final concentrations of mitotic inhibitors in culture medium: 1 µM cytosine β-D arabinofuranoside, 10 µM 5'fluoro 2'deoxyuridine, 10 µM Uridine

2. Wash poly-D-lysine and laminin coated scaffolds in DPBS twice, and place in a 12-well tissue culture plate with 4 mL mitotic inhibitor containing medium.

3. Using a p200 pipette seed 1-2 neurospheres per well for 2D neurite outgrowth assays in a volume of 10 µL or for 3D models, 5-10 neurospheres per scaffold in a volume of 50 µL.

4. Neurospheres should then be cultured for a further 10 days, during which time neurites begin to develop from the neurospheres and either radiate from the central neurosphere in 2D culture or enter the 3D growth matrix.

Culture medium should not be replaced during the 10-day neurite outgrowth phase of culture, as this may disrupt the developing neurites.

5. Following the 10 day culture period, cultures should be fixed for 1 hour in 4 % PFA at room temperature. Samples can then be analysed by immunofluorescence as detailed below.

IMMUNOFLUORESCENCE ANALYSIS AND NEURITE QUANTIFICATION

Neurite outgrowth cultures should be analysed by staining for the pan-neuronal marker, TUJ-1, which allows visualisation of the neurites. Neurites can then be quantified using image analysis software such as Image J.

Materials

Phosphate Buffered Saline (PBS; Sigma-Aldrich, cat no. P4417)
Tween 20 (Sigma-Aldrich; cat no. P1379)
Normal Goat Serum (NGS; Sigma-Aldrich, cat no. G9023)
Triton X-100 (Sigma-Aldrich, cat no. X100)
Microscope Slides (ThermoFisher Scientific, cat no. J1800AMNZ)
Hydrophobic Blocker Pen (Vector Laboratories, cat no. H4000)
VectaShield Fluorescence Mounting Medium (Vector Laboratories, cat no. H1000)
Anti- β -III-tubulin (Anti-TUJ-1, Cambridge Bioscience, cat no. 802001)
Alexafluor anti-rabbit 488 (ThermoFisher Scientific, cat no. A11070)
Hoechst 33342 (ThermoFisher Scientific, cat no. H-5370)
22 x 50 mm Coverslips (ThermoFisher Scientific, cat no. 12373128)

Immunofluorescence Staining of Scaffolds

1. Models fixed in 4 % PFA should be permeabilised by incubating with permeabilisation buffer for 20 minutes at room temperature.

2. Models can then be blocked with blocking buffer for 30 minutes at room temperature.

3. To prepare scaffolds for primary antibody incubation, scaffolds should be placed on a clean microscope slide and drawn around with a hydrophobic barrier pen.

4. The primary antibody targeted against the pan-neuronal marker TUJ-1 should be diluted in a 1:600 ratio with blocking buffer and 150 µL of diluted antibody solution should be added to each scaffold or 2D well. Scaffolds should then be incubated for 2 hours at room temperature or overnight at 4 °C in a humidified chamber, whereas 2D cultures should be incubated for one hour at room temperature.

5. Models should then be washed three times for 10 minutes each in blocking buffer.

Washes can be carried out in a 12-well tissue culture plate.

6. Secondary antibody (Alexafluor anti-rabbit 488) should be diluted in blocking buffer at a ratio of 1:600 along with the nuclear dye Hoechst which should be diluted a concentration of 1:1,000. Scaffolds should then be placed on clean microscope slides and drawn around with a hydrophobic barrier pen. Diluted secondary antibody solution should then be added to each scaffold at a volume of 150 µL and incubated for 1 hour at room temperature in a humidified chamber. 2D models should also be incubated with 150 µL secondary antibody solution for 1 hour at room temperature.

7. Models should then be washed three times for 10 minutes in blocking buffer.

8. Scaffolds should be mounted onto clean microscope slides with a drop of Vectasheild fluorescence mounting medium and topped with a coverslip. 2D samples should be stored in PBS prior to microscopic examination. Samples are now ready for microscopic analysis.

Microscopy & Image Analysis

1. Either a 5x magnification lens or a 3 x 3 tile scan using a confocal microscope can be used to capture neurite outgrowth from neurospheres cultured in 2D. Scaffolds should be

imaged from above (top view) and below (bottom view) using a confocal microscope to reduce the out of focus light from cells present on the other side of the scaffold. The 488 and 405 nm lasers should be used to detect neurite outgrowth and nuclear staining.

The main body of the neurosphere should be visible from the top view of the scaffold, whereas neurites that have penetrated the scaffold should be visible from the bottom view of the scaffold.

2. 2D images or images taken from the bottom of the scaffolds, should be opened in Image J software for analysis. The free-hand draw tool can be used in Image J to trace individual neurites that have penetrated the scaffold, and can be measured and traced by using keyboard shortcuts such as ctrl + m and ctrl + d. For 2D studies, a gird overlay should be used in conjunction with a random number generator to identify only 3 squares per image for quantification.

REAGENTS & SOLUTIONS

EC23 Stock Solution

The molecular weight of EC23 is 332.44 and initially a stock solution of 10 mM should be produced by dissolving 1 mg of EC23 powder in 300.8 µL of sterile, cell culture grade DMSO (SigmalAldrich, cat no. D5879). This initial 10 mM stock solution can then be further diluted in DMSO in a ratio of 1:1000. This produces a 0.01 mM stock solution that can be aliquoted and stored at -80 °C until required.

Poly-D-lysine Stock Solution

Reconstitute 5 mg of poly-D-lysine powder in 5 mL sterile DPBS to give a stock solution of 1 $mgmL^{-1}$.

Mitotic Inhibitor Stock Solutions

Mitotic inhibitor stock solutions were made up at 10 mM (5'fluoro 2'deoxyuridine and uridine) or 1 mM (cytosine β-D arabinofuranoside) and diluted 1:1000 in culture medium to give a final concentration of 10 µM 5'fluoro 2'deoxyuridine and uridine) or 1 µM (cytosine β-D arabinofuranoside).

5'Fluoro 2'deoxyuridine
MW = 246.19
To achieve a 10 mM stock solution, dissolve 0.12 g of powdered substance in 50 mL sterile DPBS.

Uridine
MW = 244.2
To achieve a 10 mM stock solution, dissolve 0.12 g of powdered substance in 50 mL sterile DPBS.

Cytosine β-D arabinofuranoside
MW = 243.22
To achieve a 1 mM stock solution, dissolve 0.012 g in 50 mL sterile DPBS.

Immunofluorescence Permeabalisation Buffer

500 mL PBS
500 µL Triton X-100

Immunofluorescence Blocking Buffer

495 mL PBS
5 mL NGS
50 µL Tween-20

Blocking buffer can be stored at 4 °C for 1-2 weeks. Discard if there is any evidence of precipitate.

Background Information

Impairment of neurite outgrowth is common to many neurological disorders and has a detrimental effect on neuronal connectivity[4,5,7,8,19,20]. The development of accurate *in vitro* models of neurite outgrowth is an extremely active area of research, as neurite inhibition is a poorly understood process. *In vitro* models of neuritogenesis have many applications that range from screening of potential drug targets, neurotoxicity screening and investigations into the molecular mechanisms that underpin neurite inhibition in the context of many neurological disorders[21]. For this reason, the development of a physiologically relevant, robust and reliable model of human neuritogenesis is an important advancement in the field.

Spinal cord injury (SCI) results in the formation of an inhibitory environment known as the glial scar[2,3,22]. Growth of neurites within the glial scar is inhibited due to a combination of inhibitory factors including: mechanical inhibition in the form of an astrocytic meshwork and inhibitory molecules found on myelin debris or secreted by reactive astrocytes such as, chondroitin sulphate proteoglycans (CSPGs)[3]. The in ability of neurites to develop within the area of injury, results in a loss of neuronal innervation that leads to functional deficits associated with injury[22]. Therefore, the molecular basis of CSPG-mediated neurite inhibition has been the focus of many studies and although it is thought that CSPGs act through activation of Rho A signalling, the detailed molecular mechanism of their action still remains unclear[6,10,12,23,24]. The development of robust and reproducible neurite outgrowth models, have a potential application in the study of CSPG-mediated inhibition and the screening of potential small molecule candidate to overcome such inhibition.

Many current neurite outgrowth models rely on the 2D culture of neuronal monolayers[25–27], however, not only is 2D culture far removed from the *in vivo* microenvironment[28], quantification and tracing of neurites when cultured as monolayers can be time consuming and inaccurate. Spheroid cultures offer an alternative, as neurites radiate from a central perikaryon with minimal branching, allowing for a more simple method of quantification[9,29]. In this SOP we describe a human model of neurite outgrowth that combines spheroid and 3D scaffold technology to provide a more physiologically relevant geometry to study the development of neurites, which can be used as a screening tool to assess the effect of compounds on neurite outgrowth.

Critical Parameters

Retinoid Stocks

EC23 is critical for the successful induction of neural differentiation in this culture system. Therefore, the accurate generation of 0.01 mM stock solutions is an essential step in the preparation of EC cell derived neurite outgrowth models using this methodology. Stock solutions were typically aliquoted in volumes of 100 µL and stored at -80 °C. Repeat freeze/thaw cycles should be avoided.

Cell Stocks

TERA2.cl.SP12 embryonal carcinoma cells should be maintained as 2D monolayers prior to the seeding of cells in suspension to promote the formation of spheroids for differentiation purposes. These cells should be maintained at high confluency to maintain their pluripotent phenotype, as if cell density drops, cells may spontaneously differentiate toward an epithelial-like phenotype. Cells should be used at 100 % confluence and due to the nature of their metabolism, require frequent media changes.

Troubleshooting

Table 1 lists a selection of problems that may arise during the generation of neurite outgrowth models along with common causes and solutions.

Problem	Possible Cause	Solution
TERA2.cl.SP12 cells are not adherent in 2D maintenance cultures	Incorrect heat treatment of FBS	FBS should be incubated in a 56 °C water bath for 25 minutes
Few / small spheroids in suspension culture	Too frequent medium changes Changing of culture medium too soon after seeding	Medium should be changed 4 days after initial cell seeding in suspension and then every 3-4 days throughout the remaining culture period.
Excessive cellular migration from neurospheres	Inefficient inhibition of mitosis	Check mitotic inhibitors have been diluted to the appropriate concentration
Neurospheres missing from top of scaffolds	Excessive washes during processing	Scaffolds should be gently washed during immunofluorescence preparation and rough handling may result in the dislodgement of neurospheres from the scaffold

Table 1: Troubleshooting Guide for Induction of Neurite Outgrowth from Human Pluripotent Stem Cell-Derived Neurospheres in a Novel Three-Dimensional Assay

Bibliography:

1. Da Silva & Dotti. Breaking the neuronal sphere: regulation of the actin cytoskeleton in neuritogenesis. Nat Rev Neurosci. 2002 Sep;694–704.
2. Rolls, Shechter, & Schwartz. The bright side of the glial scar in CNS repair. Nat Rev Neurosci. 2009 Mar;235–41.
3. Yiu & He. Glial inhibition of CNS axon regeneration. Nat Rev Neurosci. 2006 Aug;617–27.
4. Xu, Park, Ohtake, Li, Hayat, Liu, Selzer, Longo, & Li. Role of CSPG receptor LAR phosphatase in restricting axon regeneration after CNS injury. Neurobiol Dis. 2015 Jan;36–48.
5. Niederost, Oertle, Fritsche, McKinney, & Bandtlow. Nogo-A and myelin-associated glycoprotein mediate neurite growth inhibition by antagonistic regulation of RhoA and Rac1. J Neurosci. 2002 Dec;10368–76.
6. Gopalakrishnan, Teusch, Imhof, Bakker, Schurdak, Burns, & Warrior. Role of Rho kinase pathway in chondroitin sulfate proteoglycan-mediated inhibition of neurite outgrowth in PC12 cells. J Neurosci Res. 2008 Aug;2214–26.
7. Petratos, Li, George, Hou, Kerr, Unabia, Hatzinisiriou, Maksel, Aguilar, & Small. The beta-amyloid protein of Alzheimer's disease increases neuronal CRMP-2 phosphorylation by a Rho-GTP mechanism. Brain. 2008 Jan;90–108.

8. Postuma, He, Nunan, Beyreuther, Masters, Barrow, & Small. Substrate-bound beta-amyloid peptides inhibit cell adhesion and neurite outgrowth in primary neuronal cultures. J Neurochem. 2000 Mar;1122–30.
9. Clarke, Tams, Henderson, Roger, Whiting, & Przyborski. A robust and reproducible human pluripotent stem cell derived model of neurite outgrowth in a three-dimensional culture system and its application to study neurite inhibition. Neurochem Int.
10. Lingor, Teusch, Schwarz, Mueller, Mack, Bahr, & Mueller. Inhibition of Rho kinase (ROCK) increases neurite outgrowth on chondroitin sulphate proteoglycan in vitro and axonal regeneration in the adult optic nerve in vivo. J Neurochem. 2007 Oct;181–9.
11. Monnier, Sierra, Schwab, Henke-Fahle, & Mueller. The Rho/ROCK pathway mediates neurite growth-inhibitory activity associated with the chondroitin sulfate proteoglycans of the CNS glial scar. Mol Cell Neurosci. 2003 Mar;319–30.
12. Fujita & Yamashita. Axon growth inhibition by RhoA/ROCK in the central nervous system. Vol. 8, Frontiers in Neuroscience. 2014.8.
13. Dou & Levine. Inhibition of neurite growth by the NG2 chondroitin sulfate proteoglycan. J Neurosci. 1994 Dec;7616–28.
14. Costa, Planchenault, Charriere-Bertrand, Mouchel, Fages, Juliano, Lefrancois, Barlovatz-Meimon, & Tardy. Astroglial permissivity for neuritic outgrowth in neuron-astrocyte cocultures depends on regulation of laminin bioavailability. Glia. 2002 Feb;105–13.
15. Przyborski. Isolation of human embryonal carcinoma stem cells by immunomagnetic sorting. Stem Cells. 2001;500–4.
16. Przyborski, Smith, & Wood. Transcriptional profiling of neuronal differentiation by human embryonal carcinoma stem cells in vitro. Stem Cells. 2003;459–71.
17. Przyborski, Morton, Wood, & Andrews. Developmental regulation of neurogenesis in the pluripotent human embryonal carcinoma cell line NTERA-2. Eur J Neurosci. 2000 Oct;3521–8.
18. Przyborski, Christie, Hayman, Stewart, & Horrocks. Human embryonal carcinoma stem cells: models of embryonic development in humans. Stem Cells Dev. 2004 Aug;400–8.
19. Winner, Melrose, Zhao, Hinkle, Yue, Kent, Braithwaite, Ogholikhan, Aigner, Winkler, Farrer, & Gage. Adult neurogenesis and neurite outgrowth are impaired in LRRK2 G2019S mice. Neurobiol Dis. 2011 Mar;706–16.
20. Takenouchi, Hashimoto, Hsu, Mackowski, Rockenstein, Mallory, & Masliah. Reduced neuritic outgrowth and cell adhesion in neuronal cells transfected with human alpha-synuclein. Mol Cell Neurosci. 2001 Jan;141–50.
21. Avior, Sagi, & Benvenisty. Pluripotent stem cells in disease modelling and drug discovery. Nat Rev Mol Cell Biol. 2016 Mar;170–82.
22. Fawcett & Asher. The glial scar and central nervous system repair. Brain Res Bull. 1999 Aug;377–91.
23. Fu, Hue, & Li. Nonsteroidal anti-inflammatory drugs promote axon regeneration via RhoA inhibition. J Neurosci. 2007 Apr;4154–64.
24. Dill, Patel, Yang, Bachoo, Powell, & Li. A Molecular Mechanism for Ibuprofen-Mediated RhoA Inhibition in Neurons. Vol. 30, The Journal of neuroscience : the official journal of the Society for Neuroscience. 2010.30(3) p. 963–72.
25. Mitchell, Hanson, Quets-Nguyen, Bergeron, & Smith. A quantitative method for analysis of in vitro neurite outgrowth. J Neurosci Methods. 2007 Aug 30;350–62.
26. Radio & Mundy. Developmental neurotoxicity testing in vitro: Models for assessing chemical effects on neurite outgrowth. Neurotoxicology. 2008 May;361–76.
27. Benson, Romero, Lush, Lu, Henkemeyer, & Parada. Ephrin-B3 is a myelin-based inhibitor of neurite outgrowth. Proc Natl Acad Sci United States Am. 2005 Jul 26;10694–9.
28. Knight & Przyborski. Advances in 3D cell culture technologies enabling tissue-like structures to be created in vitro. J Anat. 2015 Dec 1;746–56.
29. Stewart, Christie, & Przyborski. Manipulation of human pluripotent embryonal carcinoma stem cells and the development of neural subtypes. Stem Cells. 2003;248–56.